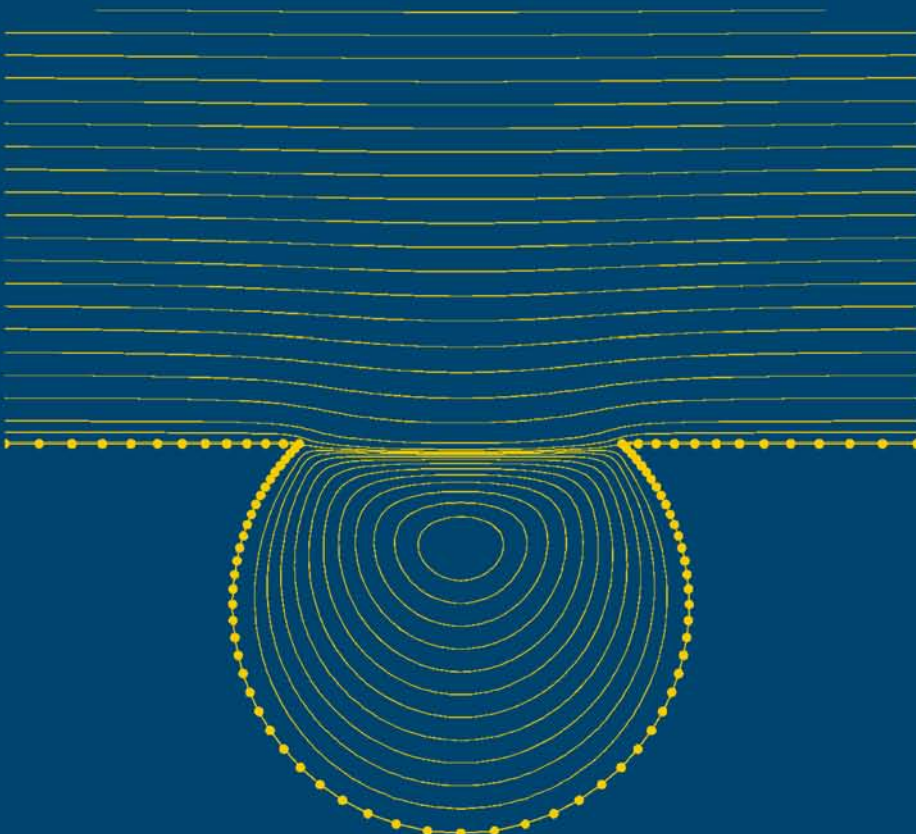


A Practical Guide to
**BOUNDARY
ELEMENTS METHODS**
with the Software Library BEMLIB



COSTAS POZRIKIDIS



CHAPMAN & HALL/CRC

A Practical Guide to
BOUNDARY
ELEMENT METHODS
with the Software Library BEMLIB

A Practical Guide to
**BOUNDARY
ELEMENT METHODS**
with the Software Library BEMLIB

C. POZRIKIDIS



CHAPMAN & HALL/CRC

A CRC Press Company
Boca Raton London New York Washington, D.C.

Library of Congress Cataloging-in-Publication Data

Pozrikidis, C.

A practical guide to boundary element methods with the software library BEMLIB / by
Costas Pozrikidis.

p. cm.

Includes bibliographical references and index.

ISBN 1-58488-323-5

1. Boundary element methods—Data processing. 2. Computer programming. I. Title.

TA347.B69 P69 2002

620'.001'51535—dc21

2002024166

This book contains information obtained from authentic and highly regarded sources. Reprinted material is quoted with permission, and sources are indicated. A wide variety of references are listed. Reasonable efforts have been made to publish reliable data and information, but the author and the publisher cannot assume responsibility for the validity of all materials or for the consequences of their use.

Neither this book nor any part may be reproduced or transmitted in any form or by any means, electronic or mechanical, including photocopying, microfilming, and recording, or by any information storage or retrieval system, without prior permission in writing from the publisher.

The consent of CRC Press LLC does not extend to copying for general distribution, for promotion, for creating new works, or for resale. Specific permission must be obtained in writing from CRC Press LLC for such copying.

Direct all inquiries to CRC Press LLC, 2000 N.W. Corporate Blvd., Boca Raton, Florida 33431.

Trademark Notice: Product or corporate names may be trademarks or registered trademarks, and are used only for identification and explanation, without intent to infringe.

Visit the CRC Press Web site at www.crcpress.com

© 2002 by Chapman & Hall/CRC

No claim to original U.S. Government works

International Standard Book Number 1-58488-323-5

Library of Congress Card Number 2002024166

Printed in the United States of America 1 2 3 4 5 6 7 8 9 0

Printed on acid-free paper

Preface

In the last 20 years, the boundary-element method (BEM) has been established as a powerful numerical technique for tackling a variety of problems in science and engineering involving elliptic partial differential equations. Examples can be drawn from the fields of elasticity, geomechanics, structural mechanics, electromagnetism, acoustics, hydraulics, low-Reynolds-number hydrodynamics, and biomechanics. The strength of the method derives from its ability to solve efficiently and accurately problems in domains with complex and possibly evolving geometry where traditional methods can be inefficient, cumbersome, or unreliable.

The purpose of this text is to provide a concise introduction to the theory and implementation of the boundary-element method, while simultaneously offering hands-on experience based on the software library *BEMLIB*. The intended audience includes professionals, researchers, and students in various branches of computational science and engineering. The material is suitable for self-study, and the text is appropriate for instruction in an introductory course on boundary-integral and boundary-element methods, or a more general course in computational science and engineering.

The software library *BEMLIB* accompanying this book contains a collection of FORTRAN 77 programs related to Green's functions and boundary-element methods for Laplace's equation, Helmholtz's equation, and Stokes flow. The main directories contain subdirectories that include main programs, assisting subroutines, and utility subroutines. Linked with drivers, the utility subroutines become stand-alone modules. The programs of *BEMLIB* explicitly illustrate how procedures and concepts discussed in the text translate into code instructions, and demonstrate the mathematical formulation and structure of boundary-element codes for a variety of applications. The output of the codes is recorded in tabular form so that it can be displayed using independent graphics, visualization, and animation applications. The codes of *BEMLIB* can be used as building blocks, and may serve as a point of departure for developing further codes. General information on *BEMLIB*, the directory contents, and instructions on how to download and compile the codes are given in Chapter 8.

Consistent with the dual nature of this book as an introductory text and a software user guide, the material is divided into two parts. The first part, Chapters 1 to 7, discusses the theory and implementation of boundary-element methods. The material includes classical topics and recent development such as the method of approximate particular solutions and the dual reciprocity method for solving inhomogeneous, nonlinear, and time-dependent equations.

The second part, Chapters 8 to 12, contains the user guide to *BEMLIB*. The user guide explains the problem formulation and numerical method of the particular problems considered, and discusses the function of the individual subprograms and codes with emphasis on implementation.

I am indebted to Audrey Hill for her assistance in the preparation of the manuscript, to Judith Kamin for skillfully and gracefully coordinating the production, and to Todd Porteous for his flawless work in setting up the hardware and configuring the software.

C. Pozrikidis

Contents

Frequently Asked Questions	xi
1 Laplace's equation in one dimension	1
1.1 Green's first and second identities and the reciprocal relation	1
1.2 Green's functions	2
1.3 Boundary-value representation	7
1.4 Boundary-value equation	8
2 Laplace's equation in two dimensions	9
2.1 Green's first and second identities and the reciprocal relation	9
2.2 Green's functions	12
2.3 Integral representation	19
2.4 Integral equations	28
2.5 Hypersingular integrals	36
2.6 Irrotational flow	44
2.7 Generalized single- and double-layer representations	47
3 Boundary-element methods for Laplace's equation in two dimensions	53
3.1 Boundary element discretization	53
3.2 Discretization of the integral representation	63
3.3 The boundary-element collocation method	74
3.4 Isoparametric cubic-splines discretization	77
3.5 High-order collocation methods	80
3.6 Galerkin and global expansion methods	86
4 Laplace's equation in three dimensions	91
4.1 Green's first and second identities and the reciprocal relation	91
4.2 Green's functions	93
4.3 Integral representation	100
4.4 Integral equations	102
4.5 Axisymmetric fields in axisymmetric domains	106
5 Boundary-element methods for Laplace's equation in three dimensions	111
5.1 Discretization	111
5.2 Three-node flat triangles	117
5.3 Six-node curved triangles	122
5.4 High-order expansions	127

6 Inhomogeneous, nonlinear, and time-dependent problems	131
6.1 Distributed source and domain integrals	132
6.2 Particular solutions and dual reciprocity in one dimension	134
6.3 Particular solutions and dual reciprocity in two and three dimensions	141
6.4 Convection – diffusion equation	150
6.5 Time-dependent problems	154
7 Viscous flow	161
7.1 Governing equations	161
7.2 Stokes flow	165
7.3 Boundary integral equations in two dimensions	171
7.4 Boundary-integral equations in three dimensions	175
7.5 Boundary-element methods	178
7.6 Interfacial dynamics	180
7.7 Unsteady, Navier-Stokes, and non-Newtonian flow	182
8 BEMLIB user guide	191
8.1 General information	191
8.2 Terms and conditions	192
8.3 Directory contents	193
9 Directory: grids	197
grid_2d	198
trgl	203
10 Directory: laplace	207
lgf_2d	209
lgf_3d	230
lgf_ax	245
flow_1d	254
flow_1d_1p	261
flow_2d	265
body_2d	270
body_ax	276
tank_2d	281
ldr_3d	287
lnm_3d	291
11 Directory: helmholtz	295
flow_1d_osc	296
12 Directory: stokes	301
sgf_2d	302
sgf_3d	329
sgf_ax	349
flow_2d	364

<code>prtcl_sw</code>	371
<code>prtcl_2d</code>	376
<code>prtcl_ax</code>	385
<code>prtcl_3d</code>	390
Appendix A Mathematical supplement	397
Appendix B Gauss elimination and linear solvers	403
Appendix C Elastostatics	407
References	413
Index	418

Frequently Asked Questions

1. What is the boundary-element method (BEM)?

The boundary-element method is a numerical method for solving partial differential equations encountered in mathematical physics and engineering. Examples include Laplace's equation, Helmholtz's equation, the convection-diffusion equation, the equations of potential and viscous flow, the equations of electrostatics and electromagnetics, and the equations of linear elastostatics and elastodynamics.

2. Is there a restriction on the type of differential equation?

In principle, the answer is negative. In practice, however, the method is efficient and thus appropriate for linear, elliptic, and homogeneous partial differential equations governing boundary-value problems in the absence of a homogeneous source.

3. What are the advantages of the boundary-element method?

Suppose that we want to find the solution of an elliptic partial differential equation in a two-dimensional domain. In the boundary-element method, we solve only for the boundary distribution of the unknown function or one of its derivatives. *It is not necessary to compute the requisite function throughout the domain of solution.* Once the unknown boundary distribution is available, the solution at any point may be produced by direct evaluation. Thus, the crux of the boundary-element method is the reduction of the dimension of the solution space with respect to physical space by one unit.

4. How is this accomplished?

The key idea is to express the solution in terms of boundary distributions of fundamental solutions of the particular differential equation considered. The fundamental solutions are Green's functions expressing the field due to a localized source. The densities of the distributions are then computed to satisfy the specified boundary conditions.

5. What is the origin of the terminology “boundary-element method”?

The name derives from the practice of discretizing the boundary of a solution domain into “boundary elements.” In the case of a two-dimensional solution domain, the

boundary is a planar line, and the boundary elements are straight segments, parabolas, circular arcs, or cubic segments. In the case of a three-dimensional solution domain, the boundary is a three-dimensional surface, and the boundary elements are flat triangles, curved triangles, or rectangles. In contrast, elements that arise from the discretization of the solution domain itself are called “finite elements.”

6. When was the boundary-element method conceived?

Integral representations of the solution of elliptic partial differential equations, including Laplace’s equation and the equations of linear elastostatics, have been known for well over a century (e.g., [33]).

In 1963, M. A. Jaswon and G. T. Symm [31, 66] demonstrated that the associated integral equations can be solved accurately and reliably using numerical methods. In 1978, C. A. Brebbia [9] formalized the boundary-integral equation method (BIEM) and introduced the terminology *boundary-element method* (BEM), which contrasted with the already established terminology *finite-element method* (FEM).

7. What are the disadvantages of the boundary-element method?

Some initial effort is required to learn the fundamental principles underlying the integral representations and the implementation of the numerical methods. An oversight in the mathematical formulation, a mistake in the implementation of the numerical methods, or an error in a code is likely to have a catastrophic effect on the accuracy of the solution.

8. How does the BEM compare with the finite-difference method (FDM) and the finite-element method (FEM)?

For linear and elliptic problems, the BEM is vastly superior in both efficiency and accuracy. Alternative methods require discretizing the whole of the solution domain, and this considerably raises the cost of the computation. Problems that can be solved on a laptop computer using the boundary-element method may require the use of a supercomputer by finite-difference and finite-element methods for the same level of accuracy.

9. What should one know before one can understand the foundation of the BEM?

General knowledge of differential and integral calculus and introductory linear algebra is required.

10. What should one know before one can write a BEM code?

General purpose numerical methods including numerical linear algebra, function interpolation, and function integration are required. The necessary topics are discussed in this book. Familiarity with a computer programming language, preferably FORTRAN, is a prerequisite.

11. How can one keep up to date with the growing literature on boundary-element methods?

The internet site: <http://www.olemiss.edu/sciencenet/benet> provides a wealth of updated information on books, journals, research, and software related to boundary-element methods.

Chapter 1

Laplace's equation in one dimension

To introduce the fundamental ideas underlying the development of the boundary-element method, we begin by considering Laplace's equation in one dimension for an unknown function $f(x)$,

$$\frac{d^2 f}{dx^2} = 0. \quad (1.1)$$

The solution is to be found over a specified interval of the x axis, $a \leq x \leq b$, subject to two boundary conditions for the function $f(x)$ or its first derivative $df(x)/dx$ at one or both ends $x = a, b$.

Using elementary calculus, we find that the general solution of (1.1) is the linear function,

$$f(x) = m x + c, \quad (1.2)$$

where the slope coefficient m and the constant c are computed by enforcing the two boundary conditions. For example, if the solution is required to satisfy $f(0) = 1$ and $f(1) = 3$, then $m = 2$ and $c = 1$.

Pretending that we are unaware of the analytical solution given in (1.2), we proceed to formulate the problem in an alternative fashion by working in four stages. First, we discuss Green's first and second identities and the reciprocal relation. Second, we introduce the Green's functions. Third, we develop a boundary-value representation. Finally, we derive a boundary-value equation that serves as a prelude to the boundary-integral equations developed in subsequent chapters for partial differential equations.

1.1 Green's first and second identities and the reciprocal relation

Multiplying the left-hand side of (1.1) by a twice-differentiable function $\phi(x)$ and rearranging, we obtain Green's first identity

$$\phi \frac{d^2 f}{dx^2} = \frac{d}{dx} [\phi \frac{df}{dx}] - \frac{d\phi}{dx} \frac{df}{dx}. \quad (1.1.1)$$

Interchanging the roles of f and ϕ , we derive the transposed form

$$f \frac{d^2 \phi}{dx^2} = \frac{d}{dx} [f \frac{d\phi}{dx}] - \frac{df}{dx} \frac{d\phi}{dx}. \quad (1.1.2)$$

Subtracting (1.1.2) from (1.1.1), we obtain Green's second identity

$$\phi \frac{d^2 f}{dx^2} - f \frac{d^2 \phi}{dx^2} = \frac{d}{dx} [\phi \frac{df}{dx} - f \frac{d\phi}{dx}]. \quad (1.1.3)$$

If functions f and ϕ both satisfy Laplace's equation (1.1), then the left-hand side of (1.1.3) vanishes, yielding the reciprocal relation

$$\frac{d}{dx} [\phi \frac{df}{dx} - f \frac{d\phi}{dx}] = 0, \quad (1.1.4)$$

Green's second identity will be our point of departure for developing the requisite boundary-value representation in Section 1.3.

1.2 Green's functions

A Green's function of the one-dimensional Laplace equation satisfies Laplace's equation (1.1) everywhere except at an arbitrarily chosen point $x = x_0$. At that point, the Green's function is singular, that is, it takes an infinite value.

By definition, the Green's function, denoted by $G(x, x_0)$, satisfies the singularly forced Laplace equation

$$\frac{d^2 G(x, x_0)}{dx^2} + \delta_1(x - x_0) = 0, \quad (1.2.1)$$

where:

- x is the variable “field point”.
- x_0 is the fixed location of the singular “point” or “pole.”
- $\delta_1(x - x_0)$ is Dirac's delta function in one dimension.

By construction, Dirac's delta function in one dimension is distinguished by the following properties:

1. $\delta_1(x - x_0)$ vanishes everywhere except at the point $x = x_0$, where it becomes infinite.
2. The integral of δ_1 with respect to x over an interval I that contains the point x_0 is equal to unity,

$$\int_I \delta_1(x - x_0) dx = 1. \quad (1.2.2)$$

This property reveals that the delta function with argument of length has units of inverse length.

3. The integral of the product of an arbitrary function $q(x)$ and the delta function over an interval I that contains the point x_0 is equal to value of the function at the singular point,

$$\int_D \delta_1(x - x_0) q(x) dx = q(x_0). \quad (1.2.3)$$

The integral of the product of an arbitrary function $q(x)$ and the delta function over an interval I that does *not* contain the point x_0 is equal to zero.

4. In formal mathematics, $\delta_1(x - x_0)$ arises from the family of test functions

$$g(x - x_0) = \left(\frac{\lambda}{\pi L^2}\right)^{1/2} \exp\left[-\lambda \frac{(x - x_0)^2}{L^2}\right], \quad (1.2.4)$$

in the limit as the dimensionless parameter λ tends to infinity; in equation (1.2.4), L is an arbitrary length,

Figure 1.2.1 shows graphs of a family of dimensionless test functions $G \equiv gL$ plotted against the dimensionless distance $X \equiv (x - x_0)/L$ for $\lambda = 1$ (dashed line), 2, 5, 10, 20, 50, 100, and 500 (dotted line). The maximum height of each graph is inversely proportional to its width, so that the area underneath each graph is equal to unity,

$$\int_{-\infty}^{\infty} g(x) dx = \left(\frac{\lambda}{\pi L^2}\right)^{1/2} \int_{-\infty}^{\infty} \exp\left(-\lambda \frac{x^2}{L^2}\right) dx = 1. \quad (1.2.5)$$

To prove this identity, we recall the definite integral associated with the error function,

$$\frac{2}{\sqrt{\pi}} \int_0^{\infty} \exp[-w^2] dw = 1, \quad (1.2.6)$$

and substitute $w = \lambda^{1/2} x/L$.

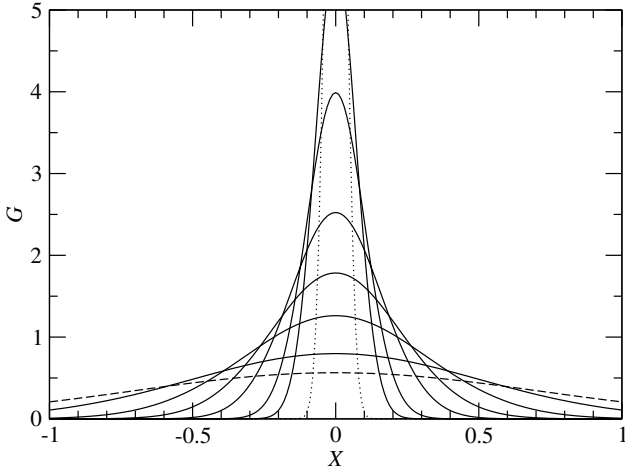


Figure 1.2.1 A family of dimensionless test functions $G \equiv g_L$ described by (1.2.4) plotted against the dimensionless distance $X \equiv (x - x_0)/L$ for $\lambda = 1$ (dashed line), 2, 5, 10, 20, 50, 100, and 500 (dotted line). In the limit as the dimensionless parameter λ tends to infinity, we recover Dirac's delta function in one dimension.

A solution of equation (1.2.1) is the piecewise linear function whose slope equal to $-\frac{1}{2}$ when $x > x_0$, and $\frac{1}{2}$ when $x < x_0$, given by

$$G(x, x_0) = \begin{cases} -\frac{1}{2}(x - x_0) & \text{if } x > x_0 \\ \frac{1}{2}(x - x_0) & \text{if } x < x_0 \end{cases}, \quad (1.2.7)$$

as depicted in Figure 1.2.2. Alternatively, we may write

$$G(x, x_0) = -\frac{1}{2} |x - x_0|. \quad (1.2.8)$$

An arbitrary constant may be added to the right-hand side of (1.2.8) without affecting the impending derivation of the boundary-value representation.

Equation (1.2.8) illustrates that the Green's function enjoys the symmetry property

$$G(x, x_0) = G(x_0, x). \quad (1.2.9)$$

We shall see in later chapters that similar symmetry properties are satisfied by Green's functions of partial differential equations involving self-adjoint differential operators, including Laplace's equation in two and three dimensions. These symmetry properties play an important role in the physical interpretation of the boundary-value and boundary-integral representations.

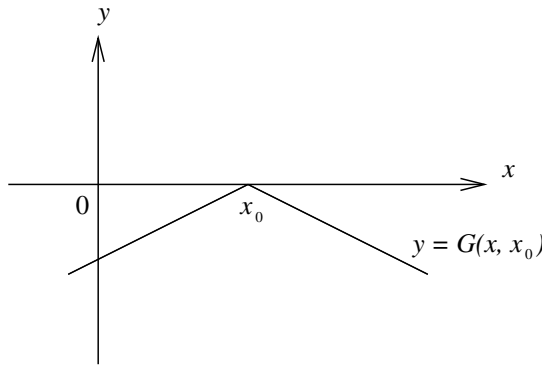


Figure 1.2.2 Graph of the Green's function of Laplace's equation in one dimension satisfying equation (1.2.1). The singular point x_0 is the pole of the Green's function.

1.2.1 Green's function dipole

Differentiating the right-hand side of (1.2.7) with respect to the field point x , we find that the derivative of the Green's function is a piecewise constant function,

$$\frac{dG(x, x_0)}{dx} = \begin{cases} -\frac{1}{2} & \text{if } x > x_0 \\ \frac{1}{2} & \text{if } x < x_0 \end{cases}. \quad (1.2.10)$$

Since the first derivative of the Green's function is discontinuous at the singular point, it is not surprising that the second derivative behaves like a delta function according to (1.2.1).

Problems

P.1.2.1 The Heaviside function

Show that the integral of $\delta_1(x' - x_0)$ with respect to x' from negative infinity to x is the shifted Heaviside function $H(x - x_0)$, which is equal to zero when $x < x_0$, and unity when $x > x_0$.

P.1.2.2 Green's function of Helmholtz's equation in one dimension

(a) Show that any two solutions of Helmholtz's equation in one dimension

$$\frac{d^2 f}{dx^2} - c f = 0, \quad (1)$$

satisfy the reciprocal relation (1.1.4); c is a real or complex constant.

(b) A Green's function of Helmholtz's equation in one dimension satisfies the equation

$$\frac{d^2G(x, x_0)}{dx^2} - c G(x, x_0) + \delta_1(x - x_0) = 0. \quad (2)$$

When $c = -\lambda^2$, where λ is a real constant, the Green's function is given by

$$G(x, x_0) = -\frac{1}{2\lambda} \sin(\lambda|x - x_0|). \quad (3)$$

When $c = \lambda^2$, where λ is a real constant, the Green's function is given by

$$G(x, x_0) = -\frac{1}{2\lambda} \sinh(\lambda|x - x_0|). \quad (4)$$

Confirm that, in the limit as λ tends to zero, the Green's functions (3) and (4) reduce to the Green's function of Laplace's equation given in (1.2.7).

P.1.2.3 Convection – diffusion in uniform flow

The steady-state temperature or species concentration field $f(x)$ in a uniform flow with constant velocity U is governed by the linear convection – diffusion equation

$$U \frac{df}{dx} = \kappa \frac{d^2f}{dx^2}, \quad (1)$$

where κ is the thermal or species diffusivity. The corresponding Green's function satisfies the equation

$$U \frac{dG(x, x_0)}{dx} = \kappa \frac{d^2G(x, x_0)}{dx^2} + \delta_1(x - x_0). \quad (2)$$

Show that

$$G(x, x_0) = \frac{1}{\kappa} H(x, x_0) \exp\left[\frac{U(x - x_0)}{2\kappa}\right], \quad (3)$$

where $H(x, x_0)$ is the Green's function of Helmholtz's equation given by the right-hand side of equation (4) of P.1.2.2 with $\lambda = |U|/(2\kappa)$. Thus,

$$G(\mathbf{x}, \mathbf{x}_0) = -\frac{1}{|U|} \sinh\left(\frac{|U||x - x_0|}{2\kappa}\right) \exp\left[\frac{U(x - x_0)}{2\kappa}\right]. \quad (4)$$

1.3 Boundary-value representation

Let us return to Green's second identity (1.1.3), and identify the function ϕ with the Green's function given in (1.2.7), where the singular point x_0 is located inside the solution domain $a < x_0 < b$. Using the definition in (1.2.1), and assuming that the function f satisfies (1.1), we find

$$f(x) \delta(x - x_0) = \frac{d}{dx} [G(x, x_0) \frac{df(x)}{dx} - f(x) \frac{dG(x, x_0)}{dx}]. \quad (1.3.1)$$

Integrating both sides of (1.3.1) with respect to x over the solution domain $[a, b]$, and using the distinctive properties of the delta function and the fundamental theorem of calculus, we obtain the representation

$$\begin{aligned} \int_a^b f(x) \delta(x - x_0) dx &= f(x_0) \\ &= [G(x, x_0) \frac{df(x)}{dx} - f(x) \frac{dG(x, x_0)}{dx}]_{x=b} \\ &\quad - [G(x, x_0) \frac{df(x)}{dx} - f(x) \frac{dG(x, x_0)}{dx}]_{x=a}. \end{aligned} \quad (1.3.2)$$

A slight rearrangement yields

$$\begin{aligned} f(x_0) &= -(\frac{df}{dx})_{x=a} G(x_0, x = a) + (\frac{df}{dx})_{x=b} G(x_0, x = b) \\ &\quad + f(x = a) (\frac{dG(x, x_0)}{dx})_{x=a} - f(x = b) (\frac{dG(x, x_0)}{dx})_{x=b}. \end{aligned} \quad (1.3.3)$$

Denoting df/dx by q , we obtain

$$\begin{aligned} f(x_0) &= -q(x = a) G(x_0, x = a) + q(x = b) G(x_0, x = b) \\ &\quad + f(x = a) (\frac{dG(x, x_0)}{dx})_{x=a} - f(x = b) (\frac{dG(x, x_0)}{dx})_{x=b}, \end{aligned} \quad (1.3.4)$$

which can be regarded as a boundary-value representation: if $f(x = a)$, $f(x = b)$, $q(x = a)$, and $q(x = b)$ are known, the right-hand side of (1.3.4) may be evaluated for any value of x_0 , thereby providing us with the solution.

Using expressions (1.2.7) and (1.2.10) for the Green's function and its derivative, we recast (1.3.4) into the explicit form

$$\begin{aligned} f(x_0) &= \frac{1}{2} q(x = a) (x_0 - a) + \frac{1}{2} q(x = b) (x_0 - b) \\ &\quad + \frac{1}{2} f(x = a) + \frac{1}{2} f(x = b). \end{aligned} \quad (1.3.5)$$

Equation (1.1) demands that the slope df/dx be constant, independent of x . Setting $q(x = a) = q(x = b) = q$, we obtain

$$f(x_0) = q \cdot (x_0 - \frac{a+b}{2}) + \frac{1}{2}[f(x=a) + f(x=b)], \quad (1.3.6)$$

which reproduces the linear solution given in (1.2).

Problem

P.1.3.1 Helmholtz's equation

Develop the counterpart of the boundary-value representation (1.3.4) for Helmholtz's equation in one dimension, equation (1) of P.1.2.2, involving the corresponding Green's function.

1.4 Boundary-value equation

In practice, boundary conditions provide us with two of the following three values:

$$f(x=b), \quad f(x=a), \quad q.$$

To compute the unknown value, we take the limit of (1.3.6) as the point x_0 approaches one of the end-points a or b , and thereby derive an algebraic relation called the “boundary-value equation.”

For example, if $f(x = b)$ and $f(x = a)$ are specified, we may evaluate (1.3.6) at $x_0 = b$, and rearrange to obtain the familiar expression for the slope of a straight line

$$q = \frac{f(x=b) - f(x=a)}{b - a}. \quad (1.4.1)$$

Substituting (1.4.1) into (1.3.6) completes the boundary-value representation.

In the case of Laplace's equation in one dimension discussed in this chapter, the boundary-value representation has provided us with an algebraic equation for an unknown boundary value.

In the case of Laplace's equation and other partial differential equations in two- and three-dimensional domains discussed in the remainder of this book, analogous formulations will result in integral equations for the boundary distribution of an unknown function. The numerical solution of these integral equations is the fundamental goal of the boundary-element method.

Chapter 2

Laplace's equation in two dimensions

Laplace's equation in two dimensions takes the form of the linear, elliptic, and homogeneous partial differential equation

$$\nabla^2 f(x, y) = 0, \quad (2.1)$$

where ∇^2 is the Laplacian operator in the xy plane defined as

$$\nabla^2 \equiv \frac{\partial^2}{\partial x^2} + \frac{\partial^2}{\partial y^2}. \quad (2.2)$$

A function that satisfies (2.1) is called harmonic.

To compute the solution of (2.1) in a certain solution domain, we require boundary conditions for the unknown function f (Dirichlet boundary condition), its normal derivative (Neumann boundary condition), or a combination thereof (mixed or Robin boundary condition) along overlapping or complementary parts of the boundary.

Following the analysis of Chapter 1, we proceed to formulate the solution in terms of an integral equation by working in four stages. First, we discuss Green's first and second identities and the reciprocal relation. Second, we introduce the Green's functions of Laplace's equation in two dimensions. Third, we develop a boundary-integral representation. Finally, we derive an integral equation that we then solve using the boundary-element method.

2.1 Green's first and second identities and the reciprocal relation

Green's first identity states that any two twice-differentiable functions $f(x, y)$ and $\phi(x, y)$ satisfy the relation

$$\phi \nabla^2 f = \nabla \cdot (\phi \nabla f) - \nabla \phi \cdot \nabla f. \quad (2.1.1)$$

Note the similarity with (1.1.1) for the corresponding problem in one dimension.

In index notation, equation (2.1.1) takes the form

$$\frac{\partial^2 f}{\partial x_i \partial x_i} = \frac{\partial}{\partial x_i} \left(\phi \frac{\partial f}{\partial x_i} \right) - \frac{\partial \phi}{\partial x_i} \frac{\partial f}{\partial x_i}, \quad (2.1.2)$$

where summation over the repeated index i is implied in the range $i = 1, 2$, corresponding to x and y (Appendix A). The proof of (2.1.2) requires elementary operations following the observation that $\nabla^2 = \nabla \cdot (\nabla f)$, that is, the Laplacian of a scalar function is equal to the divergence of its gradient (Appendix A).

Interchanging the roles of f and ϕ , we obtain the converse relation

$$f \nabla^2 \phi = \nabla \cdot (f \nabla \phi) - \nabla f \cdot \nabla \phi. \quad (2.1.3)$$

Subtracting (2.1.3) from (2.1.1), we derive Green's second identity

$$\phi \nabla^2 f - f \nabla^2 \phi = \nabla \cdot (\phi \nabla f - f \nabla \phi). \quad (2.1.4)$$

If both functions f and ϕ satisfy Laplace's equation (2.1), the left-hand side of (2.1.4) vanishes, yielding the reciprocal relation for harmonic functions

$$\nabla \cdot (\phi \nabla f - f \nabla \phi) = 0, \quad (2.1.5)$$

which is the two-dimensional counterpart of (1.1.4).

2.1.1 Integral form of the reciprocal relation

The integral form of the reciprocal relation arises by integrating both sides of the reciprocal relation (2.1.5) over an arbitrary control area A_c that is bounded by a closed line or a collection of closed lines denoted by C , as illustrated in Figure 2.1.1.

Using the divergence theorem in the plane (Appendix A), we convert the areal integral to a line integral, and thereby obtain the integral statement

$$\int \int_{A_c} (\phi \nabla f - f \nabla \phi) \cdot \mathbf{n} dA = 0, \quad (2.1.6)$$

where \mathbf{n} is the unit vector normal to C pointing into the control area, and $dA = dx dy$ is a differential area in the xy plane.

Equation (2.1.6) imposes an integral constraint on the boundary values and boundary distribution of the normal derivatives of any pair of non-singular harmonic functions f and ϕ . If we identify f with an unknown function and ϕ with a specified test function, then we can use (2.1.6) to obtain information on, and even construct, a desired solution. The most appropriate family of test functions are the Green's functions discussed next in Section 2.2.

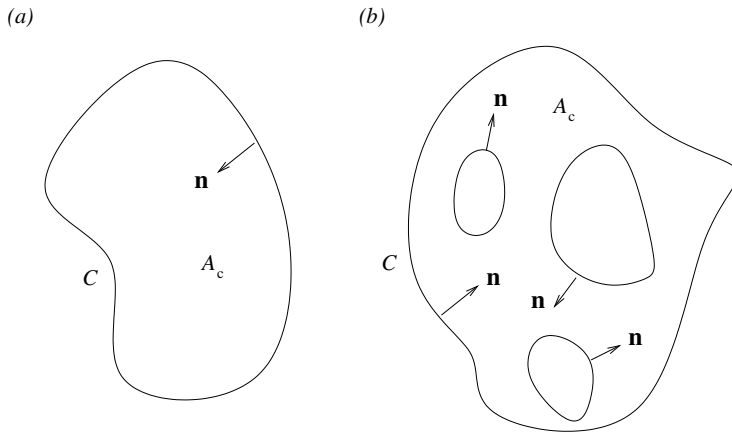


Figure 2.1.1 A control area in the xy plane enclosed by (a) a closed line, and (b) a collection of closed lines.

Problem

P.2.1.1 Kirchhoff transformation

Laplace's equation describes the steady-state distribution of temperature T in a domain occupied by a homogeneous material with uniform thermal conductivity k .

If the thermal conductivity is not constant but varies with position over the medium, then the temperature distribution is described by the generalized equation

$$\frac{\partial}{\partial x} \left(k \frac{\partial T}{\partial x} \right) + \frac{\partial}{\partial y} \left(k \frac{\partial T}{\partial y} \right) = 0, \quad (1)$$

which arises by balancing the thermal fluxes expressed by Fick's law over an infinitesimal area.

Consider heat conduction in a homogeneous material where the thermal conductivity is a function of the local temperature, that is, $k = q(T)$, where $q(T)$ is a given function, and introduce the Kirchhoff transformation

$$f(T) = \int_{T_0}^T q(\eta) d\eta, \quad \frac{df}{dT} = q(T), \quad (2)$$

where T_0 is an arbitrary reference temperature, and η is a dummy variable of integration. The function $f(T)$ is an implicit function of position through the dependence of T on x and y . Show that (a) the gradients of f and T are related by $\nabla f = k \nabla T$, and (b) $f(x, y)$ satisfies Laplace's equation (2. 1).

2.2 Green's functions

The Green's functions of Laplace's equation in two dimensions constitute a special class of harmonic functions that are singular at an arbitrary point $\mathbf{x}_0 = (x_0, y_0)$. By definition, a Green's function satisfies the singularly forced Laplace's equation

$$\nabla^2 G(\mathbf{x}, \mathbf{x}_0) + \delta_2(\mathbf{x} - \mathbf{x}_0) = 0, \quad (2.2.1)$$

where:

- $\mathbf{x} = (x, y)$ is the variable “field point.”
- $\mathbf{x}_0 = (x_0, y_0)$ is the fixed location of the “singular point” or “pole.”
- $\delta_2(\mathbf{x} - \mathbf{x}_0)$, written more explicitly as $\delta_2(x - x_0, y - y_0)$, is Dirac's delta function in two dimensions.

By construction, Dirac's delta function in two dimensions is endowed with the following properties:

1. $\delta_2(x - x_0, y - y_0)$ vanishes everywhere except at the point $x = x_0, y = y_0$, where it becomes infinite.
2. The integral of the delta function over an area D that contains the singular point (x_0, y_0) is equal to unity,

$$\int_D \delta_2(x - x_0, y - y_0) dx dy = 1. \quad (2.2.2)$$

This property illustrates that the delta function in the xy plane has units of inverse squared length.

3. The integral of the product of an arbitrary function $f(x, y)$ and the delta function over an area D that contains the singular point (x_0, y_0) is equal to the value of the function at the singular point,

$$\int_D \delta_2(x - x_0, y - y_0) f(x, y) dx dy = f(x_0, y_0). \quad (2.2.3)$$

The integral of the product of an arbitrary function $f(x, y)$ and the delta function over an area D that does *not* contain the singular point (x_0, y_0) is equal to zero.

4. In formal mathematics, $\delta_2(x - x_0, y - y_0)$ arises from the family of test functions

$$q(r) = \frac{\lambda}{\pi L^2} \exp(-\lambda \frac{r^2}{L^2}), \quad (2.2.4)$$

in the limit as the dimensionless parameter λ tends to infinity, where

$$r \equiv |\mathbf{x} - \mathbf{x}_0| = \sqrt{(x - x_0)^2 + (y - y_0)^2},$$

and L is an arbitrary length,

Figure 2.2.1 shows graphs of a family of dimensionless test functions $Q \equiv qL^2$ plotted against the dimensionless distance $X \equiv (x - x_0)/L$ for $y = y_0$, and $\lambda = 1$ (dashed line), 2, 5, 10, 20, 50, 100, and 500 (dotted line). The maximum height of each graph is inversely proportional to the square of its width, so that the area underneath each graph in the xy plane is equal to unity,

$$\begin{aligned} \int \int q(r) dx dy &= \int_0^{2\pi} \int_0^\infty q(r) r dr d\theta = 2\pi \int_0^\infty q(r) r dr \\ &= \frac{2\lambda}{L^2} \int_0^\infty \exp(-\lambda \frac{r^2}{L^2}) r dr = 1. \end{aligned} \quad (2.2.5)$$

Another way to derive this identity is to observe that

$$q(r) = g(x - x_0) g(y - y_0), \quad (2.2.6)$$

where the function g is defined in equation (1.2.4), write

$$\int \int q(r) dx dy = \left[\int_{-\infty}^\infty g(x - x_0) dx \right] \left[\int_{-\infty}^\infty g(y - y_0) dy \right], \quad (2.2.7)$$

and then use property (1.2.5).

2.2.1 Green's functions of the first kind and Neumann functions

In addition to satisfying equation (2.2.1), a Green's function of the *first kind* is required to take the reference value of zero over a contour C_G representing the boundary of a solution domain, that is,

$$G(\mathbf{x}, \mathbf{x}_0) = 0, \quad (2.2.8)$$

when the point \mathbf{x} lies on C_G .

On the other hand, a Green's function of the *second kind*, also called a *Neumann function*, is distinguished by the property that its normal derivative vanishes over the boundary C_G , that is,

$$\mathbf{n}(\mathbf{x}) \cdot \nabla G(\mathbf{x}, \mathbf{x}_0) \equiv \frac{\partial G}{\partial n}(\mathbf{x}, \mathbf{x}_0) = 0, \quad (2.2.9)$$

where the point \mathbf{x} lies on C_G .

Physically, a Green's or Neumann function may be identified with one of the following:

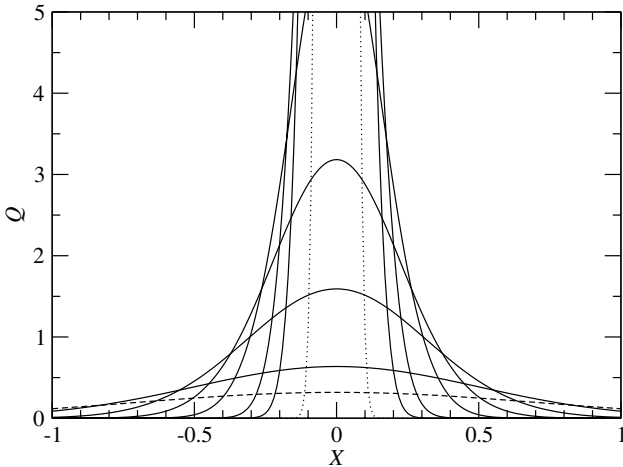


Figure 2.2.1 A family of dimensionless test functions $Q \equiv qL^2$ described by (2.2.4) plotted against the dimensionless distance $X \equiv (x - x_0)/L$ for $y = y_0$ and $\lambda = 1$ (dashed line), 2, 5, 10, 20, 50, 100, and 500 (dotted line). In the limit as the dimensionless parameter λ tends to infinity, we recover Dirac's delta function in two dimensions.

- The steady temperature field due to a *point source of heat* located at the point \mathbf{x}_0 in the presence of an isothermal or insulated boundary represented by C_G , corresponding, respectively, to the Green's function of the first or second kind.
- The steady concentration field due to a *point source of a species* located at the point \mathbf{x}_0 in the presence of an iso-concentration or impermeable boundary represented by C_G , corresponding, respectively, to the Green's function of the first or second kind.
- The harmonic potential due to a *point sink of mass* located at the point \mathbf{x}_0 in a domain of flow bounded by C_G .

2.2.2 Free-space Green's function

The free-space Green's function corresponds to an infinite solution domain in the absence of any interior boundaries. Solving equation (2.2.1) by inspection or using the Fourier transform, we find

$$G(\mathbf{x}, \mathbf{x}_0) = -\frac{1}{2\pi} \ln r, \quad (2.2.10)$$

where $r = |\mathbf{x} - \mathbf{x}_0| = [(x - x_0)^2 + (y - y_0)^2]^{1/2}$ is the scalar distance of the field point \mathbf{x} from the singular point \mathbf{x}_0 .

2.2.3 Green's functions in bounded domains

As the observation point \mathbf{x} approaches the singular point \mathbf{x}_0 , all Green's and Neumann functions exhibit a common singular behavior. Specifically, any Green's or Neumann function is composed of a singular part that is identical to the free-space Green's function given in (2.2.10), and a complementary part expressed by a harmonic function H that is non-singular throughout the domain of solution,

$$G(\mathbf{x}, \mathbf{x}_0) = -\frac{1}{2\pi} \ln r + H(\mathbf{x}, \mathbf{x}_0). \quad (2.2.11)$$

In the case of the free-space Green's function, the complementary component H vanishes. More generally, the particular form of H depends on the geometry of the boundary C_G . For certain simple boundary geometries involving straight and circular contours, the complementary function H may be found by the method of images, that is, by placing free-space Green's functions and their derivatives at strategically selected locations outside the solution domain.

For example, the Green's function for a semi-infinite domain bounded by a plane wall located at $y = w$ is given by

$$G(\mathbf{x}, \mathbf{x}_0) = -\frac{1}{2\pi} \ln r \pm \frac{1}{2\pi} \ln r^{Im}, \quad (2.2.12)$$

where

$$r = |\mathbf{x} - \mathbf{x}_0|, \quad r^{Im} = |\mathbf{x} - \mathbf{x}_0^{Im}|, \quad (2.2.13)$$

and $\mathbf{x}_0^{Im} = (x_0, 2w - y_0)$ is the image of the point \mathbf{x}_0 with respect to the wall. The plus and minus sign correspond, respectively, to the Green's function of the first kind and to the Neumann function.

2.2.4 BEMLIB directory `lgf_2d`

Subdirectory `lgf_2d` of directory `laplace` of *BEMLIB* contains subroutines that evaluate a family of Green's and Neumann functions, including the following:

- Green's function in free space.
- Singly periodic Green's function.
- Green's and Neumann functions in a semi-infinite domain bounded by a plane wall.
- Green's and Neumann functions in an infinite strip confined by two parallel plane walls.

- Neumann function in a semi-infinite strip confined by two parallel plane walls and a third wall intersecting the parallel walls at right angles.
- Neumann function in the exterior of a circle.

Most of these Green's and Neumann functions are constructed by the method of images. Details on derivation and illustration of iso-scalar contours are presented in Chapter 10.

2.2.5 Integral properties of Green's functions

Consider a singly or multiply connected control area in the xy plane, denoted by A_c , that is bounded by a closed contour or a collection of closed contours, denoted by C . The boundary C_G associated with the Green's function may be one of these contours. For the moment, we shall assume that all contours are smooth, that is, they do not exhibit corners or cusps.

Integrating (2.2.1) over the control area A_c , and using the divergence theorem and the distinctive properties of the delta function in two dimensions, we find that the Green's functions satisfy the integral identity

$$\int_C \mathbf{n}(\mathbf{x}) \cdot \nabla G(\mathbf{x}, \mathbf{x}_0) dl(\mathbf{x}) = \begin{cases} 1 & \text{when } \mathbf{x}_0 \text{ is inside } A_c \\ \frac{1}{2} & \text{when } \mathbf{x}_0 \text{ is on } C \\ 0 & \text{when } \mathbf{x}_0 \text{ is outside } A_c \end{cases}, \quad (2.2.14)$$

where the unit normal vector \mathbf{n} points *into* the control area A_c . When the singular point \mathbf{x}_0 is located on the boundary C , the improper integral on the left-hand side of (2.2.14) is a *principal-value integral*.

Using the three relations shown in (2.2.14), we derive the important identity

$$\int_C \mathbf{n}(\mathbf{x}) \cdot \nabla G(\mathbf{x}, \mathbf{x}_0) dl(\mathbf{x}) = \int_C^{PV} \mathbf{n}(\mathbf{x}) \cdot \nabla G(\mathbf{x}, \mathbf{x}_0) dl(\mathbf{x}) \pm \frac{1}{2}, \quad (2.2.15)$$

where PV denotes the principal-value integral computed by placing the evaluation point \mathbf{x}_0 precisely on C . The plus and minus sign on the right-hand side of (2.2.15) apply, respectively, when the point \mathbf{x}_0 on the left-hand side lies inside or outside the control area A_c .

2.2.6 Green's function dipole

Differentiating a Green's function with respect to the coordinates of the pole, we obtain a vectorial singularity called the Green's function dipole, given by

$$\mathbf{G}^D(\mathbf{x}, \mathbf{x}_0) \equiv \nabla_0 G(\mathbf{x}, \mathbf{x}_0) = \left[\frac{\partial G(\mathbf{x}, \mathbf{x}_0)}{\partial x_0}, \frac{\partial G(\mathbf{x}, \mathbf{x}_0)}{\partial y_0} \right], \quad (2.2.16)$$

where the subscript “0” denotes differentiation with respect to the Cartesian components of \mathbf{x}_0 . Physically, the scalar field

$$\Phi(\mathbf{x}, \mathbf{x}_0) = \mathbf{d} \cdot \nabla_0 G(\mathbf{x}, \mathbf{x}_0) \quad (2.2.17)$$

represents the temperature or concentration field due to a point source dipole of heat or species located at the point \mathbf{x}_0 . The direction and strength of the dipole are determined, respectively, by the orientation and magnitude of the arbitrary vector \mathbf{d} .

Differentiating, for example, the right-hand side of (2.2.10), we derive the two-dimensional free-space Green's function dipole,

$$G_i^D(\mathbf{x}, \mathbf{x}_0) = \frac{1}{2\pi} \frac{\hat{x}_i}{r^2}, \quad (2.2.18)$$

where $i = 1, 2$ corresponds to x and y , $\hat{\mathbf{x}} = \mathbf{x} - \mathbf{x}_0$, and $r = |\mathbf{x} - \mathbf{x}_0|$. The temperature field due to a point source dipole of heat in free space is thus given by

$$\Phi(\mathbf{x}, \mathbf{x}_0) = \frac{1}{2\pi} \frac{d_x \hat{x} + d_y \hat{y}}{r^2}, \quad (2.2.19)$$

where the scalar coefficients d_x and d_y determine the orientation and strength of the dipole in the xy plane.

2.2.7 Green's function quadruple

Higher derivatives of the Green's function with respect to the coordinates of the pole yield higher-order tensorial singularities that are multi-poles of the point source. The first three members of this family are the quadruple G^Q , the octuple G^O , and the sextupole G^S .

The free-space quadruple is given by

$$G_{ij}^Q(\mathbf{x}, \mathbf{x}_0) = \frac{\partial G_j^D(\mathbf{x}, \mathbf{x}_0)}{\partial x_{0j}} = \frac{\partial^2 G(\mathbf{x}, \mathbf{x}_0)}{\partial x_{0i} \partial x_{0j}} = -\frac{1}{2\pi} \left(\frac{\delta_{ij}}{r^2} - 2 \frac{\hat{x}_i \hat{x}_j}{r^4} \right), \quad (2.2.20)$$

where $\hat{\mathbf{x}} = \mathbf{x} - \mathbf{x}_0$ and $r = |\mathbf{x} - \mathbf{x}_0|$.

Problems

P.2.2.1 Delta function in two dimensions

Prove by direct evaluation the equality shown in the second line of (2.2.5).

P.2.2.2 Helmholtz's equation

(a) Show that any two solutions of Helmholtz's equation in two dimensions

$$\nabla^2 f(x, y) - c f(x, y) = 0, \quad (1)$$

satisfy the reciprocal relation (2.1.5); c is a real or complex constant,

(b) The Green's functions of Helmholtz's equation in two dimensions satisfy the equation

$$\nabla^2 G(\mathbf{x}, \mathbf{x}_0) - c G(\mathbf{x}, \mathbf{x}_0) + \delta_2(\mathbf{x} - \mathbf{x}_0) = 0. \quad (2)$$

- When $c = \pm i\lambda^2$, where i is the imaginary unit and λ is a real positive constant, the free-space Green's function is given by

$$G(\mathbf{x}, \mathbf{x}_0) = \frac{1}{2\pi} [\ker_0(\lambda r) \pm i \operatorname{kei}_0(\lambda r)], \quad (3)$$

where $r = |\mathbf{x} - \mathbf{x}_0|$, and \ker_0 , kei_0 are Kelvin functions (e.g., [2], p. 379).

- When $c = \lambda^2$, where λ is a real positive constant, the free-space Green's function is given by

$$G(\mathbf{x}, \mathbf{x}_0) = \frac{1}{2\pi} K_0(\lambda r), \quad (4)$$

where K_0 is a modified Bessel function (e.g., [2], p. 374).

- When $c = -\lambda^2$, where λ is a real positive constant, the free-space Green's function is given by

$$G(\mathbf{x}, \mathbf{x}_0) = -\frac{i}{4} H_0^{(2)}(\lambda r), = -\frac{1}{4} [Y_0(\lambda r) + i J_0(\lambda r)], \quad (5)$$

where $H_0^{(2)}$ is a Hankel function, and J_0 , Y_0 are, respectively, Bessel functions of the first and second kind (e.g., [2], p. 358).

With the help of a mathematical handbook, show that, in the limit as the field point \mathbf{x} approaches the singular point \mathbf{x}_0 , the real and complex Green's functions (3) to (5) reduce to the free-space Green's function of Laplace's equation given in (2.2.10).

P.2.2.3 Convection – diffusion in uniform flow

The steady-state temperature or species concentration field $f(x, y)$ in a uniform (streaming) flow with constant velocity $\mathbf{U} = (U_x, U_y)$ is governed by the linear convection – diffusion equation

$$U_x \frac{\partial f}{\partial x} + U_y \frac{\partial f}{\partial y} = \kappa \nabla^2 f, \quad (1)$$

where κ is the thermal or species diffusivity with dimensions of length squared divided by time. In vector notation, equation (1) takes the compact form $\mathbf{U} \cdot \nabla f = \kappa \nabla^2 f$. The corresponding Green's function satisfies the equation

$$U_x \frac{\partial G(\mathbf{x}, \mathbf{x}_0)}{\partial x} + U_y \frac{\partial G(\mathbf{x}, \mathbf{x}_0)}{\partial y} = \kappa \nabla^2 G(\mathbf{x}, \mathbf{x}_0) + \delta_2(\mathbf{x} - \mathbf{x}_0). \quad (2)$$

Confirm that the free-space Green's function is given by

$$G(\mathbf{x}, \mathbf{x}_0) = \frac{1}{\kappa} H(\mathbf{x}, \mathbf{x}_0) \exp\left[\frac{\mathbf{U} \cdot (\mathbf{x} - \mathbf{x}_0)}{2\kappa}\right], \quad (3)$$

where $H(\mathbf{x}, \mathbf{x}_0)$ is the Green's function of Helmholtz's equation given by the right-hand side of equation (4) of P.2.2.2 with $\lambda = |\mathbf{U}|/(2\kappa)$. Thus,

$$G(\mathbf{x}, \mathbf{x}_0) = \frac{1}{2\pi\kappa} K_0\left(\frac{|\mathbf{U}| r}{2\kappa}\right) \exp\left[\frac{\mathbf{U} \cdot (\mathbf{x} - \mathbf{x}_0)}{2\kappa}\right]. \quad (4)$$

P.2.2.4 D'Arcy equation

Verify that the Green's function of D'Arcy's equation in two dimensions

$$k_1 \frac{\partial^2 f}{\partial x^2} + k_2 \frac{\partial^2 f}{\partial y^2} = 0, \quad (1)$$

where k_1 and k_2 are two real constants with the same sign, is given by

$$G(\mathbf{x}, \mathbf{x}_0) = -\frac{1}{2\pi\sqrt{k_1 k_2}} \ln r. \quad (2)$$

What transformation does the Green's function undergo when k_1 and k_2 have different signs?

2.3 Integral representation

Applying Green's second identity (2.1.4) for a non-singular harmonic function $f(\mathbf{x})$ and a Green's function $G(\mathbf{x}, \mathbf{x}_0)$ in place of $\phi(\mathbf{x})$, and using the definition (2.2.1), we obtain

$$f(\mathbf{x}) \delta_2(\mathbf{x} - \mathbf{x}_0) = \nabla \cdot [G(\mathbf{x}, \mathbf{x}_0) \nabla f(\mathbf{x}) - f(\mathbf{x}) \nabla G(\mathbf{x}, \mathbf{x}_0)], \quad (2.3.1)$$

which is the two-dimensional counterpart of (1.3.1).

Next, we select a control area A_c that is bounded by a closed contour or a collection of contours denoted by C , as illustrated in Figure 2.1.1. When the pole of the Green's function \mathbf{x}_0 is placed outside A_c , the left-hand side of (2.3.1) is non-singular throughout A_c . Integrating both sides of (2.3.1) over A_c , and using the divergence theorem in two dimensions (Appendix A), we find

$$\int_C [G(\mathbf{x}, \mathbf{x}_0) \nabla f(\mathbf{x}) - f(\mathbf{x}) \nabla G(\mathbf{x}, \mathbf{x}_0)] \cdot \mathbf{n}(\mathbf{x}) dl(\mathbf{x}) = 0, \quad (2.3.2)$$

where dl is the differential arc length along C .

In contrast, when the \mathbf{x}_0 is placed inside A_c , the left-hand side of (2.3.1) exhibits a singularity at the point \mathbf{x}_0 . Using the distinctive properties of the delta function in two dimensions to perform the integration, we find

$$\begin{aligned} f(\mathbf{x}_0) = & - \int_C G(\mathbf{x}, \mathbf{x}_0) [\mathbf{n}(\mathbf{x}) \cdot \nabla f(\mathbf{x})] dl(\mathbf{x}) \\ & + \int_C f(\mathbf{x}) [\mathbf{n}(\mathbf{x}) \cdot \nabla G(\mathbf{x}, \mathbf{x}_0)] dl(\mathbf{x}), \end{aligned} \quad (2.3.3)$$

where the unit normal vector \mathbf{n} points *into* the control area enclosed by C , as shown in Figure 2.1.1.

Equation (2.3.3) provides us with a boundary-integral representation of a harmonic function in terms of the boundary values and the boundary distribution of the normal derivative of the harmonic function. To compute the value of f at a particular point \mathbf{x}_0 located inside a selected control area, we simply evaluate the two boundary integrals on the right-hand side of (2.3.3).

A symmetry property allows us to switch the order of the arguments of the Green's function in (2.3.3), that is, to interchange the location of the singular point and the evaluation point, writing

$$G(\mathbf{x}, \mathbf{x}_0) = G(\mathbf{x}_0, \mathbf{x}), \quad (2.3.4)$$

(see P.2.3.1). Using this property, we express (2.3.3) in the form

$$\begin{aligned} f(\mathbf{x}_0) = & - \int_C G(\mathbf{x}_0, \mathbf{x}) [\mathbf{n}(\mathbf{x}) \cdot \nabla f(\mathbf{x})] dl(\mathbf{x}) \\ & + \int_C f(\mathbf{x}) [\mathbf{n}(\mathbf{x}) \cdot \nabla G(\mathbf{x}_0, \mathbf{x})] dl(\mathbf{x}). \end{aligned} \quad (2.3.5)$$

The two integrals on the right-hand side of (2.3.5) represent boundary distributions of Green's functions and Green's function dipoles oriented perpendicular to the boundaries of the control area expressing, respectively, boundary distributions of point

sources and point-source dipoles. Making an analogy with the corresponding boundary distributions of electric charges and charge dipoles in electrostatics, we refer to these integrals as the *single-layer* and *double-layer* harmonic potentials. The densities (strength per unit length) of these potentials are equal, respectively, to the boundary distribution of the normal derivative and to the boundary values of the harmonic potential.

2.3.1 Green's third identity

Applying the integral representation (2.3.3) with the free-space Green's function given in (2.2.10), we derive Green's third identity in two dimensions,

$$f(\mathbf{x}_0) = \frac{1}{2\pi} \int_C [\ln r \nabla f(\mathbf{x}) + f(\mathbf{x}) \frac{\mathbf{x}_0 - \mathbf{x}}{r^2}] \cdot \mathbf{n}(\mathbf{x}) dl(\mathbf{x}), \quad (2.3.6)$$

where $r = |\mathbf{x} - \mathbf{x}_0|$, and the unit normal vector \mathbf{n} points into the control area enclosed by the contour C .

2.3.2 Choice of Green's functions

Green's third identity involving the free-space Green's function is applicable to any solution domain geometry. In practice, it is beneficial to work with a boundary-integral representation that involves a Green's function of the first or second kind corresponding to the particular geometry under consideration, and chosen according to the type of specified boundary conditions.

Suppose, for example, that the boundary conditions require that the function f vanishes over a contour C_G that is part of the boundary C involved in the integral representation. Implementing this boundary condition, we find that the double-layer potential over C_G is identically equal to zero. If $G(\mathbf{x}_0, \mathbf{x})$ is chosen to be the Green's function of the first kind corresponding to C_G , that is, $G(\mathbf{x}_0, \mathbf{x}) = 0$ when the evaluation point \mathbf{x} lies on C_G , then the corresponding single-layer integral is also equal to zero, yielding a simplified representation.

2.3.3 Integral representation of the gradient

It is perfectly acceptable to compute first or higher-order derivatives of the right-hand side of (2.3.3) with respect to the components of $\mathbf{x}_0 = (x_0, y_0)$, so long as the point \mathbf{x}_0 lies inside the solution domain away from the boundaries. The result is an integral representation for the gradient ∇f and for high-order tensors consisting of high-order derivatives.

Taking the first derivative of the integral representation (2.3.3) with respect to x_0 , and switching the order of differentiation and integration on the right-hand side, we

find

$$\begin{aligned} \frac{\partial f(\mathbf{x}_0)}{\partial x_0} = & - \int_C \frac{\partial G(\mathbf{x}_0, \mathbf{x})}{\partial x_0} [\mathbf{n}(\mathbf{x}) \cdot \nabla f(\mathbf{x})] dl(\mathbf{x}) \\ & + \int_C f(\mathbf{x}) [\mathbf{n}(\mathbf{x}) \cdot \nabla \frac{\partial G(\mathbf{x}_0, \mathbf{x})}{\partial x_0}] dl(\mathbf{x}), \end{aligned} \quad (2.3.7)$$

where the gradient ∇ on the right-hand side operates with respect to \mathbf{x} . Taking also the derivative with respect to y_0 and compiling the two representations, we obtain a vector integral representation for the gradient,

$$\begin{aligned} \nabla_0 f(\mathbf{x}_0) = & - \int_C \nabla_0 G(\mathbf{x}_0, \mathbf{x}) [\mathbf{n}(\mathbf{x}) \cdot \nabla f(\mathbf{x})] dl(\mathbf{x}) \\ & + \int_C f(\mathbf{x}) [\mathbf{n}(\mathbf{x}) \cdot \nabla \nabla_0 G(\mathbf{x}_0, \mathbf{x})] dl(\mathbf{x}), \end{aligned} \quad (2.3.8)$$

where the gradient ∇_0 operates with respect to the evaluation point \mathbf{x}_0 . In index notation, the representation (2.3.8) takes the form

$$\begin{aligned} \frac{\partial f(\mathbf{x}_0)}{\partial x_{0i}} = & - \int_C \frac{\partial G(\mathbf{x}_0, \mathbf{x})}{\partial x_{0i}} [\mathbf{n}(\mathbf{x}) \cdot \nabla f(\mathbf{x})] dl(\mathbf{x}) \\ & + \int_C f(\mathbf{x}) \frac{\partial^2 G(\mathbf{x}_0, \mathbf{x})}{\partial x_{0i} \partial x_j} n_j(\mathbf{x}) dl(\mathbf{x}), \end{aligned} \quad (2.3.9)$$

where summation over the repeated index j is implied on the right-hand side.

Applying the representation (2.3.9) for a constant function $f(\mathbf{x})$, we derive the vector identity

$$\int_C \frac{\partial^2 G(\mathbf{x}_0, \mathbf{x})}{\partial x_{0i} \partial x_j} n_j(\mathbf{x}) dl(\mathbf{x}) = 0. \quad (2.3.10)$$

Applying further the representation (2.3.9) for the linear function $f(\mathbf{x}) = a_i(x_i - b_i)$, where a_i are arbitrary constant coefficients and b_i are arbitrary coordinates, observing that $\mathbf{n}(\mathbf{x}) \cdot \nabla f(\mathbf{x}) = a_k n_k(\mathbf{x})$, and discarding the arbitrary constants a_k , we find

$$\begin{aligned} \delta_{ik} = & - \int_C \frac{\partial G(\mathbf{x}_0, \mathbf{x})}{\partial x_{0i}} n_k(\mathbf{x}) dl(\mathbf{x}) \\ & + \int_C (x_k - b_k) \frac{\partial^2 G(\mathbf{x}_0, \mathbf{x})}{\partial x_{0i} \partial x_j} n_j(\mathbf{x}) dl(\mathbf{x}), \end{aligned} \quad (2.3.11)$$

where δ_{ik} is Kronecker's delta (Appendix A).

Identities (2.3.10) and (2.3.11) are useful for reducing the order of the singularity of the second integral on the right-hand side of (2.3.8) in the limit as the evaluation point \mathbf{x}_0 approaches the boundary C , as will be discussed in Section 2.5.

In the case of the free-space Green's function, we depart from Green's third identity (2.3.6) and derive the more specific form of (2.3.8),

$$\begin{aligned} \nabla_0 f(\mathbf{x}_0) &= \frac{1}{2\pi} \int_C (\nabla_0 \ln r) [\mathbf{n}(\mathbf{x}) \cdot \nabla f(\mathbf{x})] dl(\mathbf{x}) \\ &\quad + \frac{1}{2\pi} \int_C f(\mathbf{x}) [\nabla_0 \left(\frac{\mathbf{x}_0 - \mathbf{x}}{r^2} \right) \cdot \mathbf{n}(\mathbf{x})] dl(\mathbf{x}), \end{aligned} \quad (2.3.12)$$

where $r = |\mathbf{x} - \mathbf{x}_0|$. Carrying out the differentiations and switching to index notation, we find

$$\begin{aligned} \frac{\partial f(\mathbf{x}_0)}{\partial x_{0i}} &= \frac{1}{2\pi} \int_C \frac{\tilde{x}_i}{r^2} [\mathbf{n}(\mathbf{x}) \cdot \nabla f(\mathbf{x})] dl(\mathbf{x}) \\ &\quad + \frac{1}{2\pi} \int_C f(\mathbf{x}) \left(\frac{\delta_{ij}}{r^2} - 2 \frac{\tilde{x}_i \tilde{x}_j}{r^4} \right) n_j(\mathbf{x}) dl(\mathbf{x}), \end{aligned} \quad (2.3.13)$$

where δ_{ij} is Kronecker's delta, and $\tilde{\mathbf{x}} = \mathbf{x}_0 - \mathbf{x}$. Comparing the two integrands with expressions (2.2.18) and (2.2.20), we conclude that the two integrals on the right-hand side of (2.3.13) and, by extension, the integrals on the right-hand side of (2.3.9), represent boundary distributions of point-source dipoles and quadruples.

Identities (2.3.10) and (2.3.11) written with the free-space Green's function take the specific forms

$$\int_C \left(\frac{\delta_{ij}}{r^2} - 2 \frac{\tilde{x}_i \tilde{x}_j}{r^4} \right) n_j(\mathbf{x}) dl(\mathbf{x}) = 0, \quad (2.3.14)$$

and

$$\delta_{ik} = - \int_C \frac{\tilde{x}_i}{r^2} n_k(\mathbf{x}) dl(\mathbf{x}) + \int_C (x_k - b_k) \left(\frac{\delta_{ij}}{r^2} - 2 \frac{\tilde{x}_i \tilde{x}_j}{r^4} \right) n_j(\mathbf{x}) dl(\mathbf{x}). \quad (2.3.15)$$

2.3.4 Representation in the presence of an interface

In engineering applications, we encounter problems involving heat conduction or species diffusion in two adjacent media labeled 1 and 2, as illustrated in Figure 2.3.1. At steady state, the individual temperature or concentration fields, denoted by $f^{(1)}$ and $f^{(2)}$, satisfy Laplace's equation (2.1).

At the interface, denoted by I , physical considerations provide us with an expression for the discontinuity in temperature of species concentration

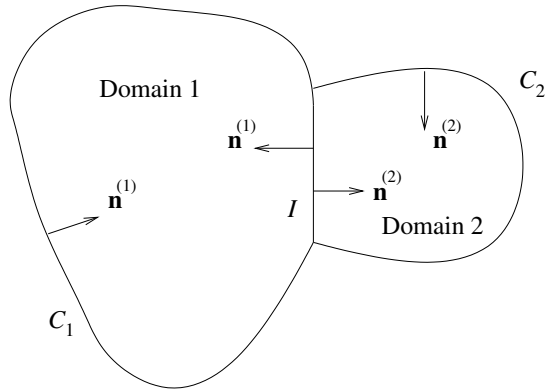


Figure 2.3.1 Illustration of a composite domain consisting of two conducting media with an interface.

$$\Delta f \equiv f^{(1)} - f^{(2)}. \quad (2.3.16)$$

For example, in heat transfer, an apparent discontinuity in temperature may arise because of imperfect mechanical contact associated with surface roughness, and may be modeled in terms of a “contact conductance.”

Moreover, an interfacial energy or mass balance provides us with an expression for the flux discontinuity

$$\begin{aligned} \Delta q &\equiv -k_1 \mathbf{n}^{(1)} \cdot \nabla f^{(1)} + k_2 \mathbf{n}^{(1)} \cdot \nabla f^{(2)} \\ &= -k_2 \mathbf{n}^{(2)} \cdot \nabla f^{(2)} + k_1 \mathbf{n}^{(2)} \cdot \nabla f^{(1)}, \end{aligned} \quad (2.3.17)$$

where k_1 and k_2 are the media conductivities or diffusion coefficients. The unit normal vectors are directed as shown in Figure 2.3.1.

Our objective is to derive an integral representation where the interfacial conditions (2.3.16) and (2.3.17) are embedded in the integral representation.

We begin by considering a point \mathbf{x}_0 in medium 1, and apply identity (2.3.2) with $C = C_2$ and the integral representation (2.3.3) with $C = C_1$ to find

$$\begin{aligned} 0 &= - \int_{C_2} G(\mathbf{x}, \mathbf{x}_0) [\mathbf{n}^{(2)}(\mathbf{x}) \cdot \nabla f^{(2)}(\mathbf{x})] dl(\mathbf{x}) \\ &+ \int_{C_2} f^{(2)}(\mathbf{x}) [\mathbf{n}^{(2)}(\mathbf{x}) \cdot \nabla G(\mathbf{x}, \mathbf{x}_0)] dl(\mathbf{x}), \end{aligned} \quad (2.3.18)$$

and

$$\begin{aligned} f^{(1)}(\mathbf{x}_0) = & - \int_{C_1} G(\mathbf{x}, \mathbf{x}_0) [\mathbf{n}^{(1)}(\mathbf{x}) \cdot \nabla f^{(1)}(\mathbf{x})] dl(\mathbf{x}) \\ & + \int_{C_1} f^{(1)}(\mathbf{x}) [\mathbf{n}^{(1)}(\mathbf{x}) \cdot \nabla G(\mathbf{x}, \mathbf{x}_0)] dl(\mathbf{x}), \end{aligned} \quad (2.3.19)$$

where the contours C_1 and C_2 include the interface I .

Decomposing the integrals over C_1 and C_2 into integrals over the interface I and integrals over the remaining part, adding (2.3.18) and (2.3.19), and recalling that along the interface $\mathbf{n}^{(2)} = -\mathbf{n}^{(1)}$, we obtain the representation

$$\begin{aligned} f^{(1)}(\mathbf{x}_0) = & -A_1 + B_1 - A_2 + B_2 \\ & - \frac{\lambda - 1}{\lambda} \int_I G(\mathbf{x}, \mathbf{x}_0) [\mathbf{n}^{(1)}(\mathbf{x}) \cdot \nabla f^{(1)}(\mathbf{x}) - \frac{1}{\lambda - 1} \frac{\Delta q}{k_1}] dl(\mathbf{x}) \\ & + \int_I \Delta f(\mathbf{x}) [\mathbf{n}^{(1)}(\mathbf{x}) \cdot \nabla G(\mathbf{x}, \mathbf{x}_0)] dl(\mathbf{x}), \end{aligned} \quad (2.3.20)$$

where $\lambda \equiv k_2/k_1$. The first four terms on the right-hand side of (2.3.20) are defined as

$$\begin{aligned} A_1 &\equiv \int_{C_1-I} G(\mathbf{x}, \mathbf{x}_0) [\mathbf{n}^{(1)}(\mathbf{x}) \cdot \nabla f^{(1)}(\mathbf{x})] dl(\mathbf{x}), \\ B_1 &\equiv \int_{C_1-I} f^{(1)}(\mathbf{x}) [\mathbf{n}^{(1)}(\mathbf{x}) \cdot \nabla G(\mathbf{x}, \mathbf{x}_0)] dl(\mathbf{x}), \\ A_2 &\equiv \int_{C_2-I} G(\mathbf{x}, \mathbf{x}_0) [\mathbf{n}^{(2)}(\mathbf{x}) \cdot \nabla f^{(2)}(\mathbf{x})] dl(\mathbf{x}), \\ B_2 &\equiv \int_{C_2-I} f^{(2)}(\mathbf{x}) [\mathbf{n}^{(2)}(\mathbf{x}) \cdot \nabla G(\mathbf{x}, \mathbf{x}_0)] dl(\mathbf{x}). \end{aligned} \quad (2.3.21)$$

Alternatively, we may multiply (2.3.18) by λ and add the resulting expression to (2.3.19) to obtain

$$\begin{aligned} f^{(1)}(\mathbf{x}_0) = & -A_1 + B_1 - \lambda A_2 + \lambda B_2 + \frac{1}{k_1} \int_I \Delta q(\mathbf{x}) G(\mathbf{x}, \mathbf{x}_0) dl(\mathbf{x}) \\ & + (1 - \lambda) \int_I [f^{(1)}(\mathbf{x}) + \frac{\lambda}{1 - \lambda} \Delta f(\mathbf{x})] [\mathbf{n}^{(1)}(\mathbf{x}) \cdot \nabla G(\mathbf{x}, \mathbf{x}_0)] dl(\mathbf{x}). \end{aligned} \quad (2.3.22)$$

Analogous representations for a point \mathbf{x}_0 that lies in medium 2 arise by straightforward changes in notation.

Simplifications have occurred because the integrals over the interface in (2.3.20) and (2.3.22) involve the discontinuities Δf and Δq and the distribution of f or its normal derivative on one side.

Problems

P.2.3.1 Symmetry of the Green's functions

Prove the symmetry property (2.3.4). *Hint:* Apply Green's second identity with the functions f and ϕ chosen to be Green's functions with singular points located at different positions, and integrate the resulting expression over a selected control area bounded by C_G .

P.2.3.2 Mean-value theorem

Consider a harmonic function $f(x, y)$ satisfying Laplace's equation (2.1), and introduce a control area enclosed by a circular contour of radius a centered at the point \mathbf{x}_0 . In plane polar coordinates (ρ, θ) centered at the point \mathbf{x}_0 , the unit normal vector pointing into the control area is given by $\mathbf{n} = (-\cos \theta, -\sin \theta)$. Moreover, $x - x_0 = a \cos \theta$, $y - y_0 = a \sin \theta$, and $r \equiv |\mathbf{x} - \mathbf{x}_0| = a$. Using these expressions, we find that Green's third identity (2.3.6) simplifies to

$$f(\mathbf{x}_0) = \frac{a}{2\pi} \int_0^{2\pi} [\ln a \nabla f(\mathbf{x}) \cdot \mathbf{n}(\mathbf{x}) + f(\mathbf{x}) \frac{1}{a}] d\theta. \quad (1)$$

Use the divergence theorem to show that the integral of the first term on the right-hand side of (1) vanishes, and thereby obtain the mean-value theorem

$$f(\mathbf{x}_0) = \frac{1}{2\pi} \int_0^{2\pi} f(\mathbf{x}) d\theta. \quad (2)$$

The right-hand side of (2) is the mean value of f over the perimeter of the circle.

P.2.3.3 Helmholtz's equation

Show that a solution of Helmholtz's equation in two dimensions, equation (1) of P.2.2.2, admits the integral representation (2.3.3), where $G(\mathbf{x}, \mathbf{x}_0)$ is the corresponding Green's function.

P.2.3.4 Linear convection – diffusion equation

The steady-state distribution of a temperature or species concentration field $f(x, y)$ in a two-dimensional flow with x and y velocity components $u_x(x, y)$ and $u_y(x, y)$

is governed by the convection – diffusion equation

$$\frac{\partial(u_x f)}{\partial x} + \frac{\partial(u_y f)}{\partial y} = \kappa \nabla^2 f, \quad (1)$$

where κ is the thermal or species diffusivity with dimensions of squared length divided by time. In vector notation, equation (1) takes the compact form

$$\nabla \cdot (\mathbf{u} f) = \kappa \nabla^2 f, \quad (2)$$

where $\mathbf{u} = (u_x, u_y)$ is the velocity vector field.

To develop a boundary-integral representation for f , we consider Green's second identity (2.1.4) and express it in the form

$$\begin{aligned} \phi [-\nabla \cdot (\mathbf{u} f) + \kappa \nabla^2 f] + \nabla \cdot (f \phi \mathbf{u}) - f [\mathbf{u} \cdot \nabla \phi + \kappa \nabla^2 \phi] \\ = \kappa \nabla \cdot (\phi \nabla f - f \nabla \phi). \end{aligned} \quad (3)$$

If f satisfies equation (1), then the expression enclosed by the first set of square brackets on the left-hand side vanishes. Rearranging the remaining terms, we obtain

$$-f [\mathbf{u} \cdot \nabla \phi + \kappa \nabla^2 \phi] = \nabla \cdot (\kappa \phi \nabla f - \kappa f \nabla \phi - f \phi \mathbf{u}). \quad (4)$$

Next, we introduce the Green's function of the adjoint of the convection – diffusion equation (1), denoted by $G^*(\mathbf{x}, \mathbf{x}_0)$, satisfying the equation

$$-\mathbf{u}(\mathbf{x}) \cdot \nabla G^*(\mathbf{x}, \mathbf{x}_0) = \kappa \nabla^2 G^*(\mathbf{x}, \mathbf{x}_0) + \delta_2(\mathbf{x} - \mathbf{x}_0). \quad (5)$$

The computation of Green's functions for uniform and linear flows is discussed in Reference [58].

(a) Identify the function ϕ in (4) with a Green's function G^* whose singular point is located inside a control area enclosed by the contour C , and work as in the text to derive the boundary-integral representation

$$\begin{aligned} f(\mathbf{x}_0) &= \int_C G^*(\mathbf{x}, \mathbf{x}_0) [\mathbf{n} \cdot (\mathbf{u} f - \kappa \nabla f)](\mathbf{x}) dl(\mathbf{x}) \\ &\quad + \kappa \int_C f(\mathbf{x}) [\mathbf{n}(\mathbf{x}) \cdot \nabla G^*(\mathbf{x}, \mathbf{x}_0)] dl(\mathbf{x}), \end{aligned} \quad (6)$$

where the unit normal vector \mathbf{n} points into the control area enclosed by C .

(b) Discuss the physical interpretation of the two integrals on the right-hand side of (6).

2.4 Integral equations

Let us return to the integral representation (2.3.4) and take the limit as the point \mathbf{x}_0 approaches a locally smooth contour C . Careful examination reveals that the single-layer potential varies continuously as the point \mathbf{x}_0 approaches and then crosses C .

Focusing on the behavior of the double-layer potential, we use identity (2.2.15) to write

$$\begin{aligned} & \lim_{\mathbf{x}_0 \rightarrow C} \left\{ \int_C f(\mathbf{x}) [\mathbf{n}(\mathbf{x}) \cdot \nabla G(\mathbf{x}_0, \mathbf{x})] dl(\mathbf{x}) \right\} \\ &= \lim_{\mathbf{x}_0 \rightarrow C} \left\{ \int_C [f(\mathbf{x}) - f(\mathbf{x}_0)] [\mathbf{n}(\mathbf{x}) \cdot \nabla G(\mathbf{x}_0, \mathbf{x})] dl(\mathbf{x}) \right. \\ &\quad \left. + f(\mathbf{x}_0) \int_C \mathbf{n}(\mathbf{x}) \cdot \nabla G(\mathbf{x}_0, \mathbf{x}) dl(\mathbf{x}) \right\} \\ &= \lim_{\mathbf{x}_0 \rightarrow C} \left\{ \int_C [f(\mathbf{x}) - f(\mathbf{x}_0)] [\mathbf{n}(\mathbf{x}) \cdot \nabla G(\mathbf{x}_0, \mathbf{x})] dl(\mathbf{x}) \right\} \\ &\quad + f(\mathbf{x}_0) \int_C^{PV} \mathbf{n}(\mathbf{x}) \cdot \nabla G(\mathbf{x}_0, \mathbf{x}) + \frac{1}{2} f(\mathbf{x}_0), \\ &= \int_C^{PV} f(\mathbf{x}) [\mathbf{n}(\mathbf{x}) \cdot \nabla G(\mathbf{x}_0, \mathbf{x})] dl(\mathbf{x}) + \frac{1}{2} f(\mathbf{x}_0), \end{aligned} \tag{2.4.1}$$

where PV denotes the principal-value integral.

Substituting (2.4.1) into (2.3.5) and rearranging the resulting expression, we find

$$\begin{aligned} f(\mathbf{x}_0) &= -2 \int_C G(\mathbf{x}, \mathbf{x}_0) [\mathbf{n}(\mathbf{x}) \cdot \nabla f(\mathbf{x})] dl(\mathbf{x}) \\ &\quad + 2 \int_C^{PV} f(\mathbf{x}) [\mathbf{n}(\mathbf{x}) \cdot \nabla G(\mathbf{x}, \mathbf{x}_0)] dl(\mathbf{x}), \end{aligned} \tag{2.4.2}$$

where the point \mathbf{x}_0 lies *precisely* on the contour C , and the unit normal vector \mathbf{n} points into the control area enclosed by C .

Written with the free-space Green's function, the integral equation (2.4.2) takes the form

$$\begin{aligned} f(\mathbf{x}_0) &= \frac{1}{\pi} \int_C \ln r [\mathbf{n}(\mathbf{x}) \cdot \nabla f(\mathbf{x})] dl(\mathbf{x}) \\ &\quad + \frac{1}{\pi} \int_C^{PV} f(\mathbf{x}) \frac{\mathbf{n}(\mathbf{x}) \cdot (\mathbf{x}_0 - \mathbf{x})}{r^2} dl(\mathbf{x}), \end{aligned} \tag{2.4.3}$$

where $r = |\mathbf{x} - \mathbf{x}_0|$. Expression (2.4.3) is Green's third identity evaluated at the boundary,

The boundary-element method is based on the following observations:

- Given the boundary distribution of the function f , equation (2.4.2) reduces to a *Fredholm integral equation of the first kind* for the normal derivative $q \equiv \mathbf{n} \cdot \nabla f$. To show this more explicitly, we recast the integral equation into the form

$$\int_C G(\mathbf{x}, \mathbf{x}_0) q(\mathbf{x}) dl(\mathbf{x}) = F(\mathbf{x}_0), \quad (2.4.4)$$

where

$$F(\mathbf{x}_0) \equiv -\frac{1}{2} f(\mathbf{x}_0) + \int_C^{PV} f(\mathbf{x}) [\mathbf{n}(\mathbf{x}) \cdot \nabla G(\mathbf{x}, \mathbf{x}_0)] dl(\mathbf{x}) \quad (2.4.5)$$

is a known source term consisting of the boundary values of f and the double-layer potential.

- Given the boundary distribution of the normal derivative $\mathbf{n} \cdot \nabla f$, equation (2.4.2) reduces to a *Fredholm integral equation of the second kind* for the boundary distribution of f . To show this more explicitly, we recast the integral equation into the form

$$f(\mathbf{x}_0) = 2 \int_C^{PV} f(\mathbf{x}) [\mathbf{n}(\mathbf{x}) \cdot \nabla G(\mathbf{x}, \mathbf{x}_0)] dl(\mathbf{x}) + \Phi(\mathbf{x}_0), \quad (2.4.6)$$

where

$$\Phi(\mathbf{x}_0) = -2 \int_C G(\mathbf{x}, \mathbf{x}_0) [\mathbf{n}(\mathbf{x}) \cdot \nabla f(\mathbf{x})] dl(\mathbf{x}) \quad (2.4.7)$$

is a known source term consisting of the single-layer potential.

The Green's function exhibits a logarithmic singularity with respect to distance of the evaluation point from the singular point. Because the order of this singularity is lower than the linear dimension of the variable of integration, the integral equation (2.4.4) is weakly singular. Consequently, the Fredholm-Riesz theory of compact operators can be applied to study the properties of the solution (e.g., [4]), and the improper integral may be evaluated accurately by numerical methods, as discussed in Chapter 3.

When C is a smooth contour with a continuously varying normal vector, as the integration point \mathbf{x} approaches the evaluation point \mathbf{x}_0 , the normal vector \mathbf{n} tends to become orthogonal to the nearly tangential vector $(\mathbf{x} - \mathbf{x}_0)$. Consequently, the numerator of the integrand of the double-layer potential on the right-hand side of (2.4.3)

behaves quadratically with respect to the scalar distance $r = |\mathbf{x} - \mathbf{x}_0|$, and a singularity does not appear. The Fredholm-Riesz theory of compact operators may then be applied to study the properties of the solution (e.g., [4]), and the principal value of the double-integral integral may be computed accurately by numerical methods, as discussed in Chapter 3.

The main goal of the boundary-element method is to generate numerical solutions to the integral equations (2.4.4) and (2.4.6). The numerical implementation of the boundary-element collocation method, to be discussed in detail in Chapter 3, involves the following steps:

1. Discretize the boundary into a collection of boundary elements, and approximate the boundary integrals with sums of integrals over the boundary elements.
2. Introduce approximations for the unknown function over the individual boundary elements.
3. Apply the integral equation at collocation points located over the boundary elements to generate a number of linear algebraic equations equal to the number of unknowns.
4. Perform the integration of the single- and double-layer potential over the boundary elements.
5. Solve the linear system for the coefficients involved in the approximation of the unknown function.

In performing and interpreting the results of a boundary-integral computation, it is important to have a good understanding of the existence and uniqueness of solution. If the integral equation does not have a solution or if the solution is not unique, poorly conditioned or singular algebraic systems with erroneous solutions will arise.

For example, analysis shows that the integral equation (2.4.6) has a unique solution only when the specified boundary distribution of the normal derivative satisfies the integral constraint

$$\int_C \mathbf{n}(\mathbf{x}) \cdot \nabla f(\mathbf{x}) dl(\mathbf{x}) = 0. \quad (2.4.8)$$

If this constraint is satisfied, any solution can be shifted uniformly by an arbitrary constant (e.g., [4, 60]). This behavior is consistent with the physical expectation that, given the temperature flux around the boundary of a conducting plate, a steady temperature field will be established only if the net rate of heat flow into the plate is zero; and if so, the temperature field can be elevated or reduced by an arbitrary constant.

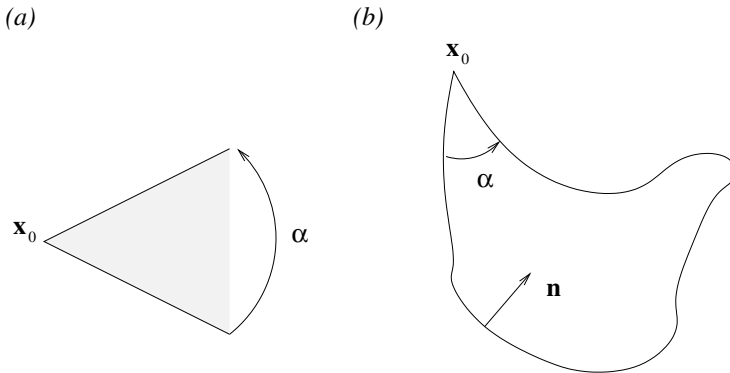


Figure 2.4.1 Illustration of (a) a wedge-shaped domain with apex at the point \mathbf{x}_0 , and (b) a control area whose boundary exhibits a corner.

2.4.1 Boundary corners

Relation (2.2.15) and subsequent relations (2.4.1) and (2.4.2) are valid only when the contour C is smooth in the neighborhood of the evaluation point \mathbf{x}_0 , that is, the curvature is finite and the unit normal vector is unique and varies continuously with respect to arc length.

To derive an integral representation at a boundary corner or cusp, we observe that the integral of the two-dimensional Dirac delta function over the infinite wedge-shaped area shown in Figure 2.4.1(a) is equal to $\alpha/(2\pi)$, where α is the aperture angle. Repeating the preceding analysis, we find that, when the point \mathbf{x}_0 is located at a boundary corner or cusp, as shown in Figure 2.4.1(b), the boundary-integral representation takes the form

$$\begin{aligned} f(\mathbf{x}_0) = & -\frac{2\pi}{\alpha} \int_C G(\mathbf{x}, \mathbf{x}_0) [\mathbf{n}(\mathbf{x}) \cdot \nabla f(\mathbf{x})] d\mathbf{l}(\mathbf{x}) \\ & + \frac{2\pi}{\alpha} \int_C^{PV} f(\mathbf{x}) [\mathbf{n}(\mathbf{x}) \cdot \nabla G(\mathbf{x}, \mathbf{x}_0)] d\mathbf{l}(\mathbf{x}). \end{aligned} \quad (2.4.9)$$

When $\alpha = \pi$, the contour is locally smooth, and (2.4.9) reduces to the standard representation (2.4.2).

When the boundary of a solution domain contains a corner or cusp, the solution of the integral equation for the function f or its normal derivative is likely to exhibit a local singularity. Numerical experience has shown that neglecting the singularity and solving the integral equations using the standard implementation of the boundary-element method are not detrimental to the overall accuracy of the computation.

To improve the accuracy of the numerical solution, the functional form of the singularity may be identified by carrying out a local analysis, and the boundary-element method may be designed to automatically probe the strength of the divergent part and effectively produce the regular part of the solution [25, 34 – 36, 63, 69]. (see also Reference [40]).

2.4.2 Shrinking arcs

It is instructive to rederive the integral representation (2.4.2) and its generalized form (2.4.9) in an alternative fashion that circumvents making use of the peculiar properties of the delta function. A key observation is that the integral identity (2.3.2) is valid so long as the evaluation point lies outside the solution domain, however close the point is to the boundaries. Written with the free-space Green's function, this identity reads

$$\frac{1}{2\pi} \int_C [\ln r \nabla f(\mathbf{x}) + f(\mathbf{x}) \frac{\mathbf{x}_0 - \mathbf{x}}{r^2}] \cdot \mathbf{n}(\mathbf{x}) dl(\mathbf{x}) = 0, \quad (2.4.10)$$

where $r = |\mathbf{x} - \mathbf{x}_0|$.

Consider a point \mathbf{x}_0 on a locally smooth contour, as illustrated in Figure 2.4.2(a), or at a boundary corner, as illustrated in Figure 2.4.2(b), and introduce a circular arc of radius ϵ and aperture angle α that serves to exclude the evaluation point \mathbf{x}_0 from the control area enclosed by C . If the contour C is locally smooth, as shown in Figure 2.4.2(a), $\alpha = \pi$; if the contour is locally cusped, $\alpha = 0$ or 2π . On the circular arc, $x - x_0 = \epsilon \cos \theta$, $y - y_0 = \epsilon \sin \theta$, $r \equiv |\mathbf{x} - \mathbf{x}_0| = \epsilon$, $n_x(\mathbf{x}) = \cos \theta$, $n_y(\mathbf{x}) = \sin \theta$, and the differential arc length is given by $dl = \epsilon d\theta$. Using these expressions, we find that the contribution of the arc to the integral on the right-hand side of (2.4.10) is

$$\frac{1}{2\pi} \int_0^\alpha \left\{ \ln \epsilon [\cos \theta \frac{\partial f}{\partial x}(\mathbf{x}) + \sin \theta \frac{\partial f}{\partial y}(\mathbf{x})] - f(\mathbf{x}) \frac{1}{\epsilon} \right\} \epsilon d\theta. \quad (2.4.11)$$

In limit as ϵ tends to zero, the product $\epsilon \ln \epsilon$ tends to vanish, the function $f(\mathbf{x})$ and its partial derivatives $\frac{\partial f}{\partial x}(\mathbf{x})$ and $\frac{\partial f}{\partial y}(\mathbf{x})$ tend to their respective values at \mathbf{x}_0 , and the right-hand side of (2.4.11) tends to the value $-\frac{\alpha}{2\pi} f(\mathbf{x}_0)$. Correspondingly, the integral over the modified contour on the right-hand side of (2.4.10) tends to its principal value computed by excluding from the integration domain a small interval of length ϵ on either side of the evaluation point \mathbf{x}_0 . Combining these results, we derive the integral representation (2.4.9), which includes the common case (2.4.2) for a smooth contour.

Our earlier observation that any Green's function is composed of the singular free-space Green's function and a non-singular complementary part can be invoked to demonstrate the general applicability of the boundary-integral equation (2.4.9).

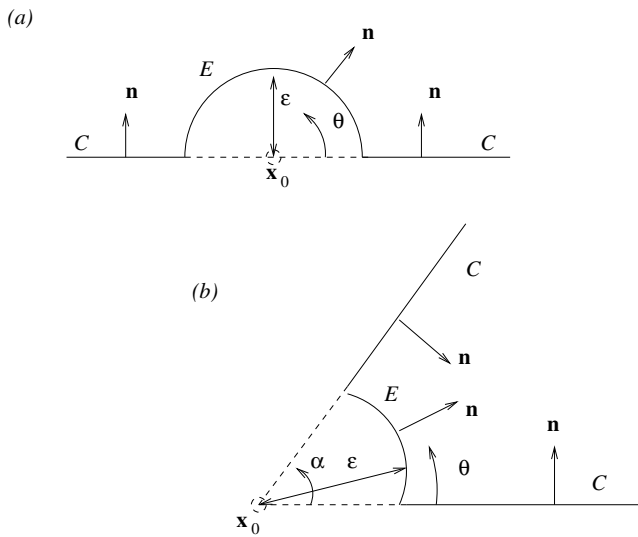


Figure 2.4.2 Derivation of the boundary-integral representation in two dimensions at a point \mathbf{x}_0 that lies (a) on a smooth contour, and (b) at a boundary corner.

Problems

P.2.4.1 Boundary corners

With reference to Figure 2.4.1(b), show that the aperture angle α can be evaluated as

$$\alpha = 2\pi \int_C^{PV} \mathbf{n}(\mathbf{x}) \cdot \nabla G(\mathbf{x}, \mathbf{x}_0) dl(\mathbf{x}). \quad (1)$$

P.2.4.2 Conduction in the presence of an interface

(a) Take the limit of the integral representation (2.3.20) as the evaluation point \mathbf{x}_0 approaches a locally smooth interface I , and thus derive boundary-integral equation.

(b) Repeat (a) for the integral representation (2.3.22).

P.2.4.3 The biharmonic equation

The biharmonic equation in two dimensions reads

$$\nabla^4 f(x, y) = 0, \quad (1)$$

where ∇^4 is the biharmonic operator defined as

$$\nabla^4 \equiv \nabla^2 \nabla^2 = \frac{\partial^4}{\partial x^4} + 2 \frac{\partial^4}{\partial x^2 \partial y^2} + \frac{\partial^4}{\partial y^4}. \quad (2)$$

The corresponding Green's function satisfies the equation

$$\nabla^4 G(\mathbf{x}, \mathbf{x}_0) + \delta_2(\mathbf{x} - \mathbf{x}_0) = 0, \quad (3)$$

where δ_2 is Dirac's delta function in the xy plane.

(a) Verify that the free-space Green's function is given by

$$G(\mathbf{x}, \mathbf{x}_0) = -\frac{1}{8\pi} r^2 (\ln r - 1), \quad (4)$$

where $r = |\mathbf{x} - \mathbf{x}_0|$.

(b) A Green's function of the biharmonic equation and its normal derivative are required to take the reference value of zero over a specified contour C_G .

Verify that the Green's function for a semi-infinite domain bounded by a plane wall located at $y = w$ is given by

$$G(\mathbf{x}, \mathbf{x}_0) = -\frac{1}{8\pi} r^2 \ln \frac{r}{r^{Im}} - \frac{y_0 - w}{4\pi} (y - w), \quad (5)$$

where $r = |\mathbf{x} - \mathbf{x}_0|$, $r^{Im} = |\mathbf{x} - \mathbf{x}_0^{Im}|$, and $\mathbf{x}_0^{Im} = (x_0, 2w - y_0)$ is the image of the singular point with respect to the wall [24].

(c) Verify that the Green's function in the interior of a circular boundary of radius a centered at the point \mathbf{x}_c is given by

$$G(\mathbf{x}, \mathbf{x}_0) = -\frac{1}{8\pi} r^2 \ln \frac{r a}{r^{Im} d} - \frac{d^2 - a^2}{16\pi a^2} (|\mathbf{x} - \mathbf{x}_c|^2 - a^2), \quad (6)$$

where $d = |\mathbf{x}_0 - \mathbf{x}_c|$, $r = |\mathbf{x} - \mathbf{x}_0|$, $r^{Im} = |\mathbf{x} - \mathbf{x}_0^{Im}|$, and

$$\mathbf{x}_0^{Im} = \mathbf{x}_c + (\mathbf{x}_0 - \mathbf{x}_c) \frac{a^2}{d^2} \quad (7)$$

is the image of the singular point with respect to the circle ([18], p. 272).

(d) Consider Green's second identity (2.1.4), and set $\phi = \nabla^2 \psi$, where ψ is a new function, to obtain

$$\nabla^2 \psi \nabla^2 f - f \nabla^4 \psi = \nabla \cdot [\nabla^2 \psi \nabla f - f \nabla (\nabla^2 \psi)]. \quad (8)$$

Using elementary calculus, we find

$$\begin{aligned}\nabla^2 \psi \nabla^2 f &= \nabla \cdot (\nabla \psi) \nabla^2 f = \nabla \cdot [\nabla \psi \nabla^2 f] - \nabla \psi \cdot \nabla (\nabla^2 f) \\ &= \nabla \cdot [\nabla \psi \nabla^2 f - \psi \nabla (\nabla^2 f)] + \psi \nabla^4 f.\end{aligned}\quad (9)$$

Replacing the first term on the left-hand side of (8) with the last expression and rearranging, we find

$$\begin{aligned}\psi \nabla^4 f - f \nabla^4 \psi \\ &= \nabla \cdot [\nabla^2 \psi \nabla f - f \nabla (\nabla^2 \psi) - \nabla \psi \nabla^2 f + \psi \nabla (\nabla^2 f)].\end{aligned}\quad (10)$$

Assuming now that the function f satisfies the biharmonic equation (1), we eliminate the first term on the left-hand side of (10). Identifying further ψ with a Green's function of the biharmonic equation, we obtain

$$\begin{aligned}f(\mathbf{x}) \delta_2(\mathbf{x} - \mathbf{x}_0) &= \nabla \cdot [G^L(\mathbf{x} - \mathbf{x}_0) \nabla f(\mathbf{x}) \\ &\quad - f(\mathbf{x}) \nabla G^L(\mathbf{x} - \mathbf{x}_0) - \nabla \psi(\mathbf{x}, \mathbf{x}_0) \omega(\mathbf{x}) + G(\mathbf{x}, \mathbf{x}_0) \nabla \omega(\mathbf{x})],\end{aligned}\quad (11)$$

where

$$G^L(\mathbf{x} - \mathbf{x}_0) \equiv \nabla^2 G(\mathbf{x} - \mathbf{x}_0) \quad (12)$$

is a Green's function of Laplace's equation, and

$$\omega \equiv \nabla^2 f. \quad (13)$$

Departing from identity (11), derive the boundary-integral representation

$$\begin{aligned}f(\mathbf{x}_0) &= - \int_C G^L(\mathbf{x}, \mathbf{x}_0) [\mathbf{n}(\mathbf{x}) \cdot \nabla f(\mathbf{x})] dl(\mathbf{x}) \\ &\quad + \int_C f(\mathbf{x}) [\mathbf{n}(\mathbf{x}) \cdot \nabla G^L(\mathbf{x}, \mathbf{x}_0)] dl(\mathbf{x}) \\ &\quad - \int_C G(\mathbf{x}, \mathbf{x}_0) [\mathbf{n}(\mathbf{x}) \cdot \nabla \omega(\mathbf{x})] dl(\mathbf{x}) \\ &\quad + \int_C \omega(\mathbf{x}) [\mathbf{n}(\mathbf{x}) \cdot \nabla G(\mathbf{x}, \mathbf{x}_0)] dl(\mathbf{x}),\end{aligned}\quad (14)$$

where the unit normal vector \mathbf{n} points into the control area enclosed by the contour C , as shown in Figure 2.1.1, and the point \mathbf{x}_0 lies inside C .

(e) Show that, when the point \mathbf{x}_0 lies on a locally smooth contour C , the integral representation (14) yields the integral equation

$$\begin{aligned}
f(\mathbf{x}_0) = & -2 \int_C G^L(\mathbf{x}, \mathbf{x}_0) [\mathbf{n}(\mathbf{x}) \cdot \nabla f(\mathbf{x})] dl(\mathbf{x}) \\
& + 2 \int_C^{PV} f(\mathbf{x}) [\mathbf{n}(\mathbf{x}) \cdot \nabla G^L(\mathbf{x}, \mathbf{x}_0)] dl(\mathbf{x}) \\
& - 2 \int_C G(\mathbf{x}, \mathbf{x}_0) [\mathbf{n}(\mathbf{x}) \cdot \nabla \omega(\mathbf{x})] dl(\mathbf{x}) \\
& + 2 \int_C \omega(\mathbf{x}) [\mathbf{n}(\mathbf{x}) \cdot \nabla G(\mathbf{x}, \mathbf{x}_0)] dl(\mathbf{x}),
\end{aligned} \tag{15}$$

where PV denotes the principal value of the double-layer potential.

(f) Derive the counterpart of (15) for a point \mathbf{x}_0 at a boundary corner.

2.5 Hypersingular integrals

Consider the integral representation for the gradient of a harmonic function in two dimensions written with the free-space Green's function, given in equation (2.3.13). Expanding the terms that have been contracted by the repeated index summation convention, we find that the x and y derivatives of the scalar field are given by

$$\begin{aligned}
\frac{\partial f(\mathbf{x}_0)}{\partial x_0} = & -\frac{1}{2\pi} \int_C \frac{x - x_0}{r^2} [\mathbf{n}(\mathbf{x}) \cdot \nabla f(\mathbf{x})] dl(\mathbf{x}) \\
& + \frac{1}{2\pi} \int_C f(\mathbf{x}) \left[\frac{n_x(\mathbf{x})}{r^2} - 2(x - x_0) \frac{(x - x_0) n_x(\mathbf{x}) + (y - y_0) n_y(\mathbf{x})}{r^4} \right] dl(\mathbf{x}),
\end{aligned} \tag{2.5.1}$$

and

$$\begin{aligned}
\frac{\partial f(\mathbf{x}_0)}{\partial y_0} = & -\frac{1}{2\pi} \int_C \frac{y - y_0}{r^2} [\mathbf{n}(\mathbf{x}) \cdot \nabla f(\mathbf{x})] dl(\mathbf{x}) \\
& + \frac{1}{2\pi} \int_C f(\mathbf{x}) \left[\frac{n_y(\mathbf{x})}{r^2} - 2(y - y_0) \frac{(x - x_0) n_x(\mathbf{x}) + (y - y_0) n_y(\mathbf{x})}{r^4} \right] dl(\mathbf{x}),
\end{aligned} \tag{2.5.2}$$

where $r = |\mathbf{x}_0 - \mathbf{x}|$.

In the limit as the evaluation point \mathbf{x}_0 approaches the contour C , as illustrated in Figure 2.5.1(a), these representations provide us with integral equations of the first

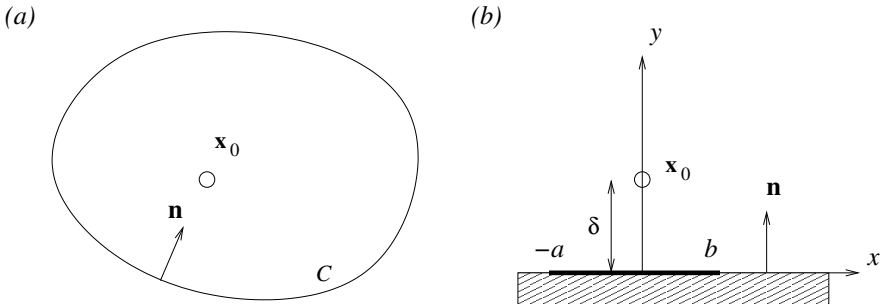


Figure 2.5.1 (a) In the limit as the evaluation point x_0 approaches the contour C , the integral representation for the gradient provides us with a “hypersingular” integral equation for the boundary distribution of the function f and its spatial derivatives. (b) Evaluation of the improper integrals over a section of a flat boundary extending between $x = -a$ and b .

or second kind for the boundary distribution of the function f and its derivatives. To derive the precise form of these integral equations, it is necessary to perform a detailed investigation of the asymptotic behavior of the integrals on the right-hand sides of (2.5.1) and (2.5.2).

2.5.1 Local analysis

It is illuminating to begin by considering the behavior of the integrals in the limit as the evaluation point x_0 approaches a locally flat boundary extending between $x = -a$ and b , as illustrated in Figure 2.5.1(b).

Writing $\mathbf{x}_0 = (0, \delta)$, $\mathbf{x} = (x, 0)$, and $\mathbf{n} = (0, 1)$, we find that the contribution of the straight segment to the integrals on the right-hand sides of (2.5.1) and (2.5.2) is

$$\begin{aligned} I^x(\delta) &= -\frac{1}{2\pi} \int_{-a}^b \frac{x}{x^2 + \delta^2} \left(\frac{\partial f}{\partial y} \right)_{x,y=0} dx \\ &\quad + \frac{\delta}{\pi} \int_{-a}^b \frac{x}{(x^2 + \delta^2)^2} f(x, y=0) dx, \end{aligned} \quad (2.5.3)$$

and

$$\begin{aligned} I^y(\delta) &= \frac{\delta}{2\pi} \int_{-a}^b \frac{1}{x^2 + \delta^2} \left(\frac{\partial f}{\partial y} \right)_{x,y=0} dx \\ &\quad + \frac{1}{2\pi} \int_{-a}^b \left[\frac{1}{x^2 + \delta^2} - \frac{2\delta^2}{(x^2 + \delta^2)^2} \right] f(x, y=0) dx. \end{aligned} \quad (2.5.4)$$

Naively putting $\delta = 0$ produces strongly singular and so-called “hypersingular” integrals whose interpretation is unclear.

To properly assess the behavior of the right-hand side of (2.5.3) in the limit as δ tends to zero, we recast it into the form

$$I^x(\delta) = I_1^x - f_y(0) I_2^x + I_3^x - f(0) I_4^x + f_x(0) I_5^x + f_{xx}(0) I_6^x, \quad (2.5.5)$$

where the subscripts x and y denote differentiation with respect to the corresponding variable, followed by evaluation at $y = 0$. We have introduced the definite integrals

$$\begin{aligned} I_1^x &\equiv -\frac{1}{2\pi} \int_{-a}^b \frac{x}{x^2 + \delta^2} [f_y(x) - f_y(0)] dx, \\ I_2^x &\equiv \frac{1}{2\pi} \int_{-a}^b \frac{x}{x^2 + \delta^2} dx, \\ I_3^x &\equiv \frac{\delta}{\pi} \int_{-a}^b \frac{x}{(x^2 + \delta^2)^2} [f(x) - f(0) - f_x(0)x - \frac{1}{2}f_{xx}(0)x^2] dx, \\ I_4^x &\equiv \frac{\delta}{\pi} \int_{-a}^b \frac{x}{(x^2 + \delta^2)^2} dx, \\ I_5^x &\equiv \frac{\delta}{\pi} \int_{-a}^b \frac{x^2}{(x^2 + \delta^2)^2} dx, \\ I_6^x &\equiv \frac{\delta}{2\pi} \int_{-a}^b \frac{x^3}{(x^2 + \delta^2)^2} dx. \end{aligned} \quad (2.5.6)$$

Using Taylor series expansions, we find that, as δ tends to zero, the integrands of I_1^x and I_3^x behave in a regular fashion, and the corresponding integrals tend to finite values.

The second integral can be evaluated exactly, and is found to be

$$I_2^x = \frac{1}{2\pi} \int_{-a/\delta}^{b/\delta} \frac{w dw}{1+w^2} = \frac{1}{4\pi} \ln \frac{b^2 + \delta^2}{a^2 + \delta^2}, \quad (2.5.7)$$

where $w \equiv x/\delta$. In the limit as δ tends to zero, I_2^x tends to the principal-value integral

$$I_2^x(0) \equiv \frac{1}{2\pi} \not{\int}_{-a}^b \frac{1}{x} dx \equiv \frac{1}{2\pi} \left(\int_{-a}^{-\epsilon} \frac{dx}{x} + \int_{\epsilon}^b \frac{dx}{x} \right)_{\epsilon \rightarrow 0}, \quad (2.5.8)$$

where the right-hand side is evaluated in the limit as the positive exclusion length ϵ tends to zero.

The fourth integral can be calculated exactly, and is found to be

$$I_4^x = \frac{\delta}{2\pi} \frac{b^2 - a^2}{(a^2 + \delta^2)(b^2 + \delta^2)}. \quad (2.5.9)$$

In the limit as δ tends to zero, this integral vanishes.

The fifth integral can be calculated exactly, and is found to be

$$I_5^x = \frac{1}{\pi} \int_{-a/\delta}^{b/\delta} \frac{w^2 dw}{(1+w^2)^2} = \frac{1}{\pi} \int_{-\arctan(a/\delta)}^{\arctan(b/\delta)} \sin^2 \theta d\theta, \quad (2.5.10)$$

where $w = \tan \theta$. In the limit as δ tend to zero, the lower and upper limits of integration with respect to θ on the right-hand side tend, respectively, to $-\pi/2$ and $\pi/2$; accordingly, I_5^x tends to 1/2.

The sixth integral is given by

$$I_6^x = \delta I_2^x - \frac{1}{2} I_4^x. \quad (2.5.11)$$

In the limit as δ tends to zero, this integral vanishes.

Combining these results, we find that, in the limit as δ tends to zero,

$$I^x(\delta) \rightarrow -\frac{1}{2\pi} \not{\int}_{-a}^b \frac{f_y(x)}{x} dx + \frac{1}{2} f_x(0), \quad (2.5.12)$$

where P denotes the principal value of the improper integral. The first term on the right-hand side of (2.5.12) expresses the “naive” evaluation of (2.5.3) for $\delta = 0$.

To examine the asymptotic behavior of the right-hand side of (2.5.4), we remove the singularity of the kernel by writing

$$\begin{aligned} I^y(\epsilon) = & I_1^y + f_y(0) I_2^y + f_{yx}(0) I_3^y + I_4^y + f(0) I_5^y + f_x(0) I_6^y \\ & + I_7^y - f(0) I_8^y - f_x(0) I_9^y - f_{xx}(0) I_{10}^y - f_{xxx}(0) I_{11}^y, \end{aligned} \quad (2.5.13)$$

where

$$\begin{aligned}
 I_1^y &\equiv \frac{\delta}{2\pi} \int_{-a}^b \frac{1}{x^2 + \delta^2} [f_y(x) - f_y(0) - f_{yx}(0)x] dx, \\
 I_2^y &\equiv \frac{\delta}{2\pi} \int_{-a}^b \frac{dx}{x^2 + \delta^2}, \quad I_3^y \equiv \frac{\delta}{2\pi} \int_{-a}^b \frac{x}{x^2 + \delta^2} dx, \\
 I_4^y &\equiv \frac{1}{2\pi} \int_{-a}^b \frac{1}{x^2 + \delta^2} [f(x) - f(0) - f_x(0)x] dx, \\
 I_5^y &\equiv \frac{1}{2\pi} \int_{-a}^b \frac{dx}{x^2 + \delta^2}, \quad I_6^y \equiv \frac{1}{2\pi} \int_{-a}^b \frac{x}{x^2 + \delta^2} dx, \\
 I_7^y &\equiv -\frac{\delta^2}{\pi} \int_{-a}^b \frac{1}{(x^2 + \delta^2)^2} [f(x) - f(0) - f_x(0)x - \frac{1}{2}f_{xx}(0)x^2 \\
 &\quad - \frac{1}{6}f_{xxx}(0)x^3] dx, \\
 I_8^y &\equiv \frac{\delta^2}{\pi} \int_{-a}^b \frac{dx}{(x^2 + \delta^2)^2}, \quad I_9^y \equiv \frac{\delta^2}{\pi} \int_{-a}^b \frac{x}{(x^2 + \delta^2)^2} dx, \\
 I_{10}^y &\equiv \frac{\delta^2}{2\pi} \int_{-a}^b \frac{x^2}{(x^2 + \delta^2)^2} dx, \quad I_{11}^y \equiv \frac{\delta^2}{3\pi} \int_{-a}^b \frac{x^3}{(x^2 + \delta^2)^2} dx.
 \end{aligned} \tag{2.5.14}$$

Using Taylor series expansions, we find that, as δ tends to zero, I_1^y , I_4^y , and I_7^y tend to finite values, I_2^y tends to $\frac{1}{2}$, I_3^y tends to zero, I_5^y diverges as $\frac{1}{2\delta}$, and I_6^y tends to a finite value associated with a principal-value integral. The integral I_8^y can be expressed in the form

$$I_8^y = I_5^y + \frac{1}{4\pi\delta} \left[\sin 2\theta \right]_{\theta=-\arctan(a/\delta)}^{\theta=\arctan(b/\delta)}. \tag{2.5.15}$$

The first term on the right-hand side counterbalances the divergent contribution of I_5^y on the right-hand side of (2.5.13). Using Taylor series expansions, we find that, as δ tends to zero, the second term on the right-hand side of (2.5.15) vanishes. The last three integrals I_9^y , I_{10}^y , and I_{11}^y tend to zero.

Combining these results, we find that, in the limit as δ tends to zero,

$$I^y(\delta) \rightarrow \frac{1}{2}f_y(0) + \frac{1}{2\pi} \text{P} \int_{-a}^b \frac{f(x) - f(0)}{x^2} dx, \tag{2.5.16}$$

where P denotes the principal-value integral.

2.5.2 Shrinking arcs

Another way of assessing the asymptotic behavior of the integral representation for the gradient is to consider a point \mathbf{x}_0 that lies on a smooth contour C and exclude it from the control area enclosed by the contour by introducing a semi-circular arc of radius ϵ , as illustrated in Figure 2.4.2(b).

On the circular arc, $x - x_0 = \epsilon \cos \theta$, $y - y_0 = \epsilon \sin \theta$, $r \equiv |\mathbf{x} - \mathbf{x}_0| = \epsilon$, $n_x(\mathbf{x}) = \cos \theta$, $n_y(\mathbf{x}) = \sin \theta$, and $dl = \epsilon d\theta$. The contribution of the arc to the right-hand side of (2.5.1) and (2.5.2) is

$$I_\epsilon^x = -\frac{1}{2\pi} \int_0^\pi \cos \theta \left[\cos \theta \frac{\partial f(\mathbf{x})}{\partial x} + \sin \theta \frac{\partial f(\mathbf{x})}{\partial y} \right] d\theta - \frac{1}{2\pi\epsilon} \int_0^\pi f(\mathbf{x}) \cos \theta d\theta, \quad (2.5.17)$$

and

$$I_\epsilon^y = -\frac{1}{2\pi} \int_0^\pi \sin \theta \left[\cos \theta \frac{\partial f(\mathbf{x})}{\partial x} + \sin \theta \frac{\partial f(\mathbf{x})}{\partial y} \right] d\theta - \frac{1}{2\pi\epsilon} \int_0^\pi f(\mathbf{x}) \sin \theta d\theta, \quad (2.5.18)$$

where the point \mathbf{x} lies on the arc.

To compute the limiting value of the right-hand side of (2.5.17) as ϵ tends to zero, we expand the function $f(\mathbf{x})$ and its derivatives in Taylor series about the evaluation point \mathbf{x}_0 , retain the leading term in the expansion of the derivatives in the first integral and the leading two terms in the expansion of $f(\mathbf{x})$ in the second integral, and perform the integration in local polar angle θ to find

$$\begin{aligned} I_\epsilon^x &\rightarrow -\frac{1}{4} f_x(0) - \frac{1}{2\pi\epsilon} f(\mathbf{x}_0) \int_0^\pi \cos \theta d\theta \\ &- \frac{1}{2\pi\epsilon} \int_0^\pi [f_x(0) \epsilon \cos \theta + f_y(0) \epsilon \sin \theta] \cos \theta d\theta = -\frac{1}{2} f_x(0). \end{aligned} \quad (2.5.19)$$

Working similarly with (2.5.18), we find

$$I_\epsilon^y \rightarrow -\frac{1}{\pi\epsilon} f(\mathbf{x}_0) - \frac{1}{2} f_y(0). \quad (2.5.20)$$

Substituting (2.5.19) and (2.5.20) into (2.5.1) and (2.5.2) with the left-hand sides set equal to zero, and rearranging, we find

$$\begin{aligned} \frac{1}{2} \frac{\partial f(\mathbf{x}_0)}{\partial x_0} &= -\frac{1}{2\pi} \int_C^{PV} \frac{x - x_0}{r^2} [\mathbf{n}(\mathbf{x}) \cdot \nabla f(\mathbf{x})] dl(\mathbf{x}) \\ &+ \frac{1}{2\pi} \int_C^{PV} f(\mathbf{x}) \left[\frac{n_x(\mathbf{x})}{r^2} - 2(x - x_0) \frac{(x - x_0) n_x(\mathbf{x}) + (y - y_0) n_y(\mathbf{x})}{r^4} \right] dl(\mathbf{x}), \end{aligned} \quad (2.5.21)$$

and

$$\begin{aligned} \frac{1}{2} \frac{\partial f(\mathbf{x}_0)}{\partial y_0} = & -\frac{1}{2\pi} \int_C^{PV} \frac{y - y_0}{r^2} [\mathbf{n}(\mathbf{x}) \cdot \nabla f(\mathbf{x})] dl(\mathbf{x}) + \lim_{\epsilon \rightarrow 0} \{ \\ & \frac{1}{2\pi} \int_C f(\mathbf{x}) \left[\frac{n_y(\mathbf{x})}{r^2} - 2(y - y_0) \frac{(x - x_0) n_x(\mathbf{x}) + (y - y_0) n_y(\mathbf{x})}{r^4} \right] dl(\mathbf{x}) \\ & - \frac{1}{\pi\epsilon} f(\mathbf{x}_0) \}. \end{aligned} \quad (2.5.22)$$

It is understood that the principal value of the quantity enclosed by the curly brackets on the right-hand side of (2.5.22) arises in the limit as ϵ tends to zero. These results are consistent with the more specific forms (2.5.12) and (2.5.16).

In the literature of boundary-element methods, the second term on the right-hand side of (2.5.22), defined in terms of a limit, is called the Hadamard or “finite part” of the unregularized integral, and is denoted by

$$\begin{aligned} & \frac{1}{2\pi} \int_C^{FP} f(\mathbf{x}) \left[\frac{n_y(\mathbf{x})}{r^2} - 2(y - y_0) \frac{(x - x_0) n_x(\mathbf{x}) + (y - y_0) n_y(\mathbf{x})}{r^4} \right] dl(\mathbf{x}) \\ & \equiv \lim_{\epsilon \rightarrow 0} \{ \frac{1}{2\pi} \int_C f(\mathbf{x}) \left[\frac{n_y(\mathbf{x})}{r^2} - 2(y - y_0) \frac{(x - x_0) n_x(\mathbf{x}) + (y - y_0) n_y(\mathbf{x})}{r^4} \right] \\ & \quad \times dl(\mathbf{x}) - \frac{1}{\pi\epsilon} f(\mathbf{x}_0) \}. \end{aligned} \quad (2.5.23)$$

Extreme caution should be exercised in using this terminology and accepting the underlying implication that the limit of a strongly singular integral automatically produces the finite part of a hypersingular integral.

Expressions (2.5.21) and (2.5.22) have been derived with reference to a local coordinate system where the y axis is normal to the contour C at the point \mathbf{x}_0 where the gradient is evaluated. The results have shown that a hypersingular integral arises in the representation of the normal derivative.

2.5.3 Hypersingular integral equations

Having confirmed the existence of the limit of the integral representation for the gradient (2.3.13) as the evaluation point \mathbf{x}_0 approaches the boundary C , provided that sufficient regularity conditions are met so that the Taylor series expansions are defined, we may proceed to derive “hypersingular integral equations” for the boundary distribution of the normal or tangential derivatives.

Taking, in particular, the limit as the point \mathbf{x}_0 approaches the contour C , and projecting the resulting expression onto the normal vector, we find

$$\begin{aligned} \frac{1}{2} n_i(\mathbf{x}_0) \frac{\partial f(\mathbf{x}_0)}{\partial x_{0_i}} &= - \int_C^{PV} n_i(\mathbf{x}_0) \frac{\partial G(\mathbf{x}_0, \mathbf{x})}{\partial x_{0_i}} [\mathbf{n}(\mathbf{x}) \cdot \nabla f(\mathbf{x})] dl(\mathbf{x}) \\ &+ \int_C^{FP} f(\mathbf{x}) n_i(\mathbf{x}_0) \frac{\partial^2 G(\mathbf{x}_0, \mathbf{x})}{\partial x_{0_i} \partial x_j} n_j(\mathbf{x}) dl(\mathbf{x}), \end{aligned} \quad (2.5.24)$$

where the notation

$$\begin{aligned} &\int_C^{FP} f(\mathbf{x}) n_i(\mathbf{x}_0) \frac{\partial^2 G(\mathbf{x}_0, \mathbf{x})}{\partial x_{0_i} \partial x_j} n_j(\mathbf{x}) dl(\mathbf{x}) \\ &\equiv \lim_{\epsilon \rightarrow 0} \left\{ \int_C f(\mathbf{x}) n_i(\mathbf{x}_0) \frac{\partial^2 G(\mathbf{x}_0, \mathbf{x})}{\partial x_{0_i} \partial x_j} n_j(\mathbf{x}) dl(\mathbf{x}) - \frac{1}{\pi \epsilon} f(\mathbf{x}_0) \right\} \end{aligned} \quad (2.5.25)$$

defines the finite part of the integral. Equation (2.5.24) is a Fredholm integral equation of the second kind for the boundary distribution of the normal derivative.

2.5.4 Regularization of hypersingular integral equations

In practice, it is beneficial to eliminate the strong singularities at the outset by regularizing the kernels with the help of integral identities.

Consider the integral representation (2.3.9) and its consequent vector identities (2.3.10) and (2.3.11). To prepare the ground for the regularization, we multiply (2.3.10) by $f(\mathbf{x}_0)$ and obtain the identity

$$0 = \int_C f(\mathbf{x}_0) \frac{\partial^2 G(\mathbf{x}_0, \mathbf{x})}{\partial x_{0_i} \partial x_j} n_j(\mathbf{x}) dl(\mathbf{x}). \quad (2.5.26)$$

Furthermore, we project (2.3.11) onto the gradient $\partial f(\mathbf{x}_0)/\partial x_{0_k}$ and set the constants b_k equal to x_{0_k} to obtain the identity

$$\begin{aligned} \frac{\partial f(\mathbf{x}_0)}{\partial x_{0_i}} &= - \int_C \frac{\partial G(\mathbf{x}_0, \mathbf{x})}{\partial x_{0_i}} \frac{\partial f(\mathbf{x}_0)}{\partial x_{0_k}} n_k(\mathbf{x}) dl(\mathbf{x}) \\ &+ \int_C \frac{\partial^2 G(\mathbf{x}_0, \mathbf{x})}{\partial x_{0_i} \partial x_j} n_j(\mathbf{x}) \frac{\partial f(\mathbf{x}_0)}{\partial x_{0_k}} (x_k - x_{0_k}) dl(\mathbf{x}). \end{aligned} \quad (2.5.27)$$

Next, we subtract (2.5.26) and (2.5.27) from (2.3.9) and find

$$0 = - \int_C \frac{\partial G(\mathbf{x}_0, \mathbf{x})}{\partial x_{0_i}} \{ \mathbf{n}(\mathbf{x}) \cdot \nabla [f(\mathbf{x}) - f(\mathbf{x}_0)] \} dl(\mathbf{x}) \\ + \int_C [f(\mathbf{x}) - f(\mathbf{x}_0) - \frac{\partial f(\mathbf{x}_0)}{\partial x_{0_k}} (x_k - x_{0_k})] \frac{\partial^2 G(\mathbf{x}_0, \mathbf{x})}{\partial x_{0_i} \partial x_j} n_j(\mathbf{x}) dl(\mathbf{x}), \quad (2.5.28)$$

where summation over the repeated index j is implied on the right-hand side. In the limit as the evaluation point \mathbf{x}_0 approaches the boundary C , the integrands on the right-hand side of (2.5.28) remain nonsingular, yielding a regularized integral equation.

Problem

P.2.5.1 Evaluation of definite integrals

Confirm the definite integrals (2.5.7), (2.5.9), and (2.5.11) given in the text.

2.6 Irrotational flow

Laplace's equation arises in the computation of a particular class of fluid flows whose velocity $\mathbf{u} = (u_x, u_y)$ may be expressed as the gradient of a scalar function ϕ , called the velocity potential, in the form

$$u_x = \frac{\partial \phi}{\partial x}, \quad u_y = \frac{\partial \phi}{\partial y}. \quad (2.6.1)$$

In vector notation,

$$\mathbf{u} = \nabla \phi. \quad (2.6.2)$$

Conversely, if the velocity field derives from a scalar function ϕ as shown in (2.6.2), then the flow is potential or irrotational (e.g., [59]).

A mass balance over an infinitesimal volume of flow occupied by an incompressible fluid shows that the velocity field is solenoidal,

$$\nabla \cdot \mathbf{u} \equiv \frac{\partial u_x}{\partial x} + \frac{\partial u_y}{\partial y} = 0. \quad (2.6.3)$$

Expressing the velocity in terms of the potential using (2.6.1), we find

$$\nabla \cdot \nabla \phi = \nabla^2 \phi = \frac{\partial^2 \phi}{\partial x^2} + \frac{\partial^2 \phi}{\partial y^2} = 0, \quad (2.6.4)$$

that is, the velocity potential satisfies Laplace's equation. The boundary-integral representation of the harmonic potential is a convenient starting point for deriving a host of results concerning the properties and computation of irrotational flow (e.g., [59]).

As a first step toward developing the boundary-integral representation, we select a *finite* control area that is enclosed by a collection of contours, denoted by C . This otherwise mundane step acquires special importance when we consider flow in an infinite or partially bounded domain where the temptation to define an infinite control area may lead to an erroneous formulation.

2.6.1 Infinite flow past a body

Consider two-dimensional potential flow past a body in an infinite domain, in the absence of circulatory motion around the body, as illustrated in Figure 2.6.1. To develop the boundary-integral representation, we split the harmonic potential into an incident component ϕ^∞ that prevails far from the body, and a disturbance component ϕ^D due to the body

$$\phi = \phi^\infty + \phi^D. \quad (2.6.5)$$

In the presence of circulatory motion, a third component must be added to the right-hand side of (2.6.5), as discussed in subdirectory `body_2d` of directory `laplace` of the *BEMLIB* user guide (Chapter 10).

Because the body is assumed to be impenetrable, far from the body the disturbance potential behaves like a point source dipole described by the gradient of the Green's function,

$$\phi^D(\mathbf{x}) \simeq \mathbf{d} \cdot \nabla_B G(\mathbf{x}, \mathbf{x}_B), \quad (2.6.6)$$

where \mathbf{d} is an *a priori* unknown constant vector, \mathbf{x}_B is a designated center of the body, and the gradient ∇_B operates with respect to \mathbf{x}_B . If the potential behaved like a point source, a non-zero amount of fluid would have to emanate from the body, which is not acceptable.

To derive the boundary-integral representation, we consider a control area that is bounded by the contour of the body C_B and a large circular contour of radius R centered at \mathbf{x}_0 , denoted by L . Applying the boundary-integral representation (2.3.3) for the disturbance potential, we find

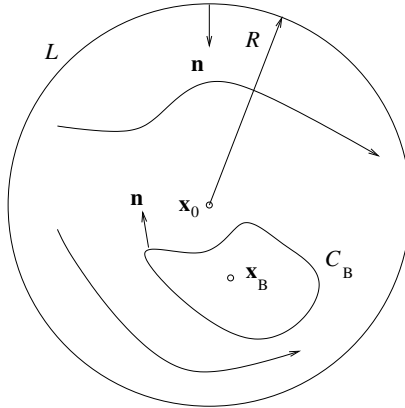


Figure 2.6.1 Potential flow past a two-dimensional body with vanishing circulation around the body. To develop the boundary-integral representation, we define a control area that is enclosed by the contour of the body C_B and a large circular contour of radius R enclosing the body centered at x_0 , denoted by L , and then let the radius of L expand to infinity.

$$\begin{aligned} \phi^D(x_0) = & - \int_{C_B, L} G(x_0, x) [\mathbf{n}(x) \cdot \nabla \phi^D(x)] dl(x) \\ & + \int_{C_B, L} \phi^D(x) [\mathbf{n}(x) \cdot \nabla G(x_0, x)] dl(x), \end{aligned} \quad (2.6.7)$$

where the unit normal vector \mathbf{n} points into the control area enclosed by the union of C_B and L , as depicted in Figure 2.6.1.

Focusing our attention on the single-layer integral over the large contour L , we note that $G(\mathbf{x}, \mathbf{x}_0) = -\frac{1}{2\pi} \ln R$ is constant and extract it from the integral. Mass conservation requires that the flow rate across any surface enclosing the body is zero, $\int_L [\mathbf{n}(x) \cdot \nabla \phi^D(x)] dl(x) = 0$. Combining these results, we find that the single-layer potential over L vanishes for any location of the evaluation point. Turning to the double-layer integral over L , we use the asymptotic behavior shown in (2.6.6) to find that, in the limit as R tends to infinity, the double-layer integral disappears. Discarding the integrals over L on the right-hand side of (2.6.7), we derive a representation for the disturbance potential in terms of potentials defined over the body contour.

2.7 Generalized single- and double-layer representations

The boundary-integral representation provides us with the solution of Laplace's equation at the point \mathbf{x}_0 in terms of boundary distributions of point sources and point-source dipoles whose strength density distributions are the boundary value and normal derivative of the solution. For simplicity, it is sometimes desirable to eliminate one of the two potentials, thereby deriving *generalized* or *indirect* boundary-integral representations with modified strength density distributions.

2.7.1 Interior fields

Consider first the solution of Laplace's equation in the interior of a closed contour C , denoted by f^{Int} , and introduce an exterior field f^{Ext} that shares with f^{Int} the boundary values over C , that is, $f^{Int} = f^{Ext}$ over C . Applying the boundary-integral representation for the interior field and the reciprocal relation for the exterior field, both at a point \mathbf{x}_0 that lies inside C , we obtain

$$\begin{aligned} f^{Int}(\mathbf{x}_0) &= - \int_C G(\mathbf{x}, \mathbf{x}_0) [\mathbf{n}(\mathbf{x}) \cdot \nabla f^{Int}(\mathbf{x})] dl(\mathbf{x}) \\ &\quad + \int_C f^{Int}(\mathbf{x}) [\mathbf{n}(\mathbf{x}) \cdot \nabla G(\mathbf{x}, \mathbf{x}_0)] dl(\mathbf{x}), \end{aligned} \quad (2.7.1)$$

and

$$\begin{aligned} 0 &= - \int_C G(\mathbf{x}, \mathbf{x}_0) [\mathbf{n}(\mathbf{x}) \cdot \nabla f^{Ext}(\mathbf{x})] dl(\mathbf{x}) \\ &\quad + \int_C f^{Ext}(\mathbf{x}) [\mathbf{n}(\mathbf{x}) \cdot \nabla G(\mathbf{x}, \mathbf{x}_0)] dl(\mathbf{x}), \end{aligned} \quad (2.7.2)$$

where the unit normal vector \mathbf{n} points toward the interior. Subtracting (2.7.2) from (2.7.1) and using the stipulated continuity condition for f across C , we obtain the single-layer representation

$$f^{Int}(\mathbf{x}_0) = -I^{SLP}(\mathbf{x}_0, \sigma), \quad (2.7.3)$$

where

$$I^{SLP}(\mathbf{x}_0, \sigma) \equiv \int_C G(\mathbf{x}, \mathbf{x}_0) \sigma(\mathbf{x}) dl(\mathbf{x}), \quad (2.7.4)$$

is the single-layer potential, and

$$\sigma(\mathbf{x}) \equiv \mathbf{n}(\mathbf{x}) \cdot \nabla [f^{Int}(\mathbf{x}) - f^{Ext}(\mathbf{x})], \quad (2.7.5)$$

is the strength density distribution. It is understood that the right-hand side of (2.7.5) is evaluated over C .

Alternatively, we introduce an exterior field f^{Ext} that shares with f^{Int} the boundary distribution of the normal derivative, $\mathbf{n}(\mathbf{x}) \cdot \nabla f^{Int}(\mathbf{x}) = \mathbf{n}(\mathbf{x}) \cdot \nabla f^{Ext}(\mathbf{x})$ over C . Working in a similar fashion, we derive a representation of the interior field in terms of a double-layer potential,

$$f^{Int}(\mathbf{x}_0) = I^{DLP}(\mathbf{x}_0, q), \quad (2.7.6)$$

where

$$I^{DLP}(\mathbf{x}_0, q) \equiv \int_C q(\mathbf{x}) [\mathbf{n}(\mathbf{x}) \cdot \nabla G(\mathbf{x}, \mathbf{x}_0)] dl(\mathbf{x}), \quad (2.7.7)$$

is the double-layer potential, and

$$q(\mathbf{x}) \equiv f^{Int}(\mathbf{x}) - f^{Ext}(\mathbf{x}), \quad (2.7.8)$$

is the strength density distribution. It is understood that the right-hand side of (2.7.8) is evaluated over C .

It is instructive to note that the boundary-integral formulation provides us with the identity

$$f^{Int}(\mathbf{x}_0) = -I^{SLP}(\mathbf{x}_0, \frac{\partial f^{Int}}{\partial n}) + I^{DLP}(\mathbf{x}_0, f^{Int}), \quad (2.7.9)$$

which identifies the strength density of the double- and single-layer potential with the boundary distribution of the harmonic function and its normal derivative.

2.7.2 Exterior fields

Similar representations can be derived for an exterior field, with one important exception. A representation of an exterior field in terms of a double-layer potential is possible only when the integrated flux is zero,

$$\int_C \mathbf{n}(\mathbf{x}) \cdot \nabla f^{Ext}(\mathbf{x}) dl(\mathbf{x}) = 0. \quad (2.7.10)$$

The physical reason is that the double-layer representation is unable to generate a field that behaves like a point source far from an interior boundary.

To overcome this limitation, the double-layer representation may be complemented with the field due to a point source expressed by the Green's function, where the singular point is located inside the interior boundary (e.g., [59]). The resulting compound representation is known as the “completed double-layer potential.”

2.7.3 Gradient of the single-layer potential

Taking the gradient of the single-layer potential (2.7.4) written with the free-space Green's function, and noting that $G(\mathbf{x}, \mathbf{x}_0) = G(\mathbf{x} - \mathbf{x}_0)$ and thus $\nabla_0 G(\mathbf{x}, \mathbf{x}_0) = -\nabla G(\mathbf{x} - \mathbf{x}_0)$, we find

$$\nabla_0 I^{SLP}(\mathbf{x}_0, \sigma) = - \int_C \nabla G(\mathbf{x}_0, \mathbf{x}) \sigma(\mathbf{x}) dl(\mathbf{x}). \quad (2.7.11)$$

To express the integral representation (2.7.11) in terms of the single- and double-layer potential, we decompose the gradient of the Green's function into its normal and tangential constituents as

$$\nabla G(\mathbf{x}_0, \mathbf{x}) = \mathbf{n} [\mathbf{n} \cdot \nabla G(\mathbf{x}_0, \mathbf{x})] + \mathbf{t} [\mathbf{t} \cdot \nabla G(\mathbf{x}_0, \mathbf{x})], \quad (2.7.12)$$

where \mathbf{t} is the unit tangent vector along C . Substituting this decomposition into the right-hand side of (2.7.11), defining

$$\mathbf{u} \equiv \sigma \mathbf{n}, \quad (2.7.13)$$

and rearranging, we obtain

$$\begin{aligned} \nabla_0 I^{SLP}(\mathbf{x}_0, \sigma) &= - \int_C \mathbf{u}(\mathbf{x}) [\mathbf{n}(\mathbf{x}) \cdot \nabla G(\mathbf{x}_0, \mathbf{x})] dl(\mathbf{x}) \\ &\quad - \int_C \mathbf{t}(\mathbf{x}) \frac{\partial G(\mathbf{x}_0, \mathbf{x})}{\partial l} \sigma(\mathbf{x}) dl(\mathbf{x}) \\ &= - \int_C \mathbf{u}(\mathbf{x}) [\mathbf{n}(\mathbf{x}) \cdot \nabla G(\mathbf{x}_0, \mathbf{x})] dl(\mathbf{x}) - \int_C \frac{\partial}{\partial l} [\mathbf{t}(\mathbf{x}) G(\mathbf{x}_0, \mathbf{x}) \sigma(\mathbf{x})] dl(\mathbf{x}) \\ &\quad + \int_C G(\mathbf{x}_0, \mathbf{x}) \frac{\partial}{\partial l} [\mathbf{t}(\mathbf{x}) \sigma(\mathbf{x})] dl(\mathbf{x}). \end{aligned} \quad (2.7.14)$$

The fundamental theorem of calculus requires that the penultimate integral in (2.7.14) is zero, yielding the identity

$$\begin{aligned} \nabla_0 I^{SLP}(\mathbf{x}_0, \sigma) &= - \int_C \mathbf{u}(\mathbf{x}) [\mathbf{n}(\mathbf{x}) \cdot \nabla G(\mathbf{x}_0, \mathbf{x})] dl(\mathbf{x}) \\ &\quad + \int_C \mathbf{v}(\mathbf{x}) G(\mathbf{x}_0, \mathbf{x}) dl(\mathbf{x}), \end{aligned} \quad (2.7.15)$$

where

$$\mathbf{v} \equiv \frac{\partial}{\partial l} (\mathbf{t} \sigma) = \kappa \sigma \mathbf{n} + \frac{\partial \sigma}{\partial l} \mathbf{t}. \quad (2.7.16)$$

The first expression on the right-hand side of (2.7.16) arises from the Frenet relation $\partial \mathbf{t} / \partial l = \kappa \mathbf{n}$, where κ is the curvature.

Equation (2.7.15) expresses the gradient of the single-layer potential as a linear combination of a single- and a double-layer potential with vectorial strength density distributions in the form

$$\nabla_0 I^{SLP}(\mathbf{x}_0, \sigma) = I^{SLP}(\mathbf{x}_0, \mathbf{v}) - I^{DLP}(\mathbf{x}_0, \mathbf{u}). \quad (2.7.17)$$

2.7.4 Gradient of the double-layer potential

To derive an analogous representation for the gradient of the double-layer potential, we work in a similar fashion and find

$$\nabla_0 I^{DLP}(\mathbf{x}_0, q) = - \int_C q(\mathbf{x}) [\mathbf{n}(\mathbf{x}) \cdot \nabla \{ \nabla G(\mathbf{x}_0, \mathbf{x}) \}] dl(\mathbf{x}). \quad (2.7.18)$$

The i th component of the gradient may be expressed in the form

$$\begin{aligned} \frac{\partial I^{DLP}(\mathbf{x}_0, q)}{\partial x_{0_i}} &= - \int_C q(\mathbf{x}) n_j(\mathbf{x}) \frac{\partial^2 G(\mathbf{x}_0, \mathbf{x})}{\partial x_j \partial x_i} dl(\mathbf{x}) \\ &= - \int_C \frac{\partial}{\partial x_i} [q(\mathbf{x}) \frac{\partial G(\mathbf{x}_0, \mathbf{x})}{\partial x_j}] n_j(\mathbf{x}) dl(\mathbf{x}) \\ &\quad + \int_C \frac{\partial q}{\partial x_i} \frac{\partial G(\mathbf{x}_0, \mathbf{x})}{\partial x_j} n_j(\mathbf{x}) dl(\mathbf{x}). \end{aligned} \quad (2.7.19)$$

To simplify this representation, we extend the density q into the complement of the solution space, use the divergence theorem to convert the penultimate integral to a domain integral, expand the integrand of the domain integral and invoke the definition of the Green's function to discard one term, and, finally, use the divergence theorem to eliminate the domain integral in favor of a contour integral. Combining the surviving terms, and reverting to vector notation, we find

$$\begin{aligned} \nabla_0 I^{DLP}(\mathbf{x}_0, q) &= \int_C [\mathbf{n}(\mathbf{x}) \times \nabla q(\mathbf{x})] \times \nabla G(\mathbf{x}_0, \mathbf{x}) dl(\mathbf{x}) \\ -\mathbf{e}_z \times \int_C \nabla G(\mathbf{x}_0, \mathbf{x}) \frac{\partial q}{\partial l}(\mathbf{x}) dl(\mathbf{x}) &= \mathbf{e}_z \times \nabla_0 I^{SLP}(\mathbf{x}_0, \frac{\partial q}{\partial l}), \end{aligned} \quad (2.7.20)$$

where $\mathbf{e}_z \equiv \mathbf{t} \times \mathbf{n}$ is the unit vector perpendicular to the xy plane. Using (2.7.15) with $\partial q/\partial l$ in place of σ , we now obtain the desired representation

$$\begin{aligned} \nabla_0 I^{DLP}(\mathbf{x}_0, q) &= \int_C \hat{\mathbf{u}}(\mathbf{x}) [\mathbf{n}(\mathbf{x}) \cdot \nabla G(\mathbf{x}_0, \mathbf{x})] dl(\mathbf{x}) \\ &\quad - \int_C \hat{\mathbf{v}}(\mathbf{x}) G(\mathbf{x}_0, \mathbf{x}) dl(\mathbf{x}), \end{aligned} \quad (2.7.21)$$

involving single- and double-layer potentials, where

$$\hat{\mathbf{u}} \equiv -\mathbf{e}_z \times \mathbf{n} \frac{\partial q}{\partial l} = \frac{\partial q}{\partial l} \mathbf{t}, \quad (2.7.22)$$

and

$$\hat{\mathbf{v}} \equiv -\mathbf{e}_z \times \frac{\partial}{\partial l} \left[\mathbf{t} \frac{\partial q}{\partial l} \right] = -\mathbf{e}_z \times [\kappa \mathbf{n} \frac{\partial q}{\partial l} + \mathbf{t} \frac{\partial^2 q}{\partial l^2}] = \kappa \frac{\partial q}{\partial l} \mathbf{t} - \frac{\partial^2 q}{\partial l^2} \mathbf{n}. \quad (2.7.23)$$

Equation (2.7.21) expresses the gradient of the single-layer potential as a linear combination of a single- and a double-layer potential with vectorial strength density distributions given in (2.7.22) and (2.7.23), in the form

$$\nabla_0 I^{DLP}(\mathbf{x}_0, q) = -I^{SLP}(\mathbf{x}_0, \hat{\mathbf{v}}) + I^{DLP}(\mathbf{x}_0, \hat{\mathbf{u}}). \quad (2.7.24)$$

When the scalar density of the double-layer potential q is constant, the vector density distributions $\hat{\mathbf{u}}$ and $\hat{\mathbf{v}}$ are both zero and the gradient of the double-layer potential vanishes. This result is consistent with the uniformity of the double-layer potential in the interior and exterior of C , as required by identity (2.2.14).

Problem

P.2.7.1 Boundary integral representation of the gradient

- (a) Follow the instructions in the text to derive the representation (2.7.20).
- (b) If $f(\mathbf{x})$ is a harmonic function, then the scalar components of its gradient $\nabla f(\mathbf{x})$ are also harmonic functions and admit the boundary-integral representation (2.7.9) with $\partial f / \partial x$ or $\partial f / \partial y$ in place of f . Thus,

$$\nabla f^{Int}(\mathbf{x}_0) = -I^{SLP}(\mathbf{x}_0, \frac{\partial \nabla f^{Int}}{\partial n}) + I^{DLP}(\mathbf{x}_0, \nabla f^{Int}). \quad (1)$$

On the other hand, taking the gradient of (2.7.9), we find

$$\nabla_0 f^{Int}(\mathbf{x}_0) = -\nabla_0 I^{SLP}(\mathbf{x}_0, \frac{\partial f^{Int}}{\partial n}) + \nabla_0 I^{DLP}(\mathbf{x}_0, f^{Int}). \quad (2)$$

Show that when (2.7.17) and (2.7.24) are substituted into equation (2), and the single- and double-layer potentials are consolidated, the result is equation (1).

Chapter 3

Boundary-element methods for Laplace's equation in two dimensions

The boundary-element method derives its name from the practice of describing the boundary of a solution domain with a collection of elementary geometrical units called boundary elements. In the case of Laplace's equation in two dimensions, the boundary elements are line segments with straight or curved shapes described in analytical form by methods of function interpolation and approximation in terms of element nodes.

Boundary discretization is the first step in the implementation of the boundary-element method. In the second step, we describe the boundary distribution of the specified or unknown functions involved in the integral representation with local interpolating or approximating polynomials. In the third step, we compute the polynomial coefficients by requiring an appropriate number of conditions originating from the integral equations.

In this chapter, we outline the implementation of these fundamental steps with reference to Laplace's equation in two dimensions. Other types of differential equations may be solved by straightforward alterations of the basic procedure.

3.1 Boundary element discretization

A variety of boundary elements are available in two dimensions. Three popular choices are linear elements with straight shapes, circular arcs, and elements of cubic splines.

3.1.1 Straight elements

Figure 3.1.1 illustrates the discretization of a boundary into a collection of N straight elements defined by the element end-points or nodes. The element labels, printed in bold, increase in the counterclockwise direction around the boundary. Since the sec-

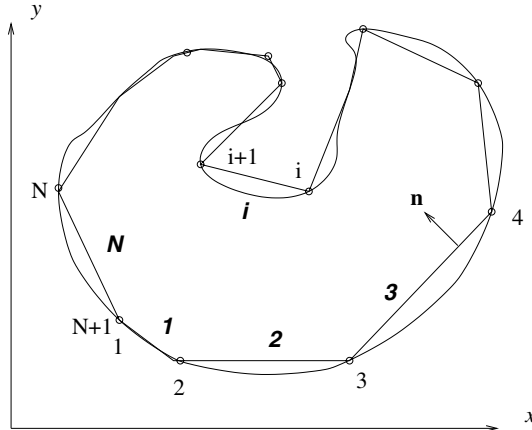


Figure 3.1.1 Discretization of a closed line, representing a two-dimensional boundary, into a collection of straight elements whose union forms a polygon.

ond end-point of an element is the first end-point of the next element, the collection of the N elements is defined by $N + 1$ distinct (unique) nodes. If the boundary is closed, as depicted in Figure 3.1.1, the first and last global nodes coincide, and the collection of the N elements is defined by N distinct nodes.

To describe the i th element, we introduce the coordinates of the element end-points

$$(x_{i,1}^E, y_{i,1}^E), \quad (x_{i,2}^E, y_{i,2}^E), \quad (3.1.1)$$

and a dimensionless parameter ξ ranging in the interval $[-1, 1]$. The coordinates of a point on the element are given by

$$\begin{aligned} x(\xi) &= \frac{1}{2} (x_{i,2}^E + x_{i,1}^E) + \frac{1}{2} (x_{i,2}^E - x_{i,1}^E) \xi, \\ y(\xi) &= \frac{1}{2} (y_{i,2}^E + y_{i,1}^E) + \frac{1}{2} (y_{i,2}^E - y_{i,1}^E) \xi. \end{aligned} \quad (3.1.2)$$

As ξ increases from -1 to 1, the point (x, y) moves from the first element end-point to the second element end-point.

Next, we introduce the array of global or unique nodes, (x_i^G, y_i^G) . Recalling that the second end-point of the i th element is the first end-point of the next element, we write

$$(x_{i,1}^E, y_{i,1}^E) = (x_i^G, y_i^G), \quad (x_{i,2}^E, y_{i,2}^E) = (x_{i+1}^G, y_{i+1}^G). \quad (3.1.3)$$

Making substitutions into (3.1.2), we derive parametric representations in terms of the global nodes.

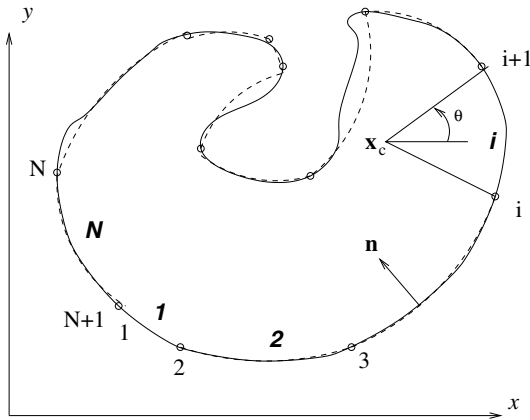


Figure 3.1.2 Discretization of a closed line, representing a two-dimensional boundary, into a collection of circular arcs drawn with dashed lines.

3.1.2 Circular arcs

Figure 3.1.2 illustrates the discretization of a boundary into a collection of N circular arcs. The element labels, printed in bold, increase in the counter-clockwise direction around the boundary.

The coordinates of the first and second end-point of the i th arc are shown in (3.1.1). Additional geometrical properties of the arc include the following:

- The coordinates of the arc center $(x_{c,i}, y_{c,i})$.
- The arc radius R_i .
- The polar angles at the first and second end-points denoted, respectively, by $\theta_{1,i}$ and $\theta_{2,i}$.

If the arc turns in the counterclockwise direction, as shown in Figure 3.1.2, $\theta_{2,i} > \theta_{1,i}$; if the arc turns in the clockwise direction, $\theta_{2,i} < \theta_{1,i}$.

A point on the i th arc is described in parametric form in terms of the polar angle θ by the equations

$$x(\theta) = x_{c,i} + R_i \cos \theta, \quad y(\theta) = y_{c,i} + R_i \sin \theta. \quad (3.1.4)$$

If the arc turns in the counterclockwise direction, $\theta_{1,i} < \theta < \theta_{2,i}$; if the arc turns in the clockwise direction, $\theta_{1,i} < \theta < \theta_{2,i}$. By definition then,

$$\begin{aligned} x_{1,i} &= x_{c,i} + R_i \cos \theta_{1,i}, & y_{1,i} &= y_{c,i} + R_i \sin \theta_{1,i}, \\ x_{2,i} &= x_{c,i} + R_i \cos \theta_{2,i}, & y_{2,i} &= y_{c,i} + R_i \sin \theta_{2,i}. \end{aligned} \quad (3.1.5)$$

To standardize the parametric representation, we introduce the dimensionless parameter ξ ranging in the interval $[-1, 1]$, and write

$$\theta(\xi) = \frac{1}{2} (\theta_{2,i} + \theta_{1,i}) + \frac{1}{2} (\theta_{2,i} - \theta_{1,i}) \xi. \quad (3.1.6)$$

As ξ increases from -1 to 1, the angle θ changes from $\theta_{i,1}$ to $\theta_{i,2}$. Correspondingly, the point $[x(\theta), y(\theta)]$ moves from the first element end-point to the second element end-point.

Substituting the right-hand side of (3.1.6) in place of θ in (3.1.4), we derive a parametric representation in terms of ξ , $[x(\xi), y(\xi)]$.

3.1.3 Cubic splines

The straight-segment and circular-arc discretizations provide us with approximate representations with discontinuous slope and curvature at the element end-points. To obtain a globally smooth representation, we introduce boundary elements defined by cubic-splines interpolation.

To implement this discretization, we describe the boundary with $N + 1$ nodes, introduce a parameter s that varies monotonically along the boundary, and assign values of s to the nodes. One sensible choice for the value of s assigned to the i th node, denoted by s_i , is the polygonal arc length, that is, the current length of the polygonal line connecting sequential nodes, measured from the first node.

In the cubic-splines representation, the i th boundary element subtended between the i th and $i + 1$ node is described in parametric form by the cubic polynomials

$$\begin{aligned} x(s) &= P_i(s) = a_i (s - s_i)^3 + b_i (s - s_i)^2 + c_i (s - s_i) + x_i^G, \\ y(s) &= P'_i(s) = a'_i (s - s_i)^3 + b'_i (s - s_i)^2 + c'_i (s - s_i) + y_i^G, \end{aligned} \quad (3.1.7)$$

where $s_i \leq s \leq s_{i+1}$. By construction, the parametric representations shown in (3.1.7) satisfy the interpolation conditions

$$x(s_i) = P_i(s_i) = x_i^G, \quad y(s_i) = P'_i(s_i) = y_i^G. \quad (3.1.8)$$

The $3N$ coefficients a_i, b_i , and c_i , where $i = 1, \dots, N$, and the corresponding $3N$ coefficients a'_i, b'_i , and c'_i , will be computed by requiring interpolation and smoothness conditions, as follows.

Consider the parametric representation for the x coordinate shown in the first equation of (3.1.7).

First, we require the interpolation condition

$$P_i(s_{i+1}) = x_{i+1}^G = x_i^G + a_i h_i^3 + b_i h_i^2 + c_i h_i, \quad (3.1.9)$$

for $i = 1, \dots, N$, where

$$h_i \equiv s_{i+1} - s_i. \quad (3.1.10)$$

Second, we require continuity of slope at the interior nodes,

$$\frac{dP_i}{ds}(s_{i+1}) = \frac{dP_{i+1}}{ds}(s_{i+1}), \quad (3.1.11)$$

for $i = 1, \dots, N - 1$. Substituting the first expression of (3.1.7) into (3.1.11), we obtain

$$3 a_i h_i^2 + 2 b_i h_i + c_i = c_{i+1}, \quad (3.1.12)$$

for $i = 1, \dots, N - 1$.

Third, we require continuity of curvature at the interior nodes,

$$\frac{d^2 P_i}{ds^2}(s_{i+1}) = \frac{d^2 P_{i+1}}{ds^2}(s_{i+1}), \quad (3.1.13)$$

for $i = 1, \dots, N - 1$. Substituting the first expression of (3.1.7) into (3.1.13), we obtain

$$6 a_i h_i + 2 b_i = 2 b_{i+1}, \quad (3.1.14)$$

for $i = 1, \dots, N$, subject to the definition

$$b_{N+1} \equiv \frac{1}{2} \frac{d^2 P_N}{ds^2}(s_{N+1}). \quad (3.1.15)$$

In summary, equations (3.1.9), (3.1.12), and (3.1.14) provide us with $3N - 1$ conditions involving $3N + 1$ unknown coefficients including b_{N+1} , and a_i, b_i, c_i , for $i = 1, \dots, N$. To balance the number of unknowns with the number of equations, we must impose two additional conditions by exercising common sense or geometrical intuition, as will be discussed later in this section.

To compute the unknown coefficients, it is expedient to proceed in three stages. First, we rearrange (3.1.14) into

$$a_i = \frac{b_{i+1} - b_i}{3 h_i}, \quad (3.1.16)$$

for $i = 1, \dots, N$. Second, we substitute this expression into (3.1.9) and solve for c_i to obtain

$$c_i = \frac{x_{i+1}^G - x_i^G}{h_i} - \frac{1}{3} h_i (b_{i+1} + 2 b_i), \quad (3.1.17)$$

for $i = 1, \dots, N$. Third, we substitute (3.1.17) and (3.1.16) into (3.1.12) and rearrange to derive a tridiagonal system of $N - 1$ equations involving the $N + 1$ coefficients b_i , $i = 1, \dots, N + 1$,

$$\frac{h_i}{3} b_i + 2 \frac{h_i + h_{i+1}}{3} b_{i+1} + \frac{h_{i+1}}{3} b_{i+2} = \frac{x_{i+2}^G - x_{i+1}^G}{h_{i+1}} - \frac{x_{i+1}^G - x_i^G}{h_i}, \quad (3.1.18)$$

for $i = 1, \dots, N - 1$. To compute these unknown coefficients, we require two additional conditions.

Periodic cubic splines

When the boundary is closed or periodic, we impose periodicity conditions for the first and second derivative at the first and last nodes expressed, respectively, by the equations

$$3 a_N h_N^2 + 2 b_N h_N + c_N = c_1, \quad b_1 = b_{N+1}. \quad (3.1.19)$$

Substituting (3.1.16) and (3.1.17) into the first of (3.1.19) to eliminate a_N , c_N , and c_1 , rearranging the resulting expression, and using the second of (3.1.19), we find

$$\frac{2}{3} (h_1 + h_N) b_1 + \frac{1}{3} h_1 b_2 + \frac{1}{3} h_N b_N = \frac{x_2^G - x_1^G}{h_1} - \frac{x_{N+1}^G - x_N^G}{h_N}. \quad (3.1.20)$$

Applying (3.1.18) for $i = 1, \dots, N - 1$, and using the second of (3.1.19) to eliminate b_{N+1} , we derive the linear system

$$\begin{bmatrix} \frac{2(h_1+h_2)}{3} & \frac{h_2}{3} & 0 & \dots & \dots & 0 \\ \frac{h_2}{3} & \frac{2(h_2+h_3)}{3} & \frac{h_3}{3} & 0 & \dots & 0 \\ \dots & \dots & \dots & \dots & \dots & \vdots \\ 0 & \dots & \frac{h_{N-3}}{3} & \frac{2(h_{N-3}+h_{N-2})}{3} & \frac{h_{N-2}}{3} & 0 \\ 0 & \dots & 0 & \frac{h_{N-2}}{3} & \frac{2(h_{N-2}+h_{N-1})}{3} & \frac{h_{N-1}}{3} \\ 0 & 0 & \dots & 0 & \frac{h_{N-1}}{3} & \frac{2(h_{N-1}+h_N)}{3} \end{bmatrix} \cdot \begin{bmatrix} b_2 \\ b_3 \\ b_4 \\ \vdots \\ b_{N-2} \\ b_{N-1} \\ b_N \end{bmatrix} = \begin{bmatrix} \frac{x_3^G - x_2^G}{h_2} - \frac{x_2^G - x_1^G}{h_1} - \frac{h_1}{3} b_1 \\ \frac{x_4^G - x_3^G}{h_3} - \frac{x_3^G - x_2^G}{h_2} \\ \vdots \\ \frac{x_{N-1}^G - x_{N-2}^G}{h_{N-2}} - \frac{x_{N-2}^G - x_{N-3}^G}{h_{N-3}} \\ \frac{x_N^G - x_{N-1}^G}{h_{N-1}} - \frac{x_{N-1}^G - x_{N-2}^G}{h_{N-2}} \\ \frac{x_{N+1}^G - x_N^G}{h_N} - \frac{x_N^G - x_{N-1}^G}{h_{N-1}} - \frac{h_N}{3} b_1 \end{bmatrix}. \quad (3.1.21)$$

If the coefficient b_1 on the right-hand side were known, we would be able to solve the tridiagonal system (3.1.21) using Thomas' algorithm discussed in Section 3.1.5, and thereby complete the cubic splines parametrization.

The proper value of b_1 ensures that equation (3.1.20) is also satisfied. To compute this value, we note that the values of b_i , $i = 2, \dots, N$, computed by solving system (3.1.21) are *linear* functions of the value b_1 , and so is the left-hand side of (3.1.20). This observation allows us to express (3.1.20) in the linear form

$$F(\alpha) \equiv \alpha b_1 + \beta = 0, \quad (3.1.22)$$

where α and β are two *a priori* unknown constants. The desired root is given by

$$b_1 = -\frac{\beta}{\alpha} = -\frac{F(0)}{F(1) - F(0)}. \quad (3.1.23)$$

The solution algorithm involves five steps:

1. Set $b_1 = 0$ on the right-hand side of (3.1.21), solve the linear system using Thomas' algorithm described in Section 3.1.5, and evaluate the difference between the left- and right-hand sides of (3.1.20); this is the value $F(0)$.
2. Set $b_1 = 1$ on the right-hand side of (3.1.21), solve the linear system using Thomas' algorithm, and evaluate the difference between the left- and right-hand sides of (3.1.20); this is the value $F(1)$.
3. Compute the proper value of b_1 from (3.1.23).
4. Compute the right-hand side of (3.1.21) using the proper value of b_1 , and solve the linear system to obtain the rest of the coefficients b_i .
5. Compute a_i and c_i using equations (3.1.16) and (3.1.17).

A similar calculation can be done for the y coordinates of the nodes, and the two sets of cubic splines coefficients for the x and y coordinates may be used to construct the parametric representation according to (3.1.7). Figure 3.1.3 shows the cubic splines representation of a closed line defined by five points.

Natural cubic splines

When the interpolated line is open, it is reasonable to demand that the curvature vanish at the end-points, and thus obtain a natural cubic spline resembling an elastic plate that is deflected under the action of an edge force.

To compute the natural spline, we apply (3.1.18) for $i = 1, \dots, N - 1$, and set $b_1 = 0$ and $b_{N+1} = 0$ to derive a system of $N - 1$ equations for the $N - 1$ unknowns b_2, \dots, b_N . The system may be solved efficiently using Thomas' algorithm described in Section 3.1.5.

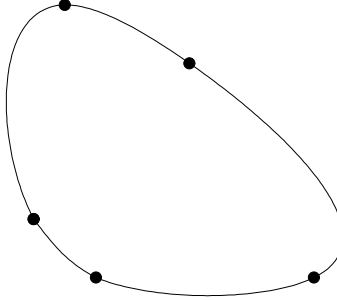


Figure 3.1.3 Cubic splines representation of a closed line defined by five points.

The solid line in Figure 3.1.4 is the natural cubic splines representation of an open line defined by five points.

Clamped-end cubic splines

An alternative to the natural-end conditions are the clamped-end conditions that specify the slope at the first and last node, denoted by α_1 and α_{N+1} . Using the cubic splines parametrization along with (3.1.16) and (3.1.17), we find

$$\begin{aligned} c_1 &= \frac{x_2^G - x_1^G}{h_1} - \frac{1}{3} h_1 (b_2 + 2 b_1) = \alpha_1, \\ 3 a_N h_N^2 + 2 b_N h_N + c_N &= \frac{x_{N+1}^G - x_N^G}{h_N} + \frac{1}{3} h_N (b_N + 2 b_{N+1}) = \alpha_{N+1}. \end{aligned} \tag{3.1.24}$$

Rearranging, we obtain

$$\begin{aligned} b_1 &= -\frac{1}{2} b_2 + \frac{3}{2 h_1} \left(\frac{x_2^G - x_1^G}{h_1} - \alpha_1 \right), \\ b_{N+1} &= -\frac{1}{2} b_N - \frac{3}{2 h_N} \left(\frac{x_{N+1}^G - x_N^G}{h_N} - \alpha_{N+1} \right). \end{aligned} \tag{3.1.25}$$

Applying (3.1.18) for $i = 1, \dots, N-1$, and using (3.1.25) to eliminate b_1 and b_{N+1} , we derive a system of $N-1$ equations for the $N-1$ unknowns b_2, \dots, b_N . The solution can be found efficiently using Thomas' algorithm described in Section 3.1.5.

The dashed line in Figure 3.1.4 is the cubic splines representation of an open line defined by five points, computed with clamped-end conditions of zero slope.

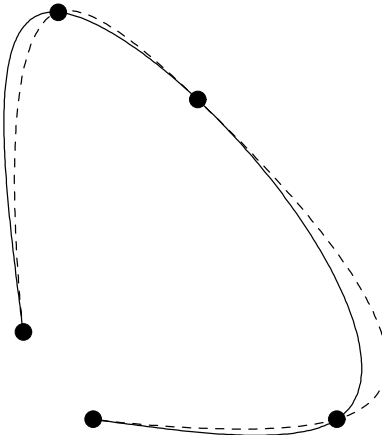


Figure 3.1.4 Cubic splines representation of an open line defined by five points.

The solid line represents the natural splines, and the dashed line represents the splines computed with clamped-end conditions of zero slope.

3.1.4 BEMLIB discretization

Subdirectory `grid_2d` of directory `grids` of `BEMLIB` contains a main program and assisting subroutines that perform the boundary-element discretization of a line consisting of a collection of straight and circular segments into a graded mesh of elements with corresponding shapes, as illustrated in Figure `grid_2d.1` of the `BEMLIB` directory guide (Chapter 9).

Subdirectory `06_interp_diff` of directory `num_meth` of `BEMLIB` contains the main program `splines_cb` and assisting subroutines that perform the boundary-element discretization of a closed or open line into cubic splines.

3.1.5 Thomas' algorithm

The tridiagonal structure of the matrix \mathbf{A} displayed on the right-hand side of equation (3.1.21) allows us to compute the solution with minimal computational effort using Thomas' algorithm.

Consider the $K \times K$ system of linear equations

$$\mathbf{T} \cdot \mathbf{x} = \mathbf{s} \quad (3.1.26)$$

for the unknown vector \mathbf{x} , where \mathbf{T} is the tridiagonal matrix

$$\mathbf{T} = \begin{bmatrix} a_1 & b_1 & 0 & 0 & 0 & \dots & 0 & 0 & 0 \\ c_2 & a_2 & b_2 & 0 & 0 & \dots & 0 & 0 & 0 \\ 0 & c_3 & a_3 & b_3 & 0 & \dots & 0 & 0 & 0 \\ \dots & \dots \\ 0 & 0 & 0 & 0 & 0 & \dots & c_{K-1} & a_{K-1} & b_{K-1} \\ 0 & 0 & 0 & 0 & 0 & \dots & 0 & c_K & a_K \end{bmatrix}, \quad (3.1.27)$$

and \mathbf{s} is a known right-hand side. Thomas' algorithm proceeds in two stages, as follows.

At the first stage, the tridiagonal system (3.1.26) is transformed to the bidiagonal system $\mathbf{T}' \cdot \mathbf{x} = \mathbf{y}$ involving the bidiagonal coefficient matrix

$$\mathbf{T}' = \begin{bmatrix} 1 & d_1 & 0 & 0 & 0 & \dots & 0 & 0 & 0 \\ 0 & 1 & d_2 & 0 & 0 & \dots & 0 & 0 & 0 \\ 0 & 0 & 1 & d_3 & 0 & \dots & 0 & 0 & 0 \\ \dots & \dots \\ 0 & 0 & 0 & 0 & 0 & \dots & 0 & 1 & d_{K-1} \\ 0 & 0 & 0 & 0 & 0 & \dots & 0 & 0 & 1 \end{bmatrix}. \quad (3.1.28)$$

At the second stage, the bidiagonal system is solved by backward substitution, that is, by solving the last equation for the last unknown x_K , and then moving upward to compute the rest of the unknowns in a sequential fashion. The combined algorithm is as follows:

Reduction to bidiagonal

$$\begin{bmatrix} d_1 \\ y_1 \end{bmatrix} = \frac{1}{a_1} \begin{bmatrix} b_1 \\ s_1 \end{bmatrix}$$

Do $i = 1, K - 1$

$$\begin{bmatrix} d_{i+1} \\ y_{i+1} \end{bmatrix} = \frac{1}{a_{i+1} - c_{i+1}d_i} \begin{bmatrix} b_{i+1} \\ s_{i+1} - c_{i+1}y_i \end{bmatrix}$$

End Do

(3.1.29)

Backward substitution

$$x_K = y_K$$

Do $i = K - 1, 1$ (step = -1)

$$x_i = y_i - d_i x_{i+1}$$

End Do

Thomas' algorithm is a special implementation of the inclusive method of Gauss elimination discussed in Appendix A, which is applicable to systems with coefficient matrices of arbitrary structure. Computational savings arise by recognizing and bypassing idle operations such as the addition of zero and the multiplication by unity.

Problems

P.3.1.1 Boundary-element discretization

- (a) Use program `grid_2d` in directory `grids` of `BEMLIB` to discretize a closed contour of your choice, and display your results.
- (b) Use program `splines_cb` in subdirectory `06_interp_diff` of directory `num_meth` of `BEMLIB` to discretize a closed contour of your choice, and display your results.

P.3.1.2 Thomas' algorithm

Subdirectory `03_lin_eq` of directory `num_meth` of `BEMLIB` includes subroutine `thomas` that solves a tridiagonal system of equations by Thomas' algorithm discussed in the text. Use the program to solve a system of your choice, and verify *a posteriori* that the solution satisfies all equations.

3.2 Discretization of the integral representation

Consider the boundary-integral representations (2.3.3) and (2.4.2) applicable, respectively, for a point \mathbf{x}_0 located inside or at the boundary of a selected control area, repeated here for convenience:

$$\begin{aligned} f(\mathbf{x}_0) = & - \int_C G(\mathbf{x}, \mathbf{x}_0) [\mathbf{n}(\mathbf{x}) \cdot \nabla f(\mathbf{x})] dl(\mathbf{x}) \\ & + \int_C f(\mathbf{x}) [\mathbf{n}(\mathbf{x}) \cdot \nabla G(\mathbf{x}, \mathbf{x}_0)] dl(\mathbf{x}), \end{aligned} \quad (3.2.1)$$

and

$$\begin{aligned} f(\mathbf{x}_0) = & -2 \int_C G(\mathbf{x}, \mathbf{x}_0) [\mathbf{n}(\mathbf{x}) \cdot \nabla f(\mathbf{x})] dl(\mathbf{x}) \\ & + 2 \int_C^{PV} f(\mathbf{x}) [\mathbf{n}(\mathbf{x}) \cdot \nabla G(\mathbf{x}, \mathbf{x}_0)] dl(\mathbf{x}). \end{aligned} \quad (3.2.2)$$

The unit normal vector \mathbf{n} points into the control area enclosed by the contour C .

Approximating the integrals over C with sums of integrals over the boundary elements E_i , $i = 1, \dots, N$, we obtain the discrete representation

$$\begin{aligned} f(\mathbf{x}_0) = & -\sum_{i=1}^N \int_{E_i} G(\mathbf{x}, \mathbf{x}_0) [\mathbf{n}(\mathbf{x}) \cdot \nabla f(\mathbf{x})] dl(\mathbf{x}) \\ & + \sum_{i=1}^N \int_{E_i} f(\mathbf{x}) [\mathbf{n}(\mathbf{x}) \cdot \nabla G(\mathbf{x}, \mathbf{x}_0)] dl(\mathbf{x}), \end{aligned} \quad (3.2.3)$$

and the discretized integral equation

$$\begin{aligned} f(\mathbf{x}_0) = & -2 \sum_{i=1}^N \int_{E_i} G(\mathbf{x}, \mathbf{x}_0) [\mathbf{n}(\mathbf{x}) \cdot \nabla f(\mathbf{x})] dl(\mathbf{x}) \\ & + 2 \sum_{i=1}^N \int_{E_i}^{PV} f(\mathbf{x}) [\mathbf{n}(\mathbf{x}) \cdot \nabla G(\mathbf{x}, \mathbf{x}_0)] dl(\mathbf{x}). \end{aligned} \quad (3.2.4)$$

Equation (3.2.4) applies at a point \mathbf{x}_0 that lies over one of the boundary elements E_i .

In addition to the geometrical boundary-element approximation, we now introduce approximations for the boundary distribution of the function $f(\mathbf{x})$ and its normal derivative $\mathbf{n}(\mathbf{x}) \cdot \nabla f(\mathbf{x})$.

3.2.1 Uniform elements

In the simplest approximation, we replace the boundary distribution of $f(\mathbf{x})$ and its normal derivative $\mathbf{n}(\mathbf{x}) \cdot \nabla f(\mathbf{x})$ with constant functions over the individual boundary elements, denoted respectively by f_i and $(\partial f / \partial n)_i$, where $i = 1, \dots, N$.

Extracting these constant values from the single- and double-layer potential on the right-hand sides of (3.2.3) and (3.2.4), we find

$$f(\mathbf{x}_0) = -\sum_{i=1}^N \alpha_i(\mathbf{x}_0) (\frac{\partial f}{\partial n})_i + \sum_{i=1}^N \beta_i(\mathbf{x}_0) f_i, \quad (3.2.5)$$

and

$$f(\mathbf{x}_0) = -2 \sum_{i=1}^N \alpha_i(\mathbf{x}_0) (\frac{\partial f}{\partial n})_i + 2 \sum_{i=1}^N \beta_i^{PV}(\mathbf{x}_0) f_i. \quad (3.2.6)$$

We have introduced the *influence coefficients*

$$\alpha_i(\mathbf{x}_0) \equiv \int_{E_i} G(\mathbf{x}, \mathbf{x}_0) dl(\mathbf{x}), \quad (3.2.7)$$

and

$$\beta_i(\mathbf{x}_0) \equiv \int_{E_i} \mathbf{n}(\mathbf{x}) \cdot \nabla G(\mathbf{x}, \mathbf{x}_0) dl(\mathbf{x}), \quad (3.2.8)$$

representing uniform distributions of point sources and point-source dipoles oriented normal to the boundary elements. This interpretation explains the somewhat unfortunate nomenclature “uniform elements” or “constant elements” favored in the boundary-element literature.

The notation $\beta_i^{PV}(\mathbf{x}_0)$ on the right-hand side of (3.2.6) signifies that, when the point \mathbf{x}_0 lies on the i th boundary element, the principal value of the integral on the right-hand side of (3.2.8) is implied.

If the element values f_i and $(\partial f / \partial n)_i$ were available, we would be able to compute the field value $f(\mathbf{x}_0)$ in terms of the influence coefficients using the discrete representation (3.2.5). Moreover, we would be able to reproduce the boundary values using the companion discrete representation (3.2.6).

To compute the influence coefficients accurately, it is necessary to classify the elements into two categories according to whether or not singularities in the integrands arise. In the remainder of this section, we discuss the computation of the influence coefficients in each category. In Section 3.3, we discuss methods of computing the element values f_i and $(\partial f / \partial n)_i$ by solving systems of linear algebraic equations.

3.2.2 Non-singular elements

Assume first that the evaluation point \mathbf{x}_0 lies off the i th element. In that case, the integrands of the constant-element influence coefficients shown in (3.2.7) and (3.2.8) are non-singular, and the integrals may be computed accurately using standard analytical or numerical methods.

Straight elements

Consider the evaluation of the influence coefficients over the i th straight element described in parametric form by the equations in (3.1.2), as illustrated in Figure 3.2.1(a). A straightforward computation shows that the differential arc length is given by

$$dl \equiv \sqrt{dx^2 + dy^2} = h_\xi d\xi, \quad (3.2.9)$$

where $-1 \leq \xi \leq 1$, and

$$h_\xi \equiv \frac{1}{2} \sqrt{(x_{i,2}^E - x_{i,1}^E)^2 + (y_{i,2}^E - y_{i,1}^E)^2} \quad (3.2.10)$$

is the metric coefficient associated with the parameter ξ . The unit normal vector is constant, denoted by $\mathbf{n}^{(i)}$.

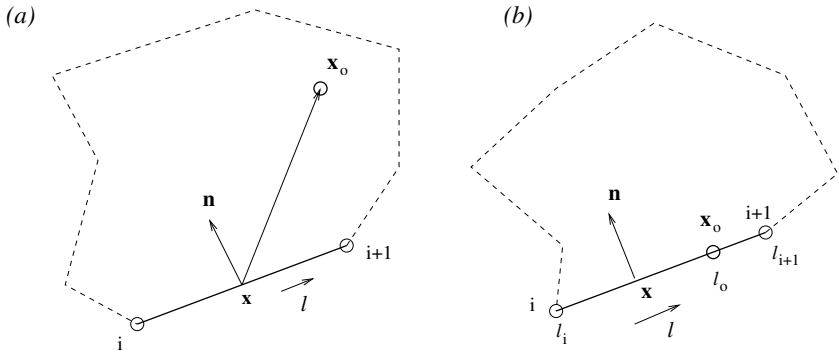


Figure 3.2.1 Evaluation of the influence coefficients over (a) a non-singular, and (b) a singular straight element. The unit normal vector points into the solution domain.

Accordingly, the influence coefficients are given by

$$\alpha_i(\mathbf{x}_0) = h_\xi \int_{-1}^1 G[x(\xi), y(\xi), x_0, y_0] d\xi, \quad (3.2.11)$$

and

$$\begin{aligned} \beta_i(\mathbf{x}_0) = h_\xi & \left\{ n_x^{(i)} \int_{-1}^1 \frac{\partial G}{\partial x}[x(\xi), y(\xi), x_0, y_0] d\xi \right. \\ & \left. + n_y^{(i)} \int_{-1}^1 \frac{\partial G}{\partial y}[x(\xi), y(\xi), x_0, y_0] d\xi \right\}. \end{aligned} \quad (3.2.12)$$

Gauss-Legendre quadrature

The integrals on the right-hand sides of (3.2.11) and (3.2.12) may be computed accurately by the *Gauss-Legendre quadrature*. In this method, the integral of a non-singular function $f(\xi)$ over the interval $[-1, 1]$ is approximated with a weighted sum of the values of the integrand at selected locations, in the form

$$\int_{-1}^1 f(\xi) d\xi \simeq \sum_{k=1}^{N_Q} f(\xi_k) w_k, \quad (3.2.13)$$

where:

- N_Q is a specified number of *quadrature base points*.
- The k th base point ξ_k is the k th root of the N_Q -degree Legendre polynomial $L_{N_Q}(\xi)$, taking values in the interval $(-1, 1)$.

- w_k is the integration weight corresponding to the k th base point. The sum of the integration weights is equal to 2 for any value of N_Q , so that, when f is a constant function, quadrature (3.2.13) produces the exact answer.

For example, when $N_Q = 1$, $\xi_1 = 0$ is the root of the first-degree Legendre polynomial, $L_1(\xi) = \xi$. The corresponding integration weight is $w_1 = 2$.

Applying the Gauss-Legendre quadrature to compute the single-layer influence coefficient defined in (3.2.11), we obtain the approximation

$$\alpha_i(\mathbf{x}_0) \simeq h_\xi \sum_{k=1}^{N_Q} G[x(\xi_k), y(\xi_k), x_0, y_0] w_k, \quad (3.2.14)$$

Mathematical handbooks and decent texts on numerical methods provide us with tables of the pairs (ξ_k, w_k) parametrized by the number of quadrature points N_Q (e.g., [60]). Subroutine `gauss_leg` in subdirectory `07_integration` of directory `mum_meth` of *BEMLIB* contains tabulated pairs for $N_Q = 1, 2, 3, 4, 5, 6, 8, 12$, and 20. Program `integral` in the same subdirectory evaluates an integral by several methods including the Gauss-Legendre quadrature.

Circular arcs

Consider next the evaluation of the influence coefficients over the i th circular arc described in parametric form in terms of the polar angle θ by the equations in (3.1.4), as illustrated in Figure 3.2.2(a). The differential arc length is given by

$$dl = \pm R_i d\theta, \quad (3.2.15)$$

where the plus sign applies when the arc turns in the counterclockwise direction, as shown in Figure 3.2.2(a), and the minus sign otherwise. Correspondingly, the unit normal vector is given by

$$\pm n_x = -\cos \theta, \quad \pm n_y = -\sin \theta. \quad (3.2.16)$$

When the arc turns in the counterclockwise direction, the normal vector points toward the arc center.

Substituting (3.1.4), (3.2.15), and (3.2.16) into the right-hand sides of (3.2.7) and (3.2.8), we obtain

$$\alpha_i(\mathbf{x}_0) = \pm R_i \int_{\theta_{1,i}}^{\theta_{2,i}} G[x(\theta), y(\theta), x_0, y_0] d\theta, \quad (3.2.17)$$

and

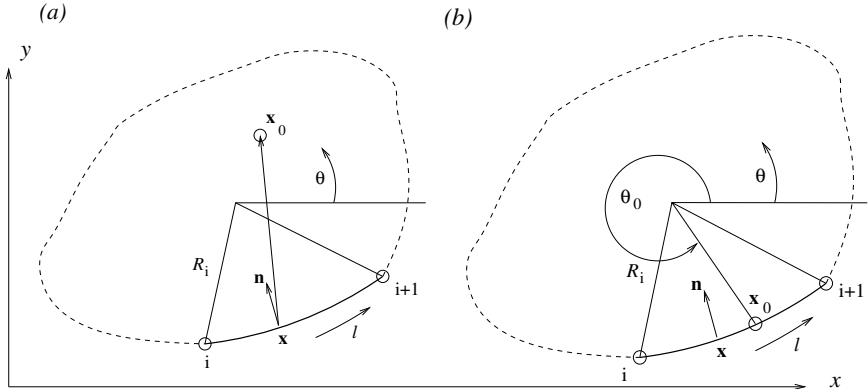


Figure 3.2.2 Evaluation of the influence coefficients over (a) a non-singular, and (b) a singular arc.

$$\begin{aligned} \beta_i(\mathbf{x}_0) = -R_i \int_{\theta_{1,i}}^{\theta_{2,i}} & \left\{ \frac{\partial G}{\partial x}[x(\theta), y(\theta), x_0, y_0] \cos \theta \right. \\ & \left. + \frac{\partial G}{\partial y}[x(\theta), y(\theta), x_0, y_0] \sin \theta \right\} d\theta, \end{aligned} \quad (3.2.18)$$

where $\theta_{i,1}$ and $\theta_{i,2}$ are the angles corresponding to the first and second end-point.

Next, we express θ in terms of ξ using the parametrization (3.1.6), and then evaluate the integrals by the Gauss-Legendre quadrature.

For example, to compute the single-layer influence coefficient, we write

$$\begin{aligned} \alpha_i(\mathbf{x}_0) &= \pm R_i \frac{\theta_{2,i} - \theta_{1,i}}{2} \int_{-1}^1 G[x(\xi), y(\xi), x_0, y_0] d\xi \\ &\simeq R_i \frac{|\theta_{2,i} - \theta_{1,i}|}{2} \sum_{k=1}^{N_Q} G[x(\xi_k), y(\xi_k), x_0, y_0] w_k. \end{aligned} \quad (3.2.19)$$

Cubic splines

The single- and double-layer influence coefficients over cubic-splines elements are computed in a similar fashion. Using the parametric forms displayed in (3.1.7), we find that the differential arc length over the i th boundary element is given by

$$dl \equiv \sqrt{dx^2 + dy^2} = h_i(s) ds, \quad (3.2.20)$$

where $s_i \leq s \leq s_{i+1}$, and

$$\begin{aligned} h_i(s) &\equiv ([3 a_i(s - s_i)^2 + 2 b_i(s - s_i) + c_i]^2 \\ &+ [3 a'_i(s - s_i)^2 + 2 b'_i(s - s_i) + c'_i]^2)^{1/2} \end{aligned} \quad (3.2.21)$$

is a position-dependent metric coefficient for the arc length. When the parameter s increases in the counterclockwise direction around the boundary, the Cartesian components of the unit normal vector are given by

$$\begin{aligned} n_x(s) &= -\frac{dy}{dl} = -\frac{1}{h_i(s)} [3 a'_i(s - s_i)^2 + 2 b'_i(s - s_i) + c'_i], \\ n_y(s) &= \frac{dx}{dl} = \frac{1}{h_i(s)} [3 a_i(s - s_i)^2 + 2 b_i(s - s_i) + c_i]. \end{aligned} \quad (3.2.22)$$

Substituting (3.1.7), (3.2.20), and (3.2.22) into the right-hand sides of (3.2.7) and (3.2.8), we derive expressions for the influence coefficients in terms of integrals with respect to the parameter s . Finally, we introduce the familiar parametrization

$$s = \frac{1}{2} (s_i + s_{i+1}) + \frac{1}{2} (s_{i+1} - s_i) \xi, \quad (3.2.23)$$

where $-1 \leq \xi \leq 1$, and compute the integrals by the Gauss-Legendre quadrature.

3.2.3 Singular elements

Consider now the computation of the influence coefficients when the evaluation point \mathbf{x}_0 lies on the i th boundary element. In this case, as the integration point \mathbf{x} approaches the evaluation point \mathbf{x}_0 , the integrands of the influence coefficients (3.2.7) and (3.2.8) exhibit, respectively, a logarithmic and an apparent higher-order singularity, and the boundary elements are classified as singular.

To simplify the treatment the singularities, we subtract the free-space kernels at the outset by recasting expressions (3.2.7) and (3.2.8) into the forms

$$\alpha_i(\mathbf{x}_0) \equiv \int_{E_i} \left(G(\mathbf{x}, \mathbf{x}_0) + \frac{1}{2\pi} \ln |\mathbf{x} - \mathbf{x}_0| \right) dl(\mathbf{x}) + \alpha_i^{FS}(\mathbf{x}_0), \quad (3.2.24)$$

and

$$\begin{aligned} \beta_i^{PV}(\mathbf{x}_0) &\equiv \int_{E_i} \mathbf{n}(\mathbf{x}) \cdot \left(\nabla G(\mathbf{x}, \mathbf{x}_0) + \frac{1}{2\pi} \frac{\mathbf{n}(\mathbf{x}) \cdot (\mathbf{x} - \mathbf{x}_0)}{|\mathbf{x} - \mathbf{x}_0|^2} \right) dl(\mathbf{x}) \\ &+ \beta_i^{PV-FS}(\mathbf{x}_0), \end{aligned} \quad (3.2.25)$$

where

$$\alpha_i^{FS}(\mathbf{x}_0) \equiv -\frac{1}{2\pi} \int_{E_i} \ln |\mathbf{x} - \mathbf{x}_0| dl(\mathbf{x}), \quad (3.2.26)$$

and

$$\beta_i^{PV-FS}(\mathbf{x}_0) \equiv -\frac{1}{2\pi} \int_{E_i}^{PV} \frac{\mathbf{n}(\mathbf{x}) \cdot (\mathbf{x} - \mathbf{x}_0)}{|\mathbf{x} - \mathbf{x}_0|^2} dl(\mathbf{x}). \quad (3.2.27)$$

The superscript FS denotes the free-space forms, and PV denotes the principal value of the double-layer integral. The first integrals on the right-hand sides of (3.2.24) and (3.2.25) are non-singular and may be computed with high accuracy using the Gauss-Legendre quadrature. The problem has been reduced to evaluating the seemingly improper free-space forms (3.2.26) and (3.2.27).

Consider the integrand of the double-layer potential on the right-hand side of (3.2.27). As the integration point \mathbf{x} approaches the evaluation point \mathbf{x}_0 , the normal vector \mathbf{n} tends to become orthogonal to the nearly tangential vectorial distance $(\mathbf{x} - \mathbf{x}_0)$. Consequently, the numerator of the fraction of the integrand behaves quadratically with respect to the scalar distance $|\mathbf{x} - \mathbf{x}_0|$, and a singularity does not appear.

The absence of a singularity explains why the computation of the principal value is so much more convenient than the computation of the limit of the double-layer potential as the evaluation point approaches the boundary.

Straight elements

Consider the evaluation of the influence coefficients over the i th straight element described in parametric form by the equations in (3.1.2), where the evaluation point \mathbf{x}_0 lies on the segment at arc length position l_0 , as illustrated in Figure 3.2.1(b).

Writing $|\mathbf{x} - \mathbf{x}_0| = |l - l_0|$ and carrying out the integration for the single-layer potential, we obtain

$$\begin{aligned} \alpha_i(\mathbf{x}_0) &= -\frac{1}{2\pi} \int_{l_i}^{l_{i+1}} \ln |l - l_0| dl \\ &= -\frac{1}{2\pi} [|l_{i+1} - l_0| (\ln |l_{i+1} - l_0| - 1) + |l_i - l_0| (\ln |l_i - l_0| - 1)]. \end{aligned} \quad (3.2.28)$$

Because the normal vector \mathbf{n} is orthogonal to the tangential vector $(\mathbf{x} - \mathbf{x}_0)$, the numerator of the fraction inside the integral of the double-layer influence coefficient vanishes, and the influence coefficient of the double-layer potential is identically equal to zero, $\beta_i^{PV-FS}(\mathbf{x}_0) = 0$.

Circular arcs

Consider next the evaluation of the influence coefficients over the i th circular arc described in parametric form in terms of the polar angle θ by the equations in (3.1.4). The evaluation point \mathbf{x}_0 lies on the arc at a location corresponding to the polar angle θ_0 , which is intermediate between the end-values θ_i and θ_{i+1} , as illustrated in Figure 3.2.2(b).

Using expressions (3.2.14) and (3.2.15) and observing that

$$|\mathbf{x} - \mathbf{x}_0| = 2 R_i \sin \frac{|\theta - \theta_0|}{2}, \quad (3.2.29)$$

we find

$$\begin{aligned} \alpha_i(\mathbf{x}_0) &\equiv - \left[\pm \frac{R_i}{2\pi} \int_{\theta_i}^{\theta_{i+1}} \ln[2 R_i \sin \frac{|\theta - \theta_0|}{2}] d\theta \right] \\ &= - \left[\pm \frac{R_i}{2\pi} \int_{\theta_i}^{\theta_{i+1}} \ln \frac{2 \sin \frac{|\theta - \theta_0|}{2}}{|\theta - \theta_0|} d\theta \pm \frac{1}{2\pi} \int_{\theta_i}^{\theta_{i+1}} \ln(R_i |\theta - \theta_0|) d(R_i \theta) \right], \end{aligned} \quad (3.2.30)$$

and

$$\begin{aligned} \beta_i^{PV-FS}(\mathbf{x}_0) &\equiv \frac{1}{8\pi} \int_{\theta_i}^{\theta_{i+1}} \frac{\cos \theta (\cos \theta - \cos \theta_0) + \sin \theta (\sin \theta - \sin \theta_0)}{\sin^2 \frac{|\theta - \theta_0|}{2}} d\theta \\ &= \frac{1}{8\pi} \int_{\theta_i}^{\theta_{i+1}} \frac{1 - \cos(\theta - \theta_0)}{\sin^2 \frac{|\theta - \theta_0|}{2}} d\theta = \frac{1}{4\pi} (\theta_{i+1} - \theta_i). \end{aligned} \quad (3.2.31)$$

The first integral in the second line of (3.2.30) is non-singular, and may be computed with high accuracy using the Gauss-Legendre quadrature. The second integral in the second line of (3.2.30) may be computed by elementary methods, as shown in (3.2.28).

Cubic-splines elements

Because the integrand of the principal-value, double-layer integral is non-singular, the corresponding influence coefficient may be computed using a standard numerical method based, for example, on the Gauss-Legendre quadrature.

To compute the influence coefficient associated with the single-layer potential, we use the parametric forms shown in (3.1.7) and expression (3.2.20) for the differential arc length. Assuming that the position of the evaluation point corresponds to the parameter value s_0 , which is intermediate between the end-point values s_i and s_{i+1} ,

of the i th boundary element,

$$\begin{aligned} \alpha_i(\mathbf{x}_0) &\equiv -\frac{1}{2\pi} \int_{E_i} \ln |\mathbf{x}(s) - \mathbf{x}(s_0)| dl(s) \\ &= -\frac{1}{2\pi} \left[\int_{s_i}^{s_{i+1}} \ln \frac{|\mathbf{x}(s) - \mathbf{x}(s_0)|}{|s - s_0|} h_i(s) ds + \int_{s_i}^{s_{i+1}} \ln |s - s_0| h_i(s) ds \right], \end{aligned} \quad (3.2.32)$$

where $h_i(s)$ is the metric coefficient defined in (3.2.21).

The integrand of the first integral in the last expression of (3.2.32) is non-singular, and the corresponding integral may be computed accurately by the Gauss-Legendre quadrature. The integrand of the second integral exhibits a logarithmic singularity that may be integrated by two methods.

In the first method, the singular behavior is removed by writing

$$\begin{aligned} &\int_{s_i}^{s_{i+1}} \ln |s - s_0| h_i(s) ds \\ &= \int_{s_i}^{s_{i+1}} \ln |s - s_0| [h_i(s) - h_i(s_0)] ds + h_i(s_0) \int_{s_i}^{s_{i+1}} \ln |s - s_0| ds. \end{aligned} \quad (3.2.33)$$

The first integral on the right-hand side may be computed by a standard numerical method, such as the Gauss-Legendre quadrature. The second integral may be computed by elementary analytical methods.

In a preferred method, the improper integral is broken up into two parts,

$$\begin{aligned} &\int_{s_i}^{s_{i+1}} \ln |s - s_0| h_i(s) ds \\ &= \int_{s_i}^{s_0} \ln |s - s_0| h_i(s) ds + \int_{s_0}^{s_{i+1}} \ln |s - s_0| h_i(s) ds \\ &= \int_0^{s_0 - s_i} \ln(\eta) h_i(s_0 - \eta) d\eta + \int_0^{s_{i+1} - s_0} \ln(\eta) h_i(s_0 + \eta) d\eta, \end{aligned} \quad (3.2.34)$$

where η is an auxiliary integration variable.

Concentrating on the first integral in the last expression of (3.2.34), we write

$$\begin{aligned} &-\int_0^{s_0 - s_i} \ln(\eta) h_i(s_0 - \eta) d\eta = -\Delta s_1 \int_0^1 \ln(\xi \Delta s_1) h_i(s_0 - \xi \Delta s_1) d\xi \\ &= -\Delta s_1 \int_0^1 \ln(\xi) h_i(s_0 - \xi \Delta s_1) d\xi - \Delta s_1 \ln(\Delta s_1) \int_0^1 h_i(s_0 - \xi \Delta s_1) d\xi, \end{aligned} \quad (3.2.35)$$

where $\Delta s_1 \equiv s_0 - s_i$, and ξ is a new auxiliary variable. The second integral in the last expression may be computed by the Gauss-Legendre quadrature. The first integral may be computed using a quadrature that is specifically designed for integrands with a logarithmic singularity.

Quadrature for logarithmic singularities

The integration quadrature for an integral with a logarithmic singularity takes the standard form

$$-\int_0^1 \ln(\xi) v(\xi) d\xi \simeq \sum_{k=1}^{N_Q} v(\xi_k) w_k, \quad (3.2.36)$$

where:

- The function $v(\xi)$ is non-singular over the integration domain $[0, 1]$.
- N_Q is a specified number of integration base points.
- ξ_k is the location of the k th base point ranging in the interval $(0, 1)$.
- w_k is the corresponding weight. The sum of the integration weights is equal to 1 for any value of N_Q , so that, when v is a constant function, quadrature (3.2.36) produces the exact answer.

Applying the quadrature to the last integral in (3.2.35), we obtain

$$-\int_0^1 \ln(\xi) h_i(s_0 - \xi \Delta s_1) d\xi \simeq \sum_{k=1}^{N_Q} h_i(s_0 - \xi_k \Delta s_1) w_k, \quad (3.2.37)$$

Mathematical handbooks and decent texts on numerical methods provide us with tables of the pairs (ξ_k, w_k) parametrized by the number of base points N_Q (e.g., [60]). Subroutine `gauss_log` in subdirectory `07_integration` of directory `num_meth` of *BEMLIB* contains tabulated pairs for $N_Q = 2, 3, 4$, and 5 . Program `integral.log` in the same directory uses the quadrature to evaluate integrals whose integrand exhibits a logarithmic singularity.

It may appear that the first method of subtracting the singularity culminating in equation (3.2.33) is comparable to the second method based on the Gaussian quadrature, but this impression is false. Performing a Taylor series expansion of the function $h_i(s)$ around the singular point s_0 , we find that, in general, the first integral in the second line of (3.2.33) behaves like $(s - s_0) \ln |s - s_0|$. As s tends to s_0 , the integrand tends to zero and a singularity does not appear. However, the derivatives of the integrand tend to become infinite in this limit, and this makes the method less accurate than its competitor.

Problems

P.3.2.1 Gauss-Legendre quadrature

Use the Gauss-Legendre quadrature with $N_Q = 1, 2, 3$, and 4 base points to integrate a sixth-degree polynomial of your choice over the interval $(-1, 1)$, and discuss the accuracy of your results.

P.3.2.2 Integrand with a log singularity

The integrand of the integral

$$\int_0^1 e^{-x^2} \ln|x - 0.5| dx \quad (1)$$

exhibits a logarithmic singularity at $x = 0.5$. Compute the integral by (a) subtracting the singularity as discussed in the text, and (b) using the Gaussian quadrature for logarithmic kernels with $N_Q = 2, 3, 4$, and 5 base points, and then compare the results of the two methods.

3.3 The boundary-element collocation method

The boundary-element discretization has provided us with the discretized integral equation (3.2.4), repeated here for convenience:

$$f(\mathbf{x}_0) = -2 \sum_{i=1}^N \alpha_i(\mathbf{x}_0) \left(\frac{\partial f}{\partial n} \right)_i + 2 \sum_{i=1}^N \beta_i^{PV}(\mathbf{x}_0) f_i. \quad (3.3.1)$$

In practice, Dirichlet boundary conditions provide us with a set of element values f_i , and Neumann boundary conditions provide us with another set of element values $(\partial f / \partial n)_i$, a total of N values. To compute the N element values that are not specified, we apply the method of point collocation.

The objective is to generate a number of equations equal to the number of unknowns N . With this goal in mind, we identify the arbitrary point \mathbf{x}_0 with the mid-point of each boundary element denoted by \mathbf{x}_j^M , where $j = 1, \dots, N$, and thereby obtain the algebraic equations

$$f(\mathbf{x}_j^M) \equiv f_j = -2 \sum_{i=1}^N \alpha_i(\mathbf{x}_j^M) \left(\frac{\partial f}{\partial n} \right)_i + 2 \sum_{i=1}^N \beta_i^{PV}(\mathbf{x}_j^M) f_i. \quad (3.3.2)$$

To simplify the notation, we introduce the single- and double-layer influence coefficients

$$A_{ji} \equiv \alpha_i(\mathbf{x}_j^M), \quad B_{ji} \equiv \beta_i^{PV}(\mathbf{x}_j^M), \quad (3.3.3)$$

and recast (3.3.2) into the form

$$\frac{1}{2} f_j = -A_{ji} f'_i + B_{ji} f_i, \quad (3.3.4)$$

where we have defined $f'_i \equiv (\frac{\partial f}{\partial n})_i$. Summation over the repeated index i is implied on the right-hand side of (3.3.4). Moving the element values f_j from the left- to the right-hand side, rearranging, and writing $f_j = \delta_{ij} f_i$, where δ_{ij} is Kronecker's delta, we obtain

$$A_{ji} f'_i = (B_{ji} - \frac{1}{2} \delta_{ji}) f_i. \quad (3.3.5)$$

The corresponding vector form is

$$\mathbf{A} \cdot \mathbf{f}' = (\mathbf{B} - \frac{1}{2} \mathbf{I}) \cdot \mathbf{f}, \quad (3.3.6)$$

where \mathbf{I} is the identity matrix. Three cases may now be recognized:

- If all element values f_i are specified, equation (3.3.6) provides us with a system of linear equations for the unknown vector of normal derivatives \mathbf{f}' .
- If all element values f'_i are specified, equation (3.3.6) provides us with a system of linear equations for the unknown vector \mathbf{f} .
- If some element values f_i and a complementary set of values f'_i are specified, equation (3.3.6) provides us with a system of linear equations for the unknowns.

Setting up the linear algebraic system (3.3.6) is the main task of the boundary-element implementation. Once this has been accomplished, the solution can be found using a linear solver based, for example, on the method of Gauss elimination or one of its alternatives discussed in Appendix A.

An important feature of the linear system arising from the boundary-element collocation method is that the coefficient matrices \mathbf{A} and \mathbf{B} are dense, that is, they are fully populated with non-zero elements. In contrast, linear systems arising from finite-difference, finite-element, and spectral-element methods are banded, that is, they contain diagonal arrays or blocks of non-zero elements, while all other elements are zero (e.g., [60]).

3.3.1 *BEMLIB* directory `laplace`

BEMLIB directory `laplace` contains codes that solve Laplace's equation in two dimensions using the constant-element collocation method discussed in this section, including the following:

- `flow_1d`
Unidirectional viscous flow through a tube with arbitrary cross-section.
- `flow_1d_1p`
Unidirectional shear flow past (a) a periodic array of cylinders with arbitrary cross-section, and (b) a periodic wall with arbitrary profile.
- `flow_2d`
Two-dimensional potential flow in an arbitrary domain.
- `body_2d`
Potential flow past, or due to the motion of, a two-dimensional body.
- `tank_2d`
Dynamical simulation of liquid sloshing in a rectangular tank.

The problem formulation and particulars of the numerical method are discussed in the corresponding sections of the *BEMLIB* user guide (Chapter 10).

Problems

P.3.3.1 Gauss elimination

Subdirectory `03_lin_eq` of directory `num_meth` of *FDLIB* includes the program `gel` that solves a system of linear equations by the method of Gauss elimination with row pivoting (Appendix A). Use the program to solve a system of your choice, and verify that the solution satisfies the equations.

P.3.3.2 *BEMLIB* codes for Laplace's equation in two dimensions

(a) Code `flow_2d` in directory `laplace` of *BEMLIB* computes two-dimensional potential flow in an arbitrary domain. Study the mathematical formulation and numerical method discussed in the corresponding section of the *BEMLIB* user guide (Chapter 10), run the code for a configuration of your choice, prepare graphs of the streamline pattern, and discuss the results of your computation.

(b) Repeat (a) for code `flow_2d_1p`. (c) Repeat (a) for code `body_2d`. (d) Repeat (a) for code `tank_2d`.

P.3.3.3 BEMLIB code for Helmholtz's equation in two dimensions

Directory `helmholtz` of *BEMLIB* contains the code `flow_2d_osc` that solves the equations of oscillatory unidirectional viscous flow inside or outside a cylindrical tube with arbitrary cross-section using the boundary-element collocation method.

Study the mathematical formulation and the numerical method discussed in the corresponding section of the *BEMLIB* user guide (Chapter 11), run the code for a tube geometry of your choice and for several oscillation frequencies, prepare graphs, and discuss the results of your computation.

3.4 Isoparametric cubic-splines discretization

The uniform-element discretization described in Sections 3.2 and 3.3 represents the simplest implementation of the boundary-element method. If a continuous boundary distribution for the function f or its normal derivative is desired, then a higher-order discretization must be applied.

In the *isoparametric* cubic-splines representation, the boundary elements are described by cubic splines interpolation, as shown in the equations displayed in (3.1.7), and the boundary distribution of f and its normal derivative over the i th element are approximated with the corresponding forms

$$f(s) \simeq R_i(s) \equiv p_i (s - s_i)^3 + q_i (s - s_i)^2 + r_i (s - s_i) + f_i, \quad (3.4.1)$$

and

$$\frac{\partial f}{\partial n}(s) \simeq R'_i(s) \equiv p'_i (s - s_i)^3 + q'_i (s - s_i)^2 + r'_i (s - s_i) + \left(\frac{\partial f}{\partial n}\right)_i, \quad (3.4.2)$$

where $s_i \leq s \leq s_{i+1}$. The $3N$ coefficients p_i , q_i , and r_i , where $i = 1, \dots, N$, and the corresponding $3N$ coefficient p'_i , q'_i , and r'_i , either are specified or must be computed using the boundary-integral equation.

3.4.1 Cardinal cubic-splines functions

Reviewing the steps involved in the computation of the cubic splines discussed in Section 3.1, we observe that the coefficients p_i , q_i , and r_i , where $i = 1, \dots, N$, are linear functions of the nodal values f_j , where $j = 1, \dots, N + 1$. Accordingly, we introduce the expressions

$$p_i = P_{ij} f_j, \quad q_i = Q_{ij} f_j, \quad r_i = R_{ij} f_j, \quad (3.4.3)$$

where summation over the repeated index j is implied in the $N + 1$ nodes defining the boundary elements. The constant matrices P_{ij} , Q_{ij} , and R_{ij} depend exclusively on the arc-length parametrization and on the element node distribution.

Substituting (3.4.3) into (3.4.1), we find

$$f(s) \simeq R_i(s) = [P_{ij} (s - s_i)^3 + Q_{ij} (s - s_i)^2 + R_{ij} (s - s_i) + \delta_{ij}] f_j, \quad (3.4.4)$$

where $s_i \leq s \leq s_{i+1}$. This expression illustrates that *all* nodal values contribute to the cubic polynomial expansion over the i th boundary element.

The union of the individual cubics, $R_i(s)$, provides us with the global approximation

$$f(s) \simeq R(s) = \sum_{j=1}^{N+1} Z_j(s) f_j, \quad (3.4.5)$$

where $Z_j(s)$ are *cardinal* cubic-splines interpolation functions with the following properties:

- $Z_j(s_j) = 1$, and $Z_j(s_k) = 0$ for $k \neq j$.
- $Z_j(s)$ is composed of piecewise cubic polynomials whose union forms a continuous function with continuous first and second derivatives.
- $Z_j(s)$ is identical to the cubic-splines approximation of a function that is equal to unity at the j th node, and zero at all other nodes.

The last property suggests a practical method of computing the cubic-splines cardinal functions. Results for a typical case are shown in Figure 3.4.1.

3.4.2 Boundary element discretization

Expressions similar to those shown in (3.4.3) can be written down for the normal derivative,

$$p'_i = P_{ij} \left(\frac{\partial f}{\partial n} \right)_j, \quad q'_i = Q_{ij} \left(\frac{\partial f}{\partial n} \right)_j, \quad r'_i = R_{ij} \left(\frac{\partial f}{\partial n} \right)_j. \quad (3.4.6)$$

Substituting (3.4.5) and its counterpart for the normal derivative into the boundary-integral representation (2.10.3) and into the boundary-integral equation (2.12.2), and extracting the nodal values from the single- and double-layer potential, we find

$$\begin{aligned} f(\mathbf{x}_0) = & - \sum_{i=1}^{N+1} \left(\frac{\partial f}{\partial n} \right)_i \int_C Z_i(s) G(\mathbf{x}, \mathbf{x}_0) dl(s) \\ & + \sum_{i=1}^{N+1} f_i \int_C Z_i(s) [\mathbf{n}(\mathbf{x}) \cdot \nabla G(\mathbf{x}, \mathbf{x}_0)] dl(s), \end{aligned} \quad (3.4.7)$$

and

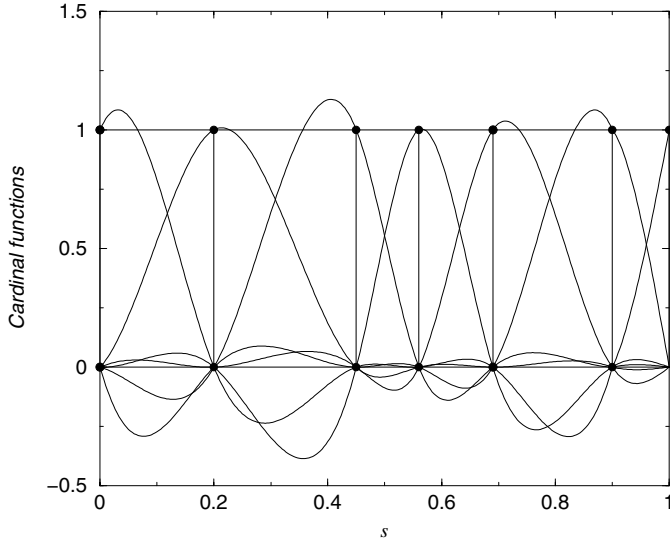


Figure 3.4.1 Periodic cubic-splines cardinal functions for $N = 6$ intervals defined by seven nodes. The i th cardinal function takes the value of unity at the i th node, and the value of zero at all other nodes.

$$\begin{aligned}
 f(\mathbf{x}_0) = & -2 \sum_{i=1}^{N+1} \left(\frac{\partial f}{\partial n} \right)_i \int_C Z_i(s) G(\mathbf{x}, \mathbf{x}_0) dl(s) \\
 & + 2 \sum_{i=1}^{N+1} f_i \int_C^{PV} Z_i(s) [\mathbf{n}(\mathbf{x}) \cdot \nabla G(\mathbf{x}, \mathbf{x}_0)] dl(s). \quad (3.4.8)
 \end{aligned}$$

The influence coefficients represented by the integrals on the right-hand sides are computed over the union of *all* boundary elements. The individual integrals over the elements may be computed using the numerical methods discussed in Section 3.2.

Consider, for example, the computation of the single-layer integral with the free-space Green's function over the i th singular element, expressed in the form

$$\int_{s_i}^{s_{i+1}} Z_i(s) G(\mathbf{x}, \mathbf{x}_0) \frac{dl}{ds} ds = -\frac{1}{2\pi} \int_{s_i}^{s_{i+1}} Z_i(s) \ln |\mathbf{x} - \mathbf{x}_i| \frac{dl}{ds} ds. \quad (3.4.9)$$

The singular integral on the right-hand side may be computed by subtracting the singularity or by using a quadrature for improper integrals with logarithmic singularity, as discussed in Section 3.3. The kernel of the principal-value, double-layer integral is non-singular, and the corresponding influence coefficient may be computed by the Gauss-Legendre quadrature.

The discretized integral equation (3.4.8) provides us with a basis for the boundary-element collocation method discussed in Section 3.3. The procedure involves applying this equation at the element end-points to generate and then solve a system of linear equations for the unknown node values of the function f or its normal derivative.

Problem

P.3.4.1 Lagrange interpolating polynomials

The N th-degree Lagrange interpolating polynomials are defined with respect to a set of $N + 1$ nodes corresponding to parameter values s_i , $i = 1, \dots, N + 1$, as

$$L_i(s) = \frac{(s - s_1)(s - s_2)\dots(s - s_{i-1})(s - s_{i+1})\dots(s - s_N)(s - s_{N+1})}{(s_i - s_1)(s_i - s_2)\dots(s_i - s_{i-1})(s_i - s_{i+1})\dots(s_i - s_N)(s - s_{N+1})}.$$

- (a) Show that these polynomials constitute a family of cardinal functions specific to the nodes.
 - (b) Prepare graphs of the Lagrange polynomials for a set of seven nodes of your choice, and discuss your results with reference to the cubic-splines cardinal functions.
-

3.5 High-order collocation methods

We have seen that two types of approximation are involved in the boundary-element method: a geometrical approximation related to the boundary discretization, and a function approximation related to the distribution of the unknown function and its normal derivative over the individual boundary elements. In the isoparametric representation discussed in Section 3.4, the two approximations were chosen to be of the same order. In practice, a high-order function approximation may be necessary over boundary elements with low-order shapes to capture rapid variations in the solution.

To implement high-order expansions, it is convenient to map the i th straight or curved element onto the interval $[-1, 1]$ of the dimensionless ξ axis, as shown in Figure 3.5.1, and introduce $M_i + 1$ native element nodes at positions $\xi_{i,j}$, where $j = 1, \dots, M_i + 1$. In the case of straight segments, circular arcs, and cubic splines, the mapping is mediated, respectively, by equations (3.1.2), (3.1.4) combined with (3.1.6), and (3.1.7) combined with (3.2.23).

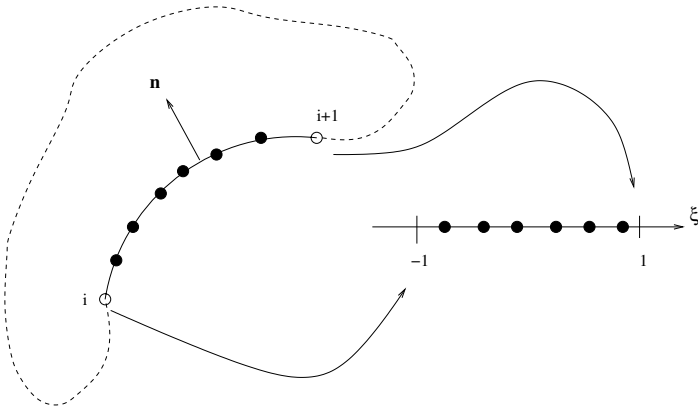


Figure 3.5.1 Mapping of the i th boundary element to the interval $[-1, 1]$ of the dimensionless ξ axis. The native element nodes are marked as filled circles.

Next, we use the native element nodes as a basis for approximating the distribution of the function f and its normal derivative with M_i -degree polynomials with respect to ξ . To simplify the logistics, we introduce the M_i -degree Lagrange interpolating polynomials

$$L_{i,j}(\xi) = \frac{(\xi - \xi_{i,1}) \cdots (\xi - \xi_{i,j-1})(\xi - \xi_{i,j+1})(\xi - \xi_{i,M_i+1})}{(\xi_{i,j} - \xi_{i,1}) \cdots (\xi_{i,j} - \xi_{i,j-1})(\xi_{i,j} - \xi_{i,j+1})(\xi_{i,j} - \xi_{i,M_i+1})}, \quad (3.5.1)$$

where $j = 1, \dots, M_i + 1$, and write

$$f(\xi) \simeq R_i(\xi) = \sum_{j=1}^{M_i+1} f_{i,j} L_{i,j}(\xi), \quad (3.5.2)$$

$$\left(\frac{\partial f}{\partial n} \right) f(\xi) \simeq R'_i(\xi) = \sum_{j=1}^{M_i+1} \left(\frac{\partial f}{\partial n} \right)_{i,j} L_{i,j}(\xi),$$

where $f_{i,j}$ and $\left(\frac{\partial f}{\partial n} \right)_{i,j}$ are the node values of the function and its normal derivative. When $M_i = 0$, the element distribution is uniform, and we recover the constant-element formulation developed in Section 3.3.

The Lagrange polynomials are cardinal functions similar to the cubic-splines cardinal functions displayed in Figure 3.4.1. By construction, the Lagrange polynomials take the value of unity at a chosen node and the value of zero at all other nodes. In terms of Kronecker's delta,

$$L_{i,j}(\xi_{i,k}) = \delta_{jk}, \quad (3.5.3)$$

where summation over i is *not* implied on the left-hand side.

Substituting the expansions shown in (3.5.2) into the boundary-integral representation (2.3.3) and into the boundary-integral equation (2.4.2), and extracting the node values from the single- and double-layer potential, we find

$$\begin{aligned} f(\mathbf{x}_0) = & - \sum_{i=1}^N \sum_{j=1}^{M_i+1} \left(\frac{\partial f}{\partial n} \right)_{i,j} \int_{E_i} L_{i,j}(\xi) G(\mathbf{x}, \mathbf{x}_0) dl(\xi) \\ & + \sum_{i=1}^N \sum_{j=1}^{M_i+1} f_{i,j} \int_{E_i} L_{i,j}(\xi) [\mathbf{n}(\mathbf{x}) \cdot \nabla G(\mathbf{x}, \mathbf{x}_0)] dl(\xi), \end{aligned} \quad (3.5.4)$$

and

$$\begin{aligned} f(\mathbf{x}_0) = & -2 \sum_{i=1}^{N+1} \sum_{j=1}^{M_i+1} \left(\frac{\partial f}{\partial n} \right)_{i,j} \int_{E_i} L_{i,j}(\xi) G(\mathbf{x}, \mathbf{x}_0) dl(\xi) \\ & + 2 \sum_{i=1}^{N+1} \sum_{j=1}^{M_i+1} f_{i,j} \int_{E_i}^{PV} L_{i,j}(\xi) [\mathbf{n}(\mathbf{x}) \cdot \nabla G(\mathbf{x}, \mathbf{x}_0)] dl(\xi). \end{aligned} \quad (3.5.5)$$

The influence coefficients on the right-hand sides are defined in terms of integrals expressing single- and double-layer potentials with polynomial strength distributions.

The discrete integral equation (3.5.5) provides us with a basis for the boundary-element collocation method discussed in Section 3.3. The procedure involves applying this equation at the element nodes, thereby generating a system of linear equations for the unknown node values of the function f or its normal derivative. The influence coefficients are computed by numerical methods similar to those discussed in Section 3.3.

3.5.1 Spectral node distribution

Analysis shows that the most accurate results are obtained when the element nodes are located at positions corresponding to the roots of orthogonal polynomials defined over the standard interval $[-1, 1]$. Examples include the Legendre, Chebyshev, Jacobi, Radau, and Lobatto polynomials. The roots of these polynomials are listed in mathematical handbooks and texts on numerical methods (e.g., [60]).

Of particular interest is the family of Lobatto polynomials defined over the interval $[-1, 1]$. The first few members of this family are

$$\begin{aligned} Lo_0(\xi) &= 1, & Lo_1(\xi) &= 3\xi, \\ Lo_2(\xi) &= \frac{3}{2}(5\xi^2 - 1), & Lo_3(\xi) &= \frac{1}{2}(35\xi^2 - 15)\xi. \end{aligned} \quad (3.5.6)$$

Having selected a member of the Lobatto family, we set $\xi_{i,1} = -1$ and $\xi_{i,M_i+1} = 1$, that is, we place two nodes at the end-points of each element, and identify the intermediate $M_i - 1$ nodes $\xi_{i,j}$, where $j = 2, \dots, M_i$, with the roots of the $(M_i - 1)$ -degree Lobatto polynomial. The shared element nodes ensure the continuity of the boundary distribution f and its normal derivative $\partial f / \partial n$ along the discretized contour and across the boundary elements. In the boundary-element literature, this property is described by the terminology “continuous element discretization.”

For example, when $M_i = 2$, we place three nodes at $\xi_{i,1} = -1$, $\xi_{i,2} = 0$, and $\xi_{i,3} = 1$; the second node corresponds to the root of $Lo_1(\xi)$. Substituting these values into (3.5.1), we find that the corresponding Lagrange polynomials are given by

$$\begin{aligned} L_{i,1}(\xi) &= \frac{1}{2} \xi (\xi - 1), & L_{i,2}(\xi) &= (1 - \xi) (1 + \xi), \\ L_{i,3}(\xi) &= \frac{1}{2} \xi (\xi + 1). \end{aligned} \tag{3.5.7}$$

Reference to (3.5.4) and (3.5.5) shows that evaluating the influence coefficients requires computing single- and double-layer potentials over the individual boundary elements with constant, linear, and quadratic strength density distributions.

3.5.2 Corner elements

When a boundary element is adjacent to a true boundary corner (but not an artificial corner due to the discretization), the boundary distribution of the function f and its normal derivative are likely to exhibit discontinuous or singular behavior, and a boundary-element distribution involving a shared corner node is not appropriate.

If the corner is the result of physical idealization, the singular behavior may be suppressed by smoothing out the geometrical discontinuity. This can be done by replacing a portion of the corner with a transverse segment, an inscribed circular arc of small radius, or another properly defined curved element.

A less invasive approach involves distributing the near-corner nodes at positions corresponding to the roots of the Radau polynomials defined over the interval $[-1, 1]$. The first few members of this family are

$$\begin{aligned} R_0(\xi) &= 1, & R_1(\xi) &= \frac{1}{2} (3 \xi - 1), & R_2(\xi) &= \frac{1}{2} (5 \xi^2 - 2 \xi - 1), \\ R_3(\xi) &= \frac{1}{8} (35 \xi^3 - 15 \xi^2 - 15 \xi + 3). \end{aligned} \tag{3.5.8}$$

If a corner occurs at the second end-point of the i th element, we set $\xi_{i,1} = -1$, that is, we place the first node at the first end-point, and identify the rest of the M_i nodes

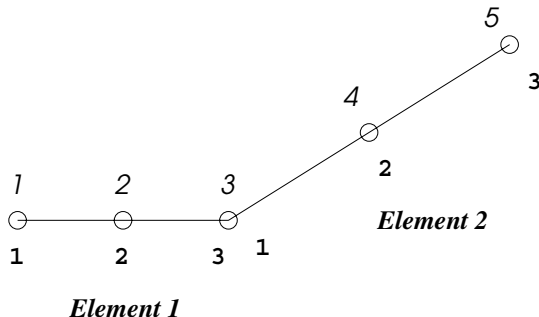


Figure 3.5.2 A two-element system illustrating the global (italic) and element (bold) node labels.

$\xi_{i,j}$, where $j = 2, \dots, M_i + 1$, with the roots of the M_i -degree Radau polynomial. For example, when $M_i = 1$, we place two nodes at $\xi_{i,1} = -1$ and $\xi_{i,2} = 1/3$; the second node corresponds to the root of $R_1(\xi)$ shown in (3.5.8). If the corner occurs at the first end-point, we replace ξ by $1 - \xi$, thereby reflecting the nodes with respect to the mid-point.

3.5.3 Assembly

When the final system of linear equations corresponding to the element nodes is being generated, the coefficient matrix and right-hand side must be defined and assembled properly to ensure that shared nodes are not counted twice.

Consider, for example, the two-element system depicted in Figure 3.5.2, where each element has three nodes, and the third node is shared by the two elements. The global node labels, printed in italic, are related to the element node labels, printed in bold, by

$$\begin{aligned} f_{1,1} &= f_1^G, & f_{1,2} &= f_2^G, & f_{1,3} &= f_3^G, \\ f_{2,1} &= f_3^G, & f_{2,2} &= f_4^G, & f_{2,3} &= f_5^G, \end{aligned} \tag{3.5.9}$$

where the superscript G denotes the global array. Accordingly, the double-layer sum shown in the second line of equation (3.5.5) takes the form of the inner vector product

$$[M_1, M_2, M_3, M_4, M_5] \cdot \begin{bmatrix} f_1^G \\ f_2^G \\ f_3^G \\ f_4^G \\ f_5^G \end{bmatrix}, \tag{3.5.10}$$

where

$$\begin{aligned}
 M_1 &\equiv \int_{E_1}^{PV} L_{1,1}(\xi) [\mathbf{n}(\mathbf{x}) \cdot \nabla G(\mathbf{x}, \mathbf{x}_0)] dl(\xi), \\
 M_2 &\equiv \int_{E_1}^{PV} L_{1,2}(\xi) [\mathbf{n}(\mathbf{x}) \cdot \nabla G(\mathbf{x}, \mathbf{x}_0)] dl(\xi), \\
 M_3 &\equiv \int_{E_1}^{PV} L_{1,3}(\xi) [\mathbf{n}(\mathbf{x}) \cdot \nabla G(\mathbf{x}, \mathbf{x}_0)] dl(\xi) \\
 &\quad + \int_{E_2}^{PV} L_{2,1}(\xi) [\mathbf{n}(\mathbf{x}) \cdot \nabla G(\mathbf{x}, \mathbf{x}_0)] dl(\xi), \\
 M_4 &\equiv \int_{E_2}^{PV} L_{2,2}(\xi) [\mathbf{n}(\mathbf{x}) \cdot \nabla G(\mathbf{x}, \mathbf{x}_0)] dl(\xi), \\
 M_5 &\equiv \int_{E_2}^{PV} L_{2,3}(\xi) [\mathbf{n}(\mathbf{x}) \cdot \nabla G(\mathbf{x}, \mathbf{x}_0)] dl(\xi).
 \end{aligned} \tag{3.5.11}$$

The algorithm involves double-looping over the elements and element nodes, while making appropriate contributions to the global influence coefficients expressed by M_i . The method is implemented by introducing a connectivity table that associates the element node labels with the global node labels. The row-vector M_i in (3.5.10) is evaluated at sequential nodes, yielding successive rows of the influence matrix corresponding to the double-layer potential. A similar computation is performed simultaneously for the influence coefficients corresponding to the single-layer potential.

3.5.4 Grid refinement

The accuracy of a boundary-element computation may be improved in two ways: (a) by increasing the number of boundary elements while keeping the order of the polynomial expansion over each element constant – this is an h -type refinement – or (b) by increasing the order of the polynomial expansion while keeping the number of elements fixed – this is a p -type refinement.

In practice, it may be desirable to keep the number of boundary elements constant and the order of the expansion fixed, and perform optimization with respect to the location of the element nodes in the spirit of r -adaptation. A drawback of this method is that, when a small or moderate number of elements is used, the optimal element distribution may be highly skewed, causing local inaccuracies or irregularities.

Grid optimization for the boundary-element method was pioneered by Ingber and Mitra [29]. The optimization process involves introducing a norm for the numerical

error, and then minimizing the error with respect to the number or position of the nodes. Error estimation and adaptive boundary-element methods have been developed by numerous subsequent authors, as reviewed in References [1, 41, 44, 46].

Problems

P.3.5.1 Lobatto polynomials

(a) Confirm that the four Lobatto polynomials listed in (3.5.6) satisfy the orthogonality condition

$$\int_{-1}^1 L_{0i}(\xi) L_{0j}(\xi) (1 - \xi^2) d\xi = \frac{2(i+1)(i+2)}{2i+3} \delta_{ij}. \quad (1)$$

(b) Write out the Lagrange interpolating polynomials corresponding to the Lobatto nodes for $M_i = 1$ and 3; the Lagrange polynomials for $M_i = 2$ are shown in (3.5.7).

P.3.5.2 Radau polynomials

(a) Confirm that the four Radau polynomials listed in (3.5.8) satisfy the orthogonality property

$$\int_{-1}^1 R_i(\xi) R_j(\xi) (1 + \xi) d\xi = \frac{2}{i+1} \delta_{ij}. \quad (1)$$

(b) Write out the Lagrange interpolating polynomials corresponding to the Radau nodes for $M_i = 1$ and 2.

3.6 Galerkin and global expansion methods

The collocation method discussed previously in this chapter is the most popular implementation of the boundary-element method. For completeness, two alternative methods are discussed in this section.

3.6.1 Galerkin boundary-element method

Consider the uniform-element discretization of the boundary-integral equation, shown in equation (3.2.6), and introduce a set of N basis functions $\Phi_i(l)$ distinguished by

the property that $\Phi_i(l)$ is equal to unity over the i th element, and zero over all other elements; l is the arc length along the discretized contour.

By construction, the constant-element discretization of the function f and its normal derivative can be expressed in the forms

$$f(l) \simeq \sum_{i=1}^N \Phi_i(l) f_i, \quad \frac{\partial f}{\partial n}(l) \simeq \sum_{i=1}^N \Phi_i(l) \left(\frac{\partial f}{\partial n} \right)_i. \quad (3.6.1)$$

Accordingly, the boundary-integral equation (3.2.6) can be expressed in the form

$$\begin{aligned} \sum_{i=1}^N f_i \Phi_i(l_0) &= -2 \sum_{i=1}^N \left(\frac{\partial f}{\partial n} \right)_i \sum_{j=1}^N \int_{E_j} \Phi_i(l) G(\mathbf{x}, \mathbf{x}_0) dl(\mathbf{x}) \\ &\quad + 2 \sum_{i=1}^N f_i \sum_{j=1}^N \int_{E_j}^{PV} \Phi_i(l) [\mathbf{n}(\mathbf{x}) \cdot \nabla G(\mathbf{x}, \mathbf{x}_0)] dl(\mathbf{x}). \end{aligned} \quad (3.6.2)$$

In the Galerkin projection method, the unknown element values are computed by projecting equation (3.6.2) onto the set of basis functions Φ_i . The projection is implemented by multiplying both sides of (3.6.2) by $\Phi_i(l_0)$, where $i = 1, \dots, N$, and integrating the product with respect to arc length l_0 around the discretized contour C defined by the union of the boundary elements.

The k th projection produces the equation

$$\sum_{i=1}^N \gamma_{ki} f_i = -2 \sum_{i=1}^N \left(\frac{\partial f}{\partial n} \right)_i \sum_{j=1}^N \alpha_{kji} + 2 \sum_{i=1}^N f_i \sum_{j=1}^N \beta_{kji}^{PV}, \quad (3.6.3)$$

where

$$\begin{aligned} \alpha_{kji} &\equiv \int_C \int_{E_j} \Phi_k(l_0) \Phi_i(l) G(\mathbf{x}, \mathbf{x}_0) dl(\mathbf{x}) dl_0, \\ \beta_{kji} &\equiv \int_C \int_{E_j} \Phi_k(l_0) \Phi_i(l) [\mathbf{n}(\mathbf{x}) \cdot \nabla G(\mathbf{x}, \mathbf{x}_0)] dl(\mathbf{x}) dl_0, \\ \gamma_{ki} &\equiv \int_C \Phi_k(l_0) \Phi_i(l_0) dl_0. \end{aligned} \quad (3.6.4)$$

The superscript PV in the last sum on the right-hand side of (3.6.3) denotes the principal value of the integral with respect to l .

Taking advantage of the finite support of the uniform-element basis functions, we write

$$\alpha_{kji} = \delta_{ij} A_{kj}, \quad \beta_{kji} = \delta_{ij} B_{kj}, \quad \gamma_{ki} = \delta_{ki} \Delta l_k, \quad (3.6.5)$$

where δ_{lm} is Kronecker's delta, Δl_k is the arc length of the k th element, and we have defined

$$\begin{aligned} A_{kj} &\equiv \int_{E_k} \int_{E_j} G(\mathbf{x}, \mathbf{x}_0) \, dl(\mathbf{x}) \, dl_0, \\ B_{kj} &\equiv \int_{E_k} \int_{E_j} [\mathbf{n}(\mathbf{x}) \cdot \nabla G(\mathbf{x}, \mathbf{x}_0)] \, dl(\mathbf{x}) \, dl_0. \end{aligned} \quad (3.6.6)$$

Substituting these expressions into (3.6.3) and simplifying, we derive the final form

$$\Delta l_k f_k = -2 \sum_{i=1}^N \left(\frac{\partial f}{\partial n} \right)_i A_{ki} + 2 \sum_{i=1}^N f_i B_{ki}^{PV}, \quad (3.6.7)$$

where summation over k is *not* implied on the left-hand side. Applying equation (3.6.7) for $k = 1, \dots, N$, we obtain a system of linear equations for the unknown element values.

Now, because of the symmetry of the Green's function, $G(\mathbf{x}, \mathbf{x}_0) = G(\mathbf{x}_0, \mathbf{x})$, the matrix A_{kj} defined in the first equation of (3.6.6) is symmetric, and so is the coefficient of the linear system for the element values of the normal derivative originating from (3.6.7). Consequently, when Dirichlet conditions are specified (Neumann problem), the Galerkin boundary-element method produces a linear system with a symmetric coefficient matrix multiplying the unknown vector of normal derivatives at the nodes. Solving this system requires a reduced amount of computational effort (e.g., [60]).

The boundary-element Galerkin method just described can be generalized by replacing the piecewise constant element basis functions $\Phi_i(l)$ with cardinal interpolation functions $Z_i(l)$ defined with respect to a set of $N + 1$ boundary-element nodes. An example is the set of cubic-splines cardinal functions discussed in Section 3.4. The counterpart of the linear system (3.6.7) is

$$\sum_{i=1}^{N+1} C_{ki} f_i = -2 \sum_{i=1}^{N+1} \left(\frac{\partial f}{\partial n} \right)_i A_{ki} + 2 \sum_{i=1}^{N+1} f_i B_{ki}^{PV}, \quad (3.6.8)$$

where

$$\begin{aligned} A_{ki} &\equiv \int_C \int_C Z_k(l_0) Z_i(l) G(\mathbf{x}, \mathbf{x}_0) \, dl(\mathbf{x}) \, dl_0, \\ B_{ki} &\equiv \int_C \int_C Z_k(l_0) Z_i(l) [\mathbf{n}(\mathbf{x}) \cdot \nabla G(\mathbf{x}, \mathbf{x}_0)] \, dl(\mathbf{x}) \, dl_0, \\ C_{ki} &\equiv \int_C \int_C Z_k(l_0) Z_i(l) \, dl_0, \end{aligned} \quad (3.6.9)$$

are Galerkin influence coefficients defined in terms of double integrals. Note that the matrix A_{ki} remains symmetric in this generalized framework.

The implementation of the Galerkin boundary-element method for the hypersingular integral equations discussed in Section 2.5 follows the basic steps outlined in this section. When Neumann boundary conditions are specified (Dirichlet problem), the method produces a linear system of algebraic equations with a symmetric coefficient matrix multiplying the vector of unknown function values at the nodes.

In spite of the additional computational effort necessary for evaluating the double integrals that arise from the Galerkin projection, the approach described in this section has certain advantages over the collocation method including ability to evaluate without ambiguity hypersingular integrals, and better accuracy for the same number of unknowns (e.g., [23]).

3.6.2 Global expansion method

In the global expansion method, the boundary distribution of the function f and its normal derivative are expressed as linear combinations of a complete set of basis functions defined over the whole of the boundary of the solution domain. The unknown coefficients of the expansions are then found by solving linear systems of equations generated by the Galerkin projection. The implementation and performance of the method are discussed in References [3, 4].

Problems

P.3.6.1 Constant-element basis functions

Express the constant-element basis functions $B_i(l)$ in terms of the Heaviside function $H(x)$, which is equal to unity when x is positive, and zero when x is negative.

P.3.6.2 Influence coefficients

Investigate whether it is possible to compute the influence coefficient A_{kj} defined in (3.6.6) by analytical methods for straight boundary elements when (a) $k = j$, and (b) $k \neq j$.

Chapter 4

Laplace's equation in three dimensions

Generalizing the theoretical framework developed in Chapter 2 for Laplace's equation in two dimensions, in this chapter, we discuss the boundary-integral formulation of Laplace's equation in three dimensions

$$\nabla^2 f(x, y, z) = 0, \quad (4.1)$$

where ∇^2 is the Laplacian operator

$$\nabla^2 \equiv \frac{\partial^2}{\partial x^2} + \frac{\partial^2}{\partial y^2} + \frac{\partial^2}{\partial z^2}. \quad (4.2)$$

A function that satisfies equation (4.1) is called harmonic.

The fundamental concepts underlying the development of boundary-integral and boundary-element methods in three dimensions are straightforward extensions of corresponding concepts in two dimensions. To avoid extensive duplication, we confine our attention to presenting the basic ideas, discussing the most important derivations, and developing formulations for axisymmetric domains.

4.1 Green's first and second identities and the reciprocal relation

Green's first identity states that any two twice-differentiable functions $f(x, y, z)$ and $\phi(x, y, z)$ satisfy the relation

$$\phi \nabla^2 f = \nabla \cdot (\phi \nabla f) - \nabla \phi \cdot \nabla f. \quad (4.1.1)$$

In index notation, equation (4.1.1) takes the form of equation (2.1.2), where summation over the repeated index i is implied in the range $i = 1, 2$, and 3 , corresponding to x, y , and z .

Interchanging the roles of f and ϕ , we obtain

$$f \nabla^2 \phi = \nabla \cdot (f \nabla \phi) - \nabla f \cdot \nabla \phi. \quad (4.1.2)$$

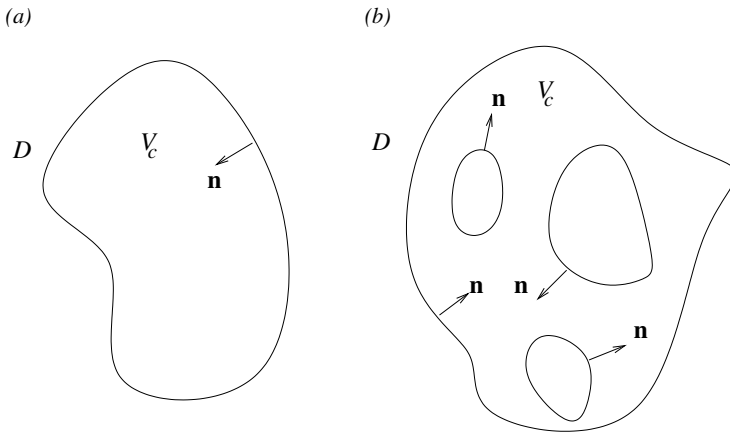


Figure 4.1.1 A control volume enclosed by (a) a closed surface, and (b) a collection of closed surfaces. The unit normal vector \mathbf{n} points into the control volume.

Subtracting (4.1.2) from (4.1.1), we derive Green's second identity

$$\phi \nabla^2 f - f \nabla^2 \phi = \nabla \cdot (\phi \nabla f - f \nabla \phi). \quad (4.1.3)$$

If both functions f and ϕ satisfy Laplace's equation (4.1), the left-hand side of (4.1.3) vanishes, yielding the reciprocal relation for nonsingular harmonic functions

$$\nabla \cdot (\phi \nabla f - f \nabla \phi) = 0, \quad (4.1.4)$$

which is the three-dimensional counterpart of (1.1.4) and (2.1.5).

4.1.1 Integral form of the reciprocal relation

The integral form of the reciprocal relation arises by integrating both sides of equation (4.1.4) over an arbitrary control volume V_c that is bounded by a closed surface or a collection of closed surfaces denoted by D , as illustrated in Figure 4.1.1.

Using the divergence theorem (Appendix A), we convert the volume integral to a surface integral, and thereby obtain the integral statement

$$\int \int_{V_c} (\phi \nabla f - f \nabla \phi) \cdot \mathbf{n} dV = 0, \quad (4.1.5)$$

where \mathbf{n} is the unit vector normal to D pointing into the control volume, and $dV = dx dy dz$ is a differential volume.

Relation (4.1.5) imposes an integral constraint on the boundary values and boundary distribution of the normal derivatives of any pair of non-singular harmonic functions f and ϕ . The boundary-integral representation for the function f arises by identifying ϕ with a Green's function.

4.2 Green's functions

The Green's functions constitute a special class of harmonic functions that are singular at an arbitrary point $\mathbf{x}_0 = (x_0, y_0, z_0)$. By definition, a Green's function of Laplace's equation in three dimensions satisfies the singularly forced Laplace's equation

$$\nabla^2 G(\mathbf{x}, \mathbf{x}_0) + \delta_3(\mathbf{x} - \mathbf{x}_0) = 0, \quad (4.2.1)$$

where:

- $\mathbf{x} = (x, y, z)$ is the variable “field point.”
- $\mathbf{x}_0 = (x_0, y_0, z_0)$ is the fixed location of the “singular point” or “pole.”
- $\delta_3(\mathbf{x} - \mathbf{x}_0)$, written more explicitly as $\delta_3(x - x_0, y - y_0, z - z_0)$, is Dirac's delta function in three dimensions.

By construction, Dirac's delta function in three dimensions is distinguished by the following properties:

1. $\delta_3(x - x_0, y - y_0, z - z_0)$ vanishes everywhere except at the point $x = x_0$, $y = y_0$, $z = z_0$, where it becomes infinite.
2. The integral of the delta function over a volume Ω that contains the singular point (x_0, y_0, z_0) is equal to unity,

$$\int_{\Omega} \delta_3(x - x_0, y - y_0, z - z_0) dx dy dz = 1. \quad (4.2.2)$$

This property illustrates that the delta function in three dimensions has units of inverse cubed length.

3. The integral of the product of an arbitrary function $f(x, y, z)$ and the delta function over a volume Ω that contains the singular point (x_0, y_0, z_0) is equal to the value of the function at the singular point,

$$\int_{\Omega} \delta_3(x - x_0, y - y_0, z - z_0) f(x, y, z) dx dy dz = f(x_0, y_0, z_0). \quad (4.2.3)$$

The integral of the product of an arbitrary function $f(x, y, z)$ and the delta function over a volume Ω that does *not* contain the singular point (x_0, y_0, z_0) is equal to zero.

4. In formal mathematics, $\delta_3(x - x_0, y - y_0, z - z_0)$ arises from the family of test functions

$$h(r) = \left(\frac{\lambda}{\pi L^2}\right)^{3/2} \exp(-\lambda \frac{r^2}{L^2}), \quad (4.2.4)$$

in the limit as the dimensionless parameter λ tends to infinity, where

$$r \equiv |\mathbf{x} - \mathbf{x}_0| = \sqrt{(x - x_0)^2 + (y - y_0)^2 + (z - z_0)^2},$$

and L is an arbitrary length,

Figure 4.2.1 shows graphs of the dimensionless test functions $H \equiv hL^3$ plotted against the dimensionless distance $X \equiv (x - x_0)/L$ for $y = y_0$, $z = z_0$, and $\lambda = 1$ (dashed line), 2, 5, 10, 20, 50, 100, and 500 (dotted line). The maximum height of each graph is inversely proportional to the cubic power of its width, so that the volume underneath each graph in three-dimensional space is equal to unity,

$$\begin{aligned} \int \int \int h(r) dx dy dz &= \int_0^\pi \int_0^{2\pi} \int_0^\infty h(r) \sin \theta r^2 dr d\varphi d\theta \\ &= 4\pi \int_0^\infty h(r) r^2 dr = 4\pi \left(\frac{\lambda}{\pi L^2}\right)^{3/2} \int_0^\infty \exp(-\lambda \frac{r^2}{L^2}) r^2 dr = 1, \end{aligned} \quad (4.2.5)$$

where (r, θ, φ) are spherical polar coordinates centered at the singular point. To prove this identity, we observe that

$$q(r) = g(x - x_0) g(y - y_0) g(z - z_0), \quad (4.2.6)$$

where the function g is defined in equation (1.2.4), write

$$\begin{aligned} \int \int \int h(r) dx dy dz &= \left[\int_{-\infty}^\infty g(x - x_0) dx \right] \left[\int_{-\infty}^\infty g(y - y_0) dy \right] \\ &\quad \times \left[\int_{-\infty}^\infty g(z - z_0) dz \right], \end{aligned} \quad (4.2.7)$$

and use property (1.2.5).

4.2.1 Green's and Neumann functions

In addition to satisfying equation (4.2.1), a Green's function of the *first kind* is required to take the reference value of zero over a surface S_G representing the boundary of a solution domain, as shown in (2.2.8), where the point \mathbf{x} lies on S_G .

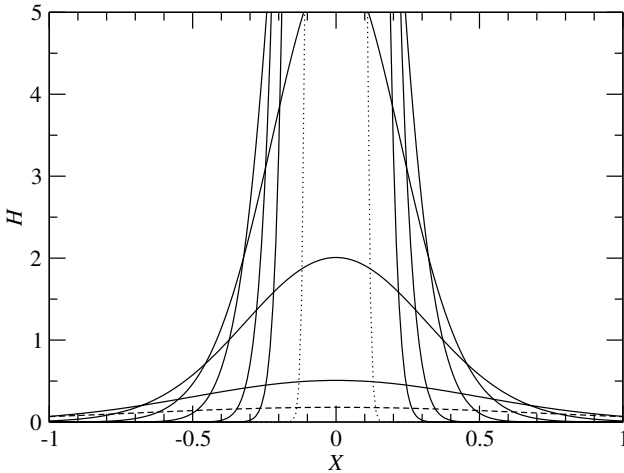


Figure 4.2.1 A family of dimensionless test functions $H \equiv hL^3$ described by (4.2.4) plotted against the dimensionless distance $X \equiv (x - x_0)/L$ for $y = y_0$, $z = z_0$, and $\lambda = 1$ (dashed line), 2, 5, 10, 20, 50, 100, and 500 (dotted line). In the limit as the dimensionless parameter λ tends to infinity, we recover Dirac's delta function in three dimensions.

A Green's function of the *second kind*, also called a *Neumann function*, is distinguished by the property that its normal derivative vanishes over the surface S_G , as shown in (2.2.9), where the point \mathbf{x} lies on S_G .

The physical interpretation of Green's and Neumann functions is discussed in Section 2.2.1.

4.2.2 The free-space Green's function

The free-space Green's function corresponds to an infinite solution domain in the absence of interior boundaries. Solving equation (4.2.1) by inspection or using the Fourier transform, we obtain

$$G(\mathbf{x}, \mathbf{x}_0) = \frac{1}{4\pi r}, \quad (4.2.8)$$

where $r = |\mathbf{x} - \mathbf{x}_0|$ is the distance of the field point \mathbf{x} from the singular point \mathbf{x}_0 .

4.2.3 Green's functions in bounded domains

As the observation point \mathbf{x} approaches the singular point \mathbf{x}_0 , all Green's and Neumann functions exhibit a common singular behavior. Specifically, any Green's or

Neumann function is composed of a singular part that is identical to the free-space Green's function given in (4.2.8), and a complementary part expressed by a harmonic function H that is non-singular throughout the domain of solution,

$$G(\mathbf{x}, \mathbf{x}_0) = \frac{1}{4\pi r} + H(\mathbf{x}, \mathbf{x}_0). \quad (4.2.9)$$

In the case of the free-space Green's function, the complementary component H vanishes. More generally, the particular form of H depends on the geometry of the boundary S_G . For certain simple boundaries geometries involving planar and spherical shapes, the complementary function H may be found by the method of images, that is, by placing free-space Green's functions and their derivatives at strategically selected positions outside the solution domain.

For example, the Green's function for a semi-infinite domain bounded by a plane wall located at $x = w$ is given by

$$G(\mathbf{x}, \mathbf{x}_0) = \frac{1}{4\pi r} \pm \frac{1}{4\pi r^{Im}}, \quad (4.2.10)$$

where $r = |\mathbf{x} - \mathbf{x}_0|$, $r^{Im} = |\mathbf{x} - \mathbf{x}_0^{Im}|$, and $\mathbf{x}_0^{Im} = (2w - x_0, y_0, z_0)$ is the image of the singular point \mathbf{x}_0 with respect to the wall. The plus and minus sign correspond, respectively, to the Green's function of the first kind and to the Neumann function.

4.2.4 BEMLIB directory `lgf_3d`

Subdirectory `lgf_3d` of directory `laplace` of *BEMLIB* contains subroutines that evaluate a family of Green's and Neumann functions in three dimensions, including the following:

- Green's function in free space.
- Green's and Neumann functions in a semi-infinite domain bounded by a plane wall.
- Neumann function in the exterior of a sphere.
- Doubly periodic Green's function.

Illustration of iso-scalar contours are presented in Chapter 10.

4.2.5 Integral properties of Green's functions

Consider a singly or multiply connected control volume, denoted by V_c , bounded by a closed surface or a collection of closed surfaces, denoted by D . The boundary S_G associated with the Green's function may be one of these surfaces. For the moment,

we shall assume that all surfaces are smooth, that is, they do not exhibit conical, edge-like or cusp-like corners.

Integrating (4.2.1) over the control volume V_c , and using the divergence theorem and the distinctive properties of the delta function in three dimensions, we find that the Green's functions satisfy the integral identity

$$\int_D \mathbf{n}(\mathbf{x}) \cdot \nabla G(\mathbf{x}, \mathbf{x}_0) dS(\mathbf{x}) = \begin{cases} 1 & \text{when } \mathbf{x}_0 \text{ is inside } V_c \\ \frac{1}{2} & \text{when } \mathbf{x}_0 \text{ is on } D \\ 0 & \text{when } \mathbf{x}_0 \text{ is outside } V_c \end{cases}, \quad (4.2.11)$$

where the unit normal vector \mathbf{n} points *into* the control volume V_c . When the point \mathbf{x}_0 is located on the boundary D , the improper integral on the left-hand side of (4.2.11) is a *principal-value integral*.

Using the three relations shown in (4.2.11), we derive the important identity

$$\int_D \mathbf{n}(\mathbf{x}) \cdot \nabla G(\mathbf{x}, \mathbf{x}_0) dS(\mathbf{x}) = \int_D^{PV} \mathbf{n}(\mathbf{x}) \cdot \nabla G(\mathbf{x}, \mathbf{x}_0) dS(\mathbf{x}) \pm \frac{1}{2}, \quad (4.2.12)$$

where PV denotes the principal-value integral computed by placing the evaluation point \mathbf{x}_0 precisely on the surface D . The plus and minus sign on the right-hand side of (4.2.12) apply, respectively, when the point \mathbf{x}_0 on the left-hand side lies inside or outside the control volume V_c .

4.2.6 Green's function dipole

Differentiating a Green's function with respect to the coordinates of the pole we obtain a vectorial singularity called the Green's function dipole, given by

$$\mathbf{G}^D \equiv \nabla_0 G(\mathbf{x}, \mathbf{x}_0) = \left[\frac{\partial G(\mathbf{x}, \mathbf{x}_0)}{\partial x_0}, \frac{\partial G(\mathbf{x}, \mathbf{x}_0)}{\partial y_0}, \frac{\partial G(\mathbf{x}, \mathbf{x}_0)}{\partial z_0} \right], \quad (4.2.13)$$

where the subscript “0” denotes differentiation with respect to the Cartesian components of \mathbf{x}_0 . Physically, the scalar field

$$\Phi(\mathbf{x}, \mathbf{x}_0) = \mathbf{d} \cdot \nabla_0 G(\mathbf{x}, \mathbf{x}_0) \quad (4.2.14)$$

represents the temperature or species concentration field due to a point source dipole of heat or species located at the point \mathbf{x}_0 . The direction and strength of the dipole are determined, respectively, by the orientation and magnitude of the vector \mathbf{d} .

Differentiating, for example, the right-hand side of (4.2.8), we derive the three-dimensional free-space point source dipole

$$G_i^D = \frac{1}{4\pi} \frac{\hat{x}_i}{r^3}, \quad (4.2.15)$$

where $i = 1, 2, 3$ corresponds to x, y, z , $\hat{\mathbf{x}} = \mathbf{x} - \mathbf{x}_0$, and $r = |\mathbf{x} - \mathbf{x}_0|$. The temperature field due to a point source dipole of heat in free space is thus given by

$$T(\mathbf{x}) = \frac{1}{4\pi} \frac{d_x \hat{x} + d_y \hat{y} + d_z \hat{z}}{r^3}, \quad (4.2.16)$$

where the scalar coefficients d_x, d_y , and d_z determine the orientation and strength of the dipole.

4.2.7 Green's function quadruple

Higher derivatives of the Green's function with respect to the coordinates of the pole yield higher-order tensorial singularities that are multi-poles of the point source. The first three members of this family are the quadruple G^Q , the octupole G^O , and the sextupole G^S .

The free-space quadrupole is given by

$$G_{ij}^Q(\mathbf{x}, \mathbf{x}_0) = \frac{\partial G_j^D(\mathbf{x}, \mathbf{x}_0)}{\partial x_{0j}} = \frac{\partial^2 G(\mathbf{x}, \mathbf{x}_0)}{\partial x_{0i} \partial x_{0j}} = -\frac{1}{4\pi} \left(\frac{\delta_{ij}}{r^3} - 3 \frac{\hat{x}_i \hat{x}_j}{r^5} \right), \quad (4.2.17)$$

where $\hat{\mathbf{x}} = \mathbf{x} - \mathbf{x}_0$ and $r = |\mathbf{x} - \mathbf{x}_0|$.

Problems

P.4.2.1 Delta function in three dimensions

Given the equality shown in the third line of (4.2.5), show that

$$\int_0^\infty e^{-u^2} u^2 du = \frac{\sqrt{\pi}}{4}. \quad (1)$$

P.4.2.2 Helmholtz's equation

(a) Show that any two non-singular solutions of Helmholtz's equation in three dimensions

$$\nabla^2 f(x, y, z) - c f(x, y, z) = 0, \quad (1)$$

satisfy the reciprocal relation (4.1.4); c is a real or complex constant.

(b) The Green's functions of Helmholtz's equation in three dimensions satisfy the equation

$$\nabla^2 G(\mathbf{x}, \mathbf{x}_0) - c G(\mathbf{x}, \mathbf{x}_0) + \delta_3(\mathbf{x} - \mathbf{x}_0) = 0. \quad (2)$$

Confirm that the free-space Green's function is given by

$$G(\mathbf{x}, \mathbf{x}_0) = \frac{1}{4\pi r} \exp(-\sqrt{c} r), \quad (3)$$

and discuss the behavior as r tends to zero or to infinity in relation to the free-space Green's function of Laplace's equation.

P.4.2.3 Convection-diffusion in uniform flow

The steady-state temperature or species concentration field $f(x, y, z)$ in a uniform (streaming) flow with constant velocity $\mathbf{U} = (U_x, U_y, U_z)$ is governed by the linear convection – diffusion equation

$$U_x \frac{\partial f}{\partial x} + U_y \frac{\partial f}{\partial y} + U_z \frac{\partial f}{\partial z} = \kappa \nabla^2 f, \quad (1)$$

where κ is the thermal or species diffusivity. In vector notation, equation (1) takes the compact form $\mathbf{U} \cdot \nabla f = \kappa \nabla^2 f$. The corresponding Green's function satisfies the equation

$$\begin{aligned} U_x \frac{\partial G(\mathbf{x}, \mathbf{x}_0)}{\partial x} + U_y \frac{\partial G(\mathbf{x}, \mathbf{x}_0)}{\partial y} + U_z \frac{\partial G(\mathbf{x}, \mathbf{x}_0)}{\partial z} \\ = \kappa \nabla^2 G(\mathbf{x}, \mathbf{x}_0) + \delta_3(\mathbf{x} - \mathbf{x}_0). \end{aligned} \quad (2)$$

Show that the free-space Green's function is given by

$$G(\mathbf{x}, \mathbf{x}_0) = \frac{1}{\kappa} H(\mathbf{x}, \mathbf{x}_0) \exp\left[\frac{1}{2\kappa} \mathbf{U} \cdot (\mathbf{x} - \mathbf{x}_0)\right], \quad (3)$$

where $H(\mathbf{x}, \mathbf{x}_0)$ is the Green's function of Helmholtz's equation given by the right-hand side of equation (3) of P.4.2.2 with $c = |\mathbf{U}|/(2\kappa)$. Thus,

$$G(\mathbf{x}, \mathbf{x}_0) = \frac{1}{4\pi\kappa r} \exp\left[-\frac{1}{2\kappa} [|\mathbf{U}| r - \mathbf{U} \cdot (\mathbf{x} - \mathbf{x}_0)]\right]. \quad (4)$$

P.4.2.4 The biharmonic equation in three dimensions

The biharmonic equation in three dimensions reads

$$\nabla^4 f(x, y, z) = 0, \quad (1)$$

where $\nabla^4 \equiv \nabla^2 \nabla^2$ is the biharmonic operator, and ∇^2 is the Laplacian operator. The corresponding Green's function satisfies the equation

$$\nabla^4 G(\mathbf{x}, \mathbf{x}_0) + \delta_3(\mathbf{x} - \mathbf{x}_0) = 0. \quad (2)$$

Verify that the free-space Green's function is given by

$$G(\mathbf{x}, \mathbf{x}_0) = \frac{r}{8\pi}, \quad (3)$$

where $r = |\mathbf{x} - \mathbf{x}_0|$.

4.3 Integral representation

Applying Green's second identity (4.1.3) for a non-singular harmonic function $f(\mathbf{x})$ and a Green's function $G(\mathbf{x}, \mathbf{x}_0)$ in place of $\phi(\mathbf{x})$, and using the definition (4.2.1), we obtain

$$f(\mathbf{x}) \delta_3(\mathbf{x} - \mathbf{x}_0) = \nabla \cdot [G(\mathbf{x}, \mathbf{x}_0) \nabla f(\mathbf{x}) - f(\mathbf{x}) \nabla G(\mathbf{x}, \mathbf{x}_0)], \quad (4.3.1)$$

which is the three-dimensional counterpart of the one- and two-dimensional forms (1.3.1) and (2.3.1).

Next, we select a control volume V_c that is bounded by a closed surface or a collection of closed surfaces denoted by D , as illustrated in Figure 4.1.1.

When the pole of the Green's function \mathbf{x}_0 is placed outside V_c , the left-hand side of (4.3.1) is non-singular throughout V_c . Integrating both sides over V_c , and using the divergence theorem (Appendix A), we find

$$\int_D [G(\mathbf{x}, \mathbf{x}_0) \nabla f(\mathbf{x}) - f(\mathbf{x}) \nabla G(\mathbf{x}, \mathbf{x}_0)] \cdot \mathbf{n}(\mathbf{x}) dS(\mathbf{x}) = 0, \quad (4.3.2)$$

where dS is the differential surface area of D .

On the other hand, when the pole \mathbf{x}_0 is placed inside V_c , the left-hand side of (4.3.1) is singular at the point \mathbf{x}_0 . Using the distinctive properties of the delta function in three dimensions to perform the integration, we find

$$\begin{aligned} f(\mathbf{x}_0) &= - \int_D G(\mathbf{x}, \mathbf{x}_0) [\mathbf{n}(\mathbf{x}) \cdot \nabla f(\mathbf{x})] dS(\mathbf{x}) \\ &\quad + \int_D f(\mathbf{x}) [\mathbf{n}(\mathbf{x}) \cdot \nabla G(\mathbf{x}, \mathbf{x}_0)] dS(\mathbf{x}), \end{aligned} \quad (4.3.3)$$

where the unit normal vector \mathbf{n} points into the control volume enclosed by D , as shown in Figure 4.1.1.

Equation (4.3.3) provides us with a boundary-integral representation of a harmonic function in terms of the boundary values and the boundary distribution of the normal

derivative. To compute the value of f at a particular point \mathbf{x}_0 located inside a selected control volume, we simply evaluate the two surface integrals on the right-hand side of (4.3.3).

A symmetry property allows us to switch the order of the arguments of the Green's function in (4.3.3), writing $G(\mathbf{x}, \mathbf{x}_0) = G(\mathbf{x}_0, \mathbf{x})$ (see P.2.3.1). Using this property, we recast (4.3.3) into the form

$$\begin{aligned} f(\mathbf{x}_0) = & - \int_D G(\mathbf{x}_0, \mathbf{x}) [\mathbf{n}(\mathbf{x}) \cdot \nabla f(\mathbf{x})] dS(\mathbf{x}) \\ & + \int_D f(\mathbf{x}) [\mathbf{n}(\mathbf{x}) \cdot \nabla G(\mathbf{x}_0, \mathbf{x})] dS(\mathbf{x}). \end{aligned} \quad (4.3.4)$$

The two integrals on the right-hand side of (4.3.4) represent boundary distributions of Green's functions and Green's function dipoles oriented perpendicular to the boundaries of the control volume, expressing boundary distributions of point sources and point source dipoles. Making an analogy with the corresponding boundary distributions of electric charges and charge dipoles in electrostatics, we refer to the two integrals as the *single-layer* and *double-layer* harmonic potential. The densities (strength per unit of surface area) of these potentials are equal, respectively, to the boundary distribution of the normal derivative and to the boundary values of the harmonic potential.

4.3.1 Green's third identity

Applying the integral representation (4.3.3) with the free-space Green's function given in (4.2.8), we derive Green's third identity in three dimensions,

$$f(\mathbf{x}_0) = \frac{1}{4\pi} \int_D \left[-\frac{1}{r} \nabla f(\mathbf{x}) + f(\mathbf{x}) \frac{\mathbf{x}_0 - \mathbf{x}}{r^3} \right] \cdot \mathbf{n}(\mathbf{x}) dS(\mathbf{x}), \quad (4.3.5)$$

where $r = |\mathbf{x} - \mathbf{x}_0|$, and the unit normal vector \mathbf{n} points into the control volume enclosed by the surface D .

4.3.2 Integral representation of the gradient

An integral representation for the gradient ∇f may be derived by repeating the analysis of Section 2.3.3 in three dimensions. The result is

$$\begin{aligned} \frac{\partial f(\mathbf{x}_0)}{\partial x_{0i}} = & - \int_D \frac{\partial G(\mathbf{x}_0, \mathbf{x})}{\partial x_{0i}} [\mathbf{n}(\mathbf{x}) \cdot \nabla f(\mathbf{x})] dS(\mathbf{x}) \\ & + \int_D f(\mathbf{x}) \frac{\partial^2 G(\mathbf{x}_0, \mathbf{x})}{\partial x_{0i} \partial x_j} n_j(\mathbf{x}) dS(\mathbf{x}), \end{aligned} \quad (4.3.6)$$

where summation over the repeated index j is implied on the right-hand side.

In the case of the free-space Green's function, we depart from Green's third identity (4.3.5) and derive the more specific form

$$\begin{aligned} \frac{\partial f(\mathbf{x}_0)}{\partial x_{0_i}} &= \frac{1}{4\pi} \int_D \frac{\tilde{x}_i}{r^3} [\mathbf{n}(\mathbf{x}) \cdot \nabla f(\mathbf{x})] dS(\mathbf{x}) \\ &\quad + \frac{1}{4\pi} \int_C f(\mathbf{x}) \left(\frac{\delta_{ij}}{r^3} - 3 \frac{\tilde{x}_i \tilde{x}_j}{r^5} \right) n_j(\mathbf{x}) dS(\mathbf{x}), \end{aligned} \quad (4.3.7)$$

where δ_{ij} is Kronecker's delta, and $\tilde{\mathbf{x}} = \mathbf{x}_0 - \mathbf{x}$. Comparing the two integrands on the right-hand side with expressions (4.2.15) and (4.2.17), we find that the corresponding integrals, and by extension the integrals in (4.3.6), represent boundary distributions of point source dipoles and quadruples.

Problems

P.4.3.1 Mean-value theorem

Consider a harmonic function $f(x, y, z)$ satisfying Laplace's equation (4.1), and introduce a control volume enclosed by a spherical surface D of radius a centered at the point \mathbf{x}_0 . Apply Green's third identity (4.3.5) to derive the mean-value theorem

$$f(\mathbf{x}_0) = \frac{1}{4\pi a^2} \int_D f(\mathbf{x}) dS(\mathbf{x}). \quad (1)$$

The right-hand side is the average value of f over the surface of the sphere.

P.4.3.2 Helmholtz's equation

Show that a solution of Helmholtz's equation in three dimensions, equation (1) of P.4.2.2, admits the integral representation (4.3.4), where $G(\mathbf{x}, \mathbf{x}_0)$ is the corresponding Green's function.

4.4 Integral equations

To derive integral equations for the boundary distribution of the harmonic function f and its normal derivative, we return to the integral representation (4.3.4), and take the limit as the evaluation point \mathbf{x}_0 approaches a locally smooth boundary D . Careful examination shows that the single-layer potential varies continuously as the point \mathbf{x}_0

approaches and then crosses D . Concentrating on the double-layer potential, we use property (4.2.12) and find

$$\begin{aligned} \lim_{\mathbf{x}_0 \rightarrow D} \int_D f(\mathbf{x}) [\mathbf{n}(\mathbf{x}) \cdot \nabla G(\mathbf{x}_0, \mathbf{x})] dS(\mathbf{x}) \\ = \int_D^{PV} f(\mathbf{x}) [\mathbf{n}(\mathbf{x}) \cdot \nabla G(\mathbf{x}_0, \mathbf{x})] dS(\mathbf{x}) + \frac{1}{2} f(\mathbf{x}_0), \end{aligned} \quad (4.4.1)$$

where PV denotes the principal-value integral.

Substituting (4.4.1) into (4.3.4) and rearranging, we find

$$\begin{aligned} f(\mathbf{x}_0) = -2 \int_D G(\mathbf{x}, \mathbf{x}_0) [\mathbf{n}(\mathbf{x}) \cdot \nabla f(\mathbf{x})] dS(\mathbf{x}) \\ + 2 \int_D^{PV} f(\mathbf{x}) [\mathbf{n}(\mathbf{x}) \cdot \nabla G(\mathbf{x}, \mathbf{x}_0)] dS(\mathbf{x}), \end{aligned} \quad (4.4.2)$$

where the point \mathbf{x}_0 lies precisely on the surface D , and the unit normal vector \mathbf{n} points into the control volume enclosed by D .

Written with the free-space Green's function, the integral equation (4.4.2) takes the form

$$\begin{aligned} f(\mathbf{x}_0) = \frac{1}{2\pi} \int_D \frac{1}{r} [\mathbf{n}(\mathbf{x}) \cdot \nabla f(\mathbf{x})] dS(\mathbf{x}) \\ + \frac{1}{2\pi} \int_D^{PV} f(\mathbf{x}) \frac{\mathbf{n}(\mathbf{x}) \cdot (\mathbf{x}_0 - \mathbf{x})}{r^3} dS(\mathbf{x}), \end{aligned} \quad (4.4.3)$$

where $r = |\mathbf{x} - \mathbf{x}_0|$.

The boundary-element method is based on the following observations:

- Specifying the boundary distribution of the function f , reduces equation (4.4.2) to a *Fredholm integral equation of the first kind* for the normal derivative $\mathbf{n} \cdot \nabla f$.
- Specifying the boundary distribution of the normal derivative $\mathbf{n} \cdot \nabla f$, reduces equation (4.4.2) to a *Fredholm integral equation of the second kind* for the boundary distribution of f .

The free-space Green's function exhibits a $1/r$ singularity, where r is the distance of the evaluation point from the singular point. Because the order of this singularity is lower than the quadratic dimension of the variable of integration, the integral equation is weakly singular. Consequently, the Fredholm-Riesz theory of compact operators may be used to study the properties of the solution (e.g., [4]), and the improper

integral may be computed accurately by numerical methods, as will be discussed in Chapter 5.

When D is a smooth surface with a continuously varying normal vector, as the integration point \mathbf{x} approaches the evaluation point \mathbf{x}_0 , the normal vector \mathbf{n} tends to become orthogonal to the nearly tangential vector $(\mathbf{x} - \mathbf{x}_0)$. Consequently, the numerator of the integrand of the double-layer potential on the right-hand side of (4.4.3) behaves quadratically with respect to the scalar distance $r = |\mathbf{x} - \mathbf{x}_0|$, and the order of the singularity is reduced from the nominal value of $1/r^2$ to the actual value of $1/r$. Because of the weak nature of the singularity, the Fredholm-Riesz theory of compact operators may be used to study the properties of the solution. The computation of the principal value of the double-layer potential, however, requires careful attention, as will be discussed in Chapter 5.

4.4.1 Boundary corners

Relation (4.2.12) and subsequent relations (4.4.1) and (4.4.2) are valid only when the surface D is smooth in the neighborhood of the evaluation point \mathbf{x}_0 , that is, D has a continuously varying normal vector.

To derive an integral representation equation at a corner point, we note that the integral of the three-dimensional Dirac delta function over the conical volume depicted in Figure 4.4.1(a) is equal to $\alpha/(4\pi)$. The solid angle α is defined as the surface area of the sector of the unit sphere that is centered at the point \mathbf{x}_0 and is enclosed by the cone. Using this property, we find that, when the point \mathbf{x}_0 lies at a boundary corner, as depicted in Figure 4.4.1(b), the boundary-integral representation takes the form

$$\begin{aligned} f(\mathbf{x}_0) = & -\frac{4\pi}{\alpha} \int_D G(\mathbf{x}, \mathbf{x}_0) [\mathbf{n}(\mathbf{x}) \cdot \nabla f(\mathbf{x})] dS(\mathbf{x}) \\ & + \frac{4\pi}{\alpha} \int_D^{PV} f(\mathbf{x}) [\mathbf{n}(\mathbf{x}) \cdot \nabla G(\mathbf{x}, \mathbf{x}_0)] dS(\mathbf{x}). \end{aligned} \quad (4.4.4)$$

When $\alpha = 2\pi$, the boundary is locally smooth, and (4.4.4) reduces to the standard representation (4.4.2).

4.4.2 Hypersingular equations

Integral equations for the boundary distribution of the gradient and normal derivative can be derived from the integral representation (4.3.6) or (4.3.7), as discussed in Section 2.5.

Taking, for example, the limit as the point \mathbf{x}_0 approaches the boundary D , and projecting the resulting expression onto the normal vector, we obtain the “hypersingular

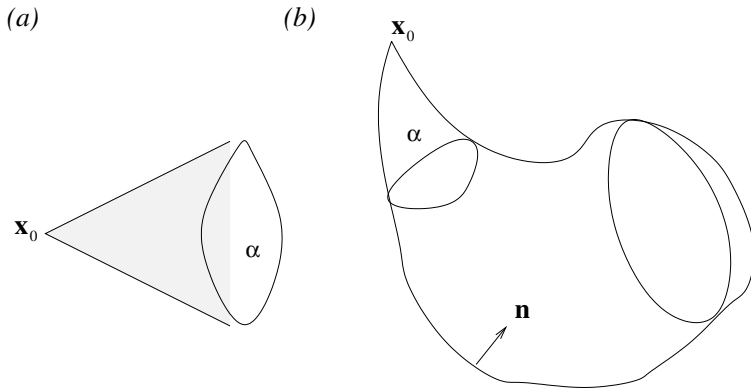


Figure 4.4.1 Illustration of (a) a conical domain with apex at the point \mathbf{x}_0 , and (b) a control volume whose boundary contains a corner.

integral equation”

$$\frac{1}{2} n_i(\mathbf{x}_0) \frac{\partial f(\mathbf{x}_0)}{\partial x_{0i}} = - \int_D^{PV} n_i(\mathbf{x}_0) \frac{\partial G(\mathbf{x}_0, \mathbf{x})}{\partial x_{0i}} [\mathbf{n}(\mathbf{x}) \cdot \nabla f(\mathbf{x})] dS(\mathbf{x}) + \int_D^{FP} f(\mathbf{x}) n_i(\mathbf{x}_0) \frac{\partial^2 G(\mathbf{x}_0, \mathbf{x})}{\partial x_{0i} \partial x_j} n_j(\mathbf{x}) dS(\mathbf{x}), \quad (4.4.5)$$

where

$$\int_D^{FP} f(\mathbf{x}) n_i(\mathbf{x}_0) \frac{\partial^2 G(\mathbf{x}_0, \mathbf{x})}{\partial x_{0i} \partial x_j} n_j(\mathbf{x}) dS(\mathbf{x}) \equiv \lim_{\epsilon \rightarrow 0} \left\{ \int_D f(\mathbf{x}) n_i(\mathbf{x}_0) \frac{\partial^2 G(\mathbf{x}_0, \mathbf{x})}{\partial x_{0i} \partial x_j} n_j(\mathbf{x}) dS(\mathbf{x}) - \frac{1}{2\epsilon} f(\mathbf{x}_0) \right\}^{PV} \quad (4.4.6)$$

is the finite part of the integral; ϵ is the radius of a small disk centered at the point \mathbf{x}_0 and excluded from the integration domain, and PV denotes the principal value of the integral enclosed by the curly brackets. Equation (4.4.5) is a Fredholm integral equation of the second kind for the boundary distribution of the normal derivative.

Problems

P.4.4.1 Conical boundaries

With reference to Figure 4.4.1(b), show that the solid angle α can be evaluated as

$$\alpha = 4\pi \int_D^{PV} \mathbf{n}(\mathbf{x}) \cdot \nabla G(\mathbf{x}, \mathbf{x}_0) dS(\mathbf{x}). \quad (1)$$

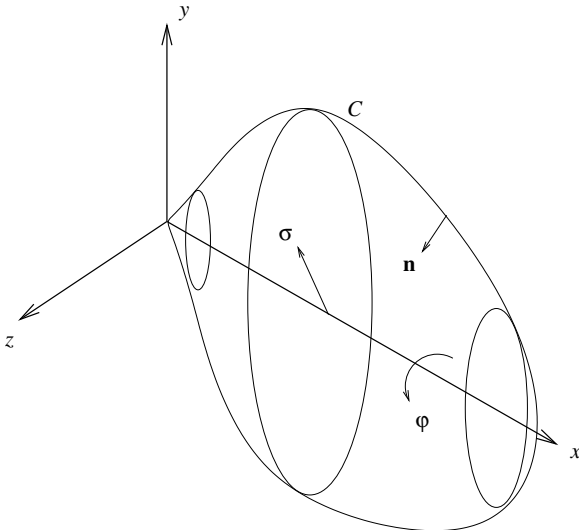


Figure 4.5.1 Illustration of an axisymmetric surface whose trace on the xy meridional plane is the contour C .

P.4.4.2 Shrinking spherical sectors

The integral representation (4.4.2) may be derived in an alternative fashion that circumvents the unusual properties of the delta function. A key observation is that the integral identity (4.3.2) is valid so long as the evaluation point lies outside the solution domain, however close the point is to the boundaries. Working as in Section 2.4.2 for the corresponding problem in two dimensions, but using a shrinking spherical sector instead of a circular arc, reproduce the representation (4.4.4).

4.5 Axisymmetric fields in axisymmetric domains

Consider Green's third identity (4.3.5), and assume that the solution domain and the solution itself are both rotationally symmetric about the x axis, as illustrated in Figure 4.5.1. Because of the axial symmetry, the meridional component of the normal vector over the boundary D vanishes, $n_\varphi = 0$, the meridional component of the gradient ∇f is zero, and the function f and the axial and radial components of ∇f depend on x and σ but not on φ .

Taking advantage of these simplifications, and expressing the differential surface

area dS in the form $\sigma d\varphi dl$, where dl is the differential arc length along the contour C of the surface in a meridional plane, we recast (4.3.5) into the form

$$\begin{aligned} f(x_0, \sigma_0) = & - \int_0^{2\pi} \int_C G(\mathbf{x}, \mathbf{x}_0) [n_x \frac{\partial f}{\partial x} + n_\sigma \frac{\partial f}{\partial \sigma}](\mathbf{x}) \sigma(\mathbf{x}) dl(\mathbf{x}) d\varphi \\ & + \int_0^{2\pi} \int_C f(\mathbf{x}) [n_x(\mathbf{x}) \frac{\partial G(\mathbf{x}, \mathbf{x}_0)}{\partial x} + n_\sigma(\mathbf{x}) \frac{\partial G(\mathbf{x}, \mathbf{x}_0)}{\partial \sigma}] \sigma(\mathbf{x}) dl(\mathbf{x}) d\varphi. \end{aligned} \quad (4.5.1)$$

An equivalent form is

$$\begin{aligned} f(x_0, \sigma_0) = & - \int_C G^{AX}(x, \sigma, x_0, \sigma_0) [n_x \frac{\partial f}{\partial x} + n_\sigma \frac{\partial f}{\partial \sigma}](\mathbf{x}) \sigma(\mathbf{x}) dl(\mathbf{x}) \\ & + \int_C f(\mathbf{x}) [n_x(\mathbf{x}) \frac{\partial G^{AX}(x, \sigma, x_0, \sigma_0)}{\partial x} + n_\sigma(\mathbf{x}) \frac{\partial G^{AX}(x, \sigma, x_0, \sigma_0)}{\partial \sigma}] \sigma(\mathbf{x}) dl(\mathbf{x}), \end{aligned} \quad (4.5.2)$$

where G^{AX} is the free-space axisymmetric Green's function defined as

$$G^{AX}(x, \sigma, x_0, \sigma_0) \equiv \frac{1}{4\pi} \int_0^{2\pi} \frac{d\varphi}{|\mathbf{x} - \mathbf{x}_0|}. \quad (4.5.3)$$

Physically, the axisymmetric Green's function represents the field at the point (x_0, σ_0) due to a ring distribution of point-source singularities of radius σ positioned at x .

In vector notation, the integral representation (4.5.2) takes the form

$$\begin{aligned} f(x_0, \sigma_0) = & - \int_C G^{AX}(x, \sigma, x_0, \sigma_0) [\mathbf{n}(\mathbf{x}) \cdot \nabla f(\mathbf{x})] \sigma(\mathbf{x}) dl(\mathbf{x}) \\ & + \int_C f(\mathbf{x}) [\mathbf{n}(\mathbf{x}) \cdot \nabla G^{AX}(x, \sigma, x_0, \sigma_0)] \sigma(\mathbf{x}) dl(\mathbf{x}), \end{aligned} \quad (4.5.4)$$

where the unit normal vector \mathbf{n} on the right-hand side points into the control area enclosed by the contour C .

The corresponding integral equation is

$$\begin{aligned} f(x_0, \sigma_0) = & -2 \int_C G^{AX}(x, \sigma, x_0, \sigma_0) [\mathbf{n}(\mathbf{x}) \cdot \nabla f(\mathbf{x})] \sigma(\mathbf{x}) dl(\mathbf{x}) \\ & + 2 \int_C^{PV} f(\mathbf{x}) [\mathbf{n}(\mathbf{x}) \cdot \nabla G^{AX}(x, \sigma, x_0, \sigma_0)] \sigma(\mathbf{x}) dl(\mathbf{x}), \end{aligned} \quad (4.5.5)$$

where PV denotes the principal-value integral.

4.5.1 Computation of the free-space axisymmetric Green's function

Expressing the position vector on the right-hand side of (4.5.3) in cylindrical polar coordinates as $y = \sigma \cos \varphi$, $z = \sigma \sin \varphi$, $y_0 = \sigma_0 \cos \varphi_0$, and $z_0 = \sigma_0 \sin \varphi_0$, we find

$$\begin{aligned}
& G^{AX}(x, \sigma, x_0, \sigma_0) \\
&= \frac{1}{4\pi} \int_0^{2\pi} \frac{d\varphi}{\sqrt{(x - x_0)^2 + (y - y_0)^2 + (z - z_0)^2}} \\
&= \frac{1}{4\pi} \int_0^{2\pi} \frac{d\varphi}{[(x - x_0)^2 + (\sigma \cos \phi - \sigma_0 \cos \phi_0)^2 + (\sigma \sin \phi - \sigma_0 \sin \phi_0)^2]^{1/2}} \\
&= \frac{1}{4\pi} \int_0^{2\pi} \frac{d(\varphi - \varphi_0)}{[(x - x_0)^2 + \sigma^2 + \sigma_0^2 - 2\sigma\sigma_0 \cos(\varphi - \varphi_0)]^{1/2}} \\
&= \frac{\sigma}{4\pi} \int_0^{2\pi} \frac{du}{[(x - x_0)^2 + \sigma^2 + \sigma_0^2 - 2\sigma\sigma_0 \cos u]^{1/2}} \\
&= \frac{1}{4\pi} \int_0^{2\pi} \frac{du}{[(x - x_0)^2 + (\sigma + \sigma_0)^2 - 4\sigma\sigma_0 \cos^2 \frac{u}{2}]^{1/2}} \\
&= \frac{1}{\pi \sqrt{(x - x_0)^2 + (\sigma + \sigma_0)^2}} \int_0^{2\pi} \frac{du}{\sqrt{1 - k^2 \cos^2 \frac{u}{2}}} \\
&= \frac{F(k)}{\pi \sqrt{(x - x_0)^2 + (\sigma + \sigma_0)^2}}, \tag{4.5.6}
\end{aligned}$$

where $u = \varphi - \varphi_0$, and

$$k^2 \equiv \frac{4\sigma\sigma_0}{(x - x_0)^2 + (\sigma + \sigma_0)^2}. \tag{4.5.7}$$

We have introduced the complete elliptic integral of the first kind

$$F(k) \equiv \int_0^{\pi/2} \frac{d\eta}{\sqrt{1 - k^2 \cos^2 \eta}}, \tag{4.5.8}$$

where η is a dummy variable of integration.

In the limit as x tends to x_0 and σ tends to σ_0 , the dimensionless variable k tends to unity, and $F(k)$ behaves like

$$F(k) \simeq \ln \frac{4}{k_1} + O(k_1^2 \ln k_1), \tag{4.5.9}$$

where

$$k_1^2 \equiv 1 - k^2 = \frac{(x - x_0)^2 + (\sigma - \sigma_0)^2}{(x - x_0)^2 + (\sigma + \sigma_0)^2}. \quad (4.5.10)$$

Substituting (4.5.10) into (4.5.9) and the result into the last expression of (4.5.6), we find that, in the limit as x tends to x_0 and σ tends to σ_0 ,

$$G^{AX}(x, \sigma, x_0, \sigma_0) \simeq -\frac{1}{2\pi\sigma_0} \ln[(x - x_0)^2 + (\sigma - \sigma_0)^2]^{1/2}. \quad (4.5.11)$$

In this limit, the integrands of the single- and double-layer potential on the right-hand sides of (4.5.4) and (4.5.5) reduce to the corresponding integrands of the boundary-integral representation for Laplace's equation in two dimensions defined over a meridional plane.

4.5.2 BEMLIB directory `lgf_ax`

Subdirectory `lgf_ax` of directory `laplace` of *BEMLIB* contains subroutines that evaluate (a) the free-space axisymmetric Green's function, and (b) the axisymmetric Green's and Neumann functions for a semi-infinite domain bounded by a plane wall that is perpendicular to the x axis.

4.5.3 Boundary-element methods

Boundary-element methods for solving Laplace's equation in axisymmetric domains are straightforward extensions of those for two-dimensional domains, as discussed in Chapter 3.

Subdirectory `body_ax` in directory `laplace` of *BEMLIB* contains a code that computes potential flow past, or due to the motion of, an axisymmetric body. The problem formulation and particulars of the numerical method are discussed in the corresponding section of the *BEMLIB* user guide (Chapter 10).

Problem

P.4.5.1 BEMLIB code `body_ax`

Study the mathematical formulation and the numerical method, and run the code in subdirectory `body_ax` of directory `laplace` of *BEMLIB* for a configuration of your choice. Prepare graphs and discuss the results of your computation.

Chapter 5

Boundary-element methods for Laplace's equation in three dimensions

In Chapter 3, we discussed the implementation of the boundary-element method for Laplace's equation in two dimensions. The general methodology involves discretizing the boundary of a selected control area into line elements with straight or curved shapes, introducing approximations for the unknown function over the individual elements, and deriving systems of linear equations for the coefficients of the local expansions by demanding the discrete satisfaction of the integral equation.

The approach can be extended in a straightforward fashion to encompass problems in three-dimensional domains where the boundary-integral formulation provides us with integral representations and integral equations defined over three-dimensional surfaces. The implementation of the boundary-element method involves discretizing the surfaces enclosing a selected control volume into three-dimensional elements with flat or curved shapes, introducing local approximations for the unknown functions in local surface coordinates, and, finally, generating and solving systems of linear equations for the coefficients of the local expansions.

In this chapter, we illustrate the implementation of these steps for the most popular class of three-dimensional elements with flat or curved triangular shapes. We shall see that an important consideration in the development of numerical methods is the accurate evaluation of the singular single- and double-layer integrals over the individual boundary elements. This concern makes the implementation of the boundary-element method in three dimensions significantly more challenging than that of its two-dimensional and axisymmetric counterparts.

5.1 Discretization

Consider the integral representation of a harmonic function in terms of the single- and double-layer potential defined over a surface D that encloses a selected control volume, as shown in equation (4.3.3). The boundary-element method involves discretizing the surface D into a collection of N boundary elements, denoted by E_i ,

where $i = 1, \dots, N$, and replacing the integrals over D with sums of integrals over the boundary elements to obtain the discrete representation

$$\begin{aligned} f(\mathbf{x}_0) = & - \sum_{i=1}^N \int_{E_i} G(\mathbf{x}, \mathbf{x}_0) [\mathbf{n}(\mathbf{x}) \cdot \nabla f(\mathbf{x})] dS(\mathbf{x}) \\ & + \sum_{i=1}^N \int_{E_i} f(\mathbf{x}) [\mathbf{n}(\mathbf{x}) \cdot \nabla G(\mathbf{x}, \mathbf{x}_0)] dS(\mathbf{x}), \end{aligned} \quad (5.1.1)$$

where the unit normal vector \mathbf{n} points into the control area enclosed by D .

5.1.1 Triangulation

Any open or closed three-dimensional surface may be triangulated, that is, divided into flat or curved triangular elements, each defined by a group of element nodes. The collection of the elements defines an unstructured surface grid defined by the global grid nodes.

Compared to a structured grid defined in global curvilinear coordinates over the whole surface, the unstructured grid has two significant advantages: the local curvilinear coordinates over each element are nonsingular, whereas the structured grid may have singular points; and the element shape and size may be readily controlled to improve the spatial resolution at selected regions. Moreover, the unstructured discretization is readily amenable to the finite-volume and finite-element formulations for solving partial differential equations in fixed or evolving domains.

As an example, we consider the triangulation of a three-dimensional surface into flat triangles, as illustrated in Figure 5.1.1. Each triangle is defined by three nodes numbered in the counterclockwise direction with respect to the normal vector, as will be discussed in Section 5.2. The surface grid is described by the following scalar labels and connectivity tables generated in the process of triangulation:

- Element labels, printed in bold in Figure 5.1.1.
- Global node labels, printed in italic in Figure 5.1.1.
- Local node labels, printed in roman for one element in Figure 5.1.1. In the case of flat triangles presently considered, the local node labels range over 1, 2, and 3. In the case of the curved triangles to be discussed in Section 5.3, the local node labels range over 1, 2, ..., 6.
- A two-dimensional array ne defined such that $ne(i, 1)$ is the number of elements sharing the i th global node. Subsequent entries,

$$ne(i, 2), \dots, ne(i, ne(i, 1) + 1),$$

are the labels of the elements sharing the i th node.

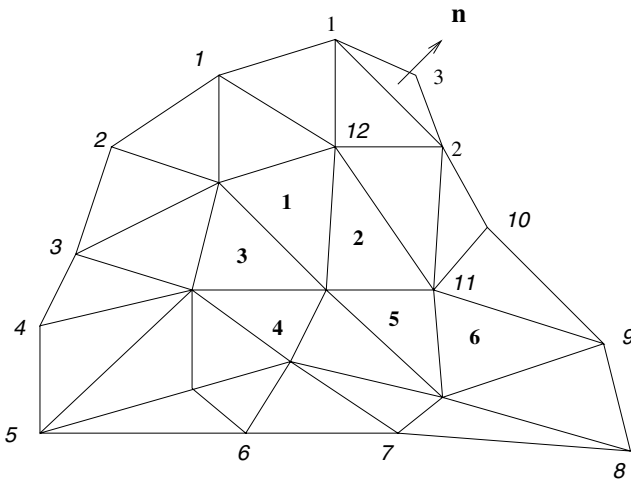


Figure 5.1.1 Triangulation of a three-dimensional surface into a grid of flat triangles defined by three nodes. The bold-faced numbers are the element labels, and the italic numbers are the global node labels. The three roman numbers 1, 2, 3, are the local node labels of the element on the right top corner.

- A two-dimensional array n defined such that $n(i, j)$ is the global label of the j local node of the i th element, where $j = 1, 2, 3$.

These records are useful for computing node from element values of surface functions and vice versa, and for performing various ancillary computations involved in the boundary-element implementation.

Suppose, for example, that a surface function has been approximated with a piecewise constant function over each element. The value of the function at the i th global node, denoted by f_i , can be approximated with the average of the values of the function on the elements that share that node, denoted by f_j^E , using the formula

$$f_i = \frac{1}{ne(i, 1)} \sum_{j=2}^{ne(i, 1)+1} f_j^E. \quad (5.1.2)$$

Several algorithms are available for triangulating planar and three-dimensional, open and closed surfaces, as reviewed in Reference [38]. The advancing-front method, in particular, can be used to perform adaptive triangulation in physical or parameter space, according to the local mean or directional curvature. The simplest discretization algorithm is based on element subdivision beginning with a hard-coded coarse pattern.

5.1.2 Successive subdivision

A closed three-dimensional surface with a compact shape can be triangulated in a recursive fashion by the process of successive element subdivision. To triangulate the surface of a sphere, we introduce a regular tetrahedron, octahedron, or icosahedron inscribed within the sphere (these are the lowest-order polyhedra whose faces are equilateral triangles), and recursively subdivide the faces of the polyhedra into four descendant faces by connecting the edge mid-points, as illustrated in Figure 5.1.2. At the end, or in the meanwhile, the new vertices and mid-points are projected onto the surface of the sphere. The final grid may then be deformed to yield a triangulated three-dimensional surface that is topologically similar to the sphere.

Program `trg1` in directory `grids` of *BEMLIB* triangulates a sphere based on the successive subdivision of an octahedron or icosahedron, and then deforms the surface grid to produce an ellipsoidal shape with specified axes ratios. Typical triangulations are shown in Figure 5.1.3.

5.1.3 Local element approximation

Having defined the boundary elements, we introduce local approximations for the distribution of the harmonic function f and its normal derivative $\mathbf{n} \cdot \nabla f$.

In the simplest implementation, we approximate both distributions with constant functions over each element, denoted respectively by f_i and $\left(\frac{\partial f}{\partial n}\right)_i$, where $i = 1, \dots, N$, yielding the discrete boundary-element representation

$$\begin{aligned} f(\mathbf{x}_0) &= - \sum_{i=1}^N \left(\frac{\partial f}{\partial n} \right)_i \int_{E_i} G(\mathbf{x}, \mathbf{x}_0) dS(\mathbf{x}) \\ &\quad + \sum_{i=1}^N f_i \int_{E_i} [\mathbf{n}(\mathbf{x}) \cdot \nabla G(\mathbf{x}, \mathbf{x}_0)] dS(\mathbf{x}). \end{aligned} \quad (5.1.3)$$

The integrals over the boundary elements on the right-hand side are the influence coefficients associated with the single- and double-layer potential.

The counterpart of the representation (5.1.3) for a point \mathbf{x}_0 that lies on one of the boundary elements is

$$\begin{aligned} f(\mathbf{x}_0) &= -2 \sum_{i=1}^N \left(\frac{\partial f}{\partial n} \right)_i \int_{E_i} G(\mathbf{x}, \mathbf{x}_0) dS(\mathbf{x}) \\ &\quad + 2 \sum_{i=1}^N f_i \int_{E_i}^{PV} [\mathbf{n}(\mathbf{x}) \cdot \nabla G(\mathbf{x}, \mathbf{x}_0)] dS(\mathbf{x}). \end{aligned} \quad (5.1.4)$$

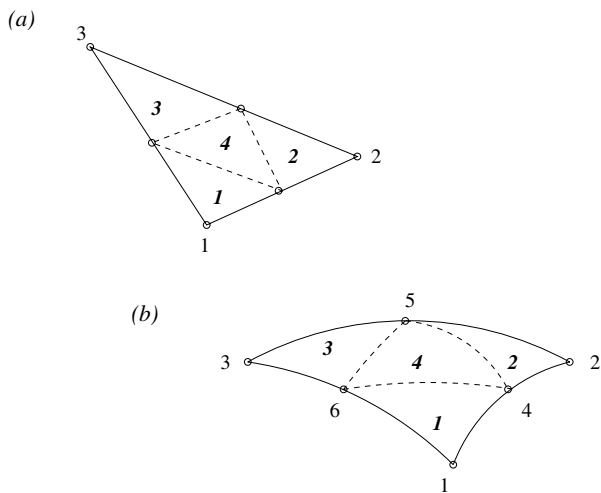


Figure 5.1.2 Subdivision of (a) a flat, and (b) a six-node curved triangle into four descendant triangles.

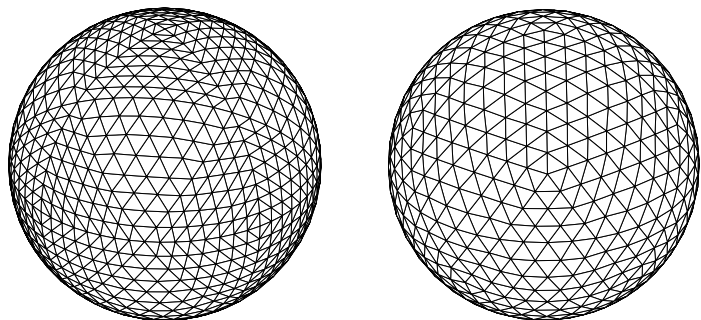


Figure 5.1.3 Triangulation of the surface of a sphere based on the successive subdivision of an octahedron (left) or icosahedron (right).

The qualified PV , denoting the principal-value integral, applies only to those elements that share the evaluation point \mathbf{x}_0 .

5.1.4 Point collocation

To compute the unknown element values of the function f or its normal derivative, we apply the discretized integral equation (5.1.4) at the mid-point of each boundary element, denoted by \mathbf{x}_j^M , where $j = 1, \dots, N$, and obtain

$$\begin{aligned} f(\mathbf{x}_j^M) &= -2 \sum_{i=1}^N \left(\frac{\partial f}{\partial n} \right)_i \int_{E_i} G(\mathbf{x}, \mathbf{x}_j^M) dS(\mathbf{x}) \\ &\quad + 2 \sum_{i=1}^N f_i \int_{E_i}^{PV} [\mathbf{n}(\mathbf{x}) \cdot \nabla G(\mathbf{x}, \mathbf{x}_j^M)] dS(\mathbf{x}). \end{aligned} \quad (5.1.5)$$

Setting $f(\mathbf{x}_j^M) = f_j$, writing $f_i = \delta_{ij} f_j$, and rearranging, we derive the algebraic relation

$$(A_{ij} - \frac{1}{2} \delta_{ij}) f_i = B_{ji} \left(\frac{\partial f}{\partial n} \right)_i, \quad (5.1.6)$$

where δ_{ij} is Kronecker's delta; summation over the repeated index i is implied on both sides of (5.1.6). We have introduced the coefficient matrices

$$A_{ij} \equiv \int_{E_i} G(\mathbf{x}, \mathbf{x}_j^M) dS(\mathbf{x}), \quad (5.1.7)$$

$$B_{ij} \equiv \int_{E_i}^{PV} [\mathbf{n}(\mathbf{x}) \cdot \nabla G(\mathbf{x}, \mathbf{x}_j^M)] dS(\mathbf{x}). \quad (5.1.8)$$

If the element values f_i are specified, equation (5.1.6) provides us with a system of linear algebraic equations for the normal derivatives $\left(\frac{\partial f}{\partial n} \right)_i$, and vice versa.

5.1.5 High-order methods

The constant-element approximation underlying expression (5.1.4) is the simplest implementation of the boundary-element method. Higher-order methods involve linear, quadratic, or high-order polynomial expansions of the surface functions over the individual boundary elements. The implementation of these methods will be discussed in Section 5.4.

Problem

P.5.1.1 Boundary-element discretization

- (a) Use program `trgl` in directory `grids` of *BEMLIB* to triangulate the surface of a spheroid of your choice, and prepare a three-dimensional illustration of the triangulated surface.
- (b) Write a subroutine called `trgl_tetra` that triangulates the surface of the unit sphere based on the successive subdivisions of a tetrahedron, and prepare three-dimensional illustrations of a triangulated surface for three levels of discretization.
-

5.2 Three-node flat triangles

In the simplest implementation of the boundary-element method, the boundary elements of a triangulated surface have flat shapes defined by three vertex nodes, as illustrated on the left of Figure 5.2.1.

To describe the surface of an element in parametric form, we map the triangle in the physical three-dimensional space to a right isosceles triangle in the $\xi\eta$ parametric plane, as shown in Figure 5.2.1. The first element node is mapped to the origin, the second is mapped to the point $\xi = 1, \eta = 0$ on the ξ axis, and the third is mapped to the point $\xi = 0, \eta = 1$ on the η axis.

The mapping from physical to parametric space is mediated by the function

$$\mathbf{x} = \mathbf{x}_1 \zeta + \mathbf{x}_2 \xi + \mathbf{x}_3 \eta, \quad (5.2.1)$$

where $\zeta = 1 - \xi - \eta$. The trio of surface variables (ξ, η, ζ) constitutes the barycentric triangle coordinates.

The tangential vectors in the directions of the ξ or η axes over the triangle are given by

$$\mathbf{e}_\xi = \frac{\partial \mathbf{x}}{\partial \xi} = \mathbf{x}_2 - \mathbf{x}_1, \quad \mathbf{e}_\eta = \frac{\partial \mathbf{x}}{\partial \eta} = \mathbf{x}_3 - \mathbf{x}_1, \quad (5.2.2)$$

the corresponding metric coefficients are given by

$$h_\xi \equiv \left| \frac{\partial \mathbf{x}}{\partial \xi} \right| = |\mathbf{x}_2 - \mathbf{x}_1|, \quad h_\eta \equiv \left| \frac{\partial \mathbf{x}}{\partial \eta} \right| = |\mathbf{x}_3 - \mathbf{x}_1|, \quad (5.2.3)$$

and the unit normal vector is given by

$$\mathbf{n} = \frac{1}{h_S} \mathbf{e}_\xi \times \mathbf{e}_\eta, \quad (5.2.4)$$

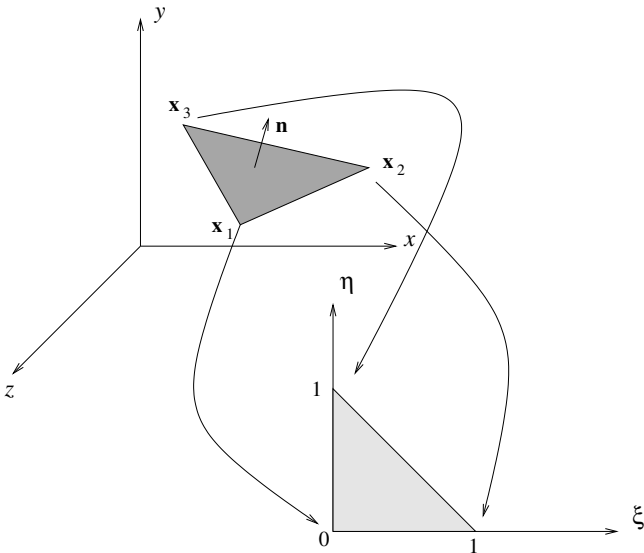


Figure 5.2.1 A flat triangle in three-dimensional space is mapped to a right isosceles triangle in the $\xi\eta$ plane.

where

$$h_S = |\mathbf{e}_\xi \times \mathbf{e}_\eta| = \text{Det} \begin{bmatrix} x_1 & x_2 & x_3 \\ y_1 & y_2 & y_3 \\ z_1 & z_2 & z_3 \end{bmatrix} \quad (5.2.5)$$

is the surface metric, and Det denotes the determinant. The surface area of the triangle is equal to $A = \frac{1}{2} h_S$. Note that all metrics and the normal vector are constant, independent of position over the surface of the triangle.

The integral of a function $f(\mathbf{x})$ over the surface of the triangle in physical space is given by

$$\int_{\text{Triangle}} f(\mathbf{x}) dS = h_S \int_0^1 \int_0^{1-\xi} f[\mathbf{x}(\xi, \eta)] d\eta d\xi. \quad (5.2.6)$$

Setting $f = 1$ and performing the integration confirms our earlier statement that the surface area of the triangle is equal to $\frac{1}{2} h_S$.

5.2.1 Non-singular triangles

If the surface function $f(\mathbf{x})$ is non-singular over the surface of the triangle, the integral (5.2.6) may be computed accurately using a quadrature that is specifically

designed for integrating over the surface of a triangle, according to the formula

$$\int_{\text{Triangle}} f(\mathbf{x}) dS \simeq \frac{1}{2} h_S \sum_{k=1}^{N_Q} f[\mathbf{x}(\xi_k, \eta_k)] w_k, \quad (5.2.7)$$

where:

- N_Q is a specified number of *quadrature base points*.
- (ξ_k, η_k) are the coordinates of the k th base point located inside or along the edges of the right isosceles triangle in parametric space.
- w_k is the integration weight corresponding to the k th base point. The sum of the integration weights is equal to unity for any value of N_Q , so that, when f is a constant function, quadrature (5.2.7) produces the exact answer.

Quadratures for integrating over triangles have been developed by several authors [12, 16]. Mathematical handbooks and texts on numerical methods provide us with tables of the triplets (ξ_k, η_k, w_k) parametrized by N_Q . Subroutine gauss_trg1 in subdirectory 07_integration of directory num_meth of *BEMLIB* contains tabulated triplets for $N_Q = 1, 3, 4, 6, 7, 9, 12$, and 13.

5.2.2 Single-layer integral over singular triangles

When the single-layer potential is evaluated at a vertex point of a flat triangle, the integrand $f(\mathbf{x})$ exhibits a $1/r$ singularity characteristic of the Green's function of Laplace's equation in three dimensions.

Suppose, for example, that the singular point is the first vertex; if it is another vertex, the nodes are temporarily relabeled. The single-layer integral over the triangle takes the form

$$\begin{aligned} I &= \int_{\text{Triangle}} \frac{q(\mathbf{x})}{|\mathbf{x} - \mathbf{x}_1|} dS \\ &= h_S \int_0^1 \int_0^{1-\xi} \frac{q[(\mathbf{x}(\xi, \eta))]}{|(\mathbf{x}_2 - \mathbf{x}_1)\xi + (\mathbf{x}_3 - \mathbf{x}_1)\eta|} d\eta d\xi \\ &= \frac{h_S}{|\mathbf{x}_2 - \mathbf{x}_1|} \int_0^1 \int_0^{1-\xi} \frac{q[(\mathbf{x}(\xi, \eta))]}{\sqrt{\xi^2 + 2B\xi\eta + C\eta^2}} d\eta d\xi, \end{aligned} \quad (5.2.8)$$

where $q(\mathbf{x})$ is a non-singular surface function, and we have defined the constants

$$B = \frac{(\mathbf{x}_3 - \mathbf{x}_1) \cdot (\mathbf{x}_2 - \mathbf{x}_1)}{|\mathbf{x}_2 - \mathbf{x}_1|^2}, \quad C = \frac{|\mathbf{x}_3 - \mathbf{x}_1|^2}{|\mathbf{x}_2 - \mathbf{x}_1|^2}. \quad (5.2.9)$$

Three methods of computing the improper single-layer integral are the following:

- Introduce plane polar coordinates in the $\xi\eta$ plane, denoted by (ρ, χ) and defined such that $\xi = \rho \cos \chi$ and $\eta = \rho \sin \chi$, express the differential area in the parametric plane as $\rho d\rho d\chi$, and recast the last expression in (5.2.8) into the form

$$I = \frac{h_S}{|\mathbf{x}_2 - \mathbf{x}_1|} \int_0^{\pi/2} \frac{\int_0^{R(\chi)} q(\rho, \chi) d\rho}{\sqrt{\cos^2 \chi + B \sin 2\chi + C \sin^2 \chi}} d\chi, \quad (5.2.10)$$

where

$$R(\chi) = \frac{1}{\cos \chi + \sin \chi}. \quad (5.2.11)$$

The change of variables has caused the singularity to disappear. The inner and outer integrals in (5.2.11) may be computed accurately by the Gauss-Legendre quadrature.

- Express the integral in the form

$$I = \frac{h_S}{|\mathbf{x}_2 - \mathbf{x}_1|} \int_0^1 \int_0^{1-\xi} \frac{g[(\mathbf{x}(\xi, \eta))]}{\sqrt{\xi^2 + \eta^2}} d\eta d\xi, \quad (5.2.12)$$

where

$$g[(\mathbf{x}(\xi, \eta))] \equiv q[(\mathbf{x}(\xi, \eta))] \left(\frac{\xi^2 + \eta^2}{\xi^2 + 2B \xi \eta + C \eta^2} \right)^{1/2}, \quad (5.2.13)$$

and compute the integral on the right-hand side of (5.2.12) using a specialized integration quadrature (e.g., [52]).

- Approximate the surface function $q[\mathbf{x}(\xi, \eta)]$ with a constant or linear function with respect to ξ and η over the triangle, and perform the integration by analytical methods (e.g., [13]).

The first method is superior in terms of accuracy and ease of implementation.

5.2.3 Double-layer integral over singular triangles

When the single-layer potential is evaluated at a point \mathbf{x}_0 that lies on a flat triangle, the integrand of the principal value of the double-layer potential associated with the free-space Green's function is identically equal to zero,

$$\mathbf{n}(\mathbf{x}) \cdot \nabla G(\mathbf{x}, \mathbf{x}_0) = \mathbf{n}(\mathbf{x}) \cdot (\mathbf{x} - \mathbf{x}_0) \frac{1}{4\pi r^3} = 0, \quad (5.2.14)$$

where $r = |\mathbf{x} - \mathbf{x}_0|$. This is because the vector $(\mathbf{x} - \mathbf{x}_0)$ lies in the plane of the triangle, and is thus perpendicular to the normal vector at any position.

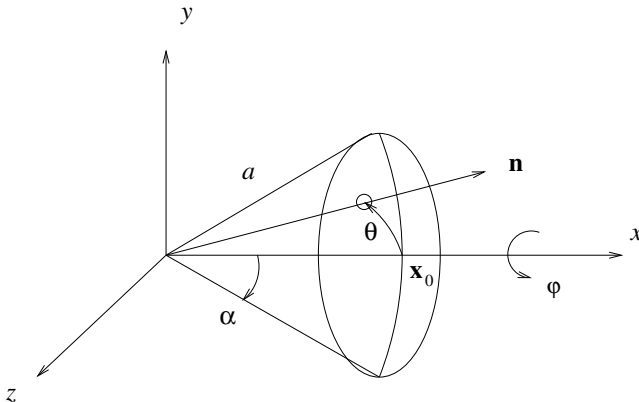


Figure 5.2.2 The double-layer potential with constant density can be evaluated analytically over a spherical cap.

The vanishing of the double-layer potential over a flat triangle is a mixed blessing. On the one hand, we do not need to evaluate the corresponding influence coefficient, and we can simply set the diagonal elements of the matrix B_{ij} introduced in (5.1.7) equal to zero. On the other hand, the associated discretization error is on the order of $\delta \kappa_m / (4\pi)$, where δ is the perimeter of the triangle and κ_m is the mean curvature of the undiscretized surface. Unless the element size is sufficiently small, this error can be substantial.

To illustrate the issue of accuracy, we consider the principal value of the double-layer integral over a spherical cap of radius a and aperture α , evaluated at the cap axis, $\theta = 0$, as depicted in Figure 5.2.2. We note that $\mathbf{n}(\mathbf{x}) \cdot (\mathbf{x} - \mathbf{x}_0) = a(1 - \cos \theta) = 2a \sin^2 \frac{\theta}{2}$ and $r = 2a \sin \frac{\theta}{2}$, and perform the integration in spherical polar coordinates to find

$$\begin{aligned} & \int_{Cap}^{PV} \mathbf{n}(\mathbf{x}) \cdot \nabla G(\mathbf{x}, \mathbf{x}_0) dS(\mathbf{x}) \\ &= \frac{1}{4\pi} \int_0^\alpha \frac{2a \sin^2 \frac{\theta}{2}}{(2a \sin \frac{\theta}{2})^3} 2\pi a^2 \sin \theta d\theta = \frac{1}{2} \sin \frac{\alpha}{2}. \end{aligned} \quad (5.2.15)$$

This formula shows that replacing a spherical cap with aperture angle $\alpha = \pi/2$ with a flat triangle anchored at three points along the circumference introduces an error on the order of 0.3, which is substantial.

Problems

P.5.2.1 Quadrature for integrating over a triangle

Use subroutine `gauss_trgl` in subdirectory `07_integration` of directory `mum_meth` of *BEMLIB* to compute the integral of a surface function over a triangle of your choice, and discuss the accuracy of your results.

P.5.2.2 Double-layer integral

Evaluate (5.2.15) for $\alpha = \pi$, and explain why the result is consistent with the integral identity (4.2.11).

5.3 Six-node curved triangles

To account for the curvature of a surface, we use boundary elements with curved sides and surfaces defined by six nodes, including three vertex nodes and three edge nodes, as illustrated on the left of Figure 5.3.1.

To describe the surface of an element in parametric form, we map each curved triangle in physical three-dimensional space to the familiar right isosceles triangle in the $\xi\eta$ plane, as illustrated in figure 5.3.1. The first element node is mapped to the origin, the second is mapped to the point $\xi = 1, \eta = 0$ on the ξ axis, the third is mapped to the point $\xi = 0, \eta = 1$ on the η axis, the fourth is mapped to the point $\xi = \alpha, \eta = 0$, the fifth is mapped to the point $\xi = \gamma, \eta = 1 - \gamma$, and the sixth is mapped to the point $\xi = 0, \eta = \beta$.

The mapping from physical to parameter space is mediated by the function

$$\mathbf{x} = \sum_{i=1}^6 \mathbf{x}_i \phi_i(\xi, \eta), \quad (5.3.1)$$

where $\phi(\xi, \eta)$ are element-node cardinal interpolation functions defined as

$$\phi_2 = \frac{1}{1-\alpha} \xi \left(\xi - \alpha + \frac{\alpha - \gamma}{1-\gamma} \eta \right),$$

$$\phi_3 = \frac{1}{1-\beta} \eta \left(\eta - \beta + \frac{\beta + \gamma - 1}{\gamma} \xi \right),$$

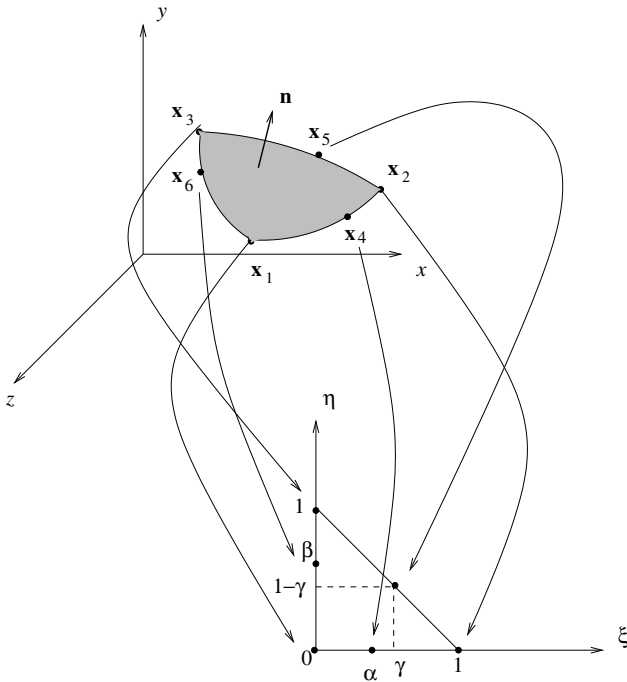


Figure 5.3.1 A curved six-node triangle in three-dimensional space is mapped to a right isosceles triangle in the $\xi\eta$ plane.

$$\phi_4 = \frac{1}{\alpha(1-\alpha)} \xi (1 - \xi - \eta),$$

$$\phi_5 = \frac{1}{\gamma(1-\gamma)} \xi \eta,$$

$$\phi_6 = \frac{1}{\beta(1-\beta)} \eta (1 - \xi - \eta),$$

$$\phi_1 = 1 - \phi_2 - \phi_3 - \phi_4 - \phi_5 - \phi_6, \quad (5.3.2)$$

and

$$\alpha = \frac{1}{1 + \frac{|\mathbf{x}_4 - \mathbf{x}_2|}{|\mathbf{x}_4 - \mathbf{x}_1|}}, \quad \beta = \frac{1}{1 + \frac{|\mathbf{x}_6 - \mathbf{x}_3|}{|\mathbf{x}_6 - \mathbf{x}_1|}}, \quad \gamma = \frac{1}{1 + \frac{|\mathbf{x}_5 - \mathbf{x}_2|}{|\mathbf{x}_5 - \mathbf{x}_3|}} \quad (5.3.3)$$

are geometrical parameters. If the edge nodes are located at the mid-points, $\alpha = 1/2$, $\beta = 1/2$, and $\gamma = 1/2$, thus yielding the simplified forms

$$\phi_1 = \zeta (2\zeta - 1), \quad \phi_2 = \xi (2\xi - 1), \quad \phi_3 = \eta (2\eta - 1),$$

$$\phi_4 = 4 \xi \zeta, \quad \phi_5 = 4 \xi \eta, \quad \phi_6 = 4 \eta \zeta, \quad (5.3.4)$$

where $\zeta = 1 - \xi - \eta$.

The tangential vectors in the directions of the ξ or η axes in physical space are given by

$$\mathbf{e}_\xi = \frac{\partial \mathbf{x}}{\partial \xi} = \sum_{i=1}^6 \mathbf{x}_i \frac{\partial \phi_i}{\partial \xi}, \quad \mathbf{e}_\eta = \frac{\partial \mathbf{x}}{\partial \eta} = \sum_{i=1}^6 \mathbf{x}_i \frac{\partial \phi_i}{\partial \eta}, \quad (5.3.5)$$

and the corresponding metric coefficients are given by

$$h_\xi(\xi, \eta) \equiv \left| \frac{\partial \mathbf{x}}{\partial \xi} \right|, \quad h_\eta(\xi, \eta) \equiv \left| \frac{\partial \mathbf{x}}{\partial \eta} \right|. \quad (5.3.6)$$

The derivatives on the right-hand side of (5.3.5) may be computed by straightforward differentiation of the expressions given in (5.3.2). The unit normal vector is given by

$$\mathbf{n}(\xi, \eta) = \frac{1}{h_S} \mathbf{e}_\xi \times \mathbf{e}_\eta, \quad (5.3.7)$$

where

$$h_S(\xi, \eta) = |\mathbf{e}_\xi \times \mathbf{e}_\eta| \quad (5.3.8)$$

is the surface metric. In contrast to the case of the three-node flat triangle, neither the metric coefficients nor the unit normal vector are constant over the surface of the six-node curved triangle.

The integral of a function $f(\mathbf{x})$ over the surface of the triangle is given by

$$\int_{Triangle} f(\mathbf{x}) dS = \int_0^1 \int_0^{1-\xi} f[\mathbf{x}(\xi, \eta)] h_S(\xi, \eta) d\eta d\xi. \quad (5.3.9)$$

5.3.1 Non-singular triangles

If the function $f(\mathbf{x})$ is non-singular over the surface of the triangle, the integral (5.3.9) may be computed accurately using a Gauss quadrature specifically designed for the triangle, according to the formula

$$\int_{Triangle} f(\mathbf{x}) dS \simeq \frac{1}{2} \sum_{k=1}^{N_Q} f[\mathbf{x}(\xi_k, \eta_k)] h_S(\xi_k, \eta_k) w_k, \quad (5.3.10)$$

as discussed in Section 5.2.

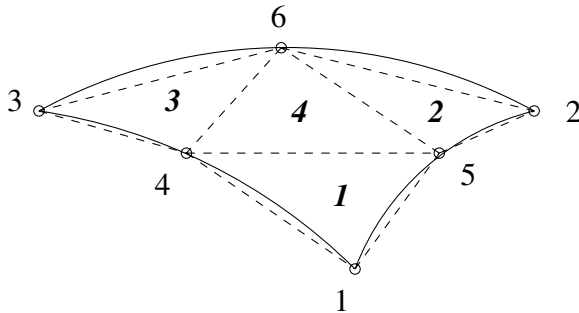


Figure 5.3.2 To evaluate the single-layer integral at a vertex node or edge node of a curved triangle, we replace the triangle with four flat triangles and perform the integration over the individual subelements.

5.3.2 Single-layer integral over singular triangles

When the single-layer potential is evaluated at a vertex or edge node, the integrand $f(\mathbf{x})$ exhibits a $1/r$ singularity characteristic of Green's function. Suppose that the singular point is the first vertex; if it is another vertex, the nodes are temporarily relabeled. Using expressions (5.3.1) and (5.3.2), we find

$$\mathbf{x} - \mathbf{x}_1 = \sum_{i=1}^6 \mathbf{x}_i [\phi_i(\xi, \eta) - \delta_{i1}]. \quad (5.3.11)$$

The single-layer integral over the triangle takes the form

$$\begin{aligned} I &= \int_{Triangle} \frac{q(\mathbf{x})}{|\mathbf{x} - \mathbf{x}_1|} dS \\ &= \int_0^1 \int_0^{1-\xi} \frac{q[(\mathbf{x}(\xi, \eta))]}{\left| \sum_{i=1}^6 \mathbf{x}_i [\phi_i(\xi, \eta) - \delta_{i1}] \right|} h_S(\xi, \eta) d\eta d\xi, \end{aligned} \quad (5.3.12)$$

where $q(\mathbf{x})$ is a non-singular surface function. The last integral may be evaluated accurately by integrating in local polar coordinates, as shown in (5.2.10).

A more efficient method of evaluating the single-layer integral at vertex and edge nodes involves breaking up the curved triangle into four flat triangles, as illustrated in figure 5.3.2, and performing the integration over the individual subelements using the methods discussed in Section 5.2. For the non-singular subelements we use a Gaussian quadrature, whereas for the singular subelements we perform the integration in local plane polar coordinates whose origin lies at the singular point.

5.3.3 Double-layer integral over singular triangles

The evaluation of the double-layer integral over a curved triangle is more challenging. Breaking up the curved triangle into four flat triangles yields vanishing sub-element contributions and incurs substantial numerical error, as discussed in Section 5.2. When the integral is evaluated at a vertex node, the $1/r$ singularity of the double-layer potential may be eliminated by performing the integration in local plane polar coordinates in the $\xi\eta$ plane. The implementation of this method for the edge nodes is less straightforward.

When D is a closed surface, the double-layer integral is computed most accurately by removing the singularity at the outset using the integral identity (4.2.11). The method is implemented by recasting the principal-value integral of the double-layer potential into the regularized form

$$\int_D^{PV} f(\mathbf{x}) [\mathbf{n}(\mathbf{x}) \cdot \nabla G(\mathbf{x}, \mathbf{x}_0)] dS(\mathbf{x}) = \int_D [f(\mathbf{x}) - f(\mathbf{x}_0)] [\mathbf{n}(\mathbf{x}) \cdot \nabla G(\mathbf{x}, \mathbf{x}_0)] dS(\mathbf{x}) + \frac{1}{2} f(\mathbf{x}_0). \quad (5.3.13)$$

Using Taylor series expansions, we find that, as the integration point \mathbf{x} approaches the evaluation point \mathbf{x}_0 , the modified integrand on the right-hand side is non-singular. The limiting value of the integrand, however, depends on the orientation of the nearly tangential vector $(\mathbf{x} - \mathbf{x}_0)$, and the integral is not entirely regular (see P.5.3.2). In practice, the integral may be computed with high accuracy using a Gauss integration quadrature for the triangle.

Problems

P.5.3.1 Cardinal interpolation functions

Verify that the i th interpolation function defined in (5.3.2) takes the value of unity at the i th node and the value of zero at all other nodes.

P.5.3.2 Regularized double-layer

Consider the regularized double-layer integral shown on the right-hand side of equation (5.3.13), computed over the spherical cap shown in Figure 5.2.2, for $f(\mathbf{x}) = c_0 + c_1 y = c_0 + c_1 \sin \theta \cos \varphi$, where c_0 and c_1 are constant coefficients. (a) Demonstrate the discontinuous behavior of the integrand at the evaluation point \mathbf{x}_0 , and (b) compute the integral by analytical methods.

5.4 High-order expansions

Equations (5.1.3) and (5.1.4) have emerged by approximating the continuous surface function f and its normal derivative $\partial f / \partial n$ with constant functions over the individual boundary elements.

To improve the accuracy of the solution, the surface distributions may be approximated with bivariate or high-order polynomials with respect to the local triangle coordinates ξ, η . The polynomial coefficients may then be found by applying the integral representation at an appropriate number of nodes in the spirit of the spectral-element method discussed in Section 3.5.

Isoparametric representations arise when the order of the polynomial expansion over a triangular element matches the order of the geometrical interpolation that defines the element.

5.4.1 Isoparametric linear expansion

When a surface has been discretized into flat triangles, as discussed in Section 5.2, we may assume that the surface function f and its normal derivative $\partial f / \partial n$ vary linearly with respect to the local triangle coordinates ξ and η , and express them in forms analogous to that shown in (5.2.1):

$$f(\xi, \eta) = f_1 \zeta + f_2 \xi + f_3 \eta, \quad (5.4.1)$$

and

$$\frac{\partial f}{\partial n}(\xi, \eta) = \left(\frac{\partial f}{\partial n} \right)_1 \zeta + \left(\frac{\partial f}{\partial n} \right)_2 \xi + \left(\frac{\partial f}{\partial n} \right)_3 \eta, \quad (5.4.2)$$

where $\zeta = 1 - \xi - \eta$, and the subscripts are the local element node labels.

Substituting these expansions into the integral equation associated with the integral representation (5.1.1), and requiring the satisfaction of the integral equation at the global nodes, we obtain a system of linear equation involving the element node values of the harmonic function and its normal derivative. Because elements share nodes, the linear system must be concatenated so that coincident element nodes are compiled into sums multiplying unique global nodes. The coefficient matrix of the linear system for the global nodes and associated right-hand side may be constructed by the following two methods:

- Substitute the linear expansions (5.4.1) and (5.4.2) into the single- and double-layer potential, extract the element nodal values from the integrals, evaluate the integrals using numerical methods, and make contributions to the appropriate

entries of the linear system for the global nodes, as dictated by the connectivity table relating local element to global grid nodes. This method is commonplace in finite element implementations.

- Generate the linear system by the method of impulses. The algorithm involves setting the value of the harmonic function and its normal derivative to unity at one cardinal node, and to zero at all other nodes, computing the single- and double-layer potential by integrating over the elements that share the cardinal node, and making appropriate entries to the coefficient matrix and to the right-hand side.

5.4.2 Isoparametric quadratic expansion

When a surface has been discretized into six-node curved triangles, as discussed in Section 5.3, we may assume that the surface function f and its normal derivative $\partial f / \partial n$ vary quadratically with respect to the local triangle coordinates ξ and η , and express them in forms analogous to that shown in (5.3.1):

$$f(\xi, \eta) = \sum_{i=1}^6 f_i \phi_i(\xi, \eta), \quad (5.4.3)$$

and

$$\frac{\partial f}{\partial n}(\xi, \eta) = \sum_{i=1}^6 \left(\frac{\partial f}{\partial n} \right)_i \phi_i(\xi, \eta). \quad (5.4.4)$$

The implementation of the collocation method follows the steps outlined in Section 5.4.1 for flat triangles.

Subdirectories `ldr_3d` and `lnm_3d` of directory `laplace` or `BEMLIB` contain boundary-element codes that solve Laplace's equation in the interior or exterior of a closed surface subject to Dirichlet or Neumann boundary conditions.

5.4.3 Spectral-element methods

The isoparametric-expansion method can be generalized in the spirit of the spectral-element-collocation method in two dimensions discussed in Section 3.5. Orthogonal polynomial expansions for triangular domains have been developed in References [15, 32]. The difficulty in computing the singular single- and double-layer integrals with sufficient accuracy has been an impediment to the implementation of these methods.

Problem**P.5.4.1 BEMLIB codes**

- (a) Use program `ldr_3d` in directory `laplace` of *BEMLIB* to solve Laplace's equation in the interior of a sphere subject to Dirichlet boundary conditions of your choice, and discuss the accuracy of the numerical method.
- (b) Repeat (a) for the exterior of a sphere.
- (c) Use program `lnm_3d` in directory `laplace` of *BEMLIB* to solve Laplace's equation in the exterior of a sphere subject to Neumann boundary conditions of your choice, and discuss the accuracy of the numerical method.
- (d) Repeat (c) for the interior of a sphere.

Chapter 6

Inhomogeneous, nonlinear, and time-dependent problems

In previous chapters, we have discussed integral representations, integral equations, and boundary-element methods for Laplace's equation in two and three dimensions, with occasional reference to Helmholtz's equation and the steady-state convection – diffusion equation. Prerequisites for applying the theoretical formulation and numerical methods to other differential equations of the general form

$$L[f(\mathbf{x})] = 0, \quad (6.1)$$

where $L[\cdot]$ is a differential operator, are the following:

- The differential operator $L[\cdot]$ is *elliptic*, that is, the solution of (6.1) is determined exclusively by data specified around the boundaries of the solution domain.
- The differential equation is *homogeneous*, that is, if the boundary data are zero, then the solution is also zero.
- The differential equation is *linear*, that is, if two functions satisfy the differential equation, then any linear combination of them will also satisfy the differential equation.
- A Green's function of the differential equation is available in analytical or readily computable form.

In real life, we encounter problems involving inhomogeneous, nonlinear, and time-dependent (parabolic or hyperbolic) equations expressing evolution from an initial state or wave propagation. Examples include the convection – diffusion equation in the presence of a distributed source, the unsteady heat conduction equation, Burgers' equation, the Navier-Stokes equation, and the wave equation. To take advantage of the benefits of the boundary-integral formulation, we must extend the theoretical foundation and numerical implementation so that we can tackle this broader class of equations.

In this chapter, we discuss the generalization of the boundary-integral formulation with emphasis on practical implementation. In Sections 6.1–6.3 we discuss the solution of linear inhomogeneous equations and the computation of domain integrals

involving Green's functions. In Section 6.4 we discuss nonlinear equations, and in Section 6.5 we review strategies for computing time-dependent solutions.

6.1 Distributed source and domain integrals

Consider the solution of a linear, elliptic, and inhomogeneous differential equation subject to an appropriate set of boundary conditions. A standard method of removing the source term that is responsible for the inhomogeneity involves three steps:

- Split the solution into a particular solution and a homogeneous solution.
- Find a particular solution by inspection or by elementary analytical methods without regard to the specified boundary conditions.
- Compute the homogeneous solution by boundary-element methods subject to modified boundary conditions that depend on the chosen particular solution.

For example, the mathematical formulation of the problem of pressure-driven unidirectional viscous flow through a tube with arbitrary cross-section is governed by Poisson's equation for the axial velocity with a constant source term that is proportional to the pressure gradient in the streamwise direction. In this case, a particular solution can be found by inspection, and the homogeneous solution satisfying Laplace's equation can be computed accurately and efficiently by boundary-element methods, as discussed in subdirectory `flow_1d` of directory `laplace` of the *BEMLIB* user guide (see Chapter 10).

More generally, the particular solution can be expressed in the form of a Newtonian potential, that is, as a domain integral of the product of (a) the source term of the differential equation, and (b) a Green's function of the corresponding homogeneous differential equation. For example, in two dimensions, a particular solution of the linear, elliptic, and inhomogeneous differential equation

$$L[f(\mathbf{x})] + s(\mathbf{x}) = 0, \quad (6.1.1)$$

involving the source term $s(\mathbf{x})$, is given by the Newtonian potential

$$N(\mathbf{x}_0) = \int \int s(\mathbf{x}) G(\mathbf{x}_0, \mathbf{x}) dx dy, \quad (6.1.2)$$

where the integral is computed over the solution domain, and $G(\mathbf{x}_0, \mathbf{x}_0)$ is the Green's function satisfying $L[G(\mathbf{x}, \mathbf{x}_0)] + \delta_2(\mathbf{x} - \mathbf{x}_0) = 0$. Operating on both sides of (6.1.2) by $L[\cdot]$ acting with respect to \mathbf{x}_0 , transferring the operation inside the integral, and

using the definition of the Green's function, we confirm that the particular solution satisfies (6.1.1).

When an exact particular solution is not available in a convenient analytical or numerical form, an approximation may be constructed by expressing the source term $s(\mathbf{x})$ as a linear combination of M interpolation or influence functions ϕ_i , concisely called basis functions, in the form

$$s(\mathbf{x}) \simeq \sum_i^M c_i \phi_i(\mathbf{x}), \quad (6.1.3)$$

where c_i are known coefficients. The basis functions are selected so that the equation $L[\hat{\phi}_i(\mathbf{x})] + \phi_i(\mathbf{x}) = 0$ may be readily solved for the parental function $\hat{\phi}_i$. Recasting (6.1.3) into the form

$$s(\mathbf{x}) \simeq -L\left[\sum_i^M c_i \hat{\phi}_i(\mathbf{x})\right] \quad (6.1.4)$$

shows that an approximate particular solution of (6.1.1) is given by

$$f^P(\mathbf{x}_0) \simeq \sum_i^M c_i \hat{\phi}_i(\mathbf{x}_0). \quad (6.1.5)$$

The particular solution (6.1.5) also arises by substituting (6.1.3) into the Newtonian potential (6.1.2), and then using the reciprocal relation for the operator $L[\cdot]$ to convert the areal integral to a boundary integral, as will be discussed in Sections 6.2 and 6.3. This indirect approach is the preferred venue in the dual reciprocity method introduced by Nardini and Brebbia [47].

Domain integrals also arise when the Green's function of a particular *homogeneous* differential equation is not available in readily computable form, and the Green's function of a simpler differential equation is used in its place.

Consider, for example, Green's second identity in two dimensions, equation (2.1.4). Assume that the function f satisfies Helmholtz's equation $\nabla^2 f = \lambda^2 f$, and identify the arbitrary function ϕ with a Green's function of Laplace's equation, denoted by $G^L(\mathbf{x}, \mathbf{x}_0)$. Working in the familiar way, we derive the boundary-integral representation (2.3.3), except that the right-hand side also contains the Newtonian potential

$$N(\mathbf{x}_0) \equiv -\lambda^2 \int \int f(\mathbf{x}) G^L(\mathbf{x}_0, \mathbf{x}) dx dy. \quad (6.1.6)$$

The domain integral has emerged by regarding the Helmholtz equation as a Poisson equation with a source term that involves the unknown function on the right-hand side.

Taking the Laplacian of both sides of (6.1.6) with respect to \mathbf{x}_0 , we find that the Newtonian potential $N(\mathbf{x}_0)$ satisfies Poisson's equation $\nabla^2 N = \lambda^2 f$ with an a

a priori unknown right-hand side. We may now apply the method of approximate particular solutions or the dual reciprocity method to derive an approximation to the Newtonian potential similar to that shown in (6.1.4). In this case, however, the coefficients c_i must be computed as part of the solution.

Problem

P.6.1.1 Transforming the domain integral to a boundary integral

Show that the domain integral (6.1.6) may be expressed as a boundary integral in the form

$$\begin{aligned} & -\lambda^2 \int_{A_c} f(\mathbf{x}) G^L(\mathbf{x}, \mathbf{x}_0) dA(\mathbf{x}) \\ &= \int_C [G^L(\mathbf{x}_0, \mathbf{x} - G^H(\mathbf{x}_0, \mathbf{x}))] [\mathbf{n}(\mathbf{x}) \cdot \nabla f(\mathbf{x})] dl(\mathbf{x}) \\ & \quad - \int_C f(\mathbf{x}) \{\mathbf{n}(\mathbf{x}) \cdot \nabla [G^L(\mathbf{x}_0, \mathbf{x} - G^H(\mathbf{x}_0, \mathbf{x}))]\} dl(\mathbf{x}), \end{aligned} \quad (1)$$

where $G^H(\mathbf{x}, \mathbf{x}_0)$ is a Green's function of Helmholtz's equation.

6.2 Particular solutions and dual reciprocity in one dimension

It is convenient to introduce the method of approximate particular solution (MAPS) and the dual reciprocity method (DRM) with reference to Poisson's equation in one dimension for an unknown function $f(x)$,

$$\frac{d^2 f}{dx^2} + s(x) = 0, \quad (6.2.1)$$

where $s(x)$ is a given source term. When $s(x) = 0$, we obtain Laplace's equation in one dimension discussed in Chapter 1. The solution of (6.2.1) is to be found over a specified interval of the x axis, $a \leq x \leq b$, subject to two boundary conditions for the function $f(x)$ or its first derivative $df(x)/dx$ at one or both ends $x = a, b$.

The general solution of (6.2.1) may be expressed as the sum of a homogeneous solution f^H satisfying Laplace's equation $d^2 f^H / dx^2 = 0$, and a particular solution f^P satisfying (6.2.1),

$$f(x) = f^H(x) + f^P(x). \quad (6.2.2)$$

6.2.1 The Newtonian potential

A particular solution is given by the Newtonian potential

$$N(x_0) \equiv \int_a^b s(x) G(x_0, x) dx, \quad (6.2.3)$$

where $G(x, x_0)$ is a Green's function of Laplace's equation in one dimension satisfying $d^2G(x, x_0)/dx^2 + \delta_1(x - x_0) = 0$, and δ_1 is Dirac's delta function in one dimension; the free-space Green's function is given by $G(x, x_0) = -\frac{1}{2} |x - x_0|$.

Taking the second derivative of (6.2.3) with respect to x_0 , transposing the order of differentiation and integration on the right-hand side, and invoking the definition of the Green's function and the properties of the delta function, we confirm that this particular solution satisfies (6.2.1).

Consider now Green's second identity in one dimension (1.1.3), and identify the function $f(x)$ with the Newtonian potential and the function $\phi(x)$ with the Green's function of Laplace's equation, where the singular point x_0 is placed inside the solution domain, $a < x_0 < b$. Using the definition of Green's function, we find

$$\begin{aligned} & -G(x, x_0) s(x) + N(x) \delta_1(x - x_0) \\ &= \frac{d}{dx} \left[G(x, x_0) \frac{dN(x)}{dx} - N(x) \frac{dG(x, x_0)}{dx} \right]. \end{aligned} \quad (6.2.4)$$

Integrating (6.2.4) with respect to x over the solution domain $[a, b]$ and using the distinctive properties of the delta function, the definition (6.2.3), and the fundamental theorem of calculus, we obtain

$$\left[G(x, x_0) \frac{dN(x)}{dx} - N(x) \frac{dG(x, x_0)}{dx} \right]_{x=a}^{x=b} = 0, \quad (6.2.5)$$

where the square brackets denote the difference of the enclosed expression evaluated at $x = b$ and a .

6.2.2 Integral representation involving a domain integral

Next, we recall the boundary-value representation of the homogeneous solution associated with the Newtonian potential, denoted by f^{HN} , and substitute the particular solution (6.2.3) into (6.2.2) to obtain

$$f(x_0) = \left[G(x, x_0) \frac{df^{HN}(x)}{dx} - f^{HN}(x) \frac{dG(x, x_0)}{dx} \right]_{x=a}^{x=b} + N(x_0). \quad (6.2.6)$$

Adding the left-hand side of (6.2.5) to the right-hand side of (6.2.6) and recalling the decomposition (6.2.2), we derive the alternative representation

$$f(x_0) = \left[G(x, x_0) \frac{df(x)}{dx} - f(x) \frac{dG(x, x_0)}{dx} \right]_{x=a}^{x=b} + N(x_0), \quad (6.2.7)$$

which is preferable in view of the specified boundary conditions for f or df/dx .

Expression (6.2.7) can be derived directly by identifying the function $\phi(x)$ in Green's second identity (1.1.3) with a Green's function whose singular point x_0 is placed inside the solution domain, $a < x_0 < b$. Assuming that $f(x)$ satisfies (6.2.1), we find

$$\begin{aligned} & -G(x, x_0) s(x) + f(x) \delta_1(x - x_0) \\ &= \frac{d}{dx} [G(x, x_0) \frac{df(x)}{dx} - f(x) \frac{dG(x, x_0)}{dx}]. \end{aligned} \quad (6.2.8)$$

Integrating (6.2.8) with respect to x over the solution domain $[a, b]$ and using the distinctive properties of the delta function and the fundamental theorem of calculus, we recover (6.2.7).

The presence of the inhomogeneous source term $s(x)$ in (6.2.1) has resulted in an integral over the domain of solution complementing the boundary-value representation expressed by the terms enclosed by the square brackets on the right-hand sides of (6.2.6) and (6.2.7).

6.2.3 MAPS with cardinal interpolation functions

To compute an approximation to the particular solution, we distribute M data points over the solution domain, x_i , $i = 1, \dots, M$, where $a \leq x_i \leq b$, introduce a corresponding set of cardinal interpolation functions $Z_i(x)$, and express the source term on the right-hand side of the Poisson equation (6.2.1) in the approximate form

$$s(x) \simeq \sum_{i=1}^M s(x_i) Z_i(x). \quad (6.2.9)$$

The cardinal interpolation functions are distinguished by the property $Z_i(x_i) = 1$ and $Z_i(x_j) = 0$ if $i \neq j$, where summation over i is *not* implied over the repeated index i . For example, $Z_i(x)$ may be identified with the cubic-splines cardinal functions discussed in Section 3.2.

Moreover, we introduce parental functions $\hat{Z}_i(x)$ associated with the cardinal interpolation functions defined over the whole of the solution domain $[a, b]$ by the relation

$$\frac{d^2 \hat{Z}_i(x)}{dx^2} + Z_i(x) = 0. \quad (6.2.10)$$

Substituting (6.2.10) into (6.2.9), we find

$$s(x) \simeq - \sum_{i=1}^M s(x_i) \frac{d^2 \hat{Z}_i(x)}{dx^2}, \quad (6.2.11)$$

which shows that an approximate particular solution of (6.2.1) is given by

$$f^P(x) \simeq \sum_{i=1}^M s(x_i) \hat{Z}_i(x). \quad (6.2.12)$$

The emerging solution procedure involves the following steps:

1. Specify the cardinal functions $Z_i(x)$ and compute the associated parental functions \hat{Z}_i using (6.2.10).
2. Compute the boundary values of the homogeneous solution f^H or df^H/dx using the specified boundary values of f or df/dx , the decomposition (6.2.2), and the approximation (6.2.12).
3. Compute the unknown boundary values of f^H or df^H/dx using the boundary-value representation

$$f^H(x) = \left[G(x, x_0) \frac{df^H(x)}{dx} - f^H \frac{dG(x, x_0)}{dx} \right]_a^b, \quad (6.2.13)$$

as discussed in Section 1.4.

4. Recover the unknown boundary values of f or df/dx based on (6.2.2) and (6.2.12).

The important benefit of this seemingly cumbersome method is that, because of the smoothness of the parental functions \hat{Z}_i , the sum on the right-hand side of (6.2.12) converges much faster with respect to M than other sums approximating the domain integrals on the left-hand side of (6.2.6) or (6.2.7).

6.2.4 DRM with cardinal interpolation functions

Alternatively, we substitute (6.2.11) into the domain integral defining the Newtonian potential (6.2.3) to obtain

$$N(x_0) \simeq - \sum_{i=1}^M \int_a^b \frac{d^2 \hat{Z}_i(x)}{dx^2} G(x_0, x) dx. \quad (6.2.14)$$

Using Green's second identity in one dimension, we recast the individual integrals on the right-hand side of (6.2.14) into the form

$$\begin{aligned} & \int_a^b \frac{d^2 \hat{Z}_i(x)}{dx^2} G(x_0, x) dx \\ &= -\hat{Z}_i(x_0) + \left[G(x_0, x) \frac{d\hat{Z}_i(x)}{dx} - \hat{Z}_i(x) \frac{dG(x_0, x)}{dx} \right]_{x=a}^{x=b}. \end{aligned} \quad (6.2.15)$$

Substituting the right-hand side of (6.2.15) into (6.2.14) and rearranging, we obtain

$$N(x_0) \simeq f^P(x_0) - \left[G(x, x_0) \frac{df^P(x)}{dx} - f^P(x) \frac{dG(x, x_0)}{dx} \right]_{x=a}^{x=b}, \quad (6.2.16)$$

where the approximate particular solution f^P is defined in (6.2.12). Finally, we substitute the right-hand side of (6.2.16) in place of the domain integral on the right-hand side of (6.2.7), use the decomposition (6.2.2), and recover the boundary-value representation (6.2.13).

As an example, we confirm the representation (6.2.16) by considering the solution of (6.2.1) over the interval $[0, 1]$ for a uniform source term $s(x) = 1$. For illustration, we choose $M = 2$, $x_1 = 0$, and $x_2 = 1$, and use the linear finite-element or B -spline cardinal interpolation functions (e.g., [60])

$$Z_1(x) = 1 - x, \quad Z_2(x) = x. \quad (6.2.17)$$

The corresponding parental functions are found by integrating (6.2.10) using elementary methods, and are given by

$$\hat{Z}_1(x) = c_1 + c_2 x - \frac{1}{2} x^2 + \frac{1}{6} x^3, \quad \hat{Z}_2(x) = c_3 + c_4 x - \frac{1}{6} x^3, \quad (6.2.18)$$

where c_1, c_2, c_3 , and c_4 are four arbitrary constants. Setting $s(x_1) = 1$ and $s(x_2) = 1$, we find that the particular solution $f^P(x)$ defined in (6.2.12) is given by

$$f^P(x) \simeq \hat{Z}_1(x) + \hat{Z}_2(x) = c_1 + c_3 + (c_2 + c_4) x - \frac{1}{2} x^2. \quad (6.2.19)$$

For these specific choices, equation (6.2.16) with $G(x, x_0) = -\frac{1}{2} |x - x_0|$ yields

$$\begin{aligned} N(x_0) &\equiv -\frac{1}{2} \int_0^1 |x - x_0| dx \\ &\simeq f^P(x_0) - \frac{1}{2} [-(1 - x_0) (\frac{df^P}{dx})_{x=1} + f^P(x=1)] \\ &\quad + \frac{1}{2} [-x_0 (\frac{df^P}{dx})_{x=0} - f^P(x=0)] = -\frac{1}{2} (x_0^2 - x_0 + \frac{1}{2}), \end{aligned} \quad (6.2.20)$$

which is exact because of the absence of error in the interpolation of the source term $s(x)$. The last expression in (6.2.20) is clearly a particular solution of (6.2.1) with unit source term.

6.2.5 MAPS and DRM with influence functions

In practice, the cardinal interpolation functions introduced in (6.2.9) and their parental functions may not be readily available. As a compromise, we introduce the approximate expansion

$$s(x) \simeq \sum_{i=1}^M \alpha_i H_i(x), \quad (6.2.21)$$

where $H_i(x)$ are specified *influence functions*, and α_i are scalar coefficients computed by requiring the interpolation condition

$$s(x_i) = \sum_{j=1}^M \alpha_j H_i(x_i), \quad (6.2.22)$$

for $j = 1, \dots, M$.

For convenience, we express the linear system (6.2.22) in the form

$$\mathbf{A} \cdot \boldsymbol{\alpha} = \mathbf{g}, \quad (6.2.23)$$

where $A_{ij} = H_i(x_j)$, the vector $\boldsymbol{\alpha}$ contains the unknown coefficients α_i , and the vector \mathbf{g} contains the known values $s(x_i)$. If the influence functions $H_i(x)$ are cardinal interpolation functions associated with the data points, then \mathbf{A} reduces to the identity matrix and the solution of (6.2.23) is simply $\boldsymbol{\alpha} = \mathbf{g}$.

Working as previously with the cardinal interpolation functions, we introduce the parental functions $\hat{H}_i(x)$ defined by the relation

$$\frac{d^2 \hat{H}_i(x)}{dx^2} + H_i(x) = 0 \quad (6.2.24)$$

and build the particular solution

$$f^P(x) \simeq \sum_{i=1}^M \alpha_i \hat{H}_i(x), \quad (6.2.25)$$

which is related to the Newtonian potential (6.2.3) by (6.2.16) (P.6.2.3).

The solution procedure involves the following steps:

1. Specify the influence functions $H_i(x)$ and compute their parental functions \hat{H}_i , or vice versa, using (6.2.24).
2. Compute the boundary values of the homogeneous solution f^H or df^H/dx using the specified boundary values of f or df/dx and the decomposition (6.2.2).
3. Compute the unknown boundary values of f^H or df^H/dx based on the boundary-value representation (6.2.13).
4. Recover the unknown boundary values of f or df/dx based on (6.2.2).

6.2.6 Cardinal functions from influence functions

It is illuminating to solve equation (6.2.23) for the unknown vector α in terms of the inverse matrix \mathbf{A}^{-1} and then substitute the result into (6.2.21) to obtain

$$s(x) = H_i(x) \mathbf{A}_{ij}^{-1} g(x_j), \quad (6.2.26)$$

where summation is implied over the repeated indices i and j in the range $1, \dots, M$. Comparing equation (6.2.26) with (6.2.9), we deduce that

$$Z_j(x) = H_i(x) \mathbf{A}_{ij}^{-1} \quad (6.2.27)$$

is a set of cardinal interpolation functions associated with the influence functions H_i . Thus, unless the matrix \mathbf{A} is singular, to each set of influence functions corresponds a set of cardinal interpolation functions whose explicit construction appears to be redundant.

In practice, however, the basis functions must be selected with care so that the condition number of the inverse matrix \mathbf{A}^{-1} is not excessively large. Otherwise, round-off error may erode the accuracy of the solution.

Problems

P.6.2.1 Linear B-spline cardinal functions

- (a) Verify that the Newtonian potential shown in (6.2.20) satisfies identity (6.2.5) with $a = 0$ and $b = 1$.
- (b) Repeat the example discussed in the text involving equations (6.2.17) to (6.2.20) for the linear source term $s(x) = x$, and discuss the accuracy of the boundary-value representation (6.2.16).

P.6.2.2 Parental cubic-splines cardinal functions

Write a program that computes the parental functions of the cardinal cubic-splines interpolation functions associated with a specified set of nodes. Prepare graphs of these functions for a set of nodes of your choice.

P.6.2.3 Particular solution and Newtonian potential

Prove that the particular solution given in (6.2.25) is related to the Newtonian potential (6.2.3) by (6.2.16).

6.3 Particular solutions and dual reciprocity in two and three dimensions

Generalizing the analysis of Section 6.2, we consider Poisson's equation in two dimensions for an unknown function $f(x, y)$,

$$\nabla^2 f + s(x, y) = 0, \quad (6.3.1)$$

where ∇^2 is the Laplacian operator in the xy plane, and $s(x, y)$ is a specified distributed source. Dirichlet or Neumann boundary conditions are provided around the boundary C of a selected control area A_c . When $s(x, y) = 0$, we obtain Laplace's equation in two dimensions discussed in Chapters 2 and 3.

The general solution of (6.3.1) may be expressed as the sum of a homogeneous solution f^H satisfying Laplace's equation $\nabla^2 f^H = 0$, and a particular solution f^P satisfying (6.3.1),

$$f(x, y) = f^H(x, y) + f^P(x, y). \quad (6.3.2)$$

6.3.1 The Newtonian potential

A particular solution of (6.3.1) is given by the Newtonian potential

$$N(x_0, y_0) \equiv \int \int_{A_c} s(x, y) G(\mathbf{x}_0, \mathbf{x}) dx dy, \quad (6.3.3)$$

where $G(\mathbf{x}, \mathbf{x}_0)$ is a Green's function of Laplace's equation in two dimensions satisfying $\nabla^2 G(\mathbf{x}, \mathbf{x}_0) + \delta_2(\mathbf{x} - \mathbf{x}_0) = 0$, and δ_2 is Dirac's delta function in the xy plane; the free-space Green's function is given by $G(\mathbf{x}, \mathbf{x}_0) = -\frac{1}{2\pi} \ln r$, where $r = |\mathbf{x} - \mathbf{x}_0|$.

Taking the Laplacian of (6.3.3) with respect to \mathbf{x}_0 , transposing the order of differentiation and integration on the right-hand side, and invoking the definition of the Green's function and the properties of the delta function, we confirm that this particular solution satisfies (6.3.1).

Next, we consider Green's second identity in two dimensions (2.1.4), and identify the function f with the Newtonian potential and the function $\phi(x, y)$ with a Green's function whose singular point \mathbf{x}_0 is located inside the selected control area A_c . Using the definition of the Green's function, we find

$$\begin{aligned} & -G(\mathbf{x}, \mathbf{x}_0) s(x, y) + N(x, y) \delta_2(\mathbf{x} - \mathbf{x}_0) \\ &= \nabla [G(\mathbf{x}, \mathbf{x}_0) \nabla N(\mathbf{x}) - N(\mathbf{x}) \nabla G(\mathbf{x}, \mathbf{x}_0)]. \end{aligned} \quad (6.3.4)$$

Integrating (6.3.4) over the control area and using the distinctive properties of the delta function, the definition (6.3.3), and the divergence theorem, we derive the identity

$$\int_C \{ G(\mathbf{x}_0, \mathbf{x}) [\mathbf{n}(\mathbf{x}) \cdot \nabla N(\mathbf{x})] - N(\mathbf{x}) [\mathbf{n}(\mathbf{x}) \cdot \nabla G(\mathbf{x}_0, \mathbf{x})] \} dl(\mathbf{x}) = 0. \quad (6.3.5)$$

6.3.2 Integral representation

Now, we recall the boundary-integral representation of the homogeneous solution associated with the Newtonian potential, denoted by f^{HN} , and substitute the particular solution (6.3.3) into (6.3.2) to obtain

$$\begin{aligned} f(\mathbf{x}_0) &= - \int_C G(\mathbf{x}_0, \mathbf{x}) [\mathbf{n}(\mathbf{x}) \cdot \nabla f^{HN}(\mathbf{x})] dl(\mathbf{x}) \\ &\quad + \int_C f^{HN}(\mathbf{x}) [\mathbf{n}(\mathbf{x}) \cdot \nabla G(\mathbf{x}_0, \mathbf{x})] dl(\mathbf{x}) + N(x_0, y_0). \end{aligned} \quad (6.3.6)$$

Adding the left-hand side of (6.3.5) to the right-hand side of (6.3.6) and recalling the decomposition (6.3.2), we derive the alternative form

$$\begin{aligned} f(\mathbf{x}_0) &= - \int_C G(\mathbf{x}_0, \mathbf{x}) [\mathbf{n}(\mathbf{x}) \cdot \nabla f(\mathbf{x})] dl(\mathbf{x}) \\ &\quad + \int_C f(\mathbf{x}) [\mathbf{n}(\mathbf{x}) \cdot \nabla G(\mathbf{x}_0, \mathbf{x})] dl(\mathbf{x}) + N(x_0, y_0), \end{aligned} \quad (6.3.7)$$

which is preferable in view of the specified boundary conditions for f or its normal derivative $\mathbf{n} \cdot \nabla f$. Expression (6.3.7) could have been derived directly by applying Green's second identity in its integral form for the function f .

6.3.3 MAPS and DRM with cardinal interpolation functions

To obtain an approximate particular solution, we distribute M data points over the control volume A_c enclosed by C , located at (x_i, y_i) , $i = 1, \dots, M$, introduce a corresponding set of cardinal interpolation functions $Z_i(x, y)$, and express the source term in the approximate form

$$s(x, y) \simeq \sum_{i=1}^M s(x_i, y_i) Z_i(x, y). \quad (6.3.8)$$

By definition, the cardinal interpolation functions are distinguished by the property $Z_i(x_i, y_i) = 1$ and $Z_i(x_j, y_j) = 0$ if $i \neq j$, where summation over the repeated

index i in *not implied*. Examples of cardinal interpolation functions include the finite element pyramid-like functions, the bivariate cardinal cubic-splines functions, the B -spline surface functions, and the regular or moving least-squares interpolation functions (e.g., [60]).

Moreover, we introduce parental functions $\hat{Z}_i(x, y)$ associated with the cardinal functions defined over the whole of the solution domain by the relation

$$\nabla^2 \hat{Z}_i(x, y) + Z_i(x, y) = 0. \quad (6.3.9)$$

Substituting (6.3.9) into (6.3.8), we find

$$s(x, y) \simeq - \sum_{i=1}^M s(x_i, y_i) \nabla^2 \hat{Z}_i(x, y), \quad (6.3.10)$$

which shows that an approximate particular solution of (6.3.1) is given by

$$f^P(x, y) \simeq \sum_{i=1}^M s(x_i, y_i) \hat{Z}_i(x, y). \quad (6.3.11)$$

The solution procedure involves the following steps:

1. Specify the cardinal functions $Z_i(x, y)$ and compute the parental functions $\hat{Z}_i(x, y)$ by solving the Poisson equation (6.3.9).
2. Compute the boundary distribution of the homogeneous solution f^H or its normal derivative using the specified boundary distribution for f or its normal derivative, the decomposition (6.3.2), and the approximation (6.3.11).
3. Compute the unknown boundary distribution of f^H or its normal derivative by solving the boundary-integral equation

$$\begin{aligned} f^H(\mathbf{x}_0) &= -2 \int_C G(\mathbf{x}_0, \mathbf{x}) [\mathbf{n}(\mathbf{x}) \cdot \nabla f^H(\mathbf{x})] dl(\mathbf{x}) \\ &\quad + 2 \int_C^{PV} f^H(\mathbf{x}) [\mathbf{n}(\mathbf{x}) \cdot \nabla G(\mathbf{x}_0, \mathbf{x})] dl(\mathbf{x}). \end{aligned} \quad (6.3.12)$$

4. Recover the unknown boundary values of f or its normal derivative based on (6.3.2) and (6.3.11).

The particular solution (6.3.11) is related to the Newtonian potential (6.3.3) by the following counterpart of expression (6.2.16)

$$\begin{aligned} N(x_0, y_0) &\simeq f^P(x_0, y_0) + \int_C G(\mathbf{x}_0, \mathbf{x}) [\mathbf{n}(\mathbf{x}) \cdot \nabla f^P(\mathbf{x})] dl(\mathbf{x}) \\ &\quad - \int_C f^P(\mathbf{x}) [\mathbf{n}(\mathbf{x}) \cdot \nabla G(\mathbf{x}_0, \mathbf{x})] dl(\mathbf{x}). \end{aligned} \quad (6.3.13)$$

Note that the right-hand side of (6.3.13) remains unchanged when a non-singular harmonic function is added to the particular solution f^P .

6.3.4 MAPS and DRM with influence functions

In practice, the cardinal interpolation functions defined in (6.3.8) may not be available. As an alternative, we introduce the approximation

$$s(x, y) \simeq \sum_{i=1}^M \alpha_i H_i(x, y), \quad (6.3.14)$$

where $H_i(x, y)$ are influence functions and α_i are scalar coefficients computed by requiring the interpolation condition

$$s(x_j, y_j) = \sum_{i=1}^M \alpha_i H_i(x_j, y_j), \quad (6.3.15)$$

for $j = 1, \dots, M$. Note that, for the right-hand side of (6.3.14) to be finite, the functions $H_i(x, y)$ must be non-singular at the data points. Thus, regularity prevents us from identifying $H_i(x, y)$ with Green's functions or any other singular functions.

For convenience, we express the linear system (6.3.15) in the form

$$\mathbf{A} \cdot \boldsymbol{\alpha} = \mathbf{g}, \quad (6.3.16)$$

where $A_{ji} = H_i(x_j, y_j)$, the vector $\boldsymbol{\alpha}$ contains the unknown coefficients α_i , and the vector \mathbf{g} contains the known values $g(x_i, y_i)$. If the influence functions $H_i(x, y)$ are cardinal interpolation functions associated with the data points, then \mathbf{A} reduces to the identity matrix and the solution of (6.3.16) is simply $\boldsymbol{\alpha} = \mathbf{g}$.

Next, we introduce parental functions $\hat{H}_i(x, y)$ associated with the interpolation functions defined by the relation

$$\nabla^2 \hat{H}_i(x, y) + H_i(x, y) = 0, \quad (6.3.17)$$

and build the particular solution

$$f^P(x, y) \simeq \sum_{i=1}^M \alpha_i \hat{H}_i(x, y). \quad (6.3.18)$$

The solution procedure involves the following steps:

1. Specify the interpolation functions $H_i(x, y)$ and compute the parental functions $\hat{H}_i(x, y)$, or vice versa, using (6.3.17). Two successfully tested choices are $H_i(x, y) = r$ and $1 + r$, where $r = [(x - x_i)^2 + (y - y_i)^2]^{1/2}$ [51]. The corresponding parental functions are $\hat{H}_i(x, y) = -\frac{1}{9}r^3$ and $-\frac{1}{4}r^2 - \frac{1}{9}r^3$.
2. Solve the linear system (6.3.16) for the coefficient vector $\boldsymbol{\alpha}$. In practice, the solution is found by Gauss elimination or singular-value decomposition (e.g., [60]). The choice of interpolation functions plays an important role in the accuracy of the solution.

3. Compute the boundary distribution of f^H or its normal derivative using the specified boundary conditions for f and the approximate particular solution (6.3.18).
4. Compute the unknown boundary distribution of f^H or its normal derivative by solving the integral equation (6.3.12).
5. Recover the unknown boundary distribution of f or its normal derivative based on (6.3.2) and (6.3.18).

6.3.5 Cardinal functions from influence functions

Solving system (6.3.16) for the unknown vector α in terms of the inverse matrix \mathbf{A}^{-1} and substituting the result into (6.3.13), we obtain

$$s(x, y) = H_i(x, y) A_{ij}^{-1} s(x_j, y_j), \quad (6.3.19)$$

where summation is implied over i and j in the range $1, \dots, M$. Comparing this equation with (6.3.8), we deduce that a set of cardinal functions associated with the influence functions H_i is given by

$$Z_j(x, y) = H_i(x, y) A_{ij}^{-1}. \quad (6.3.20)$$

Thus, unless the matrix \mathbf{A} is singular, to every set of influence functions corresponds a set of cardinal interpolation functions whose explicit construction appears to be redundant.

In practice, however, the basis functions must be selected with care so that the condition number of the inverse matrix \mathbf{A}^{-1} is not excessively large. Otherwise, round-off error may erode the accuracy of the solution.

6.3.6 Radial basis functions (RBF)

Radial basis functions (RBF) are influence functions $H_i(x, y)$ that depend only on the scalar distance of the evaluation point (x, y) from the corresponding datum point (x_i, y_i) . Equation (6.3.20) provides us with a way of constructing cardinal interpolation functions corresponding to a given set of data points from a chosen set of radial basis functions.

The proper selection of radial basis functions has been the subject of extensive discussion in the literature of boundary element and meshless methods [19-22]. Analysis has shown that radial basis functions of the type $H_i(x, y) = r$ or e^{-r^2} are appropriate, and the thin-plate spline (TPS) $H_i(x, y) = r^2 \ln r$, which is identical to the fundamental solution of the biharmonic equation, minimizes a properly defined interpolation error.

6.3.7 General implementation of the DRM

The implementation of the dual reciprocity method for other types of inhomogeneous differential equations follows the basic steps outlined in this section for Poisson's equation.

Consider, for example, the inhomogeneous Helmholtz equation in two dimensions,

$$\nabla^2 f - \lambda^2 f + s(x, y) = 0, \quad (6.3.21)$$

where λ is a constant and $s(x, y)$ is a specified distributed source. The counterpart of (6.3.17) defining the parental influence functions is

$$\nabla^2 \hat{H}_i(x, y) - \lambda^2 \hat{H}_i(x, y) + H_i(x, y) = 0. \quad (6.3.22)$$

The solution for the thin-plate spline, $H_i(r) = r^2 \ln r$, is [11]

$$\hat{H}_i(r) = \frac{4}{\lambda^4} (1 + \ln r) + \frac{r^2}{\lambda^2} \ln r + \frac{4}{\lambda} K_0(\lambda r), \quad (6.3.23)$$

where K_0 is a modified Bessel function (e.g., [2], p. 374). An approximate particular solution is given by (6.3.18); the complementary homogeneous solution may be computed by boundary-element methods.

The method of approximate particular solutions and the dual reciprocity method can be extended in a straightforward fashion to three dimensions. Suitable radial basis functions are discussed in the references cited in Section 6.3.6.

Problems

P.6.3.1 Particular solution of Poisson's equation for a radially symmetric source function

Consider Poisson's equation (6.3.1) with a radially symmetric source term $s(r)$, where $r = \sqrt{x^2 + y^2}$. Requiring that the solution respects the radial symmetry, we write $f(x, y) = f(r)$, and express the Laplacian operator in plane polar coordinates to derive the ordinary differential equation

$$\frac{1}{r} \frac{d}{dr} \left(r \frac{df}{dr} \right) + s(r) = 0. \quad (1)$$

The Newtonian potential (6.3.3) integrated over a diskoidal area of radius a centered at the origin and evaluated at the radial position r_0 , where $r_0 < a$, provides us with the particular solution

$$N(r_0) = -\frac{1}{4\pi} \int_0^{2\pi} \int_0^a s(r) \ln[(x_0 - r \cos\theta)^2 + (y_0 - r \sin\theta)^2] r dr d\theta, \quad (2)$$

where θ is the polar angle. Writing $x_0 = r_0 \cos \theta_0$, $y_0 = r_0 \sin \theta_0$, $x = r \cos \theta$, and $y = r \sin \theta$, and using elementary trigonometry, we find $(x_0 - x)^2 + (y_0 - y)^2 = r^2 + r_0^2 - 2rr_0 \cos(\theta - \theta_0)$. Substituting this expression into (2) and simplifying, we find

$$N(r_0) = -\frac{1}{2\pi} \int_0^a s(r) \left(\int_0^\pi \ln[r^2 + r_0^2 - 2rr_0 \cos u] du \right) r dr, \quad (3)$$

where $u \equiv \theta - \theta_0$. Referring to standard mathematical tables (e.g., [6], p. 293), we find that the integral with respect to u enclosed by the parentheses is equal to $2\pi \ln r$ when $r > r_0$, and $2\pi \ln r_0$ when $r < r_0$. Thus,

$$\begin{aligned} N(r_0) &= - \int_0^{r_0} s(r) (\ln r_0) r dr - \int_{r_0}^a s(r) (\ln r) r dr \\ &= \int_0^{r_0} s(r) \ln \frac{r}{r_0} r dr - \int_0^a s(r) (\ln r) r dr. \end{aligned} \quad (4)$$

The last integral is independent of r_0 and may be discarded. Setting $r = w r_0$, where w is a dimensionless parameter ranging between 0 and 1, we derive the particular solution

$$f^P(r_0) = r_0^2 \int_0^1 s(w r_0) (\ln w) w dw. \quad (5)$$

(a) Evaluate the right-hand side of (5) for $s(r) = 1 + r$, and verify that the result satisfies equation (1).

(b) Another way to derive the particular solution (5) is by integrating equation (1) twice from $r = 0$ to r_0 , finding

$$f^P(r_0) = - \int_0^{r_0} \frac{1}{r} \left(\int_0^r r' s(r') dr' \right) dr. \quad (6)$$

Setting $r' = t'r$ and $r = tr_0$, where t and t' are dimensionless parameters ranging from 0 to 1, we find

$$f^P(r_0) = -r_0^2 \int_0^1 \int_0^1 t t' s(t t' r_0) dt dt'. \quad (7)$$

To reduce the double integral to a single integral, we introduce the new variables $w \equiv tt'$ and $v = t'$, and invert these relations to obtain $t = w/v$ and $t' = v$. The Jacobian matrix of the (t, t') to (w, v) transformation is

$$\mathbf{J} \equiv \begin{bmatrix} \frac{\partial t}{\partial w} & \frac{\partial t}{\partial v} \\ \frac{\partial t'}{\partial w} & \frac{\partial t'}{\partial v} \end{bmatrix} = \begin{bmatrix} \frac{1}{v} & -\frac{w}{v^2} \\ 0 & 1 \end{bmatrix}. \quad (8)$$

Expressing the differential area in the tt' plane as $\text{Det}(\mathbf{J}) dw dv$, where “ Det ” stands for the determinant, we find

$$f^P(r_0) = -r_0^2 \int_0^1 w s(wr_0) \left(\int_w^1 \frac{1}{v} dv \right) dw. \quad (9)$$

Justify the limits of integration with respect to v and, carrying out the integration with respect to v , derive the particular solution (5).

P.6.3.2 Parental function of the TPS for Helmholtz'equation

Verify by direct substitution that (6.3.23) satisfies (6.3.22) for the TPS, $H_i(r) = r^2 \ln r$.

P.6.3.3 Moving least squares approximation (MLS)

Interpolation and approximation of a function from an unstructured set of data scattered in the xy plane is an important aspect of the method of particular solutions and the dual reciprocity method.

In one version of the method of moving least-squares interpolation (MLS) [39], a set of N data points located at (x_i, y_i) is used to construct the approximating function

$$g_N(x, y) \equiv a_1(x, y) \psi_1(x, y) + a_2(x, y) \psi_2(x, y) + a_3(x, y) \psi_3(x, y) \\ + a_4(x, y) \psi_4(x, y) + a_5(x, y) \psi_5(x, y) + a_6(x, y) \psi_6(x, y), \quad (1)$$

where $\psi_1 = 1$, $\psi_2 = x$, $\psi_3 = y$, $\psi_4 = x^2$, $\psi_5 = xy$, and $\psi_6 = y^2$ constitute a complete set of quadratic basis functions in the xy plane. The coefficient functions $a_j(x, y)$ are computed by minimizing the functional

$$E \equiv \sum_{i=1}^N w_i(x, y) [g_N(x_i, y_i) - g_i]^2 \quad (2)$$

with respect to $a_j(x, y)$, where $w_i(x, y)$ are specified influence functions associated with the data points, and $g_i = g(x_i, y_i)$ are prescribed function values at the data points.

In the standard implementation of the MLS method, the individual influence functions derive from a specified master influence function $W(p, q)$, as $w_i(x, y) = W(x - x_i, y - y_i)$. An example is the radial influence function

$$W(p, q) = \hat{W}(r) = \frac{e^{-\alpha r^2}}{r^2 + \epsilon}, \quad (3)$$

where $r = \sqrt{p^2 + q^2}$, and α, ϵ are specified parameters (e.g., [39], p. 229).

Setting $\partial E / \partial a_j = 0$ for $j = 1, \dots, 6$, we derive the matrix equation

$$\mathbf{B} \cdot \mathbf{W} \cdot \mathbf{B}^T \cdot \mathbf{a} = \mathbf{B} \cdot \mathbf{W} \cdot \mathbf{g}, \quad (4)$$

where

$$\mathbf{B} = \begin{bmatrix} \psi_1(x_1, y_1) & \psi_1(x_2, y_2) & \dots & \psi_1(x_N, y_N) \\ \psi_2(x_1, y_1) & \dots & \dots & \psi_2(x_N, y_N) \\ \dots & \dots & \dots & \dots \\ \psi_5(x_1, y_1) & \dots & \dots & \psi_5(x_N, y_N) \\ \psi_6(x_1, y_1) & \psi_6(x_2, y_2) & \dots & \psi_6(x_N, y_N) \end{bmatrix}, \quad (5)$$

is a $6 \times N$ matrix,

$$\mathbf{W} = \begin{bmatrix} w_2(x, y) & 0 & \dots & 0 \\ 0 & w_2(x, y) & \dots & 0 \\ \dots & \dots & \dots & \dots \\ 0 & 0 & \dots & w_N(x, y) \end{bmatrix}, \quad (6)$$

is an $N \times N$ diagonal matrix,

$$\mathbf{a} = \begin{bmatrix} a_1 \\ a_2 \\ \dots \\ a_6 \end{bmatrix} \quad \text{and} \quad \mathbf{g} = \begin{bmatrix} g_1 \\ g_2 \\ \dots \\ g_{N-1} \\ g_N \end{bmatrix}, \quad (7)$$

are six- and N -dimensional vectors, and the superscript T denotes the matrix transpose.

If the master influence function $\hat{W}(r)$ is singular at the origin, then the approximating function g_N interpolates through the data points.

- (a) Prepare a graph of the function $g_N(x, y)$ over the square $-1 < x < 1, -1 < y < 1$, for $N = 4$, $(x_1, y_1, g_1) = (-0.5, -0.4, 0.1)$, $(x_2, y_2, g_2) = (0.4, -0.6, 0.3)$, $(x_3, y_3, g_3) = (0.6, 0.7, 0.7)$, and $(x_4, y_4, g_4) = (-0.7, 0.2, 1.1)$, using the master influence function $W(r) = 1$.
- (b) Repeat (a) for the master influence function given in equation (3) with $\alpha = 0.10$ and $\epsilon = 0.001$.
- (c) Develop a method of computing the cardinal functions associated with the moving least-squares approximation.

6.4 Convection – diffusion equation

In Section 6.3, we discussed the solution of Poisson's equation (6.3.1) describing diffusion in the presence of a known distributed source. A generalization of Poisson's equation is the steady-state convection – diffusion equation in the presence of a distributed source,

$$u_x(x, y, f) \frac{\partial f}{\partial x} + u_y(x, y, f) \frac{\partial f}{\partial y} = \kappa \nabla^2 f + r(x, y, f), \quad (6.4.1)$$

where κ is a positive constant with dimensions of length squared divided by time, defined as the medium diffusivity; $u_x(x, y, f)$ and $u_y(x, y, f)$ are the x and y components of the velocity, and $r(x, y, f)$ is the source or production field.

Comparing equation (6.4.1) with (6.3.1), we observe that, in the extended framework presently considered, the source term depends on the *a priori* unknown solution f as well as on the unknown first spatial derivatives, and is given by

$$s(x, y, f) \equiv \frac{1}{\kappa} [-u_x(x, y, f) \frac{\partial f}{\partial x} - u_y(x, y, f) \frac{\partial f}{\partial y} + r(x, y, f)]. \quad (6.4.2)$$

This point of view provides a basis for an iterative solution procedure according to the following steps:

1. Initialize or guess the solution f .
2. Compute the right-hand side of (6.4.2).
3. Solve Poisson's equation (6.4.1) to obtain a new solution.
4. Repeat until convergence.

6.4.1 Linear convection

The most amenable class of linear problems arises when (a) the velocity field (u_x, u_y) explicitly depends on the spatial position, that is, it is independent of the unknown function f , and (b) the production term r is a linear function of f , and may thus be expressed in the form $r = a(x, y) f + b(x, y)$, where $a(x, y)$ and $b(x, y)$ are given functions. Under these conditions, the right-hand side of (6.4.2) simplifies to

$$s(x, y, f) \equiv \frac{1}{\kappa} [-u_x(x, y) \frac{\partial f}{\partial x} - u_y(x, y) \frac{\partial f}{\partial y} + a(x, y) f + b(x, y)]. \quad (6.4.3)$$

We begin formulating the solution by introducing a set of M data points distributed over the solution domain including the boundaries and an associated set of interpo-

lation or influence functions $\phi_i(x, y)$, and write

$$f(x, y) \simeq \sum_{i=1}^M \alpha_i \phi_i(x, y). \quad (6.4.4)$$

The scalar coefficients α_i are computed by requiring the interpolation conditions

$$f(x_j, y_j) = \sum_{i=1}^M \alpha_i \phi_i(x_j, y_j), \quad (6.4.5)$$

for $j = 1, \dots, M$. In vector notation, system (6.4.5) takes the compact form

$$\mathbf{B} \cdot \boldsymbol{\alpha} = \mathbf{f}, \quad (6.4.6)$$

where $B_{ij} \equiv \phi_i(x_i, y_j)$. If the influence functions ϕ_i are cardinal interpolation functions, then \mathbf{B} is the unit matrix.

Inverting (6.4.6), we obtain $\alpha_i = B_{il}^{-1} f_l$, where the superscript “-1” denotes the matrix inverse, and summation over the repeated index l is implied in the range $1, \dots, M$. Substituting this expression into (6.4.4) and switching j to i , we find

$$f(x, y) \simeq f_l B_{jl}^{-1} \phi_j(x, y), \quad (6.4.7)$$

where summation over both repeated indices j and l is implied on the right-hand side.

The spatial derivatives of f may be approximated with linear combinations of corresponding derivatives of the interpolation functions ϕ_j ,

$$\begin{aligned} \frac{\partial f(x, y)}{\partial x} &\simeq f_l B_{jl}^{-1} \frac{\partial \phi_j(x, y)}{\partial x}, \\ \frac{\partial f(x, y)}{\partial y} &\simeq f_l B_{jl}^{-1} \frac{\partial \phi_j(x, y)}{\partial y}. \end{aligned} \quad (6.4.8)$$

Substituting the approximations (6.4.4) and (6.4.8) into the right-hand side of (6.4.3), we express the source term in the form

$$s(x, y, f) \simeq \frac{1}{\kappa} \left[\sum_{l=1}^M \chi_l(x, y) f_l + b(x, y) \right], \quad (6.4.9)$$

where

$$\begin{aligned} \chi_l(x, y) &\equiv -u_x(x, y) B_{jl}^{-1} \frac{\partial \phi_j(x, y)}{\partial x} \\ &\quad - u_y(x, y) B_{jl}^{-1} \frac{\partial \phi_j(x, y)}{\partial y} + a(x, y) B_{jl}^{-1} \phi_j(x, y) \end{aligned} \quad (6.4.10)$$

are auxiliary fields defined in terms of the influence functions.

We have succeeded in expressing the convection – diffusion – production term as a linear combination of the unknown values of the solution at the data points, as shown on the right-hand side of (6.4.9). This completes the first phase of the implementation.

In the second phase, we introduce expansions similar to that shown in (6.3.14) for the individual functions $\chi_l(x, y)$ and for the function $b(x, y)$ shown on the right-hand side of (6.4.9),

$$\chi_l(x, y) \simeq \sum_{l=1}^M \alpha_i^{(l)} H_i(x, y), \quad b(x, y) \simeq \sum_{l=1}^M \alpha_i^{(0)} H_i(x, y), \quad (6.4.11)$$

for $l = 1, \dots, M$. The sets of coefficients $\alpha_i^{(l)}$, $l = 0, \dots, M$, are computed by requiring the interpolation conditions

$$\begin{aligned} b(x_j, y_j) &= \sum_{i=1}^M \alpha_i^{(0)} H_i(x_j, y_j), \\ \chi_l(x_j, y_j) &= \sum_{i=1}^M \alpha_i^{(l)} H_i(x_j, y_j), \end{aligned} \quad (6.4.12)$$

for $j = 1, \dots, M$.

An approximate particular solution of Poisson's equation (6.3.1) with the linear distributed source shown in (6.4.3) is given by

$$\begin{aligned} f^P(x, y) &\simeq \frac{1}{\kappa} \sum_{i=1}^M [\alpha_i^{(0)} + \sum_{l=1}^M \alpha_i^{(l)} f_l] \hat{H}_i(x, y) \\ &= \frac{1}{\kappa} \sum_{i=1}^M \alpha_i^{(0)} \hat{H}_i(x, y) + \frac{1}{\kappa} \sum_{l=1}^M f_l \left[\sum_{i=1}^M \alpha_i^{(l)} \hat{H}_i(x, y) \right]. \end{aligned} \quad (6.4.13)$$

The last expression illustrates the linear dependence of $\psi(x, y)$ on the unknown data values f_l . When only the last term is present on the right-hand side of (6.4.3), expression (6.4.13) takes the simplified form of (6.3.18) with $\alpha_i = \alpha_i^{(0)} / \kappa$.

The general solution of (6.4.1) is $f = f^H + f^P$, where the homogeneous solution f^H satisfies Laplace's equation $\nabla^2 f^H = 0$. Introducing the boundary-integral representation of f^H and evaluating the approximate particular solution (6.4.13) around the boundary as well as at the data points (x_j, y_j) , $i = 1, \dots, M$, we obtain a complete system of linear integral/algebraic equations for the boundary distribution of f or its normal derivative, and for the field values f_i .

As an example, we regard Helmholtz's equation $\nabla^2 f = \lambda^2 f$ as Poisson's equation forced by the source term $s(f) = -\lambda^2 f$. Comparing this expression with the standard form (6.4.3), we find $u_x = 0$, $u_y = 0$, $a(x, y) = -\kappa \lambda^2$, and $b = 0$. The intermediate functions defined in (6.4.10) take the simple forms

$$\chi_l(x, y) = -\kappa \lambda^2 B_{jl}^{-1} \phi_j(x, y). \quad (6.4.14)$$

Identifying the set of influence functions ϕ_j with the set of dual reciprocity functions H_j , and comparing expression (6.4.14) with the second of expressions (6.4.12), we find $\alpha_i^{(l)} = -\kappa \lambda^2 B_{il}^{-1}$. The particular solution is given by

$$f^P(x, y) \simeq -\lambda^2 \sum_{l=1}^M f_l \left[\sum_{i=1}^M B_{il}^{-1} \hat{H}_i(x, y) \right]. \quad (6.4.15)$$

In matrix-vector notation,

$$f^P(x, y) \simeq -\lambda^2 \hat{\mathbf{h}} \cdot \mathbf{B}^{-1} \cdot \mathbf{f}, \quad (6.4.16)$$

where the i th entry of the vector $\hat{\mathbf{h}}$ is occupied by the influence function $H_i(x, y)$, and the i th entry of the vector \mathbf{f} is the unknown field value f_i . Combining expression (6.4.16) with the boundary-integral representation for the homogeneous solution f^H , we obtain the set of equations necessary for the computation of the boundary distribution of f or its normal derivative, and for the field values f_i .

6.4.2 Nonlinear convection

Nonlinear problems arise when the right-hand side of the source term defined in (6.4.2) is a nonlinear function of the *a priori* unknown function f . The analysis provides us with nonlinear algebraic equations relating the particular solution f^P to the vector data field \mathbf{f} . Because of the nonlinearity, the solution must be found by iterative methods.

To illustrate the procedure, we consider the convection – diffusion equation with a Burgers convection term in the x direction,

$$\kappa \nabla^2 f = \gamma f \frac{\partial f}{\partial x}, \quad (6.4.17)$$

where γ is a constant. In this case, the Poisson source term is a quadratic function of f given by

$$s(f) = -\frac{\gamma}{\kappa} f \frac{\partial f}{\partial x}. \quad (6.4.18)$$

Substituting (6.4.7) and the first of (6.4.8) into the right-hand side of (6.4.18), we obtain

$$\begin{aligned} s(f) &\simeq -\frac{\gamma}{\kappa} f_l B_{jl}^{-1} \phi_j(x, y) \frac{\partial \phi_q(x, y)}{\partial x} B_{qp}^{-1} f_p \\ &\equiv \frac{1}{\kappa} f_l \chi_l(x, y, f), \end{aligned} \quad (6.4.19)$$

where summation is implied over all repeated indices in the range $1, \dots, M$, and we have introduced the linear functions of f_p

$$\chi_l(x, y, f) \equiv -\gamma B_{jl}^{-1} \phi_j(x, y) \frac{\partial \phi_q(x, y)}{\partial x} B_{qp}^{-1} f_p. \quad (6.4.20)$$

The solution may be found by iteration according to the following steps:

1. Initialize or guess the field values f_p on the right-hand side of (6.4.20), and compute the functions χ_l .
2. Introduce the second expansion of (6.4.12), and solve the linear problem as discussed in Section 6.4.1.
3. Update the field values f_p on the right-hand side of (6.4.20).
4. Repeat until convergence.

Problem

P.6.4.1 Nonlinear production

Develop an algorithm for computing the solution of the nonlinear diffusion-production equation

$$\kappa \nabla^2 f = -\gamma f^m, \quad (1)$$

for values of the exponent (a) $m = 2$ and (b) $3/2$, where γ is a positive constant.

6.5 Time-dependent problems

Laplace's equation, Poisson's equation, and the inclusive convection – diffusion equation (6.4.1) describe the steady-state or time-independent spatial distribution of a physical variable such as temperature, species concentration, or fluid momentum.

If the field changes in time, then the unknown function f depends on the spatial coordinates (x, y, z) as well as time t .

In one class of problems, physical conservation laws provide us with evolution equations involving the rate of change of a function f expressed by the first time derivative $\partial f / \partial t$. In another class of problems, Newton's second law of motion provides us with evolution equations involving particle acceleration expressed by the second time derivative $\partial^2 f / \partial t^2$.

Consider, for example, unsteady convection – diffusion in the presence of production governed by the equation

$$\frac{\partial f}{\partial t} + u_x \frac{\partial f}{\partial x} + u_y \frac{\partial f}{\partial y} + u_z \frac{\partial f}{\partial z} = \kappa \nabla^2 f + r, \quad (6.5.1)$$

which is a generalization of (6.5.1). An initial condition and boundary conditions for the unknown field f are assumed to be provided.

Three general methods are available for solving problems of this kind by boundary-integral methods:

1. Develop an integral formulation that involves the Green's function of the unsteady equation representing the field due to an impulsive source.
2. Eliminate the time dependence by applying the Laplace transform.
3. Discretize the differential equation in time by approximating the time derivative with finite differences, and apply the boundary-element method to the time-discretized equation.

We shall demonstrate the implementation of these methods with reference to the unsteady diffusion equation

$$\frac{\partial f}{\partial t} = \kappa \nabla^2 f, \quad (6.5.2)$$

which is a simplified, but not contrived, version of (6.5.1).

6.5.1 Unsteady Green's functions method

A Green's function of the unsteady diffusion equation (6.5.2) satisfies the equation

$$\frac{\partial G(\mathbf{x}, \mathbf{x}_0, t - t_0)}{\partial t} = \kappa \nabla^2 G(\mathbf{x}, \mathbf{x}_0, t - t_0) + \delta_n(\mathbf{x} - \mathbf{x}_0) \delta_1(t - t_0), \quad (6.5.3)$$

where $n = 1, 2, 3$ is the dimension of the solution space determining the form of the Laplacian and the choice of the delta function on the right-hand side. Physically, the

Green's function expresses the evolving temperature or species concentration field due to an impulsive point source of heat or species activated at time t_0 at the position \mathbf{x}_0 in a conducting or diffusive medium with uniform diffusivity κ .

The free-space Green's function is equal to zero for negative elapsed times $\hat{t} \equiv t - t_0$, and is given by

$$G(\mathbf{x}, \mathbf{x}_0, t - t_0) = \frac{1}{(4\pi\kappa \hat{t})^{n/2}} \exp\left(-\frac{r^2}{4\kappa \hat{t}}\right) \quad (6.5.4)$$

for positive elapsed times $\hat{t} \equiv t - t_0$, where $r = |\mathbf{x} - \mathbf{x}_0|$ is the distance of the evaluation point from the singular point. Green's functions of the inclusive unsteady convection – diffusion equation are discussed in Reference [58].

It will be necessary to introduce the Green's function of the adjoint of the unsteady diffusion equation, denoted by G^* , satisfying

$$-\frac{\partial G^*(\mathbf{x}, \mathbf{x}_0, t - t_0)}{\partial t} = \kappa \nabla^2 G^*(\mathbf{x}, \mathbf{x}_0, t - t_0) + \delta_n(\mathbf{x} - \mathbf{x}_0) \delta_1(t - t_0). \quad (6.5.5)$$

The adjoint free-space Green's function is equal to zero for positive elapsed times $\hat{t} \equiv t - t_0$, and is given by

$$G^*(\mathbf{x}, \mathbf{x}_0, t - t_0) = G(\mathbf{x}, \mathbf{x}_0, |t - t_0|) \quad (6.5.6)$$

for negative elapsed times $\hat{t} \equiv t - t_0$.

To develop the boundary-integral representation, we consider Green's second identity in one, two, or three dimensions, expressed by equation (1.1.3), (2.1.4), or (4.1.3), and recast it into the form

$$\begin{aligned} \phi & \left(-\frac{\partial f}{\partial t} + \kappa \nabla^2 f \right) + \frac{\partial(f \phi)}{\partial t} - f \left(\frac{\partial \phi}{\partial t} + \kappa \nabla^2 \phi \right) \\ &= \kappa \nabla \cdot (\phi \nabla f - f \nabla \phi). \end{aligned} \quad (6.5.7)$$

Next, we assume that f is a solution of (6.5.2), and thus eliminate the term enclosed by the first set of parentheses on the left-hand side of (6.5.7), and identify ϕ with the adjoint Green's function G^* to obtain

$$\frac{\partial(f G^*)}{\partial t} + f \delta_n(\mathbf{x} - \mathbf{x}_0) \delta_1(t - t_0) = \kappa \nabla \cdot (G^* \nabla f - f \nabla G^*), \quad (6.5.8)$$

for $t \leq t_0$.

For clarity, we confine our attention to the two-dimensional case, $n = 2$, select a stationary control area A_c enclosed by the contour C , and integrate (6.5.8) in space over

the control area and in time from the initial instant $t = t_s$ up to the current instant t_0+ (the plus sign denotes the upward limit). Using the distinguishing properties of the delta function $\delta_1(t - t_0)$, applying the divergence theorem to convert the area integral to a contour integral on the right-hand side, and invoking property (6.5.6), we find

$$\begin{aligned} & \left[\int \int_{A_c} f(\mathbf{x}, t) G(\mathbf{x}, \mathbf{x}_0, t_0 - t) dx dy \right]_{t=t_s}^{t=t_0+} \\ & + \int \int_{A_c} f(\mathbf{x}, t_0) \delta_2(\mathbf{x} - \mathbf{x}_0) dx dy \\ & = - \int_{t_s}^{t_0} \int_C G(\mathbf{x}, \mathbf{x}_0, t_0 - t) [\mathbf{n}(\mathbf{x}) \cdot \nabla f(\mathbf{x}, t)] dl(\mathbf{x}) dt \\ & + \int_{t_s}^{t_0} \int_C f(\mathbf{x}, t) [\mathbf{n}(\mathbf{x}) \cdot \nabla G(\mathbf{x}, \mathbf{x}_0, t_0 - t)] dl(\mathbf{x}) dt, \end{aligned} \quad (6.5.9)$$

where the unit normal vector \mathbf{n} points into the control area A_c . When evaluated at the upper limit $t = t_0+$, the Green's function vanishes, and so does the term enclosed by the first set of parentheses on the left-hand side of (6.5.9).

Placing the singular point \mathbf{x}_0 inside the control volume A_c , using the properties of the delta function to evaluate the second integral on the left-hand side of (6.5.9), and rearranging, we obtain the integral representation

$$\begin{aligned} f(\mathbf{x}_0, t_0) &= - \int \int_{A_c} f(\mathbf{x}, t_s) G(\mathbf{x}, \mathbf{x}_0, t_0 - t_s) dx dy \\ & - \int_{t_s}^{t_0} \int_C G(\mathbf{x}, \mathbf{x}_0, t_0 - t) [\mathbf{n}(\mathbf{x}) \cdot \nabla f(\mathbf{x}, t)] dl(\mathbf{x}) dt \\ & + \int_{t_s}^{t_0} \int_C f(\mathbf{x}, t) [\mathbf{n}(\mathbf{x}) \cdot \nabla G(\mathbf{x}, \mathbf{x}_0, t_0 - t)] dl(\mathbf{x}) dt, \end{aligned} \quad (6.5.10)$$

involving: (a) a domain integral whose integrand is defined in terms of the unsteady Green's function, and (b) two boundary integrals. Physically, these integrals represent the field due to diffusing point sources and point-source dipoles distributed over the boundaries of the solution in the space-time domain.

If time-independent Dirichlet boundary conditions are specified, the solution will tend to a steady state at long times. Indeed, for long elapsed times $t_0 - t_s$, the Green's function in the first integral on the right-hand side of (6.5.10) decays exponentially to zero, yielding the representation (2.3.3) with the steady Green's function, as shown in equation (1) of P.6.5.1.

6.5.2 Laplace transform method

To develop this method, we introduce the Laplace transform of the unknown function f defined as

$$\hat{f}(\mathbf{x}, s) \equiv \int_{0+}^{\infty} f(\mathbf{x}, t) e^{-st} dt, \quad (6.5.11)$$

where s is a real or complex constant whose real part is sufficiently large so that the integral on the right-hand side of (6.5.11) is finite and $0+$ denotes the upward limit. Thus, in the case of an impulsive field exhibiting a discontinuity at the initial instant, the lower limit of integration in (6.5.11) corresponds to the nontrivial state established immediately after the impulse.

Multiplying both sides of the governing equation (6.5.2) by e^{-st} , integrating with respect to time from $0+$ to infinity, and writing

$$\begin{aligned} \int_{0+}^{\infty} \frac{\partial f(\mathbf{x}, t)}{\partial t} e^{-st} dt &= [f(\mathbf{x}, t) e^{-st}]_{0+}^{\infty} - \int_{0+}^{\infty} f(\mathbf{x}, t) de^{-st} \\ &= -f(\mathbf{x}, t = 0^+) + s \int_{0+}^{\infty} f(\mathbf{x}, t) e^{-st} dt \\ &= -f(\mathbf{x}, t = 0^+) + s \hat{f}(\mathbf{x}, s), \end{aligned} \quad (6.5.12)$$

we derive the inhomogeneous Helmholtz equation

$$\kappa \nabla^2 \hat{f}(\mathbf{x}, s) - s \hat{f}(\mathbf{x}, s) + f(\mathbf{x}, t = 0^+) = 0. \quad (6.5.13)$$

Having eliminated the time dependence, we may solve equation (6.5.13) for a sequence of real or complex values for s using the methods discussed in previous sections, and then recover the solution in terms of the inverse Laplace transform by numerical methods (e.g., [14]).

Stehfest's method [65] of inverting the Laplace transform is based on the weighted-sum formula

$$f(\mathbf{x}, t) \simeq \frac{\ln 2}{t} \sum_{i=1}^{2m} \simeq c_i f(\mathbf{x}, s_i), \quad (6.5.14)$$

where m is a specified truncation level, and

$$s_i = \frac{m \ln 2}{t}, \quad (6.5.15)$$

$$c_i = (-1)^{i+m} \sum_{j=\lceil \frac{i+1}{2} \rceil}^{\text{Min}(i,m)} \frac{j^m (2j)!}{(m-j)! j! (j-1)! (i-j)! (2j-i)!}.$$

The operator $\lfloor \frac{i+1}{2} \rfloor$ denotes the integral part of the enclosed variable and the operator $\text{Min}(i, m)$ denotes the minimum of i and m .

6.5.3 Time-discretization methods

Brebbia and Walker [10] proposed approximating the time derivative in (6.5.2) with a finite difference involving two or more time levels, evaluating the right-hand side at an appropriate time instant, and then computing the solution at a new time level using the boundary-element method.

The general form of a two-time level discretization scheme is

$$\frac{f^{n+1} - f^n}{\Delta t} = \kappa \left[\beta \nabla^2 f^{n+1} + (1 - \beta) \nabla^2 f^n \right], \quad (6.5.16)$$

where β is an arbitrary parameter ranging between zero and unity, and the superscripts n and $n + 1$ denote, respectively, evaluation at time t and $t + \Delta t$. The error of the temporal discretization underlying (6.5.16) is on the order of Δt^2 when $\beta = 1/2$, and Δt otherwise.

The explicit Euler discretization, arises when $\beta = 0$, the implicit Crank-Nicolson discretization arises when $\beta = 1/2$, and the implicit Euler discretization arises when $\beta = 1$. Numerical analysis shows that, with the explicit discretization, an excessively small time step Δt is required for a stable simulation that is free of artificial oscillations (e.g. [60]). Partially implicit discretizations allow the use of larger time steps and are the standard choice in practice.

Moving the terms containing the unknown solution f^{n+1} in (6.5.16) to the left-hand side and rearranging, we obtain the inhomogeneous Helmholtz equation

$$\kappa \nabla^2 f^{n+1} - \frac{1}{\beta \Delta t} f^{n+1} = -\frac{1 - \beta}{\beta} \kappa \nabla^2 f^n - \frac{1}{\beta \Delta t} f^n. \quad (6.5.17)$$

The solution for f^{n+1} can be found for a succession of time levels by the methods discussed in previous sections, yielding the time evolution.

Problems

P.6.5.1 Steady from unsteady Green's functions

The steady field due to a permanent point source with constant strength is given by

$$\phi(\mathbf{x}, \mathbf{x}_0) = \int_{-\infty}^t G(\mathbf{x}, \mathbf{x}_0, t - t_0) dt_0. \quad (1)$$

Substitute the Green's function (6.5.4) into the integrand and carry out the integration for $n = 1, 2$, and 3 to show that $\phi(\mathbf{x}, \mathbf{x}_0)$ is, in fact, the Green's function of Laplace's equation in the corresponding dimension.

P.6.5.2 Green's functions of the wave equation

A Green's function of the wave equation satisfies the equation

$$\frac{\partial^2 G(\mathbf{x}, \mathbf{x}_0, t - t_0)}{\partial t^2} = c^2 \nabla^2 G(\mathbf{x}, \mathbf{x}_0, t - t_0) + \delta_n(\mathbf{x} - \mathbf{x}_0) \delta_1(t - t_0), \quad (1)$$

where c is the wave speed, and $n = 1, 2, 3$ is the dimension of the solution space determining the form of the Laplacian and the choice of the delta function on the right-hand side. The last term on the right-hand side of (1) has dimensions of $L^{-n} T^{-1}$, where L stands for length and T for time.

(a) Verify by direct substitution that the free-space Green's function in one dimension ($n = 1$) is given by

$$G(x, x_0, \hat{t}) = \frac{1 - H(|x - x_0| - c \hat{t})}{2c}, \quad (2)$$

where $\hat{t} \equiv t - t_0$ is the elapsed time; the Heaviside step function $H(w)$ is equal to unity when $w > 0$, and zero when $w < 0$ ([45], p. 843). Prepare graphs of the Green's function at a sequence of times and discuss its behavior.

(b) Verify by direct substitution that the free-space Green's function in two dimensions ($n = 2$) is given by

$$G(\mathbf{x}, \mathbf{x}_0, \hat{t}) = \frac{1 - H(r - c \hat{t})}{2\pi c} \frac{1}{\sqrt{r^2 - c^2 \hat{t}^2}}, \quad (3)$$

where $r = |\mathbf{x} - \mathbf{x}_0|$ is the scalar distance of the evaluation point from the singular point ([45], p. 842). Prepare graphs of the Green's function at a sequence of times, and discuss its behavior.

(c) Verify by direct substitution that the free-space Green's function in three dimensions ($n = 3$) is given by

$$G(\mathbf{x}, \mathbf{x}_0, \hat{t}) = \frac{1}{4\pi c^2 r} \delta_1\left(\frac{r}{c} - \hat{t}\right), \quad (4)$$

where $r = |\mathbf{x} - \mathbf{x}_0|$ is the scalar distance of the evaluation point from the singular point ([45], p. 838).

Equation (4) describes a spherical shell expanding away from the origin with radial velocity c .

(d) Develop an integral formulation similar to that discussed in Section 6.5.1 for the unsteady diffusion equation ([45], Ch. 7).

Chapter 7

Viscous flow

In the preceding chapters, we have discussed boundary-integral formulations and boundary-element methods for scalar differential equations, including Laplace's equation, Helmholtz's equation, and the convection – diffusion equation.

The theoretical formulation and numerical implementation can be extended in a straightforward fashion to encompass systems of coupled differential equations for vector unknowns. The boundary-integral formulation involves the familiar sequence of six steps: establish a reciprocal relation; introduce the Green's functions; develop the boundary-integral representation; derive boundary-integral equations; generate and solve linear systems of equations by collocation or Galerkin projection. Inhomogeneous, nonlinear, and time-dependent equations can be solved by the generalized boundary-integral methods discussed in Chapter 6.

In this chapter, we illustrate the procedure by discussing the boundary-integral formulation of viscous flow at low Reynolds numbers. In Appendix C, we summarize corresponding results in elastostatics in a way that parallels this chapter's discourse. The similarities in the treatment of viscous flow and elastostatics underscores the generality of the basic approach.

7.1 Governing equations

Referring to a frame of reference that is fixed in space, let us observe the flow of an incompressible fluid with velocity $\mathbf{u} = (u_x, u_y, u_z)$.

Mass conservation expressed by the continuity equation requires that the divergence of the velocity vanish (e.g., [59]),

$$\nabla \cdot \mathbf{u} \equiv \frac{\partial u_x}{\partial x} + \frac{\partial u_y}{\partial y} + \frac{\partial u_z}{\partial z} = 0. \quad (7.1.1)$$

Consider an infinitesimal surface drawn in the interior of a fluid or at the boundaries, lying in a plane that is perpendicular to the unit vector \mathbf{n} . The force per unit area acting on this surface, denoted by \mathbf{f} , is called the *traction*. By definition, the traction

depends on position in the fluid, \mathbf{x} , and on the orientation of the infinitesimal surface determined by the unit vector \mathbf{n} . To signify this dependence, we write $\mathbf{f}(\mathbf{x}, \mathbf{n})$.

Analysis reveals that the traction vector depends linearly on the normal vector,

$$f_j(\mathbf{x}, \mathbf{n}) = n_i \sigma_{ij}(\mathbf{x}), \quad (7.1.2)$$

where σ_{ij} is the *Cauchy stress tensor* (e.g., [59]); summation over the repeated index i in the spatial coordinates x, y , and z is implied on the right-hand side of (7.1.2).

Applying Newton's second law to describe the motion of a small fluid parcel, we derive Cauchy's equation of motion

$$\rho \left(\frac{\partial u_i}{\partial t} + u_j \frac{\partial u_i}{\partial x_j} \right) = \frac{\partial \sigma_{ji}}{\partial x_j} + \rho g_i, \quad (7.1.3)$$

where ρ is the fluid density [59]; summation over the repeated index j is implied on both sides. The last term, ρg_i , expresses the effect of an external long-range body force. In the case of the gravitational force, \mathbf{g} is the acceleration of gravity.

In terms of the material derivative $D/Dt \equiv \partial/\partial t + u_j \partial/\partial x_j$, the equation of motion reads (e.g., [59])

$$\rho \frac{D u_i}{D t} = \frac{\partial \sigma_{ji}}{\partial x_j} + \rho g_i. \quad (7.1.4)$$

Physically, the material derivative expresses the rate of change of a quantity experienced by an observer who rides on a point particle convected by the fluid.

In vector notation, the equation of motion takes the form

$$\rho \frac{D \mathbf{u}}{D t} \equiv \rho \left(\frac{\partial \mathbf{u}}{\partial t} + \mathbf{u} \cdot \nabla \mathbf{u} \right) = \nabla \cdot \boldsymbol{\sigma} + \rho \mathbf{g}. \quad (7.1.5)$$

If the fluid is Newtonian, the stress tensor is related to the pressure p and to the rate-of-deformation tensor by the linear constitutive equation (e.g., [59])

$$\sigma_{ij} = -\delta_{ij} p + \mu \left(\frac{\partial u_i}{\partial x_j} + \frac{\partial u_j}{\partial x_i} \right), \quad (7.1.6)$$

where μ is the fluid viscosity.

Substituting equation (7.1.6) into the equation of motion (7.1.3) and simplifying, we obtain the Navier-Stokes equation (e.g., [59])

$$\rho \left(\frac{\partial u_i}{\partial t} + u_j \frac{\partial u_i}{\partial x_j} \right) = -\frac{\partial p}{\partial x_i} + \mu \nabla^2 u_i + \rho g_i. \quad (7.1.7)$$

In vector notation,

$$\rho \left(\frac{\partial \mathbf{u}}{\partial t} + \mathbf{u} \cdot \nabla \mathbf{u} \right) = -\nabla p + \mu \nabla^2 \mathbf{u} + \rho \mathbf{g}. \quad (7.1.8)$$

In summary, the motion of an incompressible Newtonian fluid is governed by equations (7.1.1) and (7.1.8). In three dimensions, this system comprises four scalar equations for four scalar fields, including the pressure and the three components of the velocity.

7.1.1 Non-dimensionalization

To assess the relative importance of the various terms in the equation of motion, we identify a characteristic length L related to the size of the boundaries, a characteristic velocity U expressing the intensity of the flow, and a characteristic external or intrinsic time T . Next, we scale the velocity by U , all lengths by L , time by T , and the pressure by $\mu U/L$, and introduce dimensionless variables and operators denoted by a caret, defined as

$$\hat{\mathbf{u}} \equiv \frac{\mathbf{u}}{U}, \quad \hat{\mathbf{x}} \equiv \frac{\mathbf{x}}{L}, \quad \hat{\nabla} \equiv L \nabla, \quad \hat{t} \equiv \frac{t}{T}, \quad \hat{p} \equiv \frac{pL}{\mu U}. \quad (7.1.9)$$

Solving for the physical variables in terms of the dimensionless ones and substituting the result into the equation of motion, we find

$$\beta \frac{\partial \hat{\mathbf{u}}}{\partial \hat{t}} + Re \hat{\mathbf{u}} \cdot \hat{\nabla} \hat{\mathbf{u}} = -\nabla \hat{p} + \hat{\nabla}^2 \hat{\mathbf{u}} + \frac{Re}{Fr^2} \frac{\mathbf{g}}{|\mathbf{g}|}, \quad (7.1.10)$$

where

$$\beta = \frac{\rho L^2}{\mu T} \quad (7.1.11)$$

is a dimensionless *acceleration* or *frequency parameter* expressing the relative importance of inertial acceleration body forces and viscous surface forces,

$$Re = \frac{\rho U L}{\mu} \quad (7.1.12)$$

is the *Reynolds number* expressing the relative importance of inertial convective body forces and viscous surface forces, and

$$Fr = \frac{U}{\sqrt{|\mathbf{g}| L}} \quad (7.1.13)$$

is the *Froude number* expressing the relative importance of inertial convective and external body forces. The ratio Re/Fr^2 on the right-hand side of (7.1.10) expresses the relative importance of external body forces and viscous surface forces.

In the absence of external forcing, $T = L/U$, and the acceleration parameter β reduces to the Reynolds number.

7.1.2 Unsteady Stokes flow

When the Reynolds number Re is sufficiently less than unity, the second term on the left-hand side of (7.1.10) is small compared to the rest of the terms and may be neglected. Reverting to physical variables, we find that the flow is governed by the unsteady Stokes equation

$$\rho \frac{\partial \mathbf{u}}{\partial t} = -\nabla p + \mu \nabla^2 \mathbf{u} + \rho \mathbf{g} \quad (7.1.14)$$

or

$$\rho \frac{\partial \mathbf{u}}{\partial t} = \nabla \cdot \boldsymbol{\sigma} + \rho \mathbf{g}. \quad (7.1.15)$$

Physically, the unsteady Stokes equation describes flows characterized by sudden acceleration or deceleration.

Taking the Laplacian of the unsteady Stokes equation and requiring the continuity equation (7.1.1), we find that the pressure is a harmonic function,

$$\nabla^2 p = 0. \quad (7.1.16)$$

7.1.3 Stokes flow

When both dimensionless numbers β and Re are sufficiently less than unity, all terms on the left-hand side of (7.1.10) are small compared to the terms on the right-hand side and may be neglected. Reverting to physical variables, we find that the flow is governed by the Stokes equation

$$-\nabla p + \mu \nabla^2 \mathbf{u} + \rho \mathbf{g} = \mathbf{0}, \quad (7.1.17)$$

or

$$\nabla \cdot \boldsymbol{\sigma} + \rho \mathbf{g} = \mathbf{0}, \quad (7.1.18)$$

describing Stokes or creeping flow. Even though time does not appear in the Stokes equation, the flow is not necessarily steady: quasi-steady time evolution may occur because of boundary motion or changing boundary conditions.

Taking the Laplacian of the Stokes equation and using the continuity equation (7.1.1), we find that the pressure is a harmonic function, as shown in (7.1.16).

7.1.4 Modified pressure

When the body force is uniform over the domain of flow, it is convenient to eliminate the inhomogeneous term from the equation of motion by introducing the dynamic or

modified pressure

$$P \equiv p - \rho \mathbf{g} \cdot \mathbf{x}. \quad (7.1.19)$$

In terms of the modified pressure, the Stokes equation (7.1.17) assumes the homogeneous form

$$-\nabla P + \mu \nabla^2 \mathbf{u} = \mathbf{0}, \quad (7.1.20)$$

which is a convenient starting point for developing the boundary-integral formulation

Problem

P.7.1.1 Vorticity

The vorticity vector is defined as the curl of the velocity vector field (Appendix A) (e.g., [59]),

$$\boldsymbol{\omega} = \nabla \times \mathbf{u}. \quad (1)$$

When the vorticity vector vanishes throughout the domain of a flow, the flow is called potential or irrotational.

- (a) Show that the vorticity field is solenoidal, that is, $\nabla \cdot \boldsymbol{\omega} = 0$. (b) Prove the identity $\nabla^2 \mathbf{u} = -\nabla \times \boldsymbol{\omega}$, and discuss its implication on the equation of motion for irrotational flow. (c) Show that the components of the vorticity vector field in Stokes flow are harmonic functions, $\nabla^2 \boldsymbol{\omega} = \mathbf{0}$.
-

7.2 Stokes flow

To develop the boundary-integral formulation of Stokes flow, we repeat the analysis of Chapters 2 and 4 for potential flow with appropriate substitutions. The sequence of steps includes: (a) establish the Lorentz reciprocal theorem, which is the counterpart of Green's second identity, (b) introduce the Green's functions, and (c) derive integral representations and accompanying integral equations.

7.2.1 The Lorentz reciprocal relation

Consider two unrelated Newtonian flows with velocity fields \mathbf{u} and \mathbf{u}' , pressure fields p and p' , and Newtonian stress tensors σ and σ' . Working as in Chapters 2 and 4

in deriving Green's second identity for Laplace's equation, we compute the scalar projection

$$\begin{aligned} \mathbf{u}' \cdot (\nabla \cdot \sigma) &\equiv u'_j \frac{\partial \sigma_{ij}}{\partial x_i} \\ &= \frac{\partial(u'_j \sigma_{ij})}{\partial x_i} - \sigma_{ij} \frac{\partial u'_j}{\partial x_i} = \frac{\partial(u'_j \sigma_{ij})}{\partial x_i} - \left(-p \delta_{ij} + \mu \left(\frac{\partial u_i}{\partial x_j} + \frac{\partial u_j}{\partial x_i} \right) \right) \frac{\partial u'_j}{\partial x_i} \\ &= \frac{\partial(u'_j \sigma_{ij})}{\partial x_i} + p \frac{\partial u'_i}{\partial x_i} - \mu \left(\frac{\partial u_i}{\partial x_j} + \frac{\partial u_j}{\partial x_i} \right) \frac{\partial u'_j}{\partial x_i}. \end{aligned} \quad (7.2.1)$$

Invoking the continuity equation, we set $\partial u'_i / \partial x_i = 0$ and find

$$u'_j \frac{\partial \sigma_{ij}}{\partial x_i} = \frac{\partial(u'_j \sigma_{ij})}{\partial x_i} - \mu \left(\frac{\partial u_i}{\partial x_j} + \frac{\partial u_j}{\partial x_i} \right) \frac{\partial u'_j}{\partial x_i}. \quad (7.2.2)$$

Switching the order of the two flows, we obtain the converse identity

$$u_j \frac{\partial \sigma'_{ij}}{\partial x_i} = \frac{\partial(u_j \sigma'_{ij})}{\partial x_i} - \mu \left(\frac{\partial u'_i}{\partial x_j} + \frac{\partial u'_j}{\partial x_i} \right) \frac{\partial u_j}{\partial x_i}. \quad (7.2.3)$$

Subtracting (7.2.3) from (7.2.2), we derive the counterpart of Green's second identity

$$u'_j \frac{\partial \sigma_{ij}}{\partial x_i} - u_j \frac{\partial \sigma'_{ij}}{\partial x_i} = \frac{\partial}{\partial x_i} (u'_j \sigma_{ij} - u_j \sigma'_{ij}). \quad (7.2.4)$$

If the two flows satisfy the Stokes equation in the absence of a body force, the left-hand side of (7.2.4) vanishes, yielding the Lorentz reciprocal relation [42]

$$\frac{\partial}{\partial x_i} (u'_j \sigma_{ij} - u_j \sigma'_{ij}) = 0. \quad (7.2.5)$$

7.2.2 Green's functions

The Green's functions of Stokes flow provide us with velocity and pressure fields that satisfy the continuity equation, $\nabla \cdot \mathbf{u} = 0$, and the singularly forced Stokes equation

$$-\nabla p + \mu \nabla^2 \mathbf{u} + \delta_n(\mathbf{x} - \mathbf{x}_0) \mathbf{b} = \nabla \cdot \sigma + \delta_n(\mathbf{x} - \mathbf{x}_0) \mathbf{b} = \mathbf{0}, \quad (7.2.6)$$

where \mathbf{b} is a constant vector, and δ_n is the delta function in two or three dimensions, $n = 2, 3$.

Physically, the Green's functions express the flow due to a point force applied at the position \mathbf{x}_0 , in the absence or presence of boundaries; the constant vector \mathbf{b} determines the strength and orientation of the point force.

It is convenient to express the solution of (7.2.6) in the form

$$\begin{aligned} u_i(\mathbf{x}) &= \frac{1}{4\pi\mu} G_{ij}(\mathbf{x}, \mathbf{x}_0) b_j, & p(\mathbf{x}) &= \frac{1}{4\pi} p_j(\mathbf{x}, \mathbf{x}_0) b_j, \\ \sigma_{ik}(\mathbf{x}) &= \frac{1}{4\pi} T_{ijk}(\mathbf{x}, \mathbf{x}_0) b_j, \end{aligned} \quad (7.2.7)$$

in the case of two-dimensional flow ($n = 2$), and

$$\begin{aligned} u_i(\mathbf{x}) &= \frac{1}{8\pi\mu} G_{ij}(\mathbf{x}, \mathbf{x}_0) b_j, & p(\mathbf{x}) &= \frac{1}{8\pi} p_j(\mathbf{x}, \mathbf{x}_0) b_j, \\ \sigma_{ik}(\mathbf{x}) &= \frac{1}{8\pi} T_{ijk}(\mathbf{x}, \mathbf{x}_0) b_j, \end{aligned} \quad (7.2.8)$$

in the case of three-dimensional flow ($n = 3$).

The continuity equation requires that in both cases

$$\frac{\partial G_{ij}}{\partial x_i}(\mathbf{x}, \mathbf{x}_0) = 0. \quad (7.2.9)$$

The Stokes equation requires that the Green's functions satisfy the equations

$$\begin{aligned} -\frac{\partial p_j(\mathbf{x}, \mathbf{x}_0)}{\partial x_i} + \nabla^2 G_{ij}(\mathbf{x}, \mathbf{x}_0) + 4\pi \delta_{ij} \delta_2(\mathbf{x} - \mathbf{x}_0) &= 0, \\ \frac{\partial T_{ijk}(\mathbf{x}, \mathbf{x}_0)}{\partial x_k} = \frac{\partial T_{kji}(\mathbf{x}, \mathbf{x}_0)}{\partial x_k} &= -4\pi \delta_{ij} \delta_2(\mathbf{x} - \mathbf{x}_0), \end{aligned} \quad (7.2.10)$$

in the case of two-dimensional flow ($n = 2$), and

$$\begin{aligned} -\frac{\partial p_j(\mathbf{x}, \mathbf{x}_0)}{\partial x_i} + \nabla^2 G_{ij}(\mathbf{x}, \mathbf{x}_0) + 8\pi \delta_{ij} \delta_3(\mathbf{x} - \mathbf{x}_0) &= 0, \\ \frac{\partial T_{ijk}(\mathbf{x}, \mathbf{x}_0)}{\partial x_k} = \frac{\partial T_{kji}(\mathbf{x}, \mathbf{x}_0)}{\partial x_k} &= -8\pi \delta_{ij} \delta_3(\mathbf{x} - \mathbf{x}_0), \end{aligned} \quad (7.2.11)$$

in the case of three-dimensional flow ($n = 3$).

Substituting expressions (7.2.7) or (7.2.8) into the Newtonian constitutive equation (7.1.6), we find that the stress Green's function derives from the velocity and pressure Green's functions by the relation

$$T_{ijk} = -\delta_{ik} p_j + \frac{\partial G_{ij}}{\partial x_k} + \frac{\partial G_{kj}}{\partial x_i}. \quad (7.2.12)$$

Consistent with the symmetry of the stress tensor evident in (7.1.6), $T_{ijk} = T_{kji}$.

7.2.3 Free-space Green's functions

The free-space Green's function is given by

$$\begin{aligned} G_{ij}(\mathbf{x} - \mathbf{x}_0) &= -\delta_{ij} \ln r + \frac{\hat{x}_i \hat{x}_j}{r^2}, \\ p_j(\mathbf{x} - \mathbf{x}_0) &= 2 \frac{\hat{x}_j}{r^2}, \quad T_{ijk}(\mathbf{x} - \mathbf{x}_0) = -4 \frac{\hat{x}_i \hat{x}_j \hat{x}_k}{r^4}, \end{aligned} \tag{7.2.13}$$

in the case of two-dimensional flow ($n = 2$), and by

$$\begin{aligned} G_{ij}(\mathbf{x} - \mathbf{x}_0) &= \frac{\delta_{ij}}{r} + \frac{\hat{x}_i \hat{x}_j}{r^3}, \\ p_j(\mathbf{x} - \mathbf{x}_0) &= 2 \frac{\hat{x}_j}{r^3}, \quad T_{ijk}(\mathbf{x} - \mathbf{x}_0) = -6 \frac{\hat{x}_i \hat{x}_j \hat{x}_k}{r^5}, \end{aligned} \tag{7.2.14}$$

in the case of three-dimensional flow ($n = 3$), where $\hat{\mathbf{x}} \equiv \mathbf{x} - \mathbf{x}_0$ and $r = |\hat{\mathbf{x}}|$. The free-space Green's function for the velocity is known as the “Stokeslet.”

7.2.4 Green's functions in bounded domains

If the domain of a flow is bounded by a solid surface, it is convenient to use a Green's function whose velocity components G_{ij} vanish over that surface, so that the no-slip and no-penetration boundary conditions are automatically satisfied (e.g., [55]).

Subdirectory `sgf_2d` of directory `stokes` of *BEMLIB* contains a collection of subroutines that evaluate the following Green's functions of two-dimensional Stokes flow:

- Green's function for flow in free space.
- Green's function for flow in a semi-infinite domain bounded by a plane wall.
- Singly periodic Green's function in free space.
- Singly periodic Green's function for flow in a semi-infinite domain bounded by a plane wall.
- Singly periodic Green's function for flow in a channel bounded by two parallel plane walls.
- Doubly periodic Green's function.

Subdirectory `sgf_3d` of directory `stokes` of *BEMLIB* contains a collection of subroutines that evaluate the following Green's functions of three-dimensional Stokes flow:

- Green's function for flow in free space.
- Green's function for flow in a semi-infinite domain bounded by a plane wall.
- Green's function for flow in the exterior of a sphere.
- Doubly periodic Green's function.
- Triply periodic Green's function.

7.2.5 Properties of the Green's functions

The Green's functions for the velocity satisfy the symmetry property

$$G_{ij}(\mathbf{x}, \mathbf{x}_0) = G_{ji}(\mathbf{x}_0, \mathbf{x}), \quad (7.2.15)$$

which allows us to switch the location of the evaluation point and the singular point, provided that we also switch the order of the indices. To prove this property, we apply identity (7.2.4) for the velocity fields induced by two point forces whose singular points are located at different positions, integrate the resulting expression over a selected control area or volume enclosed by the contour C_G or surface S_G , and use the distinctive properties of the delta function [55].

Consider a two-dimensional flow, and integrate the continuity equation (7.2.9) over an arbitrary control area A_c enclosed by the contour C . Using the divergence theorem to convert the areal to a line integral, we find that the velocity Green's functions satisfy the integral identity

$$\int_C n_i(\mathbf{x}) G_{ij}(\mathbf{x}, \mathbf{x}_0) dl(\mathbf{x}) = 0. \quad (7.2.16)$$

Working similarly with the second equation in (7.2.10), we find that the stress Green's functions satisfy the integral identity

$$\frac{1}{4\pi} \int_C T_{ijk}(\mathbf{x}, \mathbf{x}_0) n_k(\mathbf{x}) dl(\mathbf{x}) = \begin{cases} \delta_{ij} & \text{when } \mathbf{x}_0 \text{ is inside } A_c \\ \frac{1}{2} \delta_{ij} & \text{when } \mathbf{x}_0 \text{ is on } C \\ 0 & \text{when } \mathbf{x}_0 \text{ is outside } A_c \end{cases}, \quad (7.2.17)$$

where the unit normal vector \mathbf{n} points *into* the control area enclosed by C . When the point \mathbf{x}_0 lies on the boundary C , the integral on the left-hand side of (7.2.17) is a principal-value integral.

Using the three relations shown in (7.2.19), we derive the important identity

$$\int_C T_{ijk}(\mathbf{x}, \mathbf{x}_0) n_k(\mathbf{x}) dl(\mathbf{x}) = \int_C^{PV} T_{ijk}(\mathbf{x}, \mathbf{x}_0) n_k(\mathbf{x}) dl(\mathbf{x}) \pm \frac{1}{2} \delta_{ij}, \quad (7.2.18)$$

where PV denotes the principal-value integral computed by placing the evaluation point \mathbf{x}_0 precisely on the contour C . The plus or minus sign on the right-hand side of (7.2.18) applies, respectively, when the point \mathbf{x}_0 on the left-hand side lies inside or outside the control area A_c .

The counterpart of (7.2.16) for three-dimensional flow is

$$\int_D n_i(\mathbf{x}) G_{ij}(\mathbf{x}, \mathbf{x}_0) dS(\mathbf{x}) = 0, \quad (7.2.19)$$

where D is the surface enclosing a control volume V_c , and the counterpart of (7.2.17) is

$$\frac{1}{8\pi} \int_D T_{ijk}(\mathbf{x}, \mathbf{x}_0) n_k(\mathbf{x}) dS(\mathbf{x}) = \begin{cases} \delta_{ij} & \text{when } \mathbf{x}_0 \text{ is inside } D \\ \frac{1}{2} \delta_{ij} & \text{when } \mathbf{x}_0 \text{ is on } D \\ 0 & \text{when } \mathbf{x}_0 \text{ is outside } D \end{cases}, \quad (7.2.20)$$

where the unit normal vector \mathbf{n} points *into* the control volume enclosed by D . When the point \mathbf{x}_0 is located on D , the improper integral on the left-hand side of (7.2.20) is a principal-value integral.

Using the three relations shown in (7.2.20), we derive the counterpart of (7.2.18),

$$\int_D T_{ijk}(\mathbf{x}, \mathbf{x}_0) n_k(\mathbf{x}) dS(\mathbf{x}) = \int_D^{PV} T_{ijk}(\mathbf{x}, \mathbf{x}_0) n_k(\mathbf{x}) dS(\mathbf{x}) \pm \frac{1}{2} \delta_{ij}, \quad (7.2.21)$$

where PV denotes the principal-value integral computed by placing the evaluation point \mathbf{x}_0 precisely on the surface D . The plus or minus sign on the right-hand side applies, respectively, when the point \mathbf{x}_0 on the left-hand side lies inside or outside the control volume V_c .

Problem

P.7.2.1 Computation of the free-space Stokes Green's function

To compute the free-space Green's function in two dimensions, we express it in the form

$$G_{ij} = 4\pi (\delta_{ij} \nabla^2 H - \frac{\partial^2 H}{\partial x_i \partial x_j}), \quad (1)$$

where H is a generating function. Expression (1) is motivated by the realization that the continuity equation is satisfied for any choice of H .

Moreover, we recall that the pressure is a harmonic function and set

$$p_j = -4\pi \frac{\partial G^L}{\partial x_j}, \quad (2)$$

where $G^L = -\frac{1}{2\pi} \ln r$ is the free-space Green's function of Laplace's equation. Substituting (1) and (2) along with expression $\delta_2(\mathbf{x} - \mathbf{x}_0) = -\nabla^2 G^L$ into the first equation of equation (7.2.10) and rearranging, we obtain

$$\left(\delta_{ij} \nabla^2 - \frac{\partial^2}{\partial x_i \partial x_j} \right) (\nabla^2 H - G^L) = 0. \quad (3)$$

Setting $\nabla^2 H = G^L$ and taking the Laplacian of both sides, we find that H is the Green's function of the biharmonic equation in two dimensions given by $H = -\frac{1}{8\pi} r^2 (\ln r - 1)$. Finally substituting this expression into (1), we obtain the free-space velocity Green's function displayed in the first of expressions (7.2.13).

Working in a similar fashion, compute the free-space Green's function of Stokes flow in three dimensions displayed in (7.2.14).

7.3 Boundary integral equations in two dimensions

To derive the boundary-integral representation of two-dimensional Stokes flow, we apply identity (7.2.4) for a particular Stokes flow of interest with velocity \mathbf{u} and stress σ and for the flow due to a point force, setting

$$u'_j(\mathbf{x}) = \frac{1}{4\pi\mu} G_{jm}(\mathbf{x}, \mathbf{x}_0) b_m, \quad \sigma'_{ij}(\mathbf{x}) = \frac{1}{4\pi} T_{imj}(\mathbf{x}, \mathbf{x}_0) b_m, \\ \frac{\partial \sigma'_{im}}{\partial x_i} = -\delta_2(\mathbf{x} - \mathbf{x}_0) b_m, \quad (7.3.1)$$

where \mathbf{b} is an arbitrary constant, and thus obtain the *scalar* equation

$$\delta_2(\mathbf{x} - \mathbf{x}_0) b_m u_m(\mathbf{x}) \\ = \frac{\partial}{\partial x_i} \left(\frac{1}{4\pi\mu} G_{jm}(\mathbf{x}, \mathbf{x}_0) b_m \sigma_{ij}(\mathbf{x}) - u_j(\mathbf{x}) \frac{1}{4\pi} T_{imj}(\mathbf{x}, \mathbf{x}_0) b_m \right). \quad (7.3.2)$$

Discarding the arbitrary constants b_m , we derive the *vector* equation

$$u_m(\mathbf{x}) \delta_2(\mathbf{x} - \mathbf{x}_0) = \frac{1}{4\pi\mu} \frac{\partial}{\partial x_i} [G_{jm}(\mathbf{x}, \mathbf{x}_0) \sigma_{ij}(\mathbf{x}) - \mu u_j(\mathbf{x}) T_{imj}(\mathbf{x}, \mathbf{x}_0)]. \\ (7.3.3)$$

It is enlightening to note the similarity between (7.3.3) and (2.3.1) for Laplace's equation in two dimensions.

Following the analysis of Section 2.3, we integrate (7.3.3) over a selected control area A_c that is enclosed by a closed contour or a collection of closed contours denoted by C . Using the divergence theorem to convert the areal integral to a surface integral on the right-hand side, we obtain

$$\begin{aligned} & \int \int_{A_c} u_m(\mathbf{x}) \delta_2(\mathbf{x} - \mathbf{x}_0) dx dy \\ &= -\frac{1}{4\pi\mu} \int_C G_{jm}(\mathbf{x}, \mathbf{x}_0) \sigma_{ij}(\mathbf{x}) n_i(\mathbf{x}) dl(\mathbf{x}) \\ & \quad + \frac{1}{4\pi\mu} \int_C u_j(\mathbf{x}) T_{imj}(\mathbf{x}, \mathbf{x}_0) n_i(\mathbf{x}) dl(\mathbf{x}), \end{aligned} \quad (7.3.4)$$

where the unit normal vector \mathbf{n} points into the control area enclosed by C .

Recalling the properties of the delta function in two dimensions, we find that, when the point \mathbf{x}_0 lies outside A_c , the left-hand side of (7.3.4) is zero, whereas when the point \mathbf{x}_0 lies inside A_c , the left-hand side of (7.3.4) is equal to $u_m(\mathbf{x}_0)$.

Next, we place the point \mathbf{x}_0 inside the control area, invoke the symmetry of the stress tensor to write $T_{imj} = T_{jmi}$, relabel the indices, use the symmetry property (7.2.15), and thus arrive at the boundary-integral representation of two-dimensional Stokes flow,

$$\begin{aligned} u_j(\mathbf{x}_0) &= -\frac{1}{4\pi\mu} \int_C G_{ji}(\mathbf{x}_0, \mathbf{x}) f_i(\mathbf{x}) dl(\mathbf{x}) \\ & \quad + \frac{1}{4\pi} \int_C u_i(\mathbf{x}) T_{ijk}(\mathbf{x}, \mathbf{x}_0) n_k(\mathbf{x}) dl(\mathbf{x}), \end{aligned} \quad (7.3.5)$$

where $\mathbf{f} \equiv \sigma \cdot \mathbf{n}$ is the boundary traction.

The first term on the right-hand side of (7.3.5) is the single-layer potential of Stokes flow and the second term is the double-layer potential of Stokes flow. The former represents a boundary distribution of point forces associated with the Green's function for the velocity, while the latter represents a boundary distribution of point sources and point force dipoles.

The interpretation of the double-layer potential is explained by invoking the definition (7.2.12) and observing that the Green's function for the pressure is, in fact, the velocity field due to a point source [55]. The kernel of the double-layer potential is a fundamental singular solution of the equations of Stokes flow called the *stresslet*.

7.3.1 Integral equations

Taking the limit of the representation (7.3.5) as the point \mathbf{x}_0 approaches a locally smooth contour C and using the property (7.2.18), we derive the boundary-integral

equation

$$\begin{aligned} u_j(\mathbf{x}_0) = & -\frac{1}{2\pi\mu} \int_C G_{ji}(\mathbf{x}_0, \mathbf{x}) f_i(\mathbf{x}) dl(\mathbf{x}) \\ & + \frac{1}{2\pi} \int_C^{PV} u_i(\mathbf{x}) T_{ijk}(\mathbf{x}, \mathbf{x}_0) n_k(\mathbf{x}) dl(\mathbf{x}), \end{aligned} \quad (7.3.6)$$

where PV denotes the principal value of the double-layer integral. The boundary-element method for Stokes flow is based on the following observations:

- Specifying the boundary distribution of the velocity \mathbf{u} reduces (7.3.6) to a *Fredholm integral equation of the first kind* for the distribution of the boundary traction \mathbf{f} .
- Specifying the distribution of the boundary traction \mathbf{f} reduces (7.3.6) to a *Fredholm integral equation of the second kind* for the boundary distribution of the velocity \mathbf{u} .

The Green's function exhibits a logarithmic singularity with respect to the distance of the evaluation point from the singular point. Because the order of this singularity is lower than the linear dimension of the variable of integration, the integral equation is weakly singular. The Fredholm-Riesz theory of compact operators may be then applied to study the properties of the solution, and the improper single-layer integral may be computed accurately by numerical methods.

Consider the integral equation of the second kind originating from (7.3.6), written with the free-space Green's function. When C is a smooth contour with finite curvature and continuously varying normal vector, as the integration point \mathbf{x} approaches the evaluation point \mathbf{x}_0 , the normal vector \mathbf{n} tends to become orthogonal to the nearly tangential vector $(\mathbf{x} - \mathbf{x}_0)$, the numerator of the integrand of the double-layer potential behaves quadratically with respect to the scalar distance $r = |\mathbf{x} - \mathbf{x}_0|$, and a singularity does not appear. Consequently, the Fredholm-Riesz theory of compact operators may be used to study the properties of the solution, and the principal value of the double-integral integral may be computed accurately by numerical methods.

7.3.2 Integral representation for the pressure

The integral representation for the pressure corresponding to (7.3.5) is

$$\begin{aligned} p(\mathbf{x}_0) = & -\frac{1}{4\pi} \int_C p_j(\mathbf{x}_0, \mathbf{x}) f_j(\mathbf{x}) dl(\mathbf{x}) \\ & + \frac{\mu}{4\pi} \int_C u_i(\mathbf{x}) \Pi_{ik}(\mathbf{x}, \mathbf{x}_0) n_k(\mathbf{x}) dl(\mathbf{x}), \end{aligned} \quad (7.3.7)$$

where p_j is the pressure Green's function, and Π_{ik} is the pressure field associated with the stresslet.

The free-space Green's function p_j is given in the second of equations (7.2.13); the corresponding tensor Π_{ik} is given by [55]

$$\Pi_{ik}(\mathbf{x} - \mathbf{x}_0) = 4 \left(-\frac{\delta_{ik}}{r^2} + 2 \frac{\hat{x}_i \hat{x}_k}{r^4} \right) = -4 \frac{\partial^2 \ln r}{\partial x_i \partial x_k}, \quad (7.3.8)$$

where $\hat{\mathbf{x}} \equiv \mathbf{x} - \mathbf{x}_0$ and $r = |\hat{\mathbf{x}}|$.

The vector p_j represents the field due to a point source dipole, and the tensor Π_{ik} represents the field due to a point source quadrupole. To illustrate this clearly, we recast the representation (7.3.7) into the form

$$\begin{aligned} p(\mathbf{x}_0) &= \int_C \frac{\partial G^L(\mathbf{x}_0, \mathbf{x})}{\partial x_j} f_j(\mathbf{x}) dl(\mathbf{x}) \\ &\quad + 2\mu \int_C u_i(\mathbf{x}) \frac{\partial^2 G^L(\mathbf{x}_0, \mathbf{x})}{\partial x_i \partial x_j} n_k(\mathbf{x}) dl(\mathbf{x}), \end{aligned} \quad (7.3.9)$$

where $G^L = -\frac{1}{2\pi} \ln r$ is the Green's function of Laplace's equation in two dimensions.

7.3.3 Integral representation for the stress

The integral representation for the stress corresponding to (7.3.5) is

$$\begin{aligned} \sigma_{ik}(\mathbf{x}_0) &= -\frac{1}{4\pi} \int_C T_{ijk}(\mathbf{x}_0, \mathbf{x}) f_j(\mathbf{x}) dl(\mathbf{x}) \\ &\quad + \frac{\mu}{4\pi} \int_C u_j(\mathbf{x}) \Psi_{ijkl}(\mathbf{x}, \mathbf{x}_0) n_l(\mathbf{x}) dl(\mathbf{x}), \end{aligned} \quad (7.3.10)$$

where T_{ijk} is the stress Green's function, and Ψ_{ijkl} is the stress field associated with the stresslet.

The free-space Green's function T_{ijk} is given in the third of equations (7.2.13); the corresponding tensor Ψ_{ijkl} is given by [55]

$$\begin{aligned} \Psi_{ijkl}(\mathbf{x} - \mathbf{x}_0) &= \frac{4}{r^2} \delta_{ik} \delta_{jl} + \frac{4}{r^4} (\delta_{ij} \hat{x}_k \hat{x}_l + \delta_{il} \hat{x}_k \hat{x}_j + \delta_{kj} \hat{x}_i \hat{x}_l + \delta_{kl} \hat{x}_i \hat{x}_j) \\ &\quad - 32 \frac{\hat{x}_i \hat{x}_j \hat{x}_k \hat{x}_l}{r^6}, \end{aligned} \quad (7.3.11)$$

where $\hat{\mathbf{x}} \equiv \mathbf{x} - \mathbf{x}_0$ and $r = |\hat{\mathbf{x}}|$.

7.3.4 Hypersingular integrals

Taking the limit of the representation (7.3.10) as the evaluation point \mathbf{x}_0 approaches the contour C , and projecting the limit onto the unit normal vector $\mathbf{n}(\mathbf{x}_0)$, we de-

rive an integral equation of the second kind for the boundary traction \mathbf{f} involving principal-value and hypersingular integrals (Section 2.5). As in the case of Laplace's equation, the order of the singularities may be reduced by regularization to facilitate the numerical solution

Problems

P.7.3.1 Integral identities

Show that identity (7.2.17) arises by applying (7.3.4) for uniform (streaming) flow with constant velocity and uniform pressure.

P.7.3.2 Corner points

Show that, when the evaluation point \mathbf{x}_0 lies at a boundary corner, the integral equation (7.3.6) takes the form.

$$\begin{aligned} u_j(\mathbf{x}_0) = & -\frac{1}{2\alpha\mu} \int_C G_{ji}(\mathbf{x}_0, \mathbf{x}) f_i(\mathbf{x}) dl(\mathbf{x}) \\ & + \frac{1}{2\alpha} \int_C^{PV} u_i(\mathbf{x}) T_{ijk}(\mathbf{x}, \mathbf{x}_0) n_k(\mathbf{x}) dl(\mathbf{x}), \end{aligned} \quad (1)$$

where α is the corner angle. *Hint:* Work as in Sections 2.4.1 and 2.4.2 with a shrinking circular arc.

P.7.3.3 Stresslet

Verify that the tensor Ψ_{ijlk} defined in (7.3.11) satisfies the identity

$$\frac{\partial \Psi_{ijlk}}{\partial x_i} = 0, \quad (1)$$

where summation is implied over the repeated index i .

7.4 Boundary-integral equations in three dimensions

The analysis of Section 7.3 can be repeated with obvious changes in notation to derive analogous identities, integral representations, and boundary-integral equations for three-dimensional Stokes flow.

The counterpart of the integral representation (7.3.5) is

$$\begin{aligned} u_j(\mathbf{x}_0) = & -\frac{1}{8\pi\mu} \int_D G_{ji}(\mathbf{x}_0, \mathbf{x}) f_i(\mathbf{x}) dS(\mathbf{x}) \\ & + \frac{1}{8\pi} \int_D u_i(\mathbf{x}) T_{ijk}(\mathbf{x}, \mathbf{x}_0) n_k(\mathbf{x}) dS(\mathbf{x}), \end{aligned} \quad (7.4.1)$$

where the point \mathbf{x}_0 lies inside a control volume bounded by the surface D , and the unit normal vector \mathbf{n} points inward. The first term on the right-hand side of (7.4.1) is the single-layer potential of three-dimensional Stokes flow, and the second term is the double-layer potential of three-dimensional Stokes flow.

The counterpart of the integral equation (7.3.6) for a point on a smooth surface is

$$\begin{aligned} u_j(\mathbf{x}_0) = & -\frac{1}{4\pi\mu} \int_D G_{ji}(\mathbf{x}_0, \mathbf{x}) f_i(\mathbf{x}) dS(\mathbf{x}) \\ & + \frac{1}{4\pi} \int_D^{PV} u_i(\mathbf{x}) T_{ijk}(\mathbf{x}, \mathbf{x}_0) n_k(\mathbf{x}) dS(\mathbf{x}), \end{aligned} \quad (7.4.2)$$

where PV denotes the principal value of the double-layer potential. Integral equations of the first or second kind originating from (7.4.2) are weakly singular.

7.4.1 Integral representation for the pressure

The integral representation for the pressure corresponding to (7.4.1) is

$$\begin{aligned} p(\mathbf{x}_0) = & -\frac{1}{8\pi} \int_D p_j(\mathbf{x}_0, \mathbf{x}) f_j(\mathbf{x}) dS(\mathbf{x}) \\ & + \frac{\mu}{8\pi} \int_D u_i(\mathbf{x}) \Pi_{ik}(\mathbf{x}, \mathbf{x}_0) n_k(\mathbf{x}) dS(\mathbf{x}), \end{aligned} \quad (7.4.3)$$

where p_j is the pressure Green's function, and Π_{ik} is the pressure field associated with the stresslet.

The free-space Green's function p_j is given in the second of equations (7.2.14); the corresponding tensor Π_{ik} is given by [55, 59]

$$\Pi_{ik}(\mathbf{x} - \mathbf{x}_0) = 4 \left(-\frac{\delta_{ik}}{r^3} + 3 \frac{\hat{x}_i \hat{x}_k}{r^5} \right) = -4 \frac{\partial^2}{\partial x_i \partial x_k} \left(\frac{1}{r} \right), \quad (7.4.4)$$

where $\hat{\mathbf{x}} \equiv \mathbf{x} - \mathbf{x}_0$, and $r = |\hat{\mathbf{x}}|$.

7.4.2 Integral representation for the stress

The integral representation for the stress field corresponding to (7.4.1) is

$$\begin{aligned} \sigma_{ik}(\mathbf{x}_0) = & -\frac{1}{8\pi} \int_D T_{ijk}(\mathbf{x}_0, \mathbf{x}) f_j(\mathbf{x}) dS(\mathbf{x}) \\ & + \frac{\mu}{8\pi} \int_D u_j(\mathbf{x}) \Psi_{ijkl}(\mathbf{x}, \mathbf{x}_0) n_l(\mathbf{x}) dS(\mathbf{x}), \end{aligned} \quad (7.4.5)$$

where T_{ijk} is the stress Green's function, and $\Psi_{ijkl}(\mathbf{x}, \mathbf{x}_0)$ is the stress field associated with the three-dimensional stresslet.

The free-space Green's function T_{ijk} is given in the second of equations (7.2.14); the corresponding tensor Ψ_{ijkl} is given by [55]

$$\begin{aligned} \Psi_{ijkl}(\mathbf{x} - \mathbf{x}_0) = & \frac{4}{r^3} \delta_{ik} \delta_{jl} \\ & + \frac{6}{r^5} (\delta_{ij} \hat{x}_k \hat{x}_l + \delta_{il} \hat{x}_k \hat{x}_j + \delta_{kj} \hat{x}_i \hat{x}_l + \delta_{kl} \hat{x}_i \hat{x}_j) \\ & - 60 \frac{\hat{x}_i \hat{x}_j \hat{x}_k \hat{x}_l}{r^7}, \end{aligned} \quad (7.4.6)$$

where $\hat{\mathbf{x}} \equiv \mathbf{x} - \mathbf{x}_0$ and $r = |\hat{\mathbf{x}}|$.

7.4.3 Hypersingular integrals

Taking the limit of the representation (7.4.5) as the evaluation point \mathbf{x}_0 approaches the boundary D , and projecting the limit onto the unit normal vector $\mathbf{n}(\mathbf{x}_0)$, we derive an integral equation of the second kind for the boundary traction \mathbf{f} involving principal-value and hypersingular integrals. The computation of these integrals and the solution of the integral equation are discussed in Reference [30].

7.4.4 Axisymmetric flows in axisymmetric domains

To develop an integral representation for axisymmetric flow, we work as in Section 4.5 and convert the surface integrals supporting the single- and double-layer potential to line integrals along the contours of the boundaries in a meridional plane [55].

Expressions for the axisymmetric Green's functions and the reduced forms of the boundary-integral representation and boundary-integral equation are given in subdirectory `sgf_ax` of directory `stokes` of the *BEMLIB* user guide (Chapter 12).

Problem

P.7.4.1 Corner points

Show that the counterpart of the integral equation (7.4.2) at a corner point is

$$\begin{aligned} u_j(\mathbf{x}_0) = & -\frac{1}{2\alpha\mu} \int_D G_{ji}(\mathbf{x}_0, \mathbf{x}) f_i(\mathbf{x}) dS(\mathbf{x}) \\ & + \frac{1}{2\alpha} \int_D^{PV} u_i(\mathbf{x}) T_{ijk}(\mathbf{x}, \mathbf{x}_0) n_k(\mathbf{x}) dS(\mathbf{x}), \end{aligned} \quad (1)$$

where α is the solid angle subtended by the corner.

7.5 Boundary-element methods

The implementation of the boundary-element method follows the general guidelines discussed in Chapters 3 and 5 for Laplace's equation in two and three dimensions. The main difference is that, in the case of Stokes flow, the integral equation involves vector surface functions that must be decomposed into their scalar constituents before they produce the final system of linear equations.

In the case of two-dimensional or axisymmetric flow, the boundary is discretized into planar elements such as straight segments, circular arcs, and pieces of cubic splines defined by element nodes. In the case of three-dimensional flow, the boundary is discretized into three-dimensional elements including flat and curved triangles defined by groups of surface nodes.

7.5.1 Computation of the single-layer potential

In the case of two-dimensional or axisymmetric flow, the kernel of the single-layer potential exhibits a logarithmic singularity that may be integrated by several methods, as discussed in Chapter 3.

In the case of three-dimensional flow, the kernel of the single-layer potential exhibits a weak $1/r$ singularity that may be integrated by the methods discussed in Chapter 5. For example, to compute the single-layer potential over the surface of a curved triangle defined by six nodes, we break up the element into four flat triangles, and then perform the integration analytically, use the polar integration rule for singular flat triangles, or apply an integration quadrature.

7.5.2 Computation of the double-layer potential

In the case of two-dimensional or axisymmetric flow, the integrand of the principal-value integral of the double-layer potential is non-singular or weakly singular, and the integral may be computed by standard numerical methods.

In the case three-dimensional flow, the $1/r$ singularity of the principal-value integral over a *closed* surface can be removed using identity (7.2.20), writing

$$\begin{aligned} & \int_D^{PV} u_i(\mathbf{x}) T_{ijk}(\mathbf{x}, \mathbf{x}_0) n_k(\mathbf{x}) dS(\mathbf{x}) \\ &= \int_D [u_i(\mathbf{x}) - u_i(\mathbf{x}_0)] T_{ijk}(\mathbf{x}, \mathbf{x}_0) n_k(\mathbf{x}) dS(\mathbf{x}) + 4\pi u_j(\mathbf{x}_0). \end{aligned} \quad (7.5.1)$$

As the integration point \mathbf{x} approaches the evaluation point \mathbf{x}_0 , the integrand on the right-hand side of (7.5.1) tends to a finite value that depends on the orientation of the nearly tangential vector $(\mathbf{x} - \mathbf{x}_0)$. Since a singularity does not appear, the integral may be computed with adequate accuracy using a Gaussian quadrature. A similar regularization can be performed when the point \mathbf{x}_0 lies close to, but not precisely on, the domain of integration D .

When the domain of integration is not closed, the computation of the double-layer potential is more challenging. Because the kernel $T_{ijk} n_k$ of the free-space Green's function vanishes over a flat element hosting a singular point, neglecting the surface curvature introduces significant numerical error on the order of $\delta \kappa_m / (4\pi)$, where κ_m is the mean curvature of the undiscretized surface, and δ is the element size. The implementation of the polar integration rule over curved elements is cumbersome and has not been attempted.

One way to bypass these difficulties is to introduce the closure of the open interface, apply (7.5.1), and compute the non-singular double-layer integral over the extended boundary using a quadrature [71].

7.5.3 Corner singularities

When the boundary of a flow exhibits a corner or cusp, the solution of the integral equation for the traction is likely to exhibit a local singularity. Experience has shown that neglecting the singularity and solving the integral equation using standard boundary-element methods is not detrimental to the overall accuracy of the computation.

To improve the accuracy, the functional form of the singularity may be identified by carrying out a local analysis, and the boundary-element method may be designed to automatically probe the intensity of the divergent part, and effectively produce the regular part of the solution [25, 34 – 36, 63].

Problem

P.7.5.1 BEMLIB codes for Stokes flow.

(a) Code `flow_2d` in directory `stokes` of *BEMLIB* computes two-dimensional Stokes flow in an arbitrary domain. Study the mathematical formulation and the numerical method, run the code for a boundary configuration of your choice, prepare graphs of the streamline pattern, and discuss the results of your computation. (b) Repeat (a) for code `prtcl_2d`. (c) Repeat (a) for code `prtcl_ax`. (d) Repeat (a) for code `prtcl_sw`. (e) Repeat (a) for code `prtcl_3d`.

7.6 Interfacial dynamics

The boundary-element method for Stokes flow has found extensive applications in the numerical simulation of multi-fluid flow, such as the flow of suspensions of liquid drops, capsules, and cells, and the flow of liquid films over a horizontal plane or down an inclined wall (e.g., [62]).

Consider a Stokes flow with velocity $\mathbf{U}(\mathbf{x})$ past an interface separating two fluids with different viscosities, as illustrated in Figure 7.6.1(a). The unit normal vector \mathbf{n} points into the ambient fluid labeled 1. Because the interface exhibits tangential and possibly transverse tensions, the hydrodynamic traction undergoes a discontinuity defined as

$$\Delta \mathbf{f} \equiv \mathbf{f}^{(1)} - \mathbf{f}^{(2)}, \quad (7.6.1)$$

where

$$\mathbf{f}^{(1)} \equiv \sigma^{(1)} \cdot \mathbf{n}, \quad \mathbf{f}^{(2)} \equiv \sigma^{(2)} \cdot \mathbf{n}, \quad (7.6.2)$$

and σ is the stress tensor for the respective fluid. An expression for $\Delta \mathbf{f}$ arises by performing interfacial force and torque balances [55, 62]. For a common fluid interface between two fluids exhibiting uniform surface tension γ , we find $\Delta \mathbf{f} = \gamma 2\kappa_m \mathbf{n}$, where κ_m is the mean curvature.

Our goal is to develop an integral representation involving $\Delta \mathbf{f}$, under the assumption that the velocity is continuous across the interface. To achieve this, we consider a point in fluid 1, decompose the velocity into the incident component $\mathbf{U}(\mathbf{x})$ and a disturbance component, write the boundary-integral representation for the disturbance component in fluid 1 and the reciprocal relation for the disturbance component in fluid 2, and combine the two expressions to form the difference $\Delta \mathbf{f}$ [55].

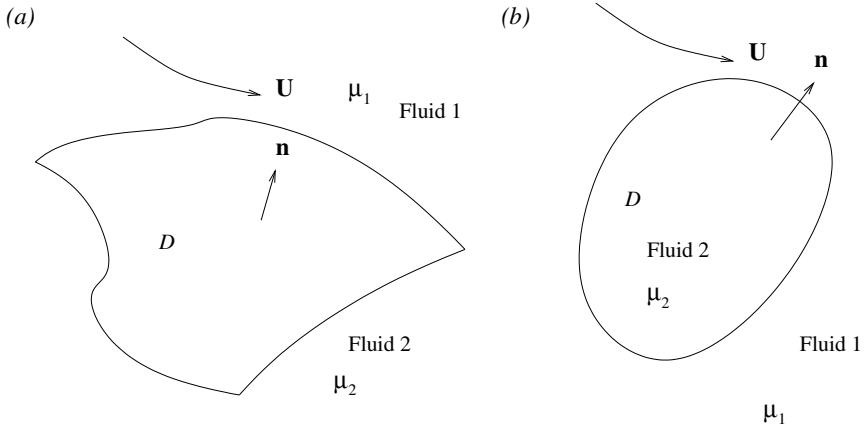


Figure 7.6.1 Stokes flow past (a) an interface separating two different fluids, and (b) a suspended drop.

In the case of three-dimensional flow past an interface D , we find that the velocity at the point \mathbf{x}_0 that lies in fluid 1 is given by the integral representation

$$\begin{aligned} u_j(\mathbf{x}_0) = & U_j(\mathbf{x}_0) - \frac{1}{8\pi\mu_1} \int_D G_{ji}(\mathbf{x}_0, \mathbf{x}) \Delta f_i(\mathbf{x}) dS(\mathbf{x}) \\ & + \frac{1-\lambda}{8\pi} \int_D u_i(\mathbf{x}) T_{ijk}(\mathbf{x}, \mathbf{x}_0) n_k(\mathbf{x}) dS(\mathbf{x}), \end{aligned} \quad (7.6.3)$$

where $\lambda = \mu_2/\mu_1$ is the viscosity ratio. The velocity at a point \mathbf{x}_0 that lies in fluid 2 is given by an identical representation, except that all terms on the right-hand side are divided by the viscosity ratio λ .

Taking the limit as the point \mathbf{x}_0 approaches the interface from either side, we derive the integral equation

$$\begin{aligned} u_j(\mathbf{x}_0) = & \frac{2}{1+\lambda} U_j(\mathbf{x}_0) - \frac{1}{4\pi\mu_1(1+\lambda)} \int_D G_{ji}(\mathbf{x}_0, \mathbf{x}) \Delta f_i(\mathbf{x}) dS(\mathbf{x}) \\ & + \frac{1-\lambda}{4\pi(1+\lambda)} \int_D^{PV} u_i(\mathbf{x}) T_{ijk}(\mathbf{x}, \mathbf{x}_0) n_k(\mathbf{x}) dS(\mathbf{x}), \end{aligned} \quad (7.6.4)$$

which is the cornerstone of the method of interfacial dynamics for Stokes flow.

When the viscosities of the two fluids are equal, $\lambda = 1$, the coefficient in front of the double-layer potential on the right-hand sides of (7.6.3) and (7.6.4) vanishes, yielding simplified representations in terms of the single-layer potential alone.

Problems

P.7.6.1 Integral equation

Work as described in the text to derive the integral equation (7.6.4).

P.7.6.2 Slip velocity

Derive the counterpart of the integral representation (7.6.3) for flow past an interface with $\Delta f = 0$ but a non-zero discontinuity in the tangential velocity.

P.7.6.3 Integral representation for two-dimensional flow

Derive the counterpart of the integral representation (7.6.3) and integral equation (7.6.4) for two-dimensional flow.

7.7 Unsteady, Navier-Stokes, and non-Newtonian flow

In Chapter 6, we discussed generalized boundary-integral methods for inhomogeneous, nonlinear, and time-dependent equations, with particular reference to Poisson's equation, the convection – diffusion equation, and the unsteady diffusion equation. Straightforward extensions of these methods allow us to develop algorithms for solving the linear equations of unsteady Stokes flow, the nonlinear equations of Navier-Stokes flow, and the equations of non-Newtonian flow.

7.7.1 Time discretization of an unsteady flow

Consider first the evolution of an unsteady flow governed by the Navier-Stokes equation (7.1.8), starting from a specified initial state. Approximating the time derivative on the right-hand side with a finite difference and the rest of the terms with weighted averages, we obtain the time-discretized equation

$$\begin{aligned} & \rho \left(\frac{\mathbf{u}^{n+1} - \mathbf{u}^n}{\Delta t} + \alpha [\mathbf{u} \cdot \nabla \mathbf{u}]^{n+1} + (1 - \alpha) [\mathbf{u} \cdot \nabla \mathbf{u}]^n \right) \\ &= -[\beta \nabla p^{n+1} + (1 - \beta) \nabla p^n] + \mu [\gamma \nabla^2 \mathbf{u}^{n+1} + (1 - \gamma) \nabla^2 \mathbf{u}^n] + \rho \mathbf{g}, \end{aligned} \quad (7.7.1)$$

where Δt is the time step, and α , β , and γ are weighting factors. The superscripts n and $n + 1$ denote that the underlying variable is evaluated, respectively, at time t_n and $t_{n+1} = t_n + \Delta t$.

Setting $\alpha = 0$, $\beta = 0$, and $\gamma = 0$, we obtain a fully explicit method that produces the solution at the new time level by direct advancement of the solution at the previous time level, without requiring inverting systems of algebraic equations. Unfortunately, because fully explicit methods are susceptible to numerical instabilities, a successful simulation requires a prohibitively small time step [59, 60].

A semi-implicit method arises by setting $\alpha = 0$, $\beta = 1$, and $\gamma = 1$, yielding

$$\rho \left(\frac{\mathbf{u}^{n+1} - \mathbf{u}^n}{\Delta t} + [\mathbf{u} \cdot \nabla \mathbf{u}]^n \right) = -\nabla p^{n+1} + \mu \nabla^2 \mathbf{u}^{n+1} + \rho \mathbf{g}. \quad (7.7.2)$$

Rearranging, we derive the inhomogeneous Brinkman equation

$$\frac{\rho}{\Delta t} \mathbf{u}^{n+1} = -\nabla p^{n+1} + \mu \nabla^2 \mathbf{u}^{n+1} + \rho \left(\frac{1}{\Delta t} \mathbf{u}^n - [\mathbf{u} \cdot \nabla \mathbf{u}]^n + \mathbf{g} \right). \quad (7.7.3)$$

The collection of the terms enclosed by the parentheses on the right-hand side are regarded as a known source field, available from the initial condition or from the solution at the previous time step.

To make the derivations more specific, we restrict our attention to two-dimensional flow and introduce the velocity and pressure Green's functions of Brinkman's equation, denoted, respectively, by G_{ij}^B and p_j^B . By definition, these Green's functions satisfy the continuity equation (7.2.9) and the singularly forced Brinkman's equation

$$-\lambda^2 G_{ij}^B(\mathbf{x}, \mathbf{x}_0) - \frac{\partial p_j^B(\mathbf{x}, \mathbf{x}_0)}{\partial x_i} + \nabla^2 G_{ij}^B(\mathbf{x}, \mathbf{x}_0) + 4\pi \delta_{ij} \delta_2(\mathbf{x} - \mathbf{x}_0) = 0, \quad (7.7.4)$$

where λ is a real positive constant with dimensions of inverse length. Equation (7.7.4) is a generalization of the first of equations (7.2.10) defining the two-dimensional Stokes flow Green's functions.

The free-space Green's function of Brinkman's equation is given by

$$G_{ij}^B(\mathbf{x} - \mathbf{x}_0) = -\delta_{ij} A(R) + \frac{\hat{x}_i \hat{x}_j}{r^2} B(R), \quad (7.7.5)$$

$$p_j^B(\mathbf{x} - \mathbf{x}_0) = 2 \frac{\hat{x}_j}{r^2},$$

with

$$A(R) = 2 \left[\frac{1}{R^2} - \frac{K_1(R)}{R} - K_0(R) \right], \quad (7.7.6)$$

$$B(R) = 2 \left[\frac{2}{R^2} - 2 \frac{K_1(R)}{R} - K_0(R) \right],$$

where $\hat{\mathbf{x}} \equiv \mathbf{x} - \mathbf{x}_0$, $r = |\hat{\mathbf{x}}|$, $R = \lambda r$, and K_0, K_1 are modified Bessel functions (e.g., [2], p. 374); the derivation is discussed in P.7.7.1.

The corresponding stress tensor is given by

$$T_{ijk}^B(\mathbf{x} - \mathbf{x}_0) = \delta_{ij} \frac{x_j}{r^2} 2[B(R) - 1] + \frac{\delta_{ij}\hat{x}_k + \delta_{kj}\hat{x}_i}{r^2} C(R) - 4 \frac{\hat{x}_i \hat{x}_j \hat{x}_k}{r^4} D(R), \quad (7.7.7)$$

where

$$C(R) = \frac{8}{R^2} - 4 K_0(R) - 2 \left(R + \frac{4}{R} \right) K_1(R), \quad (7.7.8)$$

$$D(R) = C(R) + R K_1(R).$$

In the limit as R tends to zero, the function $A(R)$ tends to $\ln R$, the functions $B(R)$ and $D(R)$ tend to unity, and the function $C(R)$ tends to vanish, yielding the free-space Green's functions of Stokes flow.

Working as in Section 7.2, we find that the solution of equation (7.7.3) is given by the integral representation

$$\begin{aligned} u_j^{n+1}(\mathbf{x}_0) &= -\frac{1}{4\pi\mu} \int_C G_{ji}^B(\mathbf{x}_0, \mathbf{x}) f_i^{n+1}(\mathbf{x}) dl(\mathbf{x}) \\ &\quad + \frac{1}{4\pi} \int_C u_i^{n+1}(\mathbf{x}) T_{ijk}^B(\mathbf{x}, \mathbf{x}_0) n_k(\mathbf{x}) dl(\mathbf{x}) \\ &\quad + \frac{\rho}{4\pi\mu} \int \int_{Flow} G_{ji}^B(\mathbf{x}_0, \mathbf{x}) b_i dx dy, \end{aligned} \quad (7.7.9)$$

where $\lambda = \sqrt{\rho/(\mu \Delta t)}$, \mathbf{b} stands for the quantity enclosed by the parentheses on the right-hand side of (7.7.3), C is a closed contour enclosing a selected area of flow, \mathbf{n} is the unit vector normal to C pointing into the flow, and $\mathbf{f} \equiv \sigma \cdot \mathbf{n}$ is the boundary traction. The domain integral on the right-hand side of (7.7.9) may be computed either directly by domain discretization followed by numerical integration, or indirectly by the method of approximate particular solutions or the dual reciprocity method discussed in Section 7.7.2.

Taking the limit as the point \mathbf{x}_0 approaches the boundary C , we derive an integral equation involving the boundary traction f_i^{n+1} and the boundary velocity u_i^{n+1} . Once this equation has been solved for the unknown boundary distribution, the velocity at the new time level can be computed by evaluating the right-hand side of (7.7.9). Details of the boundary-element implementation are discussed in Reference [49].

7.7.2 Particular solutions and dual reciprocity

The method of approximate particular solutions and the dual reciprocity method for Navier-Stokes flow are developed by working as in Chapter 6 for Poisson's, Helmholtz's, and the convection – diffusion equation.

In the case of steady flow, we set $\partial \mathbf{u} / \partial t = \mathbf{0}$ and express the Navier-Stokes equation (7.1.8) in the symbolic form

$$\nabla \cdot \boldsymbol{\sigma} + \rho \mathbf{b}(\mathbf{u}) = \mathbf{0}, \quad (7.7.10)$$

where $\boldsymbol{\sigma}$ is the stress tensor, and the forcing term

$$\mathbf{b}(\mathbf{u}) \equiv -u_j \frac{\partial \mathbf{u}}{\partial x_j} + \mathbf{g} = -\frac{\partial(u_j \mathbf{u})}{\partial x_j} + \mathbf{g} \quad (7.7.11)$$

consists of the inertial convection volume force, regarded as an *a priori* unknown body force, and the external body force; summation over the repeated index j is implied in the spatial coordinates.

In the case of two-dimensional flow, a particular solution of (7.7.10) for the velocity is given by the Newtonian potential

$$v_j(\mathbf{x}_0) \equiv \frac{\rho}{4\pi\mu} \int \int G_{ji}(\mathbf{x}_0, \mathbf{x}) b_i(\mathbf{x}) dx dy, \quad (7.7.12)$$

where G_{ij} is a Green's function of Stokes flow, and the integral is computed over the domain of flow.

To implement the dual reciprocity method, we distribute M data points (x_k, y_k) , $k = 1, \dots, M$, over the domain of flow and along the boundaries, introduce the set of interpolation or influence functions $\phi_j^{(i)}(x, y)$, where $i = 1, 2$ and $j = 1, \dots, M$, and express the velocity in the approximate form

$$u_i(x, y) \simeq \sum_{j=1}^M \beta_j^{(i)} \phi_j^{(i)}(x, y). \quad (7.7.13)$$

The coefficients $\beta_j^{(i)}$ are found by requiring the interpolation condition

$$u_i(x_k, y_k) = \sum_{j=1}^M \beta_j^{(i)} \phi_j^{(i)}(x_k, y_k) \quad (7.7.14)$$

at the boundary nodes (x_k, y_k) where the velocity is specified, and by demanding that the interpolated field (7.7.13) satisfy the continuity equation at the interior nodes. The choice of interpolation functions and further details on the interpolation procedure are discussed in Reference [17]. Substituting expansion (7.7.13) into the right-hand side of (7.7.11), we express the effective body force \mathbf{b} as a quadratic function of the interpolation coefficients $\beta_j^{(i)}$.

Next, we express the effective body force itself as a linear combination of a new set of interpolation or influence functions $H_j(x, y)$ in the form

$$b_i(x, y) = \sum_{j=1}^M \alpha_j^{(i)} H_j(x, y), \quad (7.7.15)$$

where the coefficients $\alpha_j^{(i)}$ are found by requiring appropriate interpolation conditions. A particular solution of (7.7.10) for the velocity is given by

$$u_k^P(x, y) = \sum_{j=1}^M \sum_{i=1}^2 \alpha_j^{(i)} \hat{H}_j^{(k,i)}(x, y), \quad (7.7.16)$$

where $\hat{H}_j^{(k,i)}(x, y)$ represents the k th component of a Stokes velocity field with corresponding pressure field $\hat{p}_j^{(i)}$ induced by a distributed body force acting in the i th direction; the blob-like strength density of the body force is given by the interpolation functions $H_j(x, y)$. This flow field is found by solving the inhomogeneous Stokes flow equations

$$\begin{aligned} \frac{\partial \hat{H}_j^{(k,i)}}{\partial x_k} &= 0, \\ -\frac{\partial \hat{p}_j^{(i)}}{\partial x_k} + \mu \nabla^2 \hat{H}_j^{(k,i)} + \delta_{ik} H_j(x, y) &= 0. \end{aligned} \quad (7.7.17)$$

The solution corresponding to the thin-plate spline, $H_j(r) = r^2 \ln r$, where $r = |\mathbf{x} - \mathbf{x}_j|$, is given in Reference [17].

The dual reciprocity method is motivated by the observation that the homogeneous velocity field $\mathbf{u}^H \equiv \mathbf{u} - \mathbf{u}^P$ satisfies the equations of Stokes flow, and is thus amenable to the boundary-integral formulation.

The problem has been reduced to computing the boundary velocity or traction by solving an integral equation associated with the homogeneous solution, while simultaneously computing the coefficients $\beta_j^{(i)}$ introduced in (7.7.14), as discussed in Reference [17].

7.7.3 Alternative formulations

We have discussed methods for solving the Navier-Stokes equation in primitive variables including the velocity and the pressure. Alternative formulations employ the vorticity and stream function for two-dimensional or axisymmetric flow. A recent implementation is discussed in Reference [72].

7.7.4 Non-Newtonian flow

The stresses developing in a non-Newtonian fluid obey constitutive equations that are nonlinear with respect to the components of the rate-of-deformation tensor, defined as the symmetric part of the velocity gradient tensor, $\frac{1}{2}(\partial u_i / \partial x_j + \partial u_j / \partial x_i)$. Consequently, the right-hand side of the equation of motion contains the divergence of a nonlinear extra stress tensor expressing the deviation from Newtonian behavior.

To compute a non-Newtonian flow using the boundary-element method, we regard the non-Newtonian contribution to the equation of motion as an *a priori* unknown hydrodynamic volume force and obtain the solution using an iterative method, as discussed previously in this section for Navier-Stokes flow. A recent implementation is discussed in Reference [67].

Problems

P.7.7.1 Free-space Green's function of Brinkman's equation

To compute the free-space Green's function of Brinkman's equation in two dimensions, denoted by G_{ij}^B , we introduce the generating function H defined by the expression

$$G_{ij}^B = 4\pi (\delta_{ij} \nabla^2 H - \frac{\partial^2 H}{\partial x_i \partial x_j}). \quad (1)$$

Substituting this definition into equation (7.7.4) and working as in P.7.2.1, we find that the generating function satisfies the inhomogeneous Helmholtz equation

$$(\nabla^2 - \lambda^2)H = G^L, \quad (2)$$

where $G^L = -\frac{1}{2\pi} \ln r$ is the free-space Green's function of Laplace's equation. A solution of (2) is $H = \frac{1}{\lambda^2} (G^H - G^L)$, where

$$G^H = \frac{1}{2\pi} K_0(\lambda r) \quad (3)$$

is the free-space Green's function of Helmholtz's equation, and K_0 is a modified Bessel function (P.2.2.1). Thus, the generating function is given by

$$H = \frac{1}{2\pi\lambda^2} [K_0(\lambda r) + \ln r]. \quad (4)$$

Substituting this solution into expression (1), we obtain the velocity Green's function given in (7.7.5). The pressure vector is given by the second equation of (7.7.5).

- (a) Working in a similar fashion, compute the generating function of the free-space Green's function of Brinkman's equation in three dimensions.

P.7.7.2 Oscillatory Stokes flow

Small-amplitude oscillatory Stokes flow is governed by the unsteady Stokes equation (7.1.14). The velocity and pressure fields are given by the real or imaginary part of the complex functions

$$\mathbf{u}(\mathbf{x}, t) = \mathbf{v}(\mathbf{x}) \exp(-i\Omega t), \quad p(\mathbf{x}, t) = P(\mathbf{x}) \exp(-i\Omega t), \quad (1)$$

where i is the imaginary unit, and Ω is the frequency of the oscillation. Substituting these expressions into equation (7.1.14) in the absence of a body force, we obtain the complex Brinkman equation

$$-i\Omega \rho \mathbf{v} = -\nabla P + \mu \nabla^2 \mathbf{v}, \quad (2)$$

which is to be solved together with the continuity equation $\nabla \cdot \mathbf{v} = 0$.

To compute the free-space Green's function of the complex Brinkman equation, we work as in P.7.7.1, and find that the generating function H satisfies the inhomogeneous Helmholtz equation

$$(\nabla^2 - \kappa^2)H = G^L, \quad (3)$$

where $\kappa^2 = -i\Omega\rho/\mu$ is a complex constant, and G^L is the free-space Green's function of Laplace's equation. A solution of (3) is given by $H = \frac{1}{\kappa^2} (G^H - G^L)$, where

$$G^H(\mathbf{x}, \mathbf{x}_0) = \frac{1}{2\pi} [\ker_0(\lambda r) - i \operatorname{kei}_0(\lambda r)] \quad (4)$$

is the free-space Green's function of Helmholtz's equation, $r = |\mathbf{x} - \mathbf{x}_0|$, $\lambda = \sqrt{|\Omega|\rho/\mu}$, and \ker_0 , kei_0 are Kelvin functions (P.2.2.2(b)).

Combining these results, we find that the generating function is given by

$$H = \frac{i}{2\pi\lambda^2} [\ln r + \ker_0(\lambda r) - i \operatorname{kei}_0(\lambda r)]. \quad (5)$$

Substituting this expression into the right-hand side of equation (1) of P.7.7.1, we obtain the velocity Green's function as stated in the first equation of (7.7.5) with

$$A(R) = 2 \left[\ker_0(R) - \frac{\operatorname{kei}_0'(R)}{R} \right] - 2i \left[\operatorname{kei}_0(R) - \frac{\ker_0'(R)}{R} + \frac{1}{R^2} \right], \quad (6)$$

$$B(R) = 2 \left[-\ker_0(R) + 2 \frac{\operatorname{kei}_0'(R)}{R} \right] + 2i \left[\operatorname{kei}_0(R) + 2 \frac{\ker_0'(R)}{R} + \frac{2}{R^2} \right],$$

where $R = \lambda r$ and a prime denotes a derivative with respect to R . The pressure vector is given by the second equation of (7.7.5).

Working in a similar fashion, compute the generating function of the free-space Green's function of the complex Brinkman equation in three dimensions.

Chapter 8

BEMLIB user guide

The software library *BEMLIB* contains a collection of FORTRAN 77 programs and subroutines related to Green's functions and boundary-element methods for Laplace's equation, Helmholtz's equation, and Stokes flow.

8.1 General information

At the time of printing, *BEMLIB* consists of five main directories, each containing a multitude of nested subdirectories. The contents of the subdirectories are listed in Section 8.3.

- The source codes of *BEMLIB* can be downloaded from the internet site:
<http://bemlib.ucsd.edu>
- The library has been archived using the tar UNIX facility into the tar file `bemlib.tar`. To unravel the directories on a UNIX or LINUX platform, execute the UNIX command: `tar xvf bemlib.tar`
- To unravel the directories on a Windows or Macintosh platform, double-click on the tar file and follow the instructions of the invoked application.
- The downloaded package does not contain object files or executables. An application can be built using the makefile provided in each subdirectory. A makefile is a UNIX script that instructs the operating system how to compile the main program and subroutines, and then links the object files into an executable using the linker of the f77 compiler.
- To build the application named `dehesa` on a UNIX platform, proceed to the subdirectory where the application resides and type: `make dehesa`
- To compile the code using a FORTRAN 90 compiler on a UNIX platform, make appropriate compiler call substitutions in the makefiles, or establish a symbolic link that copies the FORTRAN 90 to the FORTRAN 77 compiler call.

- To remove the object and output files of the application named `dehesa` on a UNIX platform, proceed to the subdirectory where the application resides and type: `make purge`
- To remove the object files, output files, and executable of the application named `dehesa` on a UNIX platform, proceed to the subdirectory where the application resides and type: `make clean`
- To compile and link the codes on a Windows or Macintosh platform, follow the instructions of the FORTRAN 77 or FORTRAN 90 compiler.
- *BEMLIB* is the distillation of the inclusive fluid dynamics software library *FDLIB*. The directories of *BEMLIB* have been mapped from appropriate directories of *FDLIB* through the perspective of Green's functions and boundary-element methods. The source code of *FDLIB* can be downloaded from the internet site: <http://stokes.ucsd.edu>
- A subset of *FDLIB* and *BEMLIB* has been combined with the X11 graphics library *vogle* into an integrated application that visualizes the results of the simulations. The source and binary files of the graphics library compiled for several UNIX platforms and the source code of *CFDLAB* can be downloaded from the internet site: <http://stokes.ucsd.edu>

8.2 Terms and conditions

BEMLIB, ©1999, is subject to the terms of the GNU lesser public license, as stated in the internet site: <http://www.gnu.org/copyleft/lesser.html>

The author assumes no responsibility or liability for any type of damage or mental strain that may be incurred by using any parts of this software. In no event shall the author be liable for any incidental, direct, special, or consequential damages arising out of the use of the program material. The author reserves the right to revise the program material and make changes therein from time to time without obligation to notify the user of the revision or changes. The author makes no warranties, expressed or implied, including without limitation the implied warranties of merchantability and fitness for a particular purpose, regarding the software. The author does not warrant, guarantee, or make any representations regarding the use of the software in terms of its correctness, accuracy, reliability, currentness, or otherwise. The entire risk as to the results and performance of the software is assumed by the user.

8.3 Directory contents

Directory: num_meth

Numerical methods in science and engineering.

Subdirectory	Topic
01_num_comp	General aspects of numerical computation.
02_lin_calc	Linear algebra and linear calculus.
03_lin_eq	Systems of linear algebraic equations.
04_nl_eq	Nonlinear algebraic equations.
05_eigen	Eigenvalues and eigenvectors of matrices.
06_interp_diff	Function interpolation and differentiation.
07_integration	Function integration.
08_approximation	Function approximation.
09_ode_ivp	Ordinary differential equations; initial-value problems.
10_ode_bvp	Ordinary differential equations; boundary-value problems.
11_pde	Partial differential equations.
12_spec_fnc	Computation of special functions.

This directory accompanies Reference [60].

Directory: grids

Boundary element discretization of planar lines and three-dimensional surfaces.

Subdirectory Topic

grid_2d Discretization of a planar line consisting of straight and circular segments into a nonuniform mesh of elements with corresponding shapes.

trgl Triangulation of a closed surface into an unstructured grid of quadratic elements generated by discretizing an octahedron or icosahedron.

Directory: laplace

Green's functions of Laplace's equation and boundary-element codes for problems involving Laplace's equation in two and three dimensions.

Subdirectory Topic

lgf_2d Green's and Neumann functions of Laplace's equation in two dimensions.

lgf_3d Green's and Neumann functions of Laplace's equation in three dimensions.

lgf_ax Green's and Neumann functions of Laplace's equation in axisymmetric domains.

flow_1d Unidirectional viscous flow through a tube with arbitrary cross-section.

flow_1d_1p Unidirectional periodic viscous flow past a periodic array of cylinders or a periodic wall with arbitrary cross-section.

Directory: laplace (continued)

Subdirectory	Topic
flow_2d	Two-dimensional potential flow in an arbitrary domain.
body_2d	Potential flow past, or due to the motion of, a two-dimensional body.
body_ax	Potential flow past, or due to the motion of, an axisymmetric body.
tank_2d	Dynamical simulation of liquid sloshing in a two-dimensional rectangular tank.
ldr_3d	Solution of Laplace's equation in the interior or exterior of a closed three-dimensional surface, subject to the Dirichlet boundary condition. The solution is found using a boundary-element method based on Green's third identity.
lnm_3d	Solution of Laplace's equation in the interior or exterior of a closed three-dimensional surface, subject to the Neumann boundary condition. The solution is found using a boundary-element method based on Green's third identity.

Directory: helmholtz

Boundary element codes for Helmholtz's equation.

Subdirectory	Topic
flow_1d_osc	Unidirectional oscillatory viscous flow inside or outside a cylindrical tube with arbitrary cross-section.

Directory: `stokes`

Green's functions of Stokes flow and boundary-element codes for Stokes flow in two- and three-dimensional domains.

Subdirectory	Topic
<code>sgf_2d</code>	Green's functions of two-dimensional Stokes flow.
<code>sgf_3d</code>	Green's functions of three-dimensional Stokes flow.
<code>sgf_ax</code>	Green's functions of axisymmetric Stokes flow.
<code>flow_2d</code>	Two-dimensional flow in a domain with arbitrary geometry.
<code>prtcl_sw</code>	Swirling flow due to the rotation of an axisymmetric particle.
<code>prtcl_2d</code>	Flow past a fixed bed of two-dimensional particles with arbitrary shapes, for a variety of flow configurations.
<code>prtcl_ax</code>	Flow past, or due to the motion of, a collection of axisymmetric particles for several flow configurations.
<code>prtcl_3d</code>	Flow past, or due to the motion of, a three-dimensional particle, for a variety of flow configurations.

Chapter 9

Directory: grids

This directory contains programs that perform boundary-element discretization of two-dimensional lines and three-dimensional surfaces.

Directory contents:

Subdirectory	Topic
grid_2d	Discretization of a planar line consisting of straight and circular segments into a graded mesh of boundary elements with corresponding shapes.
trg1	Triangulation of a closed surface into an unstructured grid of six-node quadratic elements generated by the successive subdivision of an octahedron or icosahedron.

Directory: **grids/grid_2d**

This directory contains programs that perform the boundary-element discretization of a planar line consisting of a collection of straight and circular segments into a graded mesh of elements with corresponding shapes, as illustrated in Figure grid_2d.1.

The discretization is an integral part of boundary-element methods for two-dimensional and axisymmetric domains.

Main program: `grid_2d`

The main program reads the properties of the boundary segments and calls the subroutines `elm_line` and `elm_arc` that perform the boundary-element discretization.

The straight segments are defined by the end-points, whereas the circular segments are defined by their center, radii, and polar angles of the end-points.

Files to be linked:

1. `elm_line`
Discretization of a straight segment into straight (linear) elements.
2. `elm_arc`
Discretization of a circular arc into circular-arc elements.

Input file: `grid_2d.dat`

Geometrical properties of the straight and circular segments.

Output file: `grid_2d.out`

Coordinates of the end-points of the linear elements, and geometrical properties of the arcs.

Subroutine: `elm_line`

The discretization of a straight segment into a graded mesh of straight (linear) elements is illustrated in Figure grid_2d.2. This subroutine produces the coordinates and the arc length at the position of the element end- and mid-points. The mid-points serve as collocation points in boundary-element methods. The call statement is:

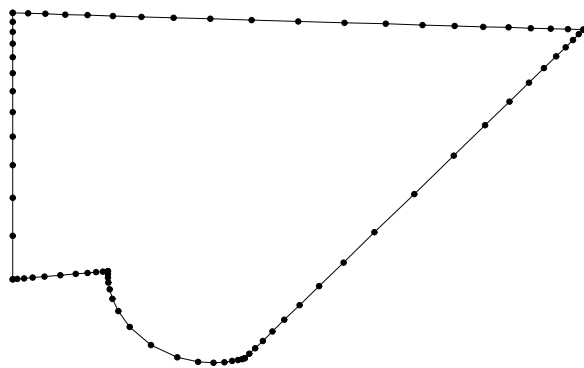


Figure grid_2d.1 Discretization of a planar line consisting of straight and circular segments into a graded mesh of elements with corresponding shapes.

elm_line

(<i>N</i>	<i>Input:</i> Number of elements along the segment.
, <i>ratio</i>	<i>Input:</i> Element stretch ratio; see Note 1.
, <i>X1, Y1</i>	<i>Input:</i> Coordinates of the first end-point.
, <i>X2, Y2</i>	<i>Input:</i> Coordinates of the second end-point.
, <i>sinit</i>	<i>Input:</i> Arc length assigned to the first end-point.
, <i>Isym</i>	<i>Input:</i> Symmetry index; see Note 1.
, <i>xe, ye, se</i>	<i>Output:</i> See Note 2.
, <i>xm, ym, sm</i>)	<i>Output:</i> See Note 3.

Notes:

1. *Isym* is a symmetry index; when it is set equal to 1, the element distribution is symmetric with respect to the mid-point of the segment; when it is set equal to 0, the distribution is non-symmetric. When *Isym* = 1 and the number of elements is odd, there is one mid-element; when *Isym* = 1 and the number of elements is even, there are two mid-elements of equal length.

When *Isym* = 0, the parameter *ratio* is the specified ratio of the length of the last element to the length of the first element. For example, when *ratio* = 0.5, the length of the last element is half the length of the first element.

When *Isym* = 1, the parameter *ratio* is the ratio of the length of the mid-element to the length of the first element. For example, when *ratio* = 2, the length of the mid-element is twice the length of the first element.

2. *xe, ye* are one-dimensional arrays containing the coordinates of the element end-nodes; *se* is a one-dimensional array containing the arc length at the position of the end-points measured along the segment from the first end-point.

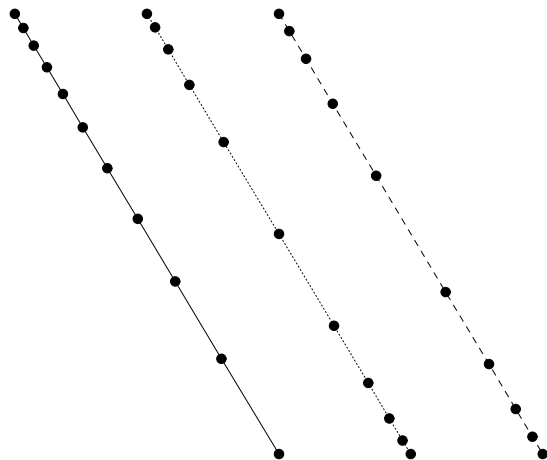


Figure grid_2d.2 Discretization of a straight segment into a graded mesh of elements. Solid line: non-symmetric distribution ($Isym = 0$); dotted line: symmetric distribution with even number of elements ($Isym = 1$); dashed line: symmetric distribution with odd number of elements ($Isym = 1$).

3. xm , ym are one-dimensional arrays containing the coordinates of the element mid-nodes located in the middle of each element. The array sm contains the arc length at the location of the mid-points measured from the first segment point.

Subroutine: elm_arc

The discretization of a circular arc into a graded mesh of circular arcs is illustrated in Figure grid_2d.3. This subroutine produces the coordinates and the arc length at the position of the element end- and mid-points. The mid-points serve as collocation points in boundary-element methods. The call statement is:

```
elm_arc
  (N
   ,ratio
   ,xcnt, ycnt
   ,radius
   ,angle1, angle2
   ,sinit
   ,Isym
   ,xe,ye,te,se
   ,xm,ym,tm,sm) Input: Number of elements along the segment.
                                Input: Element stretch ratio; see Note 1.
                                Input: Coordinates of the arc center.
                                Input: Arc radius.
                                Input: See Note 2.
                                Input: Specified arc length at the first end-point.
                                Input: Symmetry index; see Note 1.
                                Output: See Note 3.
                                Output: See Note 4.
```

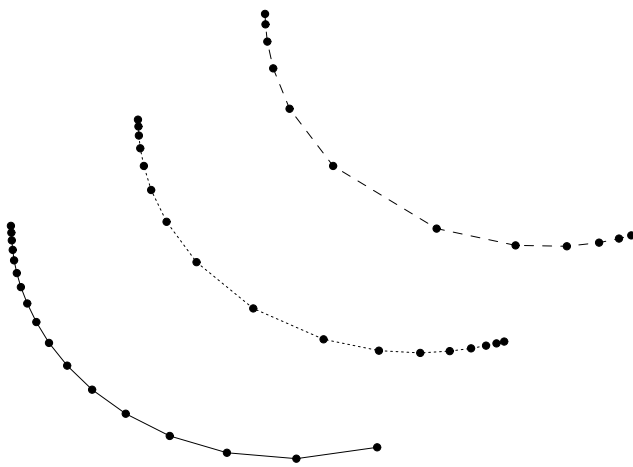


Figure grid_2d.3 Discretization of a circular segment into a graded mesh of elements. Solid line: non-symmetric distribution ($Isym = 0$); dotted line: symmetric distribution with even number of elements ($Isym = 1$); dashed line: symmetric distribution with odd number of elements ($Isym = 1$).

Notes:

1. $Isym$ is a symmetry index; when it is set equal to 1, the element distribution is symmetric with respect to the mid-point of the segment; when it is set equal to 0, the distribution is non-symmetric. When $Isym = 1$ and the number of elements is odd, there is one mid-element; when $Isym = 1$ and the number of elements is even, there are two mid-elements of equal arc length.

When $Isym = 0$, the parameter $ratio$ is the ratio of the arc length of the last element to the arc length of the first element. For example, when $ratio = 0.5$, the arc length of the last element is half the arc length of the first element.

When $Isym = 1$, the parameter $ratio$ is the ratio of the arc length of the mid-element to the arc length of the first element. For example, when $ratio = 2$, the arc length of the mid-element is twice the arc length of the first element.

2. $angle1$ and $angle2$ are the polar angles measured around the center of the arc up to the first and last end-points of the arc.
3. xe and ye are one-dimensional arrays containing the coordinates of the element end-nodes; te is an array containing polar angles of the end-nodes measured from the arc center; se is an array containing the arc length at the position of the end-points, measured along the segment with origin at the first point.

4. xm and ym are one-dimensional arrays containing the coordinates of the element mid-points, which are located at the middle of each element. The array tm contains the corresponding polar angles measured from the arc center. The array sm contains the arc length along the segment at the location of the mid-points, measured from the first segment point.

Directory: grids/trgl

This directory contains programs that perform the triangulation of a closed surface into an unstructured mesh of curved triangular quadratic defined by six nodes, as illustrated in Figure trgl.1.

The triangulation is carried out by successively subdividing the faces of a regular octahedron or icosahedron inscribed within the unit sphere into four descendant elements, thereby generating a sequence of higher-degree polyhedra, as shown in Figure trgl.2. In the process of subdivision, the edge mid-points of a parental triangle become vertex nodes of the descendant triangles. The mid-points of the edges of the newly formed descendant triangles are computed by interpolation. The descendant nodes are then projected onto the surface of the sphere to yield an ordered grid of curved triangular elements.

The parametric representation of the six-node quadratic triangles in terms of the three vertex nodes and three mid-point edge nodes is discussed in Section 5.3.

Main program: trgl

The main program calls a subroutine to triangulate the surface of the unit sphere, deforms the discretized surface to generate ellipsoids of specified aspect ratios, and then performs a series of computations based on the discrete parametric representation, including the following:

- Evaluation of the surface area and volume.
- Evaluation of the mean curvature at the nodes.
- Evaluation of the surface integral of a specified function.
- Confirmation of the orthonormality of the modified Legendre functions.
- Computation of the Cartesian surface curvature tensor.

Subroutine: trgl_octa

This subroutine generates the coordinates of the grid nodes and produces connectivity tables that relate the global and local labels of the nodes to (a) the labels of the triangular elements, and vice versa, and (b) the labels of triangles shared by the element edges. The call statement is:

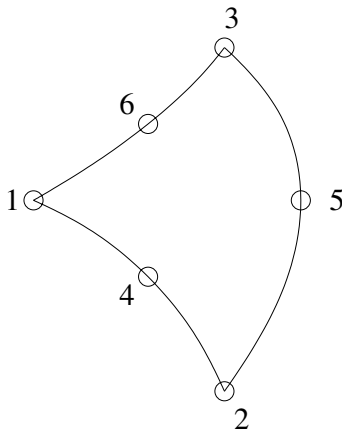


Figure trgl.1 A quadratic triangular element defined by six nodes, including three vertex nodes and three mid-nodes. The numbers displayed are the labels of the local nodes of the depicted element.

`trgl_octa`

(*Ndiv* Input: Discretization level.
 , *Npts* Output: Total number of vertex and mid-points.
 , *Nelm*) Output: Number of elements.

The integer parameter *Ndiv* provided in the input specifies the desired level of discretization: *Ndiv* = 0 gives eight elements over the whole surface of the sphere; *Ndiv* = 1 subdivides each of the eight elements into four elements to produce 32 elements, as illustrated in Figure trgl.2; similar subdivisions are performed in higher-level discretization. The total number of elements is *Nelm* = $8 \times 4^{Ndiv} - 1$.

This subroutine contains the following common blocks:

`common/points/p, ne`
`common/elmnts/n, nbe`

where:

- *p* is a two-index array defined such that $p(i, 1)$ is the *x*-coordinate of the point labeled *i*, $p(i, 2)$ is the *y*-coordinate of the point labeled *i*, and $p(i, 3)$ is the *z*-coordinate of the point labeled *i*.
- *ne* is a two-index array defined as follows: $ne(i, 1)$ is the number of elements sharing node *i*; subsequent entries, $ne(i, 2), ne(i, 3), \dots, ne(i, ne(i, 1) + 1)$, are the labels of the elements sharing the *i*th node.

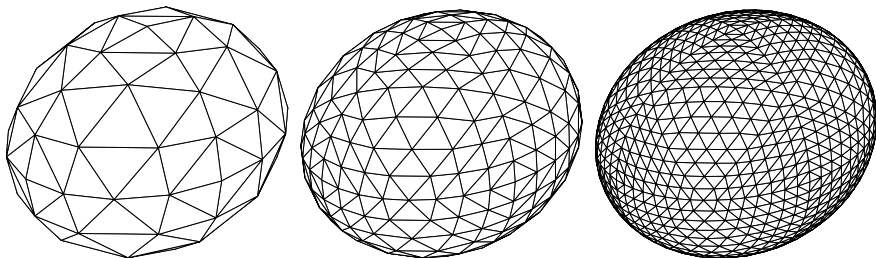


Figure trgl.2 Triangulation of the surface of a spheroid into quadratic elements defined by six nodes based on successive subdivisions of a regular octahedron, for discretization levels $Ndiv = 1, 2$, and 3 .

- n is a two-index array defined as follows: $n(i, j)$ is the global label of the node on element numbered i with local element label j , where $j = 1, \dots, 6$.

Subroutine: trgl_icos

This is similar to subroutine trgl_octa, except that the triangulation is based on the successive subdivisions of a regular icosahedron.

Files to be linked:

None for the triangulation subroutines.

The main program must be linked with the following files:

1. `cramer_33`
Solution of a 3×3 linear system by Cramer's rule.
2. `crvm_3d`
Computation of the mean curvature.
3. `gauss_trgl`
Gauss integration quadrature base points and weights for a triangle.

4. `leg_fnc_ortho`

Computation of the orthonormal set of the modified Legendre functions.

5. `srf_int_3d`

Computation of a surface integral.

6. `trgl_octa_aux`

Auxiliary subroutines that compute various geometrical properties.

7. `vtg_3d`

Computation of the tangential gradient of a vector function.

Chapter 10

Directory: laplace

This directory contains libraries of Green's and Neumann functions of Laplace's equation, and boundary-element codes that generate solutions to Laplace's equation in two and three dimensions with applications in fluid dynamics.

Directory contents:

Subdirectory	Topic
lgf_2d	Green's and Neumann functions of Laplace's equation in two dimensions.
lgf_3d	Green's and Neumann functions of Laplace's equation in three dimensions.
lgf_ax	Green's and Neumann functions of Laplace's equation in axisymmetric domains.
flow_1d	Unidirectional viscous flow through a tube with arbitrary cross-section.
flow_1d_1p	Unidirectional periodic viscous flow past a periodic array of cylinders or a periodic wall with arbitrary cross-section.
flow_2d	Two-dimensional potential flow in an arbitrary domain.
body_2d	Potential flow past, or due to the motion of, a two-dimensional body.
body_ax	Potential flow past, or due to the motion of, an axisymmetric body.
tank_2d	Dynamical simulation of liquid sloshing in a two-dimensional rectangular tank.

Directory contents (continued)

Subdirectory	Topic
ldr_3d	Solution of Laplace's equation in the interior or exterior of a three-dimensional surface, subject to the Dirichlet boundary condition. The solution is found using a boundary-element method based on Green's third identity.
lnm_3d	Solution of Laplace's equation in the interior or exterior of a three-dimensional surface, subject to the Neumann boundary condition. The solution is found using a boundary-element method based on Green's third identity.

Directory: `laplace/lgf_2d`

The Green's functions of Laplace's equation in two dimensions constitute a special class of harmonic functions that are singular at an arbitrary point $\mathbf{x}_0 = (x_0, y_0)$.

By definition, a Green's function satisfies the singularly forced Laplace's equation

$$\nabla^2 G(\mathbf{x}, \mathbf{x}_0) + \delta_2(\mathbf{x} - \mathbf{x}_0) = 0, \quad (\text{lgf_2d.1})$$

explicitly written as

$$\frac{\partial^2 G(\mathbf{x}, \mathbf{x}_0)}{\partial x^2} + \frac{\partial^2 G(\mathbf{x}, \mathbf{x}_0)}{\partial y^2} + \delta_2(\mathbf{x} - \mathbf{x}_0) = 0, \quad (\text{lgf_2d.2})$$

where:

- $\mathbf{x} = (x, y)$ is the variable “field” or “evaluation” point.
- $\mathbf{x}_0 = (x_0, y_0)$ is the fixed singular point, also called the “pole”.
- $\delta_2(\mathbf{x} - \mathbf{x}_0)$, written explicitly as $\delta_2(x - x_0, y - y_0)$, is Dirac's delta function in two dimensions.

GREEN'S FUNCTIONS OF THE FIRST KIND AND NEUMANN FUNCTIONS:

In addition to satisfying the definition (lgf_2d.1), the Green's function $G(\mathbf{x}, \mathbf{x}_0)$ or its normal derivative $\mathbf{n}(\mathbf{x}) \cdot \nabla G(\mathbf{x}, \mathbf{x}_0)$ is required to be zero when the evaluation point \mathbf{x} lies on a specified contour C_G , where $\mathbf{n}(\mathbf{x})$ is the unit vector normal to C_G .

In the first case, we have a Green's function of the first kind; in the second case, we have a Green's function of the second kind - also called a Neumann function.

PHYSICAL INTERPRETATION:

The Green's function represents the temperature or concentration field due to a point source of heat or species located at the singular point.

In fluid mechanics, the Green's function represents the velocity potential due to a point sink of mass located at the singular point. The gradient of the Green's function is the fluid velocity.

INTEGRAL IDENTITY:

A consequence of (lgf_2d.1) is that Green's functions satisfy the integral identity

$$\int_C \mathbf{n}(\mathbf{x}) \cdot \nabla G(\mathbf{x}, \mathbf{x}_0) dl(\mathbf{x}) = \begin{cases} 1 & \text{when } \mathbf{x}_0 \text{ is inside } A_c \\ \frac{1}{2} & \text{when } \mathbf{x}_0 \text{ is on } C \\ 0 & \text{when } \mathbf{x}_0 \text{ is outside } A_c \end{cases}, \quad (\text{lgf_2d.3})$$

where C is a closed loop in the xy plane enclosing the control area A_c , and the normal vector \mathbf{n} is oriented *into* the control area. When the point \mathbf{x}_0 is located precisely in the contour C , the integral on the left-hand side of (lgf_2d.3) is a principal-value integral.

BOUNDARY-INTEGRAL REPRESENTATION:

The boundary-integral representation of a harmonic function f is

$$f(\mathbf{x}_0) = - \int_C G(\mathbf{x}, \mathbf{x}_0) [\mathbf{n}(\mathbf{x}) \cdot \nabla f(\mathbf{x})] dl(\mathbf{x}) + \int_C f(\mathbf{x}) [\mathbf{n}(\mathbf{x}) \cdot \nabla G(\mathbf{x}, \mathbf{x}_0)] dl(\mathbf{x}), \quad (\text{lgf_2d.4})$$

where C is the collection of all boundaries enclosing a selected control area, and \mathbf{n} is the unit vector normal to C pointing inward.

DIRECTORY CONTENTS:

This directory contains a suite of subroutines that evaluate the following Green's and Neumann functions and their gradients:

Subroutine	Topic
lgf_2d_fs	Green's function in free space.
lgf_2d_1p	Singly periodic Green's function in free space.
lgf_2d_w	Green's and Neumann functions in a semi-infinite domain bounded by a plane wall.
lgf_2d_1p_w	Periodic Green's and Neumann functions in a semi-infinite domain bounded by a plane wall.
lgf_2d_ww	Green's and Neumann functions in an infinite strip bounded by two parallel plane walls.
lgf_2d_crc	Neumann function in the exterior of a circle.

Subroutine: lgf_2d_fs

This subroutine computes the Green's function in an infinite domain in the absence of boundaries.

The Green's function is given by

$$G(\mathbf{x}, \mathbf{x}_0) = -\frac{1}{2\pi} \ln r, \quad (1)$$

where $r = |\mathbf{x} - \mathbf{x}_0|$ is the distance of the field point \mathbf{x} from the singular point \mathbf{x}_0 .

The gradient of the Green's function is given by

$$\frac{\partial G}{\partial x} = -\frac{1}{2\pi} \frac{x - x_0}{r^2}, \quad \frac{\partial G}{\partial y} = -\frac{1}{2\pi} \frac{y - y_0}{r^2}. \quad (2)$$

Call statement:

`lgf_2d_fs`

$(Iopt$	<i>Input:</i> See Note 1.
$, x, y$	<i>Input:</i> Coordinates of the field point.
$, x_0, y_0$	<i>Input:</i> Coordinates of the singular point.
$, G$	<i>Output:</i> Green's function.
$, G_x, G_y)$	<i>Output:</i> Green's function gradient, ∇G .

Note:

1. Set $Iopt = 1$ to obtain only G ; set $Iopt \neq 1$ to also obtain G_x and G_y .

Numerical method:

The Green's function and its gradient are computed by direct evaluation of expressions (1) and (2).

Driver: `lgf_2d_fs_dr`

The driver evaluates the Green's function and verifies the integral identity (lgf_2d.3), where C is a circular contour.

Files to be linked: None.

Subroutine: lgf_2d_1p

This subroutine computes the periodic Green's function of Laplace's equation in two dimensions representing the potential due to a periodic array of point sources separated by the distance L along the x axis, as illustrated in Figure lgf_2d_1p.1. One of the singular points is located at the point $\mathbf{x}_0 = (x_0, y_0)$.

The Green's function is given by

$$G(\mathbf{x}, \mathbf{x}_0) = -\frac{1}{4\pi} \ln [2 \{ \cosh[k(y - y_0)] - \cos[k(x - x_0)] \}], \quad (1)$$

where $k = 2\pi/L$ is the wave number, and L is the period, that is, the separation between two consecutive singular points ([59], p. 358).

The gradient of the Green's function is given by

$$\begin{aligned} \frac{\partial G}{\partial x} &= -\frac{1}{2L} \frac{\sin[k(x - x_0)]}{\cosh[k(y - y_0)] - \cos[k(x - x_0)]}, \\ \frac{\partial G}{\partial y} &= -\frac{1}{2L} \frac{\sinh[k(y - y_0)]}{\cosh[k(y - y_0)] - \cos[k(x - x_0)]}. \end{aligned} \quad (2)$$

Call statement:

`lgf_2d_1p`

$(Iopt$	<i>Input:</i> See Note 1.
$, x, y$	<i>Input:</i> Coordinates of the field point.
$, x_0, y_0$	<i>Input:</i> Coordinates of the singular point.
$, L$	<i>Input:</i> Distance between the singularities.
$, G$	<i>Output:</i> Green's function.
$, G_x, G_y)$	<i>Output:</i> Green's function gradient, ∇G .

Note:

1. Set $Iopt = 1$ to obtain only G ; set $Iopt \neq 1$ to also obtain G_x and G_y .

Numerical method:

The Green's function and its gradient are computed by direct evaluation of expressions (1) and (2).

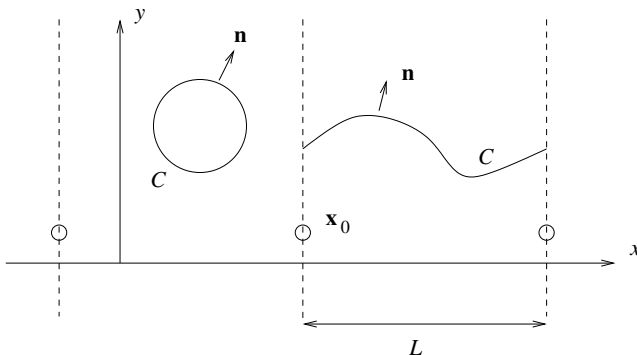


Figure lgf_2d_1p.1 The periodic Green's function represents the potential due to an array of point sources of heat or species separated by the distance L along the x axis.

Driver: `lgf_2d_1p_dr`

The driver evaluates the Green's function and verifies the integral identity (lgf_2d.3), where C is a circular contour or one period of a periodic line, as illustrated in Figure lgf_2d_1p.1.

Files to be linked: None.

Streamlines:

In fluid mechanics, the periodic Green's function represents the velocity potential due to a periodic array of point sinks. The streamline pattern is shown in Figure lgf_2d_1p.2.

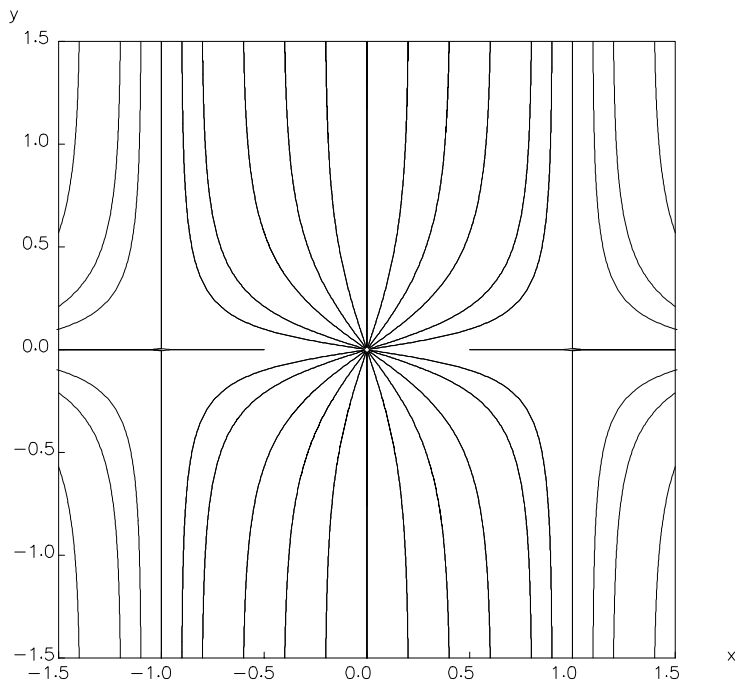


Figure lgf_2d_1p.2 Streamlines of the flow due to a periodic array of point sinks.

Subroutine: lgf_2d_w

This subroutine computes the Green's and Neumann functions of Laplace's equation in a semi-infinite domain bounded by a plane wall located at $y = wall$, as illustrated in Figure lgf_2d.w.1.

The Green's function is given by

$$G(\mathbf{x}, \mathbf{x}_0) = -\frac{1}{2\pi} \ln r \pm \frac{1}{2\pi} \ln R, \quad (1)$$

where the plus sign corresponds to the Green's function of the first kind, the minus sign corresponds to the Neumann function, $r = |\mathbf{x} - \mathbf{x}_0|$, $R = |\mathbf{x} - \mathbf{x}_0^{Im}|$, and $\mathbf{x}_0^{Im} = (x_0, 2 \times wall - y_0)$ is the location of the image of the singular point with respect to the wall.

The gradient of the Green's function is given by

$$\begin{aligned} \frac{\partial G}{\partial x} &= -\frac{1}{2\pi} \frac{x - x_0}{r^2} \pm \frac{1}{2\pi} \frac{x - x_0}{R^2}, \\ \frac{\partial G}{\partial y} &= -\frac{1}{2\pi} \frac{y - y_0}{r^2} \pm \frac{1}{2\pi} \frac{y - y_0 + 2wall}{R^2}. \end{aligned} \quad (2)$$

Call statement:

lgf_2d_w

$(Iopt$	<i>Input:</i> See Note 1.
$, Ign$	<i>Input:</i> See Note 2.
$, x, y$	<i>Input:</i> Coordinates of the field point.
$, x_0, y_0$	<i>Input:</i> Coordinates of the singular point.
$, wall$	<i>Input:</i> The wall is located at $y = wall$.
$, G$	<i>Output:</i> Green's function.
$, G_x, G_y$)	<i>Output:</i> Green's function gradient, ∇G .

Notes:

1. Set $Iopt = 1$ to obtain only G ; set $Iopt \neq 1$ to also obtain G_x and G_y .
2. Set $Ign = 1$ to obtain the Green's function of the first kind; set $Ign = 2$ to obtain the Neumann function.

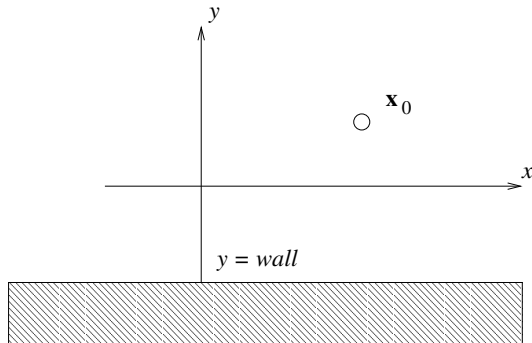


Figure lgf_2d_w.1 A semi-infinite domain bounded by a plane wall.

Numerical method:

The Green's function and its gradient are computed by direct evaluation of expressions (1) and (2).

Driver: lgf_2d_w_dr

The driver evaluates the Green's function and verifies the integral identity (lgf_2d.3), where C is a circular contour.

Files to be linked: None.

Streamlines:

In fluid mechanics, the Green's function represents the velocity potential due to a point sink placed above a wall. The streamline pattern associated with the Neumann function is shown in Figure lgf_2d_w.2.

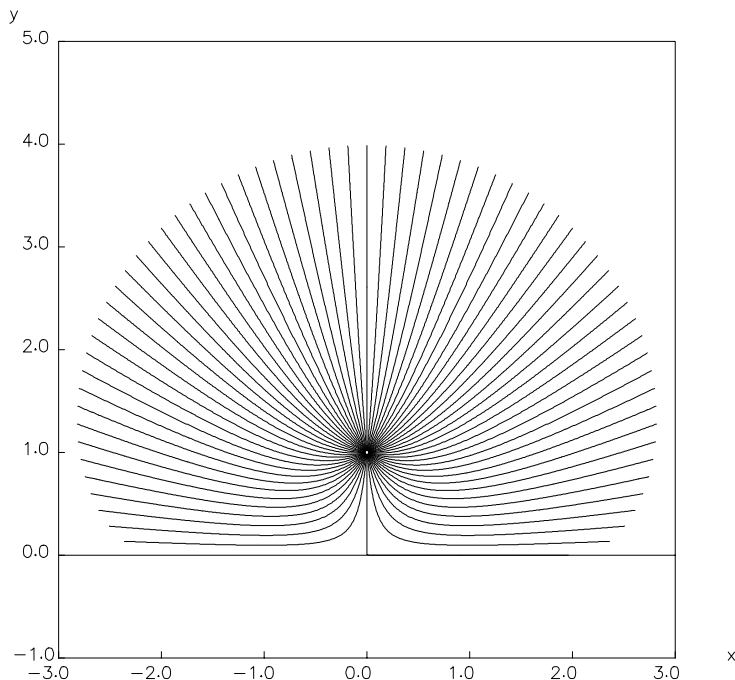


Figure lgf_2d.w.2 Streamline pattern of the flow due to a point sink placed above an impenetrable wall, expressed by the Neumann function.

Subroutine: lgf_2d_1p_w

This subroutine computes the periodic Green's and Neumann functions of Laplace's equation in a semi-infinite domain bounded by a plane wall located at $y = wall$, as illustrated in Figure lgf_2d_1p_w.1. One of the singularities is located at the point $\mathbf{x}_0 = (x_0, y_0)$.

The Green's function is given by

$$G(\mathbf{x}, \mathbf{x}_0) = -\frac{1}{4\pi} \ln[2\{\cosh[k(y - y_0)] - \cos[k(x - x_0)]\}] \\ \pm \frac{1}{4\pi} \ln[2\{\cosh[k(y - y_0^{Im})] - \cos[k(x - x_0)]\}], \quad (1)$$

where the plus sign corresponds to the Green's function of the first kind, the minus sign corresponds to the Neumann function, and $y_0^{Im} = 2 \times wall - y_0$ is the y location of the image of one singular point with respect to the wall.

The gradient of the Green's function is given by

$$\frac{\partial G}{\partial x} = -\frac{1}{2L} \frac{\sin[k(x - x_0)]}{\cosh[k(y - y_0)] - \cos[k(x - x_0)]} \\ \pm \frac{1}{2L} \frac{\sin[k(x - x_0)]}{\cosh[k(y - y_0^{Im})] - \cos[k(x - x_0)]}, \quad (2)$$

$$\frac{\partial G}{\partial y} = -\frac{1}{2L} \frac{\sinh[k(y - y_0)]}{\cosh[k(y - y_0)] - \cos[k(x - x_0)]} \\ \pm \frac{1}{2L} \frac{\sinh[k(y - y_0^{Im})]}{\cosh[k(y - y_0^{Im})] - \cos[k(x - x_0)]}.$$

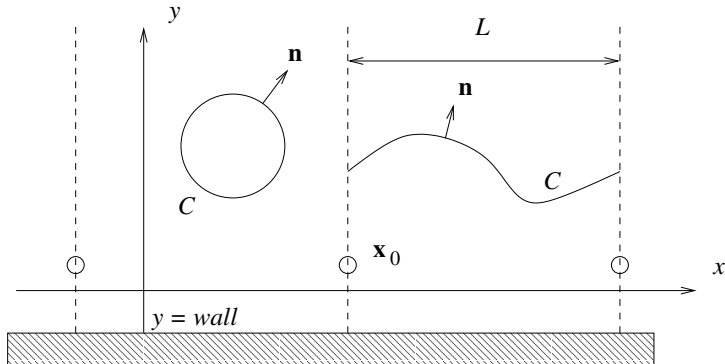


Figure lgf_2d_1p_w.1 A periodic array of singularities in a semi-infinite domain bounded by a plane wall located at $y = \text{wall}$.

Call statement:

`lgf_2d_1p_w`

$(Iopt$	<i>Input:</i> See Note 1.
$, Ign$	<i>Input:</i> See Note 2.
$, x, y$	<i>Input:</i> Coordinates of the field point.
$, x_0, y_0$	<i>Input:</i> Coordinates of the singular point.
$, L$	<i>Input:</i> Distance between the singularities.
$, wall$	<i>Input:</i> The wall is located at $y = \text{wall}$.
$, G$	<i>Output:</i> Green's function.
$, G_x, G_y)$	<i>Output:</i> Green's function gradient, ∇G .

Notes:

1. Set $Iopt = 1$ to obtain only G ; set $Iopt \neq 1$ to also obtain G_x and G_y .
2. Set $Ign = 1$ to obtain the Green's function of the first kind; set $Ign = 2$ to obtain the Neumann function.

Numerical method:

The Green's function and its gradient are computed by direct evaluation of expressions (1) and (2).

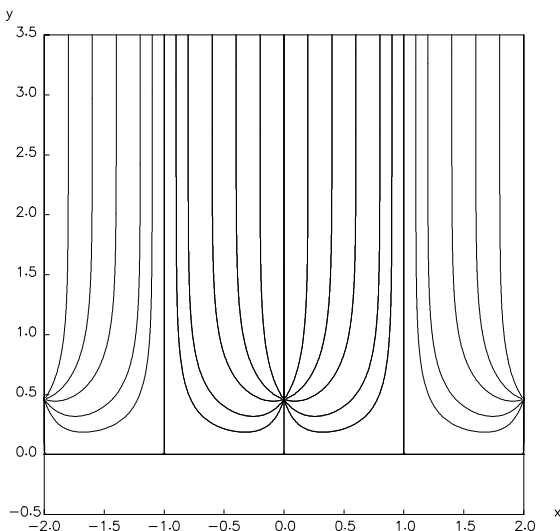


Figure lgf_2d_1p_w.2 Streamline pattern of the flow due to a periodic array of point sinks placed above an impenetrable wall, expressed by the Neumann function.

Driver: `lgf_2d_1p_w_dr`

The driver evaluates the Green's function and verifies the integral identity (lgf_2d.3), where C is a circular contour or one period of a periodic line, as illustrated in Figure lgf_2d_1p_w.1.

Files to be linked: None.

Streamlines:

In fluid mechanics, the Green's function represents the velocity potential due to a periodic array of point sinks placed above a wall. The streamline pattern associated with the Neumann function is shown in Figure lgf_2d_1p_w.2.

Subroutine: `lgf_2d_ww`

This subroutine computes the Green's and Neumann functions of Laplace's equation in an infinite strip confined between two parallel plane walls. The first wall is located at $y = wall1$ and the second wall is located at $y = wall2$, as illustrated in Figure `lgf_2d_ww.1`.

The Green's function is given by

$$\begin{aligned} G(\mathbf{x}, \mathbf{x}_0) &= -\frac{1}{4\pi} \ln[2\{\cosh[k(x - x_0)] - \cos[k(y - y_0)]\}] \\ &\quad \pm \frac{1}{4\pi} \ln[2\{\cosh[k(x - x_0)] - \cos[k(y - y_0^{Im})]\}], \end{aligned} \quad (1)$$

where:

- $k = \pi/h$ is a wave number, and $h = wall2 - wall1$ is the width of the strip.
- y_0^{Im} is the y position of the image of the singular point with respect to the upper or lower wall; thus, $y_0^{Im} = 2 \times wall1 - y_0$ or $y_0^{Im} = 2 \times wall2 - y_0$.
- The plus sign corresponds to the Green's function of the first kind, and the minus sign corresponds to the Neumann function.

The gradient of the Green's function is given by

$$\begin{aligned} \frac{\partial G}{\partial x} &= -\frac{1}{4h} \frac{\sinh[k(x - x_0)]}{\cosh[k(x - x_0)] - \cos[k(y - y_0^{Im})]} \\ &\quad \pm \frac{1}{4h} \frac{\sinh[k(x - x_0)]}{\cosh[k(x - x_0)] - \cos[k(y - y_0^{Im})]}, \end{aligned} \quad (2)$$

$$\frac{\partial G}{\partial y} = -\frac{1}{4h} \frac{\sin[k(y - y_0)]}{\cosh[k(x - x_0)] - \cos[k(y - y_0^{Im})]}$$

$$\pm \frac{1}{4h} \frac{\sin[k(y - y_0^{Im})]}{\cosh[k(x - x_0)] - \cos[k(y - y_0^{Im})]}.$$

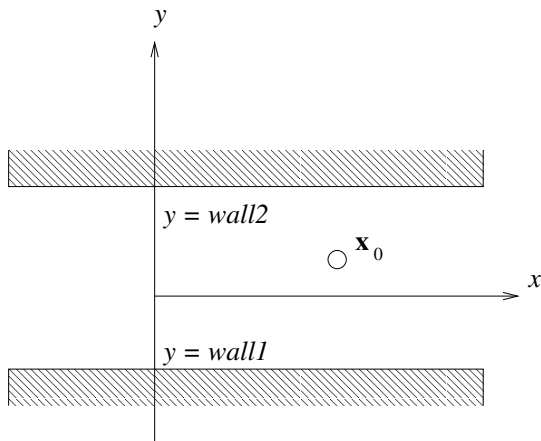


Figure lgf_2d_ww.1 An infinite strip bounded by two parallel plane walls.

Call statement:

`lgf_2d_ww`

$(Iopt$	<i>Input:</i>	See Note 1.
$, Ign$	<i>Input:</i>	See Note 2.
$, x, y$	<i>Input:</i>	Coordinates of the field point.
$, x_0, y_0$	<i>Input:</i>	Coordinates of the singular point.
$, wall1$	<i>Input:</i>	The first wall is located at $y = wall1$.
$, wall2$	<i>Input:</i>	The second wall is located at $y = wall2$.
$, G$	<i>Output:</i>	Green's function.
$, G_x, G_y)$	<i>Output:</i>	Green's function gradient, ∇G .

Notes:

1. Set $Iopt = 1$ to obtain only G ; set $Iopt \neq 1$ to also obtain G_x and G_y .
2. Set $Ign = 1$ to obtain the Green's function of the first kind; set $Ign = 2$ to obtain the Neumann function.

Numerical method:

The Green's function and its gradient are computed by direct evaluation of expressions (1) and (2).

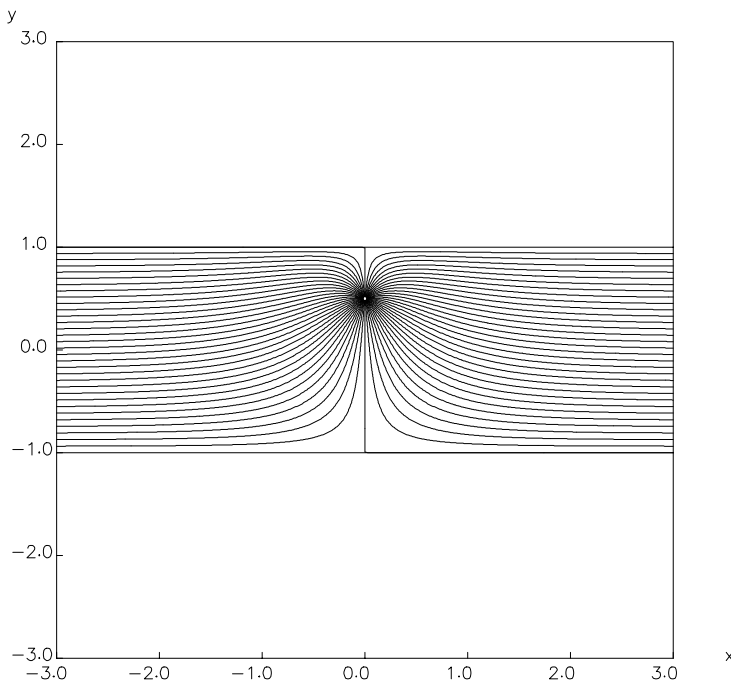


Figure lgf_2d_ww.2 Streamline pattern of the flow due to a point sink in a channel confined between two parallel impenetrable walls, expressed by the Neumann function.

Driver: lgf_2d_ww_dr

The driver evaluates the Green's function, and verifies the integral identity (lgf_2d.3), where C is a circular contour.

Files to be linked: None.

Streamlines:

In fluid mechanics, the Green's function represents the velocity potential due to a point sink in a channel confined between two parallel walls. The streamline pattern associated with the Neumann function is shown in Figure lgf_2d_ww.2.

Subroutine: lgf_2d_www

This subroutine computes the Neumann function of Laplace's equation in a semi-infinite rectangular strip confined between two parallel plane walls located at $x = wall1$ and $x = wall2$, and a third wall located at $y = wall3$ intersecting the parallel walls at right angles, as illustrated in Figure lgf_2d_www.1.

The Green's function is given by

$$G(\mathbf{x}, \mathbf{x}_0) = -\frac{1}{4\pi} \sum_{i=0}^3 \left\{ \ln[2\{\cosh[k(y - y_i)] - \cos[k(x - x_i)]\}] \right\}, \quad (1)$$

where:

- $k = \pi/h$ is a wave number, and $h = wall2 - wall1$ is the width of the strip.
- $x_1 = -x_0 + 2 \times wall1$ and $y_1 = y_0$ are the coordinates of the image of the singular point with respect to the left wall.
- $x_2 = x_0$ and $y_2 = -y_0 + 2 \times wall3$ are the coordinates of the image of the singular point with respect to the bottom wall.
- $x_3 = -x_0 + 2 \times wall1$ and $y_3 = -y_0 + 2 \times wall3$ are the coordinates of the image of the singular point with respect to the left and bottom wall.

The gradient of the Green's function is given by

$$\begin{aligned} \frac{\partial G}{\partial x} &= -\frac{1}{4h} \sum_{i=0}^3 \frac{\sinh[k(y - y_i)]}{\cosh[k(y - y_i)] - \cos[k(x - x_i)]}, \\ \frac{\partial G}{\partial y} &= -\frac{1}{4h} \sum_{i=0}^3 \frac{\sin[k(x - x_i)]}{\cosh[k(y - y_i)] - \cos[k(x - x_i)]}. \end{aligned} \quad (2)$$

Call statement:

`lgf_2d_www`

(<i>Iopt</i>	<i>Input:</i>	See Note 1.
, <i>x, y</i>	<i>Input:</i>	Coordinates of the field point.
, <i>x₀, y₀</i>	<i>Input:</i>	Coordinates of the singular point.
, <i>wall1</i>	<i>Input:</i>	The first wall is located at $x = wall1$.
, <i>wall2</i>	<i>Input:</i>	The second wall is located at $x = wall2$.
, <i>wall3</i>	<i>Input:</i>	The third wall is located at $y = wall3$.
, <i>G</i>	<i>Output:</i>	Green's function.
, <i>G_x, G_y</i>)	<i>Output:</i>	Green's function gradient ∇G .

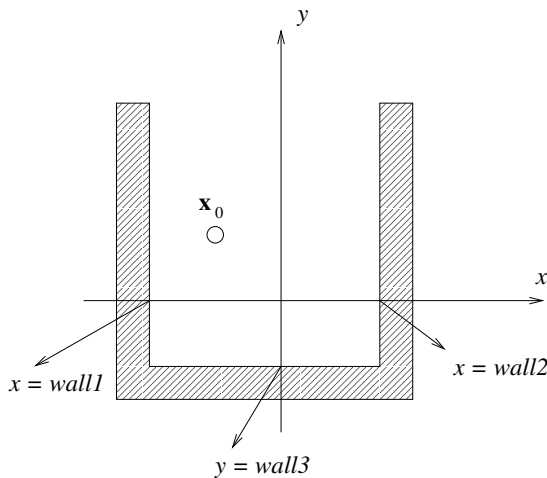


Figure lgf_2d_www.1 A semi-infinite strip extending along the y axis.

Note:

1. Set $Iopt = 1$ to obtain only G ; set $Iopt \neq 1$ to also obtain G_x and G_y .

Numerical method:

The Green's function and its gradient are computed by direct evaluation of expressions (1) and (2).

Driver: lgf_2d_www_dr

The driver evaluates the Green's function and verifies the integral identity (lgf_2d.3), where C is a circular contour.

Files to be linked: None.

Streamlines:

In fluid mechanics, the Green's function represents the velocity potential due to a point sink placed in a semi-infinite strip. The streamline pattern associated with the Neumann function is shown in Figure lgf_2d_www.2.

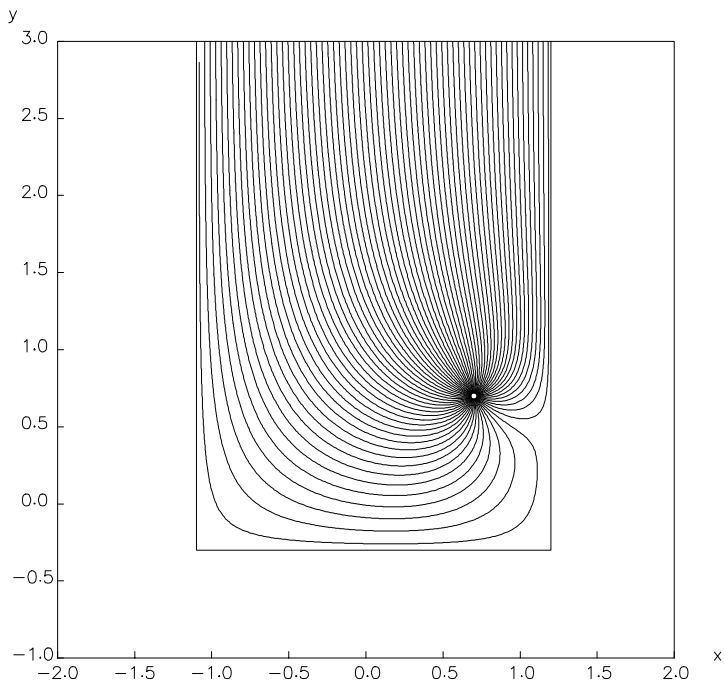


Figure lgf_2d.www.2 Streamline pattern of the flow due to a point sink in a semi-infinite strip, expressed by the Neumann function.

Subroutine: lgf_2d_crc

This subroutine computes the Neumann function of Laplace's equation in an infinite domain bounded internally by a circle of radius a centered at the point \mathbf{x}_c , as illustrated in Figure lgf_2d_crc.1.

The Neumann function is given by

$$G(\mathbf{x}, \mathbf{x}_0) = -\frac{1}{2\pi} \ln r + \frac{1}{2\pi} \ln R - \frac{1}{2\pi} \ln \rho, \quad (1)$$

where $r = |\mathbf{x} - \mathbf{x}_0|$, $R = |\mathbf{x} - \mathbf{x}_0^{Im}|$, $\rho = |\mathbf{x} - \mathbf{x}_c|$, and \mathbf{x}_0^{Im} is the inverse point of the point source with respect to the circle given by

$$\mathbf{x}_0^{Im} = \mathbf{x}_c + \frac{a^2}{|\mathbf{x}_0 - \mathbf{x}_c|^2} (\mathbf{x}_0 - \mathbf{x}_c), \quad (2)$$

([59], p. 363).

The gradient of the Neumann function is given by

$$\begin{aligned} \frac{\partial G}{\partial x} &= -\frac{1}{2\pi} \frac{x - x_0}{r^2} + \frac{1}{2\pi} \frac{x - x_0^{Im}}{R^2} - \frac{1}{2\pi} \frac{x - x_c}{\rho^2}, \\ \frac{\partial G}{\partial y} &= -\frac{1}{2\pi} \frac{y - y_0}{r^2} + \frac{1}{2\pi} \frac{y - y_0^{Im}}{R^2} - \frac{1}{2\pi} \frac{y - y_c}{\rho^2}. \end{aligned} \quad (3)$$

Call statement:

`lgf_2d_crc`

$(Iopt$	<i>Input:</i> See Note 1.
$, x, y$	<i>Input:</i> Coordinates of the field point.
$, x_0, y_0$	<i>Input:</i> Coordinates of the singular point.
$, x_c, y_c$	<i>Input:</i> Coordinates of the center of the circle.
$, a$	<i>Input:</i> Radius of the circle.
$, G$	<i>Output:</i> Neumann function.
$, G_x, G_y$	<i>Output:</i> Neumann function gradient, ∇G .

Note:

1. Set $Iopt = 1$ to obtain only G ; set $Iopt \neq 1$ to also obtain G_x and G_y .

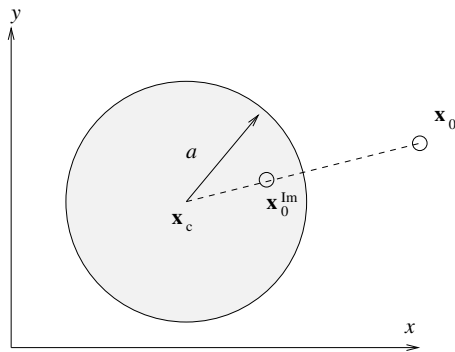


Figure lgf_2d_crc.1 Illustration of the exterior of a circle of radius a in the *xy* plane, showing the image of the pole.

Numerical method:

The Neumann function and its gradient are computed by direct evaluation of expressions (1) and (2).

Driver: `lgf_2d_crc_dr`

The driver evaluates the Neumann function and verifies the integral identity (lgf_2d.3), where C is a circular contour.

Files to be linked: None.

Streamlines:

In fluid mechanics, the Green's function represents the velocity potential due to a point sink in the exterior of a circle. The streamline pattern associated with the Neumann function is shown in Figure lgf_2d_crc.2.

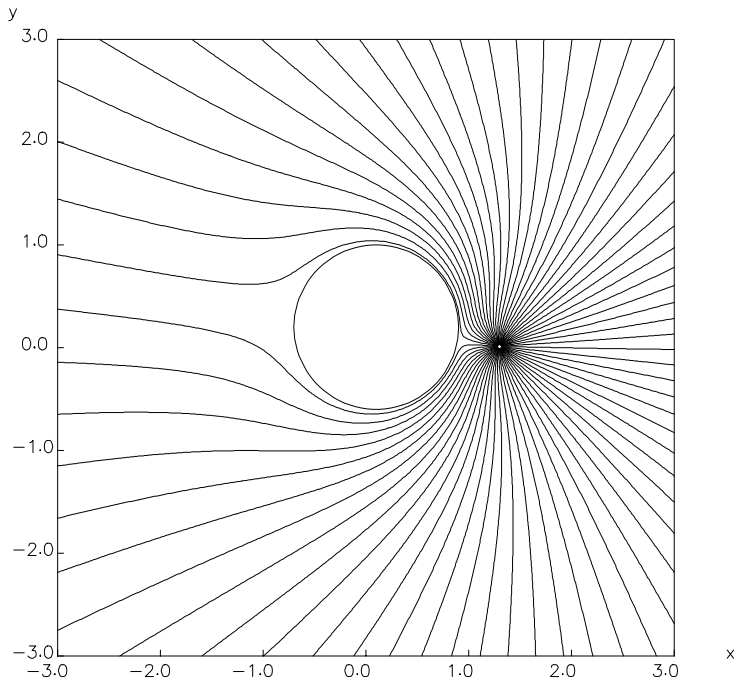


Figure lgf_2d.crc.2 Streamline pattern of the flow due to a point sink in the exterior of an impenetrable circle, expressed by the Neumann function.

Directory: `laplace/lgf_3d`

The Green's functions of Laplace's equation in three dimensions constitute a special class of harmonic functions that are singular at an arbitrary point $\mathbf{x}_0 = (x_0, y_0, z_0)$.

By definition, a Green's function satisfies the singularly forced Laplace's equation

$$\nabla^2 G(\mathbf{x}, \mathbf{x}_0) + \delta_3(\mathbf{x} - \mathbf{x}_0) = 0, \quad (\text{lgf_2d.1})$$

explicitly written as

$$\frac{\partial^2 G(\mathbf{x}, \mathbf{x}_0)}{\partial x^2} + \frac{\partial^2 G(\mathbf{x}, \mathbf{x}_0)}{\partial y^2} + \frac{\partial^2 G(\mathbf{x}, \mathbf{x}_0)}{\partial z^2} + \delta_3(\mathbf{x} - \mathbf{x}_0) = 0, \quad (\text{lgf_2d.2})$$

where:

- $\mathbf{x} = (x, y, z)$ is the variable “field” or “evaluation” point.
- $\mathbf{x}_0 = (x_0, y_0, z_0)$ is the fixed singular point, also called the “pole.”
- $\delta_3(\mathbf{x} - \mathbf{x}_0)$, written more explicitly as $\delta_3(x - x_0, y - y_0, z - z_0)$, is Dirac's delta function in three dimensions.

GREEN'S FUNCTIONS OF THE FIRST KIND AND NEUMANN FUNCTIONS:

In addition to satisfying the definition (lgf_3d.1), a Green's function $G(\mathbf{x}, \mathbf{x}_0)$ or its normal derivative $\mathbf{n}(\mathbf{x}) \cdot \nabla G(\mathbf{x}, \mathbf{x}_0)$ is required to be zero when the evaluation point \mathbf{x} lies on a specified surface S_G , where $\mathbf{n}(\mathbf{x})$ is the unit vector normal to S_G .

In the first case, we have a Green's function of the first kind; in the second case, we have a Green's function of the second kind - also called a Neumann function.

PHYSICAL INTERPRETATION:

The Green's function represents the temperature or concentration field due to a point source of heat or species located at the singular point. In fluid mechanics, the Green's function represents the harmonic potential due to a point sink of mass located at the singular point.

INTEGRAL IDENTITY:

A consequence of (lgf_3d.1) is that Green's functions satisfy the integral identity

$$\int_D \mathbf{n}(\mathbf{x}) \cdot \nabla G(\mathbf{x}, \mathbf{x}_0) dS(\mathbf{x}) = \begin{cases} 1 & \text{when } \mathbf{x}_0 \text{ is inside } V_c \\ \frac{1}{2} & \text{when } \mathbf{x}_0 \text{ is on } D \\ 0 & \text{when } \mathbf{x}_0 \text{ is outside } V_c \end{cases}, \quad (\text{lgf_2d.3})$$

where D is a closed surface enclosing the control volume V_c , and the unit normal vector \mathbf{n} points *into* the control volume.

When the point \mathbf{x}_0 is located on the surface D , the integral on the left-hand side of (lgf_3d_3) is an improper but convergent principal-value integral.

BOUNDARY-INTEGRAL REPRESENTATION:

The boundary-integral representation of a harmonic function f is

$$f(\mathbf{x}_0) = - \int_D G(\mathbf{x}, \mathbf{x}_0) \mathbf{n}(\mathbf{x}) \cdot \nabla f(\mathbf{x}) dS(\mathbf{x}) + \int_D f(\mathbf{x}) \mathbf{n}(\mathbf{x}) \cdot \nabla G(\mathbf{x}, \mathbf{x}_0) dS(\mathbf{x}), \quad (\text{lgf_2d.4})$$

where D stands for the collection of all boundaries of a selected control volume, and \mathbf{n} is the unit vector normal to D pointing inward.

DIRECTORY CONTENTS:

This directory contains a suite of subroutines that evaluate the following Green's functions and their gradients:

Subroutine	Topic
lgf_3d_fs	Green's function in free space.
lgf_3d_w	Green's and Neumann functions in a semi-infinite domain bounded by a plane wall.
lgf_3d_sph	Neumann function in the exterior of a sphere.
lgf_3d_2p	Doubly periodic Green's function.

Subroutine: lgf_3d_fs

This subroutine computes the Green's function in an infinite domain in the absence of boundaries.

The Green's function is given by

$$G(\mathbf{x}, \mathbf{x}_0) = \frac{1}{4\pi r}, \quad (1)$$

where $r = |\mathbf{x} - \mathbf{x}_0|$ is the distance between the field point \mathbf{x} and the singular point \mathbf{x}_0 .

The Cartesian components of the gradient of the Green's function are given by

$$\begin{aligned} \frac{\partial G}{\partial x} &= -\frac{1}{4\pi} \frac{x - x_0}{r^3}, \\ \frac{\partial G}{\partial y} &= -\frac{1}{4\pi} \frac{y - y_0}{r^3}, \\ \frac{\partial G}{\partial z} &= -\frac{1}{4\pi} \frac{z - z_0}{r^3}. \end{aligned} \quad (2)$$

Call statement:

lgf_3d_fs

(Iopt	<i>Input:</i> See Note 1.
, x, y, z	<i>Input:</i> Coordinates of the field point.
, x ₀ , y ₀ , z ₀	<i>Input:</i> Coordinates of the singular point.
, G	<i>Output:</i> Green's function.
, G _x , G _y , G _z)	<i>Output:</i> Green's function gradient, ∇G.

Note:

1. Set Iopt = 1 to obtain only G; set Iopt ≠ 1 to also obtain G_x, G_y, and G_z.

Numerical method:

The Green's function and its gradient are computed by direct evaluation of expressions (1) and (2).

Driver: *lgf_3d_fs_dr*

The driver evaluates the Green's function and verifies the integral identity (lgf_3d.3), where D is the surface of a sphere.

Files to be linked: None for the subroutine.

The driver requires the file *gauss_sph*, which contains quadrature base points and weights for integration over the surface of a sphere.

Subroutine: lgf_3d_w

This subroutine computes the Green's and Neumann functions of Laplace's equation in a semi-infinite domain bounded by a plane wall located at $x = wall$, as illustrated in Figure lgf_3d_w.1.

The Green's function is given by

$$G(\mathbf{x}, \mathbf{x}_0) = \frac{1}{4\pi r} \pm \frac{1}{4\pi R}, \quad (1)$$

where the minus sign corresponds to the Green's function of the first kind, the plus sign corresponds to the Neumann function, $r = |\mathbf{x} - \mathbf{x}_0|$, $R = |\mathbf{x} - \mathbf{x}_0^{Im}|$, and

$$\mathbf{x}_0^{Im} = (2 \times wall - x_0, y_0, z_0) \quad (2)$$

is the location of the image of the singular point with respect to the wall.

The gradient of the Green's function is given by

$$\begin{aligned} \frac{\partial G}{\partial x} &= -\frac{1}{4\pi} \frac{x - x_0}{r^3} \pm \frac{1}{4\pi} \frac{x - 2 \cdot wall + x_0}{R^3}, \\ \frac{\partial G}{\partial y} &= -\frac{1}{4\pi} \frac{y - y_0}{r^3} \pm \frac{1}{4\pi} \frac{y - y_0}{R^3}, \\ \frac{\partial G}{\partial z} &= -\frac{1}{4\pi} \frac{z - z_0}{r^3} \pm \frac{1}{4\pi} \frac{z - z_0}{R^3}. \end{aligned} \quad (3)$$

Call statement:

`lgf_3d_w`

$(Iopt$	<i>Input:</i> See Note 1.
$, Ign$	<i>Input:</i> See Note 2.
$, x, y, z$	<i>Input:</i> Coordinates of the field point.
$, x_0, y_0, z_0$	<i>Input:</i> Coordinates of the singular point.
$, wall$	<i>Input:</i> The wall is located at $x = wall$.
$, G$	<i>Output:</i> Green's function.
$, G_x, G_y, G_z)$	<i>Output:</i> Green's function gradient, ∇G .

Notes:

1. Set $Iopt = 1$ to obtain only G ; set $Iopt \neq 1$ to also obtain G_x , G_y , and G_z .
2. Set $Ign = 1$ to obtain the Green's function of the first kind; set $Ign = 2$ to obtain the Neumann function.

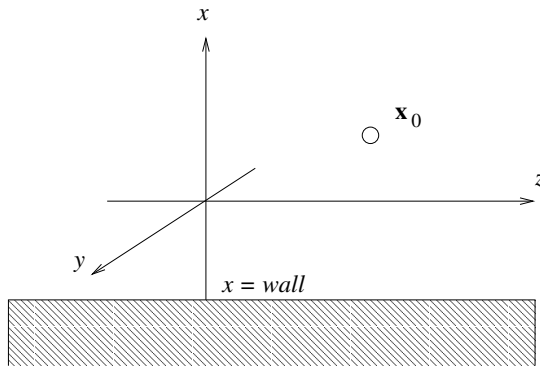


Figure lgf_3d_w.1 A semi-infinite domain bounded by a plane wall located at $x = \text{wall}$.

Numerical method:

The Green's function and its gradient are computed by direct evaluation of expressions (1) and (3).

Driver: lgf_3d_w_dr

The driver evaluates the Green's function and verifies the integral identity (lgf_3d.3), where D is the surface of a sphere.

Files to be linked:

None for the subroutine.

The driver requires the file gauss_sph, which contains quadrature base points and weights for integration over the surface of a sphere.

Streamlines:

In fluid mechanics, the Green's function represents the velocity potential due to a point sink placed above a wall. The streamline pattern corresponding to the Neumann function is shown in Figure lgf_3d_w.2.

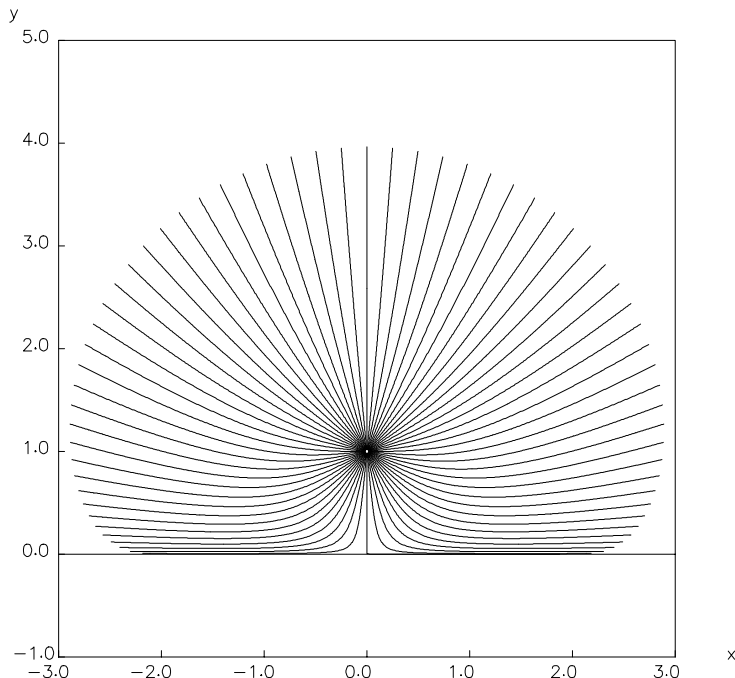


Figure lgf_3d_w.2 Streamline pattern of the flow due to a point sink placed above an impenetrable wall, expressed by the Neumann function.

Subroutine: lgf_3d_sph

This subroutine computes the Neumann function of Laplace's equation in an infinite domain bounded internally by a sphere of radius a centered at the point \mathbf{x}_c , as illustrated in Figure lgf_3d_sph.1.

The Neumann function is given by

$$G(\mathbf{x}, \mathbf{x}_0) = \frac{1}{4\pi r} + \frac{a}{|\mathbf{x}_0 - \mathbf{x}_c|} \frac{1}{4\pi R} - \frac{1}{4\pi a} \int_0^{a^2/|\mathbf{x}_0 - \mathbf{x}_c|} \frac{d\xi}{|\mathbf{x} - (\mathbf{x}_0 + \xi \mathbf{e})|}, \quad (1)$$

where $r = |\mathbf{x} - \mathbf{x}_0|$, $R = |\mathbf{x} - \mathbf{x}_0^{Im}|$, \mathbf{x}_0^{Im} is the inverse location of the point source with respect to the sphere given by

$$\mathbf{x}_0^{Im} = \mathbf{x}_c + \frac{a^2}{|\mathbf{x}_0 - \mathbf{x}_c|^2} (\mathbf{x}_0 - \mathbf{x}_c), \quad (2)$$

and $\mathbf{e} \equiv (\mathbf{x}_0 - \mathbf{x}_c)/|\mathbf{x}_0 - \mathbf{x}_c|$ is the unit vector pointing from the center of the sphere to the location of the singularity ([59], p. 335).

The gradient of the Neumann function is given by

$$\begin{aligned} \frac{\partial G}{\partial x} &= -\frac{x - x_0}{4\pi r^3} - \frac{a}{|\mathbf{x}_0 - \mathbf{x}_c|} \frac{x - x_0^{Im}}{4\pi R^3} \\ &\quad + \frac{1}{4\pi a} \int_0^{a^2/|\mathbf{x}_0 - \mathbf{x}_c|} \frac{x - x_0 + \xi e_x}{|\mathbf{x} - (\mathbf{x}_0 + \xi \mathbf{e})|^3} d\xi, \\ \frac{\partial G}{\partial y} &= -\frac{y - y_0}{4\pi r^3} - \frac{a}{|\mathbf{x}_0 - \mathbf{x}_c|} \frac{y - y_0^{Im}}{4\pi R^3} \\ &\quad + \frac{1}{4\pi a} \int_0^{a^2/|\mathbf{x}_0 - \mathbf{x}_c|} \frac{y - y_0 + \xi e_y}{|\mathbf{x} - (\mathbf{x}_0 + \xi \mathbf{e})|^3} d\xi, \end{aligned} \quad (3)$$

$$\begin{aligned} \frac{\partial G}{\partial z} &= -\frac{z - z_0}{4\pi r^3} - \frac{a}{|\mathbf{x}_0 - \mathbf{x}_c|} \frac{z - z_0^{Im}}{4\pi R^3} \\ &\quad + \frac{1}{4\pi a} \int_0^{a^2/|\mathbf{x}_0 - \mathbf{x}_c|} \frac{z - z_0 + \xi e_z}{|\mathbf{x} - (\mathbf{x}_0 + \xi \mathbf{e})|^3} d\xi. \end{aligned}$$

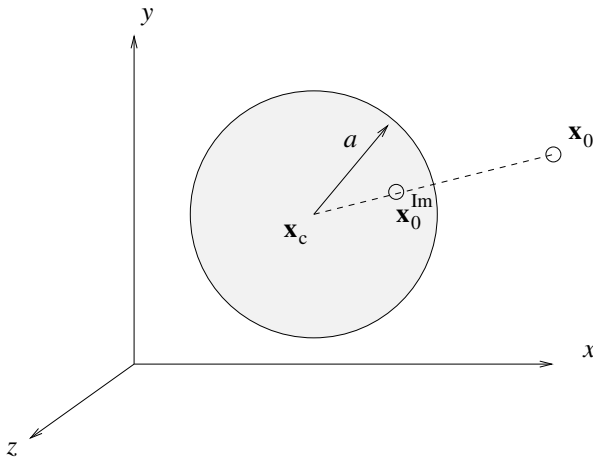


Figure lgf_3d_sph.1 A point source in the exterior of a sphere of radius a .

Call statement:

`lgf_3d_sph`

$(Iopt$	<i>Input:</i> See Note 1.
$, x, y, z$	<i>Input:</i> Coordinates of the field point.
$, x_0, y_0, z_0$	<i>Input:</i> Coordinates of the singular point.
$, x_c, y_c, z_c$	<i>Input:</i> Coordinates of the center of the sphere.
$, a$	<i>Input:</i> Radius of the sphere.
$, G$	<i>Output:</i> Neumann function.
$, G_x, G_y, G_z)$	<i>Output:</i> Neumann function gradient, ∇G .

Note:

1. Set $Iopt = 1$ to obtain only G ; set $Iopt \neq 1$ to also obtain G_x , G_y , and G_z .

Numerical method:

The Neumann function and its gradient are computed by direct evaluation of expressions (1) to (3). The integrals on the right-hand sides of (1) and (3) are computed by the trapezoidal rule [60].

Driver: `lgf_3d_sph_dr`

The driver evaluates the Neumann function and verifies the integral identity (lgf_3d.3), where D is the surface of a sphere.

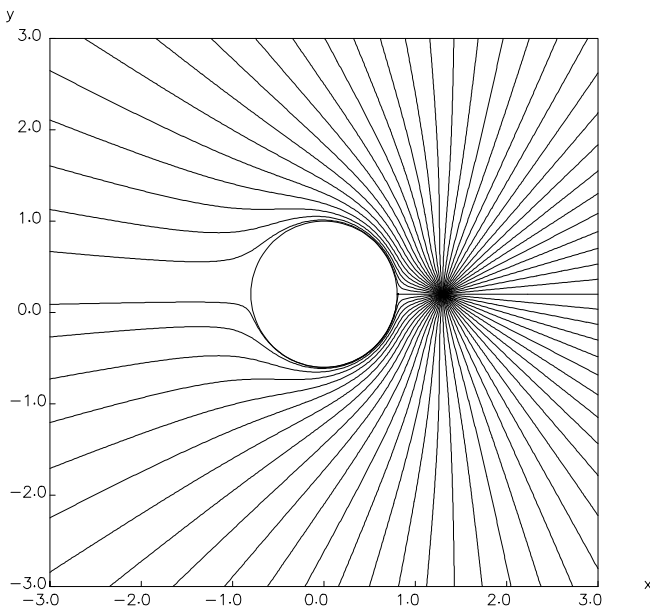


Figure lgf_3d_sph.2 Streamline pattern of the flow due to a point sink placed outside an impenetrable sphere, expressed by the Neumann function.

Files to be linked: None for the subroutine.

The driver requires the file gauss_sph, which contains quadrature base points and weights for integration over the surface of a sphere.

Streamlines:

In fluid mechanics, the Neumann function represents the velocity potential due to a point sink placed outside an impenetrable sphere. The streamline pattern is shown in Figure lgf_3d_sph.2.

Subroutine: lgf_3d_2p

This subroutine computes the doubly periodic Green's function representing the potential due to a doubly periodic array of singularities arranged in a plane that is perpendicular to the z axis, as illustrated in Figure lgf_3d_2p.1.

The singularities are located at the points $\mathbf{x}_n = \mathbf{x}_0 + \mathbf{X}_n$, where \mathbf{x}_0 is the position of an arbitrary point, \mathbf{X}_n are the vertices of a two-dimensional (planar) lattice described by

$$\mathbf{X}_n = i_1 \mathbf{a}_1 + i_2 \mathbf{a}_2, \quad (1)$$

i_1, i_2 are two integers, and $\mathbf{a}_1, \mathbf{a}_2$ are unit base vectors in the plane that is parallel to the 12 (xy) plane.

The vectorial distance of the field point \mathbf{x} from the singular point \mathbf{x}_n is defined as

$$\hat{\mathbf{x}}_n \equiv \mathbf{x} - \mathbf{x}_n. \quad (2)$$

Let \mathbf{e}_3 be the unit vector along the 3 or z axis, and $A = |\mathbf{a}_1 \times \mathbf{a}_2|$ be the area of the unit cell. As a preliminary, we introduce the reciprocal wave number base vectors

$$\mathbf{b}_1 = \frac{2\pi}{A} \mathbf{a}_2 \times \mathbf{e}_3, \quad \mathbf{b}_2 = \frac{2\pi}{A} \mathbf{e}_3 \times \mathbf{a}_2, \quad (3)$$

and define the vertices of the reciprocal wave number lattice

$$\mathbf{l}_n = j_1 \mathbf{b}_1 + j_2 \mathbf{b}_2, \quad (4)$$

where j_1 and j_2 are two integers.

The Green's function may be computed by two complementary methods depending on the location of the field point relative to the plane of the singularities.

METHOD 1: FOURIER SERIES EXPANSION

This method is useful when the field point \mathbf{x} is located sufficiently far from the plane of the singularities.

The Green's function is computed using the two-dimensional Fourier series expansion

$$G(\mathbf{x}, \mathbf{x}_0) = \frac{1}{2A} [-|\hat{\mathbf{x}}_n \cdot \mathbf{e}_z| + \sum_{\lambda, |\mathbf{l}_{\lambda}| \neq 0} \frac{\cos(\mathbf{l}_{\lambda} \cdot \hat{\mathbf{x}}_0)}{|\mathbf{l}_{\lambda}|} \exp(-|\mathbf{l}_{\lambda}| |\hat{\mathbf{x}}_0 \cdot \mathbf{e}_z|)]. \quad (5)$$

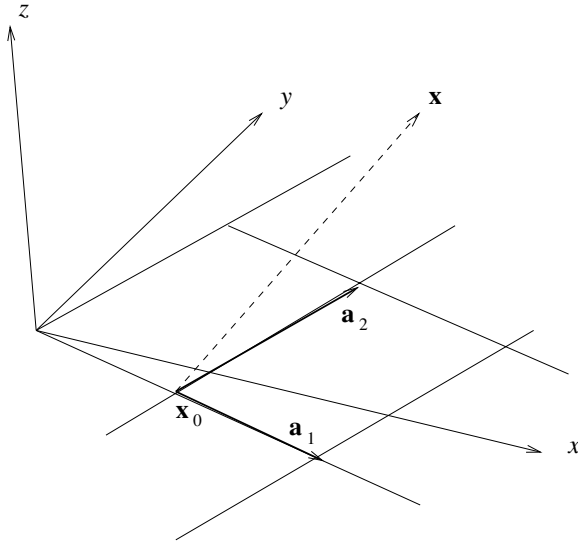


Figure lgf_3d_2p.1 A doubly periodic array of three-dimensional singularities located at the vertices of a planar lattice that is parallel to the xy plane.

Note that, when the field point \mathbf{x} is located sufficiently far from the plane of the singularities, the summed terms decay at an exponential rate.

In practical computation, the indices j_1 and j_2 defining the wave number lattice index λ are truncated to the finite range $(-\text{Max2}, \text{Max2})$.

METHOD 2: EWALD SUMMATION METHOD OF HAUTMAN AND KLEIN [27]

This method is useful when the field point \mathbf{x} is located near the plane of the singularities.

Following Hautman and Klein [27], we introduce the Ewald summation parameter ξ , and define the projection \mathbf{s} of the field point \mathbf{x} onto the plane of the singularities, and the distance of this projection from the singular point \mathbf{x}_n ,

$$\hat{\mathbf{s}}_n \equiv \mathbf{s} - \mathbf{x}_n. \quad (6)$$

The Green's function is computed in four parts, as

$$G(\mathbf{x}, \mathbf{x}_0) = \frac{1}{2A} [R(\mathbf{x}, \mathbf{x}_0) + S_0 - \frac{1}{2} |\hat{\mathbf{x}}_0 \cdot \mathbf{e}_z|^2 S_1 + \frac{3}{8} |\hat{\mathbf{x}}_0 \cdot \mathbf{e}_z|^4 S_2], \quad (7)$$

where

$$R(\mathbf{x}, \mathbf{x}_0) = \sum_n \left[\frac{1}{|\hat{\mathbf{x}}_n|} - \frac{1}{|\hat{\mathbf{s}}_n|} + \frac{1}{2} \frac{|\hat{\mathbf{x}}_0 \cdot \mathbf{e}_z|^2}{|\hat{\mathbf{s}}_n|^3} - \frac{3}{8} \frac{|\hat{\mathbf{x}}_0 \cdot \mathbf{e}_z|^4}{|\hat{\mathbf{s}}_n|^5} \right], \quad (8)$$

and the summation with respect to n runs over all singular points.

The functions S_0 , S_1 , and S_2 on the right-hand side of (7) are given by

$$\begin{aligned} S_0 &= \sum_n \frac{1 - h_0(\xi |\hat{\mathbf{s}}_n|)}{|\hat{\mathbf{s}}_n|} \\ &\quad - \frac{2\pi}{A} \frac{1}{\sqrt{\pi}\xi} + \frac{2\pi}{A} \sum_{\lambda, |\mathbf{l}_\lambda| \neq 0} \frac{\cos(\mathbf{l}_\lambda \cdot \hat{\mathbf{x}}_0)}{|\mathbf{l}_\lambda|} \operatorname{erfc}\left(\frac{|\mathbf{l}_\lambda|}{2\xi}\right), \\ S_1 &= \sum_n \frac{1 - h_1(\xi |\hat{\mathbf{s}}_n|)}{|\hat{\mathbf{s}}_n|^3} - \frac{2\pi}{A} \sum_{\lambda, |\mathbf{l}_\lambda| \neq 0} \cos(\mathbf{l}_\lambda \cdot \hat{\mathbf{x}}_0) |\mathbf{l}_\lambda| \operatorname{erfc}\left(\frac{|\mathbf{l}_\lambda|}{2\xi}\right), \\ S_2 &= \sum_n \frac{1 - h_2(\xi |\hat{\mathbf{s}}_n|)}{|\hat{\mathbf{s}}_n|^5} - \frac{2\pi}{9A} \sum_{\lambda, |\mathbf{l}_\lambda| \neq 0} \cos(\mathbf{l}_\lambda \cdot \hat{\mathbf{x}}_0) |\mathbf{l}_\lambda|^3 \operatorname{erfc}\left(\frac{|\mathbf{l}_\lambda|}{2\xi}\right), \end{aligned} \quad (9)$$

where erfc is the complementary error function computed by accurate polynomial approximations.

The splitting functions h_0 , h_1 , and h_2 on the right-hand side of equations (9) are given by

$$\begin{aligned} h_0(w) &= \operatorname{erf} w, \\ h_1(w) &= \operatorname{erf} w - \frac{2}{\sqrt{\pi}} w (1 + 2w^2) \exp(-w^2), \\ h_2(w) &= \operatorname{erf} w - \frac{2}{9\sqrt{\pi}} w (9 + 6w^2 - 4w^4 + 8w^6) \exp(-w^2), \end{aligned} \quad (10)$$

where erf is the error function computed by accurate polynomial approximations.

In practice, the indices i_1 and i_2 defined in equation (1) for summation in real space on the right-hand side of (8) and (9) are truncated to the finite range $(-\text{Max3}, \text{Max3})$ and $(-\text{Max1}, \text{Max1})$, respectively.

Similarly, the indices j_1 and j_2 defining the wave number lattice index λ on the right-hand side of (9) are truncated to the finite range $(-\text{Max2}, \text{Max2})$.

Call statement:`lgf_3d_2p`

$(Iopt$	<i>Input:</i> See Note 1.
$, Method$	<i>Input:</i> See Note 2.
$, x, y, z$	<i>Input:</i> Coordinates of the field point.
$, x_0, y_0, z_0$	<i>Input:</i> Coordinates of one singular point.
$, a_{11}, a_{12}$	<i>Input:</i> Coordinates of the first base vector.
$, a_{21}, a_{22}$	<i>Input:</i> Coordinates of the second base vector.
$, b_{11}, b_{12}$	<i>Input:</i> Coordinates of the first reciprocal base vector.
$, b_{21}, b_{22}$	<i>Input:</i> Coordinates of the second reciprocal base vector.
$, ew$	<i>Input:</i> Ewald splitting parameter ξ .
$, area$	<i>Input:</i> Area of a unit cell in the plane of the singularities.
$, Max1, Max2, Max3$	<i>Input:</i> See Note 3.
$, G$	<i>Output:</i> Green's function.
$, G_x, G_y, G_z$	<i>Output:</i> Green's function gradient, ∇G .

Notes:

1. Set $Iopt = 1$ to obtain only G ; set $Iopt \neq 1$ to also obtain G_x , G_y , and G_z .
2. Set $Method = 1$ to compute the Green's function in terms of a Fourier series; set $Method = 2$ to use the fast summation method.
3. Truncation limits for summation in real and wave number space.

Subroutine `ewald_3d_2p` must be called before subroutine `lgf_3d_2p`. Subroutine `ewald_3d_2p` computes the reciprocal wave number base vectors \mathbf{b}_1 and \mathbf{b}_2 and the area of the unit cell, and returns a recommended value for the Ewald splitting parameter ξ . The call statement is:

`ewald_3d_2p`

$(a_{11}, a_{12}$	<i>Input:</i> Coordinates of the first base vector.
$, a_{21}, a_{22}$	<i>Input:</i> Coordinates of the second base vector.
$, b_{11}, b_{12}$	<i>Input:</i> Coordinates of the first reciprocal base vector.
$, b_{21}, b_{22}$	<i>Input:</i> Coordinates of the second reciprocal base vector.
$, ew$	<i>Output:</i> Recommended Ewald splitting parameter ξ .
$, area)$	<i>Output:</i> Area of the unit cell in the plane of the singularities.

Numerical method:

The Green's function and its gradient are computed by direct evaluation of expressions (1) and (2).

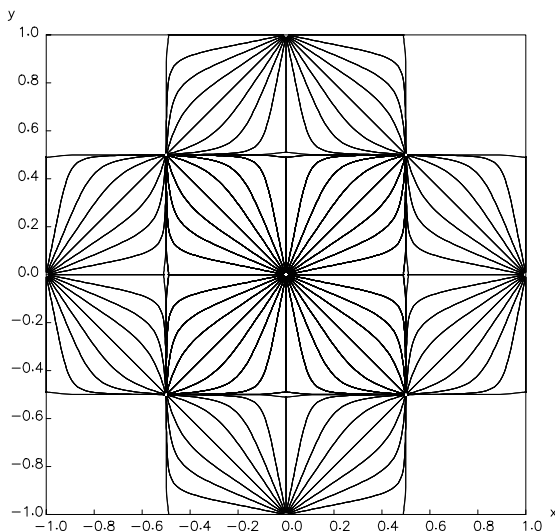


Figure lgf_3d_2p.2 Streamline pattern of the flow due to a planar square array of three-dimensional point sinks. The streamlines lie in the plane of the singularities.

Driver: `lgf_3d_2p_dr`

The driver evaluates the Green's function and verifies the integral identity (lgf_3d.3), where D is the surface of a sphere or the surface of a periodic patch.

Files to be linked: None for the subroutine.

The driver requires the file `gauss_sph`, which contains quadrature base points and weights for integration over the surface of a sphere.

Streamlines:

In fluid mechanics, the Green's function represents the velocity potential due to a doubly-periodic array of point sinks. The streamline pattern for a particular configuration is shown in Figure lgf_3d_2p.2.

Directory: `laplace/lgf_ax`

Consider the cylindrical polar coordinates (x, σ, φ) defined in Figure lgf_ax.1 with reference to the Cartesian coordinates (x, y, z) . A semi-infinite plane of constant meridional angle φ passing through the x axis is called a meridional plane.

The axisymmetric Green's functions of Laplace's equation constitute a special class of harmonic functions that are singular around a circular ring of radius σ_0 positioned at $x = x_0$. By definition, an axisymmetric Green's function satisfies the equation

$$\frac{\partial^2 G}{\partial x^2} + \frac{1}{\sigma} \frac{\partial}{\partial \sigma} \left(\sigma \frac{\partial G}{\partial \sigma} \right) + \frac{1}{\sigma_0} \delta_2(x - x_0, \sigma - \sigma_0) = 0, \quad (\text{lgf_ax.1})$$

where $G = G(x, \sigma, x_0, \sigma_0)$, and:

- (x, σ) are the axial and radial coordinates of the variable “field” or “evaluation” point.
- (x_0, σ_0) are the axial and radial coordinates of the fixed singular point representing a ring-like singularity.
- $\delta_2(x - x_0, \sigma - \sigma_0)$, is Dirac's delta function in two dimensions operating in a meridional plane of constant angle φ .

GREEN'S FUNCTIONS OF THE FIRST KIND AND NEUMANN FUNCTIONS:

In addition to satisfying the definition (lgf_ax.1), an axisymmetric Green's function $G(\mathbf{x}, \mathbf{x}_0)$ or its normal derivative $\mathbf{n}(\mathbf{x}) \cdot \nabla G(\mathbf{x}, \mathbf{x}_0)$ is required to vanish when the evaluation point \mathbf{x} lies on a specified axisymmetric surface S_G , where $\mathbf{n}(\mathbf{x})$ is the unit vector normal to S_G .

In the first case, we have a Green's function of the first kind; in the second case, we have a Neumann function - also called a Green's function of the second kind.

PHYSICAL INTERPRETATION:

The Green's function represents the temperature or concentration field due to a ring of point sources of heat or species with unit strength per arc length. In fluid mechanics, the Green's function represents the harmonic potential due to a ring of point sinks of mass.

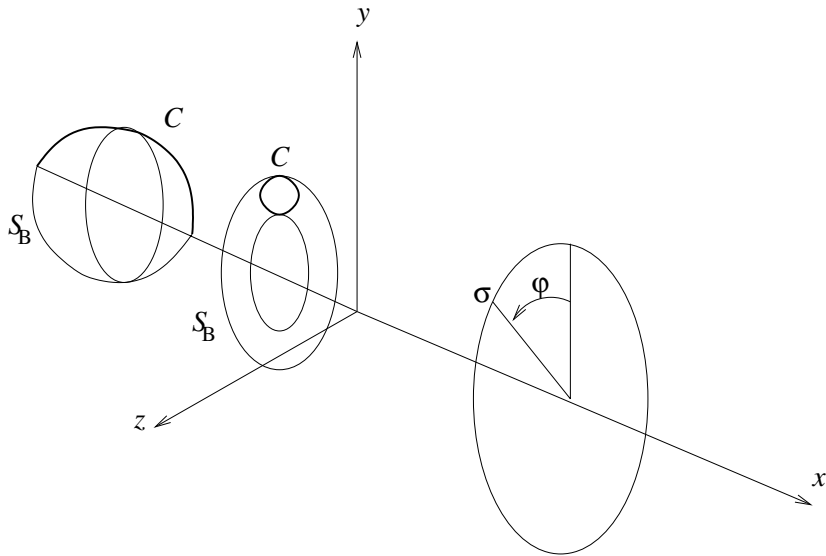


Figure lgf_ax.1 Cylindrical polar coordinates used to define the Green's functions of Laplace's equation in an axisymmetric domain.

RELATION TO THE GREEN'S FUNCTION IN THREE DIMENSIONS:

Consider the free-space axisymmetric Green's function. To demonstrate its relation to the corresponding three-dimensional Green's function presently denoted by G^{3D} , we consider the definition

$$\nabla^2 G^{3D} + \delta_3(\mathbf{x} - \mathbf{x}_0) = 0, \quad (\text{lgf_ax.2})$$

where ∇^2 is the Laplacian operator in three dimensions, and recast it into the explicit form

$$\begin{aligned} \frac{\partial^2 G^{3D}}{\partial x^2} + \frac{1}{\sigma} \frac{\partial}{\partial \sigma} \left(\sigma \frac{\partial G^{3D}}{\partial \sigma} \right) + \frac{1}{\sigma^2} \frac{\partial^2 G^{3D}}{\partial \varphi^2} \\ + \frac{1}{\sigma_0} \delta_1[\sigma_0 (\varphi - \varphi_0)] \delta_2(x - x_0, \sigma - \sigma_0) = 0. \end{aligned} \quad (\text{lgf_ax.3})$$

Integrating both sides of (lgf_ax.3) with respect to $\sigma_0 \varphi$ from 0 to $2\pi\sigma_0$ to eliminate the third term on the left-hand side, and comparing the result with (lgf_ax.1), we find

$$\begin{aligned}
G(x_0, \sigma_0, x, \sigma) &= \int_0^{2\pi} G^{3D} d\varphi = \frac{1}{4\pi} \int_0^{2\pi} \frac{d\varphi}{|\mathbf{x} - \mathbf{x}_0|} \\
&= \frac{1}{4\pi} \int_0^{2\pi} \frac{d\varphi}{\sqrt{(x - x_0)^2 + (y - y_0)^2 + (z - z_0)^2}} \\
&= \frac{1}{4\pi} \int_0^{2\pi} \frac{d\varphi}{[(x - x_0)^2 + (\sigma \cos \phi - \sigma_0 \cos \phi_0)^2 + (\sigma \sin \phi - \sigma_0 \sin \phi_0)^2]^{1/2}} \\
&= \frac{1}{4\pi} \int_0^{2\pi} \frac{d(\varphi - \varphi_0)}{[(x - x_0)^2 + \sigma^2 + \sigma_0^2 - 2\sigma\sigma_0 \cos(\varphi - \varphi_0)]^{1/2}} \\
&= \frac{1}{4\pi} \int_0^{2\pi} \frac{du}{[(x - x_0)^2 + \sigma^2 + \sigma_0^2 - 2\sigma\sigma_0 \cos u]^{1/2}} \\
&= \frac{1}{4\pi} \int_0^{2\pi} \frac{du}{[(x - x_0)^2 + (\sigma + \sigma_0)^2 - 4\sigma\sigma_0 \cos^2 \frac{u}{2}]^{1/2}} \\
&= \frac{1}{\pi \sqrt{(x - x_0)^2 + (\sigma + \sigma_0)^2}} \int_0^{2\pi} \frac{du}{\sqrt{1 - k^2 \cos^2 \frac{u}{2}}} \\
&= \frac{F(k)}{\pi \sqrt{(x - x_0)^2 + (\sigma + \sigma_0)^2}}, \tag{lgf_ax.4}
\end{aligned}$$

where $u = \varphi - \varphi_0$, and

$$k^2 \equiv \frac{4\sigma\sigma_0}{(x - x_0)^2 + (\sigma + \sigma_0)^2}. \tag{lgf_ax.5}$$

We have introduced the complete elliptic integral of the first kind

$$F(k) \equiv \int_0^{\pi/2} \frac{d\eta}{\sqrt{1 - k^2 \cos^2 \eta}}, \tag{lgf_ax.6}$$

where η is a dummy variable of integration.

The last expression in (lgf_ax.4) reveals the symmetry property

$$G(x_0, \sigma_0, x, \sigma) = G(x, \sigma, x_0, \sigma_0). \tag{lgf_ax.7}$$

Similar relations can be written for Green's functions in domains bounded by axisymmetric surfaces.

BOUNDARY-INTEGRAL REPRESENTATION:

The boundary-integral representation of a harmonic function f takes the form

$$\begin{aligned} f(x_0, \sigma_0) = & - \int_C G(x, \sigma, x_0, \sigma_0) [\mathbf{n}(\mathbf{x}) \cdot \nabla f(\mathbf{x})] \sigma(\mathbf{x}) dl(\mathbf{x}) \\ & + \int_C f(\mathbf{x}) [\mathbf{n}(\mathbf{x}) \cdot \nabla G(x, \sigma, x_0, \sigma_0)] \sigma(\mathbf{x}) dl(\mathbf{x}), \end{aligned} \quad (\text{lgf_ax.8})$$

where C stands for the collection of the contours of all boundaries of a selected solution domain in a meridional plane, and \mathbf{n} is the unit vector normal to C pointing inward.

INTEGRAL IDENTITY:

Applying (lgf_2d.8) for a constant function f , we find that the Green's function satisfies the integral identity

$$\int_C [\mathbf{n}(\mathbf{x}) \cdot \nabla G(x, \sigma, x_0, \sigma_0)] \sigma(\mathbf{x}) dl(\mathbf{x}) = \begin{cases} 1 & \text{when } \mathbf{x}_0 \text{ is inside } A_c \\ \frac{1}{2} & \text{when } \mathbf{x}_0 \text{ is on } C \\ 0 & \text{when } \mathbf{x}_0 \text{ is outside } A_c \end{cases}, \quad (\text{lgf_ax.9})$$

where C is a closed loop in a meridional plane or an open planar line beginning and ending at the x axis, both enclosing a control area A_c . In both cases, the normal vector \mathbf{n} is directed *into* the control area A_c . When the point \mathbf{x}_0 is located on the contour C , the integral on the left-hand side of (sgf_ax.9) is a principal-value integral.

DIRECTORY CONTENTS:

This directory contains the following subroutines that evaluate axisymmetric Green's functions and their gradients:

Subroutine	Topic
<code>lgf_ax_fs</code>	Green's function in free space.
<code>lgf_ax_w</code>	Green's and Neumann functions in a semi-infinite domain bounded by a plane wall.

Subroutine: lgf_ax_fs

This subroutine computes the axisymmetric Green's function in an infinite domain in the absence of boundaries.

Using the last expression of (lgf_ax.4), we find that the Green's function is given by

$$G(x, \sigma, x_0, \sigma_0) = \frac{F(k)}{\pi \sqrt{(x - x_0)^2 + (\sigma + \sigma_0)^2}}. \quad (1)$$

Differentiating the expression given in the fifth line of (lgf_ax.4), we find that the Green's function gradient is given by

$$\begin{aligned} G_x(x, \sigma, x_0, \sigma_0) &\equiv \frac{\partial G}{\partial x} = -\frac{x - x_0}{4\pi} I_{30}, \\ G_\sigma(x, \sigma, x_0, \sigma_0) &\equiv \frac{\partial G}{\partial \sigma} = -\frac{1}{4\pi} (\sigma I_{30} - \sigma_0 I_{31}), \end{aligned} \quad (2)$$

where we have defined the integrals

$$\begin{aligned} I_{30} &\equiv \int_0^{2\pi} \frac{du}{[(x - x_0)^2 + \sigma^2 + \sigma_0^2 - 2\sigma\sigma_0 \cos u]^{3/2}}, \\ I_{31} &\equiv \int_0^{2\pi} \frac{\cos u \, du}{[(x - x_0)^2 + \sigma^2 + \sigma_0^2 - 2\sigma\sigma_0 \cos u]^{3/2}}. \end{aligned} \quad (3)$$

Straightforward algebraic manipulation yields the alternative forms

$$\begin{aligned} I_{30} &= \frac{4}{[(x - x_0)^2 + (\sigma + \sigma_0)^2]^{3/2}} \frac{E(k)}{1 - k^2}, \\ I_{31} &= \frac{4}{[(x - x_0)^2 + (\sigma + \sigma_0)^2]^{3/2}} \frac{1}{k^2} [-2 F(k) + \frac{2 - k^2}{1 - k^2} E(k)], \end{aligned} \quad (4)$$

where $F(k)$ is the complete elliptic integral of the first kind defined in (lgf_ax.6), and

$$E(k) \equiv \int_0^{\pi/2} \sqrt{1 - k^2 \cos^2 \eta} \, d\eta \quad (5)$$

is the complete elliptic integral of the second kind; η is a dummy variable of integration.

Call statement:

```
lgf_ax_fs
  ( $I_{opt}$       Input: See Note 1.
   , $x, \sigma$     Input: Coordinates of the field point.
   , $x_0, \sigma_0$  Input: Coordinates of the singular point.
   , $G$           Output: Green's function.
   , $G_x, G_\sigma$ ) Output: Green's function gradient.
```

Note:

1. Set $I_{opt} = 1$ to obtain only G ; set $I_{opt} \neq 1$ to obtain G , G_x , and G_σ .

Numerical method:

The Green's function and its gradient are computed by direct evaluation using expressions (1) to (6). The complete elliptical integrals are computed using an iterative method implemented in subroutine `ell_int`.

Driver: `lgf_ax_fs_dr`

The driver evaluates the Green's function and verifies the integral identity (lgf_2d.9), where C is a circular contour.

Files to be linked:

`ell_int`: Evaluation of complete elliptic integrals of the first and second kind.

Streamlines:

In fluid mechanics, the axisymmetric Green's function represents the velocity potential due to a ring of point sinks. The streamline pattern is shown in Figure `lgf_ax_fs.1`.

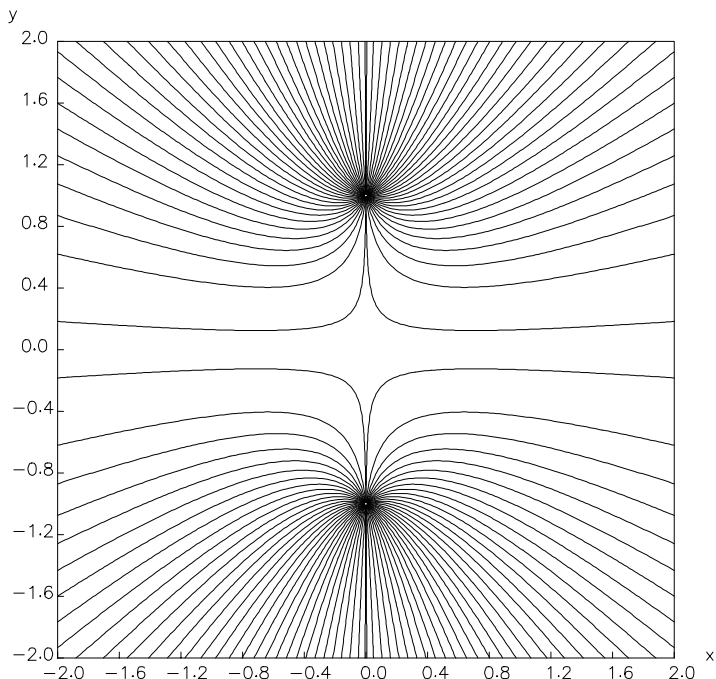


Figure lgf_ax.fs.1 Streamline pattern of the flow due to a ring of point sinks.

Subroutine: lgf_ax_w

This subroutine computes the axisymmetric Green's and Neumann functions in a semi-infinite domain bounded by a plane wall located at $x = \text{wall}$.

The Green's functions are computed as the sum of the free-space Green's function and its image with respect to the wall, located at $x = 2 \text{wall} - x_0$.

Call statement:

```
lgf_ax_w
  (Iopt      Input: See Note 1.
   ,Ign      Input: See Note 2.
   ,x,σ      Input: Coordinates of the field point.
   ,x₀,σ₀    Input: Coordinates of the singular point.
   ,wall     Input: The wall is located at  $x = \text{wall}$ .
   ,G        Output: Green's function.
   ,G_x, G_σ) Output: Green's function gradient.
```

Notes:

1. Set $Iopt = 1$ to obtain only G ; set $Iopt \neq 1$ to obtain G , G_x , and G_σ .
2. Set $Ign = 1$ to obtain the Green's function of the first kind; set $Ign = 2$ to obtain the Neumann function.

Numerical method:

The Green's function and its gradient are computed by direct evaluation using the analytical expressions for the free-space Green's function. The complete elliptical integrals are computed using an iterative method implemented in subroutine ell_int.

Driver: lgf_ax_fs_dr

The driver evaluates the Green's function and verifies the integral identity (lgf_ax.9), where C is a circular contour.

Files to be linked:

ell_int: Evaluation of complete elliptic integrals of the first and second kind.

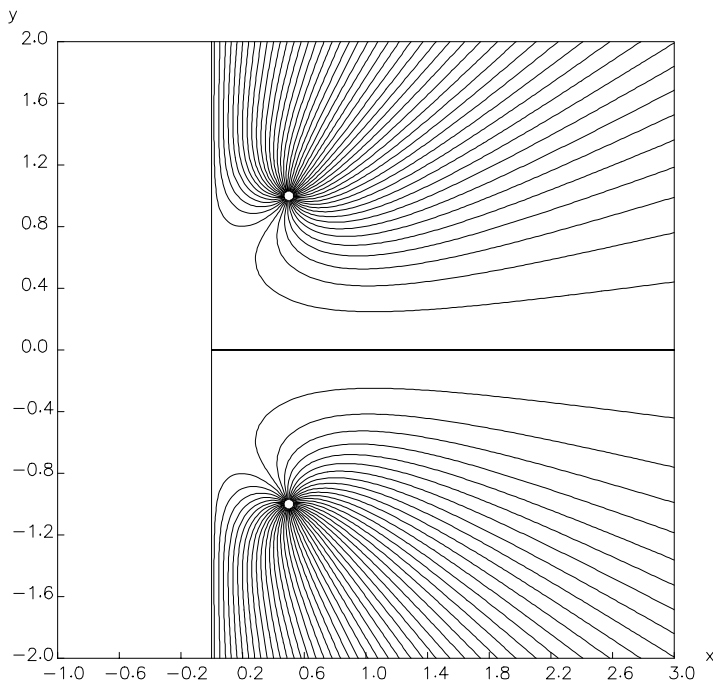


Figure lgf_ax.w.1 Streamline pattern of the flow due to a ring of point sinks in front of an impenetrable wall, expressed by the Neumann function.

Streamlines:

In fluid mechanics, the axisymmetric Green's function represents the velocity potential due to a ring of point sinks. The streamline pattern associated with the Neumann function is shown in Figure lgf_ax.w.1.

Directory: `laplace/flow_1d`

This directory contains a code that computes steady unidirectional, pressure- or gravity-driven viscous flow through a tube with arbitrary cross-section, as illustrated in Figure `flow_1d.1`.

Circular, elliptical, rectangular, and triangular tube shapes are implemented in the code. Other shapes may be included by straightforward additions and modifications.

MATHEMATICAL FORMULATION:

The equation of fluid motion for steady unidirectional viscous flow requires that the streamwise component of the velocity along the z axis, denoted by u_z , satisfies the Poisson equation [59]

$$\nabla^2 u_z = -\frac{G}{\mu} \quad (1)$$

with a constant right-hand side, where $\nabla^2 \equiv \partial^2/\partial x^2 + \partial^2/\partial y^2$ is the Laplacian operator over the tube cross-section, μ is the fluid viscosity,

$$G \equiv -\frac{dp}{dz} + \rho g_z \quad (2)$$

is the negative of the modified axial pressure gradient incorporating the effect of gravity, ρ is the fluid density, and g_z is the component of the acceleration of gravity vector along the z axis. The no-slip boundary condition requires that u_z vanish around the tube contour C in the xy plane.

To compute the solution, we decompose u_z into a particular component f^P that satisfies Poisson's equation

$$\nabla^2 f^P = -\frac{G}{\mu}, \quad (3)$$

and a homogeneous component f that satisfies Laplace's equation

$$\nabla^2 f = 0, \quad (4)$$

so that

$$u_z = f^P + f. \quad (5)$$

The non-slip boundary condition requires that $f = -f^P$ around the tube contour C .

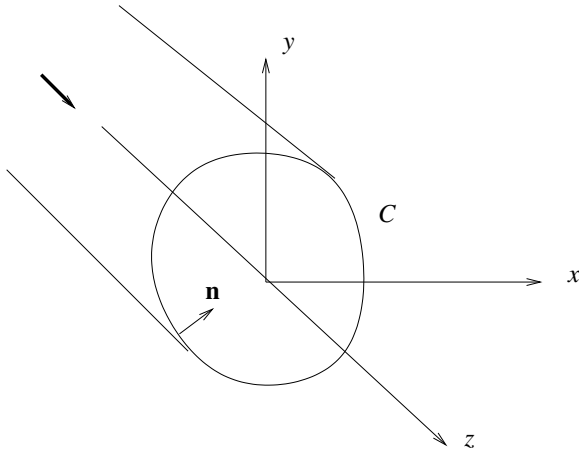


Figure flow_1d.1 Steady unidirectional flow through a tube with arbitrary cross-section computed by a boundary-element method.

It is convenient to set

$$f^P(x, y) = -\frac{G}{\mu} v(x, y), \quad (6)$$

where the function $v(x, y)$ satisfies Poisson's equation $\nabla^2 v = 1$. The no-slip boundary condition requires that $f = -f^P = Gv/\mu$ around the tube contour C .

Moreover, it is convenient to express v in the quadratic form

$$v(x, y) = \frac{1}{2} [\alpha (x - x_R)^2 + (1 - \alpha) (y - y_R)^2], \quad (7)$$

where α is an arbitrary constant parameter, and (x_R, y_R) are the coordinates of an arbitrary reference point in the xy plane. Straightforward differentiation confirms that the function q satisfies Poisson's equation $\nabla^2 v = 1$, for any value of α , as required.

Using the boundary-integral formulation, we find that the homogeneous component f at a point \mathbf{x}_0 inside the tube is given by the integral representation

$$\begin{aligned} f(\mathbf{x}_0) = & - \int_C G(\mathbf{x}, \mathbf{x}_0) \frac{\partial f(\mathbf{x})}{\partial n} dl(\mathbf{x}) \\ & + \int_C f(\mathbf{x}) [\mathbf{n}(\mathbf{x}) \cdot \nabla G(\mathbf{x}, \mathbf{x}_0)] dl(\mathbf{x}), \end{aligned} \quad (8)$$

where $\partial f / \partial n = \mathbf{n} \cdot \nabla f$ is the normal derivative of f , \mathbf{n} is the unit normal vector pointing into the tube, and $G(\mathbf{x}, \mathbf{x}_0) = -\frac{1}{2\pi} \ln |\mathbf{x} - \mathbf{x}_0|$ is the free-space Green's function of Laplace's equation in two dimensions.

Substituting the boundary condition $f = -f^P = Gv/\mu$ around C in the double-layer potential, we obtain the more explicit representation

$$\begin{aligned} f(\mathbf{x}_0) &= - \int_C G(\mathbf{x}, \mathbf{x}_0) \frac{\partial f(\mathbf{x})}{\partial n} dl(\mathbf{x}) \\ &\quad + \frac{G}{\mu} \int_C v(\mathbf{x}) [\mathbf{n}(\mathbf{x}) \cdot \nabla G(\mathbf{x}, \mathbf{x}_0)] dl(\mathbf{x}). \end{aligned} \quad (9)$$

Next, we take the limit as the point \mathbf{x}_0 approaches the tube contour C , express the limit of the double-layer potential on the right-hand side in terms of its principal value, and rearrange to derive an integral equation of the first kind for the normal derivative $\partial f / \partial n$,

$$\begin{aligned} &\int_C G(\mathbf{x}, \mathbf{x}_0) \frac{\partial f(\mathbf{x})}{\partial n} dl(\mathbf{x}) \\ &= -\frac{G}{2\mu} v(\mathbf{x}_0) + \frac{G}{\mu} \int_C^{PV} v(\mathbf{x}) [\mathbf{n}(\mathbf{x}) \cdot \nabla G(\mathbf{x}, \mathbf{x}_0)] dl(\mathbf{x}), \end{aligned} \quad (10)$$

where the point \mathbf{x}_0 lies on C , and PV denotes the principal value.

UNIQUENESS OF SOLUTION:

The solution of the integral equation (10) is unique only when the transfinite diameter of the tube contour C , denoted by ρ_C , is different from unity (in the case of a circle, ρ_C is equal to the circle radius) [70]. If ρ_C is equal to unity, then any solution can be shifted by an arbitrary constant. This superficial difficulty can be avoided by rescaling the contour at the outset, so that ρ_C becomes different from unity.

Another way of removing the non-uniqueness of solution is to impose the integral constraint

$$\int_C \frac{\partial f(\mathbf{x})}{\partial n} dl(\mathbf{x}) = 0. \quad (11)$$

If $\rho_C \neq 1$, this constraint is automatically satisfied.

COMPUTATION OF THE FLOW RATE:

Green's second identity in the plane states that any two non-singular functions $f(x, y)$ and $v(x, y)$ satisfy the relation

$$\iint_{A_c} (f \nabla^2 v - v \nabla^2 f) dA = \oint_C \mathbf{n} \cdot (v \nabla f - f \nabla v) dl, \quad (12)$$

where C is the boundary of a region A_c in the xy plane, and \mathbf{n} is the unit vector normal to C pointing inward. Assuming that the function f satisfies Laplace's equation $\nabla^2 f = 0$ and the function v satisfies Poisson's equation $\nabla^2 v = 1$, we derive an expression for the areal integral of f ,

$$\int \int_{A_c} f \, dA = \oint_C \mathbf{n} \cdot [v \nabla f - f \nabla v] \, dl. \quad (13)$$

Using the boundary condition $f = -f^P = Gv/\mu$ around C , we obtain

$$\int \int_{A_c} f \, dA = \oint_C \mathbf{n} \cdot [v \nabla(f - \frac{G}{\mu} v)] \, dl = \oint_{A_c} \mathbf{n} \cdot [v \nabla u_z] \, dl. \quad (14)$$

Next, we express the particular solution f^P as the divergence of the vector function \mathbf{h} , writing $f^P = -(G/\mu) \nabla \cdot \mathbf{h}$. For the particular choices (6) and (7), the scalar components of \mathbf{h} are given by $h_x = \alpha x^3/(6\mu)$ and $h_y = (1 - \alpha) y^3/(6\mu)$. Using the divergence theorem, we write

$$\int \int_{A_c} f^P \, dA = \frac{G}{\mu} \oint_C \mathbf{n} \cdot \mathbf{h} \, dl. \quad (15)$$

Finally, we use the decomposition (5), take into consideration (14) and (15), identify A_c with the tube cross-section, and thus derive an expression for the axial flow rate in the boundary-integral form

$$\begin{aligned} Q \equiv \int \int_{A_c} u_z \, dA &= \int \int_{A_c} (f + f^P) \, dA \\ &= \oint_C \mathbf{n} \cdot (v \nabla u_z + \frac{G}{\mu} \mathbf{h}) \, dl. \end{aligned} \quad (16)$$

Once the normal derivative of u_z around the tube is known, the integral on the right-hand side of (16) may be computed by elementary numerical methods.

NUMERICAL METHOD:

The tube contour C is discretized into a collection of N boundary elements E_i defined by $N + 1$ marker points, where $i = 1, \dots, N$. The boundary elements may be straight segments or circular arcs. Approximating the homogeneous solution and its normal derivative with constant functions over each element, we obtain a discretized version of the integral equation (10),

$$\begin{aligned} \sum_{i=1}^N \left(\frac{\partial f}{\partial n} \right)_i \int_{E_i} G(\mathbf{x}, \mathbf{x}_0) \, dl(\mathbf{x}) \\ = -\frac{G}{2\mu} v(\mathbf{x}_0) + \frac{G}{\mu} \sum_{i=1}^N v_i \int_{E_i}^{PV} \mathbf{n}(\mathbf{x}) \cdot \nabla G(\mathbf{x}, \mathbf{x}_0) \, dl(\mathbf{x}), \end{aligned} \quad (17)$$

where the subscript i denotes that the corresponding variable is evaluated at the i th boundary element.

Next, we identify the point \mathbf{x}_0 with the mid-point of each element, denoted by \mathbf{x}_j^M , where j is the element label, set $v(\mathbf{x}_j^M) = v_j$, and obtain a system of linear equations for the unknown values $(\partial f / \partial n)_i$,

$$\begin{aligned} \sum_{i=1}^N \left(\frac{\partial f}{\partial n} \right)_i & \int_{E_i} G(\mathbf{x}, \mathbf{x}_j^M) dl(\mathbf{x}) \\ &= -\frac{G}{2\mu} v_j + \frac{G}{\mu} \sum_{i=1}^N v_i \int_{E_i}^{PV} \mathbf{n}(\mathbf{x}) \cdot \nabla G(\mathbf{x}, \mathbf{x}_j^M) dl(\mathbf{x}), \end{aligned} \quad (18)$$

for $j = 1, \dots, N$. The linear system (18) is solved by Gauss elimination.

COMPUTATION OF THE SHEAR STRESS:

Using the decomposition (5) and the definition (6), we find that the shear stress over the i th boundary element is given by

$$\sigma_{sh} = \mu \left(\frac{\partial f}{\partial n} \right)_i - G (\mathbf{n} \cdot \nabla v)_i. \quad (19)$$

Integrating the shear stress along the tube perimeter, we obtain the drag force. A global force balance requires that the drag force be equal to the negative of the pressure gradient G multiplied by the tube cross-sectional area. This property may be used to confirm the accuracy of the solution.

COMPUTATION OF THE VELOCITY AT A POINT IN THE FLOW:

The homogeneous component of the velocity at a point \mathbf{x}_0 inside the tube is computed using the discretized boundary-integral representation

$$\begin{aligned} f(\mathbf{x}_0) &= - \sum_{i=1}^N \left(\frac{\partial f}{\partial n} \right)_i \int_{E_i} G(\mathbf{x}, \mathbf{x}_0) dl(\mathbf{x}) \\ &\quad + \frac{G}{\mu} \sum_{i=1}^N v_i \int_{E_i} \mathbf{n}(\mathbf{x}) \cdot \nabla G(\mathbf{x}, \mathbf{x}_0) dl(\mathbf{x}). \end{aligned} \quad (20)$$

The total velocity is computed from the decomposition (5) and the definition (6).

Main program: flow_1d

The main program solves the integral equation (10) for the distribution of the normal derivative of the homogeneous component of the velocity, computes the flow rate along the tube, and evaluates the velocity at a specified point in the flow.

Files to be linked:

1. **elm_arc**
Discretization of a circular segment into arc elements.
2. **elm_line**
Discretization of a straight segment into straight (linear) elements.
3. **flow_1d_geo**
Discretization of the boundary geometry.
4. **flow_1d_sdlp**
Evaluation of the single- and double-layer harmonic potential over the boundary elements.
5. **flow_1d_vel**
Evaluation of the velocity at a specified point in the flow.
6. **gauss_leg**
Base points and weights for the Gauss-Legendre quadrature.
7. **gel**
Solution of a linear algebraic system by Gauss elimination.
8. **lgf_2d_fs**
Free-space Green's function of Laplace's equation.

Input files:

1. **circle.dat**
Parameters for flow through a circular tube.
2. **contour.dat**
Specified nodes of the tube contour.
3. **ellipse.dat**
Parameters for flow through an elliptical tube.
4. **rectangle.dat**
Parameters for flow through a rectangular tube.
5. **triangle.dat**
Parameters for flow through a triangular tube.

Output files:

1. `flow_1d.elm`
Boundary element distribution.
2. `flow_1d.trc`
Distribution of boundary shear stress.
3. `flow_1d.vel`
Recording of the velocity at a point in the flow.

Directory: `laplace/flow_1d_1p`

This directory contains a code that computes unidirectional shear flow over a periodic array of cylinders or a periodic wall, as illustrated in Figure `flow_1d_1p.1`. Far above the cylinders or the periodic wall, the velocity profile tends to become linear with respect to y . Far below the cylinders, the velocity tends to a constant value parallel to the array, called the “drift velocity.”

MATHEMATICAL FORMULATION:

The equation of fluid motion requires that the axial component of the velocity in the direction of the z axis, denoted by u_z , satisfy Laplace’s equation

$$\nabla^2 u_z = 0, \quad (1)$$

which is to be solved subject to:

1. The boundary condition $u_z = 0$ over the surface of the cylinders or periodic wall.
2. The far-field condition $u_z \simeq \gamma y$ as $y \rightarrow \infty$, where γ is a specified constant shear rate.

Using the boundary-integral formulation, we find that the z component of the velocity at a point $\mathbf{x}_0 = (x_0, y_0)$ that lies in the domain of flow may be expressed in the integral form [61]

$$u_z(\mathbf{x}_0) = -\frac{1}{\mu} \int_C G(\mathbf{x}, \mathbf{x}_0) q(\mathbf{x}) dl(\mathbf{x}) + G y_0 + U_{Slip}, \quad (2)$$

where:

- U_{Slip} is an *a priori* unknown slip velocity.
- C is the contour of one cylinder or one period of the wall.
- $q = \mu \mathbf{n} \cdot \nabla u_z$ is the wall shear stress.
- \mathbf{n} is the unit normal vector pointing into the flow.
- $G(\mathbf{x}, \mathbf{x}_0)$ is the singly periodic upward-biased Green’s function of Laplace’s equation given by

$$G(\mathbf{x}, \mathbf{x}_0) = -\frac{1}{4\pi} \ln[2\{\cosh[k(y - y_0)] - \cos[k(x - x_0)]\}] - \frac{y - y_0}{2L}. \quad (3)$$

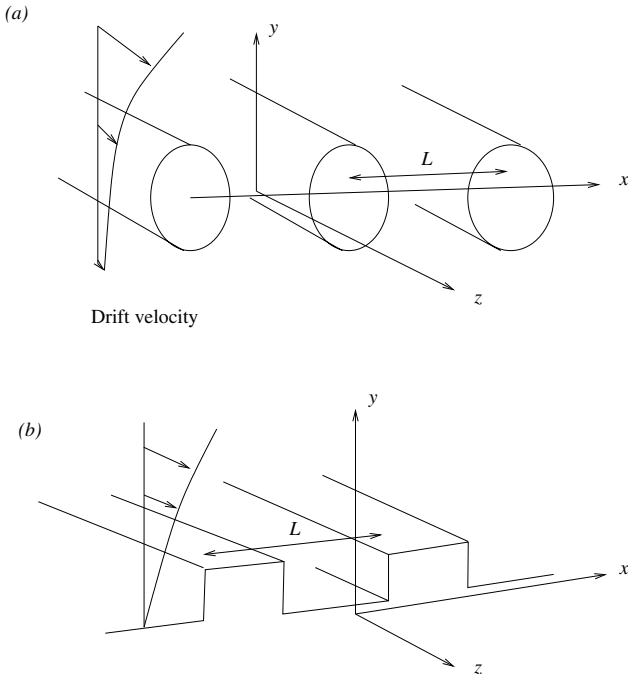


Figure flow_1d_1p.1 Unidirectional shear flow (a) over a periodic array of cylinders, and (b) past a periodic wall.

- $k = 2\pi/L$ is the wave number, and L is the period of the flow identified with the separation between the singular points.

A global force balance requires

$$\int_C q \, dl = \mu \gamma L. \quad (4)$$

Applying the integral representation (2) at a point \mathbf{x}_0 located at the surface of a cylinder or periodic wall and requiring the no-slip boundary condition, we obtain an integral equation of the first kind for the boundary shear stress,

$$\int_C G(\mathbf{x}, \mathbf{x}_0) f(\mathbf{x}_0) \, dl(\mathbf{x}) - \mu U_{Slip} = \mu \gamma y_0, \quad (5)$$

supplemented by the integral constraint (4).

Using the properties of the Green's function, we find that, far below the cylinders,

the velocity tends to the *a priori* unknown drift velocity U_{Drift} given by

$$U_{Drift} = U_{Slip} + \frac{1}{\mu L} \int_C f y \, dl. \quad (6)$$

The integral on the right-hand side of (6) is evaluated after the solution of the integral equation (5) has been found.

Numerical method:

The surface of a cylinder or one period of the wall is discretized into a collection of boundary elements, and the wall shear stress f is approximated with a constant function over each element. Applying the integral equation (5) at the mid-point of each element, we obtain a system of linear equations for the element values of the shear stress. The linear system is solved by the method of Gauss elimination.

Once the solution has been found, the velocity at a point in the flow is computed using the discrete form of the boundary-integral representation (2).

Main program: flow_1d_1p

The main program solves an integral equation of the first kind for the distribution of the boundary shear stress and computes the slip and drift velocities.

Files to be linked:

1. `elm.arc`
Discretization of a circular segment into arc elements.
2. `elm.line`
Discretization of a straight segment into straight (linear) elements.
3. `flow_1d_1p.geo`
Discretization of the boundary geometry.
4. `flow_1d_1p_slp`
Evaluation of the single-layer potential over the boundary elements.
5. `flow_1d_1p_vel`
Evaluation of the velocity at a specified point in the flow.
6. `gauss_leg`
Base points and weights for the Gauss-Legendre quadrature.
7. `gel`
Solution of a linear algebraic system by Gauss elimination.

8. `lgf_2d_1p`
Singly periodic Green's function of Laplace's equation.

Input files:

1. `circle.dat`
Parameters for flow over an array of circular cylinders.
2. `ellipse.dat`
Parameters for flow over an array of elliptical cylinders.
3. `prt_rec.dat`
Parameters for flow over a periodic wall with rectangular protrusions.
4. `rec.dat`
Parameters for flow over an array of rectangular cylinders.
5. `triangle.dat`
Parameters for flow over an array of triangular cylinders.

Output files:

1. `flow_1d_1p(elm`
Boundary element distribution.
2. `flow_1d_1p(trc`
Distribution of boundary shear stress.
3. `flow_1d_1p.vel`
Recording of the velocity at a point in the flow.

Directory: `laplace/flow_2d`

This directory contains a code that computes potential flow in a two-dimensional domain with arbitrary geometry. Several types of flows and domain geometries implemented in the code are illustrated in Figure `flow_2d.1`. Other configurations can be included by straightforward additions and modifications.

Figure `flow_2d.1(a)` shows the streamline pattern of streaming (uniform) flow past a circular cavity on a plane wall in the presence of a parallel upper wall. Figure `flow_2d.1(b)` shows the streamline pattern of streaming flow past a rectangular cavity in a semi-infinite domain. Figure `flow_2d.1(c)` shows the streamline pattern of streaming flow over a circular protrusion.

MATHEMATICAL FORMULATION:

The velocity \mathbf{u} is decomposed into a far-field component prevailing far from the wall denoted by \mathbf{u}^∞ , expressing uniform (streaming) flow along the x axis, and a disturbance component denoted by \mathbf{u}^D , so that

$$\mathbf{u} = \mathbf{u}^\infty + \mathbf{u}^D. \quad (1)$$

The disturbance velocity is described in terms of the gradient of a single-valued disturbance harmonic potential ϕ^D , so that $\mathbf{u}^D = \nabla\phi^D$. The decomposition (1) then becomes

$$\mathbf{u} = \mathbf{u}^\infty + \nabla\phi^D. \quad (2)$$

Requiring the no-penetration boundary condition $\mathbf{u} \cdot \mathbf{n} = 0$ over the boundaries of the flow, where \mathbf{n} is the unit normal vector, we derive a boundary condition for the normal derivative of the disturbance potential,

$$\mathbf{n} \cdot \nabla\phi^D \equiv \frac{\partial\phi^D}{\partial n} = -\mathbf{u}^\infty \cdot \mathbf{n}. \quad (3)$$

Using the standard boundary-integral representation, we find that the disturbance potential satisfies the integral equation of the second kind

$$\begin{aligned} \phi^D(\mathbf{x}_0) = & -2 \int_C G(\mathbf{x}, \mathbf{x}_0) [\mathbf{n}(\mathbf{x}) \cdot \nabla\phi^D(\mathbf{x})] dl(\mathbf{x}) \\ & + 2 \int_C^{PV} \phi^D(\mathbf{x}) [\mathbf{n}(\mathbf{x}) \cdot \nabla G(\mathbf{x}, \mathbf{x}_0)] dl(\mathbf{x}), \end{aligned} \quad (4)$$

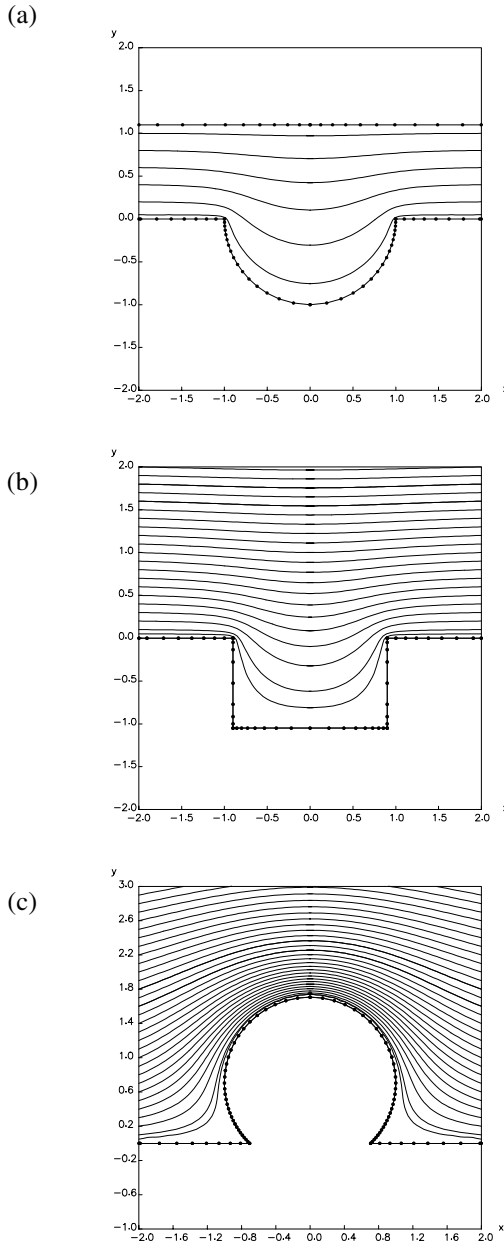


Figure flow_2d.1 Streamline patterns of potential streaming flow over a circular or rectangular cavity and past a circular protrusion. The dark circles are the end-points of the boundary elements.

where the contour C includes all boundaries of the flow, the point \mathbf{x}_0 lies on C , \mathbf{n} is the unit vector normal to C pointing into the flow, and $G(\mathbf{x}, \mathbf{x}_0)$ is the free-space Green's function. Implementing the boundary condition (3) and rearranging (4), we obtain

$$\begin{aligned} \phi^D(\mathbf{x}_0) - 2 \int_C^{PV} \phi^D(\mathbf{x}) [\mathbf{n}(\mathbf{x}) \cdot \nabla G(\mathbf{x}, \mathbf{x}_0)] dl(\mathbf{x}) \\ = 2 \mathbf{u}^\infty \cdot \int_C G(\mathbf{x}, \mathbf{x}_0) \mathbf{n}(\mathbf{x}) dl(\mathbf{x}). \end{aligned} \quad (5)$$

NUMERICAL METHOD:

The boundaries of the flow are discretized into a collection of N boundary elements denoted by E_i , $i = 1, \dots, N$. The boundary elements can be straight segments or circular arcs. The disturbance potential and its normal derivative are approximated with constant functions over the i th element denoted respectively by ϕ_i^D and $(\frac{\partial \phi^D}{\partial n})_i = -\mathbf{u}^\infty \cdot \mathbf{n}^{(i)}$, where $\mathbf{n}^{(i)}$ is the normal vector evaluated at the element mid-point. Note that the normal vector is constant over straight element.

Subject to these approximations, the integral equation (5) assumes the discretized form

$$\begin{aligned} \phi^D(\mathbf{x}_0) - 2 \sum_{i=1}^N \phi_i^D \int_{E_i}^{PV} \mathbf{n}(\mathbf{x}) \cdot \nabla G(\mathbf{x}, \mathbf{x}_0) dl(\mathbf{x}) \\ = 2 \mathbf{u}^\infty \cdot \sum_{i=1}^N \mathbf{n}^{(i)} \int_{E_i} G(\mathbf{x}, \mathbf{x}_0) dl(\mathbf{x}). \end{aligned} \quad (6)$$

Identifying the point \mathbf{x}_0 with the mid-point of the j th element, denoted by \mathbf{x}_j^M , we derive a system of linear equations for the N unknown values ϕ_i^D ,

$$\begin{aligned} \phi_j^D - 2 \sum_{i=1}^N \phi_i^D \int_{E_i}^{PV} \mathbf{n}(\mathbf{x}) \cdot \nabla G(\mathbf{x}, \mathbf{x}_j^M) dl(\mathbf{x}) \\ = 2 \mathbf{u}^\infty \cdot \sum_{i=1}^N \mathbf{n}^{(i)} \int_{E_i} G(\mathbf{x}, \mathbf{x}_j^M) dl(\mathbf{x}), \end{aligned} \quad (7)$$

where $j = 1, \dots, N$.

To illustrate the structure of the linear system explicitly, we collect the two terms on the left-hand side of (7) and rearrange to find

$$\begin{aligned}
& \sum_{i=1}^N \phi_i^D \left[\frac{1}{2} \delta_{ij} - \int_{E_i}^{PV} \mathbf{n}(\mathbf{x}) \cdot \nabla G(\mathbf{x}, \mathbf{x}_j^M) dl(\mathbf{x}) \right] \\
& = \mathbf{u}^\infty \cdot \sum_{i=1}^N \mathbf{n}^{(i)} \int_{E_i} G(\mathbf{x}, \mathbf{x}_j^M) dl(\mathbf{x}). \tag{8}
\end{aligned}$$

The integrals on the left- and right-hand sides of (8) are computed by numerical methods, and the linear system is solved by the method of Gauss elimination.

COMPUTATION OF THE VELOCITY AT A POINT IN THE FLOW:

To obtain the velocity at a point in the flow, we evaluate the gradient of the disturbance potential on the right-hand side of equation (2) using centered differences. The disturbance potential itself is evaluated using the discretized integral representation

$$\begin{aligned}
\phi^D(\mathbf{x}_0) &= \mathbf{u}^\infty \cdot \sum_{i=1}^N \mathbf{n}^{(i)} \int_{E_i} G(\mathbf{x}, \mathbf{x}_0) dl(\mathbf{x}) \\
&\quad + \sum_{i=1}^N \phi_i^D \int_{E_i} \mathbf{n}(\mathbf{x}) \cdot \nabla G(\mathbf{x}, \mathbf{x}_0) dl(\mathbf{x}), \tag{9}
\end{aligned}$$

where the point \mathbf{x}_0 lies in the domain of flow.

Main program: `flow_2d`

The main program solves an integral equation of the second kind for the boundary distribution of the disturbance potential and generates streamlines originating from specified points in the flow.

Files to be linked:

1. `elm_arc`
Discretization of a circular segment into arc elements.
2. `elm_line`
Discretization of a straight segment into straight (linear) elements.
3. `flow_2d_geo`
Discretization of the boundary geometry.
4. `flow_2d_sdlp`
Evaluation of the single-and double-layer harmonic potential over boundary elements.

5. **flow_2d.vel**
Evaluation of the velocity at a specified point in the flow.
6. **gauss_leg**
Base points and weights for the Gauss-Legendre quadrature.
7. **gel**
Solution of a linear algebraic system by Gauss elimination.
8. **lgf_2d_fs**
Green's function of Laplace's equation in free space.

Input files:

1. **cvt_crc.dat**
Parameters for flow over a circular cavity on a plane wall.
2. **cvt_rec.dat**
Parameters for flow over a rectangular cavity on a plane wall.
3. **prt_crc.dat**
Parameters for flow over a circular protrusion on a plane wall.

Output files:

1. **flow_2d.str**
Streamlines.
2. **flow_2d.out**
Boundary distribution of the disturbance potential.
3. **flow_2d.prof**
Velocity profile.

Directory: `laplace/body_2d`

This directory contains a code that computes potential flow past a two-dimensional body with arbitrary geometry, with vanishing or non-zero circulation around the body, as illustrated in Figure `body_2d.1`. The flow occurs in an infinite domain of flow or a semi-infinite domain bounded by a plane wall located at $y = wall$ where the no-penetration condition is required.

Several body geometries implemented in the code are illustrated in Figure `body_2d.1`; others can be included by straightforward modifications.

MATHEMATICAL FORMULATION:

The velocity \mathbf{u} is decomposed into three parts as

$$\mathbf{u} = \mathbf{u}^\infty + \mathbf{v} + \mathbf{u}^D, \quad (1)$$

where:

- \mathbf{u}^∞ is the far-field component prevailing far from the body, expressing uniform (streaming) flow along the x axis.
- \mathbf{v} is the velocity field due to a point vortex with specified strength situated at the body interior (e.g., [59]). In the case of flow in a semi-infinite domain bounded by an infinite plane wall, \mathbf{v} also includes the image of the point vortex with respect to the wall, included to satisfy the no-penetration condition over the wall.
- \mathbf{u}^D is a disturbance flow component expressed by the gradient of the single-valued disturbance harmonic potential ϕ^D ,

$$\mathbf{u}^D = \nabla \phi^D. \quad (2)$$

Requiring the no-penetration boundary condition $\mathbf{u} \cdot \mathbf{n} = 0$ around the contour of the body in the xy plane, where \mathbf{n} is the unit vector normal to the body, we derive a boundary condition for the normal derivative of the disturbance potential,

$$\mathbf{n} \cdot \nabla \phi^D \equiv \frac{\partial \phi^D}{\partial n} = -(\mathbf{u}^\infty + \mathbf{v}) \cdot \mathbf{n}. \quad (3)$$

Using the standard boundary-integral formulation, we find that the disturbance potential satisfies the integral equation of the second kind

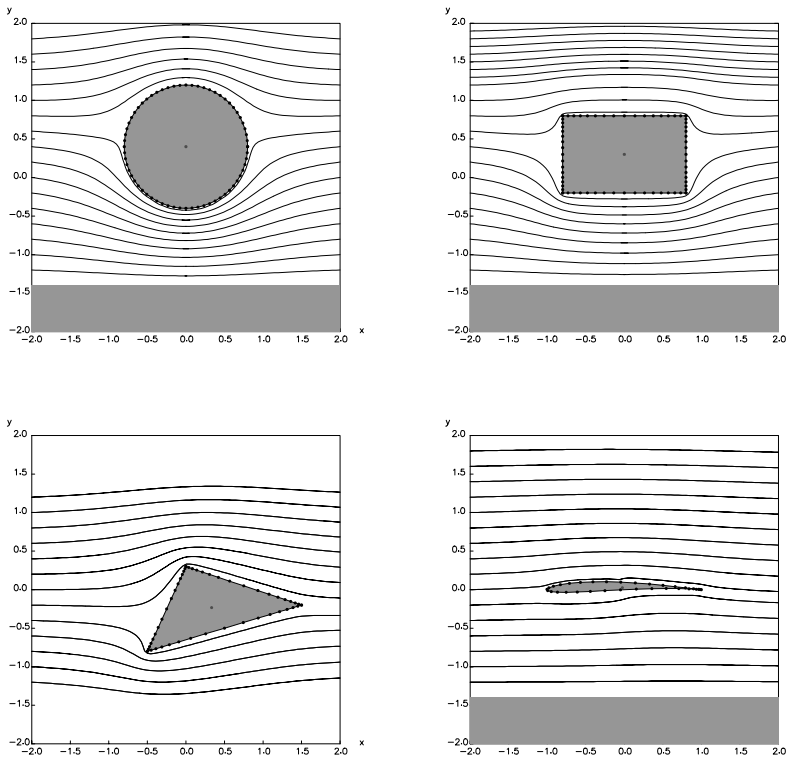


Figure body_2d.1 Streamlines of flow past a circle, a rectangle, a triangle, and a Joukowski airfoil.

$$\begin{aligned} \phi^D(\mathbf{x}_0) = & -2 \int_C G(\mathbf{x}, \mathbf{x}_0) [\mathbf{n}(\mathbf{x}) \cdot \nabla \phi^D(\mathbf{x})] dl(\mathbf{x}) \\ & + 2 \int_C^{PV} \phi^D(\mathbf{x}) [\mathbf{n}(\mathbf{x}) \cdot \nabla G(\mathbf{x}, \mathbf{x}_0)] dl(\mathbf{x}), \end{aligned} \quad (4)$$

where $G(\mathbf{x}, \mathbf{x}_0)$ is a Green's function of Laplace's equation in two dimensions, and the point \mathbf{x}_0 lies on the contour of the body C .

Inserting the boundary condition (3) into (4) and rearranging, we obtain

$$\begin{aligned} \phi^D(\mathbf{x}_0) - 2 \int_C^{PV} \phi^D(\mathbf{x}) [\mathbf{n}(\mathbf{x}) \cdot \nabla G(\mathbf{x}, \mathbf{x}_0)] dl(\mathbf{x}) \\ = 2 \int_C (\mathbf{u}^\infty + \mathbf{v}) \cdot \mathbf{n}(\mathbf{x}) G(\mathbf{x}, \mathbf{x}_0) dl(\mathbf{x}). \end{aligned} \quad (5)$$

NUMERICAL METHOD:

The contour of the body is discretized into a collection of N boundary elements denoted by E_i , $i = 1, \dots, N$. The boundary elements can be straight segments or circular arcs. The disturbance potential and its normal derivative are assumed to be constant over the i th element denoted respectively by ϕ_i^D and

$$\left(\frac{\partial \phi^D}{\partial n} \right)_i = -(\mathbf{u}^\infty + \mathbf{v}^{(i)}) \cdot \mathbf{n}^{(i)}, \quad (6)$$

where $\mathbf{n}^{(i)}$ and $\mathbf{v}^{(i)}$ are the normal vector and velocity induced by the point vortex evaluated at the mid-point of the i th element.

Subject to these approximations, the integral equation (5) assumes the discretized form

$$\begin{aligned} \phi^D(\mathbf{x}_0) - 2 \sum_{i=1}^N \phi_i^D \int_{E_i}^{PV} \mathbf{n}(\mathbf{x}) \cdot \nabla G(\mathbf{x}, \mathbf{x}_0) dl(\mathbf{x}) \\ = 2 \sum_{i=1}^N (\mathbf{u}^\infty + \mathbf{v}^{(i)}) \cdot \mathbf{n}^{(i)} \int_{E_i} G(\mathbf{x}, \mathbf{x}_0) dl(\mathbf{x}). \end{aligned} \quad (7)$$

Identifying the point \mathbf{x}_0 with the mid-point of the j th element, denoted by \mathbf{x}_j^M , we obtain a system of linear equations for the unknown values ϕ_i^D ,

$$\begin{aligned} \phi_j^D - 2 \sum_{i=1}^N \phi_i^D \int_{E_i}^{PV} \mathbf{n}(\mathbf{x}) \cdot \nabla G(\mathbf{x}, \mathbf{x}_j^M) dl(\mathbf{x}) \\ = 2 \sum_{i=1}^N (\mathbf{u}^\infty + \mathbf{v}^{(i)}) \cdot \mathbf{n}^{(i)} \int_{E_i} G(\mathbf{x}, \mathbf{x}_j^M) dl(\mathbf{x}), \end{aligned} \quad (8)$$

where $j = 1, \dots, N$. To illustrate the structure of the linear system more clearly, we collect the two terms on the left-hand side, and rearrange to find

$$\begin{aligned}
& \sum_{i=1}^N \phi_i^D \left[\frac{1}{2} \delta_{ij} - \int_{E_i}^{PV} \mathbf{n}(\mathbf{x}) \cdot \nabla G(\mathbf{x}, \mathbf{x}_j^M) dl(\mathbf{x}) \right] \\
& = \sum_{i=1}^N (\mathbf{u}^\infty + \mathbf{v}^{(i)}) \cdot \mathbf{n}^{(i)} \int_{E_i} G(\mathbf{x}, \mathbf{x}_j^M) dl(\mathbf{x}). \tag{9}
\end{aligned}$$

The integrals in (9) are computed by numerical methods and the linear system is solved by Gauss elimination.

TANGENTIAL VELOCITY:

The normal component of the disturbance velocity along the boundary contour is computed by solving an integral equation. The tangential component is computed by differentiating the disturbance potential with respect to arc length using numerical methods. The tangential component is then added to the normal component velocity to yield the total disturbance velocity. The total velocity is computed from the decomposition expressed by equation (1).

COMPUTATION OF THE VELOCITY AT A POINT IN THE FLOW:

To obtain the velocity at a point in the flow, we compute the gradient of the disturbance potential on the right-hand side of equation (2) using centered differences. The disturbance potential is evaluated using the discretized integral representation

$$\begin{aligned}
\phi^D(\mathbf{x}_0) &= \sum_{i=1}^N (\mathbf{u}^\infty + \mathbf{v}^{(i)}) \cdot \mathbf{n}^{(i)} \int_{E_i} G(\mathbf{x}, \mathbf{x}_0) dl(\mathbf{x}) \\
&+ \sum_{i=1}^N \phi_i^D \int_{E_i} \mathbf{n}(\mathbf{x}) \cdot \nabla G(\mathbf{x}, \mathbf{x}_0) dl(\mathbf{x}), \tag{10}
\end{aligned}$$

where the point \mathbf{x}_0 lies in the domain of flow.

Main program: body_2d

The main program solves an integral equation of the second kind for the boundary distribution of the disturbance potential, computes the boundary distribution of the pressure coefficient and the force exerted on the body [60], and generates streamlines originating from specified points in the flow.

Files to be linked:

1. `elm_arc`
Discretization of a circular segment into arc elements.
2. `elm_line`
Discretization of a straight segment into straight (linear) elements.
3. `body_2d_geo`
Discretization of the boundary geometry.
4. `body_2d_sdlp`
Evaluation of the single- and double-layer harmonic potential over boundary elements.
5. `body_2d_vel`
Evaluation of the velocity at a specified point in the flow.
6. `gauss_leg`
Base points and weights for the Gauss-Legendre quadrature.
7. `gel`
Solution of a linear algebraic system by Gauss elimination.
8. `lgf_2d_fs`
Green's function of Laplace's equation in free space.
9. `lgf_2d_w`
Green's function of Laplace's equation for a semi-infinite domain bounded by a plane wall.

Input files:

1. `airfoil.dat`
Parameters for flow past an airfoil. Boundary element nodes for Joukowski airfoils are generated by program `joukowski` included in this directory.
2. `circle.dat`
Parameters for flow past a circular cylinder.
3. `rectangle.dat`
Parameters for flow past a rectangular cylinder.
4. `triangle.dat`
Parameters for flow past a triangular cylinder.

Output files:

1. **body_2d.str**
Streamlines.
2. **body_2d.out**
Boundary distribution of the disturbance potential and tangential velocity.

Directory: `laplace/body_ax`

This directory contains a code that computes potential flow past an axisymmetric, compact (singly connected) or toroidal (doubly connected) body with arbitrary geometry, as illustrated in Figure `body_ax.1`. The problem formulation allows for non-zero circulation around the toroidal body.

Two body geometries implemented in the code are illustrated in Figure `body_ax.1`; other geometries can be included by straightforward additions and modifications.

MATHEMATICAL FORMULATION:

The velocity \mathbf{u} is decomposed into three parts as

$$\mathbf{u} = \mathbf{u}^\infty + \mathbf{v} + \mathbf{u}^D, \quad (1)$$

where:

- \mathbf{u}^∞ is the far-field component prevailing far from the body, expressing uniform (streaming) flow along the x axis of symmetry.
- \mathbf{v} is the velocity due to a line vortex ring with specified strength situated in the interior of the body, generating circulation around the toroidal body. In the case of flow past a compact body, this component is inconsequential, and serves only to modify the disturbance velocity.
- \mathbf{u}^D is a disturbance velocity expressed by the gradient of the single-valued harmonic potential ϕ^D ,

$$\mathbf{u}^D = \nabla \phi^D. \quad (2)$$

Requiring the no-penetration boundary condition $\mathbf{u} \cdot \mathbf{n} = 0$ around the contour of the body in a meridional plane of constant angle φ , where \mathbf{n} is the unit vector normal to the body, we derive a boundary condition for the normal derivative of the disturbance potential,

$$\mathbf{n} \cdot \nabla \phi^D \equiv \frac{\partial \phi^D}{\partial n} = -(\mathbf{u}^\infty + \mathbf{v}) \cdot \mathbf{n}. \quad (3)$$

Using the standard boundary-integral formulation, we find that the disturbance potential satisfies the integral equation of the second kind

$$\begin{aligned} \phi^D(\mathbf{x}_0) = & -2 \int_C G(\mathbf{x}, \mathbf{x}_0) [\mathbf{n}(\mathbf{x}) \cdot \nabla \phi^D(\mathbf{x})] dl(\mathbf{x}) \\ & + 2 \int_C^{PV} \phi^D(\mathbf{x}) [\mathbf{n}(\mathbf{x}) \cdot \nabla G(\mathbf{x}, \mathbf{x}_0)] dl(\mathbf{x}), \end{aligned} \quad (4)$$

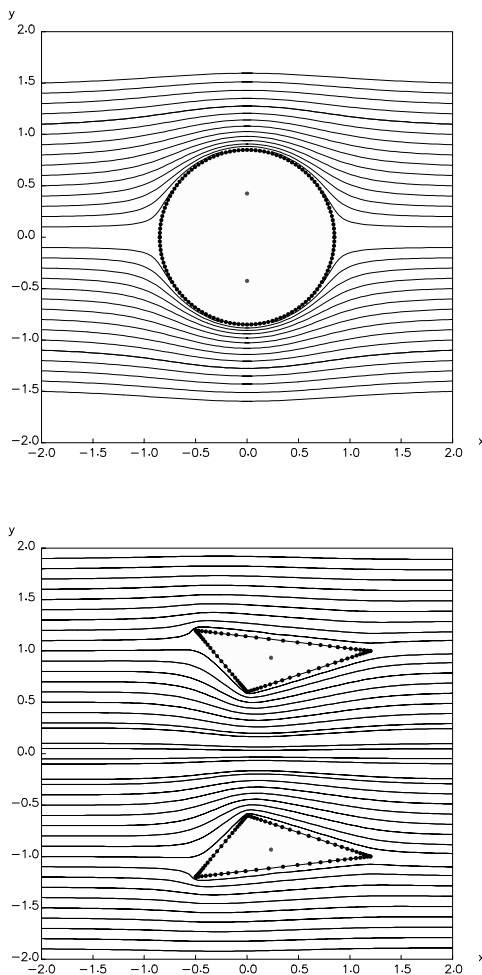


Figure body_ax.1 Streamlines of flow past a sphere and a triangular torus computed by code body_ax. The marks inside the body correspond to the trace of the circulation-producing line vortex ring.

where $G(\mathbf{x}, \mathbf{x}_0)$ is the free-space Green's function of Laplace's equation in an ax-symmetric domain, and the point \mathbf{x}_0 lies on the contour of the body C .

Inserting the boundary condition (3) into (4) and rearranging, we obtain

$$\begin{aligned} \phi^D(\mathbf{x}_0) - 2 \int_C^{PV} \phi^D(\mathbf{x}) [\mathbf{n}(\mathbf{x}) \cdot \nabla G(\mathbf{x}, \mathbf{x}_0)] dl(\mathbf{x}) \\ = 2 \int_C (\mathbf{u}^\infty + \mathbf{v}) \cdot G(\mathbf{x}, \mathbf{x}_0) \mathbf{n}(\mathbf{x}) dl(\mathbf{x}). \end{aligned} \quad (5)$$

NUMERICAL METHOD:

The contour of the body in a meridional plane is discretized into a collection of N boundary elements denoted by E_i , $i = 1, \dots, N$. The boundary elements can be straight segments or circular arcs. The disturbance potential and its normal derivative are approximated with constant functions the i th element denoted respectively by ϕ_i^D and

$$\left(\frac{\partial \phi_i^D}{\partial n} \right)_i = -(\mathbf{u}^\infty + \mathbf{v}^{(i)}) \cdot \mathbf{n}^{(i)}, \quad (6)$$

where $\mathbf{n}^{(i)}$ and $\mathbf{v}^{(i)}$ are the normal vector and velocity induced by the line vortex ring evaluated at the mid-point of the i th element.

i th element.

Subject to these approximations, the integral equation (5) assumes the discretized form

$$\begin{aligned} \phi^D(\mathbf{x}_0) - 2 \sum_{i=1}^N \phi_i^D \int_{E_i}^{PV} \mathbf{n}(\mathbf{x}) \cdot \nabla G(\mathbf{x}, \mathbf{x}_0) dl(\mathbf{x}) \\ = 2 \sum_{i=1}^N (\mathbf{u}^\infty + \mathbf{v}^{(i)}) \cdot \mathbf{n}^{(i)} \int_{E_i} G(\mathbf{x}, \mathbf{x}_0) dl(\mathbf{x}). \end{aligned} \quad (7)$$

Identifying the point \mathbf{x}_0 with the mid-point of the j th element denoted by \mathbf{x}_j^M , where $j = 1, \dots, N$, we obtain a system of linear equations for the unknown values ϕ_i^D ,

$$\begin{aligned} \phi_j^D - 2 \sum_{i=1}^N \phi_i^D \int_{E_i}^{PV} \mathbf{n}(\mathbf{x}) \cdot \nabla G(\mathbf{x}, \mathbf{x}_j^M) dl(\mathbf{x}) \\ = 2 \sum_{i=1}^N (\mathbf{u}^\infty + \mathbf{v}^{(i)}) \cdot \mathbf{n}^{(i)} \int_{E_i} G(\mathbf{x}, \mathbf{x}_j^M) dl(\mathbf{x}), \end{aligned} \quad (8)$$

where $j = 1, \dots, N$.

To illustrate the structure of the linear system more clearly, we collect the two terms on the left-hand side of (8) and rearrange to obtain

$$\begin{aligned} \sum_{i=1}^N \phi_i^D & [\frac{1}{2} \delta_{ij} - \int_{E_i}^{PV} \mathbf{n}(\mathbf{x}) \cdot \nabla G(\mathbf{x}, \mathbf{x}_j^M) dl(\mathbf{x})] \\ & = \sum_{i=1}^N (\mathbf{u}^\infty + \mathbf{v}^{(i)}) \cdot \mathbf{n}^{(i)} \int_{E_i} G(\mathbf{x}, \mathbf{x}_j^M) dl(\mathbf{x}). \end{aligned} \quad (9)$$

The integrals in equation (9) are computed by numerical methods and the linear system is solved by Gauss elimination.

TANGENTIAL VELOCITY:

The normal component of the disturbance velocity along the boundary contour is computed by solving an integral equation. The tangential component is computed numerically by differentiating the disturbance potential with respect to arc length along the contour. The tangential component is then added to the normal component to yield the total disturbance velocity. The total velocity is computed from the decomposition expressed by equation (1).

COMPUTATION OF THE VELOCITY AT A POINT IN THE FLOW:

To obtain the velocity at a point in the flow, we compute the gradient of the disturbance potential on the right-hand side of equation (2) using centered differences. The disturbance potential is evaluated using the discretized integral representation

$$\begin{aligned} \phi^D(\mathbf{x}_0) & = \sum_{i=1}^N (\mathbf{u}^\infty + \mathbf{v}^{(i)}) \cdot \mathbf{n}^{(i)} \int_{E_i} G(\mathbf{x}, \mathbf{x}_0) dl(\mathbf{x}) \\ & + \sum_{i=1}^N \phi_i^D \int_{E_i} \mathbf{n}(\mathbf{x}) \cdot \nabla G(\mathbf{x}, \mathbf{x}_0) dl(\mathbf{x}), \end{aligned} \quad (10)$$

where the point \mathbf{x}_0 lies in the domain of flow.

Main program: body_ax

The main program solves an integral equation of the second kind for the boundary distribution of the disturbance potential, computes the boundary distribution of the pressure coefficient and the force exerted on the body [60], and generates streamlines originating from specified points in the flow.

Files to be linked:

1. `elm_arc`
Discretization of a circular segment into arc elements.
2. `elm_line`
Discretization of a straight segment into straight (linear) elements.
3. `body_ax_geo`
Discretization of the boundary geometry.
4. `body_ax_sdlp`
Evaluation of the single- and double-layer harmonic potential over boundary elements.
5. `body_ax_vel`
Evaluation of the velocity at a specified point in the flow.
6. `ell_int`
Evaluation of complete elliptic integrals of the first and second kind.
7. `gauss_leg`
Base points and weights for the Gauss-Legendre quadrature.
8. `gel`
Solution of a linear algebraic system by Gauss elimination.
9. `lgf_ax_fs`
Free-space Green's function of Laplace's equation in an axisymmetric domain.
10. `lvr_ax_fs`
Potential and velocity due to a line vortex ring.

Input files:

1. `sphere.dat`
Parameters for flow past a sphere.
2. `torus_trgl.dat`
Parameters for flow past a triangular torus.

Output files:

1. `body_ax.str`
Streamlines.
2. `body_2d.out`
Boundary distribution of the disturbance potential and tangential velocity.

Directory: `laplace/tank_2d`

This directory contains a code that simulates the sloshing of a liquid inside a two-dimensional rectangular tank executing arbitrary motion, as illustrated in Figure `tank_2d.1`. The free surface exhibits constant surface tension.

When the free surface and velocity field are symmetric with respect to the mid-plane, the no-penetration condition at the vertical walls is equivalent to a periodicity boundary condition, and the motion describes spatially periodic, standing, forced, gravity or capillary waves.

MATHEMATICAL FORMULATION:

The velocity field is described in terms of the harmonic velocity potential ϕ that satisfies Laplace's equation $\nabla^2\phi = 0$, subject to the no-penetration condition $\mathbf{n} \cdot \nabla\phi = 0$ at the left, bottom, and right walls.

The velocity potential along the free surface evolves according to Bernoulli's equation for irrotational flow

$$\frac{D\phi}{Dt} = \frac{1}{2} |\mathbf{u}|^2 - \frac{P_{atm} + \gamma\kappa}{\rho} + \mathbf{g} \cdot \mathbf{x} - \frac{d\mathbf{V}}{dt} \cdot \mathbf{x}, \quad (1)$$

(e.g., [59], pp. 487 – 489), where:

- D/Dt is the material derivative (also called the substantial derivative) expressing the rate of change of a variable following the motion of material point particles.
- t stands for time.
- $|\mathbf{u}|^2 = \nabla\phi \cdot \nabla\phi$ is the square of the magnitude of the velocity.
- P_{atm} is the atmospheric pressure.
- γ is the surface tension.
- κ is the curvature of the free surface.
- ρ is the density of the liquid.
- \mathbf{g} is the acceleration of gravity vector.
- \mathbf{x} is the position vector defined with respect to an arbitrary origin.
- \mathbf{V} is the tank velocity.

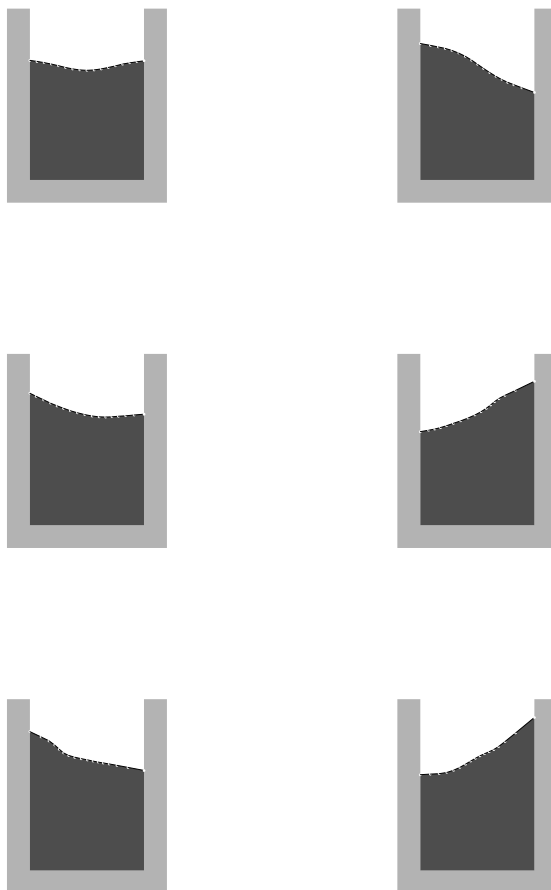


Figure tank_2d.1 Stages in the sloshing of a liquid in a rectangular tank simulated by a boundary-element method. The time sequence is from left to right and top to bottom.

Using the standard boundary-integral representation, we find that the harmonic potential and its normal derivative along the free surface satisfy the integral equation

$$\begin{aligned}\phi(\mathbf{x}_0) = & -2 \int_C G(\mathbf{x}, \mathbf{x}_0) [\mathbf{n}(\mathbf{x}) \cdot \nabla \phi(\mathbf{x})] dl(\mathbf{x}) \\ & + 2 \int_C^{PV} \phi(\mathbf{x}) [\mathbf{n}(\mathbf{x}) \cdot \nabla G(\mathbf{x}, \mathbf{x}_0)] dl(\mathbf{x}),\end{aligned}\quad (2)$$

where C represents the free surface, the point \mathbf{x}_0 lies on C , \mathbf{n} is the unit vector normal to C pointing into the flow, and $G(\mathbf{x}, \mathbf{x}_0)$ is the Neumann function of Laplace's equation for a semi-infinite strip confined between the left, bottom, and right walls. The satisfaction of the no-penetration boundary condition along the walls is implicit in the derivation of the integral equation (2).

The evolution of the free surface from a specified initial state may then be computed as follows:

- Compute the evolution of the harmonic potential along the free surface using Bernoulli's equation (1).
- Solve the integral equation (2) for the normal derivative $\mathbf{n}(\mathbf{x}) \cdot \nabla \phi(\mathbf{x})$ expressing the normal component of the velocity.
- Compute the tangential derivative of the potential expressing the tangential component of the velocity.
- Having obtained the normal and tangential components of the velocity over the free surface, evolve the position of the free surface.

NUMERICAL METHOD:

The free surface is traced with a collection of marker points that move with the fluid velocity fluid or with the component of the fluid velocity normal to the free surface. In the first case, the marker points are material point particles, whereas in the second case they are computational markers.

The free surface is approximated with a polygonal line passing through the instantaneous position of the marker points. The straight segments connecting pairs of adjacent marker points are moving boundary elements.

The harmonic potential and its normal derivative are approximated with constant functions, denoted respectively by ϕ_i and $(\frac{\partial \phi}{\partial n})_i$ over the i th element. Subject to this approximation, the integral equation (2) assumes the discretized form

$$\begin{aligned} & \sum_{i=1}^N \left(\frac{\partial \phi}{\partial n} \right)_i \int_{E_i} G(\mathbf{x}, \mathbf{x}_0) dl(\mathbf{x}) \\ &= -\frac{1}{2} \phi(\mathbf{x}_0) + \sum_{i=1}^N \phi_i \int_{E_i}^{PV} \mathbf{n}(\mathbf{x}) \cdot \nabla G(\mathbf{x}, \mathbf{x}_0) dl(\mathbf{x}), \end{aligned} \quad (3)$$

where N is the number of boundary elements.

Identifying the point \mathbf{x}_0 with the mid-point of the j th element denoted by \mathbf{x}_j^M , and setting $\phi(\mathbf{x}_j^M) = \phi_j$, we derive a system of linear equations for the N unknown values $(\frac{\partial \phi}{\partial n})_i$,

$$\begin{aligned} & \sum_{i=1}^N \left(\frac{\partial \phi}{\partial n} \right)_i \int_{E_i} G(\mathbf{x}_j^M, \mathbf{x}_0) dl(\mathbf{x}) \\ &= -\frac{1}{2} \phi_j + \sum_{i=1}^N \phi_i \int_{E_i}^{PV} \mathbf{n}(\mathbf{x}) \cdot \nabla G(\mathbf{x}_j^M, \mathbf{x}_0) dl(\mathbf{x}) \\ &= \sum_{i=1}^N \phi_i \left[\int_{E_i}^{PV} \mathbf{n}(\mathbf{x}) \cdot \nabla G(\mathbf{x}_j^M, \mathbf{x}_0) dl(\mathbf{x}) - \frac{1}{2} \delta_{ij} \right], \end{aligned} \quad (4)$$

where $j = 1, \dots, N$. The integrals in expression (4) are computed by numerical methods and the linear system is solved by Gauss elimination.

MOTION OF MARKER POINTS:

When the marker points move with the fluid velocity, the position of the element end-points is updated using the differential equation $d\mathbf{x}/dt = \mathbf{u}$ whose scalar components are

$$\frac{dx_i}{dt} = u_x(x_i, y_i), \quad \frac{dy_i}{dt} = u_y(x_i, y_i). \quad (5)$$

The free-surface velocity is computed using the decomposition

$$\mathbf{u} = \frac{\partial \phi}{\partial n} \mathbf{n} + \frac{\partial \phi}{\partial l} \mathbf{t}, \quad (6)$$

where l is the arc length along the free surface measured in the direction of the unit tangent vector \mathbf{t} . The tangential derivative of the potential is computed by quadratic differentiation with respect to arc length. Correspondingly, the rate of change of the harmonic potential is given by the right-hand side of (1).

Alternatively, when the marker points move with the velocity of the fluid normal to the free surface, system (5) is replaced by

$$\frac{dx_i}{dt} = \left(\frac{\partial \phi}{\partial n}\right)_i n_x(x_i, y_i), \quad \frac{dy_i}{dt} = \left(\frac{\partial \phi}{\partial n}\right)_i n_y(x_i, y_i), \quad (7)$$

and the rate of change of the harmonic potential is given by the modified evolution equation

$$\frac{d\phi}{dt} = |\mathbf{u} \cdot \mathbf{n}|^2 - \frac{1}{2} |\mathbf{u}|^2 - \frac{P_{atm} + \gamma\kappa}{\rho} + \mathbf{g} \cdot \mathbf{x}. \quad (8)$$

Other features of the numerical method include:

- The free-surface curvature is computed using the expression $\kappa = x_{ll}y_l - y_{ll}x_l$, where the subscript l denotes a tangential derivative with respect to arc length computed by quadratic interpolation.
- The velocity of the left and right contact line represented by the first and last marker point is computed by linear or quadratic extrapolation along the free surface.
- To prevent the onset of numerical instabilities, the position of the marker points and the corresponding values of the potential are smoothed after a specified number of steps using the formula

$$\hat{f}_i = \frac{1}{16} (-f_{i-2} + 4f_{i-1} + 10f_i + 4f_{i+1} - f_{i+2}), \quad (9)$$

where f is a smoothed variable and a caret denotes the smoothed value.

- To emulate viscous dissipation, the term $-\mu\phi$ is added to the right-hand sides of the evolution equations (1) and (8), where μ is a damping coefficient.

Main program: tank_2d

The main program performs a dynamical simulation from a specified initial state.

Files to be linked:

1. gauss_leg
Base points and weights for the Gauss-Legendre quadrature.
2. gel
Solution of a linear algebraic system by Gauss elimination.
3. lgf_2d.www
Neumann function of Laplace's equation in a semi-infinite rectangular strip.

4. `tank_2d_sd1p`

Evaluation of the single- and double-layer harmonic potential over the boundary elements.

Input files:1. `tank_2d.dat`

Specification of flow parameters.

2. `tank_2d.inp`

Restart file.

Output files:1. `tank_2d.xy`

Coordinates of free-surface marker points, and distribution of velocity and potential along the free surface at different times.

2. `tank_2d.rst`

Data for restarting a simulation.

Directory: `laplace/ldr_3d`

This directory contains a code that solves Laplace's equation in the interior or exterior of a closed three-dimensional surface subject to the Dirichlet boundary condition that specifies the surface distribution of the unknown function, as illustrated in Figure ldr_3d.1.

The solution is found by solving an integral equation of the first kind originating from Green's third identity, using a boundary-element method.

MATHEMATICAL FORMULATION:

We seek a scalar function f in the interior or exterior of a closed surface D satisfying Laplace's equation in three dimensions,

$$\nabla^2 f = 0, \quad (1)$$

subject to the Dirichlet boundary condition

$$f(\mathbf{x}) = g(\mathbf{x}), \quad (2)$$

where the point \mathbf{x} lies on D , and $g(\mathbf{x})$ is a specified surface function. In the case of the exterior problem, $f(\mathbf{x})$ is required to vanish at infinity.

The boundary-integral formulation provides us with the integral representation

$$f(\mathbf{x}_0) = \pm \left[- \int_D G(\mathbf{x}, \mathbf{x}_0) [\mathbf{n}(\mathbf{x}) \cdot \nabla f(\mathbf{x})] dS(\mathbf{x}) + \int_D f(\mathbf{x}) [\mathbf{n}(\mathbf{x}) \cdot \nabla G(\mathbf{x}, \mathbf{x}_0)] dS(\mathbf{x}) \right], \quad (3)$$

where:

- The point \mathbf{x}_0 lies in the solution domain (interior or exterior of D).
- $G(\mathbf{x}, \mathbf{x}_0) = 1/(4\pi|\mathbf{x} - \mathbf{x}_0|)$ is the free-space Green's function of Laplace's equation in three dimensions.
- \mathbf{n} is the unit vector normal to the surface D pointing *outward*.
- The plus sign on the right-hand side of (3) corresponds to the exterior problem and the minus sign corresponds to the interior problem.

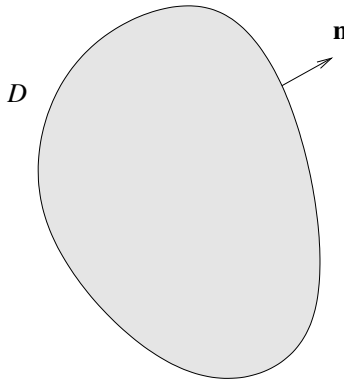


Figure 1dr_3d.1 Solution of Laplace's equation in the interior or exterior of a three-dimensional surface subject to the Dirichlet boundary condition, computed by a boundary-element method based on Green's third identity.

Taking the limit as the point \mathbf{x}_0 approaches the surface D and expressing the limit of the double-layer potential in terms of its principal value, we obtain an integral equation of the first kind for the normal derivative $\mathbf{n}(\mathbf{x}) \cdot \nabla f(\mathbf{x})$,

$$\begin{aligned} & \int_D G(\mathbf{x}, \mathbf{x}_0) [\mathbf{n}(\mathbf{x}) \cdot \nabla f(\mathbf{x})] dS(\mathbf{x}) \\ &= \int_D^{PV} f(\mathbf{x}) [\mathbf{n}(\mathbf{x}) \cdot \nabla G(\mathbf{x}, \mathbf{x}_0)] dS(\mathbf{x}) - \frac{\pm 1}{2} f(\mathbf{x}_0), \end{aligned} \quad (4)$$

where PV denotes the principal value of the double-layer integral. The plus or minus sign on the right-hand side of (4) correspond to the exterior or interior problem.

NUMERICAL METHOD:

The surface D is discretized into a grid of six-node curved triangles. All geometrical variables and the unknown function are approximated with quadratic functions over each triangle with respect to local triangle coordinates. The integral equation (4) is then applied at the grid nodes to obtain a system of linear equations for the node values of the normal derivative $\mathbf{n}(\mathbf{x}) \cdot \nabla f(\mathbf{x})$.

The linear system is generated by the method of impulses: to compute the influence matrix, we set the value of $\mathbf{n}(\mathbf{x}) \cdot \nabla f(\mathbf{x})$ equal to unity at one node, while setting it at zero at all other nodes, compute the single-layer potential at all nodes, and repeat sequentially for all nodes. The linear system is then solved by Gauss elimination.

The single-layer integral over the non-singular and singular elements is computed using a triangle quadrature and the polar integration rule, respectively.

The principal value of the double-layer integral on the right-hand side of (4) is computed using the identity

$$\begin{aligned} & \int_D^{PV} f(\mathbf{x}) [\mathbf{n}(\mathbf{x}) \cdot \nabla G(\mathbf{x}, \mathbf{x}_0)] dS(\mathbf{x}) \\ &= \int_D [f(\mathbf{x}) - f(\mathbf{x}_0)] [\mathbf{n}(\mathbf{x}) \cdot \nabla G(\mathbf{x}, \mathbf{x}_0)] dS(\mathbf{x}) - \frac{\pm 1}{2} f(\mathbf{x}_0). \end{aligned} \quad (5)$$

The non-singular integral on the right-hand side of (5) is computed by the Gauss triangle quadrature.

After the integral equation has been solved, the function f at a point in the solution domain (exterior or interior of D) is computed using the integral representation (3).

Main program: ldr_3d

The main program solves the integral equation (4) for the distribution of the normal derivative of the unknown function and computes the solution at a specified point using the integral representation.

Files to be linked:

1. gauss_leg
Base points and weights for the Gauss-Legendre quadrature.
2. gauss_trg1
Base points and weights for integration over a triangle.
3. gel
Solution of a linear algebraic system by Gauss elimination.
4. ld1p_3d
Computation of the principal value of the double-layer potential at the grid nodes.
5. ldr_3d_geo
Various auxiliary computations regarding geometry.
6. lgf_3d_fs
Free-space Green's function of Laplace's equation in three dimensions.
7. lsdlpp_3d
Computation of the nonsingular single- and double-layer potential at a point in the solution domain.

8. `lslp_3d`
Computation of the single-layer potential at the grid nodes.
9. `trgl_octa`
Triangulation of the unit sphere into a mesh of curved triangles descending from the octahedron.

Input file:

1. `ldr_3d.dat`
Specification of problem parameters.

Output file:

1. `ldr_3d.out`
Computed values of the normal derivative of the surface function f at the nodes.

Directory: `laplace/lnm_3d`

This directory contains a code that solves Laplace's equation in the interior or exterior of a closed three-dimensional surface subject to the Neumann boundary condition that specifies the surface distribution of the normal derivative of the unknown function, as illustrated in Figure lnm_3d.1.

The solution is found by solving an integral equation of the second kind emerging from Green's third identity, using a boundary-element method.

MATHEMATICAL FORMULATION:

We seek a scalar function f in the interior or exterior of a closed surface D satisfying Laplace's equation in three dimensions,

$$\nabla^2 f = 0, \quad (1)$$

subject to the Neumann boundary condition

$$\mathbf{n}(\mathbf{x}) \cdot \nabla f(\mathbf{x}) = g(\mathbf{x}), \quad (2)$$

where the point \mathbf{x} lies on D , \mathbf{n} is the unit normal vector pointing *outward*, and $g(\mathbf{x})$ is a specified surface function. In the case of the exterior problem, $f(\mathbf{x})$ is required to vanish at infinity.

The boundary-integral formulation provides us with the integral representation

$$f(\mathbf{x}_0) = \pm \left[- \int_D G(\mathbf{x}, \mathbf{x}_0) [\mathbf{n}(\mathbf{x}) \cdot \nabla f(\mathbf{x})] dS(\mathbf{x}) + \int_D f(\mathbf{x}) [\mathbf{n}(\mathbf{x}) \cdot \nabla G(\mathbf{x}, \mathbf{x}_0)] dS(\mathbf{x}) \right], \quad (3)$$

where:

- The point \mathbf{x}_0 lies in the solution domain (interior or exterior of D).
- $G(\mathbf{x}, \mathbf{x}_0) = 1/(4\pi|\mathbf{x} - \mathbf{x}_0|)$ is the free-space Green's function of Laplace's equation in three dimensions.
- \mathbf{n} is the unit vector normal to the surface D pointing *outward*.
- The plus sign on the right-hand side of (3) corresponds to the exterior problem and the minus sign corresponds to the interior problem.

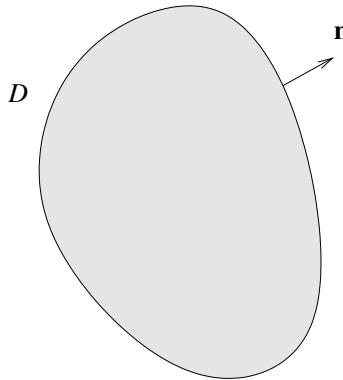


Figure Inm_3d.1 Solution of Laplace's equation in the interior or exterior of a three-dimensional surface subject to Neumann boundary conditions, computed using a boundary-element method based on Green's third identity.

Taking the limit as the point \mathbf{x}_0 approaches the surface D and expressing the limit of the double-layer potential in terms of its principal value, we obtain an integral equation of the second kind for the surface distribution of $f(\mathbf{x})$,

$$\int_D^{PV} f(\mathbf{x}) [\mathbf{n}(\mathbf{x}) \cdot \nabla G(\mathbf{x}, \mathbf{x}_0)] dS(\mathbf{x}) - \frac{1}{2} f(\mathbf{x}_0) = \pm \int_D G(\mathbf{x}, \mathbf{x}_0) [\mathbf{n}(\mathbf{x}) \cdot \nabla f(\mathbf{x})] dS(\mathbf{x}), \quad (4)$$

where PV denotes the principal value of the double-layer integral. The plus or minus sign on the left-hand side of (4) corresponds to the exterior or interior problem.

The integral equation (4) for the interior problem has a solution only if the specified distribution of the normal derivative satisfies the solvability condition

$$\int_D \mathbf{n}(\mathbf{x}) \cdot \nabla f(\mathbf{x}) dS(\mathbf{x}) = \int_D g(\mathbf{x}) dS(\mathbf{x}) = 0. \quad (5)$$

When this condition is satisfied, the integral equation has an infinite number of solutions that differ by an arbitrary constant.

NUMERICAL METHOD:

See corresponding section in directory `laplace/ldr_3d`. Because the integral equation (4) for the interior problem does not have a unique solution, the solution of the linear system for the node values of f is unreliable.

Main program: lnm_3d

The main program solves the integral equation (4) for the boundary distribution of the unknown function and computes the solution at a specified point using the integral representation.

Files to be linked:

1. gauss_leg
Base points and weights for the Gauss-Legendre quadrature.
2. gauss_trgl
Base points and weights for integration over a triangle.
3. gel
Solution of a linear algebraic system by Gauss elimination.
4. ld1p_3d
Computes the principal value of the double-layer potential at the grid nodes.
5. lnm_3d_geo
Various auxiliary computations regarding geometry.
6. lgf_3d_fs
Free-space Green's function of Laplace's equation in three dimensions.
7. lsdlpp_3d
Computes the nonsingular single- and double-layer potential at a point in the solution domain.
8. ls1p_3d
Computes the single-layer potential at the grid nodes.
9. trgl_octa
Triangulation of the unit sphere into a mesh of curved triangles descending from the octahedron.

Input file:

1. lnm_3d.dat
Specification of problem parameters.

Output file:

1. lnm_3d.out
Numerical values of the function f at the surface nodes.

Chapter 11

Directory: helmholtz

This directory contains a code that solves the complex Helmholtz equation in two dimensions describing unidirectional oscillatory viscous flow inside or outside a cylindrical tube.

Directory contents:

Subdirectory	Topic
<code>flow_1d_osc</code>	Unidirectional oscillatory viscous flow inside or outside a cylindrical tube with arbitrary cross-section.

Directory: `helmholtz/flow_1d_osc`

This directory contains a code that computes unidirectional oscillatory viscous flow inside or outside a cylindrical tube with arbitrary cross-section, as illustrated in Figure `flow_1d_osc.1`.

Circular, elliptical, rectangular, and triangular tube shapes are implemented in the code. Other shapes can be included by straightforward modifications.

MATHEMATICAL FORMULATION:

The equation of fluid motion for internal or external unsteady unidirectional viscous flow requires that, in the absence of a pressure gradient and significant gravitational effects, the streamwise component of the velocity along the z axis, denoted by u_z , satisfy the unsteady diffusion equation

$$\rho \frac{\partial u_z}{\partial t} = \mu \nabla^2 u_z, \quad (1)$$

where ρ is the fluid density, t stands for time, $\nabla^2 \equiv \partial^2/\partial x^2 + \partial^2/\partial y^2$ is the Laplacian operating over the tube cross-section in the xy plane, and μ is the fluid viscosity. If the tube moves parallel to its generators with velocity $U(t)$, the no-slip boundary condition requires that $u_z = U(t)$ around the tube contour.

In the case of oscillatory flow, the tube wall and fluid velocity can be expressed as the real or imaginary part of the complex functions

$$U(t) = A e^{-i\Omega t}, \quad u_z(x, y, t) = w(x, y) e^{-i\Omega t}, \quad (2)$$

where Ω is the angular frequency of the oscillations, i is the imaginary unit, A is a constant amplitude, and $w(x, y)$ is the complex amplitude of the fluid velocity. The non-slip boundary condition requires $w = A$ around the tube contour C .

Substituting the expressions shown in (2) into the governing equation (1) and discarding the complex exponentials, we obtain the complex Helmholtz equation

$$\nabla^2 w + i \frac{\Omega \rho}{\mu} w = 0. \quad (3)$$

Using the boundary-integral formulation, we find that the complex function w at a point \mathbf{x}_0 located in the domain of flow is given by the integral representation

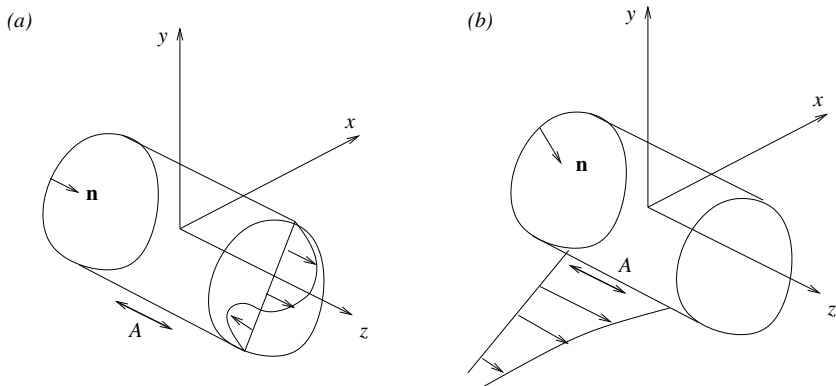


Figure flow_1d_osc.1 Unsteady unidirectional flow inside or outside a tube with arbitrary cross-section due to longitudinal boundary oscillation; (a) internal, and (b) external flow.

$$\pm w(\mathbf{x}_0) = - \int_C G(\mathbf{x}, \mathbf{x}_0) \frac{\partial w}{\partial n}(\mathbf{x}) dl(\mathbf{x}) + \int_C \mathbf{n}(\mathbf{x}) \cdot \nabla G(\mathbf{x}, \mathbf{x}_0) w(\mathbf{x}) dl(\mathbf{x}), \quad (4)$$

where:

- $\partial w / \partial n = \mathbf{n} \cdot \nabla w$ is the normal derivative of w .
- \mathbf{n} is the unit normal vector pointing into the tube.
- $G(\mathbf{x}, \mathbf{x}_0)$ is the free-space Green's function of Helmholtz's equation (3) given by

$$G(\mathbf{x}, \mathbf{x}_0) = \frac{1}{2\pi} [\mathrm{k} \mathrm{er}_0(\delta r) + i \mathrm{k} \mathrm{ei}_0(\delta r)], \quad (5)$$

$r = |\mathbf{x} - \mathbf{x}_0|$, $\delta = (\Omega\rho/\mu)^{1/2}$ is the Stokes layer thickness, and $\mathrm{k} \mathrm{er}_0$, $\mathrm{k} \mathrm{ei}_0$ are Kelvin functions.

- The plus and minus sign on the left-hand side of (4) apply, respectively, in the case of interior or exterior flow.

Implementing the boundary condition $w = A$ around C , we obtain the more specific representation

$$\begin{aligned} \pm w(\mathbf{x}_0) = & - \int_C G(\mathbf{x}, \mathbf{x}_0) \frac{\partial w}{\partial n}(\mathbf{x}) dl(\mathbf{x}) \\ & + A \int_C \mathbf{n}(\mathbf{x}) \cdot \nabla G(\mathbf{x}, \mathbf{x}_0) dl(\mathbf{x}). \end{aligned} \quad (6)$$

Taking the limit as the \mathbf{x}_0 approaches the tube contour C and expressing the limit of the double-layer potential on the right-hand side in terms of its principal value, we obtain an integral equation of the first kind for the normal derivative $\partial w / \partial n$,

$$\int_C G(\mathbf{x}, \mathbf{x}_0) \frac{\partial w}{\partial n}(\mathbf{x}) dl(\mathbf{x}) = A \int_C^{PV} \mathbf{n}(\mathbf{x}) \cdot \nabla G(\mathbf{x}, \mathbf{x}_0) dl(\mathbf{x}) - \frac{\pm A}{2}, \quad (7)$$

where the point \mathbf{x}_0 lies on C , and PV denotes the principal value of the double-layer potential.

NUMERICAL METHOD:

The tube contour C is discretized into a collection of N boundary elements E_i defined by $N + 1$ marker points, where $i = 1, \dots, N$. The boundary elements may be straight segments or circular arcs. Approximating the normal derivative of w with a constant function over each element, we obtain a discretized version of the integral equation (7):

$$\begin{aligned} \sum_{i=1}^N \left(\frac{\partial w}{\partial n} \right)_i \int_{E_i} G(\mathbf{x}, \mathbf{x}_0) dl(\mathbf{x}) \\ = A \sum_{i=1}^N \int_{E_i}^{PV} \mathbf{n}(\mathbf{x}) \cdot \nabla G(\mathbf{x}, \mathbf{x}_0) dl(\mathbf{x}) - \frac{\pm A}{2}. \end{aligned} \quad (8)$$

Next, we identify the point \mathbf{x}_0 with the mid-point of each element denoted by \mathbf{x}_j^M , where j is the element label, and thereby obtain a complex system of linear equations for the unknown complex values $(\partial w / \partial n)_i$,

$$\begin{aligned} \sum_{i=1}^N \left(\frac{\partial w}{\partial n} \right)_i \int_{E_i} G(\mathbf{x}, \mathbf{x}_j^M) dl(\mathbf{x}) \\ = A \sum_{i=1}^N \int_{E_i}^{PV} \mathbf{n}(\mathbf{x}) \cdot \nabla G(\mathbf{x}, \mathbf{x}_j^M) dl(\mathbf{x}) - \frac{\pm A}{2}, \end{aligned} \quad (9)$$

for $j = 1, \dots, N$.

The unknown complex values $(\partial w / \partial n)_i$ and the linear system (9) are decomposed into its real and imaginary parts, and the expanded system of $2N$ real equations is solved by Gauss elimination.

COMPUTATION OF THE VELOCITY AT A POINT IN THE FLOW:

The velocity at a point x_0 located in the domain of flow is computed using the discretized form of the boundary-integral representation (6).

Main program: flow_1d_osc

The main program solves the integral equation (7) for the distribution of the normal derivative of the complex function w and evaluates the complex amplitude of the velocity at a specified point in the flow.

Files to be linked:

1. elm_arc
Discretization of a circular segment into arc elements.
2. elm_line
Discretization of a straight segment into straight (linear) elements.
3. flow_1d_osc_geo
Discretization of the boundary geometry.
4. flow_1d_osc_sdlp
Evaluation of the single- and double-layer Helmholtz potential over the boundary elements.
5. flow_1d_osc_vel
Evaluation of the velocity at a specified point in the flow.
6. gauss_leg
Base points and weights for the Gauss-Legendre quadrature.
7. gel
Solution of a linear algebraic system by Gauss elimination.
8. hgfs_2dc_fs
Green's function of the Helmholtz equation in two dimensions with a complex coefficient multiplying the linear forcing term.
9. ker_kei_0
Evaluation of the Kelvin functions, \ker_0 , kei_0 , and their derivatives.

Input files:

1. `circle.dat`
Parameters for flow through a circular tube.
2. `ellipse.dat`
Parameters for flow through an elliptical tube.
3. `rectangle.dat`
Parameters for flow through a rectangular tube.
4. `triangle.dat`
Parameters for flow through a triangular tube.

Output files:

1. `flow_1d_osc(elm)`
Boundary element distribution.
2. `flow_1d_osc(trc)`
Distribution of the complex boundary shear stress (traction).
3. `flow_1d_osc.vel`
Recording of the velocity at a point in the flow.

Chapter 12

Directory: stokes

This directory contains libraries of Green's functions and boundary-element codes for Stokes flow.

Directory contents:

Subdirectory	Topic
sgf_2d	Green's functions of two-dimensional Stokes flow.
sgf_3d	Green's functions of three-dimensional Stokes flow.
sgf_ax	Green's functions of axisymmetric Stokes flow.
flow_2d	Two-dimensional flow in a domain with arbitrary geometry.
prtcl_sw	Swirling flow due to the steady rotation of an axisymmetric particle.
prtcl_2d	Flow past a fixed bed of two-dimensional particles with arbitrary shapes, for a variety of configurations.
prtcl_ax	Flow past, or due to the motion of, a collection of axisymmetric particles.
prtcl_3d	Flow past, or due to the motion of, a three-dimensional particle, for a variety of configurations.

Directory: **stokes/sgf_2d**

The velocity, pressure, and stress Green's functions of two-dimensional Stokes flow, denoted respectively by G_{ij} , p_j , and T_{ijk} , where the indices i , j , and k range over 1 and 2 corresponding to x and y , are defined such that the velocity at the field point $\mathbf{x} = (x, y)$ induced by a two-dimensional point force with strength \mathbf{b} located at the singular point $\mathbf{x}_0 = (x_0, y_0)$ is given by

$$u_i(\mathbf{x}) = \frac{1}{4\pi\mu} G_{ij}(\mathbf{x}, \mathbf{x}_0) b_j = \frac{1}{4\pi\mu} G_{ji}(\mathbf{x}_0, \mathbf{x}) b_j, \quad (\text{sgf_2d.1})$$

where μ is the fluid viscosity. The associated pressure and stress fields are given by

$$p(\mathbf{x}) = \frac{1}{4\pi} p_j(\mathbf{x}, \mathbf{x}_0) b_j, \quad (\text{sgf_2d.2})$$

and

$$\sigma_{ik}(\mathbf{x}) = \frac{1}{4\pi} T_{ijk}(\mathbf{x}, \mathbf{x}_0) b_j. \quad (\text{sgf_2d.3})$$

Using the Newtonian constitutive equation, we find that the stress Green's function derives from the pressure and velocity Green's function by the relation

$$T_{ijk} = \delta_{ik} p_j + \frac{\partial G_{ij}}{\partial x_k} + \frac{\partial G_{kj}}{\partial x_i}. \quad (\text{sgf_2d.4})$$

By definition, the velocity and pressure Green's functions satisfy the equations

$$\begin{aligned} \frac{\partial G_{ij}}{\partial x_i} &= 0, \\ -\frac{\partial p_j}{\partial x_i} + \frac{\partial^2 G_{ij}}{\partial x^2} + \frac{\partial^2 G_{ij}}{\partial y^2} &= -4\pi \delta_{ij} \delta_2(\mathbf{x} - \mathbf{x}_0), \end{aligned} \quad (\text{sgf_2d.5})$$

originating, respectively, from the continuity equation and the Stokes equation; δ_{ij} is Kronecker's s delta, and δ_2 is Dirac's delta function in two dimensions.

Correspondingly, the stress Green's function satisfies the equation

$$\frac{\partial T_{ijk}}{\partial x_k} = \frac{\partial T_{kji}}{\partial x_k} = -4\pi \delta_{ij} \delta_2(\mathbf{x} - \mathbf{x}_0). \quad (\text{sgf_2d.6})$$

INTEGRAL IDENTITIES:

Mass conservation requires that the velocity Green's function satisfy the integral identity

$$\int_C n_i(\mathbf{x}) G_{ij}(\mathbf{x}, \mathbf{x}_0) dl(\mathbf{x}) = 0, \quad (\text{sgf_2d.7})$$

where C is a closed loop in the xy plane enclosing the control area A_c . To derive (sgf_2d.7), we integrate the first equation in (sgf_2d.5) over A_c and use the divergence theorem to convert the areal integral to a line integral.

The stress Green's function satisfies the integral identity

$$\int_C T_{ijk}(\mathbf{x}, \mathbf{x}_0) n_k(\mathbf{x}) dl(\mathbf{x}) = \begin{cases} \delta_{ij} & \text{when } \mathbf{x}_0 \text{ is inside } A_c \\ \frac{1}{2} \delta_{ij} & \text{when } \mathbf{x}_0 \text{ is on } C \\ 0 & \text{when } \mathbf{x}_0 \text{ is outside } A_c \end{cases}, \quad (\text{sgf_2d.8})$$

originating from the second equation in (sgf_2d.5); the unit normal vector \mathbf{n} points *into* the control area enclosed by the contour C . When the point \mathbf{x}_0 is located on C , the principal-value integral is implied on the left-hand side of (sgf_2d.8).

BOUNDARY-INTEGRAL REPRESENTATION:

The boundary-integral representation for the velocity of a two-dimensional Stokes flow is

$$\begin{aligned} u_j(\mathbf{x}_0) = & -\frac{1}{4\pi\mu} \int_C G_{ji}(\mathbf{x}_0, \mathbf{x}) f_i(\mathbf{x}) dl(\mathbf{x}) \\ & + \frac{1}{4\pi} \int_C u_i(\mathbf{x}) T_{ijk}(\mathbf{x}, \mathbf{x}_0) n_k(\mathbf{x}) dl(\mathbf{x}), \end{aligned} \quad (\text{sgf_2d.9})$$

where C denotes the collection of all contours enclosing a selected control area in the flow, \mathbf{n} is the unit vector normal to C pointing into the control area, and $\mathbf{f} \equiv \sigma \cdot \mathbf{n}$ is the boundary traction.

BOUNDARY-INTEGRAL EQUATION:

The boundary-integral equation corresponding to (sgf_2d.9) is

$$\begin{aligned} u_j(\mathbf{x}_0) = & -\frac{1}{2\pi\mu} \int_C G_{ji}(\mathbf{x}_0, \mathbf{x}) f_i(\mathbf{x}) dl(\mathbf{x}) \\ & + \frac{1}{2\pi} \int_C^{PV} u_i(\mathbf{x}) T_{ijk}(\mathbf{x}, \mathbf{x}_0) n_k(\mathbf{x}) dl(\mathbf{x}), \end{aligned} \quad (\text{sgf_2d.10})$$

where the point \mathbf{x}_0 lies on C , and PV denotes the principal-value integral.

DIRECTORY CONTENTS:

This directory contains a suite of subroutines that evaluate the following family of Green's functions:

Subroutine	Topic
<code>sgf_2d_fs</code>	Green's function for flow in free space.
<code>sgf_2d_w</code>	Green's function for flow in a semi-infinite domain bounded by a plane wall.
<code>sgf_2d_1p</code>	Singly periodic Green's function in free space.
<code>sgf_2d_1p_w</code>	Singly periodic Green's function for flow in a semi-infinite domain bounded by a plane wall.
<code>sgf_2d_1p_ww</code>	Singly periodic Green's function for flow in a channel bounded by two parallel plane walls.
<code>sgf_2d_2p</code>	Doubly periodic Green's function.

Subroutine: sgf_2d_fs

This subroutine computes the Green's function for an infinite domain of flow in the absence of boundaries. The streamline pattern of the induced flow is depicted in Figure sgf_2d_fs.1.

The Green's function is given by

$$\begin{aligned} G_{ij}(\hat{\mathbf{x}}) &= -\delta_{ij} \ln r + \frac{\hat{x}_i \hat{x}_j}{r^2}, \\ p_j(\hat{\mathbf{x}}) &= 2 \frac{\hat{x}_j}{r^2}, \\ T_{ijk}(\hat{\mathbf{x}}) &= -4 \frac{\hat{x}_i \hat{x}_j \hat{x}_k}{r^4}, \end{aligned} \quad (1)$$

where $\hat{\mathbf{x}} \equiv \mathbf{x} - \mathbf{x}_0$ and $r = |\mathbf{x} - \mathbf{x}_0|$ are the vectorial and scalar distance of the field point \mathbf{x} from the singular point \mathbf{x}_0 , respectively.

Call statement:

sgf_2d_fs

(Iopt	Input:	See Note 1.
, x, y	Input:	Coordinates of the field point.
, x_0, y_0	Input:	Coordinates of the singular point (point force).
, G_{xx}, G_{xy}	Output:	Velocity Green's function.
, G_{yx}, G_{yy}	Output:	Velocity Green's function.
, p_x, p_y	Output:	Pressure Green's function.
, T_{xxx}, T_{xxy}	Output:	Stress Green's function.
, T_{yxx}, T_{yxy}	Output:	Stress Green's function.
, T_{xyx}, T_{xyy}	Output:	Stress Green's function.
, T_{yyx}, T_{yyy})	Output:	Stress Green's function.

Note:

1. Set Iopt = 1 to obtain only G_{ij} ; set Iopt $\neq 1$ to obtain G_{ij} , p_j , and T_{ijk} .

Numerical method:

The Green's function is computed by direct evaluation of expressions (1).

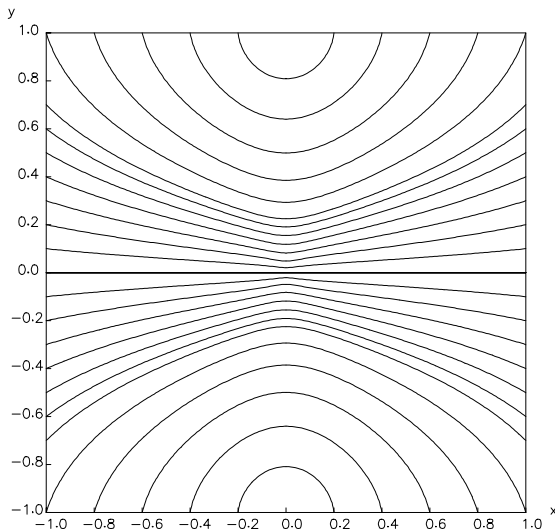


Figure sgf_2d_fs.1 Streamline pattern of the flow induced by a two-dimensional point force oriented along the x axis, in free space.

Driver: sgf_2d_fs_dr

The driver evaluates the Green's function and verifies the integral identities (sgf_2d.7,8), where C is a circular contour.

Files to be linked: None.

Subroutine: sgf_2d_w

This subroutine computes the Green's function for a semi-infinite domain of flow bounded by a plane wall located at $y = wall$, as illustrated in Figure sgf_2d_w.1. The streamline pattern of the induced flow is depicted in Figure sgf_2d_w.2.

The velocity Green's function is given by

$$\begin{aligned} G_{ij}(\mathbf{x}, \mathbf{x}_0) &= G_{ij}^{FS}(\mathbf{x} - \mathbf{x}_0) - G_{ij}^{FS}(\mathbf{x} - \mathbf{x}_0^{Im}) \\ &\quad + 2 h_0^2 D_{ij}(\mathbf{x} - \mathbf{x}_0^{Im}) - 2 h_0 Q_{ij}(\mathbf{x} - \mathbf{x}_0^{Im}), \end{aligned} \tag{1}$$

(e.g., [55], p. 93), where:

- G_{ij}^{FS} is the free-space Green's function.
- $\mathbf{x}_0^{Im} = (x_0, 2 \times wall - y_0)$ is the image of the point force with respect to the wall.
- $h_0 = y_0 - wall$ is the distance of the point force from the wall.
- The tensors D_{ij} and Q_{ij} represent, respectively, potential dipoles and point-force doublets, and are given by

$$\begin{aligned} D_{ij}(\mathbf{w}) &= \pm \frac{\partial}{\partial w_j} \left(\frac{w_i}{|\mathbf{w}|^2} \right) = \pm \left(\frac{\delta_{ij}}{|\mathbf{w}|^2} - 2 \frac{w_i w_j}{|\mathbf{w}|^4} \right), \\ Q_{ij}(\mathbf{w}) &= \pm \frac{\partial G_{ij}^{FS}}{\partial w_j} = w_2 D_{ij} \pm \frac{\delta_{j2} w_i - \delta_{i2} w_j}{|\mathbf{w}|^2}. \end{aligned} \tag{2}$$

The plus sign applies when $j = 1$, corresponding to the x direction, and the minus sign applies when $j = 2$, corresponding to the y direction.

The pressure Green's function is given by

$$p_j(\mathbf{x}, \mathbf{x}_0) = p_j^{FS}(\mathbf{x} - \mathbf{x}_0) - p_j^{FS}(\mathbf{x} - \mathbf{x}_0^{Im}) - 2 h_0 p_j^Q(\mathbf{x} - \mathbf{x}_0^{Im}), \tag{3}$$

where p_j^{FS} is the free-space pressure Green's function, and

$$p_x^Q(\mathbf{w}) = -4 \frac{w_x w_y}{|\mathbf{w}|^4}, \quad p_y^Q(\mathbf{w}) = -2 \frac{w_x^2 - w_y^2}{|\mathbf{w}|^4}, \tag{4}$$

is the pressure field corresponding to the point-force doublets.

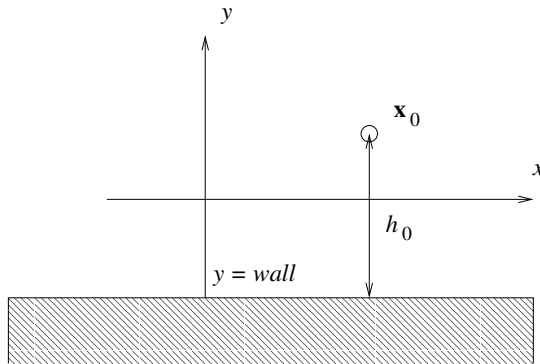


Figure sgf_2d_w.1 A two-dimensional point force in a semi-infinite domain of flow bounded by a plane wall located at $y = \text{wall}$.

The stress Green's function follows from the preceding expressions using the definition (sgf_2d.4).

Call statement:

`sgf_2d_w`

$(Iopt$	<i>Input:</i> See Note 1.
$, x, y$	<i>Input:</i> Coordinates of the field point.
$, x_0, y_0$	<i>Input:</i> Coordinates of the singular point (point force).
$, \text{wall}$	<i>Input:</i> The wall is located at $y = \text{wall}$.
$, G_{xx}, G_{xy}$	<i>Output:</i> Velocity Green's function.
$, G_{yx}, G_{yy}$	<i>Output:</i> Velocity Green's function.
$, p_x, p_y$	<i>Output:</i> Pressure Green's function.
$, T_{xxx}, T_{xxy}$	<i>Output:</i> Stress Green's function.
$, T_{yxx}, T_{yxy}$	<i>Output:</i> Stress Green's function.
$, T_{xyx}, T_{xyy}$	<i>Output:</i> Stress Green's function.
$, T_{yyx}, T_{yyy}$)	<i>Output:</i> Stress Green's function.

Note:

1. Set $Iopt = 1$ to obtain only G_{ij} ; set $Iopt \neq 1$ to obtain G_{ij} , p_j , and T_{ijk} .

Numerical method:

The Green's function is computed by direct evaluation of expressions (1) to (4).

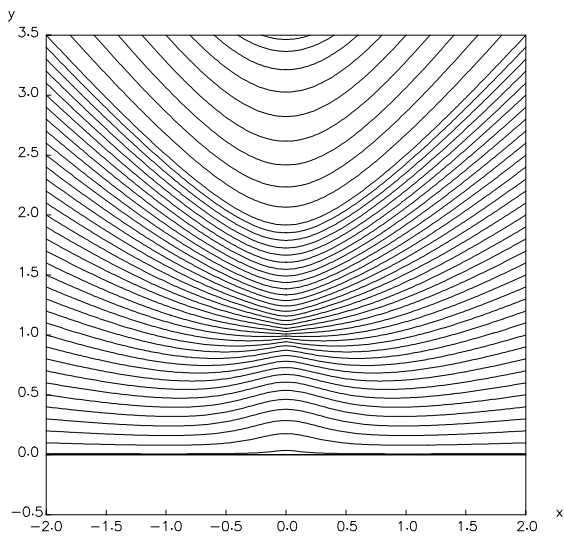
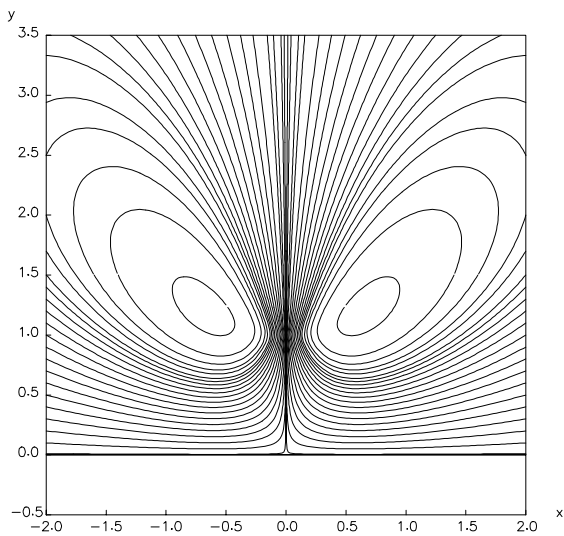


Figure sgf_2d_w.2 Streamline pattern of the flow due to a two-dimensional point force oriented normal (top) or parallel (bottom) to a plane wall.

Driver: sgf_2d_w_dr

The driver evaluates the Green's function and verifies the integral identities (sgf_2d.7,8), where C is a circular contour.

Files to be linked: None.

Subroutine: sgf_2d_1p

This subroutine computes the singly periodic Green's function in free space representing the flow due to an infinite periodic array of point forces separated by the distance L along the x axis, as illustrated in Figure sgf_2d_1p.1. One of the point forces is located at the point $\mathbf{x}_0 = (x_0, y_0)$. The streamline pattern of the induced flow is depicted in Figure sgf_2d_1p.2.

The velocity Green's function is given by

$$\begin{aligned} G_{xx}(\hat{\mathbf{x}}) &= -A(\hat{\mathbf{x}}) - \hat{y} \frac{\partial A(\hat{\mathbf{x}})}{\partial \hat{y}} + 1, \\ G_{xy}(\hat{\mathbf{x}}) &= \hat{y} \frac{\partial A(\hat{\mathbf{x}})}{\partial \hat{x}}, \\ G_{yx}(\hat{\mathbf{x}}) &= \hat{y} \frac{\partial A(\hat{\mathbf{x}})}{\partial \hat{x}}, \\ G_{yy}(\hat{\mathbf{x}}) &= -A(\hat{\mathbf{x}}) + \hat{y} \frac{\partial A(\hat{\mathbf{x}})}{\partial \hat{y}}, \end{aligned} \quad (1)$$

where $\hat{\mathbf{x}} \equiv \mathbf{x} - \mathbf{x}_0$,

$$A(\hat{\mathbf{x}}) = \frac{1}{2} \ln\{2[\cosh(k(y - y_0)) - \cos(k(x - x_0))]\}, \quad (2)$$

$k = 2\pi/L$ is the wave number, and L is the period of the flow, that is, the separation between two consecutive singular points ([55], pp. 94 – 95).

Carrying out the differentiation, we find

$$\begin{aligned} \frac{\partial A(\hat{\mathbf{x}})}{\partial \hat{x}} &= \frac{1}{2} \frac{\sin[k(x - x_0)]}{\cosh[k(y - y_0)] - \cos[k(x - x_0)]}, \\ \frac{\partial A(\hat{\mathbf{x}})}{\partial \hat{y}} &= \frac{1}{2} \frac{\sinh[k(y - y_0)]}{\cosh[k(y - y_0)] - \cos[k(x - x_0)]}. \end{aligned} \quad (3)$$

The pressure Green's function is given by

$$p_x(\hat{\mathbf{x}}) = 2 \frac{\partial A(\hat{\mathbf{x}})}{\partial \hat{x}}, \quad p_y(\hat{\mathbf{x}}) = 2 \frac{\partial A(\hat{\mathbf{x}})}{\partial \hat{y}}. \quad (4)$$

The stress Green's function follows from equation (sgf_2d.4).

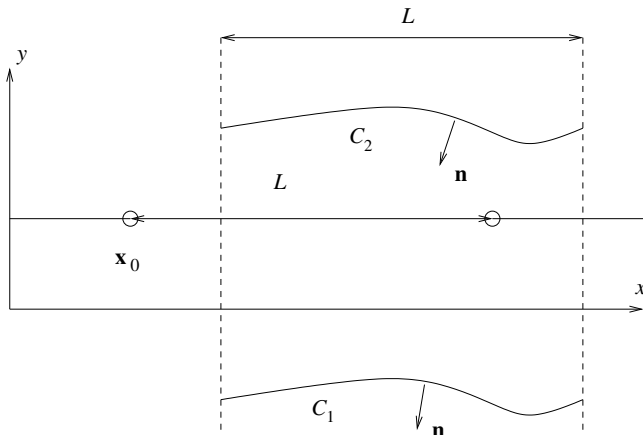


Figure sgf_2d_1p.1 A singly periodic array of point forces separated by the distance L along the x axis.

INTEGRAL IDENTITIES:

Consider two open contours C_1 and C_2 extending over one period of the flow, as illustrated in Figure sgf_2d_1p.1. The unit normal vector \mathbf{n} is oriented as shown in the figure. The stress Green's function satisfies the integral identities:

$$\int_{C_1} T_{ijk}(\mathbf{x}, \mathbf{x}_0) n_k(\mathbf{x}) dl(\mathbf{x}) = 2\pi \delta_{ij}, \quad (5)$$

$$\int_{C_1} T_{ijk}(\mathbf{x}_0, \mathbf{x}) n_k(\mathbf{x}) dl(\mathbf{x}) = -2\pi \delta_{ij}, \quad (6)$$

$$\int_{C_2} T_{ijk}(\mathbf{x}, \mathbf{x}_0) n_k(\mathbf{x}) dl(\mathbf{x}) = -2\pi \delta_{ij}, \quad (7)$$

$$\int_{C_2} T_{ijk}(\mathbf{x}_0, \mathbf{x}) n_k(\mathbf{x}) dl(\mathbf{x}) = -2\pi \delta_{ij}. \quad (8)$$

Call statement:**sgf_2d_1p**

$(Iopt$	<i>Input:</i> See Note 1.
$, x, y$	<i>Input:</i> Coordinates of the field point.
$, x_0, y_0$	<i>Input:</i> Coordinates of a singular point (point force).
$, L$	<i>Input:</i> Distance between the point forces (period).
$, G_{xx}, G_{xy}$	<i>Output:</i> Velocity Green's function.
$, G_{yx}, G_{yy}$	<i>Output:</i> Velocity Green's function.
$, p_x, p_y$	<i>Output:</i> Pressure Green's function.
$, T_{xxx}, T_{xxy}$	<i>Output:</i> Stress Green's function.
$, T_{yxx}, T_{yxy}$	<i>Output:</i> Stress Green's function.
$, T_{xyx}, T_{xyy}$	<i>Output:</i> Stress Green's function.
$, T_{yyy}, T_{yyy}$	<i>Output:</i> Stress Green's function.

Note:

1. Set $Iopt = 1$ to obtain only G_{ij} ; set $Iopt \neq 1$ to obtain G_{ij} , p_j , and T_{ijk} .

Numerical method:

The Green's function is computed by direct evaluation of expressions (1) to (4).

Driver: sgf_2d_w_dr

The driver evaluates the Green's function and verifies (a) the integral identities (sgf_2d.7,8), where C is a circular contour, and (b) the integral identities (5) to (8).

Files to be linked: None.

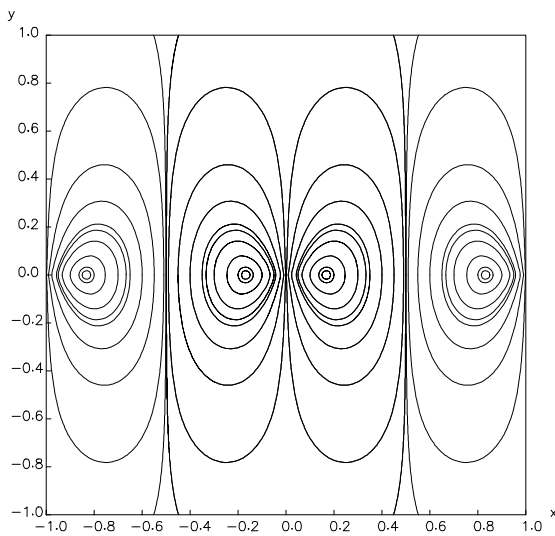
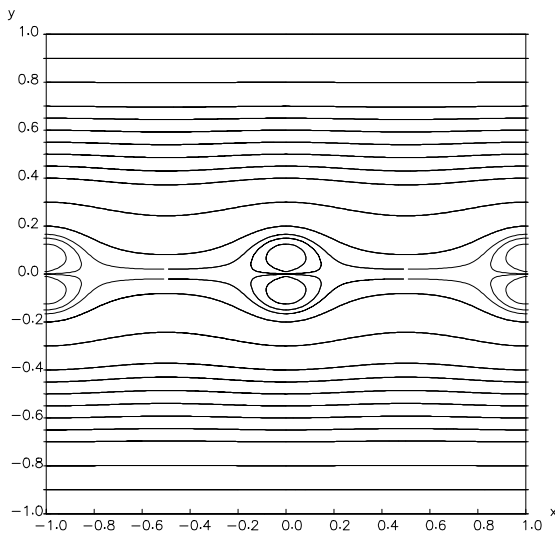


Figure sgf_2d_1p.2 Streamline pattern of the flow due to a periodic array of two-dimensional point forces oriented parallel (top) or normal (bottom) to the plane of the array.

Subroutine: sgf_2d_1p_w

This subroutine computes the singly periodic Green's function for flow in a semi-infinite domain bounded by a plane wall located at $y = \text{wall}$. The singular points are separated by the distance L along the x axis, as illustrated in Figure sgf_2d_1p_w.1. One of the point forces is located at the point $\mathbf{x}_0 = (x_0, y_0)$. The streamline pattern of the induced flow is depicted in Figure sgf_2d_1p_w.2

The velocity Green's function is given by

$$\begin{aligned} G_{ij}(\mathbf{x}, \mathbf{x}_0) &= G_{ij}^P(\mathbf{x} - \mathbf{x}_0) - G_{ij}^P(\mathbf{x} - \mathbf{x}_0^{Im}) \\ &\quad + 2 h_0^2 D_{ij}(\mathbf{x} - \mathbf{x}_0^{Im}) - 2 h_0 Q_{ij}(\mathbf{x} - \mathbf{x}_0^{Im}), \end{aligned} \quad (1)$$

([55], pp. 95 – 96), where:

- G_{ij}^P is the periodic Green's function computed by subroutine sgf_2d_1p.
- $\mathbf{x}_0^{Im} = (x_0, 2 \times \text{wall} - y_0)$ is the image of the point force with respect to the wall.
- $h_0 = y_0 - \text{wall}$ is the distance of the point force from the wall.
- The tensors D_{ij} and Q_{ij} represent, respectively, a periodic array of potential dipoles and point-force doublets, and are given by

$$\begin{aligned} D_{xx}(\mathbf{x}) &= A_{yy}, & D_{xy}(\mathbf{x}) &= A_{xy}, \\ D_{yx}(\mathbf{x}) &= -A_{xy}, & D_{yy}(\mathbf{x}) &= A_{yy}, \end{aligned} \quad (2)$$

and

$$\begin{aligned} Q_{xx}(\mathbf{x}) &= -y A_{yy}, & Q_{xy}(\mathbf{x}) &= -A_x - y A_{xy}, \\ Q_{yx}(\mathbf{x}) &= -A_x + y A_{xy}, & Q_{yy}(\mathbf{x}) &= Q_{xx}(\mathbf{x}) = -y A_{yy}, \end{aligned} \quad (3)$$

where a subscript denotes a partial derivative with respect to the corresponding variable. The function $A(\mathbf{x})$ is defined in equation (2) of subroutine sgf_2d_1p.

The pressure Green's function is given by

$$p_j(\mathbf{x}, \mathbf{x}_0) = p_j^P(\mathbf{x} - \mathbf{x}_0) - p_j^P(\mathbf{x} - \mathbf{x}_0^{Im}) - 2 h_0 p_j^Q(\mathbf{x} - \mathbf{x}_0^{Im}), \quad (4)$$

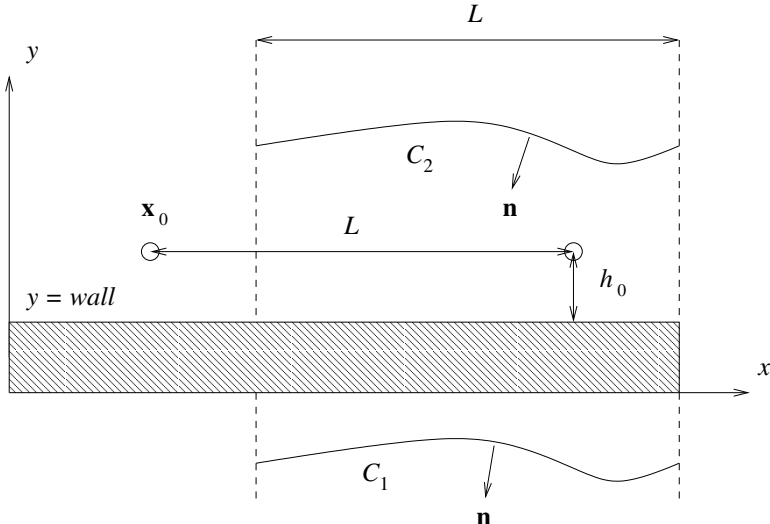


Figure sgf_2d_1p.w.1 A periodic array of point forces separated by the distance L along the x axis in a semi-infinite domain of flow bounded by a plane wall located at $y = \text{wall}$.

where p_j^P is the singly periodic pressure Green's function given in equations (4) of sgf_2d_1p, and

$$p_x^Q(\mathbf{w}) = 2 A_{xy}(\mathbf{w}), \quad p_y^Q(\mathbf{w}) = -2 A_{yy}(\mathbf{w}), \quad (5)$$

is the pressure field corresponding to the point-force doublets.

The stress Green's function follows from the preceding expressions and equation (sgf_2d.4).

INTEGRAL IDENTITIES:

Consider two open contours C_1 and C_2 extending over one period of the flow, as illustrated in Figure sgf_2d_1p.w.1. The unit normal vector \mathbf{n} is oriented as shown in the figure.

The stress Green's function satisfies the integral identities:

$$\int_{C_1} T_{ijk}(\mathbf{x}, \mathbf{x}_0) n_k(\mathbf{x}) dl(\mathbf{x}) = 0, \quad (6)$$

$$\int_{C_1} T_{ijk}(\mathbf{x}_0, \mathbf{x}) n_k(\mathbf{x}) dl(\mathbf{x}) = -4\pi \delta_{ij}, \quad (7)$$

$$\int_{C_2} T_{ijk}(\mathbf{x}, \mathbf{x}_0) n_k(\mathbf{x}) dl(\mathbf{x}) = -4\pi \delta_{ij}, \quad (8)$$

$$\int_{C_2} T_{ijk}(\mathbf{x}_0, \mathbf{x}) n_k(\mathbf{x}) dl(\mathbf{x}) = 0. \quad (9)$$

Call statement:

sgf_2d_1p_w

$(Iopt$	<i>Input:</i> See Note 1.
$, x, y$	<i>Input:</i> Coordinates of the field point.
$, x_0, y_0$	<i>Input:</i> Coordinates of a singular point (point force).
$, wall$	<i>Input:</i> The wall is located at $y = wall$.
$, L$	<i>Input:</i> Distance between the point forces (period L).
$, G_{xx}, G_{xy}$	<i>Output:</i> Velocity Green's function.
$, G_{yx}, G_{yy}$	<i>Output:</i> Velocity Green's function.
$, p_x, p_y$	<i>Output:</i> Pressure Green's function.
$, T_{xxx}, T_{xxy}$	<i>Output:</i> Stress Green's function.
$, T_{yxx}, T_{yxy}$	<i>Output:</i> Stress Green's function.
$, T_{xyx}, T_{xyy}$	<i>Output:</i> Stress Green's function.
$, T_{yyy}, T_{yyy}$	<i>Output:</i> Stress Green's function.

Note:

1. Set $Iopt = 1$ to obtain only G_{ij} ; set $Iopt \neq 1$ to obtain G_{ij} , p_j , and T_{ijk} .

Numerical method:

The Green's function is computed by direct evaluation of expressions (1) to (4).

Driver: sgf_2d_w_dr

The driver evaluates the Green's function and verifies (a) the integral identities (sgf_2d.7,8) where C is a circular contour, and (b) the integral identities (6) to (9).

Files to be linked: None.

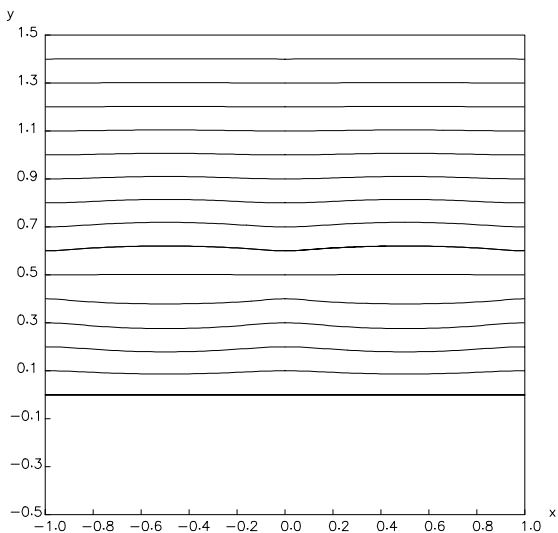
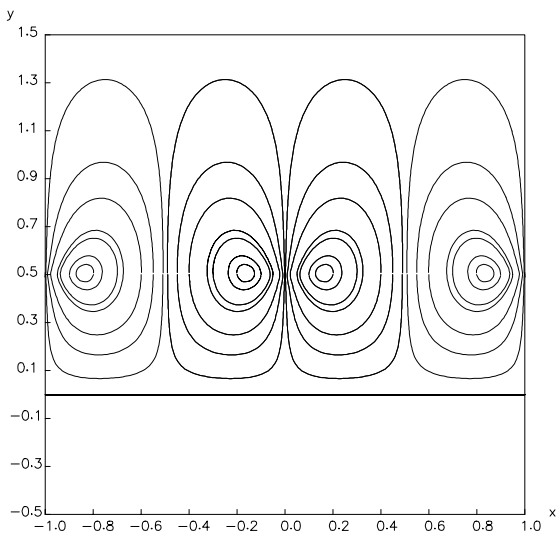


Figure sgf_2d_1p_w.2 Streamline pattern of the flow due to a periodic array of point forces oriented normal (top) and parallel (bottom) to a wall. In this case, the separation between the point forces is equal to twice their distance from the wall.

Subroutine: sgf_2d_1p_ww

This subroutine computes the singly periodic Green's function for flow in a channel bounded by two parallel plane walls located at $y = \pm h$, as illustrated in Figure sgf_2d_1p_ww.1. The singular points are deployed along the x axis and are separated by the distance L . One of the point forces is located at the point $\mathbf{x}_0 = (x_0, y_0)$. The streamline pattern of the induced flow is depicted in Figure sgf_2d_ww.2.

Closed-form but lengthy expressions for the Green's function are given in References [73] and [55] (pp. 96 – 99). The Green's function for channel flow has one degree of freedom; an arbitrary parabolic flow accompanied by a pressure drop may be added to G_{xx} and p_x to yield another perfectly acceptable Green's function. To remove this ambiguity, either the flow rate along the channel or the pressure drop across each period must be specified.

Call statement:

sgf_2d_1p_ww

(<i>Iopt</i>	<i>Input:</i> See Note 1.
, <i>Iqpd</i>	<i>Input:</i> See Note 2.
, <i>x</i> , <i>y</i>	<i>Input:</i> Coordinates of the field point.
, <i>x</i> ₀ , <i>y</i> ₀	<i>Input:</i> Coordinates of a singular point (point force).
, <i>L</i>	<i>Input:</i> Distance between the point forces (period).
, <i>N</i>	<i>Input:</i> See Note 3.
, <i>h</i>	<i>Input:</i> Channel semi-width.
, <i>G</i> _{xx} , <i>G</i> _{xy}	<i>Output:</i> Velocity Green's function.
, <i>G</i> _{yx} , <i>G</i> _{yy}	<i>Output:</i> Velocity Green's function.
, <i>p</i> _x , <i>p</i> _y	<i>Output:</i> Pressure Green's function.
, <i>T</i> _{xxx} , <i>T</i> _{xyy}	<i>Output:</i> Stress Green's function.
, <i>T</i> _{yxz} , <i>T</i> _{yyz}	<i>Output:</i> Stress Green's function.
, <i>T</i> _{xyx} , <i>T</i> _{xyy}	<i>Output:</i> Stress Green's function.
, <i>T</i> _{yyx} , <i>T</i> _{yyy})	<i>Output:</i> Stress Green's function.

Notes:

1. Set *Iopt* = 1 to obtain only G_{ij} ; set *Iopt* \neq 1 to obtain G_{ij} , p_j , and T_{ijk} .
2. Set *Iqpd* = 0 to obtain a Green's function with zero pressure drop, but non-zero flow rate. Set *Iqpd* = 1 to obtain a Green's function with zero flow rate, but non-zero pressure drop.
3. The Green's function is defined in terms of infinite series, as discussed in Reference [55], pp. 96 – 99 (see also [73]). The integer *N* is the truncation limit for summing in real space.

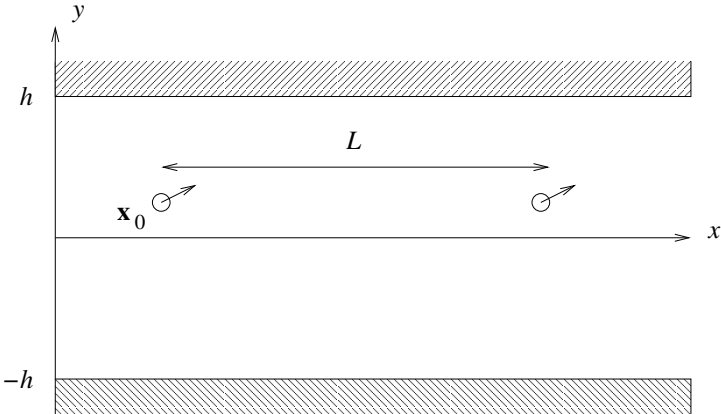


Figure sgf_2d_1p_ww.1 A singly periodic array of point forces separated by the distance L along the x axis in a two-dimensional channel bounded by two parallel plane walls located at $y = \pm h$.

FLOW RATE OF THE INDUCED FLOW:

Consider a periodic array of point forces with strength \mathbf{b} , and assume that the pressure drop of the induced flow vanishes across each period. The corresponding axial flow rate is given by

$$Q = \frac{2\pi h^2}{L\mu} \left(1 - \frac{y_0^2}{h^2}\right) b_x, \quad (1)$$

where μ is the fluid viscosity, and y_0 is the lateral position of a point force. Note that, when the point forces are placed on either wall, $y_0 = \pm h$, the flow vanishes and the flow rate ceases.

Numerical method:

The Green's function is computed by direct evaluation of expressions provided in Reference [55] (pp. 96 – 99).

An option is provided for computing the Green's function by trilinear interpolation with respect to y_0 , y , and $x - x_0$, where (x_0, y_0) are the coordinates of one point force in the periodic array, and (x, y) are the coordinates of the evaluation point. Interpolation is carried out for the desingularized component of the Green's function

$$\begin{aligned} G'_{ij} &\equiv G^{2D-1P-WW}_{ij}(x, y, x_0, y_0) - G^{2D-1P-W}_{ij}(x, y, x_0, y_0; +h) \\ &\quad - G^{2D-1P-W}_{ij}(x, y, x_0, y_0; -h) + G^{FS}_{ij}(x, y, x_0, y_0), \end{aligned} \quad (2)$$

where $G_{ij}^{2D-1P-W}(x, y, x_0, y_0; w)$ is the singly periodic Green's function of Stokes flow in a semi-infinite domain bounded by a plane wall located at $y = w$, and $G_{ij}^{FS}(x, y, x_0, y_0)$ is the free-space Green's function. The components of the desingularized Green's function G'_{ij} behave smoothly near the point force and in the vicinity of either wall, and this benefits the accuracy of the interpolation.

The complementary components expressed by the three terms on the right-hand side of (11) are available in closed form and are computed by direct evaluation [55].

The look-up tables for interpolating the desingularized Green's function G'_{ij} are generated by program `sgf_2d_1p_ww_glut` included in this directory.

Driver: `sgf_2d_1p_ww_dr`

The driver performs pointwise evaluations, tests the integral identities (`sgf_2d.7,8`) and generates velocity, pressure, and stress field profiles. Input data are read from the file `sgf_2d_1p_ww.dat`.

The Green's function is evaluated either directly or by trilinear interpolation through look-up tables. When the Green's function is computed by interpolation, the driver reads the look-up tables from the file `sgf_2d_1p_ww_glut` which is generated by program `sgf_2d_1p_ww_glut` included in this directory.

Files to be linked: None for the subroutine.

The driver must be linked with subroutine `sgf_2d_1p_ww_int` that evaluates the Green's function by interpolation through look-up tables, and also with subroutines `sgf_2d_1p_w` and `sgf_2d_fs` that evaluate Green's functions.

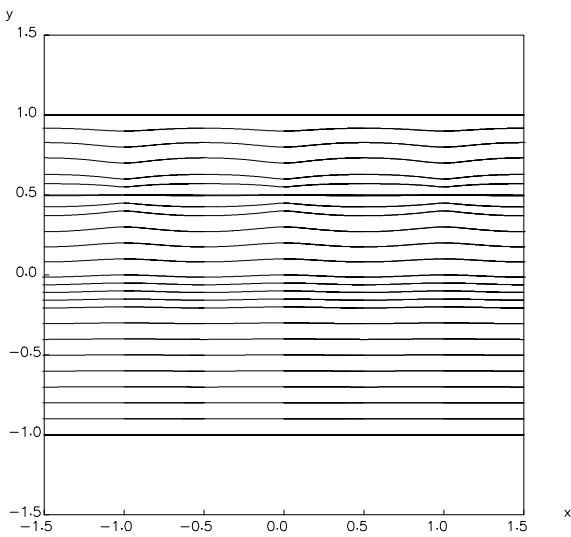
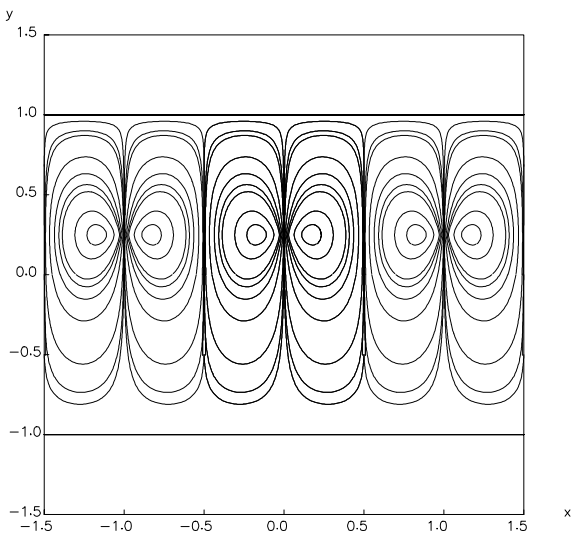


Figure sgf_2d_1p_ww.2 Streamline pattern of the flow due to a periodic array of two-dimensional point forces in a channel. The point forces are oriented normal (top) or parallel (bottom) to the walls. The pressure drop over each period vanishes in both cases ($I_{qpd} = 0$).

Subroutine: sgf_2d_2p

This subroutine computes the doubly-periodic Green's function of two-dimensional Stokes flow. The point forces are deployed at the vertices of a two-dimensional lattice defined by the base vectors $\mathbf{a}^{(1)}$ and $\mathbf{a}^{(2)}$, as depicted in Figure sgf_2d_2p.1. The streamline pattern of the induced flow is depicted in Figure sgf_2d_2p.2.

One of the point forces is located at the point $\mathbf{x}_0 = (x_0, y_0)$, and the n th point force is located at the point $\mathbf{x}^{(n)} = (x_n, y_n)$, where

$$x^{(n)} = x_0 + i a_x^{(1)} + j a_x^{(2)}, \quad y^{(n)} = y_0 + i a_y^{(1)} + j a_y^{(2)}, \quad (1)$$

i and j are two integers, and the index n is defined in terms of the indices i and j by double summation.

Following the Ewald summation method, we find that the velocity Green's function is given by [68]

$$\begin{aligned} G_{ij}(\mathbf{x}, \mathbf{x}_0) &= \sum_n \{ \delta_{ij} \left[\frac{1}{2} E(\hat{r}_n^2) - \exp(-\hat{r}_n^2) \right] + \frac{(x_i - x_i^{(n)})(x_j - x_j^{(n)})}{r_n^2} e^{-\hat{r}_n^2} \} \\ &\quad + \frac{\pi}{A_c} \sum_m \frac{4 + \hat{k}^{(m)2}}{k^{(m)2}} \left(\delta_{ij} - \frac{k_i^{(m)} k_j^{(m)}}{k^{(m)2}} \right) \\ &\quad \times \exp\left(-\frac{1}{4} \hat{k}^{(m)2}\right) \cos[\mathbf{k}^{(m)} \cdot (\mathbf{x} - \mathbf{x}_0)]. \end{aligned} \quad (2)$$

The first sum on the right-hand side of (2) with respect to n runs over the point forces, and the second sum with respect to m runs over the vertices of the reciprocal lattice in wave-number space. The base vectors of the reciprocal lattice are given by

$$\mathbf{b}^{(1)} = \frac{2\pi}{A_c} \mathbf{a}^{(2)} \times \mathbf{e}_z, \quad \mathbf{b}^{(2)} = \frac{2\pi}{A_c} \mathbf{e}_z \times \mathbf{a}^{(1)}, \quad (3)$$

where $A_c = |\mathbf{a}^{(1)} \times \mathbf{a}^{(2)}|$ is the area of the unit cell in physical space.

The vertices of the reciprocal lattice are located at $\mathbf{k}^{(m)} = (k_x^{(m)}, k_y^{(m)})$, where

$$k_x^{(m)} = i b_x^{(1)} + j b_x^{(2)}, \quad k_y^{(m)} = i b_y^{(1)} + j b_y^{(2)}, \quad (4)$$

i and j are two integers, and the index m is defined in terms of i and j using double-summation. The singular wave number corresponding to $i = 0$ and $j = 0$ is excluded from the second sum in (2).

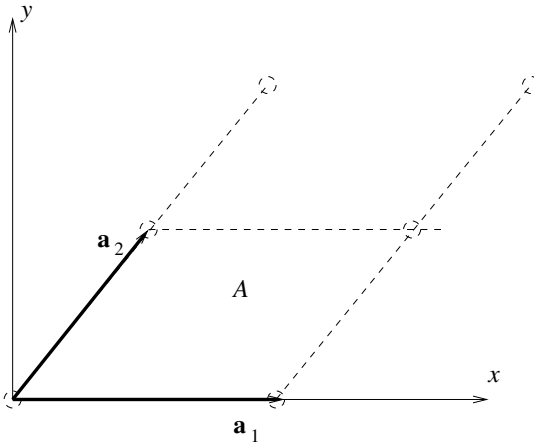


Figure sgf_2d_2p.1 A doubly periodic array of two-dimensional point forces deployed at the vertices of a two-dimensional lattice parallel to the xy plane.

The rest of the symbols in (2) are defined as follows:

- $r_n = \sqrt{(x - x_n)^2 + (y - y_n)^2}$ is the distance of the evaluation point from the n th point force, and $\hat{r}_n = \xi r_n$ is the corresponding reduced dimensionless distance.
- $k^{(m)} = |\mathbf{k}^{(m)}|$ is the length of the m th wave number vector, and $\hat{k}^{(m)} \equiv k^{(m)}/\xi$ is the reduced length of the m th wave number.
- E is the exponential integral computed by accurate polynomial approximations.
- ξ is the Ewald splitting parameter with dimensions of inverse length, determining the balance of the sums in real and reciprocal space.

The right-hand side of (2) is independent of the selected value of ξ . As ξ tends to zero, we obtain a representation in terms of sums in real space alone, whereas as ξ tends to infinity, we obtain a representation in terms of a double Fourier series in reciprocal wave number space.

The pressure Green's function is given by [68]

$$\begin{aligned}
 p_j(\mathbf{x}, \mathbf{x}_0) &= \frac{4\pi}{A_c} (x_j - x_{0_j}) + 2 \sum_n \frac{x_j - x_j^{(n)}}{r_n^2} e^{-\hat{r}_n^2} \\
 &\quad + \frac{4\pi}{A_c} \sum_m \frac{k_j^{(m)}}{\hat{k}^{(m)2}} \exp(-\frac{1}{4}\hat{k}^{(m)2}) \sin[\mathbf{k}^{(m)} \cdot (\mathbf{x} - \mathbf{x}_0)].
 \end{aligned} \tag{5}$$

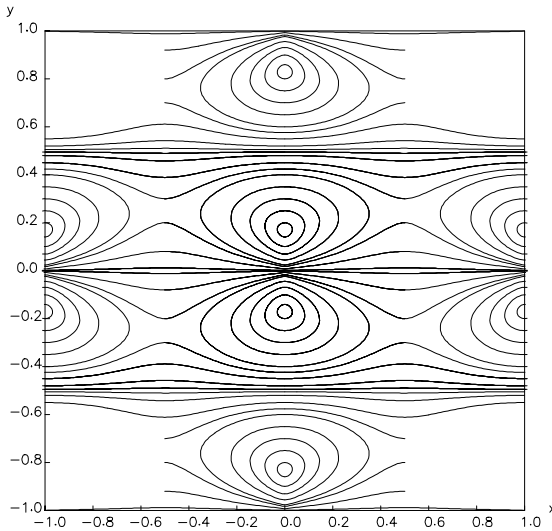


Figure sgf_2d_2p.2 Streamlines of the flow due to a doubly periodic array of two-dimensional point forces located at the vertices of a square lattice in the xy plane.

The first term on the right-hand side of (5) contributes a linear pressure field that balances the force imparted to the fluid by the point forces, thereby satisfying the force balance over each periodic cell.

The stress Green's function is given by [68]

$$\begin{aligned}
 T_{ijl}(\mathbf{x}, \mathbf{x}_0) = & -\delta_{il} \frac{4\pi}{A_c} (x_j - x_{0j}) + 2\xi^2 \sum_n [\delta_{jl}(x_i - x_i^{(n)}) + \delta_{ij}(x_l - x_l^{(n)}) \\
 & - 2(1 + \frac{1}{\hat{r}_n^2}) \frac{(x_i - x_i^{(n)})(x_j - x_j^{(n)})(x_l - x_l^{(n)})}{r_n^2}] e^{-\hat{r}_n^2} \\
 & + \frac{4\pi}{A_c} \sum_m \left[\frac{1}{k^{(m)}} \left(1 + \frac{\hat{k}^{(m)2}}{4} \right) \left(2 \frac{k_i^{(m)} k_j^{(m)} k_l^{(m)}}{k^{(m)3}} - \frac{\delta_{ij} k_l^{(m)} + \delta_{lj} k_i^{(m)}}{k^{(m)}} \right) \right. \\
 & \left. - \delta_{il} \frac{k_j^{(m)}}{k^{(m)}} \right] \exp \left(-\frac{1}{4} \hat{k}^{(m)2} \right) \sin [\mathbf{k}^{(m)} \cdot (\mathbf{x} - \mathbf{x}_0)]. \quad (6)
 \end{aligned}$$

The first term on the right-hand side of (6) incorporates the linear variation of the normal stresses due to the pressure.

It is reassuring to confirm that, in terms of the stress tensor, the Green's function for the pressure is given by

$$p_j(\mathbf{x}, \mathbf{x}_0) = -\frac{1}{2} T_{iji}(\mathbf{x}, \mathbf{x}_0), \quad (7)$$

as required by the Newtonian constitutive equation.

Call statement:

`sgf_2d_2p`

$(Iopt$	<i>Input:</i> See Note 1.
$, x, y$	<i>Input:</i> Coordinates of the field point.
$, x_0, y_0$	<i>Input:</i> Coordinates of one singular point (point force).
$, a_{11}, a_{12}$	<i>Input:</i> Coordinates of the first base vector.
$, a_{21}, a_{22}$	<i>Input:</i> Coordinates of the second base vector.
$, b_{11}, b_{12}$	<i>Input:</i> Coordinates of the first reciprocal base vector.
$, b_{21}, b_{22}$	<i>Input:</i> Coordinates of the second reciprocal base vector.
$, ew$	<i>Input:</i> Ewald splitting parameter ξ .
$, area$	<i>Input:</i> Area of the unit cell in the xy plane.
$, Max_1, Max_2$	<i>Input:</i> Summation limits in real and reciprocal space.
$, G_{xx}, G_{xy}$	<i>Output:</i> Velocity Green's function.
$, G_{yx}, G_{yy}$	<i>Output:</i> Velocity Green's function.
$, p_x, p_y$	<i>Output:</i> Pressure Green's function.
$, T_{xxx}, T_{xxy}$	<i>Output:</i> Stress Green's function.
$, T_{yxx}, T_{yyx}$	<i>Output:</i> Stress Green's function.
$, T_{xyx}, T_{xyy}$	<i>Output:</i> Stress Green's function.
$, T_{yyx}, T_{yyy}$	<i>Output:</i> Stress Green's function.

Note:

1. Set $Iopt = 1$ to obtain only G_{ij} ; set $Iopt \neq 1$ to obtain G_{ij} , p_j , and T_{ijk} .

PREREQUISITES:

Subroutines `ewald_2d`, `qqq_2d`, and `vvv_2d` must be called *in this particular order*, before subroutine `sgf_2d_2p`, as shown in the driver.

When multiple Green's function evaluations with the same lattice base vectors are to be performed, it is not necessary to call the three subroutines each time, but just once before the first evaluation.

Calling `vvv_2d` is necessary only if the pressure and stress Green's functions are required ($Iopt = 2$).

Subroutine ewald_2d:

This subroutine produces the reciprocal base vectors \mathbf{b}_1 and \mathbf{b}_2 in wave number space, and the area of the unit cell of the lattice in real space. It also returns a recommended value for the Ewald parameter ξ . The call statement is:

ewald_2p

(a_{11}, a_{12} *Input*: Coordinates of the first base vector.
 $, a_{21}, a_{22}$ *Input*: Coordinates of the second base vector.
 $, b_{11}, b_{12}$ *Output*: Coordinates of the first reciprocal base vector.
 $, b_{21}, b_{22}$ *Output*: Coordinates of the second reciprocal base vector.
 $, ew$ *Output*: Ewald splitting parameter ξ .
 $, area$) *Output*: Area of the unit cell in the xy plane.

Subroutine qqq_2d:

This subroutine produces a matrix used for computing the velocity Green's function G_{ij} by summing in the wave number space. The call statement is:

qqq_2p

(b_{11}, b_{12} *Input*: Coordinates of the first reciprocal base vector.
 $, b_{21}, b_{22}$ *Input*: Coordinates of the second reciprocal base vector.
 $, Max_2$ *Input*: Summation limit in wave number space.
 $, ew)$ *Input*: Ewald splitting parameter ξ .

The output is passed through a common block, as shown in the source code.

Subroutine vvv_2d:

This subroutine produces a matrix used for computing the pressure and stress Green's functions p_i and T_{ijk} by summing in the wave number space. The call statement is:

vvv_2p

(b_{11}, b_{12} *Input*: Coordinates of the first reciprocal base vector.
 $, b_{21}, b_{22}$ *Input*: Coordinates of the second reciprocal base vector.
 $, Max_2$ *Input*: Summation limit in wave number space.
 $, ew)$ *Input*: Ewald splitting parameter ξ .

The output is passed through a common block, as shown in the source code.

Numerical method:

The Green's function is computed by direct evaluation using expressions (1) to (6).

An option is provided for computing the Green's function by trilinear interpolation

with respect to $x - x_0$, $y - y_0$, and a_{21} , where (x_0, y_0) are the coordinates of one point force in the periodic array, and (x, y) are the coordinates of the evaluation point. It is assumed that all lengths have been scaled, and the orientation of the lattice has been chosen so that $a_{11} = 1$, $a_{12} = 0$ and $a_{22} = 1$.

The look-up tables are generated by program `sgf_2d_2p_glut` included in this directory.

Driver: `sgf_2d_2p_dr`

The driver performs pointwise evaluations and tests the integral identities (sgf_2d.7,8). Input data are read from the file `sgf_2d_2p.dat`.

The Green's function is evaluated either directly or by trilinear interpolation through look-up tables. When the Green's function is computed by trilinear interpolation, the driver reads the look-up tables from the file `sgf_2d_2p.glut` which is generated by program `sgf_2d_2p_glut` included in this directory.

Files to be linked:

The main subroutine must be linked with subroutine `exp_int` that evaluates the exponential integral E_1 .

The driver must be linked with subroutine `sgf_2d_2p_int` that computes the Green's function by interpolation through look-up tables.

Directory: `stokes/sgf_3d`

The velocity, pressure, and stress Green's functions of three-dimensional Stokes flow, denoted respectively, by G_{ij} , p_j , and T_{ijk} , where the indices range over 1, 2, and 3 corresponding to x , y , and z , are defined such that the velocity field at the field point $\mathbf{x} = (x, y, z)$ induced by a three-dimensional point force with strength \mathbf{b} placed at the singular point $\mathbf{x}_0 = (x_0, y_0, z_0)$ is given by

$$u_i(\mathbf{x}) = \frac{1}{8\pi\mu} G_{ij}(\mathbf{x}, \mathbf{x}_0) b_j = \frac{1}{8\pi\mu} G_{ji}(\mathbf{x}_0, \mathbf{x}) b_j, \quad (\text{sgf_3d.1})$$

where μ is the fluid viscosity. The associated pressure and stress fields are given by

$$p(\mathbf{x}) = \frac{1}{8\pi} p_j(\mathbf{x}, \mathbf{x}_0) b_j, \quad (\text{sgf_3d.2})$$

and

$$\sigma_{ik}(\mathbf{x}) = \frac{1}{8\pi} T_{ijk}(\mathbf{x}, \mathbf{x}_0) b_j. \quad (\text{sgf_3d.3})$$

Using the Newtonian constitutive equation, we find

$$T_{ijk} = \delta_{ik} p_j + \frac{\partial G_{ij}}{\partial x_k} + \frac{\partial G_{kj}}{\partial x_i}. \quad (\text{sgf_3d.4})$$

By definition, the velocity and pressure Green's functions satisfy the equations

$$\frac{\partial G_{ij}}{\partial x_i} = 0, \quad (\text{sgf_3d.5})$$

$$-\frac{\partial p_j}{\partial x_i} + \left(\frac{\partial^2 G_{ij}}{\partial x^2} + \frac{\partial^2 G_{ij}}{\partial y^2} + \frac{\partial^2 G_{ij}}{\partial z^2} \right) = -8\pi \delta_{ij} \delta_3(\mathbf{x} - \mathbf{x}_0),$$

originating, respectively, from the continuity equation and the Stokes equation; δ_{ij} is Kronecker's delta, and δ_3 is Dirac's delta function in three dimensions.

Correspondingly, the stress Green's function satisfies the equation

$$\frac{\partial T_{ijk}}{\partial x_k} = \frac{\partial T_{kji}}{\partial x_k} = -8\pi \delta_{ij} \delta_3(\mathbf{x} - \mathbf{x}_0). \quad (\text{sgf_3d.6})$$

INTEGRAL IDENTITIES:

Mass conservation expressed by the continuity equation requires that the velocity Green's functions satisfy the integral identity

$$\int_D n_i(\mathbf{x}) G_{ij}(\mathbf{x}, \mathbf{x}_0) dS(\mathbf{x}) = 0, \quad (\text{sgf_3d.7})$$

where D is a closed surface enclosing a control volume V_c . To derive (sgf_3d.7), we integrate the first equation of (sgf_3d.5) over V_c , and use the divergence theorem to convert the volume integral to a surface integral.

The stress Green's functions satisfy the integral identity

$$\int_D T_{ijk}(\mathbf{x}, \mathbf{x}_0) n_k(\mathbf{x}) dS(\mathbf{x}) = \begin{cases} \delta_{ij} & \text{when } \mathbf{x}_0 \text{ is inside } D \\ \frac{1}{2} \delta_{ij} & \text{when } \mathbf{x}_0 \text{ is on } D \\ 0 & \text{when } \mathbf{x}_0 \text{ is outside } D \end{cases}, \quad (\text{sgf_3d.8})$$

originating from the second of (sgf_3d.5), where the normal vector \mathbf{n} points *into* the control volume enclosed by the surface D . When the point \mathbf{x}_0 is located on D , the principal-value integral is implied on the left-hand side of (sgf_3d.8).

BOUNDARY-INTEGRAL REPRESENTATION:

The boundary-integral representation for the velocity of a three-dimensional Stokes flow is

$$\begin{aligned} u_j(\mathbf{x}_0) = & -\frac{1}{8\pi\mu} \int_D G_{ji}(\mathbf{x}_0, \mathbf{x}) f_i(\mathbf{x}) dS(\mathbf{x}) \\ & + \frac{1}{8\pi} \int_D u_i(\mathbf{x}) T_{ijk}(\mathbf{x}, \mathbf{x}_0) n_k(\mathbf{x}) dS(\mathbf{x}), \end{aligned} \quad (\text{sgf_3d.9})$$

where D is the collection of all surfaces enclosing a selected control volume in the flow, \mathbf{n} is the unit vector normal to D pointing into the control volume, and $\mathbf{f} \equiv \sigma \cdot \mathbf{n}$ is the boundary traction.

BOUNDARY-INTEGRAL EQUATION:

The boundary-integral equation corresponding to (sgf_3d.9) is

$$\begin{aligned} u_j(\mathbf{x}_0) = & -\frac{1}{4\pi\mu} \int_D G_{ji}(\mathbf{x}_0, \mathbf{x}) f_i(\mathbf{x}) dS(\mathbf{x}) \\ & + \frac{1}{4\pi} \int_D^{PV} u_i(\mathbf{x}) T_{ijk}(\mathbf{x}, \mathbf{x}_0) n_k(\mathbf{x}) dS(\mathbf{x}), \end{aligned} \quad (\text{sgf_3d.10})$$

where the point \mathbf{x}_0 lies on D , and PV denotes the principal-value integral.

DIRECTORY CONTENTS:

This directory contains a suite of subroutines that evaluate the following family of Green's functions:

Subroutine	Topic
<code>sgf_3d_fs</code>	Green's function for flow in free space.
<code>sgf_3d_w</code>	Green's function for flow in a semi-infinite domain bounded by an infinite plane wall.
<code>sgf_3d_sph</code>	Green's function for flow in the exterior of a sphere.
<code>sgf_3d_2p</code>	Doubly periodic Green's function.
<code>sgf_3d_3p</code>	Triply periodic Green's function.

Subroutine: sgf_3d_fs

This subroutine computes the Green's function for an infinite domain of flow in the absence of boundaries. The streamline pattern of the induced flow is depicted in Figure sgf_3d_fs.1.

The Green's function is given by

$$\begin{aligned} G_{ij}(\hat{\mathbf{x}}) &= \frac{\delta_{ij}}{r} + \frac{\hat{x}_i \hat{x}_j}{r^3}, \\ p_j(\hat{\mathbf{x}}) &= 2 \frac{\hat{x}_j}{r^3}, \\ T_{ijk}(\hat{\mathbf{x}}) &= -6 \frac{\hat{x}_i \hat{x}_j \hat{x}_k}{r^5}, \end{aligned} \quad (1)$$

where $\hat{\mathbf{x}} \equiv \mathbf{x} - \mathbf{x}_0$ and $r = |\mathbf{x} - \mathbf{x}_0|$ are the vectorial and scalar distance of the field point \mathbf{x} from the singular point \mathbf{x}_0 , respectively.

Call statement:

sgf_3d_fs

(Iopt	<i>Input:</i> See Note 1.
, x, y, z	<i>Input:</i> Coordinates of the field point.
, x ₀ , y ₀ , z ₀	<i>Input:</i> Coordinates of the singular point (point force).
, G _{xx} , G _{xy} , G _{xz}	<i>Output:</i> Velocity Green's function.
, G _{yx} , G _{yy} , G _{yz}	<i>Output:</i> Velocity Green's function.
, G _{zx} , G _{zy} , G _{zz}	<i>Output:</i> Velocity Green's function.
, p _x , p _y , p _z	<i>Output:</i> Pressure Green's function.
, T _{xxx} , T _{xyx} , T _{xzx}	<i>Output:</i> Stress Green's function.
, T _{yxy} , T _{yxz} , T _{zxz}	<i>Output:</i> Stress Green's function.
, T _{xyx} , T _{xyy} , T _{xyz}	<i>Output:</i> Stress Green's function.
, T _{yyy} , T _{yyz} , T _{zyz}	<i>Output:</i> Stress Green's function.
, T _{xzx} , T _{xzy} , T _{xzz}	<i>Output:</i> Stress Green's function.
, T _{zyz} , T _{yzz} , T _{zzz})	<i>Output:</i> Stress Green's function.

Note:

1. Set Iopt = 1 to obtain only G_{ij} ; set Iopt ≠ 1 to obtain G_{ij} , p_j , and T_{ijk} .

Numerical method:

The Green's function is computed by direct evaluation of expressions (1).

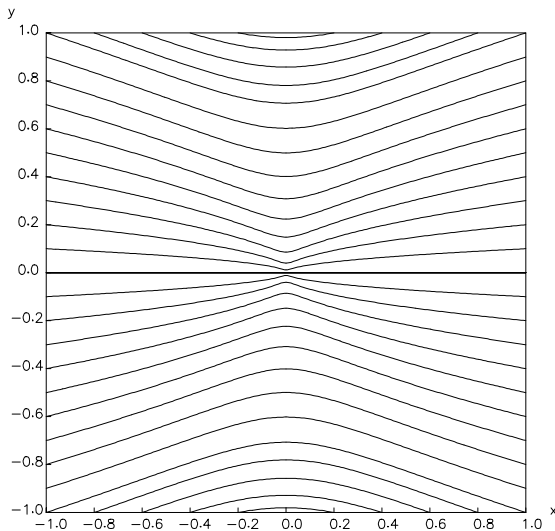


Figure sgf_3d_fs.1 Streamlines of the flow induced by a three-dimensional point force oriented along the x axis, in free space.

Driver: sgf_3d_fs_dr

The driver evaluates the Green's function and verifies the integral identities (sgf_3d.7,8), where D is the surface of a sphere.

Files to be linked: None for the subroutine.

The driver is linked with subroutine gauss_sph which contains tables of quadrature base points and weights for integration over the surface of a sphere.

Subroutine: sgf_3d_w

This subroutine computes the Green's function for a semi-infinite domain of flow bounded by a plane wall located at $x = \text{wall}$, as illustrated in Figure sgf_3d_w.1. The streamline pattern of the induced flow is depicted in Figure sgf_3d_w.2.

The velocity Green's function is given by

$$\begin{aligned} G_{ij}(\mathbf{x}, \mathbf{x}_0) &= G_{ij}^{FS}(\mathbf{x} - \mathbf{x}_0) - G_{ij}^{FS}(\mathbf{x} - \mathbf{x}_0^{Im}) \\ &\quad + 2 h_0^2 D_{ij}(\mathbf{x} - \mathbf{x}_0^{Im}) - 2 h_0 Q_{ij}(\mathbf{x} - \mathbf{x}_0^{Im}), \end{aligned} \quad (1)$$

[7, 8] (see also Reference [55], p. 84), where:

- G_{ij}^{FS} is the free-space Green's function.
- $\mathbf{x}_0^{Im} = (2 \times \text{wall} - x_0, y_0, z_0)$ is the image of the point force with respect to the wall.
- $h_0 = x_0 - \text{wall}$ is the distance of the point force from the wall.
- The tensors D_{ij} and Q_{ij} represent, respectively, potential dipoles and point-force doublets, and are given by

$$\begin{aligned} D_{ij}(\mathbf{w}) &= \pm \frac{\partial}{\partial w_i} \left(\frac{w_j}{|\mathbf{w}|^3} \right) = \pm \left(\frac{\delta_{ij}}{|\mathbf{w}|^3} - 3 \frac{w_i w_j}{|\mathbf{w}|^5} \right), \\ Q_{ij}(\mathbf{w}) &= \pm \frac{\partial G_{i1}^{FS}}{\partial w_j} = w_1 D_{ij} \pm \frac{\delta_{j1} w_i - \delta_{i1} w_j}{|\mathbf{w}|^3}. \end{aligned} \quad (2)$$

The minus sign applies for $j = 1$, corresponding to the x direction, and the minus sign applies for $j = 2, 3$, corresponding to the y and z directions.

The pressure Green's function is given by

$$p_j(\mathbf{x}, \mathbf{x}_0) = p_j^{FS}(\mathbf{x} - \mathbf{x}_0) - p_j^{FS}(\mathbf{x} - \mathbf{x}_0^{Im}) - 2 h_0 p_j^Q(\mathbf{x} - \mathbf{x}_0^{Im}), \quad (3)$$

where p_j^{FS} is the free-space pressure Green's function, and

$$\begin{aligned} p_x^Q(\mathbf{w}) &= -2 \frac{-2 w_x^2 + w_y^2 + w_z^2}{|\mathbf{w}|^5}, \\ p_y^Q(\mathbf{w}) &= -6 \frac{w_x w_y}{|\mathbf{w}|^5}, \quad p_z^Q(\mathbf{w}) = -6 \frac{w_x w_z}{|\mathbf{w}|^5}, \end{aligned} \quad (4)$$

is the pressure field corresponding to the point-force doublets.

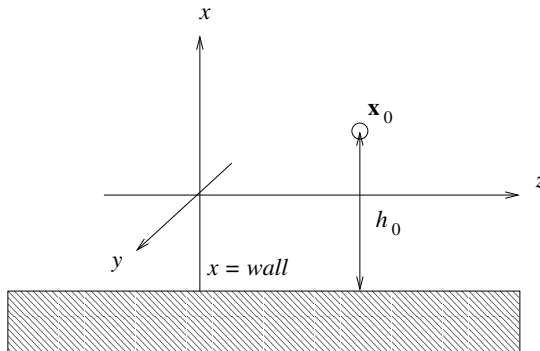


Figure sgf_3d_w.1 Flow due to a point force in semi-infinite domain bounded by a plane wall located at $x = \text{wall}$.

The stress Green's function follows from the preceding expressions and equation (sgf_3d.4).

Call statement:

sgf_3d_w

(Iopt	Input: See Note 1.
, \$x, y, z\$	Input: Coordinates of the field point.
, \$x_0, y_0, z_0\$	Input: Coordinates of the singular point (point force).
, wall	Input: The wall is located at $x = \text{wall}$.
, \$G_{xx}, G_{xy}, G_{xz}\$	Output: Velocity Green's function.
, \$G_{yx}, G_{yy}, G_{yz}\$	Output: Velocity Green's function.
, \$G_{zx}, G_{zy}, G_{zz}\$	Output: Velocity Green's function.
, \$p_x, p_y, p_z\$	Output: Pressure Green's function.
, \$T_{xxx}, T_{xxy}, T_{xxz}\$	Output: Stress Green's function.
, \$T_{yxy}, T_{yxz}, T_{zzz}\$	Output: Stress Green's function.
, \$T_{xyx}, T_{xyy}, T_{xyz}\$	Output: Stress Green's function.
, \$T_{yyy}, T_{yyz}, T_{zyz}\$	Output: Stress Green's function.
, \$T_{zxz}, T_{xzy}, T_{xzz}\$	Output: Stress Green's function.
, \$T_{zyz}, T_{yzz}, T_{zzz}\$)	Output: Stress Green's function.

Note:

1. Set $Iopt = 1$ to obtain only G_{ij} ; set $Iopt \neq 1$ to obtain G_{ij} , p_j , and T_{ijk} .

Numerical method:

The Green's function is computed by direct evaluation of expressions (1) to (4).

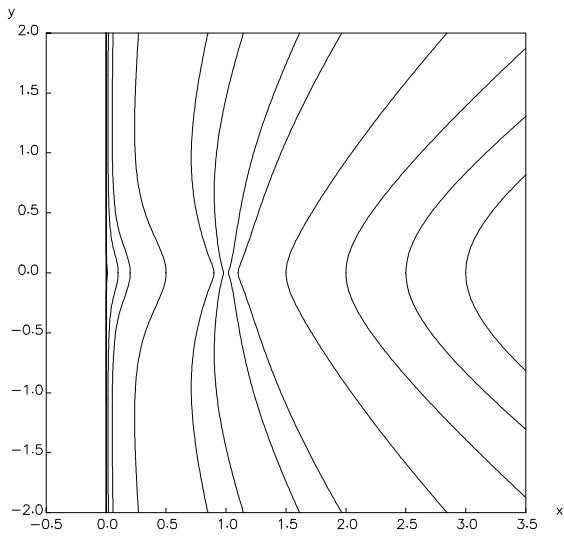
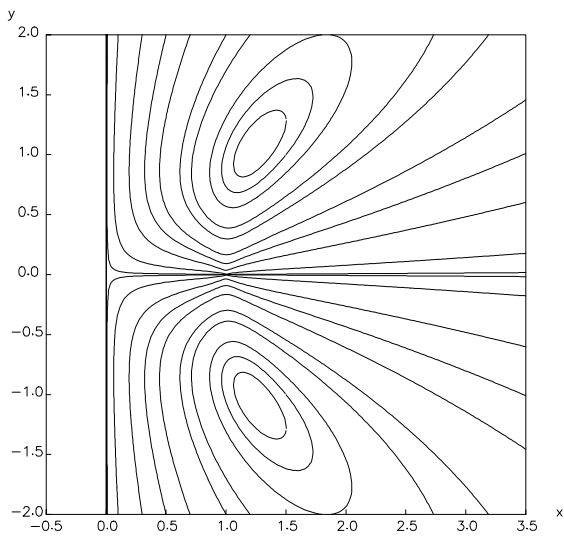


Figure sgf_3d_w.2 Streamline pattern of the flow induced by a three-dimensional point force oriented normal (top) or parallel (bottom) to a plane wall located at $x = 0$.

Driver: *sgf_3d_w_dr*

The driver evaluates the Green's function and verifies the integral identities (sgf_3d.7,8), where D is the surface of a sphere.

Files to be linked: None for the subroutine.

The driver is linked with subroutine *gauss_sph* which contains tables of quadrature base points and weights for integration over the surface of a sphere.

Subroutine: sgf_3d_sph

This subroutine computes the Green's function in the exterior of a sphere. The streamline pattern of the induced flow is depicted in Figure sgf_3d_sph.1.

Closed-form expressions for the velocity Green's function have been derived by Oseen [50], and are discussed in References [28, 37, 48] and [55], p. 87.

Call statement:

sgf_3d_sph

(x, y, z)	<i>Input:</i> Coordinates of the field point.
$, x_0, y_0, z_0$	<i>Input:</i> Coordinates of the singular point (point force).
$, x_c, y_c, z_c$	<i>Input:</i> Coordinates of the center of the sphere.
$, a$	<i>Input:</i> Radius of the sphere.
$, G_{xx}, G_{xy}, G_{xz}$	<i>Output:</i> Velocity Green's function.
$, G_{yx}, G_{yy}, G_{yz}$	<i>Output:</i> Velocity Green's function.
$, G_{zx}, G_{zy}, G_{zz}$	<i>Output:</i> Velocity Green's function.

Numerical method:

The Green's function is computed by direct evaluation of expressions provided in the aforementioned references.

Driver: sgf_3d_sph_dr

The driver evaluates the Green's function and verifies the integral identity (sgf_3d.7), where D is the surface of a sphere.

Files to be linked: None for the subroutine.

The driver is linked with subroutine gauss_sph which contains tables of quadrature base points and weights for integration over the surface of a sphere.

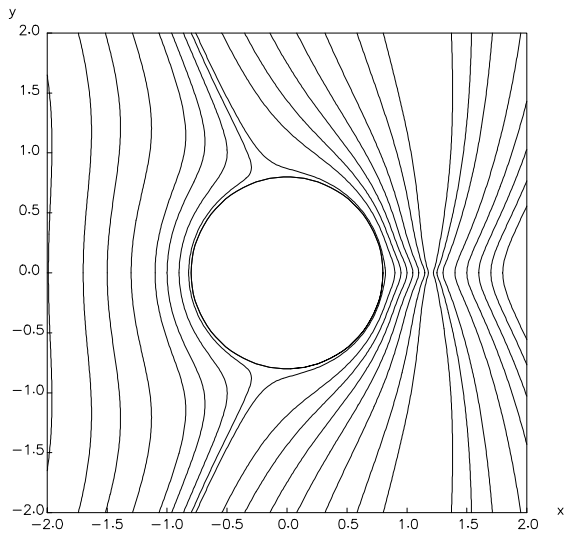
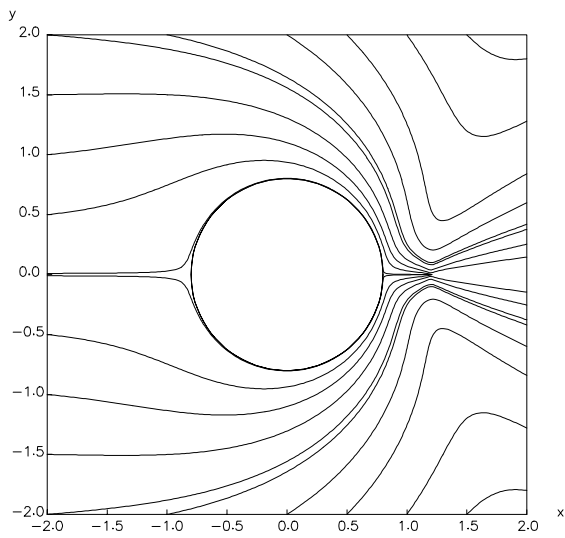


Figure sgf_3d_sph.2 Streamline pattern of the flow due to a three-dimensional point force in front of a sphere pointing in the radial (top) or azimuthal (bottom) direction.

Subroutine: sgf_3d_2p

This subroutine computes the doubly periodic Green's function representing the flow induced by a planar lattice of three-dimensional point forces, as illustrated in Figure sgf_3d_2p.1. The point forces are deployed at the vertices of a two-dimensional lattice described by two base vectors \mathbf{a}_1 and \mathbf{a}_2 parallel to the xy plane. One of the point forces is located at the point $\mathbf{x}_0 = (x_0, y_0, z_0)$. The streamline pattern of the induced flow is depicted in Figure sgf_3d_2p.2.

The Green's function may be computed by two methods: a Fourier series expansion appropriate for large distances from the array, and a rapidly converging Ewald summation method, as discussed in Reference [57].

Call statement:

sgf_3d_2p

(Method	<i>Input:</i> See Note 1.
, eps	<i>Input:</i> A small number used for numerical differentiation.
, x, y, z	<i>Input:</i> Coordinates of the field point.
, x_0, y_0, z_0	<i>Input:</i> Coordinates of the singular point (point force).
, a_{11}, a_{12}	<i>Input:</i> Coordinates of the first base vector.
, a_{21}, a_{22}	<i>Input:</i> Coordinates of the second base vector.
, b_{11}, b_{12}	<i>Input:</i> Coordinates of the first reciprocal base vector.
, b_{21}, b_{22}	<i>Input:</i> Coordinates of the second reciprocal base vector.
, ew	<i>Input:</i> Ewald summation parameter ξ .
, Max_1, Max_2	<i>Input:</i> Summation limits in real and wave number space.
, G_{xx}, G_{xy}, G_{xz}	<i>Output:</i> Velocity Green's function.
, G_{yx}, G_{yy}, G_{yz}	<i>Output:</i> Velocity Green's function.
, G_{zx}, G_{zy}, G_{zz}	<i>Output:</i> Velocity Green's function.

Note:

1. Set *Method* = 1 to compute the Green's function in terms of Fourier series; set *Method* = 2 to use the fast summation method developed in Reference [57].

PREREQUISITE:

Subroutine `ewald_3d_2p` must be called before subroutine `sgf_3d_2p`, as shown in the driver. This subroutine produces the reciprocal wave number base vectors \mathbf{b}_1 and \mathbf{b}_2 , the area of the unit cell in real space, and returns a recommended value for the Ewald splitting parameter ξ .

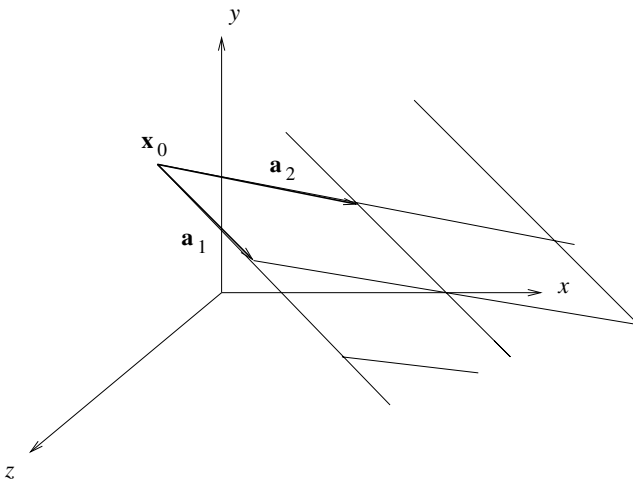


Figure sgf_3d_2p.1 A doubly periodic planar lattice of three-dimensional point forces located at the vertices of a planar lattice that is parallel to the xy plane. The structure of the lattice is defined by the base vectors \mathbf{a}_1 and \mathbf{a}_2 .

When multiple Green's function evaluations with the same lattice base vectors are to be performed, it is not necessary to call `ewald_3d_2p` each time, but just once before the first evaluation. The call statement is:

```
ewald_3d_2p
    (a11, a12) Input: Coordinates of the first base vector.
    , a21, a22 Input: Coordinates of the second base vector.
    , b11, b12 Output: Coordinates of the first reciprocal base vector.
    , b21, b22 Output: Coordinates of the second reciprocal base vector.
    , ew        Output: Ewald splitting parameter  $\xi$ .
    , area)    Output: Area of the unit cell in physical space.
```

Numerical method:

The Green's function is computed by direct evaluation using analytical expressions given in Reference [57].

Driver: sgf_3d_2p_dr

The driver evaluates the Green's function and verifies the integral identity (sgf_3d.7), where D is the surface of a sphere.

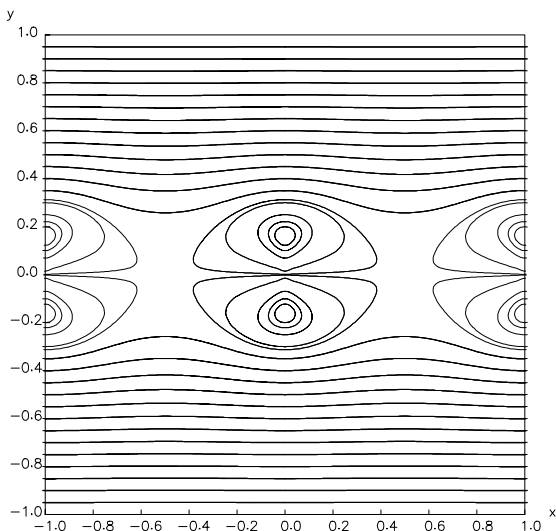


Figure sgf_3d_2p.2 Streamlines of the flow induced by a planar square lattice of three-dimensional point forces. The streamlines lie in a plane that is perpendicular to the plane of the point forces and passes through a file of point forces.

Files to be linked: None for the subroutine.

The driver must be linked with subroutine gauss_sph which contains tables of quadrature base points and weights for integration over the surface of a sphere.

Subroutine: sgf_3d_3p

This subroutine computes the triply periodic Green's function of three-dimensional Stokes flow representing the flow due to a periodic array of point forces deployed at the vertices of a three-dimensional lattice defined by the base vectors $\mathbf{a}^{(1)}$, $\mathbf{a}^{(2)}$, and $\mathbf{a}^{(3)}$, as illustrated in Figure sgf_3d_3p.1. The streamline pattern of the induced flow is depicted in Figure sgf_3d_3p.2.

One of the point forces is located at the point $\mathbf{x}_0 = (x_0, y_0, z_0)$, and the n th point force is located at the point $\mathbf{x}^{(n)} = (x_n, y_n, z_n)$, where

$$x^{(n)} = x_0 + i a_x^{(1)} + j a_x^{(2)} + k a_x^{(3)}, \quad y^{(n)} = y_0 + i a_y^{(1)} + j a_y^{(2)} + k a_y^{(3)},$$

$$z^{(n)} = z_0 + i a_z^{(1)} + j a_z^{(2)} + k a_z^{(3)}, \quad (1)$$

i , j , and k are three integers, and the index n is defined in terms of i , j and k using a triple summation formula.

Following Ewald's summation method [5, 26, 57], we find that the velocity Green's function tensor is given by

$$\begin{aligned} G_{ij}(\mathbf{x}, \mathbf{x}_0) = & \sum_n \left\{ \left[\operatorname{erfc}(\hat{r}_n) + \frac{2}{\sqrt{\pi}} \hat{r}_n (2 \hat{r}_n^2 - 3) e^{-\hat{r}_n^2} \right] \frac{\delta_{ij}}{r_n} \right. \\ & + \left[\operatorname{erfc}(\hat{r}_n) + \frac{2}{\sqrt{\pi}} \hat{r}_n (1 - 2 \hat{r}_n^2) e^{-\hat{r}_n^2} \right] \frac{(x_i - x_i^{(n)})(x_j - x_j^{(n)})}{r_n^3} \} \\ & + \frac{8\pi}{V_c} \sum_m \frac{1}{k^{(m)2}} \left(1 + \frac{1}{4} \hat{k}^{(m)2} + \frac{1}{8} \hat{k}^{(m)4} \right) \exp\left(-\frac{1}{4} \hat{k}^{(m)2}\right) \\ & \times \left(\delta_{ij} - \frac{k_i^{(m)} k_j^{(m)}}{k^{(m)2}} \right) \cos[\mathbf{k}^{(m)} \cdot (\mathbf{x} - \mathbf{x}_0)]. \end{aligned} \quad (2)$$

The first sum on the right-hand side of (2) with respect to n runs over the point forces, and the second sum with respect to m runs over the vertices of the reciprocal lattice in wave-number space. All terms on the right-hand side of (2) have dimensions of inverse length.

The base vectors of the reciprocal lattice are given by

$$\begin{aligned} \mathbf{b}^{(1)} &= \frac{2\pi}{V_c} \mathbf{a}^{(2)} \times \mathbf{a}^{(3)}, & \mathbf{b}^{(2)} &= \frac{2\pi}{V_c} \mathbf{a}^{(3)} \times \mathbf{a}^{(1)}, \\ \mathbf{b}^{(3)} &= \frac{2\pi}{V_c} \mathbf{a}^{(1)} \times \mathbf{a}^{(2)}, \end{aligned} \quad (3)$$

where $V_c = (\mathbf{a}^{(1)} \times \mathbf{a}^{(2)}) \cdot \mathbf{a}^{(3)}$ is the volume of a unit cell.

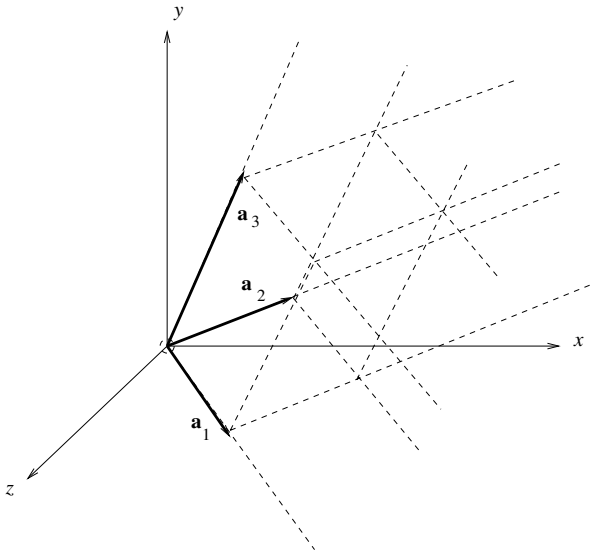


Figure sgf_3d_3p.1 A triply periodic array of three-dimensional point forces located at the vertices of a lattice.

The vertices of the reciprocal lattice are located at $\mathbf{k}^{(m)} = (k_x^{(m)}, k_y^{(m)}, k_z^{(m)})$, where

$$k_x^{(m)} = i b_x^{(1)} + j b_x^{(2)} + l b_x^{(3)}, \quad k_y^{(m)} = i b_y^{(1)} + j b_y^{(2)} + l b_y^{(3)},$$

$$k_z^{(m)} = i b_z^{(1)} + j b_z^{(2)} + l b_z^{(3)}, \quad (4)$$

and the index m is defined in terms of i , j and l using triple-summation. The singular wave number corresponding to $i = 0$, $j = 0$, and $l = 0$ is excluded from the second sum in (2).

The rest of the symbols in (2) are defined as follows:

- $r_n = \sqrt{(x - x_n)^2 + (y - y_n)^2 + (z - z_n)^2}$ is the distance of the evaluation point from the n th point force, and $\hat{r}_n = \xi r_n$ is the reduced dimensionless distance.
- $k^{(m)} \equiv |\mathbf{k}^{(m)}|$ is the length of the m th wave number vector, and $\hat{k}^{(m)} = \frac{k^{(m)}}{\xi}$ is the dimensionless wave number.
- erfc is the complementary error function.
- ξ is the Ewald splitting parameter with dimensions of inverse length, determining the balance of the sums in real and reciprocal space.

The right-hand side of (2) is independent of the selected value of ξ . As ξ tends to zero, we obtain a representation in terms of sums in real space, whereas as ξ tends to infinity, we obtain a representation in terms of a double Fourier series in reciprocal wave number space.

The pressure Green's function is given by

$$\begin{aligned}
 p_j(\mathbf{x}, \mathbf{x}_0) = & \frac{8\pi}{V_c} (x_j - x_{0j}) \\
 & + \sum_n [2 \operatorname{erfc}(\hat{r}_n) + \frac{4}{\sqrt{\pi}} \hat{r}_n (1 + 4 \hat{r}_n^2 - \frac{4}{3} \hat{r}_n^4) e^{-\hat{r}_n^2}] \frac{x_j - x_j^{(n)}}{r_n^3} \\
 & + \frac{8\pi}{V_c} \sum_m (1 - \frac{1}{6} \hat{k}^{(m)2} - \frac{1}{12} \hat{k}^{(m)4}) \frac{k_j^{(m)}}{k^{(m)2}} \exp(-\frac{\hat{k}^{(m)2}}{4}) \sin[\mathbf{k}_m \cdot (\mathbf{x} - \mathbf{x}_0)].
 \end{aligned} \tag{5}$$

The first term on the right-hand side of (5) contributes a linear pressure field that balances the force imparted to the fluid by the point forces, thereby satisfying the force balance over each periodic cell.

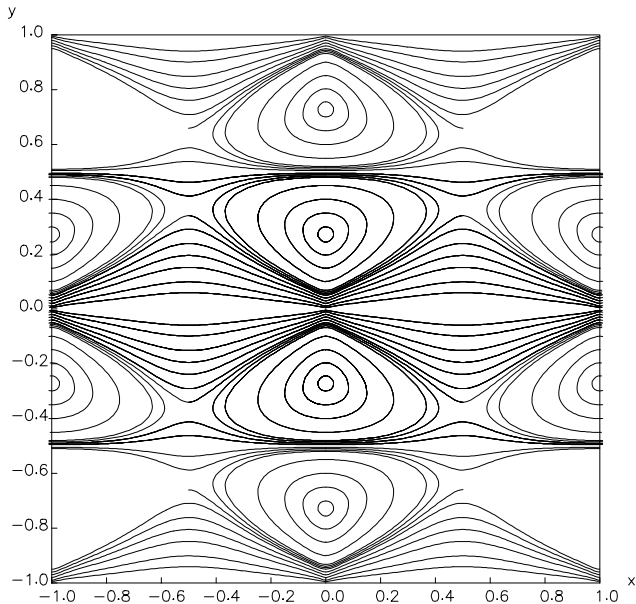


Figure sgf_3d_3p.2 Streamlines of the flow induced by a triply periodic array of three-dimensional point forces located at the vertices of a cubic lattice. The streamlines lie in a plane of point forces.

The stress Green's function is given by

$$\begin{aligned}
 T_{ijl}(\mathbf{x}, \mathbf{x}_0) = & -\delta_{il} \frac{8\pi}{V_c} (x_j - x_{0j}) \\
 & - \sum_n \left\{ \frac{8}{\sqrt{\pi}} \xi^3 [\delta_{jl}(x_i - x_i^{(i)}) + \delta_{ij}(x_l - x_l^{(n)}) + \delta_{il}(x_j - x_j^{(n)})] e^{-\hat{r}_n^2} \right. \\
 & \quad \left. + [6 \operatorname{erfc}(\hat{r}_n) + \frac{4}{\sqrt{\pi}} \hat{r}_n (3 + 2 \hat{r}_n^2 - 4 \hat{r}_n^4) e^{-\hat{r}_n^2}] \right. \\
 & \quad \left. \times \frac{(x_i - x_i^{(n)})(x_j - x_j^{(n)})(x_l - x_l^{(l)})}{r_n^5} \right\} \\
 & + \frac{8\pi}{V_c} \sum_m [2 (1 + \frac{1}{4} \hat{k}^{(m)2} + \frac{1}{8} \hat{k}^{(m)4}) \frac{k_i^{(m)} k_j^{(m)} k_l^{(m)}}{k^{(m)4}} \\
 & - \frac{\delta_{ij} k_l^{(m)} + \delta_{lj} k_i^{(m)} + \delta_{il} k_j^{(m)}}{k^{(m)2}}] \exp(-\frac{\hat{k}^{(m)2}}{4}) \sin[\mathbf{k}_m \cdot (\mathbf{x} - \mathbf{x}_0)]. \tag{6}
 \end{aligned}$$

The first term on the right-hand side of (6) incorporates the linear variation of the normal stress due to the pressure.

Call statement:

`sgf_3d_3p`

$(Iopt$	<i>Input:</i> See Note 1.
$, x, y, z$	<i>Input:</i> Coordinates of the field point.
$, x_0, y_0, z_0$	<i>Input:</i> Coordinates of one singular point (point force).
$, a_{11}, a_{12}, a_{13}$	<i>Input:</i> Coordinates of the first base vector.
$, a_{21}, a_{22}, a_{23}$	<i>Input:</i> Coordinates of the second base vector.
$, a_{31}, a_{32}, a_{33}$	<i>Input:</i> Coordinates of the third base vector.
$, b_{11}, b_{12}, b_{13}$	<i>Input:</i> Coordinates of the first reciprocal base vector.
$, b_{21}, b_{22}, b_{23}$	<i>Input:</i> Coordinates of the second reciprocal base vector.
$, b_{31}, b_{32}, b_{33}$	<i>Input:</i> Coordinates of the third reciprocal base vector.
$, ew$	<i>Input:</i> Ewald splitting parameter ξ .
$, vlm$	<i>Input:</i> Volume of the unit cell in the physical space.
$, Max_1, Max_2$	<i>Input:</i> Summation limits in real and wave number space.
$, G_{xx}, G_{xy}, G_{xz}$	<i>Output:</i> Velocity Green's function.
$, G_{yx}, G_{yy}, G_{yz}$	<i>Output:</i> Velocity Green's function.
$, G_{zx}, G_{zy}, G_{zz}$	<i>Output:</i> Velocity Green's function.
$, p_x, p_y, p_z$	<i>Output:</i> Pressure Green's function.

, $T_{xxx}, T_{xxy}, T_{xxz}$ *Output:* Stress Green's function.
, $T_{yxy}, T_{yxz}, T_{zzx}$ *Output:* Stress Green's function.
, $T_{xyx}, T_{xyy}, T_{xyz}$ *Output:* Stress Green's function.
, $T_{yyy}, T_{yyz}, T_{zyz}$ *Output:* Stress Green's function.
, $T_{xzx}, T_{xzy}, T_{xzz}$ *Output:* Stress Green's function.
, $T_{yzy}, T_{yzz}, T_{zzz}$) *Output:* Stress Green's function.

Note:

1. Set $Iopt = 1$ to obtain only G_{ij} ; set $Iopt \neq 1$ to obtain G_{ij} , p_j , and T_{ijk} .

PREREQUISITES:

Subroutines `ewald_3d`, `qqq_3d`, and `vvv_3d` must be called *in this particular order*, before subroutine `sgf_3d_3p`, as shown in the driver.

If multiple Green's function evaluations with the same lattice base vectors are to be performed, it is not necessary to call the three subroutines each time, but just once before the first evaluation.

Calling `vvv_3d` is necessary only if the pressure and stress Green's functions are required ($Iopt = 2$).

Subroutine `ewald_3d`:

This subroutine produces the reciprocal wave number space base vectors \mathbf{b}_1 , \mathbf{b}_2 , \mathbf{b}_3 , and the volume of the unit cell of the lattice in real space. It also returns a recommended value for the Ewald parameter ξ . The call statement is:

`ewald_3d`

(a_{11}, a_{12}, a_{13} *Input:* Coordinates of the first base vector.
, a_{21}, a_{22}, a_{23} *Input:* Coordinates of the second base vector.
, a_{31}, a_{32}, a_{33} *Input:* Coordinates of the third base vector.
, b_{11}, b_{12}, b_{13} *Output:* Coordinates of the first reciprocal base vector.
, b_{21}, b_{22}, b_{23} *Output:* Coordinates of the second reciprocal base vector.
, b_{31}, b_{32}, b_{33} *Output:* Coordinates of the third reciprocal base vector.
, ew *Output:* Ewald splitting parameter ξ .
, vlm) *Output:* Volume of the unit cell in physical space.

Subroutine `qqq_3d`:

This subroutine produces a matrix used for computing the velocity Green's function G_{ij} by summing in the wave number space. The call statement is:

`qqq_3p`

(b_{11}, b_{12}, b_{13} *Input:* Coordinates of the first reciprocal base vector.
 $, b_{21}, b_{22}, b_{23}$ *Input:* Coordinates of the second reciprocal base vector.
 $, b_{31}, b_{32}, b_{33}$ *Input:* Coordinates of the third reciprocal base vector.
 $, Max_2$ *Input:* Summation limit in wave number space.
 $, ew)$ *Input:* Ewald splitting parameter ξ .

The output is passed through a common block, as shown in the source code.

Subroutine vvv_3d:

This subroutine produces a matrix used for computing the pressure and stress Green's functions p_i and T_{ijk} by summing in the wave number space. The call statement is:

`vvv_3d`

(b_{11}, b_{12}, b_{13} *Input:* Coordinates of the first reciprocal base vector.
 $, b_{21}, b_{22}, b_{23}$ *Input:* Coordinates of the second reciprocal base vector.
 $, b_{31}, b_{32}, b_{33}$ *Input:* Coordinates of the third reciprocal base vector.
 $, Max_2$ *Input:* Summation limit in wave number space.
 $, ew)$ *Input:* Ewald splitting parameter ξ .

The output is passed through a common block, as shown in the source code.

Numerical method: `sgf_3d_3p_dr`

The Green's function is computed by direct evaluation of expressions (1) to (6).

Driver: `sgf_3d_3p_dr`

The driver evaluates the Green's function and verifies the integral identities (`sgf_3d.7,8`), where D is the surface of a sphere.

Files to be linked: None for the subroutine.

The driver is linked with subroutine `gauss_sph` which contains tables of quadrature base points and weights for integration over the surface of a sphere.

Directory: `stokes/sgf_ax`

Consider the cylindrical polar coordinates (x, σ, φ) illustrated in Figure sgf_ax.1, defined with respect to the Cartesian coordinates (x, y, z) . A semi-infinite plane of constant angle φ passing through the x axis is called a meridional plane.

The velocity, pressure, and stress Green's functions of axisymmetric Stokes flow denoted respectively by $G_{\alpha\beta}$, p_α , and $T_{\alpha\beta\gamma}$, where the Greek indices range over 1 and 2 corresponding to x and σ , are defined such that the velocity at the point \mathbf{x} due to a ring of point forces with strength per unit length \mathbf{b} piercing a meridional plane at the point \mathbf{x}_0 , is given by

$$u_\alpha(\mathbf{x}) = \frac{1}{8\pi\mu} G_{\alpha\beta}(\mathbf{x}, \mathbf{x}_0) b_\beta, \quad (\text{sgf_ax.1})$$

where μ is the fluid viscosity. The associated pressure and stress fields are given by

$$p(\mathbf{x}) = \frac{1}{8\pi} p_\beta(\mathbf{x}, \mathbf{x}_0) b_\beta, \quad (\text{sgf_ax.2})$$

and

$$\sigma_{\alpha\gamma}(\mathbf{x}) = \frac{1}{8\pi} Q_{\alpha\beta\gamma}(\mathbf{x}, \mathbf{x}_0) b_\beta. \quad (\text{sgf_ax.3})$$

INTEGRAL IDENTITIES:

Mass conservation requires that the axisymmetric Green's functions for the velocity satisfy the integral identity

$$\int_C n_\alpha(\mathbf{x}) G_{\alpha\beta}(\mathbf{x}, \mathbf{x}_0) \sigma dl(\mathbf{x}) = 0, \quad (\text{sgf_ax.4})$$

for $\beta = x$ or σ , where C is the closed trace of an axisymmetric surface in a meridional plane, and \mathbf{n} is the unit vector normal to C pointing *inward*.

The stress Green's functions satisfy the integral identity

$$\frac{1}{8\pi\sigma_0} \int_C Q_{\alpha\beta\gamma}(\mathbf{x}, \mathbf{x}_0) n_\alpha(\mathbf{x}) \sigma dl(\mathbf{x}) = \begin{cases} \delta_{\beta\gamma} & \text{when } \mathbf{x}_0 \text{ is inside } C \\ \frac{1}{2} \delta_{\beta\gamma} & \text{when } \mathbf{x}_0 \text{ is on } C \\ 0 & \text{when } \mathbf{x}_0 \text{ is outside } C \end{cases}. \quad (\text{sgf_ax.5})$$

When the point \mathbf{x}_0 is located on C , the principal-value integral is implied on the left-hand side of (sgf_ax.5).

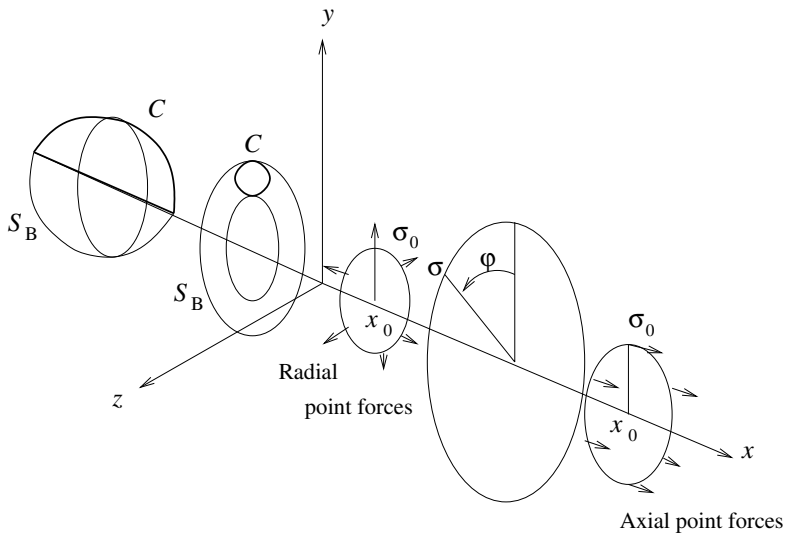


Figure sgf_ax.1 Cylindrical polar coordinates used to define the Green's functions of axisymmetric Stokes flow.

BOUNDARY-INTEGRAL REPRESENTATION:

The boundary integral representation for the axial and radial velocity components of an axisymmetric Stokes flow is

$$u_\alpha(\mathbf{x}_0) = -\frac{1}{8\pi\mu} \int_C G_{\alpha\beta}(\mathbf{x}_0, \mathbf{x}) f_\beta(\mathbf{x}) dl(\mathbf{x}) + \frac{1}{8\pi} \int_C Q_{\alpha\beta\gamma}(\mathbf{x}_0, \mathbf{x}) u_\beta(\mathbf{x}) n_\gamma(\mathbf{x}) dl(\mathbf{x}), \quad (\text{sgf_ax.6})$$

where C denotes the union of the contours of all axisymmetric surfaces enclosing a selected area of flow in a meridional plane, \mathbf{n} is the unit vector normal to C pointing into the control area, and $\mathbf{f} \equiv \sigma \cdot \mathbf{n}$ is the boundary traction.

BOUNDARY-INTEGRAL EQUATION:

The boundary integral equation corresponding to (sgf_ax.6) is

$$u_\alpha(\mathbf{x}_0) = -\frac{1}{4\pi\mu} \int_C G_{\alpha\beta}(\mathbf{x}_0, \mathbf{x}) f_\beta(\mathbf{x}) dl(\mathbf{x}) + \frac{1}{4\pi} \int_C^{PV} Q_{\alpha\beta\gamma}(\mathbf{x}_0, \mathbf{x}) u_\beta(\mathbf{x}) n_\gamma(\mathbf{x}) dl(\mathbf{x}), \quad (\text{sgf_ax.7})$$

where the point \mathbf{x}_0 lies on C , and PV denotes the principal-value integral.

FURTHER INTEGRAL IDENTITIES:

Applying the boundary-integral representation (sgf_ax.6) for rigid-body translation along the x axis, we derive the integral identities

$$\int_C G_{\alpha\beta}(\mathbf{x}_0, \mathbf{x}) n_\beta(\mathbf{x}) dl(\mathbf{x}) = 0, \quad (\text{sgf_ax.8})$$

and

$$\frac{1}{8\pi} \int_C Q_{\alpha x\gamma}(\mathbf{x}_0, \mathbf{x}) n_\gamma(\mathbf{x}) dl(\mathbf{x}) = \begin{cases} -\delta_{\alpha x} & \text{when } \mathbf{x}_0 \text{ is inside } C \\ -\frac{1}{2} \delta_{\alpha x} & \text{when } \mathbf{x}_0 \text{ is on } C \\ 0 & \text{when } \mathbf{x}_0 \text{ is outside } C \end{cases}, \quad (\text{sgf_ax.9})$$

which complement the integral identities (sgf_ax.4) and (sgf_ax.5).

DESINGULARIZATION OF THE DOUBLE-LAYER POTENTIAL:

The principal value of the axisymmetric double-layer potential expressed by the second integral on the right-hand side of (sgf_ax.7) may be desingularized by writing

$$\begin{aligned} & \int_C^{PV} Q_{\alpha\beta\gamma}(\mathbf{x}_0, \mathbf{x}) u_\beta(\mathbf{x}) n_\gamma(\mathbf{x}) dl(\mathbf{x}) \\ &= \int_C Q_{\alpha x\gamma}(\mathbf{x}_0, \mathbf{x}) [u_\beta(\mathbf{x}) - u_\beta(\mathbf{x}_0)] n_\gamma(\mathbf{x}) dl(\mathbf{x}) - 4\pi\delta_{\alpha x} u_x(\mathbf{x}_0) \\ &+ \int_C [Q_{\alpha\sigma\gamma}(\mathbf{x}_0, \mathbf{x}) u_\sigma(\mathbf{x}) - P_{\alpha\gamma}(\mathbf{x}_0, \mathbf{x}) u_\sigma(\mathbf{x}_0)] n_\gamma(\mathbf{x}) dl(\mathbf{x}) - 4\pi\delta_{\alpha\sigma} u_\sigma(\mathbf{x}_0), \end{aligned} \quad (\text{sgf_ax.10})$$

where $P_{\alpha\gamma}$ is a new tensor satisfying the identity

$$\frac{1}{8\pi} \int_C P_{\alpha\gamma}(\mathbf{x}, \mathbf{x}_0) n_\gamma(\mathbf{x}) dl(\mathbf{x}) = \begin{cases} -\delta_{\alpha\sigma} & \text{when } \mathbf{x}_0 \text{ is inside } C \\ -\frac{1}{2} \delta_{\alpha\sigma} & \text{when } \mathbf{x}_0 \text{ is on } C \\ 0 & \text{when } \mathbf{x}_0 \text{ is outside } C \end{cases}. \quad (\text{sgf_ax.11})$$

The tensor $P_{\alpha\gamma}$ is evaluated by the subroutines included in this directory.

DIRECTORY CONTENTS:

Directory `sgf_ax` contains the following subroutines and their drivers:

Subroutine	Topic
<code>sgf_ax_fs</code>	Green's function for flow in free space.
<code>sgf_ax_w</code>	Green's function for flow in a semi-infinite domain bounded by a plane wall.
<code>sgf_ax_1p</code>	Singly periodic Green's function.
<code>sgf_ax_1p_ct</code>	Periodic Green's function for flow inside a cylindrical tube with circular cross-section.

Subroutine: sgf_ax_fs

This subroutine computes the Green's function for an infinite domain of flow in the absence of boundaries. The streamline pattern of the induced flow is depicted in Figure sgf_ax_fs.1.

Analytical expressions for the Green's function in terms of complete elliptic integrals of the first and second kind are given in References [53] and [55], pp. 38 – 41.

Call statement:
sgf_ax_fs

$(Iopt$	<i>Input:</i> See Note 1.
$, x_0, \sigma_0$	<i>Input:</i> Coordinates of the singular point.
$, x, \sigma$	<i>Input:</i> Coordinates of the field point.
$, G_{xx}, G_{x\sigma}$	<i>Output:</i> Velocity Green's function.
$, G_{\sigma x}, G_{\sigma\sigma}$	<i>Output:</i> Velocity Green's function.
$, Q_{xxx}, Q_{x\sigma\sigma}$	<i>Output:</i> Stress Green's function.
$, Q_{x\sigma x}, Q_{x\sigma\sigma}$	<i>Output:</i> Stress Green's function.
$, Q_{\sigma xx}, Q_{\sigma x\sigma}$	<i>Output:</i> Stress Green's function.
$, Q_{\sigma\sigma x}, Q_{\sigma\sigma\sigma}$	<i>Output:</i> Stress Green's function.
$, P_{xx}, P_{x\sigma}$	<i>Output:</i> See Note 2.
$, P_{\sigma x}, P_{\sigma\sigma}$	<i>Output:</i> See Note 2.
$, Iaxis)$	<i>Input:</i> See Note 3.

Notes:

1. Set $Iopt = 1$ to obtain only $G_{\alpha\beta}$; set $Iopt \neq 1$ to obtain $G_{\alpha\beta}$, p_β , and $T_{\alpha\beta\gamma}$.
2. This matrix is introduced in equation (sgf_ax.10).
3. $Iaxis = 1$ indicates that $\sigma_0 = 0$, and $Iaxis = 0$ indicates otherwise. In the first case, simplified formulae are used to compute the Green's functions.

Numerical method:

The Green's function is computed by direct evaluation of analytical expressions. The complete elliptical integrals are evaluated by an iterative method.

Driver: sgf_ax_fs_dr

The driver evaluates the Green's functions and verifies the integral identities (sgf_ax.4,5,8,9,11), where C is a circular contour.

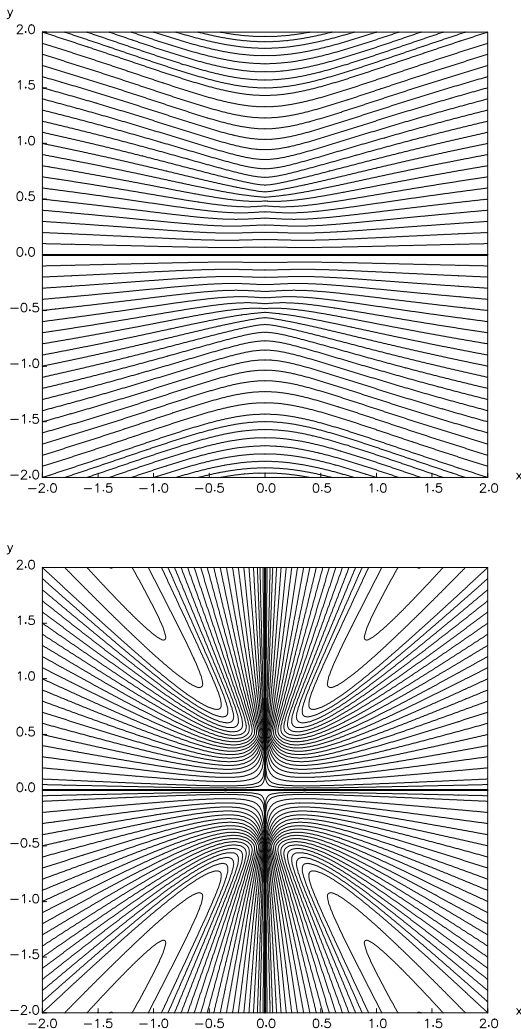


Figure sgf_ax_fs.1 Streamline pattern of the flow induced by a ring of point forces pointing in the axial (top) or radial (bottom) direction. In the dimensionless units of these graphs, the radius of the ring is 0.5.

Files to be linked:

`ell_int`: Evaluation of complete elliptic integrals of the first and second kind.

Subroutine: sgf_ax_w

This subroutine computes the Green's function for a semi-infinite domain of flow bounded by a plane wall located at $x = wall$. The streamline pattern of the induced flow is depicted in Figure sgf_ax_w.1.

Analytical expressions for the Green's function in terms of complete elliptic integrals of the first and second kind are given in Reference [54].

Call statement:
sgf_ax_w

$(Iopt$	<i>Input:</i> See Note 1.
$, x_0, \sigma_0$	<i>Input:</i> Coordinates of the singular point (point force).
$, x, \sigma$	<i>Input:</i> Coordinates of the field point.
$, wall$	<i>Input:</i> The wall is located at $x = wall$.
$, G_{xx}, G_{x\sigma}$	<i>Output:</i> Velocity Green's function.
$, G_{\sigma x}, G_{\sigma\sigma}$	<i>Output:</i> Velocity Green's function.
$, Q_{xxx}, Q_{xx\sigma}$	<i>Output:</i> Stress Green's function.
$, Q_{x\sigma x}, Q_{x\sigma\sigma}$	<i>Output:</i> Stress Green's function.
$, Q_{\sigma xx}, Q_{\sigma x\sigma}$	<i>Output:</i> Stress Green's function.
$, Q_{\sigma\sigma x}, Q_{\sigma\sigma\sigma}$	<i>Output:</i> Stress Green's function.
$, P_{xx}, P_{x\sigma}$	<i>Output:</i> See Note 2.
$, P_{\sigma x}, P_{\sigma\sigma}$	<i>Output:</i> See Note 2.
$Iaxis)$	<i>Input:</i> See Note 3.

Notes:

1. Set $Iopt = 1$ to obtain only $G_{\alpha\beta}$; set $Iopt \neq 1$ to obtain $G_{\alpha\beta}$, p_β , and $T_{\alpha\beta\gamma}$.
2. This matrix is introduced in equation (sgf_ax.10).
3. $Iaxis = 1$ indicates that $\sigma_0 = 0$, and $Iaxis = 0$ indicates otherwise. In the first case, simplified formulae are used to compute the Green's function.

Numerical method:

The Green's function is computed by direct evaluation of analytical expressions. The complete elliptical integrals are evaluated by an iterative method.

Driver: sgf_ax_w_dr

The driver evaluates the Green's function and verifies the integral identities (sgf_ax.4,5,8,9,11), where C is a circular contour.

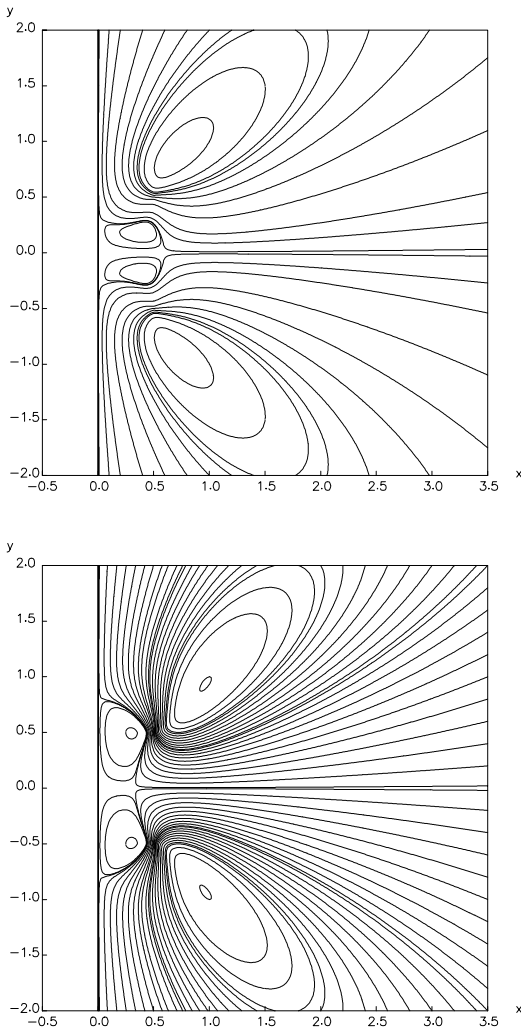


Figure sgf_ax_w.1 Streamline pattern of the flow induced by a ring of point forces pointing in the axial (top) or radial (bottom) direction, in the presence of a plane wall located at $x = 0$. In the dimensionless units of these graphs, the ring is positioned at $x = 0.5$ and its radius is equal to 0.5.

Files to be linked:

`ell_int`: Evaluation of complete elliptic integrals of the first and second kind.

Subroutine: sgf_ax_1p

This subroutine computes the periodic Green's function in free space representing the flow due to an array of rings of point forces separated by the distance L along the x axis, as illustrated in Figure sgf_ax_1p.1. The streamline pattern of the induced flow is depicted in Figure sgf_ax_1p.2.

The Green's function is computed by summing non-periodic free-space Green's functions produced by subroutine sgf_ax_fs over the one-dimensional array. For example,

$$G_{\alpha\beta}(x, \sigma, x_0, \sigma_0) = \sum_{k=-N}^{k=N} c_k G_{\alpha\beta}^{FS}(x, \sigma, x_0 + k L, \sigma_0), \quad (1)$$

where the superscript FS denotes the free-space Green's function, L is the distance between two consecutive rings, N is a specified truncation level, $c_k = 1$ for $k = -N+1, \dots, -1, 0, 1, \dots, N-1$, $c_{-N} = 1/2$, and $c_N = 1/2$.

The axial component G_{xx} decays like $4\pi\sigma_0/|(x_0 + k L) - x|$. To prevent the corresponding sum from diverging, we evaluate instead the regularized form

$$G_{xx}(x, \sigma, x_0, \sigma_0) = \sum_{k=-N}^{k=N} [c_k G_{xx}^{FS}(x, \sigma, x_0 + k L, \sigma_0) - \frac{4\pi\sigma_0}{|x_0 + (k + \frac{1}{2}) L|}]. \quad (2)$$

This modification is permissible because the last term within the sum is independent of the field-point coordinates (x, σ) . It is assumed that the denominator of the last term in (2) does not vanish for any value of k . If it does, the term enclosed by the parentheses should be modified.

The summed terms in equations (1) and (2) decay like $1/k^2$. Using the error formula for the trapezoidal rule, we find that the error due to the truncation of the sums behaves like δ/N , where δ is a constant (e.g., [60], Ch. 1). Accordingly, the error corresponding to the sequence of truncation levels

$$N_0 = N, \quad N_1 = m N, \quad N_2 = m^2 N, \quad \dots \quad (3)$$

where N and m are two specified integers, satisfies the linear relation

$$E(N_k) = \frac{1}{m} E(N_{k-1}). \quad (4)$$

The convergence may then be accelerated by Aitken's extrapolation (e.g., [60], Ch. 1).

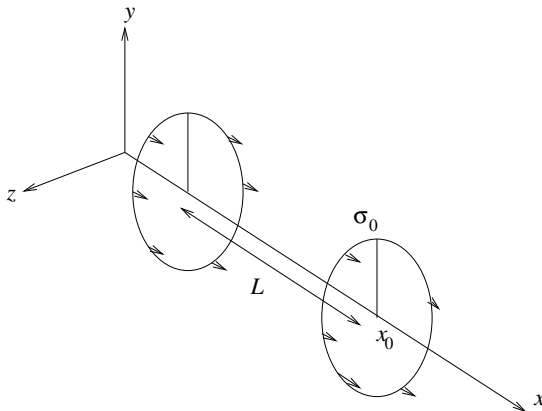


Figure sgf_ax_1p.1 A periodic array of rings of point forces separated by the distance L along the x axis, pointing in the axial or radial direction.

Call statement:

`sgf_ax_1p`

$(Iopt$	<i>Input:</i> See Note 1.
$,x_0, \sigma_0$	<i>Input:</i> Coordinates of the singular point (point force).
$,x, \sigma$	<i>Input:</i> Coordinates of the field point.
$,L$	<i>Input:</i> Separation between the point-force rings.
$,Nsum, Np$	<i>Input:</i> See Note 2.
$,G_{xx}, G_{x\sigma}$	<i>Output:</i> Velocity Green's function.
$,G_{\sigma x}, G_{\sigma\sigma}$	<i>Output:</i> Velocity Green's function.
$,Q_{xxx}, Q_{xx\sigma}$	<i>Output:</i> Stress Green's function.
$,Q_{x\sigma x}, Q_{x\sigma\sigma}$	<i>Output:</i> Stress Green's function.
$,Q_{\sigma xx}, Q_{\sigma x\sigma}$	<i>Output:</i> Stress Green's function.
$,Q_{\sigma\sigma x}, Q_{\sigma\sigma\sigma}$	<i>Output:</i> Stress Green's function.
$,P_{xx}, P_{x\sigma}$	<i>Output:</i> See Note 3.
$,P_{\sigma x}, P_{\sigma\sigma}$	<i>Output:</i> See Note 3.
$,Iaxis)$	<i>Input:</i> See Note 4.

Notes:

1. Set $Iopt = 1$ to obtain only $G_{\alpha\beta}$; set $Iopt \neq 1$ to obtain $G_{\alpha\beta}$, p_β , and $T_{\alpha\beta\gamma}$.
2. $Nsum$ is the truncation limit N defined in equation (1). Np is the integer m defined in the equations displayed in (3).
3. This matrix is introduced in equation (sgf_ax.10).
4. $Iaxis = 1$ indicates that $\sigma_0 = 0$, and $Iaxis = 0$ indicates otherwise. In the first case, simplified formulae are used to compute the Green's function.

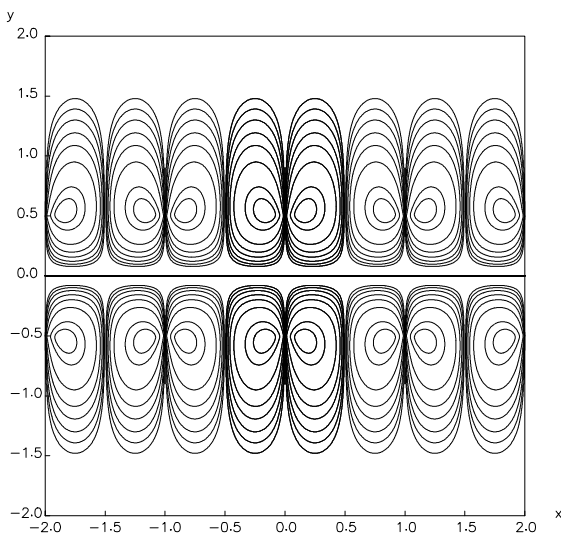
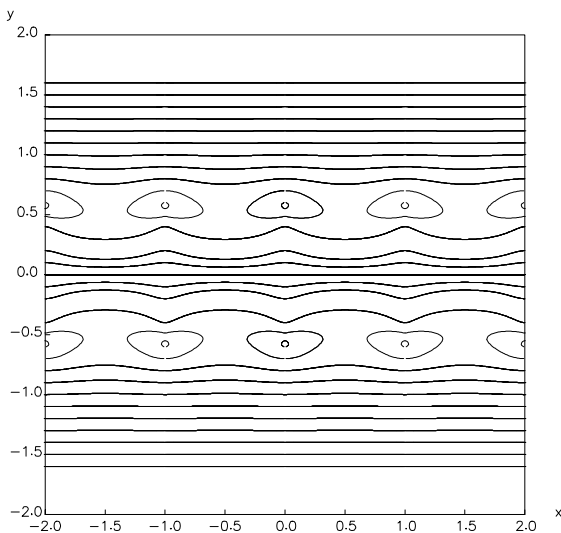


Figure sgf_ax_1p.2 Streamline pattern of the flow induced by a periodic array of rings of point forces pointing in the axial (top) or radial (bottom) direction. In the dimensionless units of these graphs, the radius of the ring is 0.5 and the period is 1.0.

Driver: `sgf_ax_1p_dr`

The driver evaluates the Green's function and verifies the integral identities (`sgf_ax.4,5,8,9`), where C is a circular contour or one period of a periodic line in a meridional plane.

Files to be linked:

1. `sgf_ax_fs`: Computation of the free-space axisymmetric Green's function.
2. `ell_int`: Evaluation of complete elliptic integrals of the first and second kind.

Subroutine: sgf_ax_1p_ct

This subroutine computes the periodic Green's function of axisymmetric Stokes flow representing the flow due to a periodic array of rings of point forces in the interior of a circular cylinder, as illustrated in Figure sgf_ax_1p_ct.1.

The derivation of the Green's function for the velocity in terms of infinite sums involving modified Bessel functions is discussed in Reference [56], pp. 89 – 92. The Green's function is defined such that, when the point forces are oriented in the axial direction, the flow rate of the induced flow vanishes.

Call statement:

sgf_ax_1p_ct

$(x, \sigma$	<i>Input:</i> Coordinates of the field point.
$, x_0, \sigma_0$	<i>Input:</i> Coordinates of a singular point.
$, a$	<i>Input:</i> Tube radius.
$, L$	<i>Input:</i> Separation between the point-force rings.
$, Nsum, Np$	<i>Input:</i> See Note 1.
$, G_{xx}, G_{x\sigma}$	<i>Output:</i> Velocity Green's function.
$, G_{\sigma x}, G_{\sigma\sigma}$)	<i>Output:</i> Velocity Green's function.

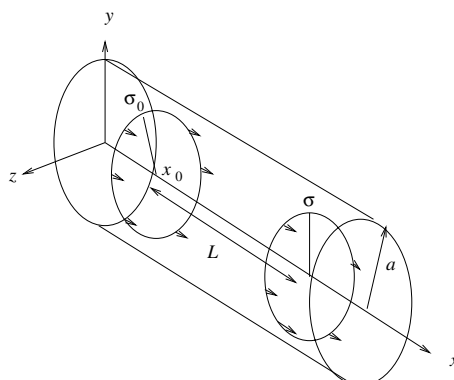


Figure sgf_ax_1p_ct.1 Axisymmetric flow induced by a periodic array of rings of point forces inside a cylindrical tube.

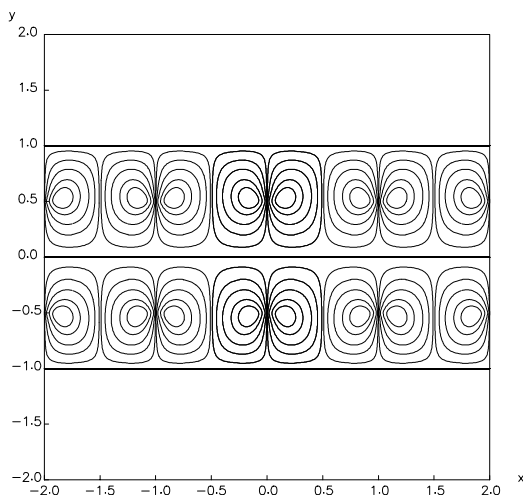
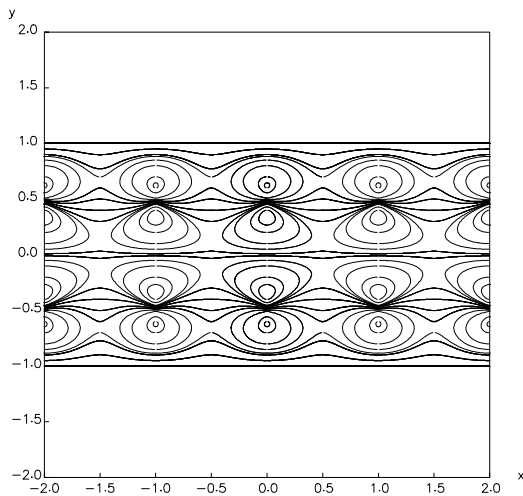


Figure sgf_ax_1p_ct.2 Streamline pattern of the flow induced by a periodic array of rings of point forces pointing in the axial (top) or radial (bottom) direction inside a circular tube. In the dimensionless units of these graphs, the radius of the ring is 0.5, the period is 1.0, and the tube radius is 1.0.

Note:

1. N_{sum} is the truncation limit of an infinite sum involved in the computation of the Green's function. N_p is the integer m defined in equations (3) of directory `sgf_ax_1p`, used to expedite the summation.

Driver: `sgf_ax_1p_ct_dr`

The driver evaluates the Green's function and verifies the integral identities (sgf_ax.4,8) where C is a circular contour.

Files to be linked:

1. `bessel_I01K01`
Evaluation of modified Bessel functions.
2. `ell_int`
Evaluation of complete elliptic integrals of the first and second kind.

Directory: `stokes/flow_2d`

This directory contains a code that computes Stokes flow in a two-dimensional domain with arbitrary geometry. Several types of flows and domain geometries implemented in the code are illustrated in Figures `flow_2d.1` and `flow_2d.2`. Other configurations may be included by straightforward modifications.

Figure `flow_2d.1(a, b)` illustrates streamline patterns for shear flow past a cavity or a protuberance on a plane wall. Figure `flow_2d.2(a)` illustrates the streamline pattern of shear flow past an inclined square held stationary above a plane wall. Figure `flow_2d.2(b)` illustrates the streamline pattern of shear flow over a periodic array of cylinders, with the shear rate vanishing far below the cylinders.

MATHEMATICAL FORMULATION FOR FLOW PAST A WALL WITH A DEPRESSION OR PROJECTION, AND FLOW PAST A CYLINDER:

In the case of shear flow over a cavity or protuberance on a plane wall, as illustrated in Figure `flow_2d.1(a, b)`, possibly in the presence of an upper plane wall that is parallel to the lower wall, and shear flow past a cylindrical body above a plane wall, possibly in the presence of an upper plane wall parallel to the lower wall, as illustrated in Figure `flow_2d.2(a)`, the velocity field \mathbf{u} is decomposed into a far-field component prevailing far from the wall, denoted by \mathbf{u}^∞ , and a disturbance component, denoted by \mathbf{u}^D , so that

$$\mathbf{u} = \mathbf{u}^\infty + \mathbf{u}^D. \quad (1)$$

The unperturbed component expresses unidirectional shear flow along the x axis with a linear or parabolic velocity profile described by

$$u_x^\infty = \gamma y + \frac{\delta}{2\mu} y^2, \quad u_y^\infty = 0, \quad (2)$$

where γ is the shear rate at the wall located at $y = 0$, δ is the pressure gradient, and μ is the fluid viscosity. The associated pressure field is given by

$$p^\infty = \delta x. \quad (3)$$

The velocity is required to satisfy the no-slip and no-penetration boundary condition $\mathbf{u} = \mathbf{0}$ over all boundaries. Consequently, the disturbance velocity is required to satisfy the boundary condition $\mathbf{u}^D = -\mathbf{u}^\infty$.

Using the boundary condition for the disturbance velocity, we find that the velocity at a point $\mathbf{x}_0 = (x_0, y_0)$ that lies in the domain of flow is given by the boundary-integral representation

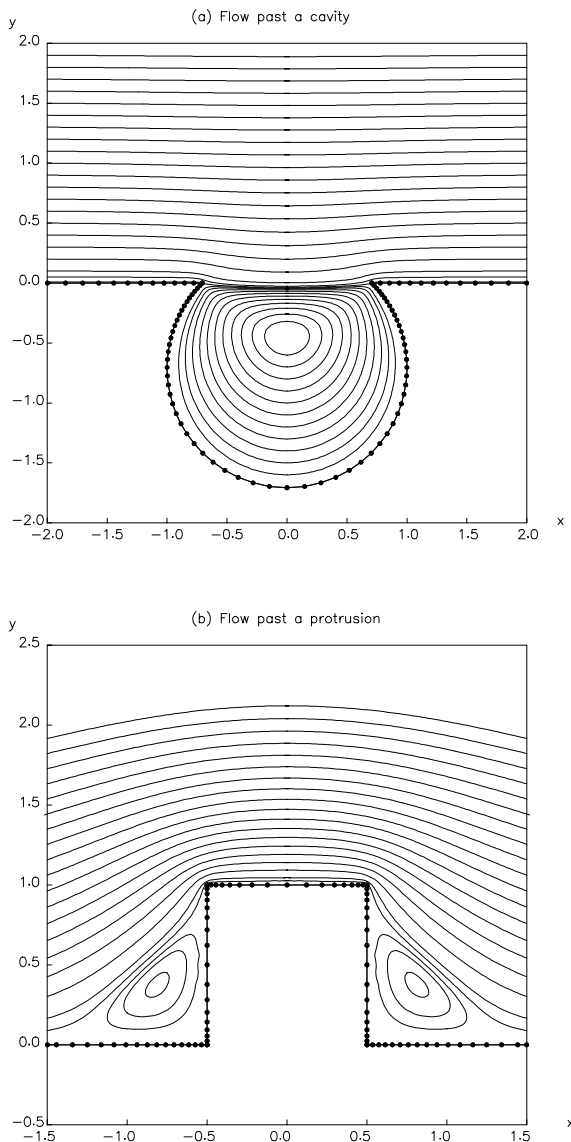


Figure flow_2d.1 Flows implemented in code flow_2d: shear flow past (a) a cavity or (b) a protrusion on a plane wall, possibly in the presence of an upper plane wall in the configuration of channel flow.

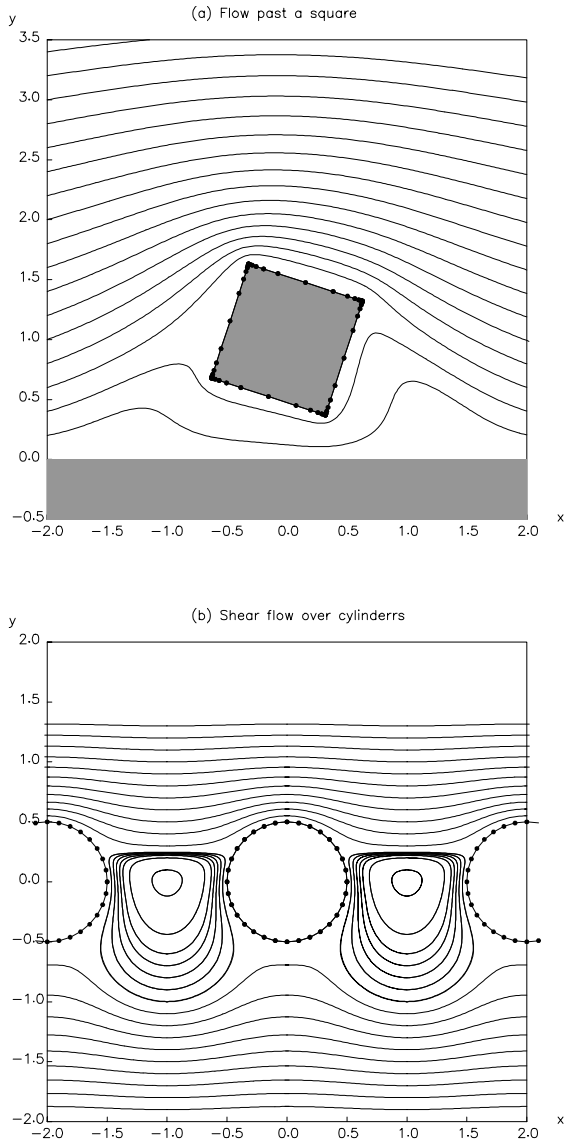


Figure flow_2d.2 Flows implemented in code flow_2d: (a) shear flow past a square above a plane wall, and (b) shear flow over a periodic array of circular cylinders.

$$u_j(\mathbf{x}_0) = u_j^\infty(\mathbf{x}_0) - \frac{1}{4\pi\mu} \int_C G_{ji}(\mathbf{x}_0, \mathbf{x}) f_i^D(\mathbf{x}) dl(\mathbf{x}) \\ - \frac{1}{4\pi} \int_C u_i^\infty(\mathbf{x}) T_{ijk}(\mathbf{x}, \mathbf{x}_0) n_k(\mathbf{x}) dl(\mathbf{x}), \quad (4)$$

where:

- \mathbf{f}^D is the disturbance component of the hydrodynamic traction.
- C is the collection of all boundaries of the flow, including the surface of the lower wall and the surface of the upper plane wall if present.
- \mathbf{n} is the unit vector normal to C pointing into the flow.
- G_{ij} and T_{ijk} are the free-space velocity and stress Green's functions.

Applying equation (4) at a point \mathbf{x}_0 located on C , we obtain an integral equation of the first kind for the disturbance boundary traction \mathbf{f}^D ,

$$\frac{1}{2\pi\mu} \int_C G_{ji}(\mathbf{x}_0, \mathbf{x}) f_i^D(\mathbf{x}) dl(\mathbf{x}) \\ = u_j^\infty(\mathbf{x}_0) - \frac{1}{2\pi} \int_C^{PV} u_i^\infty(\mathbf{x}) T_{ijk}(\mathbf{x}, \mathbf{x}_0) n_k(\mathbf{x}) dl(\mathbf{x}), \quad (5)$$

where PV denotes the principal value of the double-layer potential.

MATHEMATICAL FORMULATION FOR FLOW OVER AN ARRAY OF CYLINDERS:

In the case of infinite simple shear flow over a periodic array of cylinders, as illustrated in Figure flow_2d.2(b), the velocity at a point \mathbf{x}_0 that lies in the domain of flow is given by the boundary-integral representation [61]

$$u_j(\mathbf{x}_0) = U_{Slip} \delta_{jx} - \frac{1}{4\pi\mu} \int_C G_{ji}(\mathbf{x}, \mathbf{x}_0) f_i(\mathbf{x}) dl(\mathbf{x}), \quad (6)$$

where:

- \mathbf{f} is the hydrodynamic traction.
- U_{Slip} is an *a priori* unknown slip velocity.
- C stands for the contour of one cylinder.
- \mathbf{n} is the unit normal vector pointing into the flow.
- G_{ij} is the upward biased singly periodic Green's function of Stokes flow.

A global force balance requires

$$\int_C f_i \, dl = \mu \gamma L \delta_{ix}, \quad (7)$$

where L is the period of the flow (distance between two consecutive cylinders), and γ is the shear rate of the flow far above the cylinders.

Applying the integral representation (6) at a point \mathbf{x}_0 located at a cylinder's surface C , we obtain an integral equation for the traction, accompanied by the integral constraint (7).

Far below the cylinders, the velocity tends to an *a priori* unknown drift velocity given by

$$U_{Drift} = U_{Slip} + \frac{1}{\mu L} \int_C f_x \, y \, dl. \quad (8)$$

The integral on the right-hand side of (8) is evaluated after the solution of the integral equation (6) has been computed.

NUMERICAL METHOD:

The boundaries of the flow are discretized into a collection of straight or circular boundary elements, and the disturbance or total traction, \mathbf{f}^D or \mathbf{f} , and velocity \mathbf{u}^∞ are approximated with constant functions over each element. Applying the integral equation at the mid-point of each element, we obtain a system of linear equations for the element values of the traction. The linear system is solved by Gauss elimination.

Once the solution has been found, the velocity at a point in the flow is computed using the discrete form of the boundary-integral representation. Streamlines are generated by integrating the ordinary differential equations governing the motion of point particles using the fourth-order Runge-Kutta method.

Main program: `flow_2d`

The main program solves integral equations of the first kind for the distribution of the boundary traction or disturbance boundary traction, and computes velocity profiles and streamlines originating from specified points in the flow.

Files to be linked:

1. `elm_arc`
Discretization of a circular segment into arc elements.
2. `elm_line`
Discretization of a straight segment into straight (linear) elements.

3. **flow_2d_geo**
Discretization of the boundary geometry.
4. **flow_2d_sdlp**
Evaluation of the single- and double-layer potential over the boundary elements.
5. **flow_2d_vel**
Evaluation of the velocity at a specified point in the flow.
6. **gauss_leg**
Base points and weights for the Gauss-Legendre quadrature.
7. **gel**
Solution of a linear algebraic system by Gauss elimination.
8. **sgf_2d_1p**
Singly periodic Green's function of Stokes flow.
9. **sgf_2d_fs**
Green's function of Stokes flow in free space.
10. **sgf_2d_w**
Green's function of Stokes flow in a semi-infinite domain bounded by a plane wall.

Input files:

1. **circle.dat**
Parameters for shear flow past a circular cylinder above a plane wall.
2. **circle_1p.dat**
Parameters for shear flow over a periodic array of cylinders.
3. **cvt_crc.dat**
Parameters for shear flow over a circular cavity on a plane wall.
4. **cvt_rec.dat**
Parameters for shear flow over a rectangular cavity on a plane wall.
5. **prt_crc.dat**
Parameters for shear flow over a circular protrusion on a plane wall.
6. **prt_rec.dat**
Parameters for shear flow over a rectangular protrusion on a plane wall.
7. **square.dat**
Parameters for shear flow past a rectangular cylinder above a plane wall.

Output files:

1. `flow_2d.str`
Streamlines.
2. `flow_2d.out1`
Boundary traction.
3. `flow_2d.out2`
Recording of force and torque on an object.
4. `flow_2d.prof`
Velocity profile.

Directory: `stokes/prtcl_sw`

This directory contains a code that computes swirling flow due to the rotation of an axisymmetric particle around its axis with angular velocity Ω in an infinite viscous fluid, as illustrated in Figure `prtcl_sw.1`.

MATHEMATICAL FORMULATION:

Consider the spherical polar coordinates (x, σ, φ) depicted in Figure `prtcl_sw.1`. When inertial effects are negligible, the azimuthal component of the velocity $u_\varphi(x, \sigma)$ satisfies the equation (e.g., [59])

$$\frac{\partial^2 u_\varphi}{\partial x^2} + \frac{1}{\sigma} \frac{\partial}{\partial \sigma} \left(\sigma \frac{\partial u_\varphi}{\partial \sigma} \right) - \frac{u_\varphi}{\sigma^2} = 0, \quad (1)$$

and is subject to the no-slip boundary condition

$$u_\varphi = \Omega \sigma \quad (2)$$

over the particle surface.

The solution can be expressed in the boundary-integral form

$$\begin{aligned} u_\varphi(\mathbf{x}_0) = & - \int_C G(\mathbf{x}, \mathbf{x}_0) [\mathbf{n}(\mathbf{x}) \cdot \nabla u_\varphi(\mathbf{x})] dl(\mathbf{x}) \\ & + \int_C u_\varphi(\mathbf{x}) [\mathbf{n}(\mathbf{x}) \cdot \nabla G(\mathbf{x}, \mathbf{x}_0)] dl(\mathbf{x}), \end{aligned} \quad (3)$$

where C is the particle contour in a plane of constant meridional angle φ , and \mathbf{n} is the unit vector normal to C pointing into the fluid. The kernel $G(\mathbf{x}, \mathbf{x}_0)$ is the free-space axisymmetric Green's function of equation (1), defined as the solution of the equation

$$\frac{\partial^2 G}{\partial x^2} + \frac{1}{\sigma} \frac{\partial}{\partial \sigma} \left(\sigma \frac{\partial G}{\partial \sigma} \right) - \frac{G}{\sigma^2} + \delta_2(x - x_0, \sigma - \sigma_0) = 0, \quad (4)$$

where δ_2 is the delta function in a meridional plane.

It can be shown that the Green's function defined in (4) derives from the free-space Green's function of Laplace's equation in three dimensions denoted by G^{L3D} , as

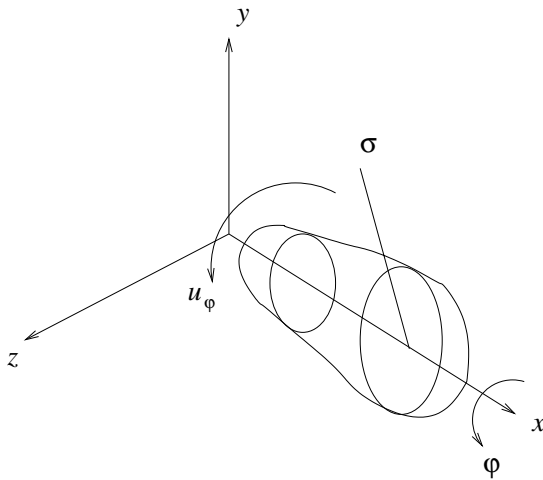


Figure prtcl_sw.1 Swirling flow due to the rotation of an axisymmetric particle in an infinite viscous fluid.

$$\begin{aligned}
 G(x, \sigma, x_0, \sigma_0) &= \sigma \int_0^{2\pi} G^{L3D} \cos(\varphi - \varphi_0) d\varphi = \frac{\sigma}{4\pi} \int_0^{2\pi} \frac{\cos(\varphi - \varphi_0) d\varphi}{|\mathbf{x} - \mathbf{x}_0|} \\
 &= \frac{\sigma}{4\pi} \int_0^{2\pi} \frac{\cos(\varphi - \varphi_0) d\varphi}{\sqrt{(x - x_0)^2 + (y - y_0)^2 + (z - z_0)^2}} \\
 &= \frac{\sigma}{4\pi} \int_0^{2\pi} \frac{\cos(\varphi - \varphi_0) d\varphi}{[(x - x_0)^2 + (\sigma \cos \phi - \sigma_0 \cos \phi_0)^2 + (\sigma \sin \phi - \sigma_0 \sin \phi_0)^2]^{1/2}} \\
 &= \frac{\sigma}{4\pi} \int_0^{2\pi} \frac{\cos(\varphi - \varphi_0) d(\varphi - \varphi_0)}{[(x - x_0)^2 + \sigma^2 + \sigma_0^2 - 2\sigma\sigma_0 \cos(\varphi - \varphi_0)]^{1/2}} \\
 &= \frac{\sigma}{4\pi} \int_0^{2\pi} \frac{\cos u du}{[(x - x_0)^2 + \sigma^2 + \sigma_0^2 - 2\sigma\sigma_0 \cos u]^{1/2}} \\
 &= \frac{\sigma}{4\pi} \int_0^{2\pi} \frac{\cos u du}{[(x - x_0)^2 + (\sigma + \sigma_0)^2 - 4\sigma\sigma_0 \cos^2 \frac{u}{2}]^{1/2}} \\
 &= \frac{\sigma}{\pi \sqrt{(x - x_0)^2 + (\sigma + \sigma_0)^2}} \int_0^{2\pi} \frac{\cos u du}{\sqrt{1 - k^2 \cos^2 \frac{u}{2}}},
 \end{aligned} \tag{5}$$

where $u = \varphi - \varphi_0$, and

$$k^2 \equiv \frac{4 \sigma \sigma_0}{(x - x_0)^2 + (\sigma + \sigma_0)^2}. \quad (6)$$

Expressing the last expression in (5) in terms of the complete elliptic integral of the first and second kind defined, respectively, as

$$F(k) \equiv \int_0^{\pi/2} \frac{d\eta}{\sqrt{1 - k^2 \cos^2 \eta}}, \quad E(k) \equiv \int_0^{\pi/2} \sqrt{1 - k^2 \cos^2 \eta} d\eta, \quad (7)$$

where η is a dummy variable of integration, we find that the Green's function is given by

$$G(x, \sigma, x_0, \sigma_0) = \frac{\sigma}{\pi \sqrt{(x - x_0)^2 + (\sigma + \sigma_0)^2}} \frac{(2 - k^2)F(k) - 2E(k)}{k^2}. \quad (8)$$

Substituting the boundary condition (2) into the double-layer potential on the right-hand side of (3), we find

$$\begin{aligned} u_\varphi(\mathbf{x}_0) = & - \int_C G(\mathbf{x}, \mathbf{x}_0) [\mathbf{n}(\mathbf{x}) \cdot \nabla u_\varphi(\mathbf{x})] dl(\mathbf{x}) \\ & + \Omega \int_C \sigma [\mathbf{n}(\mathbf{x}) \cdot \nabla G(\mathbf{x}, \mathbf{x}_0)] dl(\mathbf{x}). \end{aligned} \quad (9)$$

Next, we apply the reciprocal theorem, choosing as control volume the volume occupied by the particle, and thus convert the double-layer to a single-layer potential. Rearranging, we derive the single-layer representation

$$u_\varphi(\mathbf{x}_0) = - \int_C G(\mathbf{x}, \mathbf{x}_0) \{ \mathbf{n}(\mathbf{x}) \cdot \nabla [u_\varphi(\mathbf{x}) - \Omega \sigma] \} dl(\mathbf{x}), \quad (10)$$

which is equivalent to

$$u_\varphi(\mathbf{x}_0) = - \frac{1}{\mu} \int_C G(\mathbf{x}, \mathbf{x}_0) f_\varphi(\mathbf{x}) dl(\mathbf{x}), \quad (11)$$

where μ is the fluid viscosity, and

$$f_\varphi \equiv \mu \mathbf{n}(\mathbf{x}) \cdot \nabla [u_\varphi(\mathbf{x}) - \Omega \sigma] = \mu [n_x \frac{\partial u_\varphi}{\partial x} + n_\sigma \sigma \frac{\partial}{\partial \sigma} (\frac{u_\varphi}{\sigma})] \quad (12)$$

is the shear stress on the particle surface.

The axial torque exerted on the particle due to the shear stress is given by

$$M_x = 2\pi \int_C f_\varphi \sigma^2 dl. \quad (13)$$

NUMERICAL METHOD:

The particle contour in the upper xy meridional plane is discretized into a collection of boundary elements that may be straight segments or circular arcs, and the shear stress is approximated with a constant function over each element.

Applying the integral equation (11) at collocation points located at the mid-points of the boundary elements, we obtain a system of linear algebraic equations for the element shear stress. The solution is computed by the method of Gauss elimination.

Main program: prtcl_sw

The main program solves the integral equation (11) for the distribution of the shear stress, and computes the torque exerted on the particle.

Files to be linked:

1. `elm_arc`
Discretization of a circular segment into arc elements.
2. `elm_line`
Discretization of a straight segment into straight (linear) elements.
3. `ell_int`
Computation of complete elliptic integrals of the first and second kind.
4. `gauss_leg`
Base points and weights for the Gauss-Legendre quadrature.
5. `gel`
Solution of a linear algebraic system by Gauss elimination.
6. `prtcl_sw_geo`
Boundary element discretization.
7. `prtcl_sw_slp`
Computation of the single-layer potential over boundary elements.

Input files:

1. `sphere.dat`
Parameters for flow due to the rotation of a sphere.
2. `spheroid.dat`
Parameters for flow due to the rotation of a spheroid.

3. torus_trg1.dat

Parameters for flow due to the rotation of a triangular torus.

Output files:

1. pertcl_sw.trc

Distribution of boundary traction.

2. pertcl_sw.xy

Boundary-element distribution around the particle contour.

Directory: `stokes/prtcl_2d`

This directory contains a code that computes flow past a collection of two-dimensional rigid particles with arbitrary shapes for a variety of configurations, as illustrated in Figure `prtcl_2d.1`, including the following:

- A solitary or periodic collection of particles in semi-infinite shear flow bounded by a plane wall, as illustrated in Figure `prtcl_2d.1(a, b)`.
- A periodic collection of particles in a channel bounded by two parallel plane walls, as illustrated in Figure `prtcl_2d.1(c)`.
- A doubly periodic collection of particles in streaming (unidirectional) flow, as illustrated in Figure `prtcl_2d.1(d)`.

MATHEMATICAL FORMULATION:

The fluid velocity \mathbf{u} is decomposed into an incident component, denoted by \mathbf{u}^∞ , and a disturbance component due to the presence of the particles, denoted by \mathbf{u}^D , such that

$$\mathbf{u} = \mathbf{u}^\infty + \mathbf{u}^D. \quad (1)$$

The incident component is defined as follows:

- In the case of shear flow past a solitary or periodic collection of particles in a semi-infinite domain of flow bounded by a plane wall located at $y = w$, as illustrated in Figure `prtcl_2d.1(a, b)`,

$$u_x^\infty = \gamma(y - w) + \frac{\delta}{2\mu}(y - w)^2, \quad u_y^\infty = 0, \quad (2)$$

where γ is the shear rate at the wall, δ is the pressure gradient, and μ is the fluid viscosity. The associated pressure field is given by

$$p^\infty = \delta x. \quad (3)$$

- In the case of shear- or pressure-driven flow past a periodic collection of particles in a channel bounded by two parallel plane walls located at $y = \pm h$, as illustrated in Figure `prtcl_2d.1(c)`,

$$u_x^\infty = U_1 + (U_2 - U_1) \frac{y + h}{2h} + \frac{\delta}{2\mu}(h^2 - y^2), \quad u_y^\infty = 0, \quad (4)$$

where U_1 and U_2 are the velocities of the lower and upper wall, h is the channel semi-width, and δ is the pressure gradient. The associated pressure field is given by (3).

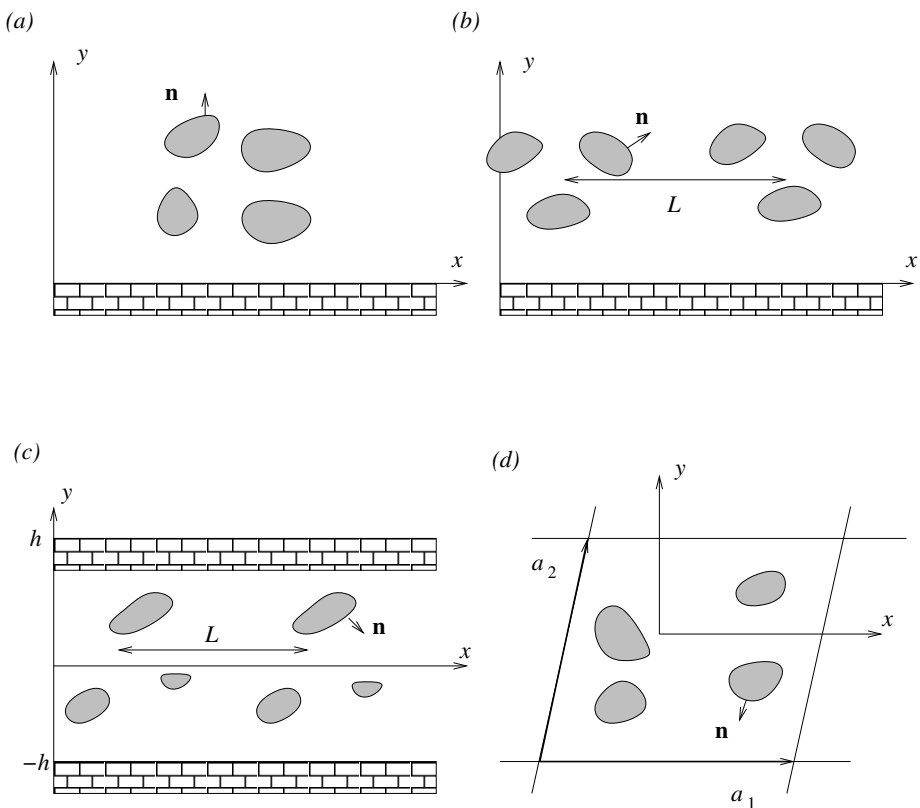


Figure prtcl_2d.1 Schematic illustration of: (a) an isolated collection of particles in semi-infinite shear flow bounded by a plane wall; (b) a periodic collection of particles in semi-infinite shear flow bounded by a plane wall; (c) a periodic collection of particles in a channel bounded by two parallel plane walls; and (d) a doubly-periodic collection of particles in streaming (uniform) flow.

- In the case of uniform (streaming) flow past a doubly periodic lattice of particles, as illustrated in Figure prtcl_2d.1(d),

$$u_x^\infty = U, \quad u_y^\infty = 0, \quad (5)$$

where U is a constant velocity. The associated pressure field is uniform.

The velocity is required to satisfy the no-slip and no-penetration boundary condition $\mathbf{u} = \mathbf{0}$ on the surfaces of the particles and on the boundaries of the flow. Consequently, the disturbance velocity is required to satisfy the boundary condition $\mathbf{u}^D = -\mathbf{u}^\infty$ on the surfaces of the particles and on the boundaries of the flow.

Using the boundary-integral formulation and enforcing the boundary conditions, we express the velocity at a point in the flow as

$$\begin{aligned} u_j(\mathbf{x}_0) &= u_j^\infty(\mathbf{x}_0) - \frac{1}{4\pi\mu} \sum_{q=1}^{N_p} \int_{C_q} G_{ij}(\mathbf{x}, \mathbf{x}_0) f_i^D(\mathbf{x}) dl(\mathbf{x}) \\ &\quad - \frac{1}{4\pi} \sum_{q=1}^{N_p} \int_{C_q} u_i^\infty(\mathbf{x}, \mathbf{x}_0) T_{ijk}(\mathbf{x}, \mathbf{x}_0) n_k(\mathbf{x}) dl(\mathbf{x}), \end{aligned} \quad (6)$$

where N_p is the number of particles, C_q is the contour of the q th particle, and \mathbf{n} is the unit normal vector pointing into the fluid.

Applying the reciprocal relationship for the incident flow over the area occupied by each particle (e.g., [55]), we derive the alternative single-layer representation

$$u_j(\mathbf{x}_0) = u_j^\infty(\mathbf{x}_0) - \frac{1}{4\pi\mu} \sum_{q=1}^{N_p} \int_{C_q} G_{ij}(\mathbf{x}, \mathbf{x}_0) f_i(\mathbf{x}) dl(\mathbf{x}). \quad (7)$$

Taking the limit as the point \mathbf{x}_0 approaches the surface of the m th particle and requiring the boundary conditions, we obtain integral equations of the first kind for the disturbance or total traction,

$$\begin{aligned} &\sum_{q=1}^{N_p} \int_{C_q} G_{ij}(\mathbf{x}, \mathbf{x}_0) f_i^D(\mathbf{x}) dl(\mathbf{x}) \\ &= 2\pi\mu u_j^\infty(\mathbf{x}_0) - \mu \sum_{q=1}^{N_p} \int_{C_q}^{PV} u_i^\infty(\mathbf{x}, \mathbf{x}_0) T_{ijk}(\mathbf{x}, \mathbf{x}_0) n_k(\mathbf{x}) dl(\mathbf{x}), \end{aligned} \quad (8)$$

and

$$\sum_{q=1}^{N_p} \int_{C_q} G_{ij}(\mathbf{x}, \mathbf{x}_0) f_i(\mathbf{x}) dl(\mathbf{x}) = 4\pi\mu u_j^\infty(\mathbf{x}_0), \quad (9)$$

where PV on the right-hand side of (8) denotes the principal value of the double-layer integral.

UNIQUENESS OF SOLUTION OF THE INTEGRAL EQUATION:

Mass conservation for the flow due to a point force situated at the point \mathbf{x}_0 requires the integral identity

$$\int_{C_q} G_{ij}(\mathbf{x}, \mathbf{x}_0) n_i(\mathbf{x}) dl(\mathbf{x}) = 0, \quad (10)$$

for $q = 1, \dots, N_p$. This identity suggests that any solution of the integral equation (8) or (9) over the contour of each particle may be enhanced with an arbitrary multiple of the unit normal vector. Thus, the integral equation has an infinite number of solutions parametrized by N_p scalar constants.

A symmetry property allows us to switch the arguments of the Green's function, provided that we also switch the order of the indices. Using this property, we recast identity (10) into the form

$$\int_{C_q} G_{ij}(\mathbf{x}, \mathbf{x}_0) n_j(\mathbf{x}_0) dl(\mathbf{x}_0) = 0, \quad (11)$$

which suggests the solvability condition

$$\int_{C_q} R_j(\mathbf{x}_0) n_j(\mathbf{x}_0) dl(\mathbf{x}_0) = 0, \quad (12)$$

where R_j is the right-hand side of (8) or (9). Condition (12) is satisfied for any incompressible incident flow.

Numerical method:

The contour of each particle is discretized into boundary elements with straight, circular, or elliptical shapes. The components of the element traction and the incident velocity are approximated with constant functions over each boundary element. Applying the integral equation (8) or (9) at the mid-point of each element, we obtain a system of linear equations

$$\mathbf{A} \cdot \mathbf{w} = \mathbf{b}, \quad (13)$$

where \mathbf{A} is the “master influence matrix” whose elements are defined in terms of integrals of the Green's function over the boundary elements, and the unknown vector \mathbf{w} contains the x and y components of the traction over the elements. The size of the system (13) is equal to twice the total number of boundary elements over all particle contours.

UNIQUENESS OF SOLUTION:

The discrete form of the integral identity (11) is

$$\mathbf{A}^{(q)} \cdot \mathbf{e}^{(q)} = \mathbf{0}, \quad (14)$$

where:

- $\mathbf{e}^{(q)}$ is the discrete right eigenvector for the q particle consisting of the x and y components of the normal vector at the mid-points of the boundary elements around the particle contour.
- The matrix $\mathbf{A}^{(q)}$ is the diagonal block of the master linear matrix corresponding to the q th particle. All entries of the matrix $\mathbf{A}^{(q)}$ are defined in terms of integrals of the single-layer potential over the boundary elements of the q th particle.

When the particle contour is polygonal, the normal vector is constant over each element and identity (14) is satisfied up to the numerical error due to the numerical integration. More generally, (14) is satisfied up to the discretization error. In either case, the linear system (13) is precisely or nearly singular, and normalization or preconditioning is required.

SINGULAR PRECONDITIONING AND REGULARIZATION:

The discrete form of the solvability condition (12) is

$$\mathbf{v}^{(q)} \cdot \mathbf{b} = 0, \quad (15)$$

where $\mathbf{v}^{(q)}$ is the discrete left eigenvector of the influence matrix for the q th particle, containing the x and y components of the normal vector at the mid-points of the boundary elements around the particle contour multiplied by the element arc length. In further discussion, we shall tacitly assume that $\mathbf{v}^{(q)}$ has been normalized so that its Euclidean norm is equal to unity.

When the particle contour is polygonal and the vector \mathbf{b} is constant, corresponding, for example, to a uniform incident flow, the left eigenvector $\mathbf{v}^{(q)}$ satisfies the discrete form of the solvability condition (15) to machine precision. More generally, (15) is satisfied up to the discretization error.

Using the integral identity (10), we derive the discrete identity

$$\mathbf{v}^{(q)} \cdot \mathbf{A}^{(q)} = \mathbf{0}. \quad (16)$$

When the particle contour is polygonal, the normal vector is constant over each element and identity (16) is satisfied up to the numerical error incurred by the numerical integration. More generally, (16) is satisfied up to the discretization error.

One way to regularize the master linear system (13) is by applying “singular preconditioning”. This is implemented by premultiplying both sides with a preconditioning matrix \mathbf{P} defined as

$$\mathbf{P} \equiv (\mathbf{I} - \mathbf{V}^{(1)} \mathbf{V}^{(1)^T}) \cdot (\mathbf{I} - \mathbf{V}^{(2)} \mathbf{V}^{(2)^T}) \cdot \dots \cdot (\mathbf{I} - \mathbf{V}^{(N_p)} \mathbf{V}^{(N_p)^T}), \quad (17)$$

where $\mathbf{V}^{(q)}$ is the extended discrete left eigenvector for the q th particle. All elements of this vector are equal to zero, except for the elements in the boundary element block for the q th particle that are equal to the corresponding elements of the discrete left eigenvector $\mathbf{v}^{(q)}$.

After singular preconditioning, system (13) is transformed to

$$\mathbf{A}^P \cdot \mathbf{w} = \mathbf{b}^P, \quad (18)$$

where

$$\mathbf{A}^P \equiv \mathbf{P} \cdot \mathbf{A}, \quad \mathbf{b}^P \equiv \mathbf{P} \cdot \mathbf{b}. \quad (19)$$

Note that $\mathbf{V}^{(q)}$ is an exact left eigenvector of the singular matrix \mathbf{A}^P corresponding to the vanishing eigenvalue, and the solvability condition

$$\mathbf{V}^{(q)} \cdot \mathbf{b}^P = 0 \quad (20)$$

is satisfied to machine accuracy. Thus, singular preconditioning guarantees the exact satisfaction of the discrete solvability condition (15) while representing the mildest possible modification of the discretized governing equations.

After singular preconditioning, the master linear system is regularized by discarding one linear equation corresponding to an arbitrary collocation point over each particle, and replacing it with the discrete form of the integral constraint

$$\int_{C_q} \mathbf{f} \cdot \mathbf{n} dl = c_q, \quad (21)$$

for $q = 1, \dots, N_p$, where c_q is an arbitrary constant. Regularization removes the N_p degrees of freedom in the solution of the integral equation and allows us to solve a perfectly well-posed problem.

Singular preconditioning is activated by setting the input flag: $Iprec = 1$. Regularization is activated by setting the input flag: $Ireg = 1$.

ITERATIVE SOLUTION OF THE MASTER LINEAR SYSTEM:

The master linear system is solved by a physically motivated iterative method based on the equation

$$\mathbf{D} \cdot \mathbf{w}^{(k+1)} = \mathbf{N} \cdot \mathbf{w}^{(k)} + \mathbf{b}, \quad (22)$$

where the matrix \mathbf{D} consists of diagonal blocks corresponding to particle clusters, and $\mathbf{N} \equiv \mathbf{A} - \mathbf{D}$. The iterations are carried out by computing the inverses of the diagonal blocks comprising the matrix \mathbf{D} , and then explicitly solving for $\mathbf{x}^{(k+1)}$ by carrying out matrix multiplications.

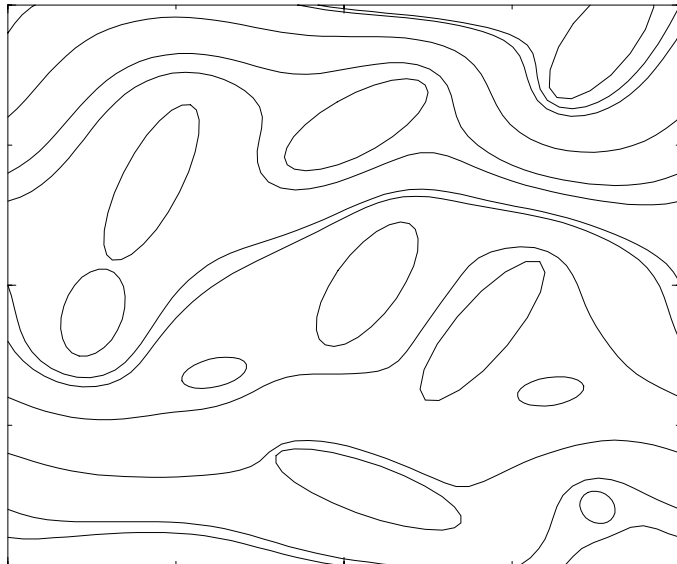


Figure prtcl_2d.2 Streamline pattern of doubly periodic Stokes flow past a collection of two-dimensional particles.

When the particles are well separated, and each block contains one particle, only a few iterations are necessary to obtain the solution with accuracy comparable to the round off error. When particle clusters are present, achieving rapid convergence or even convergence at all requires that the diagonal blocks contain particle clusters.

STREAMLINES:

Streamlines are drawn by integrating the differential equations governing the motion of point particles in the fluid using the second- or fourth-order Runge-Kutta method. The velocity is computed using the discrete version of the single-layer integral representation (6). A streamline pattern of doubly periodic flow is illustrated in figure prtcl_2d.2.

Main program: `flow_2d`

The main program solves the integral equation (8) or (9) for the distribution of the disturbance or traction over the particle surfaces, and computes streamlines originating from specified points in the flow.

Files to be linked:

1. `exp_int`
Computation of the exponential integral required by `sgf_2d_2p`.
2. `gauss_leg`
Base points and weights for the Gauss-Legendre quadrature.
3. `gel_inv`
Computation of the inverse of a matrix by Gauss elimination.
4. `prtcl_2d_aux`
Subroutines to precondition and reduce the master linear system.
5. `prtcl_2d_geo`
Discretization of particle contours.
6. `prtcl_2d_sdlp`
Evaluation of the single- and double-layer potential over the boundary elements.
7. `prtcl_2d_strml`
Computes a streamline originating from a specified point in the flow.
8. `prtcl_2d_sys`
Generates and solves by iteration the master linear system.
9. `prtcl_2d_vel`
Evaluates the velocity at a point in the flow.
10. `sgf_2d_1p_w`
Periodic Green's function of Stokes flow in a semi-infinite domain bounded by a plane wall.
11. `sgf_2d_1p_ww`
Periodic Green's function of Stokes flow for an infinite strip bounded by two parallel walls.
12. `sgf_2d_2p`
Doubly periodic Green's function of Stokes flow.
13. `sgf_2d_fs`
Green's function of Stokes flow in free space.
14. `sgf_2d_w`
Green's function of Stokes flow in a semi-infinite domain bounded by a plane wall.

Input files:

1. `prtcl_2d.dat`
Problem selection and specification of input parameters.
2. `prtcl_2d.geo.dat`
Particle position, orientation, and geometry. Particle distributions are generated by program `prtcl_2d_gen` included in this directory.
3. `prtcl_2d.inp.dat`
Collocation points and boundary traction (read to generate streamlines without solving the integral equation).
4. `strml.dat`
Starting points for drawing streamlines.

Output files:

1. `prtcl_2d.xy`
Collocation points and traction at boundary elements.
2. `prtcl_2d.error`
Transient error in the iterative solution of the master linear system.
3. `prtcl_2d.strml`
Recording of boundary and particle contours and streamlines.

Directory: `stokes/prtcl_ax`

This directory contains a code that computes axisymmetric flow past, or due to the axial motion of, a collection of particles with arbitrary shapes for several flow configurations, including the following:

- Uniform axial flow past a collection of stationary particles, and flow due to particle translation along the x axis, as illustrated in Figure `prtcl_ax.1(a)`.
- Flow due to particle translation normal to an infinite plane wall, as illustrated in Figure `prtcl_ax.1(b)`.
- Poiseuille flow past a periodic collection of stationary particles, and flow due to particle translation along the axis of a circular tube, as illustrated in Figure `prtcl_ax.1(c)`.

MATHEMATICAL FORMULATION:

Consider the cylindrical polar coordinates (x, σ, φ) defined in Figure `prtcl_ax.1`. We begin by decomposing the fluid velocity \mathbf{u} into an incident component denoted by \mathbf{u}^∞ , and a disturbance component due to the presence of the particles denoted by \mathbf{u}^D , such that

$$\mathbf{u} = \mathbf{u}^\infty + \mathbf{u}^D. \quad (1)$$

If the flow is due to the motion of the particles, the incident component vanishes. In the case of pressure-driven Poiseuille flow illustrated in Figure `prt_ax.1.(c)`, the radial and meridional components of the incident velocity vanish, and the axial component is given by

$$u_x^\infty = -\frac{dp}{dx} \frac{1}{4\mu} (\sigma^2 - a^2), \quad (2)$$

where a is the tube radius, μ is the fluid viscosity, and dp/dx is the constant streamwise pressure gradient.

The velocity is required to satisfy the no-slip and no-penetration boundary conditions on the surfaces of the particles as well as on the boundaries of the flow, stating that the fluid velocity is equal to the boundary velocity.

Using the boundary-integral formulation for axisymmetric Stokes flow, and implementing the no-slip and no-penetration boundary conditions, we express the velocity

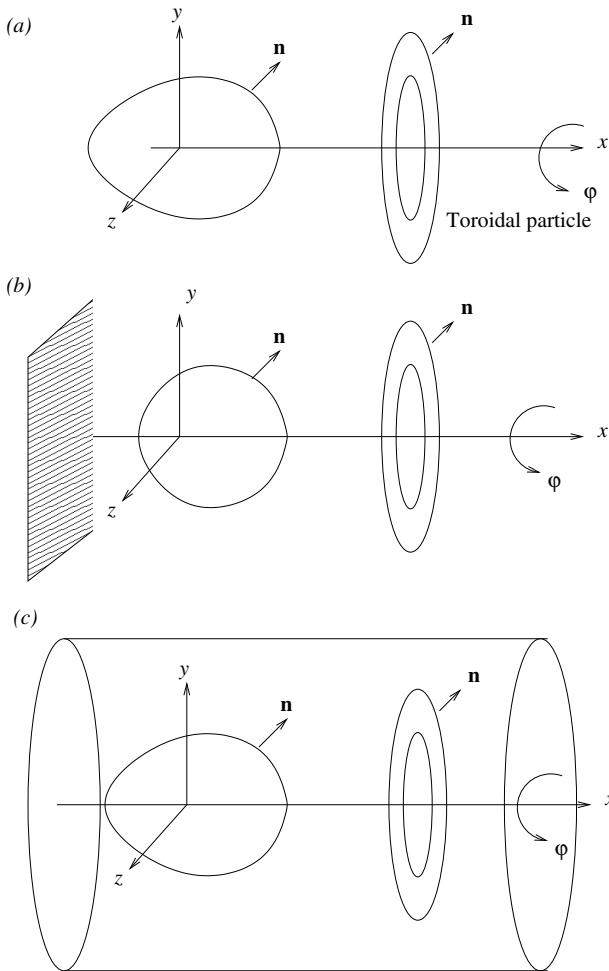


Figure prtcl_ax.1 Schematic illustration of axisymmetric flow past, or due to the axial motion of, a collection of rigid particles.

at a point \mathbf{x}_0 in the flow in the integral form

$$u_\alpha(\mathbf{x}_0) = u_\alpha^\infty(\mathbf{x}_0) - \frac{1}{8\pi\mu} \sum_{q=1}^{N_p} \int_{C_q} G_{\alpha\beta}(\mathbf{x}_0, \mathbf{x}) f_\beta(\mathbf{x}) dl(\mathbf{x}), \quad (3)$$

where N_p is the number particles, C_q is the contour of the q th particle in a meridional plane, \mathbf{n} is the unit normal vector pointing into the fluid, and Greek indices run over x and σ .

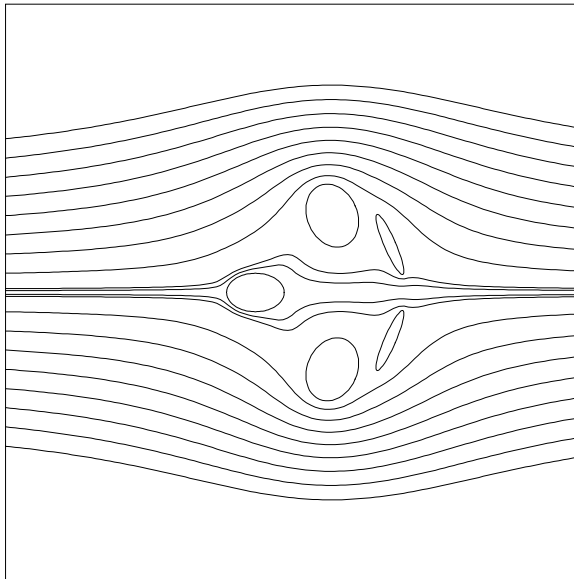


Figure prtcl_ax.2 Streamline pattern of axisymmetric Stokes flow past a compact and two toroidal particles.

Taking the limit as the point x_0 approaches the surface of the m th particle and enforcing the boundary conditions, we reduce the integral representation (3) to an integral equation of the first kind for the distribution of the particle traction.

The integral equation has an infinite number of solutions. Any particular solution over each particle surface may be enhanced with an arbitrary multiple of the normal vector, as discussed in directory prtcl_2d.

NUMERICAL METHOD:

The numerical method is similar to that discussed in directory prtcl_2d for the analogous problem of two-dimensional flow, involving singular preconditioning, reduction, and iterative solution of the master linear system.

Main program: flow_ax

The main program solves the integral equation (3) for the distribution of the disturbance traction over the particle contours, and computes streamlines originating from specified points in the flow. A streamline pattern is illustrated in figure prtcl_ax.2.

Files to be linked:

1. `bess_I01K01`
Evaluates the modified Bessel functions required by `sgf_ax_1p_ct`.
2. `ell_int`
Evaluates complete elliptic integrals of the first and second kind.
3. `gauss_leg`
Base points and weights for the Gauss-Legendre quadrature.
4. `gel_inv`
Computation of the inverse of a matrix by Gauss elimination.
5. `prtcl_ax_aux`
Subroutines to precondition and reduce the master linear system.
6. `prtcl_ax_geo`
Discretization of particle contours.
7. `prtcl_ax_slp`
Evaluation of the single-layer potential over the boundary elements.
8. `prtcl_ax_strml`
Computes a streamline originating from a specified point in the flow.
9. `prtcl_ax_sys`
Generates and solves by iteration the master linear system.
10. `prtcl_ax_vel`
Evaluates the velocity at a point in the flow.
11. `sgf_ax_fs`
Axisymmetric Green's function for flow in free space.
12. `sgf_ax_w`
Axisymmetric Green's function for flow bounded by a plane wall.
13. `sgf_ax_1p_ct`
Axisymmetric Green's function for periodic flow inside a circular tube.

Input files:

1. `prtcl_ax.dat`
Problem selection and specification of input parameters.
2. `prtcl_ax_geo.dat`
Particle position and geometry.

3. `prtcl_ax.inp.dat`
Collocation points and boundary traction (read to generate streamlines without solving the integral equation).
4. `strml.dat`
Starting points for drawing streamlines.

Output files:

1. `prtcl_ax.xy`
Collocation points and traction at boundary elements.
2. `prtcl_ax.error`
Transient error in the iterative solution of the master linear system.
3. `prtcl_ax.strml`
Recording of boundary and particle contours and streamlines.

Directory: `stokes/prtcl_3d`

This directory contains a code that computes flow past, or due to the motion of, a solitary particle or periodic collection of three-dimensional particles with arbitrary shapes for a variety of configurations, including the following:

- Flow past, or due to the motion of, a solitary particle in an infinite domain of flow, as illustrated in Figure `prtcl_3d.1(a)`.
- Flow past, or due to the motion of, a solitary particle in a semi-infinite domain of flow bounded by a plane wall, as illustrated in Figure `prtcl_3d.1(b)`.
- Streaming (uniform) flow past a triply periodic array of particles representing an ordered porous medium, as illustrated in Figure `prtcl_3d.1(c)`. The periodicity of the lattice is determined by the three base vectors \mathbf{a}_1 , \mathbf{a}_2 , and \mathbf{a}_3 .
- Streaming flow normal to a doubly periodic array of particles arranged in a plane, representing a screen, as illustrated in Figure `prtcl_3d.1(d)`. The periodicity of the array is determined by the base vectors \mathbf{a}_1 and \mathbf{a}_2 .
- Simple shear flow past a doubly periodic array of particles arranged in a plane, representing a sieve [61], as illustrated in Figure `prtcl_3d.1(d)`. The periodicity of the array is determined by the base vectors \mathbf{a}_1 and \mathbf{a}_2 .

MATHEMATICAL FORMULATION:

The fluid velocity \mathbf{u} is decomposed into an incident component, denoted by \mathbf{u}^∞ , and a disturbance component due to the presence or motion of the particles, denoted by \mathbf{u}^D , such that

$$\mathbf{u} = \mathbf{u}^\infty + \mathbf{u}^D. \quad (1)$$

When the flow is due to the motion of the particles, the incident velocity vanishes.

Using the boundary-integral formulation and enforcing the boundary conditions, we express the velocity at a point \mathbf{x}_0 in the flow in terms of a single-layer potential,

$$u_j(\mathbf{x}_0) = u_j^\infty(\mathbf{x}_0) - \frac{1}{8\pi\mu} \int_D G_{ij}(\mathbf{x}, \mathbf{x}_0) f_i(\mathbf{x}) dS(\mathbf{x}), \quad (2)$$

where μ is the fluid viscosity, D is the particle surface, \mathbf{n} is the unit normal vector pointing into the fluid, and G_{ij} is the velocity Green's function corresponding to the particular flow under consideration.

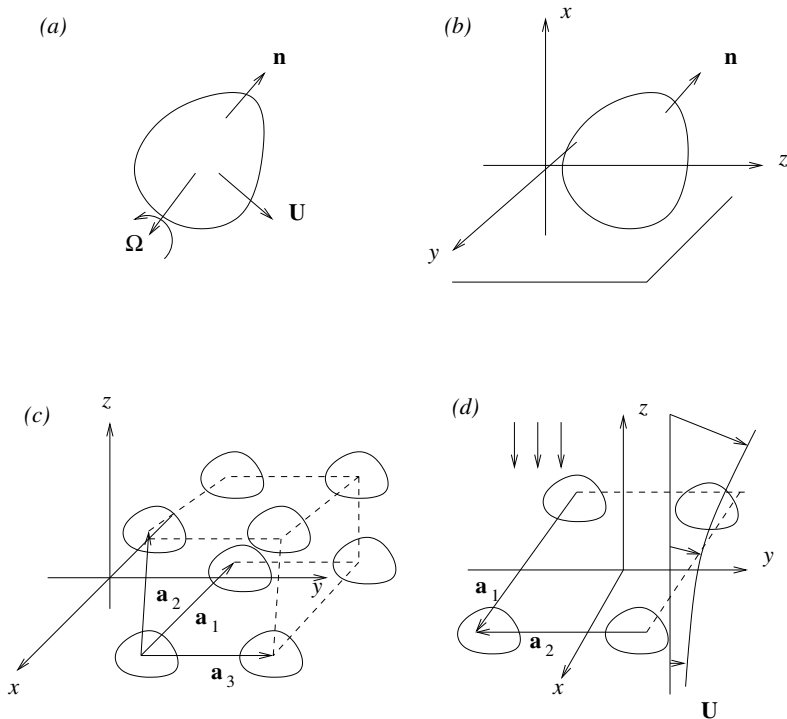


Figure prtcl_2d.1 Schematic illustration of flow past, or due to the motion of, (a) a solitary particle in an infinite domain of flow, (b) a solitary particle in a semi-infinite domain of flow bounded by a plane wall, (c) a particle that belongs to a triply periodic array; (d) uniform flow normal to, or shear flow past, a doubly periodic array of particles representing a screen.

Taking the limit as the point x_0 approaches the particle surface, and requiring the boundary conditions, we obtain an integral equation of the first kind for the boundary traction.

In the case of shear flow past a planar lattice illustrated in Figure prtcl_3d.1(d), the x and y components of the right-hand side of (2) contain two *a priori* unknown drift velocities $U_x^{-\infty}$ and $U_y^{-\infty}$. Requiring that the shear rate vanish far below the array and performing a force balance over one period, we find

$$\int_D f_x \, dS = \mu \gamma_x A, \quad \int_D f_y \, dS = \mu \gamma_y A, \quad (3)$$

where A is the area of the unit lattice cell, and γ_x, γ_y are the shear rates far above

the array in the directions of the x and y axes [61]. The equations in (3) provide us with conditions necessary for the computation of $U_x^{-\infty}$ and $U_y^{-\infty}$.

UNIQUENESS OF SOLUTION OF THE INTEGRAL EQUATION:

Mass conservation for the flow due to a point force situated at the point \mathbf{x}_0 requires the integral identity

$$\int_D G_{ij}(\mathbf{x}, \mathbf{x}_0) n_i(\mathbf{x}) dS(\mathbf{x}) = 0, \quad (4)$$

which suggests that any solution of the integral equation (2) may be enhanced with an arbitrary multiple of the unit normal vector. Thus, the integral equation has an infinite number of solutions parametrized by an arbitrary scalar constant.

A symmetry property allows us to switch the arguments of the Green's function, provided that we also switch the order of the indices. Using this property, we recast identity (4) into the form

$$\int_D G_{ij}(\mathbf{x}, \mathbf{x}_0) n_j(\mathbf{x}_0) dS(\mathbf{x}_0) = 0, \quad (5)$$

which suggests the solvability condition

$$\int_{C_q} u_j^\infty(\mathbf{x}_0) n_j(\mathbf{x}_0) dl(\mathbf{x}_0) = 0. \quad (6)$$

Condition (6) is satisfied for any incompressible incident flow.

NUMERICAL METHOD:

The particle surface is discretized into a collection of six-node curved triangles arising from the successive subdivisions of an octahedron. Approximating the components of the traction with constant functions over each element, and applying the integral equation (2) at collocation points located at the centroid of each element, we obtain the linear system

$$\mathbf{A} \cdot \mathbf{w} = \mathbf{b}, \quad (7)$$

where \mathbf{A} is an influence matrix whose elements are defined in terms of integrals of the Green's function over the boundary elements, and the unknown vector \mathbf{w} contains the x , y , and z components of the traction over the boundary elements. The size of system (7) is equal to three times the number of boundary elements.

In the case of shear flow past a two-dimensional particle array, as illustrated in Figure prtel_3d.1(d), the scalar drift velocities $U_x^{-\infty}$ and $U_y^{-\infty}$ are appended to the vector \mathbf{w} , and the linear system is augmented with the two scalar constraints expressed by (3).

UNIQUENESS OF SOLUTION:

The discrete form of the integral identity (4) is

$$\mathbf{A} \cdot \mathbf{e} = \mathbf{0}, \quad (8)$$

where \mathbf{e} is the discrete right eigenvector consisting of the x , y , and z components of the normal vector at the mid-points of the boundary elements.

When the particle contour is polyhedral, the normal vector is constant over each element and identity (8) is satisfied up to the numerical error due to the numerical integration. More generally, (8) is satisfied up to the discretization error. In either case, the linear system (7) is precisely or nearly singular, and normalization or preconditioning is required.

SINGULAR PRECONDITIONING AND REGULARIZATION:

The discrete form of the solvability condition (6) is

$$\mathbf{v} \cdot \mathbf{b} = \mathbf{0}, \quad (9)$$

where \mathbf{v} is the discrete left eigenvector containing the x , y , and z components of the normal vector at the mid-points of the boundary elements multiplied by the element surface areas. In further discussion, we shall tacitly assume that \mathbf{v} has been normalized so that its Euclidean norm is equal to unity.

When the particle contour is polyhedral and the vector \mathbf{b} is constant, corresponding, for example, to a uniform incident flow, the left eigenvector \mathbf{v} satisfies the discrete form of the solvability condition (9) to machine precision. More generally, (9) is satisfied up to the discretization error.

Using the integral identity (5), we derive the discrete identity

$$\mathbf{v} \cdot \mathbf{A} = \mathbf{0}, \quad (10)$$

When the particle contour is polyhedral, the normal vector is constant over each element and identity (10) is satisfied up to the numerical error incurred by the numerical integration. More generally, (10) is satisfied up to the discretization error.

One way to regularize the linear system (7) is by applying “singular preconditioning”, implemented by premultiplying both sides by the preconditioning matrix

$$\mathbf{P} \equiv \mathbf{I} - \mathbf{v}\mathbf{v}. \quad (11)$$

After singular preconditioning, system (7) is transformed into

$$\mathbf{A}^P \cdot \mathbf{w} = \mathbf{b}^P, \quad (12)$$

where

$$\mathbf{A}^P \equiv \mathbf{P} \cdot \mathbf{A}, \quad \mathbf{b}^P \equiv \mathbf{P} \cdot \mathbf{b}. \quad (13)$$

Note that \mathbf{v} is an exact left eigenvector of the singular matrix \mathbf{A}^P corresponding to the vanishing eigenvalue, and the solvability condition

$$\mathbf{V}^{(q)} \cdot \mathbf{b}^P = \mathbf{0} \quad (14)$$

is satisfied to machine accuracy. Thus, singular preconditioning guarantees the exact satisfaction of the discrete solvability condition (9) while representing the mildest possible modification of the discretized governing equations.

After singular preconditioning, the master linear system is regularized by discarding one linear equation corresponding to an arbitrary collocation point over the particle, and replacing it with the discrete form of the integral constraint

$$\int_D \mathbf{f} \cdot \mathbf{n} \, dS = 1. \quad (15)$$

Regularization removes the one-parameter degree of freedom in the solution of the integral equation, and allows us to solve a well-posed problem.

Singular preconditioning is activated by setting the input flag: $Iprec = 1$. Regularization is activated by setting the input flag: $Ireg = 1$.

Main program: flow_2d

The main program solves an integral equation of the first kind for the distribution of the traction over the particle surface, and computes various quantities relevant to the selected type of flow.

In the case of flow due to the motion of a particle, the program computes the grand resistance tensor [55].

Files to be linked:

1. cond_num
Condition number of a matrix.
2. gauss_leg
Base points and weights for the Gauss-Legendre quadrature.
3. gauss_trgl
Base points and weights for integrating over a triangle.
4. gel_mrhs
Gauss elimination of a linear system with multiple right-hand sides.

5. `gel_power`
Gauss elimination required by the power method for inverse iterations.
6. `prtcl_3d_geo`
Various assisting subroutines concerning geometry.
7. `prtcl_3d_prec`
Preconditioning of the linear system resulting from the boundary-element method.
8. `power`
Power method for computing eigenvalues, required by `cond_num`.
9. `prtcl_3d_slp`
Computes the single-layer potential over the boundary elements.
10. `sgf_3d_fs`
Green's function of Stokes flow in free space.
11. `sgf_3d_w`
Green's function for semi-infinite flow bounded by a plane wall.
12. `sgf_3d_3p`
Green's function for triply periodic flow.
13. `sgf_3d_2p`
Green's function for doubly periodic flow.
14. `trgl_octa`
Triangulation of a sphere based on the successive subdivisions of an octahedron.

Input file:

1. `prtcl_3d.dat`
Problem selection and specification of input parameters.

Output file:

1. `prtcl_3d.out`
Various recordings.

Appendix A

Mathematical supplement

A.1 INDEX NOTATION

In index notation, a vector \mathbf{u} in the N th dimensional space is denoted as u_i , where $i = 1, \dots, N$, a two-dimensional matrix \mathbf{A} is denoted as A_{ij} , where the indices run over appropriate ranges, and a three-dimensional matrix \mathbf{T} is denoted as T_{ijk} ; similar notation is used for higher-dimensional matrices.

Einstein's repeated-index summation convention states that, if a subscript appears twice in an expression involving products, then summation over that subscript is implied in its range. Under this convention,

$$\begin{aligned} u_i v_i &\equiv u_1 v_1 + u_2 v_2 + \dots + u_N v_N, \\ A_{ii} &\equiv A_{11} + A_{22} + \dots + A_{NN}, \end{aligned} \tag{A.1.1}$$

where N is the maximum value of the index i . The first expression defines the inner product of the pair of vectors \mathbf{u} and \mathbf{v} .

A.2 KRONECKER'S DELTA

Kronecker's delta δ_{ij} represents the identity or unit matrix: $\delta_{ij} = 1$ if $i = j$, and $\delta_{ij} = 0$ if $i \neq j$. Using this definition, we find

$$\begin{aligned} u_i \delta_{ij} &= u_j, & A_{ij} \delta_{jk} &= A_{ik}, & \delta_{ij} A_{jk} \delta_{kl} &= A_{il}, \\ \delta_{ij} \delta_{jk} \delta_{kl} &= \delta_{il}, & \delta_{ii} &= N, \end{aligned} \tag{A.2.1}$$

where N is the maximum value of the index i .

If x_i is a set of N independent variables, then

$$\frac{\partial x_i}{\partial x_j} = \delta_{ij}, \quad \frac{\partial x_i}{\partial x_i} = N. \tag{A.2.2}$$

A.3 ALTERNATING TENSOR

The alternating tensor ϵ_{ijk} , where all three indices range over 1, 2, and 3, is defined such that $\epsilon_{ijk} = 0$ if any two indices have the same value, $\epsilon_{ijk} = 1$ if the indices are arranged in one of the cyclic orders 123, 312, or 231, and $\epsilon_{ijk} = -1$ otherwise. Thus,

$$\begin{aligned}\epsilon_{132} &= -1, & \epsilon_{122} &= 0, & \epsilon_{ijj} &= 0, \\ \epsilon_{ijk} &= \epsilon_{jki} = \epsilon_{kij}.\end{aligned}\tag{A.3.1}$$

Two useful properties of the alternating matrix are

$$\begin{aligned}\epsilon_{ijk} \epsilon_{ijl} &= 2 \delta_{kl}, \\ \epsilon_{ijk} \epsilon_{ilm} &= \delta_{jl} \delta_{km} - \delta_{jm} \delta_{kl}.\end{aligned}\tag{A.3.2}$$

A.4 TWO- AND THREE-DIMENSIONAL VECTORS

The inner product of a pair of two- or three-dimensional vectors **a** and **b** is a scalar defined as $s \equiv \mathbf{a} \cdot \mathbf{b} = a_i b_i$. If the inner product vanishes, then the two vectors are orthogonal. The inner product is equal to the product of the lengths of the two vectors and the cosine of the angle subtended between the vectors in their plane.

The outer product of a pair of two- or three-dimensional vectors **a** and **b** is a new vector **c** $\equiv \mathbf{a} \times \mathbf{b}$ given by the determinant of a matrix,

$$\mathbf{c} \equiv \begin{bmatrix} \mathbf{e}_1 & \mathbf{e}_2 & \mathbf{e}_3 \\ a_1 & a_2 & a_3 \\ b_1 & b_2 & b_3 \end{bmatrix},\tag{A.4.1}$$

where \mathbf{e}_i are unit vectors in the subscripted directions. If the outer product vanishes, then the two vectors are parallel. The magnitude of the outer product is equal to the product of the lengths of the vectors **a** and **b**, and the sine of the angle subtended between these vectors in their plane. The outer product is oriented normal to the plane of **a** and **b**, and its direction is determined by the right-handed rule applied to the ordered triplet **a**, **b**, and **c**.

The triple scalar product of the ordered triplet of vectors **a**, **b**, and **c** is the scalar $s \equiv (\mathbf{a} \times \mathbf{b}) \cdot \mathbf{c} = (\mathbf{c} \times \mathbf{a}) \cdot \mathbf{b} = (\mathbf{b} \times \mathbf{c}) \cdot \mathbf{a}$, which is equal to the determinant of the matrix

$$\begin{bmatrix} a_1 & a_2 & a_3 \\ b_1 & b_2 & b_3 \\ c_1 & c_2 & c_3 \end{bmatrix}.\tag{A.4.2}$$

A.5 DEL OR NABLA OPERATOR

The Cartesian components of the *del* or *nabla* operator ∇ are the partial derivatives with respect to the corresponding coordinates,

$$\nabla \equiv \left(\frac{\partial}{\partial x}, \frac{\partial}{\partial y}, \frac{\partial}{\partial z} \right). \quad (\text{A.5.1})$$

In two dimensions, only the x and y derivatives appear.

A.6 GRADIENT AND DIVERGENCE

If f is a scalar function of position \mathbf{x} , then its gradient ∇f is a vector defined as

$$\nabla f = \mathbf{e}_x \frac{\partial f}{\partial x} + \mathbf{e}_y \frac{\partial f}{\partial y} + \mathbf{e}_z \frac{\partial f}{\partial z}, \quad (\text{A.6.1})$$

where \mathbf{e}_i are unit vectors in the directions of the subscripted axes.

The Laplacian of the scalar function f is a scalar defined as

$$\nabla \cdot (\nabla f) \equiv \nabla^2 f = \frac{\partial^2 f}{\partial x^2} + \frac{\partial^2 f}{\partial y^2} + \frac{\partial^2 f}{\partial z^2}. \quad (\text{A.6.2})$$

The Laplacian is equal to the divergence of the gradient. The divergence of a vector function of position $\mathbf{F} = (F_x, F_y, F_z)$ is a scalar defined as

$$\nabla \cdot \mathbf{F} = \frac{\partial F_i}{\partial x_i} = \frac{\partial F_x}{\partial x} + \frac{\partial F_y}{\partial y} + \frac{\partial F_z}{\partial z}. \quad (\text{A.6.3})$$

If $\nabla \cdot \mathbf{F}$ vanishes at every point, then the vector field \mathbf{F} is called *solenoidal*.

The gradient of the vector field \mathbf{F} , denoted by $\mathbf{U} \equiv \nabla \mathbf{F}$, is a two-dimensional matrix with elements

$$U_{ij} = \frac{\partial F_j}{\partial x_i}. \quad (\text{A.6.4})$$

The divergence of \mathbf{F} is equal to the trace of \mathbf{U} , which is equal to the sum of the diagonal elements.

The curl of the vector field \mathbf{F} , denoted as $\nabla \times \mathbf{F}$, is another vector field computed according to the usual rules of the outer vector product, treating the del operator as a regular vector, yielding

$$\nabla \times \mathbf{F} = \mathbf{e}_x \left(\frac{\partial F_z}{\partial y} - \frac{\partial F_y}{\partial z} \right) + \mathbf{e}_y \left(\frac{\partial F_x}{\partial z} - \frac{\partial F_z}{\partial x} \right) + \mathbf{e}_z \left(\frac{\partial F_y}{\partial x} - \frac{\partial F_x}{\partial y} \right). \quad (\text{A.6.5})$$

A.7 VECTOR IDENTITIES

If f is a scalar function and \mathbf{F}, \mathbf{G} are two vector functions, we can show by working in index notation that

$$\nabla \cdot (f \mathbf{F}) = f \nabla \cdot \mathbf{F} + \mathbf{F} \cdot \nabla f, \quad (\text{A.7.1})$$

$$\nabla \cdot (\mathbf{F} \cdot \mathbf{G}) = \mathbf{F} \cdot \nabla \mathbf{G} + \mathbf{G} \cdot \nabla \mathbf{F} + \mathbf{F} \times (\nabla \times \mathbf{G}) + \mathbf{G} \times (\nabla \times \mathbf{F}), \quad (\text{A.7.2})$$

$$\nabla \cdot (\mathbf{F} \times \mathbf{G}) = \mathbf{G} \cdot \nabla \times \mathbf{F} - \mathbf{F} \cdot \nabla \times \mathbf{G}, \quad (\text{A.7.3})$$

$$\nabla \times (\mathbf{F} \times \mathbf{G}) = \mathbf{F} \nabla \cdot \mathbf{G} - \mathbf{G} \nabla \cdot \mathbf{F} + \mathbf{G} \cdot \nabla \mathbf{F} - \mathbf{F} \cdot \nabla \mathbf{G}, \quad (\text{A.7.4})$$

$$\nabla \times (\nabla f) = \mathbf{0}, \quad (\text{A.7.5})$$

$$\nabla \cdot (\nabla \times \mathbf{F}) = 0, \quad (\text{A.7.6})$$

$$\nabla \times (\nabla \times \mathbf{F}) = \nabla (\nabla \cdot \mathbf{F}) - \nabla^2 \mathbf{F}. \quad (\text{A.7.7})$$

A.8 DIVERGENCE THEOREM IN SPACE

Let V_c be an arbitrary control volume that is bounded by the closed surface D , and \mathbf{n} be the unit vector that is normal to D pointing *outward*.

The Gauss divergence theorem states that the volume integral of the divergence of any differentiable vector function $\mathbf{F} = (F_x, F_y, F_z)$ over V_c is equal to the flow rate of \mathbf{F} across D ,

$$\int_{V_c} \nabla \cdot \mathbf{F} dV = \int_D \mathbf{F} \cdot \mathbf{n} dS. \quad (\text{A.8.1})$$

Making the three sequential choices $\mathbf{F} = (f, 0, 0)$, $\mathbf{F} = (0, f, 0)$, and $\mathbf{F} = (0, 0, f)$, where f is a differentiable scalar function, we obtain the vector form of the divergence theorem

$$\int_{V_c} \nabla f dV = \int_D f \mathbf{n} dS. \quad (\text{A.8.2})$$

The particular choices $f = x$, $f = y$, or $f = z$ yield the volume of V_c in terms of a surface integral of the x , y , or z component of the normal vector.

Setting $\mathbf{F} = \mathbf{a} \times \mathbf{G}$, where \mathbf{a} is a constant vector and \mathbf{G} is a differentiable function, and then discarding the arbitrary constant \mathbf{a} , we obtain the new identity

$$\int_{V_c} \nabla \times \mathbf{G} dV = \int_D \mathbf{n} \times \mathbf{G} dS. \quad (\text{A.8.3})$$

A.9 DIVERGENCE THEOREM IN THE PLANE

Let A_c be an arbitrary control area in the xy plane that is bounded by the closed contour C , and \mathbf{n} be the unit vector that is normal to C pointing *outward*.

The Gauss divergence theorem states that the areal integral of the divergence of any two-dimensional differentiable vector function $\mathbf{F} = (F_x, F_y)$ over A_c is equal to the flow rate of \mathbf{F} across C ,

$$\int_{A_c} \nabla \cdot \mathbf{F} dA = \int_C \mathbf{F} \cdot \mathbf{n} dl, \quad (\text{A.9.1})$$

where l is the arc length along C .

Making the sequential choices $\mathbf{F} = (f, 0)$ and $\mathbf{F} = (0, f)$, where f is a differentiable scalar function, we obtain the vector form of the divergence theorem

$$\int_{A_c} \nabla f dA = \int_C f \mathbf{n} dl. \quad (\text{A.9.2})$$

The particular choices $f = x$ or $f = y$ yield the area of A_c in terms of a line integral of the x or y component of the normal vector.

A.10 STOKES' THEOREM

Let C be an arbitrary closed loop with unit tangent vector \mathbf{t} , D be an arbitrary surface bounded by C , and \mathbf{n} be the unit vector that is normal to D and is oriented according to the right-handed rule with respect to \mathbf{t} and with reference to a designated side of D . As we look at the designated side of D , the normal vector points towards us and the tangent vector describes a counterclockwise path.

Stokes' theorem states that the circulation of a differentiable vector function \mathbf{F} along C is equal to the flow rate of the curl of \mathbf{F} across D ,

$$\int_C \mathbf{F} \cdot \mathbf{t} dl = \int_D (\nabla \times \mathbf{F}) \cdot \mathbf{n} dS, \quad (\text{A.10.1})$$

where l is the arc length along C .

Setting $F = \mathbf{a} \times \mathbf{G}$, where \mathbf{a} is a constant vector and \mathbf{G} is a differentiable function, expanding out the integrand on the right-hand side of (A.10.1), and then discarding

the arbitrary constant \mathbf{a} , we obtain the new identity

$$\int_C \mathbf{G} \times \mathbf{t} \, dl = \int_D [\mathbf{n} \nabla \cdot \mathbf{G} - (\nabla \mathbf{G}) \cdot \mathbf{n}] \, dS. \quad (\text{A.10.2})$$

Appendix B

Gauss elimination and linear solvers

Consider a system of N linear algebraic equations for the N unknown scalar variables x_1, x_2, \dots, x_N ,

$$\begin{aligned} A_{1,1} x_1 + A_{1,2} x_2 + \dots + A_{1,N-1} x_{N-1} + A_{1,N} x_N &= b_1, \\ A_{2,1} x_1 + A_{2,2} x_2 + \dots + A_{2,N-1} x_{N-1} + A_{2,N} x_N &= b_2, \\ \dots, \\ A_{N,1} x_1 + A_{N,2} x_2 + \dots + A_{N,N-1} x_{N-1} + A_{N,N} x_N &= b_N, \end{aligned} \tag{B.1}$$

where $A_{i,j}$, $i = 1, 2, \dots, N$ and $j = 1, 2, \dots, N$, are given coefficients, and b_i are given constants. In matrix notation, the system (B.1) takes the compact form

$$\mathbf{A} \cdot \mathbf{x} = \mathbf{b}, \tag{B.2}$$

where \mathbf{A} is the $N \times N$ coefficient matrix

$$\mathbf{A} = \begin{bmatrix} A_{1,1} & A_{1,2} & \dots & A_{1,N-1} & A_{1,N} \\ A_{2,1} & A_{2,2} & \dots & A_{2,N-1} & A_{2,N} \\ \dots & & & & \\ A_{N-1,1} & A_{N-1,2} & \dots & A_{N-1,N-1} & A_{N-1,N} \\ A_{N,1} & A_{N,2} & \dots & A_{N,N-1} & A_{N,N} \end{bmatrix}, \tag{B.3}$$

and \mathbf{b} is the N -dimensional vector

$$\mathbf{b} = \begin{bmatrix} b_1 \\ b_2 \\ \dots \\ b_{N-1} \\ b_N \end{bmatrix}. \tag{B.4}$$

The most general way of solving system (B.2) is by the method of Gauss elimination. The idea is to solve the first equation in (B.1) for the first unknown x_1 , and use the expression for x_1 thus obtained to eliminate x_1 from all subsequent equations. We then retain the first equation as is, and replace all subsequent equations with their descendants that do not contain x_1 .

At the second stage, we solve the second equation for the second unknown x_2 , and use the expression for x_2 thus obtained to eliminate x_2 from all subsequent equations.

We then retain the first and second equations, and replace all subsequent equations with their descendants, which do not contain x_1 or x_2 . Continuing in this manner, we arrive at the last equation, which contains only the last unknown x_N .

Having completed the elimination, we compute the unknowns by the method of *backward substitution*. First, we solve the last equation for x_N , which thus becomes a known. Second, we solve the penultimate equation for x_{N-1} , which also becomes a known. Continuing in the backward direction, we scan the reduced system until we have evaluated all unknowns.

Immediately before the m th equation has been solved for the m th unknown, where $m = 1, \dots, N - 1$, the linear system takes the form

$$\begin{bmatrix} A_{1,1}^{(m)} & A_{1,2}^{(m)} & \cdots & \cdots & \cdots & A_{1,N}^{(m)} \\ 0 & A_{2,2}^{(m)} & \cdots & \cdots & \cdots & A_{2,N}^{(m)} \\ 0 & 0 & \cdots & \cdots & \cdots & \cdots \\ 0 & 0 & A_{m-1,m-1}^{(m)} & A_{m-1,m}^{(m)} & \cdots & A_{m-1,N}^{(m)} \\ 0 & \cdots & 0 & A_{m,m}^{(m)} & \cdots & A_{m,N}^{(m)} \\ 0 & \cdots & 0 & \cdots & \cdots & \cdots \\ 0 & \cdots & 0 & A_{N,m}^{(m)} & \cdots & A_{N,N}^{(m)} \end{bmatrix} \begin{bmatrix} x_1 \\ x_2 \\ x_3 \\ \vdots \\ x_{N-1} \\ x_N \end{bmatrix} = \begin{bmatrix} b_1^{(m)} \\ b_2^{(m)} \\ b_3^{(m)} \\ \vdots \\ b_{N-1}^{(m)} \\ b_N^{(m)} \end{bmatrix}, \quad (\text{B.5})$$

where $A_{i,j}^{(m)}$ are intermediate coefficients, and $b_i^{(m)}$ are intermediate right-hand sides. The first equation of (B.5) is identical to the first equation of (B.1) for any value of m ; subsequent equations are different, except at the first step corresponding to $m = 1$.

A difficulty arises when the diagonal element $A_{m,m}^{(m)}$ is nearly or precisely equal to zero, for then we may no longer solve the m th equation for x_m , as required. The failure of the method, however, does *not* imply that the system does not have a solution. To circumvent this difficulty, we simply rearrange the equations or relabel the unknowns so as to bring the m th unknown to the m th equation, using the method of *pivoting*. If there is no way we can make this happen, then the matrix \mathbf{A} is singular, and the linear system has either no solution or an infinite number of solutions.

In the method of *row pivoting*, potential difficulties are bypassed by switching the m th equation in the system (B.5) with the subsequent k th equation, where $k > m$. The value k is chosen so that $|A_{k,m}^{(m)}|$ is the maximum value of the elements in the m th column below the diagonal, $A_{i,m}^{(m)}$, for $i \geq m$. If $A_{i,m}^{(m)} = 0$ for all $i \geq m$, then the linear system does not have a unique solution, and the matrix \mathbf{A} is singular.

In practice, the size of the system (B.1) can be on the order of $10^4 \times 10^4$ or even higher. For such large systems, the method of Gauss elimination requires a prohibitive amount of computational time. The practical need for solving systems of large size has motivated the development of a host of alternative numerical methods for general or specific applications (e.g., [60]).

A class of iterative methods search for the solution vector \mathbf{x} by making steps in the N -dimensional space toward carefully chosen or even optimal directions. Subdirectory `03_lin_eq` of directory `num_meth` of *BEMLIB* includes programs that solve linear systems with symmetric coefficient matrices by the method of *conjugate gradients*, and linear systems with non-symmetric coefficient matrices using the method of *biconjugate gradients* (e.g., [60]).

The generalized minimal residual method (GMRES) [64] has been used successfully for solving large linear systems arising from boundary element implementations in a variety of applications.

Appendix C

Elastostatics

The theory of elasticity is discussed in texts of solid mechanics and continuum mechanics, including Love's classical treatise [43]. In this appendix, we review the fundamental equations of steady-state linear elasticity required for developing the boundary integral formulation.

C.1 DISPLACEMENT, TRACTION, AND EQUILIBRIUM

An elastic medium initially at equilibrium deforms to a new configuration under the action of forces acting over its volume or at the boundary. After deformation, a material point particle initially at \mathbf{X} is displaced to the new position $\mathbf{X} + \mathbf{v}$, where \mathbf{v} is the *displacement vector*.

Consider an infinitesimal surface in the medium that is perpendicular to the unit normal vector \mathbf{n} in the deformed state. The force per unit area exerted on this surface, denoted by \mathbf{t} , is called the *traction*. The traction vector depends on position \mathbf{x} and orientation of the infinitesimal surface determined by the unit normal vector \mathbf{n} . To signify this dependence, we write $\mathbf{t}(\mathbf{x}, \mathbf{n})$.

Analysis shows that the traction depends linearly on the unit normal vector,

$$t_j = n_i \sigma_{ij}, \quad (\text{C.1.1})$$

where the matrix of proportionality coefficients σ_{ij} is the *Cauchy stress tensor*. Summation over the repeated index i with respect to the spatial coordinates x , y , and z is implied on the right-hand side of (C.1.1).

A balance of forces requires that, at steady state, the Cauchy stress tensor satisfy the equilibrium equation

$$\frac{\partial \sigma_{ij}}{\partial x_j} + \rho b_i = 0, \quad (\text{C.1.2})$$

where ρ is the density, and summation over the repeated index j is implied on the left-hand side. The last term ρb_i expresses the effect of a long-range body force acting on the material. In the case of the gravitational force field, \mathbf{b} is the acceleration of gravity.

In vector notation, the equilibrium equation (C.1.2) reads

$$\nabla \cdot \sigma + \rho \mathbf{b} = \mathbf{0}. \quad (\text{C.1.3})$$

C.2 LINEAR ELASTICITY

The distribution of stresses in a deformed body depends on the displacement field and on the properties of the material. If the body behaves like a linearly elastic medium, then the constitutive equation relating stress to deformation takes the form

$$\sigma_{ij} = \lambda \delta_{ij} \frac{\partial v_k}{\partial x_k} + \mu \left(\frac{\partial v_i}{\partial x_j} + \frac{\partial v_j}{\partial x_i} \right), \quad (\text{C.2.1})$$

where λ, μ are the Lamé constants. Summation over the repeated index k is implied in the first term on the right-hand side of (C.2.1). In terms of the modulus of elasticity E and Poisson's ratio ν , the Lamé constants are given by

$$\mu = \frac{E}{2(1+\nu)}, \quad \lambda = \frac{E\nu}{(1+\nu)(1-2\nu)}. \quad (\text{C.2.2})$$

Poisson's ratio for homogeneous materials takes values in the range $[-1, 1/2]$. If the material is incompressible, $\nu = 1/2$.

Substituting the constitutive equation (C.2.1) into the equilibrium equation (C.1.3), we derive Navier's equation

$$\mu \nabla^2 \mathbf{v} + (\mu + \lambda) \nabla \alpha + \rho \mathbf{b} = \mathbf{0}, \quad (\text{C.2.3})$$

where

$$\alpha \equiv \nabla \cdot \mathbf{v} \quad (\text{C.2.4})$$

is the dilatation due to the deformation.

Using the relations in (C.2.2), we find $\mu + \lambda = E/[2(1+\nu)(1-2\nu)] = \mu/(1-2\nu)$, and derive the alternative form of Navier's equation

$$\mu \nabla^2 \mathbf{v} + \frac{\mu}{1-2\nu} \nabla \alpha + \rho \mathbf{b} = \mathbf{0}. \quad (\text{C.2.5})$$

C.3 THE GALERKIN VECTOR

It is sometimes convenient to express the displacement field in terms of the Galerkin vector \mathbf{g} defined by the relation

$$\mathbf{v} \equiv \frac{1}{\mu} \left[\nabla^2 \mathbf{g} - \frac{1}{2(1-\nu)} \nabla (\nabla \cdot \mathbf{g}) \right]. \quad (\text{C.3.1})$$

Substituting this expression into Navier's equation (C.2.5), we find that the Galerkin vector satisfies the inhomogeneous biharmonic equation

$$\nabla^4 \mathbf{g} + \rho \mathbf{b} = \mathbf{0}, \quad (\text{C.3.2})$$

where $\nabla^4 \equiv \nabla^2 \nabla^2$ is the biharmonic operator in two or three dimensions.

C.4 BETTI'S RECIPROCAL RELATION

Consider two unrelated deformed states of a material with displacement fields \mathbf{v} and \mathbf{v}' and corresponding stress fields by σ and σ' . Straightforward analysis following the discussion of Section 7.2 for Stokes flow yields the counterpart of Green's second identity

$$v'_j \frac{\partial \sigma_{ij}}{\partial x_i} - v_j \frac{\partial \sigma'_{ij}}{\partial x_i} = \frac{\partial}{\partial x_i} (v'_j \sigma_{ij} - v_j \sigma'_{ij}). \quad (\text{C.4.1})$$

In the absence of a body force, $\mathbf{b} = \mathbf{0}$, the equilibrium equation (C.1.3) requires that the left-hand side vanish, yielding Betti's reciprocal relation

$$\frac{\partial}{\partial x_i} (v'_j \sigma_{ij} - v_j \sigma'_{ij}) = 0. \quad (\text{C.4.2})$$

C.5 GREEN'S FUNCTIONS

The Green's functions of linear elasticity represent the displacement and stress fields induced by a point load. By definition, these singular fields satisfy the forced equilibrium equation

$$\begin{aligned} \mu \nabla^2 \mathbf{v} + \frac{\mu}{1 - 2\nu} \nabla \alpha + \mathbf{c} \delta_n(\mathbf{x} - \mathbf{x}_0) \\ = \nabla \cdot \sigma + \mathbf{c} \delta_n(\mathbf{x} - \mathbf{x}_0) = \mathbf{0}, \end{aligned} \quad (\text{C.5.1})$$

where $\alpha \equiv \nabla \cdot \mathbf{v}$ is the dilatation, \mathbf{c} is an arbitrary constant vector, and δ_n is the delta function in two or three dimensions, $n = 2$ or 3 .

For convenience, we express the solution of (C.5.1) in the form

$$\begin{aligned} v_i &= \frac{1}{8\pi\mu(1-\nu)} G_{ij}(\mathbf{x}, \mathbf{x}_0) c_j, \\ \sigma_{ik} &= \frac{1}{8\pi(1-\nu)} T_{ijk}(\mathbf{x}, \mathbf{x}_0) c_j, \end{aligned} \quad (\text{C.5.2})$$

in two dimensions ($n = 2$), and

$$\begin{aligned} v_i &= \frac{1}{16\pi\mu(1-\nu)} G_{ij}(\mathbf{x}, \mathbf{x}_0) c_j, \\ \sigma_{ik} &= \frac{1}{16\pi(1-\nu)} T_{ijk}(\mathbf{x}, \mathbf{x}_0) c_j, \end{aligned} \quad (\text{C.5.3})$$

in three dimensions ($n = 3$).

Substituting these expressions into (C.5.1) and discarding the arbitrary constants c_j , we find

$$\begin{aligned} \nabla^2 G_{ij}(\mathbf{x}, \mathbf{x}_0) + \frac{1}{1-2\nu} \frac{\partial^2 G_{kj}(\mathbf{x}, \mathbf{x}_0)}{\partial x_i \partial x_k} &= -8\pi(1-\nu) \delta_{ij} \delta_2(\mathbf{x} - \mathbf{x}_0), \\ \frac{\partial T_{ijk}(\mathbf{x}, \mathbf{x}_0)}{\partial x_k} &= -8\pi(1-\nu) \delta_{ij} \delta_2(\mathbf{x} - \mathbf{x}_0), \end{aligned} \quad (\text{C.5.4})$$

in two dimensions ($n = 2$), and

$$\begin{aligned} \nabla^2 G_{ij}(\mathbf{x}, \mathbf{x}_0) + \frac{1}{1-2\nu} \frac{\partial^2 G_{kj}(\mathbf{x}, \mathbf{x}_0)}{\partial x_i \partial x_k} &= -16\pi(1-\nu) \delta_{ij} \delta_3(\mathbf{x} - \mathbf{x}_0), \\ \frac{\partial T_{ijk}(\mathbf{x}, \mathbf{x}_0)}{\partial x_k} &= -16\pi(1-\nu) \delta_{ij} \delta_3(\mathbf{x} - \mathbf{x}_0), \end{aligned} \quad (\text{C.5.5})$$

in three dimensions ($n = 3$).

C.6 FREE-SPACE GREEN'S FUNCTION IN TWO DIMENSIONS (KELVIN STATE)

The free-space Green's function in two dimensions is given by

$$G_{ij}(\mathbf{x} - \mathbf{x}_0) = -\delta_{ij} (3 - 4\nu) \ln r + \frac{\hat{x}_i \hat{x}_j}{r^2}, \quad (\text{C.6.1})$$

where ν is the Poisson ratio, $\hat{\mathbf{x}} \equiv \mathbf{x} - \mathbf{x}_0$, and $r = |\hat{\mathbf{x}}|$.

The associated stress tensor is

$$T_{ijk}(\mathbf{x} - \mathbf{x}_0) = 2(1-2\nu) \frac{\delta_{ik} \hat{x}_j - \delta_{ij} \hat{x}_k - \delta_{kj} \hat{x}_i}{r^2} - 4 \frac{\hat{x}_i \hat{x}_j \hat{x}_k}{r^4}. \quad (\text{C.6.2})$$

When $\nu = 1/2$, these Green's functions reduce to the free-space velocity and stress Green's functions of two-dimensional Stokes flow.

C.7 FREE-SPACE GREEN'S FUNCTION IN THREE DIMENSIONS (KELVIN STATE)

The free-space Green's function in three dimensions is given by

$$G_{ij}(\mathbf{x} - \mathbf{x}_0) = (3 - 4\nu) \frac{\delta_{ij}}{r} + \frac{\hat{x}_i \hat{x}_j}{r^3}, \quad (\text{C.7.1})$$

where ν is the Poisson ratio, $\hat{\mathbf{x}} \equiv \mathbf{x} - \mathbf{x}_0$, and $r = |\hat{\mathbf{x}}|$.

The associated stress tensor is

$$T_{ijk}(\mathbf{x} - \mathbf{x}_0) = 2(1 - 2\nu) \frac{\delta_{ik} \hat{x}_j - \delta_{ij} \hat{x}_k - \delta_{kj} \hat{x}_i}{r^3} - 6 \frac{\hat{x}_i \hat{x}_j \hat{x}_k}{r^5}. \quad (\text{C.7.2})$$

When $\nu = 1/2$, these Green's functions reduce to the free-space velocity and stress Green's functions of three-dimensional Stokes flow.

C.8 INTEGRAL REPRESENTATION IN TWO DIMENSIONS (SOMIGLIANA'S IDENTITY)

In the absence of a body force, the boundary-integral representation of the displacement field in two dimensions takes the form

$$\begin{aligned} v_j(\mathbf{x}_0) = & -\frac{1}{8\pi\mu(1-\nu)} \int_C G_{ij}(\mathbf{x}, \mathbf{x}_0) t_i(\mathbf{x}) dl(\mathbf{x}) \\ & + \frac{1}{8\pi(1-\nu)} \int_C v_i(\mathbf{x}) T_{ijk}(\mathbf{x}, \mathbf{x}_0) n_k(\mathbf{x}) dl(\mathbf{x}), \end{aligned} \quad (\text{C.8.1})$$

where C is the contour of a selected control area, the unit normal vector \mathbf{n} points into the control area, and the point \mathbf{x}_0 lies inside the control area. If the point \mathbf{x}_0 lies outside the control area, the left-hand side of (C.8.1) is equal to zero.

The associated integral equation is

$$\begin{aligned} v_j(\mathbf{x}_0) = & -\frac{1}{4\pi\mu(1-\nu)} \int_C G_{ij}(\mathbf{x}, \mathbf{x}_0) t_i(\mathbf{x}) dl(\mathbf{x}) \\ & + \frac{1}{4\pi(1-\nu)} \int_C^{PV} v_i(\mathbf{x}) T_{ijk}(\mathbf{x}, \mathbf{x}_0) n_k(\mathbf{x}) dl(\mathbf{x}), \end{aligned} \quad (\text{C.8.2})$$

where the point \mathbf{x}_0 lies on a locally smooth contour C , PV denotes the principal-value integral, and the unit normal vector \mathbf{n} points into the control area enclosed by the contour C .

C.9 INTEGRAL REPRESENTATION IN THREE DIMENSIONS (SOMIGLIANA'S IDENTITY)

In the absence of a body force, the boundary-integral representation of the displacement field in three dimensions takes the form

$$\begin{aligned} v_j(\mathbf{x}_0) = & -\frac{1}{16\pi\mu(1-\nu)} \int_D G_{ij}(\mathbf{x}, \mathbf{x}_0) t_i(\mathbf{x}) dS(\mathbf{x}) \\ & + \frac{1}{16\pi(1-\nu)} \int_D v_i(\mathbf{x}) T_{ijk}(\mathbf{x} - \mathbf{x}_0) n_k(\mathbf{x}) dS(\mathbf{x}), \end{aligned} \quad (\text{C.9.1})$$

where D is the boundary of a selected control volume, the unit normal vector \mathbf{n} points into the control volume, and the point \mathbf{x}_0 lies inside the control volume. If the point \mathbf{x}_0 lies outside the control volume, the left-hand side of (C.9.1) is equal to zero.

The associated integral equation is

$$\begin{aligned} v_j(\mathbf{x}_0) = & -\frac{1}{8\pi\mu(1-\nu)} \int_D G_{ij}(\mathbf{x}, \mathbf{x}_0) t_i(\mathbf{x}) dS(\mathbf{x}) \\ & + \frac{1}{8\pi(1-\nu)} \int_D^{PV} v_i(\mathbf{x}) T_{ijk}(\mathbf{x}, \mathbf{x}_0) n_k(\mathbf{x}) dS(\mathbf{x}), \end{aligned} \quad (\text{C.9.2})$$

where the point \mathbf{x}_0 lies on a locally smooth surface D , PV denotes the principal-value integral, and the unit normal vector \mathbf{n} points into the control volume enclosed by the surface D .

References

- [1] ABE, K. and SAKURABA, S., 1999, An hr -adaptive boundary element for water free-surface problems, *Eng. Anal. Bound. Elem.*, **23**, 223-232.
- [2] ABRAMOWITZ, M. and STEGUN, I. A., 1965, *Handbook of Mathematical Functions*, Dover, New York.
- [3] ATKINSON, K. E., 1990, A survey of boundary integral equation methods for the numerical solution of Laplace's equation in three dimensions, in *Numerical Solution of Integral Equations*, Goldberg, M. A., Editor, Plenum Press, New York.
- [4] ATKINSON, K. E., 1997, *The Numerical Solution of Integral Equations of the Second Kind*, Cambridge University Press.
- [5] BEENAKKER, C. W. L., 1986, Ewald sums of the Rotne-Prager tensor, *J. Chem. Phys.*, **85**, 1581-1582.
- [6] BEYER, W. H., 1986, *Standard Mathematical Tables*, 27th Edition, CRC Press, Boca Raton, FL.
- [7] BLAKE, J. R., 1971, A note on the image system for a Stokeslet near a no-slip boundary, *Proc. Camb. Phil. Soc.*, **70**, 303-310.
- [8] BLAKE, J. R. and CHWANG, A. T., 1974, Fundamental singularities of viscous flow, *J. Eng. Math.*, **8**, 23-29.
- [9] BREBBIA, C. A., 1978, *The Boundary Element Method for Engineers*, Pentech Press, London.
- [10] BREBBIA, C. A. and WALKER, S., 1980, *Boundary Element Techniques in Engineering*, Newnes-Butterworths, London.
- [11] CHEN, C. S., RASHED, Y. F., and GOLBERG, M. A., 1998, A mesh free method for linear diffusion equations, *Num. Heat Transf.*, **33**, 469-486.
- [12] COWPER, G. R., 1973, Gaussian quadrature formulas for triangles, *Int. J. Num. Meth. Eng.*, **7**, 405-408.
- [13] DAVEY, K. and HINDUJA, S., 1989, Analytical integration of linear three-dimensional triangular elements in BEM, *Appl. Math. Model.*, **13**, 450-461.
- [14] DAVIES, B. and MARTIN, B., 1979, Numerical inversion of Laplace transform: a survey and comparison of methods, *J. Comp. Phys.*, **33**, 1-32.
- [15] DUBINER, M., 1991, Spectral methods on triangles and other domains, *J. Sci. Comp.*, **6**, 345-390.

- [16] DUNAVANT, D. A., 1985, High degree efficient symmetrical Gaussian rules for the triangle, *Int. J. Num. Meth. Eng.*, **21**, 1129-1148.
- [17] FLOREZ, W. F. and POWER, H., 2001, Comparison between continuous and discontinuous boundary elements in the multidomain dual reciprocity method for the solution of the two-dimensional Navier-Stokes equations, *Eng. Anal. Bound. Elem.*, **25**, 57-69.
- [18] GARABEDIAN, P. R., 1964, *Partial Differential Equations*, John Wiley & Sons, New York.
- [19] GOLBERG, M. A., 1995, The numerical evaluation of particular solutions in the BEM – a review, *Bound. Elem. Comm.*, **6**, 99-106.
- [20] GOLBERG, M. A. and CHEN, C. S., 1994, The theory of radial basis functions applied to the BEM for inhomogeneous partial differential equations, *Bound. Elem. Comm.*, **5**, 57-61.
- [21] GOLBERG, M. A. and CHEN, C. S., 2000, Preface to a special issue on the dual reciprocity method, *Bound. Elem. Comm.*, **5**, 5111-512.
- [22] GOLBERG, M. A., CHEN, C. S., and BOWMAN, H., 1999, Some recent results and proposals for the use of radial basis functions in the BEM. *Eng. Anal. Bound. Elem.* **23**, 285-296.
- [23] GRAY, L. J., 1998, Evaluation of singular and hypersingular Galerkin integrals: direct limits and symbolic computation, in *Advances in Boundary Elements*, V. Sladek and J. Sladek, Editors, Computational Mechanics Publications, Southampton.
- [24] HANSEN, E. B., 1987, Stokes flow down a wall into an infinite pool, *J. Fluid Mech.*, **178**, 243-256.
- [25] HANSEN E. B. and KELMANSON, M. A., 1994, An integral equation justification of the boundary conditions of the driven-cavity problem, *Comput. Fluids*, **23**, 225-240.
- [26] HASIMOTO, H., 1959, On the periodic fundamental solutions of the Stokes equations and their application to viscous flow past a cubic array of spheres, *J. Fluid Mech.*, **5**, 317-328.
- [27] HAUTMAN, J. and KLEIN, M. L., 1992, An Ewald summation method for planar surfaces and interfaces, *Molecular Phys.*, **75**, 379-395.
- [28] HIGDON, J. J. L., 1979, A hydrodynamic analysis of flagellar propulsion, *J. Fluid Mech.*, **90**, 685-711.
- [29] INGBER, M. S. and MITRA, A. K., 1986, Grid optimization for the boundary element method, *Int. J. Num. Meth. Fluids*, **23**, 2121-2136.
- [30] INGBER, M. S. and MONDY, L. A., 1993, Direct second-kind boundary integral formulation for Stokes flow problems, *Comput. Mech.*, **11**, 11-27.

- [31] JASWON, M. A., 1963, Integral equations methods in potential theory. I., *Proc. Roy. Soc. A*, **275**, 23-32.
- [32] KARNIADAKIS, G. E. and SHERWIN, S. J., 1999, *Spectral/hp Element Methods for CFD*, Oxford University Press, New York.
- [33] KELLOGG, O. D., 1929, *Foundations of Potential Theory*, Reprinted by Dover, New York (1954).
- [34] KELMANSON, M. A., 1983, Modified integral equation solution of viscous flows near sharp corners, *Comput. Fluids*, **11**, 307-324.
- [35] KELMANSON, M. A., 1983, An integral equation method for the solution of singular Stokes flow problems, *J. Comp. Phys.*, **51**, 139-158.
- [36] KELMANSON, M. A. and LONGSDALE, B., 1995, Annihilation of boundary singularities via suitable Green's functions, *Comput. Math. Appl.*, **29**, 1-7.
- [37] KIM, S. and KARRILA, S. J., 1991, *Microhydrodynamics: Principles and Selected Applications*, Butterworth-Heinemann, Boston.
- [38] KWAK, S. and POZRIKIDIS, C., 1998, Adaptive triangulation of evolving, closed or open surfaces by the advancing-front method, *J. Comp. Phys.*, **145**, 61-88.
- [39] LANCASTER, P. and ŠALKAUSKAS, K., 1986, *Curve and Surface Fitting. An Introduction*, Academic Press, San Diego.
- [40] LESNIC, D., ELLIOTT, L., and INGHAM, D. B., 1994, Treatment of singularities in exterior fluid domains with corners using the boundary-element method, *Comput. Fluids*, **23**, 817-827.
- [41] LIAPIS, S., 1994, A review of error estimation and adaptivity in the boundary-element method, *Eng. Anal. Bound. Elem.*, **14**, 315-323.
- [42] LORENTZ, H. A., 1896, Eene algemeene stelling omtrent de beweging eener vloeistof met wrijving en eenige daaruit afgeleide gevolgen, *Zit. K. Akad. W. Amsterdam*, **5**, 168-195; Ein allgemeiner satz, die bewegung einer reibenden flüssigkeit betreffend, nebst einigen anwendungen desselben, *Abhandlungen über Theoretische Physik*, Leipzig (1907), pp. 23-42; See also: A general theorem concerning the motion of a viscous fluid and a few consequences derived from it, *H. A. Lorentz Collected Papers*, Martinus Nijhoff Publishers, Haque (1937).
- [43] LOVE, A. E. H., 1944, *A Treatise on the Mathematical Theory of Elasticity*, Reprinted by Dover, New York.
- [44] MACKERLE, J., 1993, Mesh generation and refinement for FEM and BEM – a bibliography (1990 – 1993), *Fin. Elem. Anal. Des.*, **15**, 177-188.
- [45] MORSE, P. M. and FESHBACH, H., 1953, *Methods of Theoretical Physics, Part I.*, McGraw Hill, New York.

- [46] MUCI-KÜCHLER K. H. and MIRANDA-VALENZUELA J. C., 2001, Guest editorial, *Eng. Anal. Bound. Elem.*, **25**, 477-487.
- [47] NARDINI, D. and BREBBIA, C. A., 1982, A new approach to free vibration analysis using boundary elements, in *Boundary Element Methods in Engineering*, Brebbia, C. A., Ed., Springer-Verlag, Berlin.
- [48] NIGAM, S. D. and SRINIVASAN, V., 1975, No-slip images in a sphere, *J. Math. Phys. Sci.*, **9**, 389-398.
- [49] OCCHIALINI, J. M., MULDOWNNEY, G. P., and HIGDON, J. J. L., 1992, Boundary integral/spectral element approaches to the Navier-Stokes equations, *Int. J. Num. Meth. Fluids*, **15**, 1361-1381.
- [50] OSEEN, C. W., 1927, *Hydrodynamik*, Akademische Verlag, Leipzig.
- [51] PARTRIDGE, P. W., BREBBIA, C.A., and WROBEL, L. C., 1992, *The Dual Reciprocity Boundary Element Method*, Computational Mechanics Publications, Southampton.
- [52] PINA, H. L. G., FERNANDES, J. L. M., and BREBBIA, C. A., 1981, Some numerical integration formulae over triangles and squares with a $1/R$ singularity, *Appl. Math. Model.*, **5**, 209-211.
- [53] POZRIKIDIS, C., 1990, The instability of a moving viscous drop, *J. Fluid Mech.*, **210**, 1-21.
- [54] POZRIKIDIS, C., 1990, The deformation of a liquid drop moving normal to a plane wall. *J. Fluid Mech.*, **215**, 331-363.
- [55] POZRIKIDIS, C., 1992, *Boundary Integral and Singularity Methods for Linearized Viscous Flow*, Cambridge University Press, Cambridge.
- [56] POZRIKIDIS, C., 1992, The buoyancy-driven motion of a train of viscous drops within a cylindrical tube, *J. Fluid Mech.*, **237**, 627-648.
- [57] POZRIKIDIS, C., 1996, Computation of periodic Green's functions of Stokes flow, *J. Eng. Math.*, **30**, 79-96.
- [58] POZRIKIDIS, C., 1997, Unsteady heat or mass transport from a suspended particle at low Péclet number. *J. Fluid Mech.*, **334**, 111-133.
- [59] POZRIKIDIS, C., 1997, *Introduction to Theoretical and Computational Fluid Dynamics*, Oxford University Press, New York.
- [60] POZRIKIDIS, C., 1998, *Numerical Computation in Science and Engineering*, Oxford University Press, New York.
- [61] POZRIKIDIS, C., 2001, Shear flow over a particular or fibrous plate, *J. Eng. Math.*, **39**, 3-24.
- [62] POZRIKIDIS, C., 2001, Interfacial Dynamics for Stokes flow, *J. Comp. Phys.*, **169**, 250-301.

- [63] POZRIKIDIS, C., 2002, Boundary-element grid optimization for Stokes flow with corner singularities, *J. Fluids Eng.*, in press.
- [64] SAAD, Y. and SCHULTZ, M. H., 1986, GMRES: a generalized minimal residual algorithm for solving nonsymmetric linear systems, *SIAM J. Sci. Stat. Comput.*, **7**, 856-869.
- [65] STEHFEST, C., 1970, Numerical inversion of the Laplace transform, *Commun. ACS*, **13**, 47-49; 624.
- [66] SYMM, G. T., 1963, Integral equations methods in potential theory. II., *Proc. Roy. Soc. A*, **275**, 33-46.
- [67] TOOSE, E. M. et al., 1996, Axisymmetric non-Newtonian drops treated with a boundary-integral method, *J. Eng. Math.*, **30**, 131-150.
- [68] VAN DE VORST, G. A. L., 1996, Integral formulation to simulate the viscous sintering of a two-dimensional lattice of periodic unit cells, *J. Eng. Math.*, **30**, 97-118.
- [69] XANTHIS, L. S., BERNAL, M. J. M., and ATKINSON, C., 1981, The treatment of singularities in the calculation of stress intensity factors using the boundary integral equation method, *Comp. Meth. Appl. Mech. Eng.*, **26**, 285-304.
- [70] YAN, Y. and SLOAN, I. H., 1988, On integral equations of the first kind with logarithmic kernels, *J. Int. Eq. Appl.*, **1**, 549-579.
- [71] YON, S. and POZRIKIDIS, C., 1999, Deformation of a liquid drop adhering to a plane wall: Significance of the drop viscosity and the effect of an insoluble surfactant, *Phys. Fluids*, **11**, 1297-1308.
- [72] YOUNG, D. L., YANG, S. K., and ELDHO, T. I., 2000, Solution of the Navier-Stokes equations in velocity-vorticity form using a Eulerian-Lagrangian boundary element method, *Int. J. Num. Meth. Fluids*, **34**, 627-650.
- [73] ZHOU, H. and POZRIKIDIS, C., 1993, The flow of suspensions in channels: single files of drops, *Phys. Fluids A*, **5**, 311-324.

Index

BEMLIB

 directory contents, 193
 user guide, 191

acceleration parameter, 163
advancing-front method, 113
alternating tensor, 398
assembly of the influence matrix, 84
axisymmetric

 harmonic functions, 106
 Stokes flow, 177

barycentric coordinates, 117
Bernoulli's equation, 281
Betti's reciprocal relation, 409
biconjugate gradients, 405
biharmonic equation

 in three dimensions, 99
 in two dimensions, 33

body_2d, 270

body_ax, 276

boundary element

 at a corner, 83
 circular arc, 55, 67, 71
 constant, 64
 continuous, 83
 cubic splines, 56, 68, 71, 73
 curved triangle, 122
 discretization, 197
 flat triangle, 117
 non-singular, 65
 singular, 69
 straight, 53, 65, 70
 subdivision, 114
 uniform, 64

boundary-element method
 for Laplace's equation
 axisymmetric, 106

 in three dimensions, 111
 in two dimensions, 53
for Stokes flow, 178
Galerkin, 86
 symmetric, 88
global expansions, 89
high order, 127
 in two dimensions, 116
boundary-integral equation
 for Laplace's equation
 at a corner, 31, 104
 axisymmetric, 107
 for the gradient, 42, 104
 in three dimensions, 102
 in two dimensions, 28
 for Stokes flow
 axisymmetric, 350
 for the pressure, 173, 176
 for the stress, 174, 177
 in three dimensions, 176
 in two dimensions, 173
 with an interface, 181
 for the biharmonic equation
 in two dimensions, 36
 in elasticity, 411, 412
boundary-integral representation
 completed, 48
 for Laplace's equation
 axisymmetric, 107
 for the gradient, 101
 in three dimensions, 100
 in two dimensions, 19
 with an interface, 23
 for Stokes flow
 at a corner, 178
 axisymmetric, 350
 for the pressure, 173, 176

- for the stress, 174, 177
- in three dimensions, 176
- in two dimensions, 172
- for the biharmonic equation, 35
- generalized, 47
- in elasticity, 411, 412
- indirect, 47
- boundary-value equation, 8
- Brinkman's equation, 183
 - complex, 188
- Burgers equation, 153
- cardinal functions
 - cubic splines, 77
 - in one dimension, 136
 - in two dimensions, 142
- Cauchy
 - equation of motion, 162
 - stress tensor
 - in a fluid, 162
 - in elasticity, 407
- collocation method
 - in three dimensions, 116
 - in two dimensions, 74
- conjugate gradients, 405
- connectivity table, 85, 112
- contact conductance, 24
- continuity equation, 161
- continuous element, 83
- convection – diffusion
 - in one dimension, 6
 - in three dimensions, 99
 - in two dimensions, 18, 26, 150
 - unsteady, 155
- corner
 - elements, 83
 - in Stokes flow, 178
 - singularity
 - for Laplace's equation, 31
 - in Stokes flow, 179
- Crank-Nicolson method, 159
- creeping flow, 164
- cubic splines, 56
 - clamped-end, 60
 - isoparametric, 77
- periodic, 58–60
- curl of a vector, 399
- D'Arcy equation, 19
- del operator, 399
- delta function
 - in one dimension, 2
 - in three dimensions, 93
 - in two dimensions, 12
- dilatation, 408
- dipole of a source
 - in three dimensions, 97
 - in two dimensions, 16
- Dirac delta function
 - in one dimension, 2
 - in three dimensions, 93
 - in two dimensions, 12
- Dirichlet boundary condition, 9
- discretization
 - of a line in a plane, 198
 - of a surface, 111
 - of an integral equation
 - in three dimensions, 114
 - in two dimensions, 63
- divergence
 - of a vector function, 399
 - theorem, 400
- double-layer potential
 - of Laplace's equation
 - gradient of, 50
 - in three dimensions, 101
 - in two dimensions, 21
 - of Stokes flow
 - in three dimensions, 176
 - in two dimensions, 172
- dual reciprocity method, 133
 - for viscous flow, 185
 - in one dimension, 134
 - in two and three dimensions, 141
- Einstein summation convention, 397
- elasticity, 407
 - modulus of, 408
- elastostatics, 407
- explicit Euler method, 159

- extra stress tensor, 187
- finite part of an integral, 42
- flow
 - Navier-Stokes, 162
 - oscillatory, 188, 296
 - shear
 - past a periodic wall, 261
 - past an array of cylinders, 261
 - Stokes, 164
 - streaming, 18
 - through a tube, 254
 - unsteady Stokes, 164
- flow_1d, 254
- flow_1d_1p, 261
- flow_1d_osc, 296
- flow_2d, 265, 364
- Fredholm
 - Riesz theory, 29, 30
 - integral equation
 - hypersingular, 43, 105
 - of the first kind, 29, 103
 - of the second kind, 29, 103
- Frenet relation, 49
- Froude number, 163
- Galerkin
 - boundary-element method, 86
 - symmetric, 88
 - vector, 408
- Gauss
 - Legendre quadrature, 66
 - divergence theorem, 400
 - elimination, 75, 76, 403
- global expansion, 89
- gradient
 - of a scalar, 399
 - of a vector, 399
- Green's function
 - in elasticity, 409
 - free-space, 410, 411
 - of Brinkman's equation, 184, 187, 188
 - of D'Arcy's equation, 19
 - of Helmholtz's equation
 - in one dimension, 5
 - in three dimensions, 98
 - in two dimensions, 17
- of Laplace's equation
 - axisymmetric, 108, 245
 - dipole, 16, 97
 - in one dimension, 2
 - in three dimensions, 93, 230
 - in two dimensions, 12, 209
 - quadruple, 17, 98
- of Stokes flow, 166
 - axisymmetric, 349
 - free-space, 168, 170
 - in three dimensions, 329
 - in two dimensions, 302
 - oscillatory, 188
- of the biharmonic equation
 - in three dimensions, 99
 - in two dimensions, 34
- of the convection – diffusion equation, 156
 - in one dimension, 6
 - in two dimensions, 18, 27
- of the unsteady diffusion equation, 155
- of the wave equation, 160
- symmetry, 4, 20, 26, 169
- unsteady, 155
- Green's identity
 - first
 - in one dimension, 1
 - in three dimensions, 91
 - in two dimensions, 9
 - second
 - in one dimension, 2
 - in three dimensions, 92
 - in two dimensions, 10
 - third
 - in three dimensions, 101
 - in two dimensions, 21
- grid
 - on a surface, 112
 - optimization, 85
 - refinement, 85
- grid_2d, 198

- Hadamard part of an integral, 42
Heaviside function, 5
Helmholtz's equation, 102, 148
 in one dimension, 5
 in three dimensions, 98
 in two dimensions, 17, 26, 77
 inhomogeneous, 146
hypersingular
 integral, 36, 104, 174
 integral equation, 42, 89
- icosahedron, 114
implicit Euler method, 159
impulses, method of, 128
index notation, 397
influence
 coefficients, 64, 114
 functions, 139
inhomogeneous equations, 131
inner vector product, 397, 398
integration quadrature
 for log singularity, 73
 Gauss-Legendre, 66
interface, 23
 in a potential field, 23
 in Stokes flow, 180
interfacial dynamics, 180
interpolation functions
 for a six-node triangle, 122
 for a three-node triangle, 117
irrotational flow, 44
isoparametric expansion, 127
- Kelvin state
 in three dimensions, 411
 in two dimensions, 410
Kirchhoff transformation, 11
Kronecker's delta, 397
- Lagrange
 interpolating polynomials, 80, 81
Lamé constants, 408
Laplace transform, 158
Laplace's equation, 207
 in one dimension, 1
- in three dimensions, 91, 287, 291
 in two dimensions, 9
Laplacian of a scalar, 399
ldr_3d, 287
least squares approximation
 moving, 148
Legendre polynomials, 66
lgf_2d, 209
lgf_2d_1p, 212
lgf_2d_1p_w, 218
lgf_2d_1p_ww, 221
lgf_2d_1p_www, 223
lgf_2d_crc, 227
lgf_2d_fs, 211
lgf_2d_w, 215
lgf_3d, 230
lgf_3d_2p, 240
lgf_3d_fs, 232
lgf_3d_sph, 237
lgf_3d_w, 234
lgf_ax, 245
lgf_ax_fs, 249
lgf_ax_w, 252
lnm_3d, 291
Lobatto polynomials, 82, 86, 89
Lorentz reciprocal relation, 165
- mapping
 of a curved triangle, 122
 of a flat triangle, 117
material derivative, 162, 281
mean value theorem
 in three dimensions, 102
 in two dimensions, 26
modulus of elasticity, 408
- nabla operator, 399
Navier equation, 408
Navier-Stokes equation, 162, 182
 time discretized, 182
 unsteady, 182
Neumann boundary condition, 9
Newtonian fluid, 162
Newtonian potential, 132, 135, 141, 185

- non-dimensionalization, 163
- non-Newtonian flow, 187
- nonlinear equations, 131, 153
- octahedron, 114
- outer vector product, 398
- particular solution
 - for viscous flow, 185
 - in one dimension, 134
 - in two and three dimensions, 141
- Poisson's
 - equation
 - in one dimension, 134
 - in two dimensions, 141, 146
 - ratio, 408
- potential flow, 44
 - in a tank, 281
 - in an arbitrary domain, 265
 - past a two-dimensional body, 270
 - past an axisymmetric body, 276
- pressure, 162
 - modified, 164
- prtcl_2d, 376
- prtcl_3d, 390
- prtcl_ax, 385
- prtcl_sw, 371
- quadrature
 - for integrating over a triangle, 119
 - for log singularity, 73
 - Gauss-Legendre, 66
- quadruple of a source
 - in three dimensions, 98
 - in two dimensions, 17
- Radau polynomials, 83, 86
- radial basis functions, 145
- RBF, 145
- reciprocal relation
 - Betti's in elasticity, 409
 - for Helmholtz's equation, 17
 - for Laplace's equation
 - in one dimension, 2
 - in three dimensions, 92
- in two dimensions, 10
- for Stokes flow, 165
- refinement
 - h*-type, 85
 - p*-type, 85
 - r*-type, 85
- regularization
 - of a hypersingular integral, 43
 - of the double-layer potential, 126, 179
- Reynolds number, 163
- Robin boundary condition, 9
- sgf_2d, 302
- sgf_2d_1p, 311
- sgf_2d_1p_w, 315
- sgf_2d_1p_ww, 319
- sgf_2d_2p, 323
- sgf_2d_fs, 305
- sgf_2d_w, 307
- sgf_3d, 329
- sgf_3d_2p, 340
- sgf_3d_3p, 343
- sgf_3d_fs, 332
- sgf_3d_sph, 338
- sgf_3d_w, 334
- sgf_ax, 349
- sgf_ax_1p, 357
- sgf_ax_1p_ct, 361
- sgf_ax_fs, 353
- sgf_ax_w, 355
- shear flow, 261
- single-layer potential
 - of Laplace's equation
 - for the gradient, 49
 - in three dimensions, 101
 - in two dimensions, 21
 - of Stokes flow
 - in three dimensions, 176
 - in two dimensions, 172
- sloshing of a fluid in a tank, 281
- smoothing
 - of a corner, 83
 - of a function, 285
- solenoidal vector field, 399

- Somigliana's identity, 411
- spectral-element method
 - in three dimensions, 128
 - in two dimensions, 82
- splines
 - cubic, 56
 - thin-plate, 145, 148, 186
- Stehfest's method, 158
- Stokes flow, 161, 164, 301
 - axisymmetric, 177
 - past particles, 385
 - in an arbitrary domain, 364
 - oscillatory, 188
 - swirling, 371
 - three-dimensional
 - past particles, 390
 - two-dimensional
 - past particles, 376
 - unsteady, 164
- Stokes' theorem, 401
- Stokeslet, 168
- stresslet, 172
 - in three dimensions
 - pressure of, 176
 - stress of, 177
 - in two dimensions
 - pressure of, 174
 - stress of, 174
- successive subdivision, 114
- tank_2d, 281
- tetrahedron, 114
- thin-plate spline, 145, 148, 186
- Thomas's algorithm, 61
- time-dependent problems, 154
- time-discretization, 159
- TPS, 145, 148, 186
- traction
 - in a fluid, 161
 - in a solid, 407
- trgl, 203
- triangle
 - curved, 122
 - flat, 117
- triangulation, 112, 203
- adaptive, 113
- triple scalar vector product, 398
- tube flow, 254
- vector identities, 400
- vector product
 - inner, 397, 398
 - outer, 398
 - triple scalar, 398
- viscosity, 162
- viscous flow, 161
- wave equation, 160